Developing new antimicrobials for the treatment of tuberculosis and mycetoma through open source drug discovery

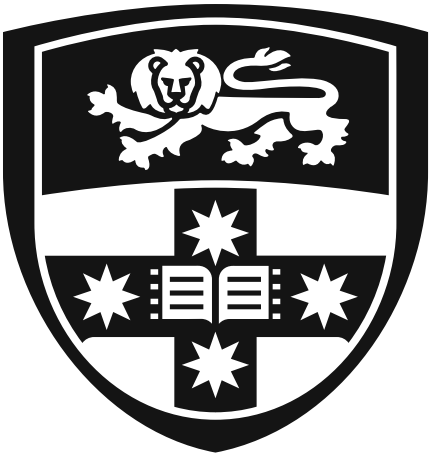

Klementine Jacqueline Burrell-Sander

A thesis submitted in fulfilment of the requirements for the degree of Doctor of Philosophy (Science)

The University of Sydney

School of Chemistry, Faculty of Science

2026

Statement of originality

This is to certify that the content of this thesis is my own work. This thesis has not been submitted for any other degree or purpose.

I certify that the intellectual content of this thesis is the product of my own work, and that all assistance received in preparing this thesis and all sources have been acknowledged.

Klementine Jacqueline Burrell-Sander

This research was supported by an Australian Government Research Training Program (RTP) Scholarship.

Abstract

Diseases that predominantly affect people in poorer nations have been historically neglected by the profit-motivated pharmaceutical industry. Tuberculosis (TB) and mycetoma are two examples of such diseases. Despite being the most fatal infectious disease globally, there has been relatively little innovation in the treatment of TB in the past four decades, and drug-resistant strains of TB are becoming an increasing concern. Mycetoma is a condition caused by either bacteria (actinomycetoma) or fungi (eumycetoma), resulting in tumour-like growths that disfigure and disable those affected. Actinomycetoma is currently treated with a harsh and lengthy drug regime which increases the likelihood of patient non-compliance, leading to the bacteria developing resistance to the antibiotics in use. Meanwhile, the curative rate of antifungals used against eumycetoma is estimated to be as low as 25%, even with treatment also including surgical intervention.

Open source drug discovery (OSDD) is a research model that aims to accelerate the development of new treatments for neglected diseases by following the principles of open science, which include sharing data openly and encouraging collaboration at all levels. This thesis describes the progress of two OSDD projects in mycetoma and TB research. Chapter 1 outlines the pathology and existing treatment of mycetoma and TB, and presents the foundation and development of open science practices, including citizen science.

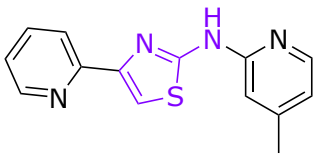

I

Previous work had identified that 2-aminothiazole derivative **I** showed promising activity against *Madurella mycetomatis*, the primary causative agent of eumycetoma. Chapter 2 describes the synthesis of a compound library of 2-aminothiazole analogues through an educational citizen science program embedded into undergraduate and secondary school curricula. Chapter 3 investigates the bioactivity of this compound library against *M. mycetomatis* through both *in vitro* cell viability assays and *in vivo* testing in a larval model. Structure-activity relationships and potential mechanisms of action are discussed. Substitutions are generally well-tolerated, but removal of nitrogen from either of the 6-membered rings causes a dramatic decrease in activity.

Chapter 4 reports cross-screening of the same compound library against both *Mycobacterium tuberculosis* (*Mtb*), the causative agent of TB, and three bacteria commonly responsible for actinomycetoma, *Nocardia brasiliensis*, *Actinomadura madurae* and *Streptomyces somaliensis*. This chapter also details the development of a resazurin-based viability assay for actinomycetoma that can be used to accelerate both susceptibility testing with existing antibiotics and drug discovery efforts to find novel therapeutic agents.

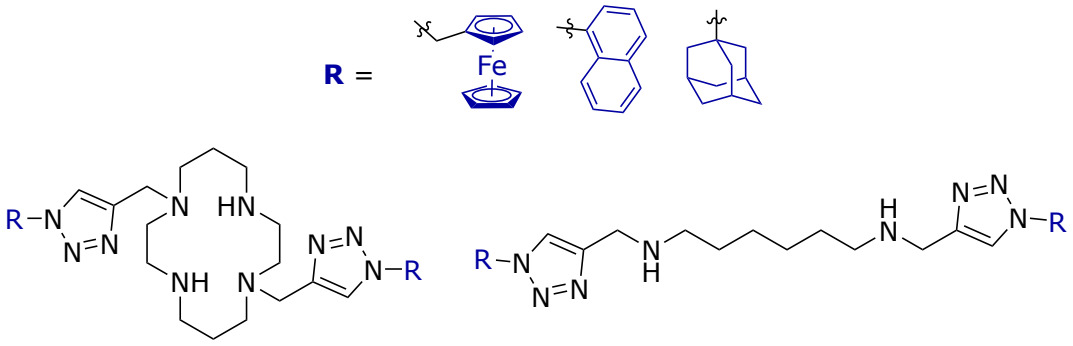

Chapter 5 focuses on the synthesis of novel anti-tubercular agents derived from bis-naphthyl functionalised cyclam analogues found to have potent activity against *Mtb*. Preliminary structure-activity relationship studies analyse the effect of changes to the pendant group and the polyamine core, with naphthyl, ferrocenyl and adamantyl groups being appended to cyclam and various 'open cyclam' linear polyamine scaffolds. Biological screening of these analogues indicated that ferrocene and adamantane are tolerated as three-dimensional bioisosteres of the planar naphthyl groups, but failed to elucidate a clear trend between biological activity and changes to the polyamine core.

Statement of student contribution

The work described in this thesis was conducted by the author in the School of Chemistry at the University of Sydney under the supervision of Prof. Peter Rutledge and Prof. Alice Motion, and at the Erasmus Medical Center in Rotterdam under the supervision of A. Prof. Wendy van de Sande.

High-resolution electrospray ionisation and all atmospheric pressure chemical ionisation mass spectrometry data were acquired by Dr. Nicholas Proschogo and his staff at the Mass Spectrometry Facility in the School of Chemistry. High-field ^{1}H and ^{13}C NMR spectra were acquired by Dr. Ian Luck and his staff at the Magnetic Resonance Facility at Sydney Analytical.

The Breaking Good workshops, including the synthetic route to the 2-aminothiazoles and selection of target compounds for 2021 and 2022 cohorts, were initially developed by Dr Kymberley Scroggie of the University of Sydney. Purification and characterisation of compounds made by the 2021 undergraduate cohort and 2022 high school cohort was also performed by Dr Kymberley Scroggie. Purification and characterisation of compounds from the 2023 high school cohort, 2024 high school cohort and 2024 undergraduate cohort was completed with the aid of Dr Anita Marfavi, Dr Julius Adamson and Dr James Lloyd respectively. Additional 2-aminothiazole compounds were provided by Dr Peter Rayner of the University of York and Dr Erika Loizidou of the University College London.

The i*n vitro* and *in vivo* screening processes described in Chapter 3 were developed by A. Prof. Wendy van de Sande of the Erasmus Medical Center. Unless otherwise stated, testing was performed in collaboration with members of the van de Sande group, primarily Dr Jingyi Ma and Dounia el-Yachioui.

Resazurin fluorescence assays for testing against *Mtb* described in Chapters 4 and 5 were developed by Prof. Jamie Triccas and Dr Gayathri Nagalingam of the Centenary Institute and Charles Perkins Centre. Testing described in Chapter 3 was performed by Dr Diana Quan of the Centenary Institute, and testing described in Chapter 5 was performed by Dr Maxwell Stevens, also of the Centenary Institute.

All other work described in this thesis was my own, including all figures, tables, graphs and schemes not otherwise referenced.

Statement of AI Use

To the best of my knowledge, no content produced by generative AI tools has been used in the preparation of this thesis.

Acknowledgements

Choosing to start a PhD is a funny thing. It may seem like a deeply individualistic goal – after all, you're trying to become the top expert in a specific niche area – but for me, the process of obtaining this degree has been an exercise in realising how much we benefit from each other. The building of knowledge has always worked best as a group endeavour, and I've never realised this more so than in the past four years. I cannot begin to name everything I have learnt, whether from hallway chats or in friendly arguments over cheap sparkling wine, from students less experienced than me or from professors – I have truly benefited so much from the people around me, and I wish I could thank every one of you. Ultimately, doing this degree has changed my perspective on myself, other people and the world around me, and I'd like to think it's for the better.

Peter and Alice, thank you for the enthusiasm, trust and kindness you have always showed me. I am so grateful to have had supervisors who don't just share my values, but model them openly and encourage us to do the same. You've taught me so much while allowing me the freedom to make my own decisions, and I am certain it's made me a better researcher and person.

Thanks to the SCOPE and Rutledge groups across the years for complimenting my cakes and supporting me through my various complaints. Carlota and Sim, thank you for keeping things interesting in the lab and at the pub in that first year of my PhD in particular – you made life fun. Larissa, Gen and Olivia – thank you for all the times you let me whinge about the same old problems and show you cat photos while you were trying to get your work done. And Olivia, it goes without saying that SUCS was never the same without you.

Dounia, you almost single-handedly kept me sane and cheerful during my stint at Erasmus. Thank you for never judging me for being clueless about something biological and for keeping me stocked with excellent reading material.

Jen and Seb, thank you for reminding me that there is in fact a life outside of academia, and for always being ready to hate on AI (and other things) with me. You've always helped me to find some perspective in this silly, stressful world.

Tom, you'd absolutely come second place if having coffee and alcoholic beverages with me while complaining about uni was a competition. Thank you for always being willing to help

me out, whether it was with basic chemistry, arcane university knowledge or an introduction to someone else. Thank you for being there since all the way back in 2017.

Leila, you're a mad genius and a proper friend. Thank you for being so genuine and keen to lend a hand, from the time you emailed me with additions to my list of dessert slices right up to proofreading part of this very thesis.

And now my family – what is there to say? I don't think any of us quite expected me to end up here, but I know I would never have made it this far without the love and support from all three of you. Audrey, thank you for always wanting to share what you love – I'm so glad you encouraged me to follow you to USyd. Mum and Dad, I swear I didn't mean to extend the academic stress of high school into almost ten years of university. I can't promise I'll stop now, but thank you a million times over for talking me through my catastrophising, celebrating my achievements and being so proud of me no matter what. I love you all.

Finally, my beloved Julius, thank you for always having the conviction in me that I sorely lacked. You were so calm and helpful whenever I was stressed, so sweet when I was down and so utterly confident in me at all times that I ended up actually believing that I could do a PhD in chemistry. Now here I am – and I absolutely could not have done it without you.

Table of Contents

Abbreviations and symbols

°C	Degrees Celsius
µg	Microgram(s)
µL	Microlitre(s)
µM	Micromolar
2-AT	2-aminothiazole
Ad	Adamantane
APCI	Atmospheric pressure chemical ionisation
ATP	Adenosine triphosphate
AUC	Area under curve
$B_{AC}2$	Base-catalysed acyl bond cleavage
$B_{AL}2$	Base-catalysed alkoxy bond cleavage
BG	Breaking Good
Boc	*Tert*-butyloxycarbonyl
CFU	Colony-forming units
CLSI	Clinical and Laboratory Standards Institute
cm^{-1}	Wavenumber(s)
CO-ADD	Community for Open Antimicrobial Drug Discovery
CuAAC	Cu(I)-catalysed azido-alkyne click coupling reaction
CYP51	Cytochrome P-450 51
d	Days
d	Doublet
D3	Distributed drug discovery

DBU	1,8-diazabicyclo(5.4.0)undec-7-ene
DCAD	Di-*p*-chlorobenzyl azodicarboxylate
DCM	Dichloromethane
DEAD	Diethyl azodicarboxylate
DHODH	Dihydroorotate dehydrogenase
DIAD	Diisopropyl azodicarboxylate
DIPEA	*N*,*N*-Diisopropylethylamine
DMF	*N*,*N*-Dimethylformamide
DMSO	Dimethyl sulfoxide
DNA	Deoxyribonucleic acid
DNDi	Drugs for Neglected Diseases initiative
DPPA	Diphenylphosphoryl azide
DST	Drug susceptibility testing
DS-TB	Drug-susceptible tuberculosis
E. coli	Escherichia coli
EP	Efflux pump
EPI	Efflux pump inhibitor
eq.	Equivalent(s)
ER	Estrogen receptor
ERG11	Sterol 14-demethylase
ESI	Electrospray ionisation
et al.	And others
EUCAST	European Committee on Antimicrobial Susceptibility Testing
FAIR	Findability, Accessibility, Interoperability and Reusability

Fc	Ferrocene
g	Gram(s)
G. mellonella	*Galleria mellonella*
GSK	GlaxoSmithKline
h	Hour(s)
HIV	Human immunodeficiency virus
HRMS	High-resolution mass spectrometry
IC_{50}	Inhibitory concentration 50%
in situ	Within the original context
in vacuo	Within a vacuum
in vitro	Within a laboratory vessel
in vivo	Within a living organism
IR	Infrared
J	Coupling constant
K_{Ca}	Calcium-activated potassium channels
L	Litre(s)
LRMS	Low-resolution mass spectrometry
M	Molecular ion
M	Unspecified metal
M	Molar
m	Multiplet
m.p.	Melting point
m/z	Mass-to-charge ratio
MDR-TB	Multi-drug-resistant tuberculosis

MeCN	Acetonitrile
MHz	Megahertz
MIC	Minimum inhibitory concentration (lowest dose required to achieve complete inhibition)
MIC_{50}	Minimum inhibitory concentration 50% (species-wide)
min	Minute(s)
mL	Millilitre(s)
mm	Millimetre(s)
mM	Millimolar
mmol	Millimole(s)
MMV	Medicines for Malaria Venture
MOPS	3-(*N*-morpholino) propanesulfonic acid
Mtb	*Mycobacterium tuberculosis*
MTS	(3-(4,5-di methyl thiazol-2-yl)-2,5-diphenyltetrazolium bromide)
MycetOS	Open Source Mycetoma
NAD+	Nicotinamide adenine dinucleotide cation
NADH	Nicotinamide adenine dinucleotide
NBS	*N*-bromosuccinimide
NC	Negative control
NDH-2	Type II NADH:quinone oxidoreductase
nm	Nanometre(s)
nM	Nanomolar
NMR	Nuclear magnetic resonance

Ns	2-nitrosulfonamide
NTD	Neglected tropical disease
OSDD	Open source drug discovery
OSM	Open Source Malaria
OSTB	Open Source Tuberculosis
p.t.	Proton transfer
PC	Positive control
pH	Hydrogen ion concentration, logarithm
ppm	Parts per million
*p*TSA	*para*-toluenesulfonic acid
q	Quartet
R	Variable group
RNA	Ribonucleic acid
RND	Resistance nodulation cell division
RPMI	Roswell Park Memorial Institute
RR-TB	Rifampicin-resistant tuberculosis
rt	Room temperature
s	Second(s)
s	Singlet
SAR	Structure-activity relationships
spp.	Several species
t	Triplet
TAM	Tamoxifen
TB	Tuberculosis

TFA	Trifluoroacetic acid
THF	Tetrahydrofuran
TLC	Thin-layer chromatography
TMS	Trimethyl silyl
UCL	University College London
UNESCO	United Nations Educational, Scientific and Cultural Organization
UV	Ultraviolet
WHO	World Health Organization
XDR-TB	Extremely drug-resistant tuberculosis
XTT	(2,3-bis-(2-methoxy-4-nitro-5-sulfophenyl)-2H-tetrazolium-5-carboxanilide)
Z	Variable group
δ	Chemical shift

1 Introduction

1.1 Open science

It is a truth near universally acknowledged that the current scientific model presents undesirable challenges. The modern system of patents, journal publications and competitive research funding encourages an environment of secrecy and individualism, with scientists incentivised to withhold results and key information rather than share their work openly.[1–4]

Previously, physical distance and limited means of communication resulted in scientific inefficiency.[5] Perhaps the most famous example of this is that of Newton and Leipzig, now generally accepted to have both independently invented calculus in the late seventeenth century.[6] Who is to say what further leaps in mathematics could have been made if only these prodigies had put their two heads together instead of working separately to solve the same issue?

Despite having largely overcome the limitations of distance with modern communications technology, science remains hindered by the constraints of profit-driven models of research.[7] When projects and careers rely on precarious funding, it is not surprising that scientists are wary of sharing ideas, data and results.

Open science is a repudiation of the secrecy, elitism and closed-mindedness that has encroached on scientific research in the past century or so. The United Nations Educational, Scientific and Cultural Organization (UNESCO) has produced the following official definition:

"Open science is a set of principles and practices that aim to make scientific research from all fields accessible to everyone for the benefits of scientists and society as a whole. Open science is about making sure not only that scientific knowledge is accessible but also that the production of that knowledge itself is inclusive, equitable and sustainable."[8]

Open knowledge scholar Eva Méndez envisioned open science as a living organism with its foundations in the goals of cross-collaboration, fostering principles of research integrity and democratising the field by opening it to all.[9] These sub-practices, then, can be seen as branches of the open science "tree" (**Figure 1.1**), with each having different offshoots that have led to diverse innovations, from shadow libraries to science in schools. Making science open is not just lofty idealism, it is rooted in a desire to do better science.

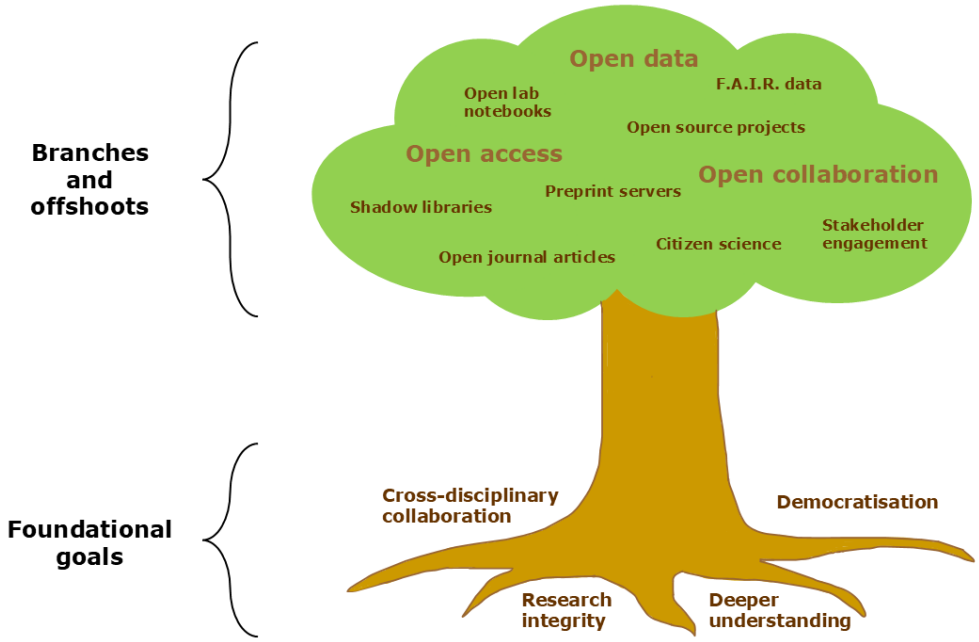

Figure 1.1 – Depiction of the Open Science "tree" adapted from Eva Mendez's Open Science Mushroom.[9]

Open science practices have emerged from the base goals of improved collaboration, integrity and democracy, and are now posited to improve efficiency, accelerate research and reduce redundancy. There is mounting evidence to support these claims across many disciplines and levels of research.[10–14] Open practices have been found to improve communication, regulation and monitoring processes in various fields,[12] and open science principles have underpinned various notable scientific achievements, from the Human Genome Project to the development of drugs for COVID-19.[15,16] In 2025, a comprehensive scoping review on the academic impact of open science found positive effects on many key areas, including efficiency, reproducibility and quality.[17] Making science more open may also help address inequalities of access and recognition by giving scholars around the world more avenues to find, use and disseminate new findings.[18]

1.1.1 Defining open science

Usually, open science is recognised as a patchwork of different sub-practices, including *open collaboration*, *open access* and *open data*, though some methods may overlap between these fields. [19] Within the open science movement, specific applications of these principles and

related terminology can vary, especially between different fields of research. In this work, the following terms are applied as defined below, and may differ from terminology used elsewhere.

Open data is the practice of making all data available for scrutiny and re-use by other researchers. Scientific organisations around the world have supported a movement towards open data,[20] with many encouraging researchers to follow the FAIR principles of Findability, Accessibility, Interoperability and Reusability.[21] These principles aim to ensure that data, digital tools and protocols are shared in a way that allows other researchers to access them easily, whether their goal is to assess claims made on the basis of the data, use the data for their own project or simply learn from the processes being used. In brief, this means data should be shared in appropriate, broadly accessible formats, methods should give full and sufficient detail for reproducibility, and metadata, such as timestamps or categorisation data, should be included where relevant.[21] There is a clear benefit to science as a whole in following these guidelines. Firstly, open data allows scientists to access valuable information without repeating efforts already undertaken by their peers, thus reducing costs and saving labour.[15] Secondly, having data that can be easily reviewed by other experts reduces the impact of research based on faulty data collection or analysis, whether due to unscrupulous practices or genuine error.[22]

Open access refers to making research publicly available, usually by removing paywalls from scientific journals that prevent scholars and members of the public from being able to read articles directly. These paywalls have been accused of perpetuating inequity in publishing, as researchers with less funding cannot stay up to date with new research as easily as their peers.[3,23,24] In 2011, computer scientist Alexandra Elbakyan attempted to combat this bias by launching Sci-Hub, a website that aims to provide completely free access to all published research papers, regardless of copyright and paywalls. The online "shadow library" has enjoyed enormous success ever since, with thousands of papers downloaded daily. Data shared by Elbakyan in 2015 indicated that in a six-month period, millions of papers were requested across the world, with the number of requests often disproportionately high in countries with lower socioeconomic status (**Figure 1.2**) – presumably due to researchers in these countries having less funding to spend on paywalled journals.[25]

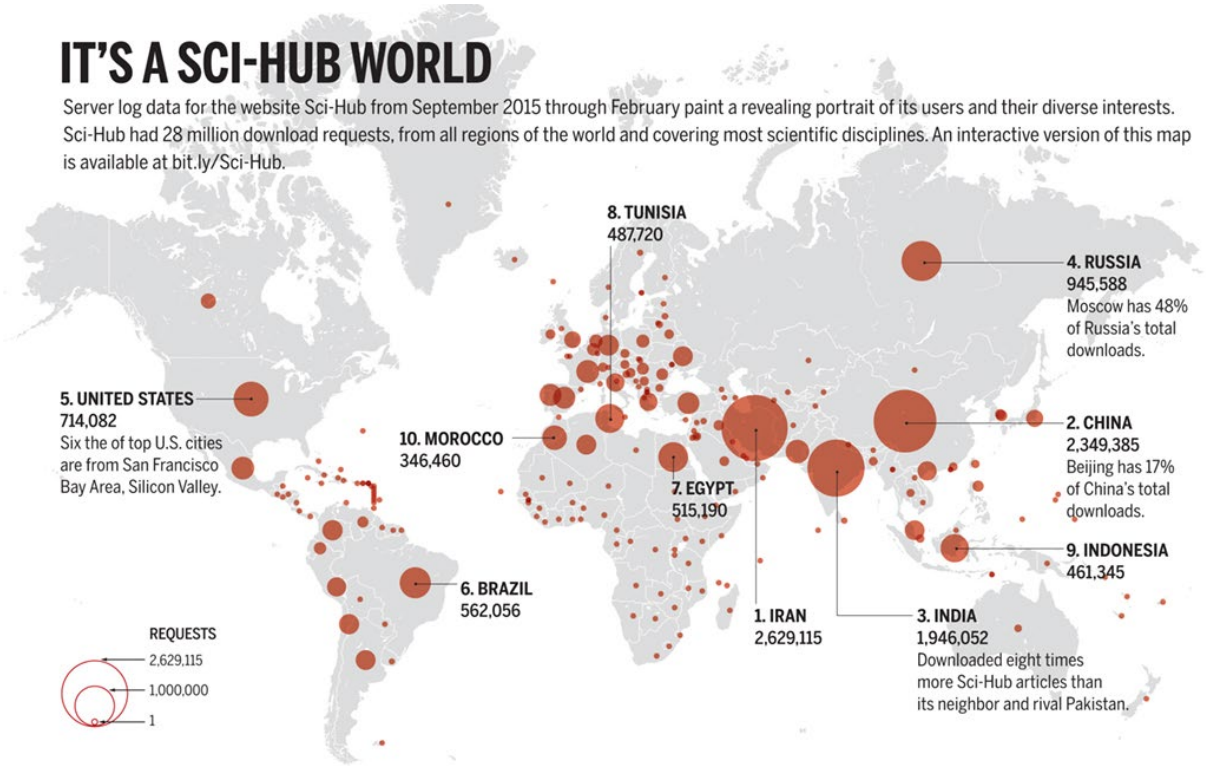

Figure 1.2 – Sci-Hub usage across the globe during September, 2015. Data provided by Sci-Hub founder Alexandra Elbakyan, visualised by Elbakyan and Bohannon and reproduced under CC BY 4.0.[25]

More broadly, a 2022 study found that over 50% of the researchers surveyed had used Sci-Hub or similar "scholarly piracy" methods to obtain research articles. While there are legal concerns about such practices, their growing prevalence is likely a factor behind the introduction of "open access" articles in scientific journals, where scholars pay a higher publishing fee to the journal in exchange for the journal removing paywalls to the article. This has generally been seen as a sign of progress for the open science movement, though questions remain about the ethics of making it more expensive to do better science.[23,26] In any case, open access articles are now offered by all major scientific publishing companies.

The dawn of the preprint server is also considered a revolutionary moment in the history of scientific access. Preprint servers are freely accessible online repositories where scientists are encouraged to uploaded complete articles prior to the peer review process. This allows scientific data to be disseminated much more rapidly than the traditional model, in which weeks or months might pass before an article is deemed worthy of publication.[27] Despite fears that sharing unreviewed work might result in the propagation of "bad science" – that is, science that *wouldn't* pass the peer review process – most evidence suggests that sharing preprints can

actually improve the quality of the final article by allowing immediate, interactive discussion of the paper's contents.[28] Uptake of the preprint model has varied across disciplines, with the largest server, ArXiv, being hugely popular in the fields of physics and mathematics, while the biggest servers for chemistry (ChemRxriv) and biology (bioRxiv) are both more recent developments and less widely used.[27,28]

Finally, *open collaboration* is perhaps the most poorly defined of the terms under consideration. In some cases, it can refer simply to collaboration between research groups or institutions,[29] and in others to participation from a broad range of stakeholders or community members.[30] In essence, open collaboration is about sharing the actual research process with a larger audience so that alterations can be made as the research occurs. This differs from open access and open data in that changes or suggestions can be incorporated into ongoing work, resulting in richer, better developed projects.[1] A well-established example of open collaboration can be found in the world of computing, where open source programs make the underlying code public and encourage the community to adapt the code for their own specific requirements or suggest improvements to the existing project. Making a project open source is thus not purely altruistic, as community feedback can identify and solve errors and generally contribute to a better functioning program.

As the advantages of this model have become apparent, open science has been embraced both within the scientific community and by government and public sectors.[18] The Directory of Open Access Journals logged over 1,500 scientific journals offering open access publishing in 2021, which translates to over a million articles on topics from astrophysics to zoology.[31] Government research sectors across the world have endorsed the FAIR data principles, including the European Open Science Cloud,[32] and the US Government's National Institute of Health,[33] with the Australian Research Data Commons requiring all publicly funded research to adhere to FAIR guidelines.[34] The uptake of open collaboration is difficult to measure, as implementation can vary hugely, but many fields certainly boast flourishing open science communities in which collaboration is encouraged at various levels. Even if open science is not yet the dominant research mode across the globe, it is growing rapidly and certainly seems to be here to stay.

1.1.1 Open source drug discovery

Naturally, uptake of open science principles is not evenly distributed throughout the various scientific disciplines, and some practices are more popular than others. Although chemists were quick to embrace open access articles and preprints in the late nineties,[35] the percentage of chemistry articles published in open access journals is now far outstripped by those in biological and life sciences.[36] In medicinal chemistry especially, the patent model is the main means by which companies protect their intellectual property and recoup the costs of research and development.[37,38] Confidentiality is therefore greatly valued and sharing data too openly can be perceived as a threat to a company's businesses model, making it difficult to enact the principles of open science.[38,39] Nonetheless, there are a growing number of open science initiatives specific to medicinal chemistry, from open source tools to analyse pharmacological patents to the application of machine learning approaches.[40–42]

Pharmaceutical development is traditionally a heavily profit-driven field in which diseases with greater potential for financial return on investment tend to receive significantly more attention.[43] Typically, this translates to a focus on so-called diseases of the wealthy – those which primarily affect people in higher-income countries who are likely to be able to afford expensive, prolonged treatments. Meanwhile, conditions that have very low patient populations or are more prominent in lower-income countries are relatively understudied, as patients are generally less able to afford treatments with the hefty price tag required to make pharmaceutical research profitable.[44]

This phenomenon is so widespread that a subset of diseases with minimal profit potential have been categorised as neglected tropical diseases (NTDs) due to the comparative lack of investment in research on them.[43] NTDs are usually caused by exposure to microorganisms as a result of inadequate infrastructure and public health measures, such as poor waste management or overcrowded housing.[45] Examples include parasitic infections like leishmaniasis or fungal infections like eumycetoma and sporotrichosis.[46,47] In contrast, malaria and tuberculosis (TB), while both primarily affecting people in underfunded countries, are usually distinguished as "diseases of poverty" but not considered NTDs because of the considerable efforts made by governments to combat them.[48,49] These efforts reflect the enormous burden that malaria and TB represent to developing countries' economies and health systems.[45]

It is these conditions that have most attracted the attention of open science, and led to the evolution of new modes of drug discovery.[43,50] Apart from this cruel bias against 'non-lucrative' diseases, the current model of research suffers from a second serious flaw – a people problem. The pharmaceutical sciences rely heavily on work performed by private companies or academic institutions in wealthy countries, and is famously secretive about ongoing research.[51] This necessarily limits innovation and collaboration to a circumscribed network of experts, where projects cannot benefit from the knowledge of scientists, clinicians and even members of the public from outside of that network.

Throughout the history of medicine, countless invaluable contributions have come from outside the established field of experts. A classic example is that of traditional knowledge of medicine and natural products, which has historically not been recognised as science yet has contributed to the development of countless drugs, from the everyday aspirin derived from willow bark to the first-line anti-malarial drug artemisinin, identified from the sweet wormwood used in traditional Chinese medicine.[52] These contributions can also be serendipitous, as when anaesthetist John Snow revolutionised understanding of infectious disease by identifying contaminated water as the cause of the infectious disease cholera.[53] Open source drug discovery (OSDD) thus presents an opportunity to make pharmaceutical development more egalitarian and more efficient by leveraging the efforts of community members and researchers from diverse disciplines, institutions and countries.[54]

Now, a growing number of drug discovery programmes have committed to open science goals of access and transparency, with some going further and developing projects based on open collaboration and knowledge-sharing.[51] Professor Mat Todd used the term open source drug discovery (OSDD) to describe projects which encourage open collaboration throughout the scientific process rather than only sharing final data and findings. The first project operating under this name was a community-based effort to find new ways to synthesise praziquantel, a drug used as the first-line treatment for the NTD schistosomiasis.[55] In 2011, Todd outlined guiding principles for current and future OSDD projects, dubbed the "Six laws of open source drug discovery", as follows:

1. All data and ideas are freely shared
2. Anyone may participate at any level
3. There will be no patents
4. Suggestions are the best form of criticism

5. Public discussion is more valuable than private email
6. An open project is bigger than, and not owned by, any given lab

The guidelines highlight the importance of accessibility, collaboration and openness, and have been used as the basis for drug discovery projects in malaria (Open Source Malaria - OSM),[56] tuberculosis (Open Source Tuberculosis - OSTB),[57] mycetoma (Open Source Mycetoma - MycetOS) and antibiotic resistance (Open Source Antibiotics) (**Figure 1.3**).[58,59]

Figure 1.3 – Logos for four OSDD projects following Todd's guidelines. From left to right: Open Source Malaria, Open Source Tuberculosis, Open Source Antibiotics, Open Source Mycetoma.

However, there are numerous projects that follow most or all of these OSDD guidelines while not using the term themselves. In 2008, another early pioneer of the concept, William Scott, coined the alliterative name *distributed drug discovery* or *D3*, for a project in which university students in different countries worked to synthesise chemical libraries of biologically active compounds.[60] In 2025, the most widely-used alternative appears to be *open drug discovery*, as used by the Community for Open Antimicrobial Drug Discovery (CO-ADD) which provides free-of-charge screening of compounds against a range of microbial targets, and collaborates with researchers from other fields to proceed through the drug discovery process.[61]

Notably, some organisations or programmes simply dub their work to be *open science* or a similarly broad term, rather than use a specific moniker. For instance, the Medicines for Malaria Venture (MMV) has a branch called MMV Open, which supplies drug discovery software and compound libraries free of charge to drug discovery researchers on the condition that any scientific findings resulting from screening are made publicly available.[62] They have also collaborated directly with the OSM project, as well as supporting various other open science initiatives. Similarly, the Drugs for Neglected Diseases initiative (DNDi) cites their commitment to *"sharing research data, knowledge and costs"* and has supported the MycetOS

project, as well as other drug discovery ventures around leishmaniasis, schistosomiasis and other NTDs.[63]

The COVID Moonshot programme is perhaps the most convincing argument for OSDD, despite not formally adopting that description. In January 2020, Zhang and colleagues sequenced the COVID-19 genome and gave permission for it to be shared publicly. Within just 15 days of its release, structural biologists around the world had identified the main protease Mpro (3CL-protease) and potential inhibitors, and the project was made fully public in March that year.[64,65] By 2023, thousands of relevant compounds had been identified, synthesised and analysed, and data from the project was used to identity ensitrelvir as a treatment that could be repurposed for COVID-19 as early as 2022.[65]

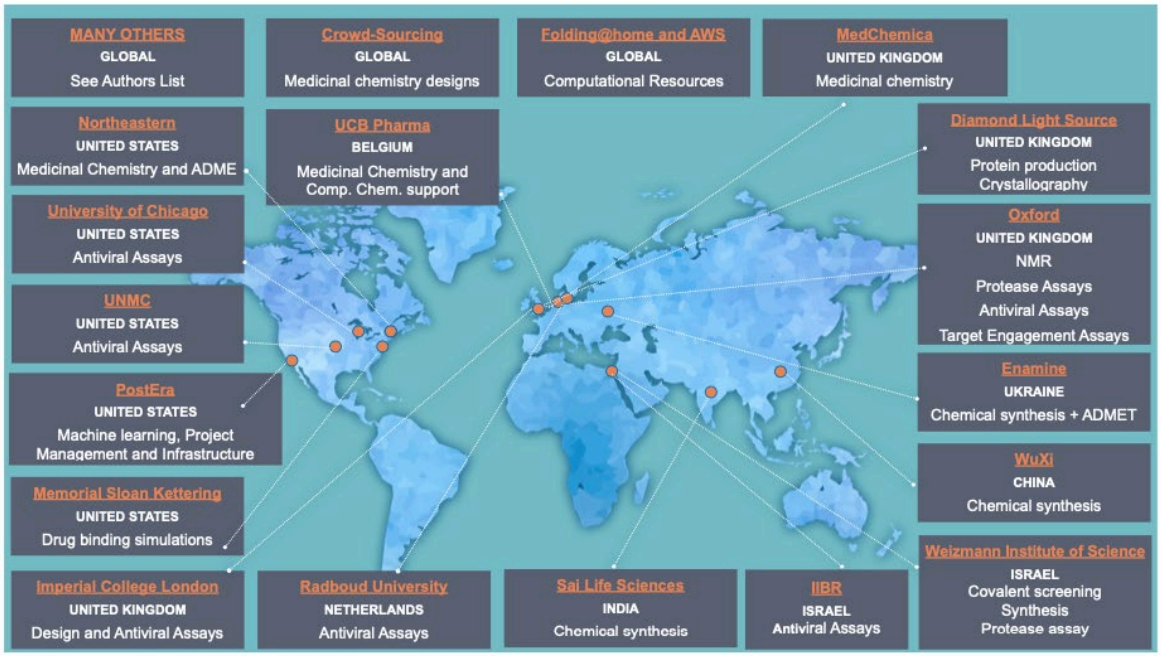

Figure 1.4 – Contributions to the COVID Moonshot program from across the globe. Adapted from the COVID Moonshot Consortium under CC BY 4.0.[16]

COVID Moonshot represents a dramatic acceleration of the typical drug discovery pipeline, which can take years or even decades to identify and evaluate new treatments, and has been recognised as an exemplar of how open collaboration can benefit patients around the world.[66] **Figure 1.4** showcases the range of collaborators involved in the project, with people participating from diverse geographical locations, institutions and disciplines.

Beyond finding new treatments for coronaviruses, the Moonshot project has served to both publicise and popularise the concept of OSDD, with proponents using it as a prime example of

why a global effort should be made to deal with diseases that affect any part of the world – in the case of COVID-19, collaboration became a matter of self-preservation as much as humanitarianism. There is now growing interest in the field as a means of making drug discovery not just more efficient, but also more democratic and equitable.

1.1.2 Citizen science

Citizen science, sometimes called participatory science, is another important domain of open science, and one that has historically intersected with OSDD efforts. Although citizen science hasn't always been recognised as a facet of open science, this perception is gradually changing, as evidenced by its inclusion in the UNESCO Recommendation on Open Science.[67]

The Australian Citizen Science Association defines citizen science as *"public participation and collaboration in scientific research with the aim to increase scientific knowledge"*, and projects are typically considered to be citizen science if they involve members of the public carrying out some part of research that is typically done by trained scientists.[68] This encompasses a huge range of activities across the natural sciences, including sample collection, environmental monitoring, data analysis and more. To cite just a few examples, participants might collect samples of river water to assess water quality (WaterWatch Australia),[69] record observations of weather conditions or animal sightings (Citizen Weather Observer Program, iNaturalist)[70,71] or analyse spectroscopic data to identify cosmic phenomena (Galaxy Zoo, RAD@home).[72] Citizen science projects vary in size, discipline and level of participation, but are increasingly popular with both governments and the community.[73,74]

Defining the beginning of citizen science is close to impossible, as the twentieth century model of research relies on a context of institutional learning, governmental funding and academic rigour that did not exist in previous centuries.[75] Although barriers such as financial means and biases against gender, race and class certainly impacted the research done in the past, the very word *scientist* only dates from 1834, and fans of Mary Shelley may remember that in 1818, Dr Frankenstein attends lectures on *natural philosophy* about potassium and boron.[76] This apparently benign change of nomenclature heralded a new understanding of science as *practical* work done as a profession, rather than the *practice* of questioning and probing the natural world (which was often achieved through observation and experimentation).[77] It is only in recent decades that the scientific community has begun to formally recognise the efforts of

community members, and there is increasing acknowledgement that the work done by dedicated amateurs can be just as valuable as that of professionals.[78]

As in any field, there are differing opinions on the role and scope of citizen science even among its advocates. Many experts feel that a citizen science approach leads to richer data and more accurate representation of the subject being studied.[79] For some, citizen science represents a hitherto underutilised resource, especially when a project can benefit from observations or activities that people do anyway, like taking photos of wildlife or solving puzzles.[80] Others champion citizen science for its capacity to democratise and universalise scientific research,[79] which can be summarised broadly by two objectives. Firstly, participating in citizen science not only builds awareness of important issues but also enables the community to develop relevant skillsets, improve their science literacy and become active in shaping the environments they live in.[73] Secondly, giving voices to marginalised individuals can lead to important progress in fields directly affecting them – and in others that do not. Unfortunately, these same individuals often face more barriers to participating in formal scientific training and research, whether this be due to prejudice, lack of access or cultural norms. Citizen science has been proposed as an alternative avenue for people in these positions to bring their ideas and experiences to research in diverse fields, especially if projects are designed with the goal of overcoming such barriers.[81–83]

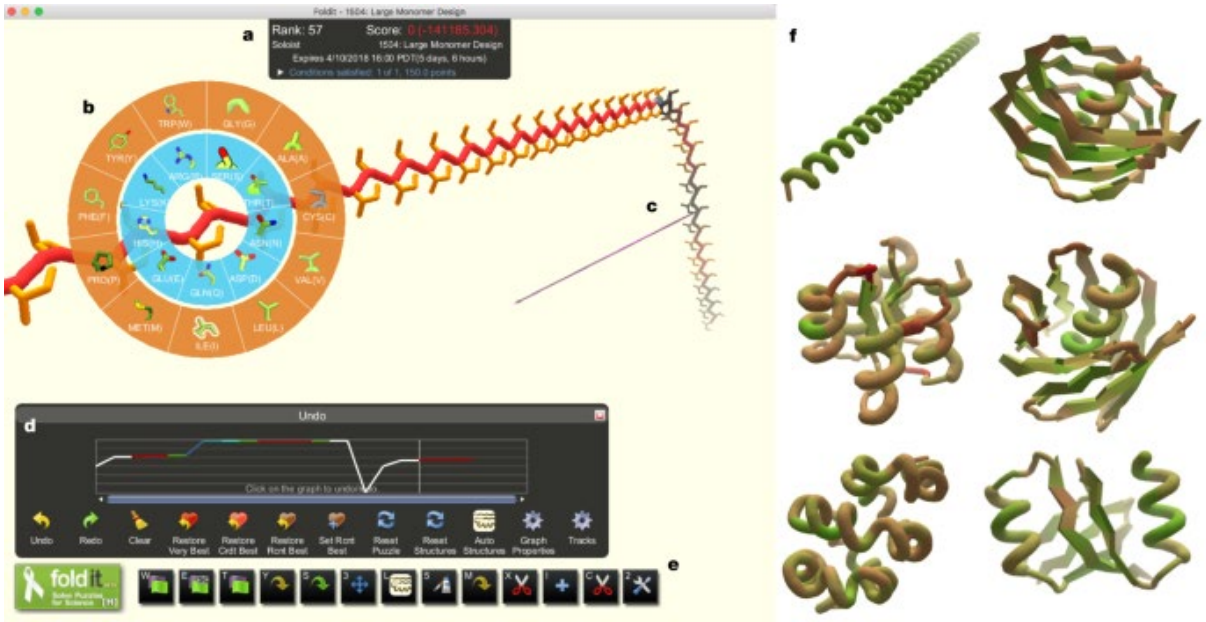

Figure 1.5 – Screenshot from the Foldit citizen science game showing user interface with 3-D protein structures. Adapted from Koepnick *et al.*, 2019 with permission.[84]

Citizen science has enjoyed a surge in popularity in recent years, with many high-profile projects developing citizen science branches, and governments around the world dedicating funding to research with citizen science opportunities.[73] In 2024, many citizen scientists were thrilled to see biochemist Robert Baker become a joint recipient of the Nobel Prize for Chemistry for his work on computational protein design.[85] This work included a rich history of contributions via citizen science, beginning in 2004 when Baker launched Rosetta@home, a software program that enabled volunteers to use their personal computers to perform calculations to predict protein folding. A few years later, interest from these volunteers prompted his team to create Foldit, an online video game in which players interact with 3D models to solve protein folding problems, as shown in **Figure 1.5**.[86] Foldit gameplay has consistently generated valuable scientific findings since its release in 2008, with players even becoming authors on scientific papers in recognition of their contributions.[87]

However, adoption of citizen science varies dramatically across different disciplines due to both societal and scientific factors, as certain disciplines lend themselves more easily to public participation. Research that relies on large amounts of data being collected or analysed, such as astronomy and ecology, can incorporate volunteer participation relatively easily provided they can access appropriate technological infrastructure.[78] In other fields, running experiments or collecting data may require specialised skills or expensive equipment, or involve significant safety risks to researchers or the subjects of a study. While there are undoubtedly still ways for the public to contribute to these disciplines, as Baker's success with Foldit demonstrates, it can require specially designed projects or a restricted scope of work.

Despite the initial challenges of incorporating citizen science into research, the field is only continuing to grow.[88] One of the largest citizen science platforms, Zooniverse, introduced 65 new projects in 2019-2020;[78] and boasts nearly 3 million registered volunteers as of 2024.[89] The impetus behind this demand may vary, from institutions seeing it as a two-in-one research-and-outreach opportunity to a genuine desire to involve communities and innovate research, but citizen science is undeniably on the rise.

1.1.3 Science communication, outreach, participation and education

One setting in which citizen science is increasing in popularity is formal education, from primary through to tertiary. The exact goals of implementing citizen science can differ between educators and researchers,[90] but broadly involve increasing student engagement with and knowledge of science by providing an opportunity for genuine participation in the scientific process. It is well-established that students engage better with science content that they consider relevant to themselves, whether this is on a personal, societal or vocational level.[91] Lüsse and colleagues suggest that citizen science is most useful for establishing the societal relevance of scientific knowledge and demystifying the otherwise rather nebulous concept of "research".[92] By harnessing an individual's external motivations, citizen projects are proposed to improve the person's continuing understanding of, interest in and support for scientific endeavours. This relationship is illustrated in **Figure 1.6**, with potential motivations including a prior interest in a given topic, the desire to solve a problem – like reducing pollution so that outdoor spaces are more pleasant to use – or simply educational and training obligations.

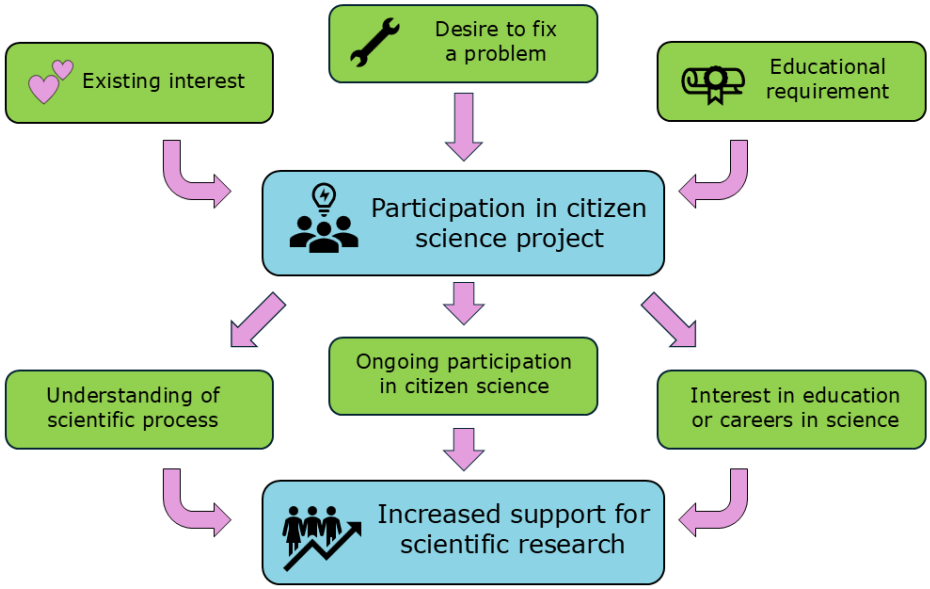

Figure 1.6 – Proposed model of motivations for and impacts of citizen science participation.

Developing this kind of positive relationship with science is important beyond just encouraging students to pursue scientific careers. Scientists are increasingly struggling to accurately communicate their work to the public in the context of social media, viral disinformation and

the so-called "attention economy",[93–95] yet both government funding and community support for research projects can hinge on how well non-scientists understand a given project. The perils of such discrepancies between policy makers, voting populations and researchers has been made painfully apparent with the recent defunding of many scholarly grants in the US.[96] While many of the grants are clearly targeted for political purposes – particularly those related to gender and racial diversity – hundreds of seemingly apolitical scientific projects, with goals like improving organ transplants or treating Alzheimer's disease, have also been cancelled or delayed.[97] Improving personal connections to science is just one way to resist the distrust in science that leads to such devastating decisions.[93,94]

Globally, there are hundreds if not thousands of citizen science projects running in classrooms, from primary schools to the university level.[98] Although uptake is high, the constraints of educational settings result in different benefits and limitations as compared to projects conducted within the general community.[73] Participation is often limited to set periods, such as a prescribed number of lessons or weeks, and skill levels will necessarily vary depending on the age of the students. The difficulty of satisfying both research goals and learning outcomes as required by curricula is also well-documented.[90] Beyond community-level societal impacts of increasing participation, implementing citizen science in schools may serve to aid the projects themselves. Introducing citizen science projects in an educational setting can improve their reach, allowing them to access audiences who might not choose to interact with such programmes – if they are even aware of them – without the external motivation of completing a course.[73,99] These experiences can spur students to continue participating in citizen science beyond the completion of the course, and even spark interest in pursuing science education at higher levels.[99,100]

Notably, some of these issues are alleviated in the university setting, as participation is less limited by class scheduling, and it may be easier to align the science of a given project with the curriculum of a tertiary-level science course. It is therefore unsurprising that some of the more ambitious education citizen science projects have been those involving university cohorts. This is illustrated by three OSDD projects implemented around the world – the D^3 program, the Bush Medicine Project and Breaking Good.

In 2005, William Scott and Martin O'Donnell launched the D^3 programme for undergraduate students at Indiana University-Purdue University Indianapolis, combining computational chemistry, synthetic chemistry and biological testing to create new chemical compounds with

pharmaceutical potential.[60] The project eventually expanded to include students working in Russia, Spain, Poland and other US universities, and has resulted in multiple peer-reviewed papers with students as co-authors.[101]

In Australia, Federation University's Bush Medicine Project takes a similarly cross-disciplinary approach, with students across the relevant subject areas working together to collect, extract and screen natural products from indigenous plants traditionally used for healing by local Aboriginal communities.[102] The Bush Medicine Project is conducted in partnership with the Aboriginal Education Centre, making it an excellent example of how citizen science can furnish scholars with richer knowledge by working with people who have historically been excluded from traditional research spheres.

Finally, Breaking Good is a citizen science initiative that aims to *"empower members of the public to be active researchers in projects that will improve human health"*, founded by Alice Motion in 2015. The initiative includes multiple programs with differing levels of involvement, one of which was a collaboration with OSM to run a drug discovery programme embedded within the University of Sydney's first-year undergraduate Chemistry course. In the Advanced Chemistry program, high-achieving students are given the opportunity to carry out semi-independent projects rather than repeating "tried and true" experiments with known outcomes. Between 2015 and 2018, students worked in small groups to synthesise and purify triazolopyrazine compounds with potential anti-malarial activity, which were evaluated for activity against *P. falciparum*, the primary causative agent of malaria.[103] The students' compounds contributed directly to increased understanding of the triazolopyridine series, and is awaiting publication.

These projects are presented here as successful case studies of how citizen science can be incorporated into educational settings to further scientific goals. There are, of course, many positive stories to be found in citizen science, but these OSDD examples stand out for their scientific complexity and direct impact on the relevant fields of research, with students contributing directly to live and authentic ongoing projects in drug discovery.

1.2 Mycetoma

Mycetoma is an NTD affecting the skin that can be caused by both bacteria and fungi. It is typically observed in tropical and sub-tropical areas around the globe. Most countries reporting mycetoma cases are within the latitudes 15° S and 30° N, sometimes known as the mycetoma belt (**Figure 1.7**). While the highest numbers of cases are reported in Sudan and Mexico,[104] screening practices and epidemiological data collection vary extensively between different countries, and true prevalence is likely to be much higher than the reported case numbers.[105]

The disease initially presents as tumefaction, which is a painless swelling in the affected area that eventually develops discharging sinuses. This discharge includes grains, which are protective structures formed around microcolonies of the causative organism that measure between 0.3 and 1 mm in size. If left untreated, the infection can lead to limb deformation through destruction of subcutaneous tissue, and amputation may be required to prevent the spread of disease.[106]

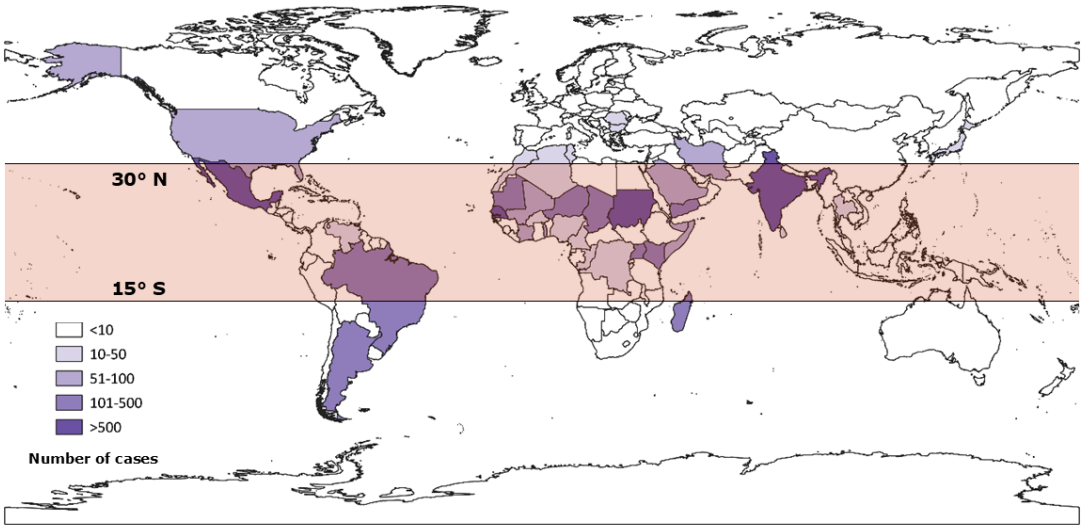

Figure 1.7 – Global distribution of mycetoma with number of cases reported by country and mycetoma belt between 15° S and 30° N shown in red. Adapted from Emery and Denning, 2020 under CC BY 4.0[105]

The prevailing theory of transmission is traumatic inoculation, in which a pathogenic agent is introduced into the tissue by a thorn or splinter in the environment. This accounts for the most common presentation of infection in the foot or lower limbs and explains the disproportionate representation in impoverished areas where people are more likely to have inadequate footwear or other protective equipment while working outdoors. Mycetoma presents a significant health

and economic burden in endemic areas, as infection often results in disability and even death.[107] Mycetoma almost exclusively affects people in low socio-economic backgrounds, with most patients being outdoor labourers in developing countries,[108] and is therefore not prioritised by the global pharmaceutical industry despite the high rates of associated disability and morbidity.

1.2.1 Mycetoma pathology and diagnosis

Treatment of mycetoma is complicated by the sheer number of different pathogens that can cause similar clinical presentations. Eumycetoma is the name given to disease caused by fungal agents and accounts for 75% of cases around the world, with up to 85% of these cases attributed to the species *Madurella mycetomatis* (*M. mycetomatis),* though over a dozen fungal genera have been identified as causative organisms. In contrast, infection caused by bacteria, known as actinomycetoma, is limited to three different genera of bacteria (*Actinomyces, Nocardia* and *Streptomyces*), with the most prominent bacterial pathogen varying greatly by geographic distribution.[105]

Table 1.1 – Grain colour and causative agents with percent of cases caused. Percent given within subclass, <1% not shown. Data from van de Sande, 2013 and van de Sande and Fahal, 2024.[109,110]

Subtype	Colour	Causative agent
Eumycetoma	Black	*Madurella mycetomatis* (85.3)
		Falciformispora senegalensis (3.5)
		Trematosphaeri grisea (1.4)
	White/pale yellow	*Scedosprium boydii* (1.0)
Actinomycetoma	White	*Nocardia brasiliensis* (39.5)
		Nocardia asteroides (2.2)
	White/pale yellow	*Actinomadura madurae* (12.0)
		Nocardia spp. (7.5)
		Nocardia otidiscaviarum (1.0)
	Yellow-brown	*Streptomyces somaliensis* (13.7)
	Red	*Actinomadura pelletieri* (12.0)

Bacterial and fungal infections naturally require different medication, and species-level variations in resistance mechanisms give rise to even greater differentiation, making correct diagnosis crucial for appropriate treatment. The colour of the grains discharged by the affected area can be used to identify the causative organism at the genus level, with fungal agents

usually resulting in black or red grains, and bacterial agents producing white or yellow grains (**Table 1.1**). This simple visual diagnosis can be useful for directing initial diagnosis, especially in under-resourced settings, but can be misleading. For instance, pale yellow grains usually indicate a bacterial causative agent, which would be treated with antibiotics, but are also produced by the fungal pathogen *Scedosporium boydii*.[106]

Species-level identification is achieved predominantly through tissue biopsy and histopathological examination, and less often via grain culturing. Recently, genomic sequencing of cultured grains has enabled comprehensive characterisation of species associated with mycetoma and may be key to developing effective new treatments.[111]

Since the 1980s, actinomycetoma has been treated with the Welsh regimen, a combined drug therapy of trimethoprim/ sulfamethoxazole (co-trimoxazole) and amikacin sulfate prescribed in a cyclical dosing regimen to limit renal and hepatic toxicity. Variations to this regimen in case of resistance or contraindication include carbapenem antibiotics like imipenem and meropenem or amoxicillin-clavulanic acid in place of amikacin, and require a longer regimen of 45 – 90 days.[112] The majority of actinomycetoma cases respond well to this treatment, with a cure rate of over 90%, and surgical intervention rarely required.[112]

In recent years, there has been concern about the rise in antibiotic resistance, and some researchers have called for the introduction of routine drug susceptibility testing (DST) before determining a treatment regime.[113] Currently, testing is performed following generalised guidelines laid out by the Clinical and Laboratory Standards Institute (CLSI), which recommends visual reading of plates.[114] Visual analysis can require specialised training and gives qualitative, rather than quantitative results, making it more difficult to scale up for high-throughput screening of compounds with potential antibiotic activity. This may contribute to the lack of innovation in therapeutics against actinomycetoma.

Eumycetoma is much more challenging to treat, with a cure rate of just 25 - 30% reported in 2023 despite surgical intervention in almost all cases.[115] This is largely attributed to a lack of curative drugs, with antifungals serving only to encapsulate and reduce lesions prior to surgical removal. In addition, treatment regimens typically run over months to years, resulting in poor adherence and high recurrence rates.[116]

Compared to the sizeable armoury of antibiotics available, there are vanishingly few antifungals, with just six classes of antifungal agents approved for use (**Table 1.2**). This is

broadly explained by the eukaryotic nature of fungi, with fungal cells sharing many characteristics with mammalian cells. There are simply fewer enzymes and biological pathways for medicinal chemists to target without causing harm to the human host.[117]

Table 1.2 – Classes of antifungals currently approved for use in humans and their mechanism of action.

Class	Mechanism	Members
Polyenes	Bind ergosterol, forming pores in cell membrane[117,118]	Amphotericin B Natamycin Nystatin
Pyrimidine analogues	Inhibit DNA and protein biosynthesis[117]	5-fluorocytosine
Azoles*	Bind CYP51 enzyme to directly inhibit ergosterol synthesis[119]	Clotrimazole (first generation) Ketoconazole (second generation) Itraconazole (third generation) Fosravuconazole (fourth generation) Oteseconazole (fifth generation)
Allylamines and benzylamines	Bind squalene oxidase (upstream of CYP51) to inhibit ergosterol synthesis[117,118]	Terbinafine Naftitine Butenafine
Echinocandins	Inhibit β-(1,3)-glucan synthase[117,120]	Caspofungin Anidulafungin Micafungin Rezafungin
Triterpenoids	Inhibit β-(1,3)-glucan synthase[117,120]	Ibrexafungerp

*There are currently approximately 40 azole-derived antifungals. A representative of each generation is given here, following the classification of Shafiei et al.[119]

Currently, three of the six classes (polyenes, azoles and allylamines) target fungal membrane synthesis by sequestering or inhibiting the synthesis of ergosterol, an analogue of cholesterol that is essential for fungal membrane structure.[118] The prodrug 5-fluorocytosine alone comprises the fourth class, and acts to disrupt the biosynthesis of fungal DNA and subsequent protein synthesis following metabolism into the nucleoside analogue 5-fluorouracil. The final two classes – the echinocandins and the most recent addition to the antifungal arsenal, terpenoids – exert their effect by inhibiting the enzyme β-(1,3)-glucan synthase to limit production of the β-(1,3)-glucan required for fungal cell wall integrity.[117,120]

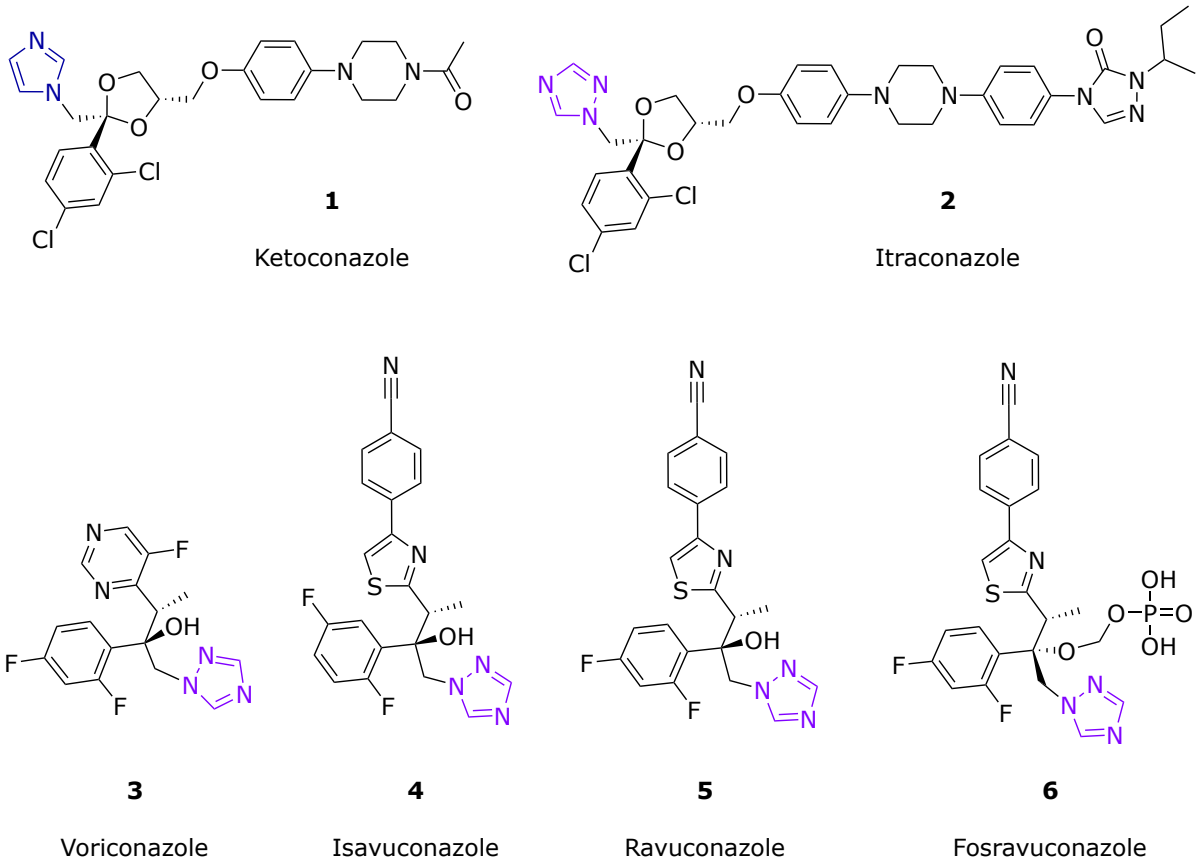

Figure 1.8 – Structures of azole drugs **1 – 6** commonly used to treat eumycetoma with azole moiety highlighted in blue (diazole) or purple (triazole).

Most of the drugs used to treat eumycetoma belong to the azole class (**Figure 1.8**), which work by binding to the cytochrome P-450 enzyme CYP51. CYP51 mediates the synthesis of ergosterol, an essential component of the fungal cell membrane, so inhibition of the enzyme prevents fungal growth.[119,121] Ketoconazole **1** was previously the first line treatment until its restriction due to potential hepatic and adrenal toxicity through off-target inhibition of other cytochrome P-450 enzymes.[108,119] Itraconazole **2** is now considered the gold standard for low income countries, though ketoconazole is still used in some countries as it remains a more affordable option.[116] Unfortunately, itraconazole resistance has been observed in *Madurella fahalii* and *Medicopsis romeroi*,[122] likely as a result of mutations in the ERG11 gene that encodes CYP51, a common cause of azole resistance in other fungi.[123] This finding reinforces the value of species-level identification prior to beginning treatment.

Other azoles commonly used include voriconazole **3**, isavuconazole **4**, ravuconazole **5**, and its prodrug fosravuconazole **6**.[108,112] In 2024, the first randomised, controlled and double-blind trial of treatments for eumycetoma found weekly administration of fosravuconazole to be

similarly effective as twice daily administration of itraconazole.[116] This was a promising result, as reducing the frequency of administration could improve adherence and thereby increase cure rates. Interestingly, the authors of this 2024 study also reported higher than usual efficacy rates for itraconazole and have theorised this may be due to higher adherence rates than are seen in clinical practice.

Beyond the azoles, only a handful of other drugs are used with any frequency or efficacy. Terbinafine, an over the counter treatment for fungal skin infections like athlete's foot, appears to be prescribed more than itraconazole in some locations despite having lower reported efficacy.[124] Liposomal amphotericin B was one of the first antifungals used and has been employed to treat eumycetoma in the past, but is rarely recommended due to the high risk of serious and even fatal side effects.[121,125] The echinocandin caspofungin and nucleoside analogue 5-fluorocytosine are also sometimes used despite a lack of clinical evidence for their efficacy against this ailment.[112]

A recent contender in the fight against eumycetoma is the first-in-class antifungal olorofim, a member of the orotomide family that has shown excellent activity against a range of fungal pathogens since being reported in 2016.[126,127] The orotomides target dihydroorotate dehydrogenase (DHODH), an enzyme that is essential in the pyrimidine biosynthesis pathway. Olorofim reversibly inhibits DHODH to inhibit pyrimidine synthesis, thus preventing DNA and RNA production. Although this pathway is common between fungal and mammalian cells, the human DHODH enzyme is significantly different in structure to fungal DHOD, and olorofim has been found to inhibit the fungal analogue with over 2000-fold potency compared to the human protein.[126] Olorofim is a potent *in vitro* inhibitor of *M. mycetomatis*, and has shown *in vivo* activity comparable to ravuconazole and other azoles in pre-clinical studies.[128] As of 2025, olorofim has reached phase 3 clinical trials for use in patients with invasive aspergillosis infections and has been proposed as a new treatment for various fungal diseases, including eumycetoma, pending the outcome of these trials.[127]

1.2.2 Eumycetoma drug screening

One significant hurdle to the development of antifungals for eumycetoma is the difficulty of testing new drug candidates. A standard phenotypic drug discovery pipeline starts with *in vitro* screening of compound libraries to determine their inhibitory concentration 50% (IC_{50}) or

minimum inhibitory concentration (MIC). (IC_{50} is the concentration of drug required to inhibit 50% of the pathogenic organism, while MIC is the concentration needed or inhibit it completely.) Potent compounds move into lead development and promising compounds will typically undergo further *in vitro* testing, such as cytotoxicity evaluation to assess how the compounds affect host cells, before entering *in vivo* studies. This approach requires an *in vitro* screening assay that is both robust and, ideally, a good indicator of *in vivo* efficacy.

While a colorimetric *in vitro* assay specific to eumycetoma was developed in 2005,[129] in the two decades since then, it has become evident that the assay does not predict *in vivo* efficacy or correspond well to clinical results. For example, colorimetric assay results indicate that *M. mycetomatis* is less susceptible to amphotericin B than to itraconazole and other azoles,[129] but *in vivo* models suggest that amphotericin B is far more effective at prolonging host survival than any of the azoles tested.[130] Confoundingly, the azoles are used with greater efficacy in clinical treatment than amphotericin B,[108] possibly due to the serious systemic side effects of the latter.

The lack of correlation between *in vitro* and clinical results has been attributed to the formation of grains during eumycetoma infection.[130] The grains encapsulate the fungus with a layer of hard cement-like material, which is believed to hinder penetration of fungicidal agents.[131] Although the exact mechanism is unclear, grain formation seems to require interactions between the causative agent and host immune system, and therefore does not occur in standard *in vitro* models.[132] The development of an *in vitro* grain model is therefore a high-priority target for eumycetoma research, as it is believed that this would better reflect the potential antifungal activity of drug candidates.

In the meantime, the eumycetoma pipeline relies heavily on the first step of *in vivo* testing to refine hit compounds and determine their viability as anti-mycetoma agents.[133] To this end, compounds are initially tested in the larvae of *Galleria mellonella,* the greater wax moth. This species is used extensively in antifungal drug development due to the relative ease and rapidity of testing they afford in comparison to mammalian models.[134] The use of the larval model also obviates the need for *in vitro* cytotoxic screening, as toxicity screening in the larvae provides a good indication of a compound's likely impact on host cells.

1.2.3 Eumycetoma drug discovery

Despite the urgent need for more effective treatments for eumycetoma, there is limited investigation of novel drug candidates. Almost all published work relies on biological testing by just a single lab: work done by Wendy van de Sande and her team in Rotterdam, the Netherlands. Research has been further stymied by recent devastating political events, with the Mycetoma Research Centre in Khartoum, Sudan destroyed in early 2025 during the ongoing Sudanese civil war.[135] In addition, drug discovery is currently restricted to phenotypic screening, although new proteomic analysis of *M. mycetomatis* from van de Sande's lab has identified a handful of kinases as potential targets for future work.[131]

Natural products have been a fruitful source of new antifungals for decades, and scholars working in Sudan and Egypt have discovered a handful of plant essential oils with favourable activity against both *M. mycetomatis* and *A. madurae*, a common actinomycetoma causative agent. Dual activity against two common causative agents is highly desirable, but the precise chemical components responsible for this activity are yet to be determined.[136]

In the realm of small molecules, six new series of compounds for lead optimisation have been reported in recent years, five of these stemming from work undertaken by MycetOS. A prime example of OSDD, the MycetOS consortium was established in 2018 by Wendy van de Sande at the Erasmus Medical Center in Rotterdam and Mat Todd, then at the University of Sydney.[137] MycetOS offers researchers around the world the opportunity to screen compounds and natural products against eumycetoma pathogens, on the proviso that results are shared following the open-access model detailed above. This collaborative endeavour has included screening multiple open-access compound libraries, such as the MMV Stasis and Pathogen Boxes, the Oncode Drug Repurposing library, and others, for their efficacy against *M. mycetomatis*.[46,59,133,138] Research to date has focused on structure-activity relationship (SAR) studies, in which minor modifications are made to the chemical structure of a compound in order to determine which motifs or structural elements are most crucial for biological activity.

MycetOS Series 1 (**Figure 1.9**) consists of analogues of the known fungicide fenarimol **7**, investigation of which was initiated by the potent *in vitro* activity of **8 (**MMV689244) from the MMV Pathogen Box. Although this compound did not prolong survival in the larvae model, four closely related analogues from the same library were subsequently tested *in vivo* and resulted in significantly improved host survival.[59] Following these results, 125 fenarimol

derivatives were donated for screening by Epichem, an Australian chemical company, and dozens of others have been synthesised by academic researchers. These studies suggest that fenarimols likely exert antifungal activity through inhibition of the same CYP51 enzyme targeted by azole-based drugs.[139] Current activity on this series has therefore shifted to homology studies exploring the interactions of fenarimol analogues with *M. mycetomatis* CYP51 proteins.

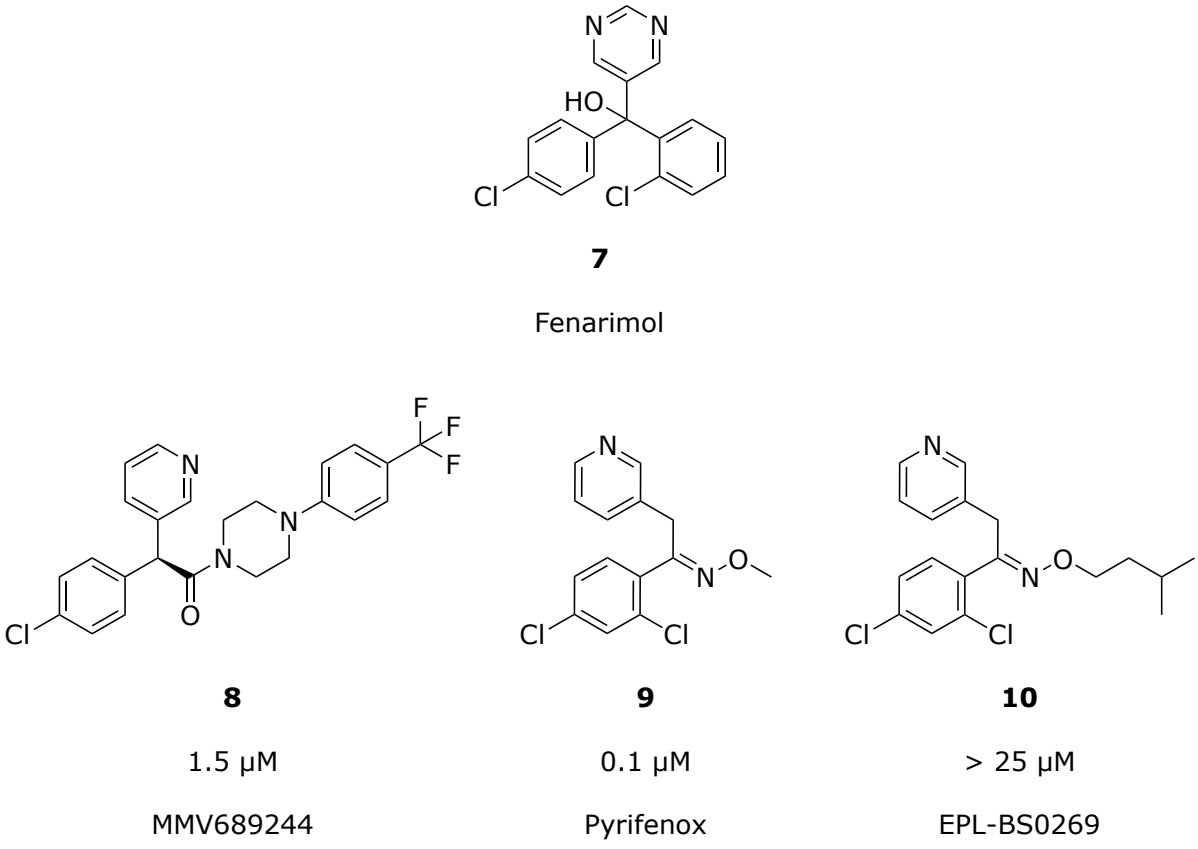

Figure 1.9 – Series 1 and series 6 compounds of interest fenarimol **7**, fenarimol analogue **8** (MMV689244), pyrifenox **9** and ketoxime analogue **10** with IC_{50} against *M. mycetomatis*.

Investigations with Series 1 led to the genesis of Series 6 (**Figure 1.9**) following an unexpected result from the Epichem library screening, which included compounds closely related to pyrifenox **9**, a well-established fungicide used in agriculture.[140] In particular, the compound EPL-BS0269 **10** showed excellent activity. Pyrifenox is characterized by two aromatic rings and a ketoxime functional group joined by a central carbon, similar to the fenarimol core structure in which three aromatic rings are joined by a central carbon. Series 6 was thus pursued to further explore the ketoxime motif, already associated with azole antifungals and thought to be implicated in CYP51 inhibition.[141,142]

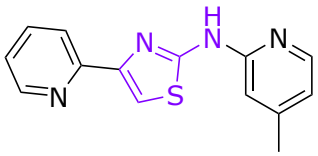

11

0.7 μM

Figure 1.10 – Series 2 lead compound **11** (MMV006357) with 2-aminothiazole core highlighted in purple and IC_{50} against *M. mycetomatis*.

While the Pathogen Box yielded a total of 12 hits against *M. mycetomatis*, screening of the Stasis box revealed just one potent compound, 2-aminothiazole (2-AT) derivative **11**, known as MMV006357 (**Figure 1.10**). This motif is well-established in drug discovery and present in many approved drugs including anti-cancer agents, anti-inflammatories and antibiotics.[143,144] The specific *N*-aryl-4-aryl-2-aminothiazole structure of MMV006357 is concurrently under investigation for application against various diseases including leishmaniasis and tuberculosis, but has not been explored in detail as an antifungal until now.[47,145,146] While the mechanism of action is not well understood in any of the aforementioned conditions, there is speculation that MMV006357's potent inhibition of calcium-activated ion channels may be related to its biological activity.[147]

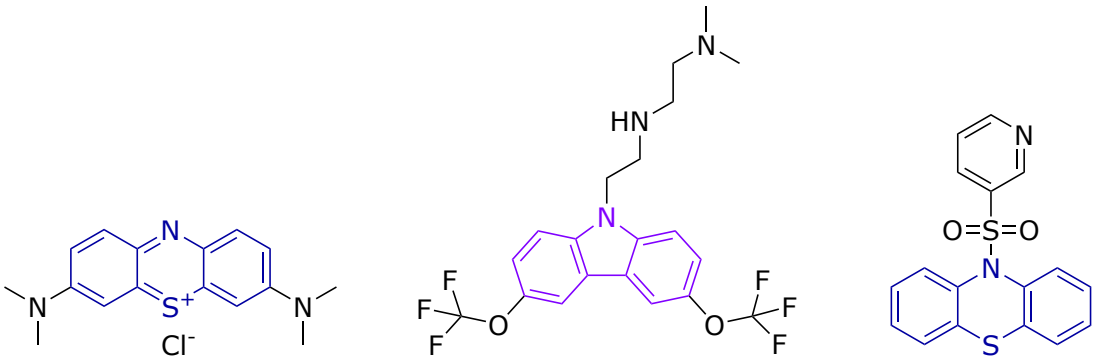

12

2.1 μM

13

3.9 μM

14

< 25 μM

Figure 1.11 – Series 3 compounds of interest, methylene blue chloride **12,** curaxin **13** and phenothiazine analogue **14** with IC_{50} against *M. mycetomatis*. Phenothiazine core shown in blue and curaxin core shown in purple.

MycetOS Series 3 (**Figure 1.11**) is based on phenothiazine, a tricyclic thiazine compound known best as the central motif of the antihistamine promethazine and anti-psychotic medications like chlorpromazine. Methylene blue (**12**), a phenothiazine-based compound, was

found to have promising *in vitro* activity when a set of compounds contributed by Dr Bernhard Biersack of the University of Bayreuth was screened. This led to the screening of 15 structurally similar curaxin compounds, such as **13**, synthesised by researchers from Northeastern University in the United States for an anti-amoebic drug discovery project collaboration with the DNDi.[148]

Since 2023, undergraduate students at the University of York in the United Kingdom have synthesised dozens of phenothiazine analogues during their studies, allowing initial SAR studies to be conducted. One such derivative, **14**, is shown as an example (**Figure 1.11**). Currently, little is known about the mechanism of action of this compound class against *M. mycetomatis*.

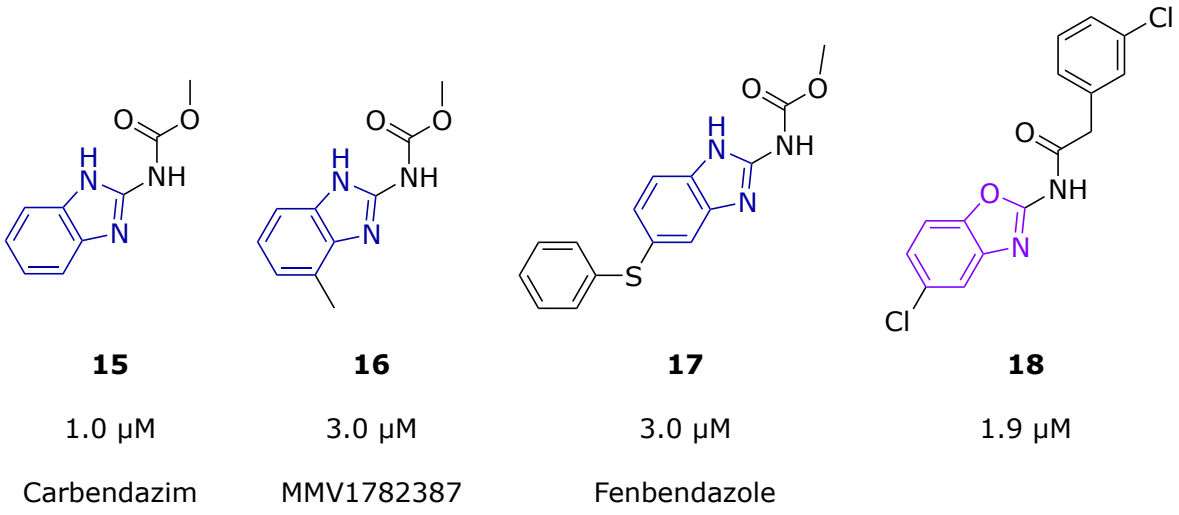

Figure 1.12 – Series 5 compounds of interest carbendazim **15**, related analogue **16**, fenbendazole **17** and benzoxazole analogue **18** with IC_{50} against *M. mycetomatis*. Benzimidazole core highlighted in blue and benzoxazole core highlighted in purple.

MycetOS Series 5 (**Figure 1.12**) derives from screening of the MMV Pandemic Response box, which identified three compounds with benzimidazole carbamate cores that significantly improved larvae survival.[133] Two were established drugs: carbendazim **15** is a commonly used agricultural fungicide, like pyrifenox,[149] while fenbendazole **17** is a broad-spectrum anthelmintic used to treat a variety of parasitic worms.[150] Another compound identified, MMV1782387 (**16**) is not a previously known drug, but varies in structure from carbendazim only by the addition of a single methyl group.[133] After these results were published, researchers in New Zealand flagged their similarity to a series of compounds with benzoxazole cores being synthesised by university students as part of a DNDi open drug discovery project; analogue **18** is given as an example. Subsequent screening against *M. mycetomatis* confirmed that these

benzoxazole compounds had similar activity to the benzimidazole analogues, and SAR studies are now underway.

Finally, the only known series developed externally to MycetOS was reported by Elkheir and colleagues and consists of compounds based on an imidazo[1,2-*b*]pyridazine scaffold (**Figure 1.13**).[151] Although significant SAR studies have been performed, screening of these compounds has been limited to *in vitro* assays and to date there is no evidence of their efficacy in larvae or other animal models. However, the imidazopyridazine core is very similar, both structurally and electronically, to the benzimidazole cores seen in Series 5. Both are flat, fused-ring heterocycles rich in electron density, and are common motifs in drug discovery.[152,153] The SAR studies on this family of compounds may therefore be relevant to the Series 5 analogues previously discussed.

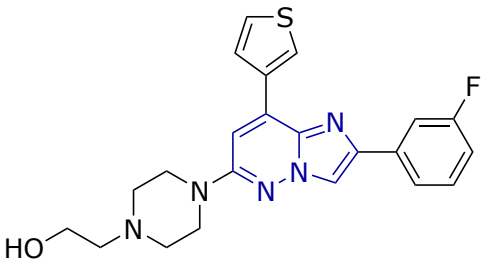

19

0.9 μM

Figure 1.13 – The most potent compound **19** described by Elkheir and colleagues with IC_{50} against *M. mycetomatis*. Imidazo[1,2-*b*]pyridazine core highlighted in blue.[151]

The majority of compounds in Series 3 and 5 have been synthesised by undergraduate students as part of their university degrees, demonstrating the mutual benefits of incorporating authentic scientific goals into education. The benzoxazoles of Series 5 were originally produced in collaboration with the Open Synthesis Network as part of a project to find new therapies against Leishmania parasites.[154] After some of these early compounds were shared with the MycetOS working group, students synthesised a number of additional compounds specifically designed with eumycetoma in mind. The Series 3 phenothiazine analogues were made during self-directed student projects in which the unit coordinators collaborated directly with the MycetOS team to identify relevant targets and organise screening.

Overall, the work carried out through the MycetOS consortium showcases the utility of an OSDD approach for a neglected disease, with five active avenues of research initiated through

the consortium in the space of seven years. None of these series would have been possible without collaboration from multiple researchers, institutions and student cohorts.

1.3 Tuberculosis

Tuberculosis (TB) is one of the world's most well-known diseases, with its origins dating back at least 5000 years.[155] In the time since, it has been given many names, attributed to diverse causes, and treated by innumerable methods, with varying efficacy.[155] It is only in the past 150 years that society has identified the causative agent, the bacterium *Mycobacterium tuberculosis* (*Mtb*), and developed cures to eradicate the disease, rather than merely treating the symptoms.[155] Now, though we are armed with a plethora of antibiotics to use against this insidious bacterium, TB remains the deadliest infectious disease worldwide, having only briefly yielded this title to the COVID-19 virus in 2020, 2021 and 2022.[156] Both social and biological factors have contributed to the persistence of TB, particularly its deeply inequitable distribution coupled with its ability to remain undetected in the body for years or decades, known as latent diease.[157]

Latent TB occurs when an individual is infected with the *Mtb* bacterium but has no symptoms of disease, making diagnosis very difficult. Once the bacterium begins to replicate, symptoms such as coughing and chest pain will present, indicating the onset of active TB. Typically, TB affects the lungs, where it slowly destroys lung tissue to the point that the patient can no longer breathe unaided.[158] However, TB can also manifest in other parts of the body, causing conditions known collectively as extrapulmonary TB. Extrapulmonary TB presents with different symptoms depending on the part of the body affected, but can be equally fatal.[159]

1.3.1 Background and prevalence

The World Health Organisation (WHO) estimates that around a quarter of the world's population is infected with latent TB.[160] Only 5 –10% of those infected will develop active disease, but even this proportion represents millions of people, with the WHO estimating that 10.8 million people became ill with TB in 2023 alone. In the same year, 1.25 million people died from TB, a disease that is both curable and preventable.[156]

The unfortunate reality is that TB is considered a disease of poverty, with many of those affected simply being unable to take precautions to protect themselves from disease or access the curative treatments it requires. TB is an airborne disease, meaning that minute droplets expelled through coughing or sneezing can remain in the air and be inhaled by people in proximity to the patient.[158] Infection therefore spreads rapidly in places with overcrowding, insufficient ventilation and a lack of appropriate protective equipment.[161]

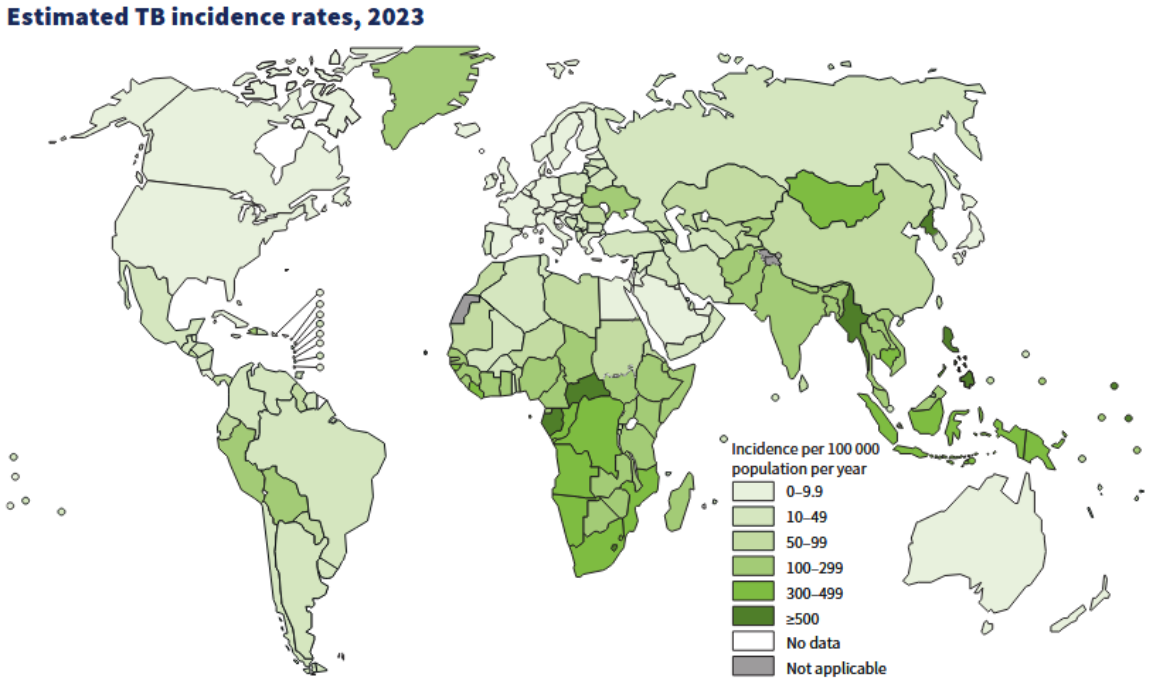

Figure 1.14 – Estimated global TB incidence rates in 2023, from WHO Tuberculosis report 2024, reproduced under CC BY-NC-SA 3.0 IGO.

Unfortunately, these conditions are far more prevalent in poorer and less developed nations, and this is reflected in the distribution of disease around the world (**Figure 1.14**). In the 30 countries with the highest TB burden, cases vary between 150 and 400 per 100,000 people, while elsewhere the rate is less than 10 cases per 100,000. According to WHO estimates, 69% of new TB cases in 2023 occurred in South-East Asia and Africa, while just 5.3% were in Europe and the Americas. India, Indonesia, the Philippines, Pakistan and Nigeria, the top five countries by TB abundance, represent over half of the global TB burden.[156] In short, the spread of disease is deeply inequitable, with the countries most affected generally being those least equipped to combat it.

Another factor in the distribution of disease is the high rate of comorbidity with human immunodeficiency virus (HIV), which is also far more prevalent in less developed countries

due to a lack of education and resources.[162] TB is the primary cause of death for people with HIV, and HIV infection is thought to be one of the main causes of latent TB developing into active disease, with around 13% of those who died from TB in 2023 also infected with HIV.[156,158] The treatments of both diseases are therefore closely linked, which can cause complications when trying to find drug regimens suitable for people with both conditions.

Although TB disproportionately affects low-income countries, its infectious nature means that it can rapidly become an issue for higher-income nations as well. Migration from high TB burden countries to low-burden countries is increasingly common, whether due to globalisation or because of conflict. While many wealthy countries screen new arrivals for active TB through chest X-rays and sputum smears, screening for latent TB is expensive and time-consuming, and as a result is less commonly employed.[163] Relatively small outbreaks of TB in high-income countries are regularly reported,[164] and in 2025 the US state of Kansas reported one of the largest outbreaks in the country's history, with dozens of active cases and at least two deaths.[165] Ultimately, reduction in TB rates in the regions with the highest disease burden will likely benefit not just those countries, but also the rest of the world.

1.3.2 Disease pathology, treatment and resistance

The unusual pathology of TB complicates treatment, with latent infection posing the biggest challenge. Sharma *et al.* define four stages of TB infection: macrophage response, growth, immune control, and lung cavitation, summarised in **Figure 1.15**.[157] Initially, *Mtb* enters the respiratory tract where it is engulfed by alveolar macrophages that attempt to destroy it through phagocytosis. Instead, the bacteria continue to grow inside the macrophage while lymphocytes prompt a cell-mediated immune response that encapsulates the infected macrophages to protect the rest of the body. The resulting cluster of immune cells with *Mtb* bacteria within is called a granuloma, a hallmark of the disease.[158,166]

Within the granuloma, the bacteria can evade the host immune system and may remain dormant for many years. This is known as latent infection, and in healthy patients, disease may not progress further. However, given the 'right' conditions – such as malnutrition, immunosuppression or concurrent infections like sepsis and HIV – the bacteria will begin to replicate rapidly, with the granuloma core now acting as a nutrient source to encourage bacterial growth. This results in the formation of holes in the lung tissue known as cavitary lesions,

which are the primary cause of common symptoms of chest pain and haemoptysis (coughing up blood).[157,158] At this stage, the infection is considered active TB.

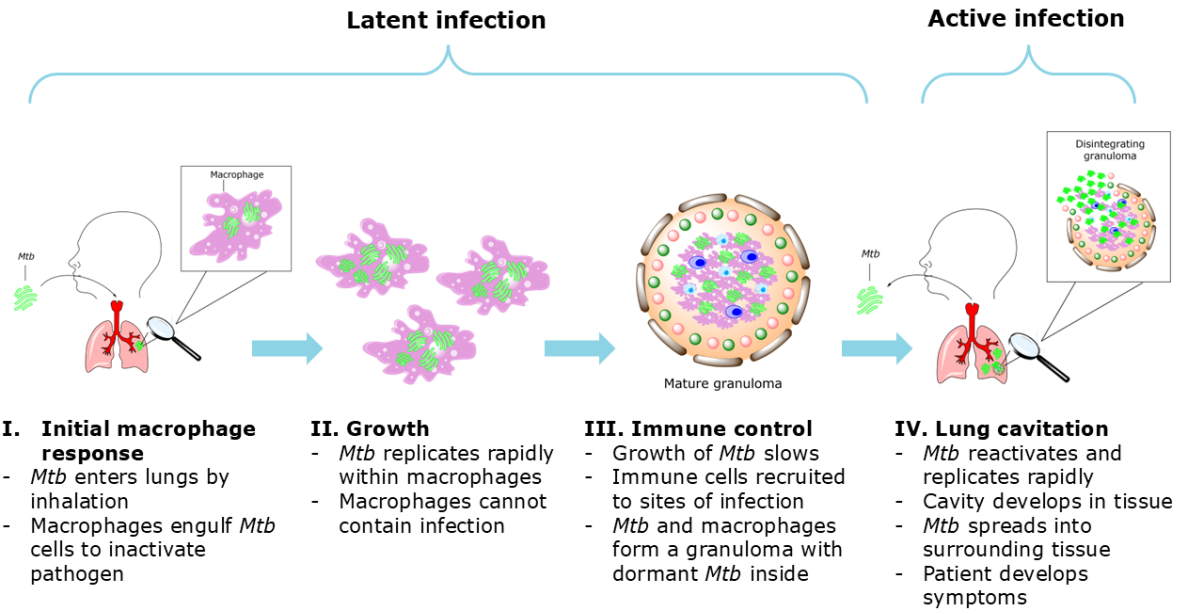

Figure 1.15 – The four stages of TB infection as described by Sharma *et al.*, 2021[157] with illustrations adapted from Alsayed and Gunosewoyo, 2023 under CC BY 4.0.[158]

Importantly, active TB can recur after initial treatment, even if symptoms have been resolved. This is generally due to the presence of dormant bacteria, left unharmed by antibiotics that typically target actively replicating bacteria.[167,168] Once the patient is no longer being treated for active infection, the dormant bacilli can start to replicate and grow once again. Therefore, modern treatment plans involve combinations of drugs to target both replicating and dormant bacteria.[167]

The current gold standard treatment for drug-susceptible TB (DS-TB) stipulates two months of treatment with four different antibiotics, rifampicin, isoniazid, ethambutol and pyrazinamide (**Figure 1.16**), followed by a four-month sterilisation period with rifampicin and isoniazid alone.[169] The initial cocktail targets both dormant and active bacteria, while the remaining four months of treatment focuses on the dormant bacteria only.[158] Understandably, patient compliance can be low due to a high likelihood of unwanted side effects, exceedingly long treatment duration and perceived lack of necessity.[158] However, when followed correctly, cure rates are greater than 85% and relapse is minimal.[156,169]

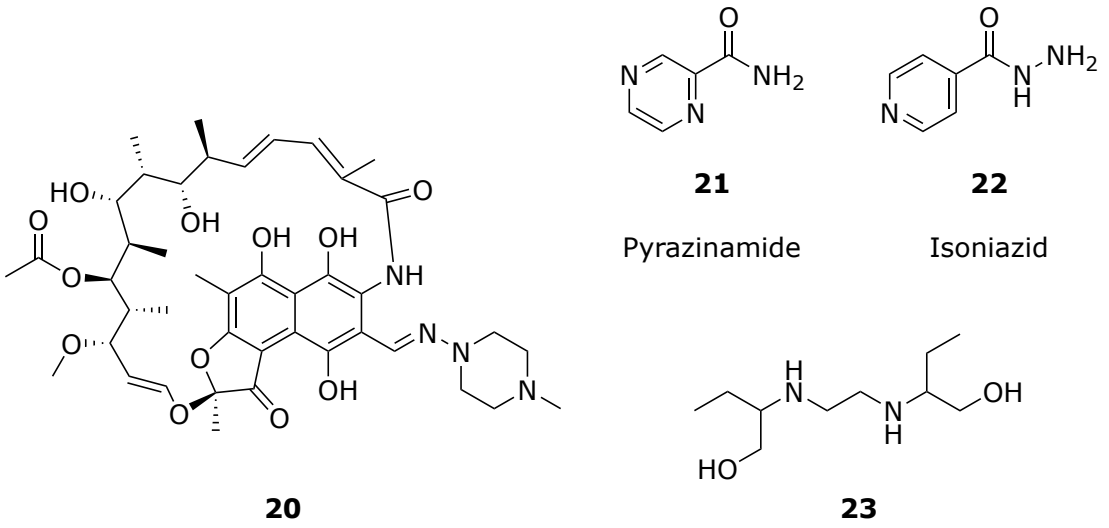

Figure 1.16 – Structures of first-line treatments for drug-susceptible TB: rifampicin **20**, pyrazinamide **21**, isoniazid **22** and ethambutol **23**.

Unfortunately, an increasing number of patients are contracting drug-resistant strains, often as a result of imperfect adherence to therapeutic regimens.[158,170] Rifampicin-resistant TB (RR-TB) and multi-drug resistant TB (MDR-TB defined as strains resistant to both rifampicin and isoniazid), are estimated to account for just over 19% of current TB cases, with approximately 400,000 people thought to have contracted RR/MDR-TB in 2023.[156] Although alternative drugs can be used, the treatment regimens are long, harsh and inaccessible, usually requiring at least one drug to be taken *via* injection.[171]

Even more concerningly, the WHO has now defined two further categories of resistance, namely pre-extensively drug resistant TB (pre-XDR-TB) and extensively drug resistant TB (XDR-TB), with the latter showing resistance to rifampicin as well as at least one fluoroquinolone and either bedaquiline or linezolid.[172] While XDR-TB and pre-XDR-TB currently represent a minority of cases (the WHO reported just under 30,000 detected cases in 2023), these numbers may be a significant underestimation of actual rates, and they are growing.[172] Treatment success rates for MDR-TB and XDR-TB are reported between 36% and 79%, with some studies finding cure rates as low as 30% for XDR-TB.[173,174]

Treating drug-resistant bacterial infections is not trivial. While new drugs can be initially effective, bacteria gradually develop resistance mechanisms through genetic mutations, necessitating the constant development of novel treatments. For instance, RR-TB is linked to mutations in *rpoB*, a gene that encodes part of the RNA polymerase targeted by rifamycins.[175]

Therefore, the range of TB drugs currently used target multiple different pathways, including cell wall biosynthesis, protein synthesis, and DNA replication. The mechanisms of action for the various classes of drugs used against TB are outlined in **Table 1.3**.

Table 1.3 – Mechanisms and classes of current TB drugs, as described by Dookie *et al*., 2018 and Patel *et al.*, 2025. *Denotes first-line treatment.

Target of inhibition	Class	Drugs
RNA polymerase	Rifamycins	Rifampicin* Rifabutin Rifapentine
Cell wall synthesis (arabinogalactan)	-	Ethambutol*
Cell wall synthesis (Mycolic acid)	-	Isoniazid*
Cell wall synthesis (Mycolic acid)	Thioamides[176]	Ethionamide Prothionamide
Cell wall synthesis (Mycolic acid)	Nitroimidazoles	Delamanid Pretomanid Metronidazole
Cell wall synthesis (D-alanine ligase)	D-alanine analogues	Cycloserine Terizidone
Cell wall synthesis (penicillin-binding proteins)	Carbapenems	Meropenem Imipenem
Protein synthesis (50S ribosomal subunit)	Oxazolidinones	Linezolid
Protein synthesis (30S ribosomal subunit)	Aminoglycosides	Amikacin Streptomycin Kanamycin
DNA gyrase	Fluoroquinolones	Levofloxacin Gatifloxacin Ofloxacin Moxifloxacin
DNA precursor synthesis	-	*Para*-amino salicylic acid
ATP synthesis	Diarylquinolines	Bedaquiline
Unknown	Nicotinamide analogues	Pyrazinamide*

Each of the first-line antitubercular drugs acts on a different target, with ethambutol and isoniazid both preventing cell wall synthesis through the inhibition of arabinogalactan and mycolic acid respectively.[173] Rifampicin, a member of the rifamycin family, is a macrocyclic antibiotic that exerts bactericidal effects by binding RNA-polymerase to prevent RNA synthesis. Rifapentine and rifabutin, both from the same class, are occasionally also used to treat TB.[177] Pyrazinamide is a pro-drug and must be metabolised into pyrazinoic acid to have antibacterial activity, but its exact mechanism of action remains unclear despite the drug's clinical use since 1954.[169]

Therapeutic plans should ultimately be determined by the resistance pattern of the individual patient, to both maximise the likelihood of cure and limit the development of further resistance.[170] Modern diagnostic techniques can now identify resistance in individual patients through susceptibility testing and molecular detection of genetic mutations.[170] Xpert MTB/RIF is an assay that uses the polymerase chain reaction assay and can identify rifampicin resistance in a matter of hours,[178] and similar assays are being developed to identify resistance to isoniazid and fluoroquinolones.[179] However, in countries with high TB burden and under-resourced healthcare systems, these methods are not always put into practice, and even with improved recognition of DR-TB strains, current therapies are clearly not adequate.

For now, all forms of DR-TB are primarily observed in low-income, high burden countries, where resistance is often acquired through incomplete adherence to treatment. If case numbers continue to rise, however, the rate of person-to-person transmission rises too, and DR-TB outbreaks in wealthier countries become increasingly likely.[174] The development of new antibiotics with novel mechanisms of action is therefore a global necessity, and should be a universal priority.

1.3.3 Emerging anti-tubercular agents

Only two new classes of antitubercular agents have been approved in the last 40 years, with only one targeting a novel pathway: the diarylquinoline bedaquiline, which inhibits ATP synthesis.[180] Delamanid and pretomanid are the two currently utilised members of the second approved class, nitroimidazoles, which bind mycolic acid to prevent cell wall formation (a similar mechanism of action to established anti-TB drugs isoniazid or ethionamide).[181] While these three additions to the clinical arsenal have proved invaluable for treating DR-TB strains, there is still urgent need for compounds with novel mechanisms of action, all the more so as resistance to bedaquiline is already being reported in high burden countries.[182]

Even though TB is classified as a disease of poverty, there is considerable investment and research into new anti-tubercular agents. Beyond purely altruistic drivers, a new compound with activity against TB would likely find application in treating other bacterial infections, as many existing TB drugs are indicated for use in other conditions.[183–185] This may partially account for the continuing investment from the profit-driven pharmaceutical industry, which

might otherwise neglect a market in which most patients would not be able to afford expensive medications.

Of course, many studies of anti-tubercular activity will not continue beyond the lead optimisation stage, due to toxicity concerns, poor pharmacokinetic profiles or other complications. While dozens of patents have been filed for novel anti-tubercular agents over recent decades, a few classes stand out for their novel mechanisms of action, with a handful of new compounds having reached various stages of clinical evaluation (**24 – 28**, **Figure 1.16**).

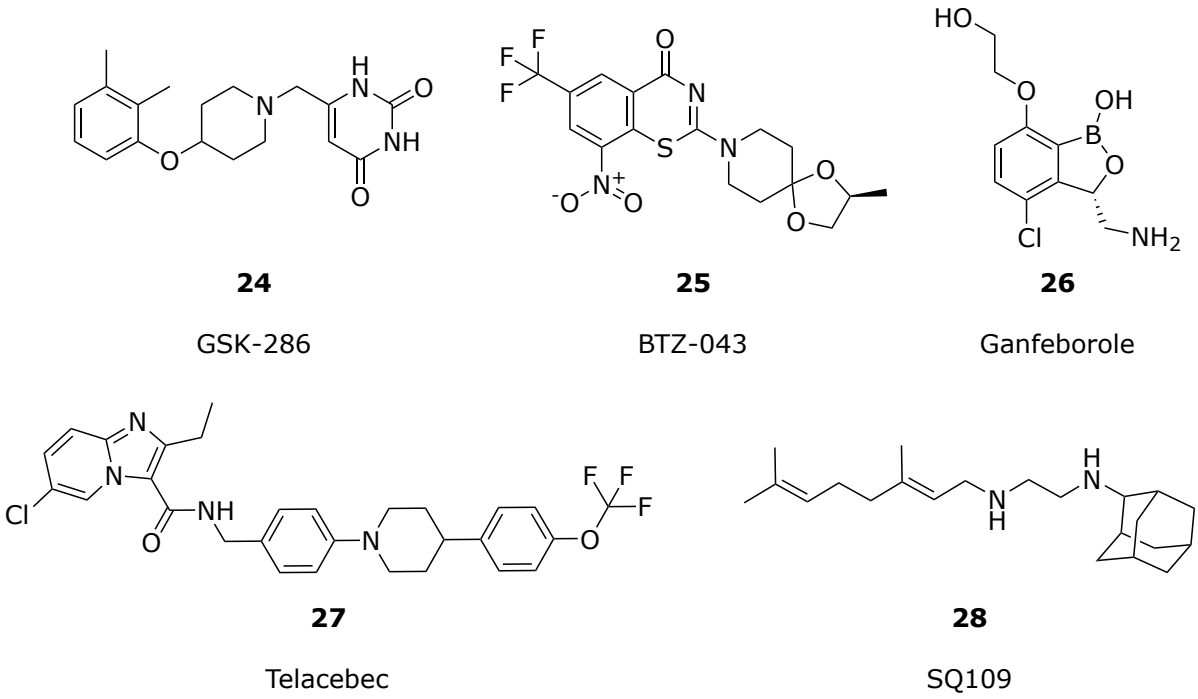

Figure 1.17 – Chemical structures of five antitubercular compounds currently undergoing clinical evaluation: **24** (GSK-286), **25** (BTZ-043), **26** (Ganfeborole), **27 (**Telacebec, i.e. Q203) and **28 (**SQ109).

Outlined in **Table 1.4**, these therapies variously target cholesterol metabolism, cell wall synthesis, protein synthesis and oxidative phosphorylation pathways.[186–190] SQ109 (**28**), a linear amine derived from ethambutol, has a multi-pronged mechanism of action, being able to inhibit ATP synthesis and biosynthesis of vitamin K, as well as affecting cell wall production through inhibition of the MmpL3 mycolic acid transporter protein.[190] As of 2025, benzothiazone **25** and Telacebec (**27**) have passed initial phase 2 trials, but phase 3 trials have not yet commenced.[189,191]

Table 1.4 – Compounds with novel mechanisms of action against *Mtb* currently in clinical evaluation.

Compound	Structural class	Target	Pathway affected	Clinical trials
GSK-286[182,186]	4-aryloxypiperidine	Rv1625c	Cholesterol metabolism	Phase 1
BTZ-043[191]	Benzothiazone	DpreE1	Cell wall synthesis	Passed phase 1b/2a
pBTZ-169[187,192] **(Macazinone)**	Benzothiazone	DpreE1	Cell wall synthesis	Phase 2
Ganfeborole[193]	Benzoxaborole	Leucyl-tRNA	Protein synthesis	Phase 2
SQ109[190]	1,2-ethylenediamine	Mmpl3	Cell wall synthesis, ATP synthesis, vitamin K synthesis	Phase 2
Q203[188,189] **(Telacebec)**	Imidazopyridine amine	Cytochrome bc_1	Oxidative phosphorylation	Passed phase 2

Another busy area of antitubercular research is the development of adjuvant or adjunct therapies, where a compound may not have bactericidal or bacteriostatic effects, but can improve the potency or pharmacokinetic properties of a drug that does have antibiotic activity.[194] The co-administration of penicillin antibiotics with clavulanic acid is a classic example, as the clavulanic acid covalently binds and inhibits beta-lactamase enzymes that would otherwise destroy the active penicillin antibiotic. Within the TB space, efflux pump inhibitors (EPIs), which block transporter proteins to increase intracellular levels of another drug, have been the primary avenue of interest.[195]

Bacterial efflux pumps (EPs) are well-characterised and many have been identified as factors in antibiotic resistance. Indeed, resistance to three of the first-line TB drugs, ethambutol, rifampicin and isoniazid, has been linked to specific EPs, and even the more recently approved drug bedaquiline has encountered resistance associated with the resistance nodulation cell division (RND) family of EPs.[195]

This strong correlation between EPs and resistance has led to the investigation of EPIs as adjuvant therapies, starting by repurposing drugs approved for other conditions (**Figure 1.17**). This is an attractive approach as it can save on the high costs of research and safety trials, and drugs can be made available to patients far more rapidly than those developed from scratch.[196]

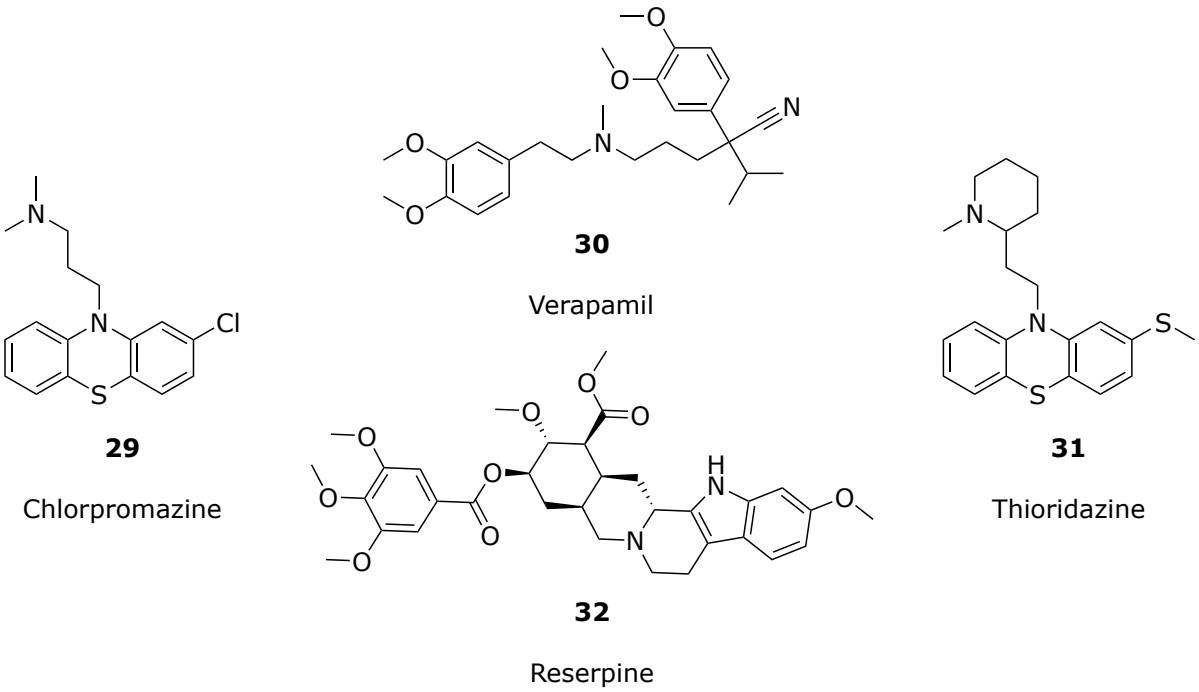

Figure 1.18 – Chemical structures of existing drugs **29 – 32** with potential application as anti-tubercular agents.

Verapamil (**30**) and reserpine (**32**) are traditionally used to treat high blood pressure and related conditions, and chlorpromazine (**29**) and thioridazine (**31**) were developed as antipsychotics. All four have been shown to increase potency of existing TB drugs *in vitro*, and are being explored as potential adjunct therapies for the treatment of DR-TB strains.[195,197–199] However, there is limited clinical evidence for their effectiveness so far, and associated toxicity has been a particular concern for the phenothiazines.[200] There is an ongoing effort to find or develop new EPIs that have similarly synergistic effects without the unwanted toxicity.[195]

1.3.4 Open Source Tuberculosis and open cyclams

The OSTB consortium, founded by medicinal chemist Mat Todd, seeks to develop new anti-tubercular agents through an OSDD approach. Since its inception in 2013, a total of four series of compounds have been explored, with one series remaining under active investigation (**Figure 1.19**). The 'Spiros', a family of spirocyclic compounds identified by high-throughput screening of a compound library from GlaxoSmithKline (GSK) formed the basis of Series 1, but was abandoned due to safety concerns during *in vivo* studies.[57,201,202] Series 2 was sourced from the library and featured compounds with a benzimidazole core, and in 2015 the screening of a second library from GSK led to the development of Series 3 with compound OSTBS83 as

a lead. Both series were eventually discontinued due to synthetic complexities and lack of promising activity.[202,203]

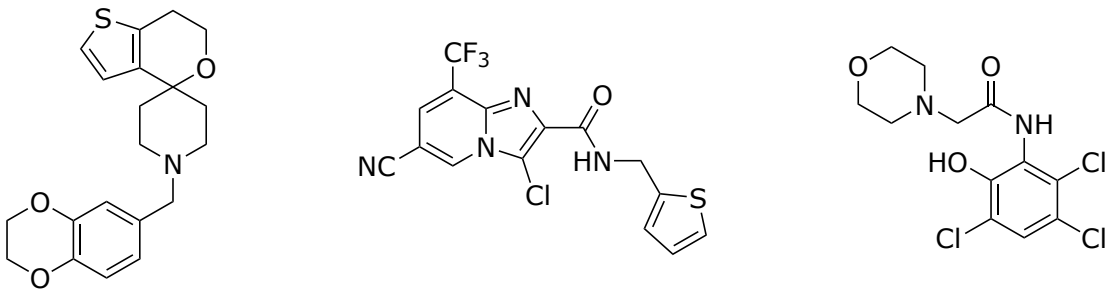

33 **34** **35**

Figure 1.19 – Chemical structures of lead compounds from previous OSTB investigations: **33** (Series 1), **34** (Series 2) and **35** (Series 3).

Series 4, known as the 'open cyclams', originated from studies on the macrocyclic polyamine **36**, known as cyclam (**Figure 1.20**). Cyclam is a well-established scaffold in coordination chemistry and biomedicine, with analogues being used in radio-imaging, biological sensing and photo-electron catalysis, among other applications.[204–206] In 1997, the discovery of a bi-cyclam compound, **37**, with potent anti-HIV activity precipitated interest in cyclam as a therapeutic agent, with cyclam-based compounds being investigated as treatments for rheumatoid arthritis, and cancer.[207–209] Since then, their medicinal applications have grown to encompass anti-viral and antibacterial activity, gene therapy, anti-cancer activity and diagnostic radiopharmaceuticals.[208]

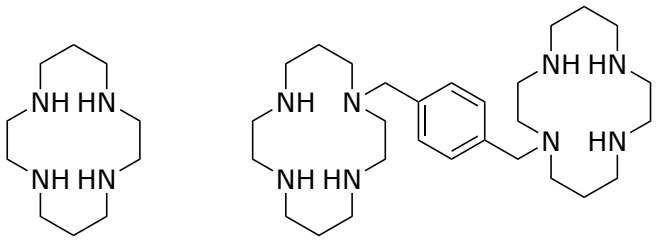

36 **37**

Figure 1.20 – Chemical structures of cyclam **32** and bi-cyclam **33.**

Phenotypic screening of 1,8-difunctionalised cyclam metal complexes by the Rutledge and Todd groups revealed their potent anti-tubercular activity, with MICs commensurate with those of first-line TB drugs.[210] Compounds **38 – 40** (**Figure 1.21**) maintained potency even against

strains of TB with resistance to rifampicin, ethambutol and isoniazid, indicating a different mechanism of action to all three drugs. Initial cytotoxicity assays showed minimal toxicity to THP-1 macrophage-like human cells, meaning that these compounds can inhibit bacterial growth without damaging human cells.[210]

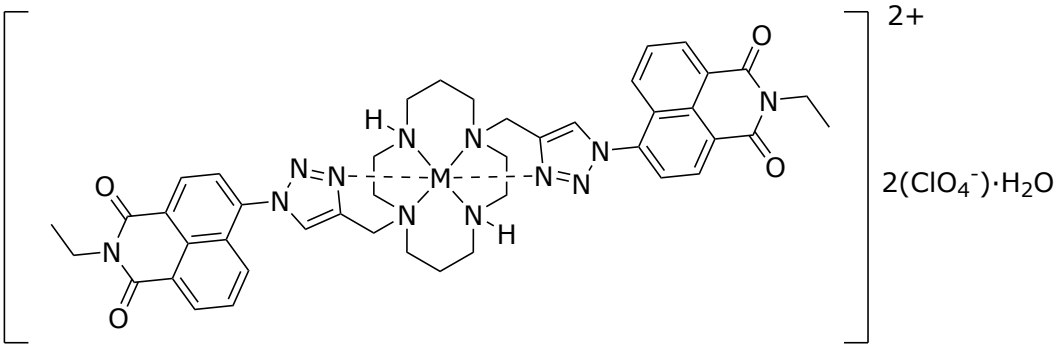

38: M = no metal, TFA salt
39: M = Cu
40: M = Zn

Figure 1.21 – Structures of cyclam-based lead compounds: the amine salt **38** and its copper(II) and zinc(II) complexes as the perchlorate salts (**39** and **40** respectively). All three compounds were found to have a *minimum* IC_{50} of 6.25 μM against *Mtb* H37Rv.

SAR studies were then conducted to explore the effects of the triazole linker, coordinated metal ion, and the nature of the pendant groups (**Figure 1.22**). Minor changes to the linker and the co-ordination of different metal ions had relatively little effect on activity, and the pendant groups thus became the focus of further exploration.[211] Results indicated that activity was largely retained with various bulky, hydrophobic pendant groups, including carboranes and the synthetically simpler 1-naphthyl motif.[211,212]

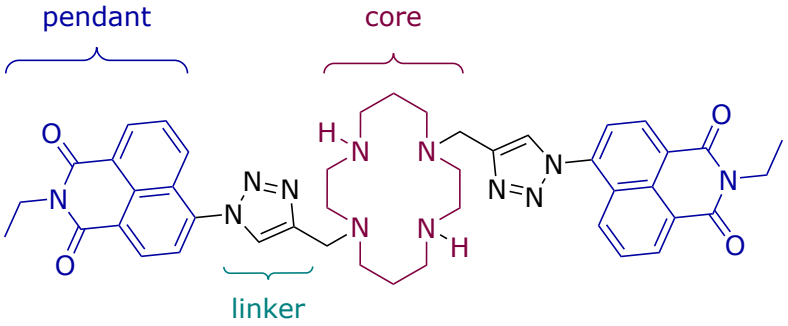

Figure 1.22 – Generalised structure of 1,8-difunctionalised cyclam compounds with cyclam core (maroon), triazole linker (green) and naphthalimide pendants (blue). Adapted from Spain *et al.*, 2018.[211]

Eventually, synthetic complexities led to a re-evaluation of the existing SAR, and the macrocyclic core was substituted with a series of linear polyamines in the hope of mimicking the structure and function of the cyclam core while offering greater synthetic flexibility. The polyamine backbone is also reminiscent of the first-line TB drug ethambutol and its derivative SQ109. A series of nine linear analogues were synthesised using polyamines of varying chain length and number of amines. Gratifyingly, some of these compounds did show comparable activity against drug-susceptible *Mtb*, with the most potent compound **41** being equally potent to the most potent cyclam derivative (**Figure 1.23**).[213] These compounds became the basis of OSTB Series 4, named for their similarity to their macrocyclic cousins.

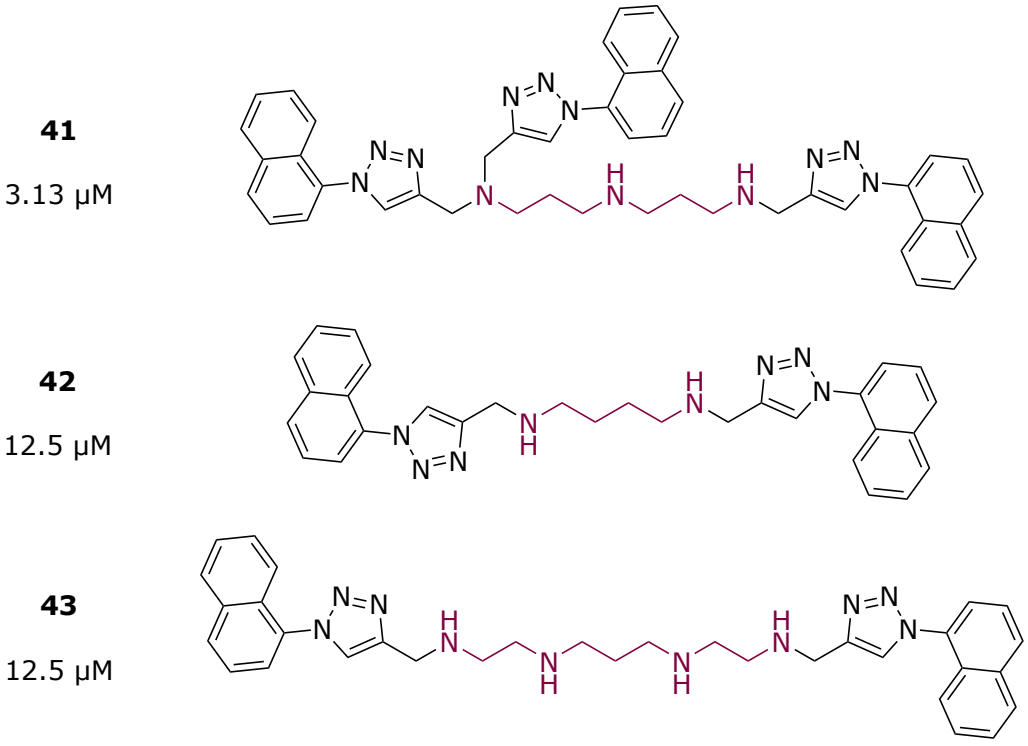

Figure 1.23 - The three most potent open cyclam compounds **41** – **43** synthesised by Batten, with *minimum* IC_{50} against *Mtb* H37Rv.

Difficulties controlling alkylation and purifying the open cyclam compounds meant that several of the *bis*-alkylated target compounds were not synthesised. Instead, several *tris* and *tetra*-alkylated analogues were obtained, with one of the *tris* derivatives, **41**, ultimately having the most potent activity. Unfortunately, no clear SAR trends could be determined due to the irregular patterns of chain length, number of amines and degree of alkylation in the final compounds.

1.4 Project aims

This study applies an open science approach to the exploration of new antifungal and antibiotic agents, incorporating citizen science educational programs and the development of new synthetic routes and biological screening assays to probe the SAR of 2-aminothiazoles against eumycetoma and open cyclam compounds against TB.

1.4.1 Probing SAR of the open cyclam series

Within the OSTB project, this work aims to determine how changes to the open cyclam core and pendant groups affect the activity of the series (**Figure 1.24**). Uncovering how these factors relate to antitubercular activity is an important step towards determining the mechanism of action of these polyamines.

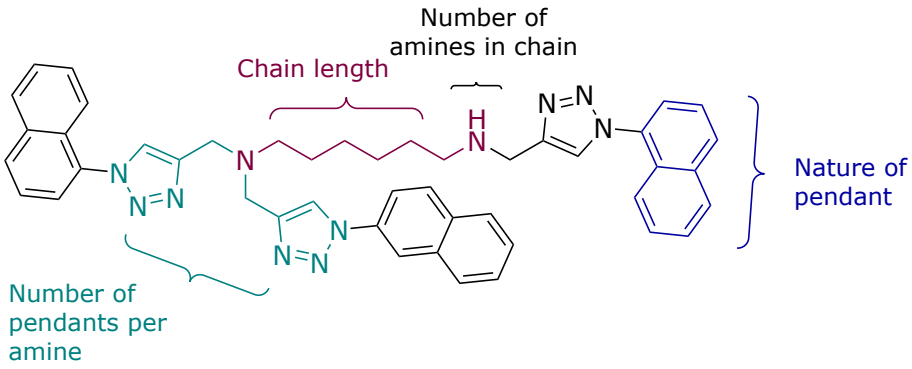

Figure 1.24 – Areas of potential SAR exploration for open cyclams.

Alterations to the core under investigation include chain length and the number of amines within the chain, while both the nature and number of pendant groups is assessed through the synthesis of open cyclam analogues with naphthyl, ferrocenyl and adamantyl pendants. A secondary focus is the development of straightforward and reliable synthetic routes to these compounds.

1.4.2 Formation of a 2-aminothiazole compound library

The SAR of 2-ATs as anti-eumycetoma agents is explored through the synthesis of a library of 2-AT analogues. The selected targets probe aromatic substituents and cyclic isosteres on both the C-2 and C-4 pyridine rings (**Figure 1.25**), with the primary objective being to identify the

most potent antifungal compounds and thus shed light on the mechanism of action of MycetOS Series 2.

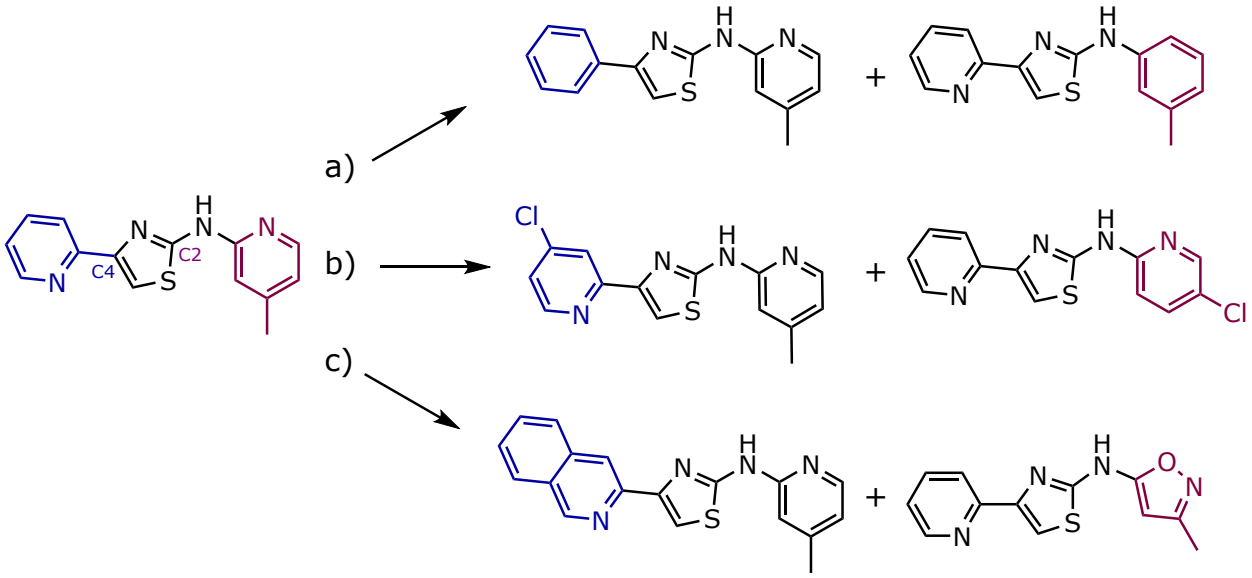

Figure 1.25 – Avenues of SAR exploration for 2-ATs: a) Replacement of pyridine rings, b) Aromatic substitution, c) Insertion of cyclic isosteres.

A significant proportion of the analogues in the library also form part of the citizen science program Breaking Good. These programs are embedded into secondary and tertiary curricula through the development of workshops, laboratory sessions and learning resources, and allow students to participate in the synthesis of target compounds.

1.4.3 Screening of 2-aminothiazoles against actinomycetoma causative agents

Finally, the 2-AT analogues are cross-screened for antibiotic activity against a representative sampling of the most common actinomycetoma pathogens across the world, *Actinomadura madurae, N. brasiliensis* and *S. somaliensis*. To this end, a novel biological assay that allows rapid assessment of antibiotic activity is developed.

2 Breaking Good: a citizen science approach to drug discovery

The foundations for the Breaking Good initiative commenced at the University of Sydney in 2015 when founder Prof Alice Motion, developed a research project in open source drug discovery for the undergraduate teaching labs.[103] The name Breaking Good was formalised when Motion and Prof Matthew Todd worked with teachers and Year 12 students at Sydney Grammar School to synthesize Daraprim, an antiparasitic and antimalarial drug, in the school's laboratory. A year prior, the American marketing rights for the drug had been sold to a new company, Turing Pharmaceuticals, which chose to raise the price per tablet from $13.50 USD to an eyewatering $750 USD.[214] This price hike unsurprisingly reduced access to the drug, which is most commonly used to treat toxoplasmosis in people living with HIV. The Breaking Good team synthesised the active ingredient at a cost of less than $2 AUD per tablet, aiming to draw attention to Turing Pharmaceutical's massive profit margin and highlighting the deeply inequitable effect that this price hike had on patients.[215]

Since then, Breaking Good has grown to encompass online learning activities, high school workshops centred around accessibility of essential medicines (E$$ENTIAL MEDICINE$) and the Advanced Chemistry program in which high-achieving undergraduate students generated compounds for the OSM project. By 2020, it was decided that the triazolopyrazine series of compounds would no longer be investigated, and new synthetic targets were required. However, determining a new area of research for a citizen science project is not necessarily trivial.

Creating a successful citizen science project in any research area requires careful planning to ensure that meaningful science can be conducted while respecting the needs and abilities of the community involved.[216] While cost, safety and length of synthesis are concerns for any synthetic project, the Advanced Chemistry program has strict time constraints, with just five lab sessions of three hours allotted to the program, and limited budget. In addition, students generally have very little experience with chemical synthesis or with handling hazardous substances.

Therefore, target compounds are limited to those which can be made entirely through reactions that are rapid, straightforward and reliable, without requiring specialist equipment. The

reagents should be appropriately safe for students to handle with supervision, and economical enough to buy at scale. Finally, the compounds generated should advance scientific knowledge, such as by contributing to SAR studies, and ideally as part of an open science project.

2.1 MycetOS Series 2 and the undergraduate lab

The 2-AT derivative **11** had been reported by the MycetOS community as a promising lead for the treatment of eumycetoma, but no progress had yet been made on investigating this compound. MycetOS series 2 proved to be an ideal focus for the Advanced Chemistry program, as 2-AT analogues can be generated in just three steps from commercially available materials, and many variations in substituent type and position can be introduced without altering the synthetic pathway.

The Hantzsch synthesis of thiazoles from an α-haloketone and thioamide has been used without significant alteration since the 19th century and remains one of the most efficient ways to produce these compounds (**Scheme 2.1**). Using a functionalised thiourea in place of the thioamide allows facile introduction of the C-4 amine and aromatic ring, while a functionalised haloketone similarly provides access to the ring at the C-2 position (**Scheme 2.1**).

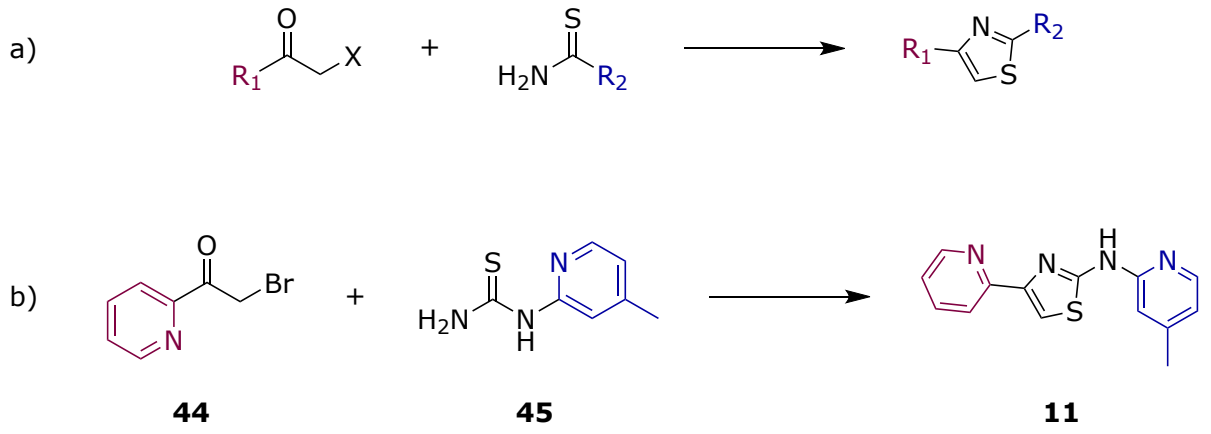

Scheme 2.1 – a) Generalised Hantzsch synthesis and b) synthesis of lead compound **11** from bromoketone **44** and thiourea **45.**

In general, the necessary haloketones can be purchased commercially or made *via* halogenation of the parent ketone. Typically, the bromoketone is preferred, both for its greater reactivity and relative ease of synthesis comparative to the chloroketone.

There are several routes to the functionalised thioureas, with a common method being the two-step reaction of an amine with benzoyl isothiocyanate and hydrolysis of the subsequent thiourea.[217] Although thioureas can be formed from aqueous isothiocyanate alone, the resonance offered by the carbonyl encourages the formation of thioureas with more sterically hindered amines.[218] The resulting di-functionalised thiourea is vulnerable to hydrolysis of the carbonyl group, yielding the desired, mono-functionalised thiourea.

Benzoyl thiocyanate **47** is rapidly generated *in situ* from the reaction of benzoyl chloride **46** and potassium isothiocyanate in acetone (**Scheme 2.2**). Addition of the requisite amine results in the precipitation of the benzoyl thiourea, which is isolated by pouring the reaction mixture into ice water and collecting the solid *in vacuo*.

Hydrolysis of the benzoyl thiourea is achieved trivially by stirring the compound in aqueous sodium hydroxide, with complete dissolution generally indicating reaction completion within 15 – 30 minutes. The free thiourea is obtained with high purity by vacuum filtration, as the benzoate side product remains in solution at high pH. Finally, the free thiourea and the appropriate bromoketone are heated at reflux in ethanol until TLC analysis indicates consumption of starting material. The product is precipitated using saturated sodium carbonate solution to adjust the pH to approximately 8.

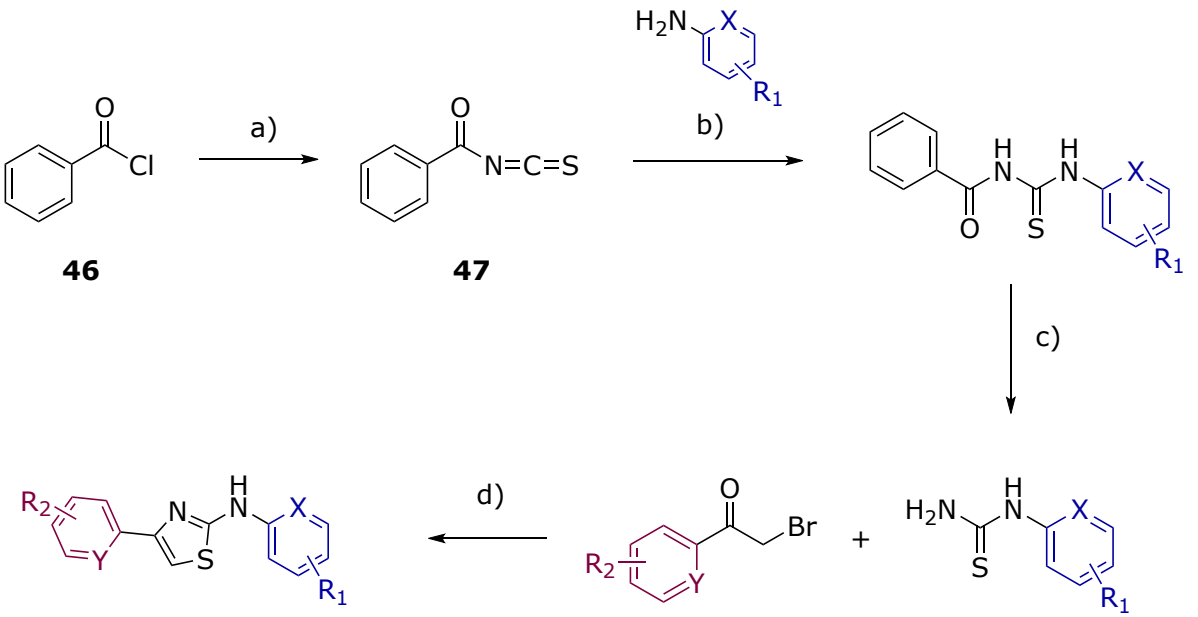

Scheme 2.2 - Generalised reaction scheme for synthesis of 2-aminothiazole derivatives. a) Acetone, 60°C, 15 mins. b) Acetone, 60°C, 1 – 3 hrs. c) NaOH (2.5 M), 80°C, 15 – 30 mins. d) Ethanol, 60°C, 1 – 3 hrs.

Each of these reactions can be adapted to fit the three-hour lab sessions of the undergraduate course. As not all bromoketones and amines are suitable for students to handle, targets were selected in part by the hazards of the starting materials required. Generally, compounds with category 1 or 2 health hazards were avoided, unless the hazard could be sufficiently mitigated by use of minimal quantities and personal protective equipment.

2.1.1 Program

Advanced Chemistry labs are run across five three-hour lab sessions, with four synthesis-focused labs followed by a characterisation workshop in the final session. In the synthesis sessions, students set up reactions with guidance from demonstrators, monitored those reactions using TLC analysis, and performed workups to isolate their products. After the final 2-AT product was isolated, students conducted IR spectroscopy on their own samples to confirm the identity of the molecule.

Once students had synthesised the targets, the samples were collected and fully characterised by ^{1}H and ^{13}C NMR spectroscopy, HPLC analysis and mass spectrometry. In cases where the student sample was not obtained with > 95% purity, a small quantity of the sample was first purified by Breaking Good researchers. The characterisation data collected by researchers was then presented in the final lab session, and students were guided through the analysis of the data, as the 2-AT targets are much more complex than the molecules students would typically be asked to identify.

Although the characterisation methods used differ slightly from those taught as part of the undergraduate curriculum, collecting alternative data would both increase the workload for teaching staff or researchers, and reduce the authenticity of the process. For instance, students are generally familiar with fragmentation analysis mass spectrometry from hard ionisation sources, but soft ionisation methods such as electrospray ionisation or atmospheric-pressure chemical ionisation are commonly used in the field,[219] and are easier to obtain in the specific setting of the School of Chemistry. This gives students an insight into real-life scientific practices and how they might differ from the theory taught in a classroom, while also providing an extension opportunity for high-achieving students.

Once the students' samples were fully characterised and adequately purified, the compounds were screened for antifungal activity against *M. mycetomatis* by collaborators in the Netherlands. Initially, the intention was for students to receive the biological data on their own compounds, but the lengthy process of antifungal testing made this unfeasible. Instead, demonstrators shared results obtained for the compounds made by the previous cohort, to illustrate how their work was part of a larger, ongoing project. In addition, this provided an opportunity to discuss the process of target selection, as students could see how their own target molecules were directly related to the results of previous years.

Between 2022 and 2024, approximately ~240 students completed the Advanced Chemistry lab course, collectively synthesising 32 analogues for MycetOS Series 2. The biological activity of these compounds is discussed in Chapter 3.

2.1.2 Synthesis

The 2021 and 2022 cohorts produced a series of C-4 phenyl analogues of the lead compound **11** (**Figure 2.1**) as well as both pyridinyl and phenyl C-2 analogues (**Figure 2.2**). Pleasingly, those made with phenyl rings at the C-4 position were obtained in exceptional (> 95%) purity from precipitation alone. The derivatives with pyridine rings in the same position, however, required considerable purification, which was complicated by their poor solubility in most organic solvents. While it is well known that purification of amines can be tedious,[220] it was surprising that the pyridinyl amine affected purification more dramatically than the secondary amine, given their relative basicity.

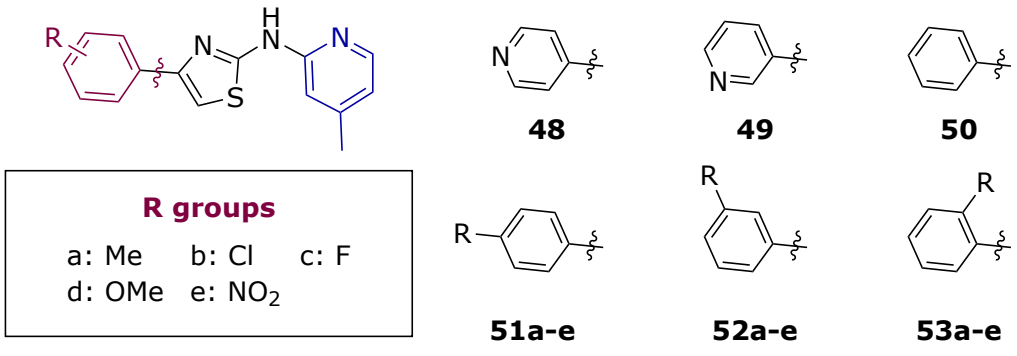

Figure 2.1 – C-4 phenyl analogues made by Advanced Chemistry students in 2021 and 2022.

All molecules were eventually isolated by automated column chromatography using varying ratios of either DCM, methanol and ammonium hydroxide, or petroleum benzine, ethyl acetate and triethylamine. Without the inclusion of base in the eluent, the compounds adhered to the silica and could not be separated.

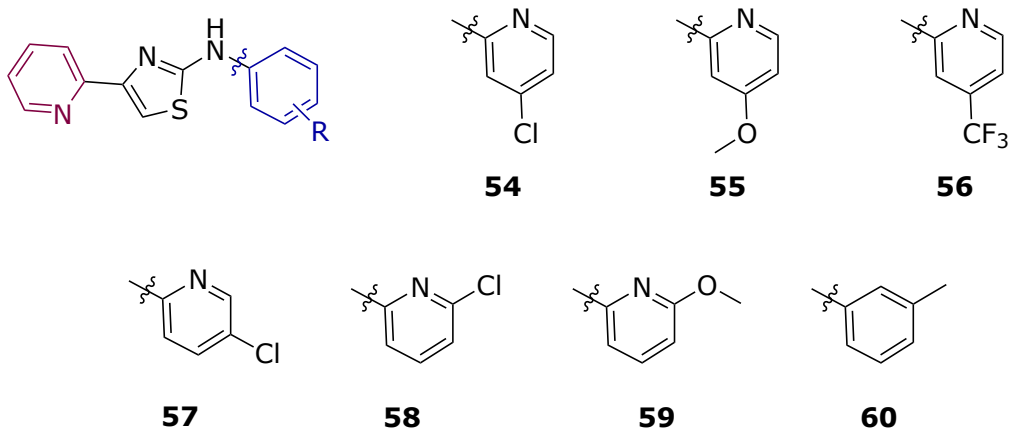

Figure 2.2 – C-2 phenyl and pyridinyl analogues made by Advanced Chemistry students in 2021 and 2022.

Five analogues with substituted pyridines at the C-4 position were therefore selected as targets for the 2023 cohort (**Figure 2.3**).[221] Compounds **61a** and **61b** were chosen to explore the effect of halogen substitution around the ring, with **61c** included as a substitute for the more desirable 4-bromo analogue, as the corresponding ketone could not be sourced.

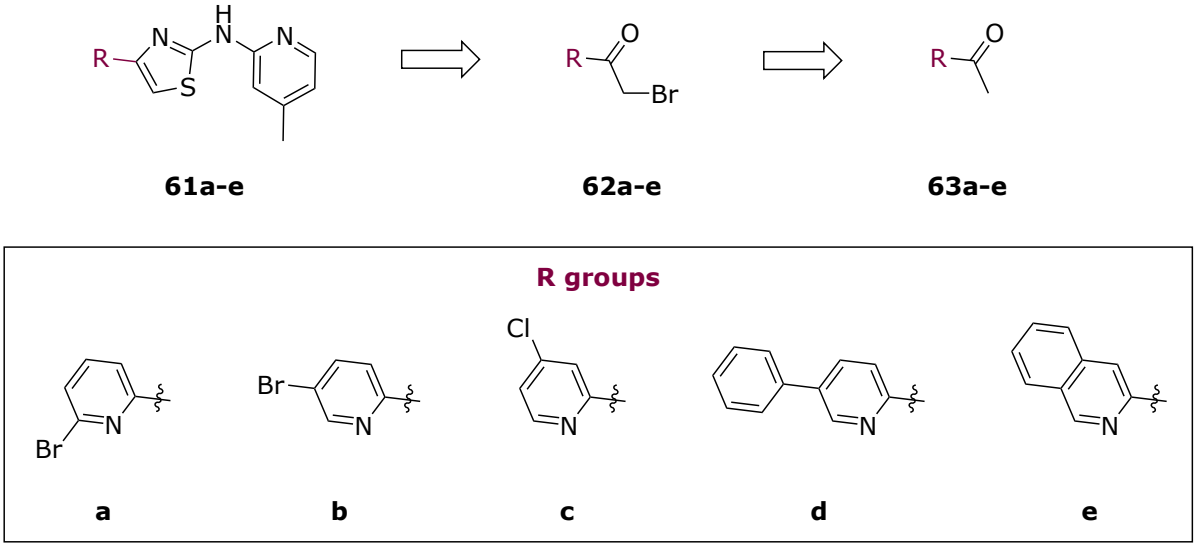

Scheme 2.3 – Retrosynthetic pathway for C-4 pyridinyl analogues to be made by the Advanced Chemistry cohort of 2023.

The targets **61d** and **61e** were designed to probe the effect of increased size, despite the parent ketones not being commercially available. In the literature, ketone **63d** has previously been synthesised using a Suzuki coupling and the same method was applied successfully here.[1,2] (**Scheme 2.4**). Phenylboronic acid **64** and 2-acetyl-5-bromopyridine **63b** were dissolved in toluene and water and combined with potassium carbonate and a tetrakis(triphenylphosphine)palladium(0) catalyst. After stirring under nitrogen at 105°C for 22 hours, the mixture was extracted with ethyl acetate crude and dried over magnesium sulfate to yield **63d** as a lumpy orange-white solid. Excess phenylboronic acid was removed by dissolving the solid in DCM and filtering it through a silica plug to give the desired compound as a pale-yellow solid in excellent yield.

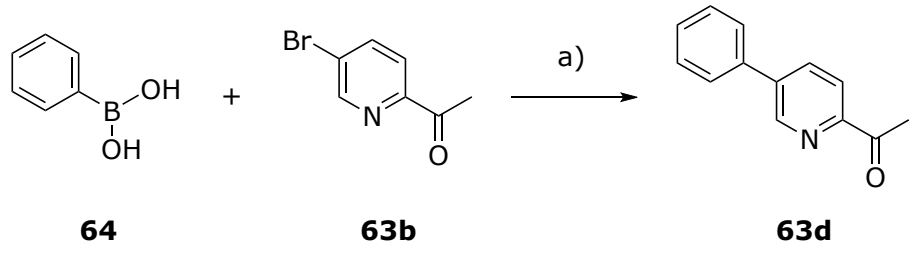

64 **63b** **63d**

Scheme 2.4 – Synthesis of **63d** from boronic acid **64** and ketone **63b**. a) $Pd(PPh_3)_4$, K_2CO_3, toluene/H_2O, 105°C, 22 h, 99%.

Various methods have been employed to produce quinoline ketone **63e**, typically using quinaldic acid **65** as a starting point and proceeding *via* methyl esterification, Claisen condensation and decarboxylation of the subsequent ester (**Scheme 2.5**).[222,223] The methyl ester **66** was prepared by dissolving **65** in methanol with sulfuric acid and stirring at 65°C for 22 hours to yield the methyl quinaldate **66** as a white crystalline solid in good yield. Following the method of Chan *et al.*, **66** was then converted to the 3-oxobutanoate ester **67** by stirring with potassium *tert*-butoxide in ethyl acetate at room temperature. The reaction occurred almost immediately, as evidenced by the formation of bright yellow precipitate, but when the mixture was worked up after 20 minutes of stirring, the crude product was highly impure and resulted in low yield after purification by automated column chromatography. Increasing reaction time to one hour resulted in an improved, but still poor yield of just 46% after purification, with TLC and ^{1}H NMR analysis indicating the presence of a secondary product. This material, thought to be a decomposition product, was isolated from the desired compound, but could not be definitively identified by ^{1}H NMR and spectrometric analysis.

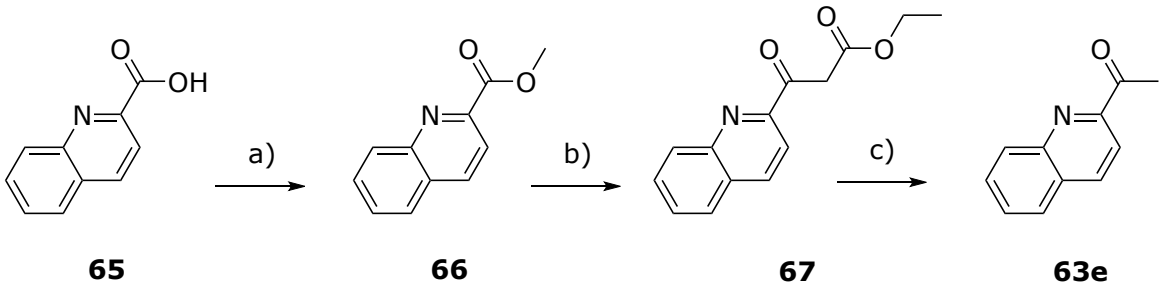

Scheme 2.5 – Synthesis of 2-acetyl quinoline **63e** from commercial reagent **65**. a) H_2SO_4 (18.4 M), MeOH, 65°C, 22 h, 82%. b) KO^{t}Bu, EtOAc, rt, 1 h, 46%. c) HCl (1M), 1,4-dioxane, 100°C, 18 h, 76%.

Despite this disappointing yield, sufficient quantity was obtained to continue with the reduction to the desired 2-acetylquinoline. Compound **67** was dissolved in 1,4-dioxane and treated with aqueous hydrochloric acid at 100°C, to cleave the ethyl ester moiety and access the desired ketone *via* decarboxylation. Ketone **63e** was afforded in good yield as a crystalline brown solid and used without further purification.

Bromination was first attempted on ketone **63a** using hydrobromic acid and elemental bromine in glacial acetic acid (**Scheme 2.6**), a well-established method that has previously been used to synthesize pyridinyl α-bromoketones with good yields.[224] However, the initial reaction proceeded slowly and gave only moderate yields, leading to the investigation of *N*-bromosuccinimide (NBS) as an alternative brominating agent.

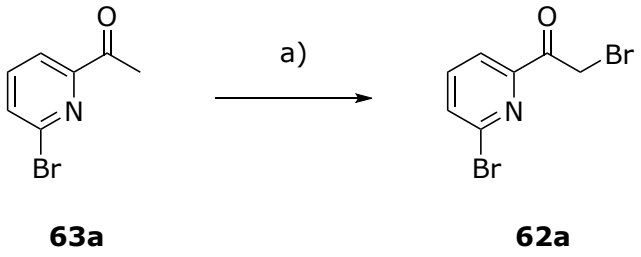

Scheme 2.6 – Bromination of ketone **61a** using hydrobromic acid and elemental bromine. a) HBr, Br_2, glacial acetic acid, rt, 24 h. 67%.

NBS is favoured for α-bromination of various carbonyl derivatives as it can deliver high yields without affecting functional groups that might be sensitive to attack by elemental bromine. In proposed mechanisms, activation of NBS by a Lewis or Brønsted acid catalyst (**71**) leads to reduction of the NBS **(72**) and formation of a bromocation that is highly susceptible to attack by nucleophiles, and reacts rapidly with enolates **(69**) to give the α-bromo product (**Scheme 2.7**).[225–227] The dibromo product can easily be obtained by increasing the equivalents of NBS

used. Various acid catalysts have been used in the literature, including ionic liquids and functionalised silica gels as well as more traditional catalysts like magnesium perchlorate and trihaloisocyanuric acids.[225,226,228] As high yields are reported with the comparatively accessible and economical *para*-toluenesulfonic acid (*p*TSA), this unremarkable Brønsted acid was the catalyst of choice.[229–231]

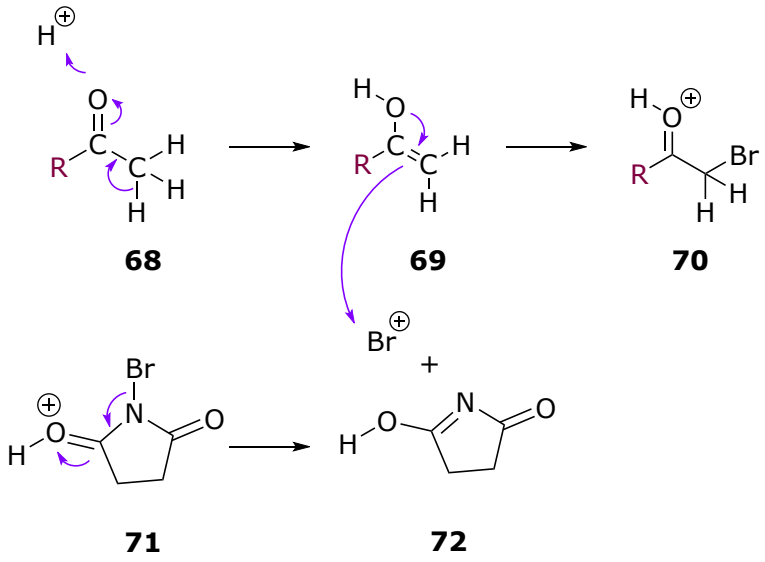

Scheme 2.7 – Proposed mechanism of bromination with NBS and an acid catalyst.

NBS and *p*TSA were added to the parent ketone **63a** dissolved in acetonitrile and the solution was stirred at 80°C for 24 hours (**Scheme 2.8**). Analysis by TLC and ^{1}H NMR indicated that both the mono-bromo- and di-bromoketone had been formed, with the combined yield of 95% calculated by quantitative NMR analysis. As the di-bromoketone can partake in the same Hantzsch reaction, and indeed theoretically will react more rapidly than its mono-brominated counterpart, no attempt was made to separate the two products.

The improved yield and comparative safety of the NBS reaction made it the obvious choice for brominating the remaining ketones, and compounds **62b**, **62c** and **62d** were produced in good to excellent yields following an identical method. However, the same approach resulted in poor yield for **62e**, with ^{1}H NMR analysis suggesting that as much as half of the starting material remained unreacted after 48 hours of stirring. Previous studies have found that aryl ketones with electron-withdrawing groups had reduced yields, yet the halogen-substituted analogues had consistently better yields than the quinoline derivative.[227,228] Steric hindrance is unlikely to be the culprit, as the spatially analogous naphthalene ketone is obtained in high yields in the literature, and the similarly bulky **63d** was also obtained in good yield under the same

conditions. One study using a different catalyst did find that using methanol as a solvent and adding the NBS portion-wise resulted in an overall increase in yields, regardless of substitution, but this unfortunately could not be tested due to time pressures.[227]

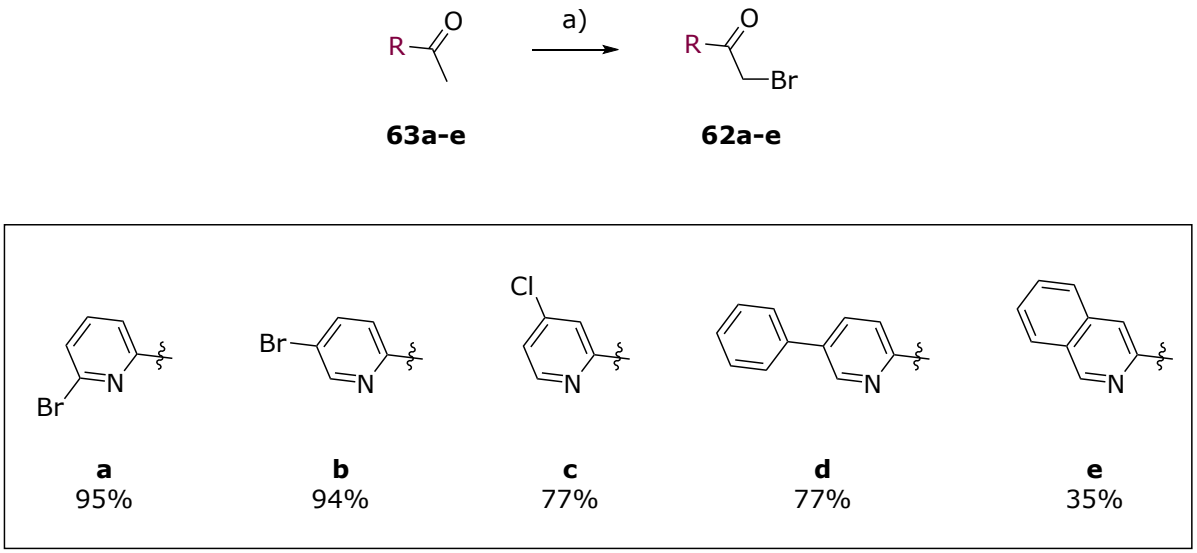

Scheme 2.8 – Synthesis of α-bromoketones **62a-e** from parent ketones **63a-e**, with combined yields of mono- and di-brominated products. a) NBS, pTSA, acetonitrile, 80°C, 24 – 48 h.

With the necessary bromoketones in hand, the Advanced Chemistry students of 2023 were able to produce the five target compounds **61a-e** without complication. HPLC analysis of the crude products revealed that only **61a**, which was obtained as a yellow powder, was sufficiently pure for immediate biological testing. Fortunately, only minor impurities were present in the remaining compounds, which were purified with relative ease according to the procedures described above to yield **61e** as a dark yellow powder and **61b-d** as orange-brown solids.

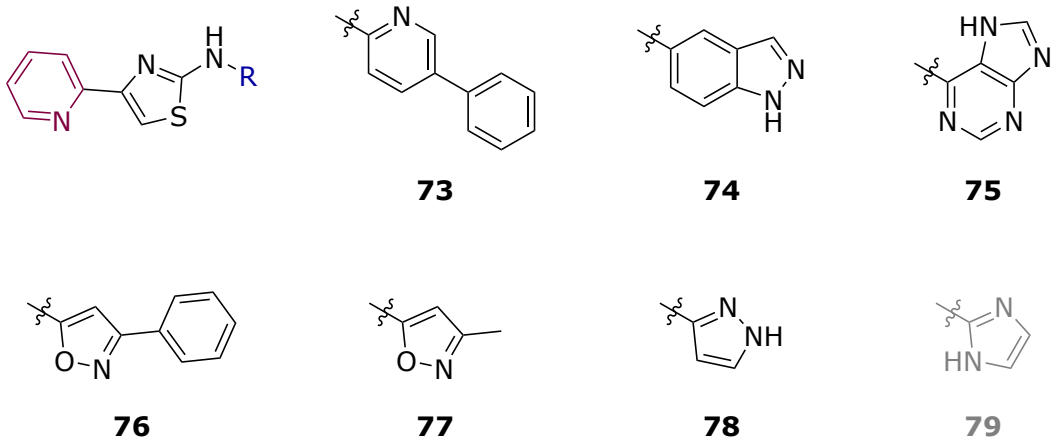

Figure 2.3 – Final compounds **73 - 79** selected for Advanced Chemistry students in 2024.

The time investment required to synthesize precursors at the scale demanded by the Advanced Chemistry program (10 – 15 g per cohort) was deemed too considerable to repeat in the following year. Therefore, the targets for the students of 2024 needed to be achieved using only commercially available materials. The dearth of α-bromoketones on the market made exploration of the C-4 ring far more attractive, and a series of targets incorporating different heterocycles was devised. Analogue **73** was particularly chosen for its comparison with **61e** as it would achieve the same goal of probing the effect of added bulk, but in a new direction, while the remaining targets **74 – 79** were selected principally by availability (**Figure 2.3**).

This selection proved less reliable, with **74 - 76** being obtained as highly impure products with low yields, and **79** not being successfully isolated at all. Targets **73** and **77** both precipitated cleanly and in reasonable quantity, and **78** was obtained in good yield though with suboptimal purity. Compounds **74**, **76** and **78** were successfully purified by column chromatography, but **75** could only be isolated using preparative HPLC.

2.2 Synthetic chemistry in a high school context

With the Advanced Chemistry program firmly established as an organic chemistry citizen project embedded within the university curriculum, attention turned towards developing a similar program suitable for secondary school students. There is abundant evidence that involving students in authentic scientific processes can influence their perception of science and their relationship with it.[92,99,232] However, despite the growing recognition of the benefits of citizen science, there are relatively few projects with substantial chemistry components, with a recent unpublished review finding that just 4.51% of school-based citizen science programs are chemistry-related.[233] Those that do exist typically focus on analytical skills, such as determining measuring contaminant levels in water or soil, likely because these are generally simpler to organise around the restrictions of time and safety that constrain a school cohort.[234]

Synthetic chemistry in particular is hugely underrepresented, with no active projects listed by the Australian Citizen Science Association.[235] This is attributed to several factors, including safety concerns when using hazardous chemicals and the need for specialty equipment and training. For a project to contribute to scientific knowledge, students must be able to create compounds with a genuine application in research, or otherwise generate new data, such as by

testing reaction conditions. Effectively, this means that synthetic chemistry citizen science projects require close collaboration with researchers who can identify appropriate target compounds and advise on how to achieve the synthesis of these targets.

Prior research by the Learning by Doing team, a group of researchers with a focus on citizen science in education, identified various barriers to the implementation of citizen science in schools, including lack of awareness and support for teachers, and the need for curriculum alignment.[236] Many teachers expressed a desire to participate in citizen science projects, but found it difficult to cover the required syllabus while also devoting time to projects without a clear and explicit connection to the required content. This was especially cited as a barrier to participating in citizen science in the final years of school, when students and teachers alike are overloaded with content and assessment.

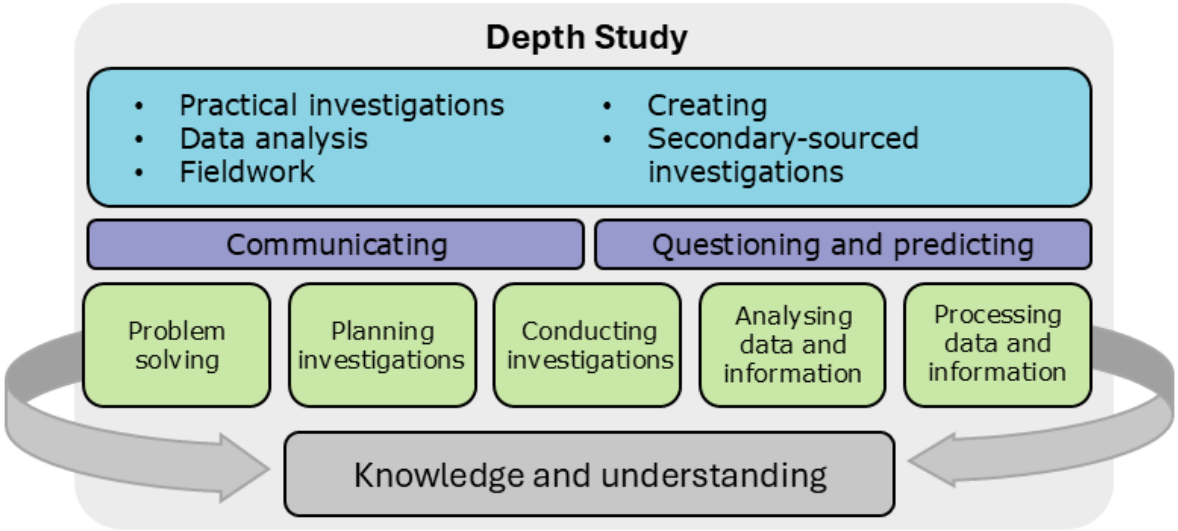

Figure 2.4 – Depth Study investigations (blue), core Working Scientifically skills (purple) and additional Working Scientifically skills (green). Adapted from NESA, 2017.

These findings indicated that citizen science projects that directly align with curriculum would be more successfully integrated into schools.[236] In collaboration with secondary school educators, the Breaking Good team identified components in the New South Wales Stage 6 Chemistry curriculum, which dictates the requirements for students in their final two years of school, that could be integrated into a citizen science program. Currently, all Stage 6 science subjects call for a Depth Study in which fundamental scientific processes, referred to as "Working Scientifically" skills, are addressed (**Figure 2.4**). Students must perform the core Working Scientifically skills of *Questioning and predicting* and *Communicating* (purple), and

at least two additional Working Scientifically skills (green) through investigations carried out across 15 hours of course time.[237] These investigations can be practical, such as conducting lab experiments or doing fieldwork, or based on analysis of secondary sources, but should be genuine scientific investigations.

Although this last mandate can be seen as recognition of the importance of authentic science, there is some evidence that teachers may find the challenges of implementation to outweigh the benefits, as projects can require significant background expertise and time investments.[238] It was therefore decided to adapt the existing Advanced Chemistry program into a chemistry workshop that fulfilled the requirements of the NSW Depth Study, thus offering teachers an opportunity to incorporate citizen science into their classrooms while simultaneously fulfilling the demanding requirements of the syllabus.

2.2.1 Program

Several changes were made to the existing program to make it more appropriate for school students in terms of safety, time demands and curriculum. Broadly, this was achieved by reducing the number of experiments to just one reaction, simplifying certain procedures and redesigning learning materials to be aligned with the Year 12 Chemistry curriculum.

The final result is a two-part workshop, with a synthetic chemistry experience on the first day followed by a spectroscopy analysis workshop delivered at the school the following week. Students are hosted in the University of Sydney chemistry teaching labs, where they carry out the same Hantzsch synthesis performed by undergraduate students and isolate their final products. Spectroscopic data is then collected by researchers and presented to students in the second workshop, giving them the chance to put their data analysis to the test and determine whether their product has been made successfully. As with the undergraduate program, the compounds made by students are then purified where necessary and sent for biological screening.

The core Working Scientifically skills of *Questioning and predicting* and *Communicating* are facilitated by discussions with researchers and demonstrators during the workshop, with resources provided to teachers before and after the workshop to give context and updates. The laboratory-based component allows students to develop skills in *Conducting investigations* and

Problem solving, while the spectroscopy workshop provides an opportunity for both *Processing* and *Analysing data and information*. The Breaking Good program as Depth Study therefore covers six of the seven Working Scientifically skills described in the Year 12 curriculum (**Figure 2.4**), giving teachers ample room to devise assessment that fits the requirements of their individual school and assessment landscape.

One major difference between the undergraduate and secondary school programs is the required starting materials. While the undergraduate program can, for the most part, rely strictly on purchased materials, this is not feasible for the secondary school program with its reduced experimental load. Instead, the necessary thioureas are synthesised by Breaking Good researchers prior to the workshops, following the same scheme used in the undergraduate lab. This represents a considerable workload for the team, but also enables much greater flexibility, as targets would otherwise be limited only to molecules which can be made in a single step from commercially available reagents.

The Breaking Good synthetic workshops have been run three times across 2022 to 2024, with three different secondary schools participating. Two of the three schools were academically selective, and all three were government-funded public schools. Selecting public schools to participate was a deliberate decision, as government funded schools often lack the resources enjoyed by private, independent schools that can enable more engaging and memorable projects. In this time, approximately 500 students were involved in the synthesis of 24 molecules, approximately half of which were novel compounds.

2.2.2 Synthesis

Initially, the targets selected for the high school workshops were variations on the C-2 ring (**Figure 2.6**), as the workshop was devised alongside the Advanced Chemistry program. In 2022, four of the six targets selected were synthesised with excellent purity (**86 - 89**), but two failed to precipitate out of solution when attempted by students (**90** and **91**). However, both were later extracted from the pooled student filtrates, and were purified by automated column chromatography.

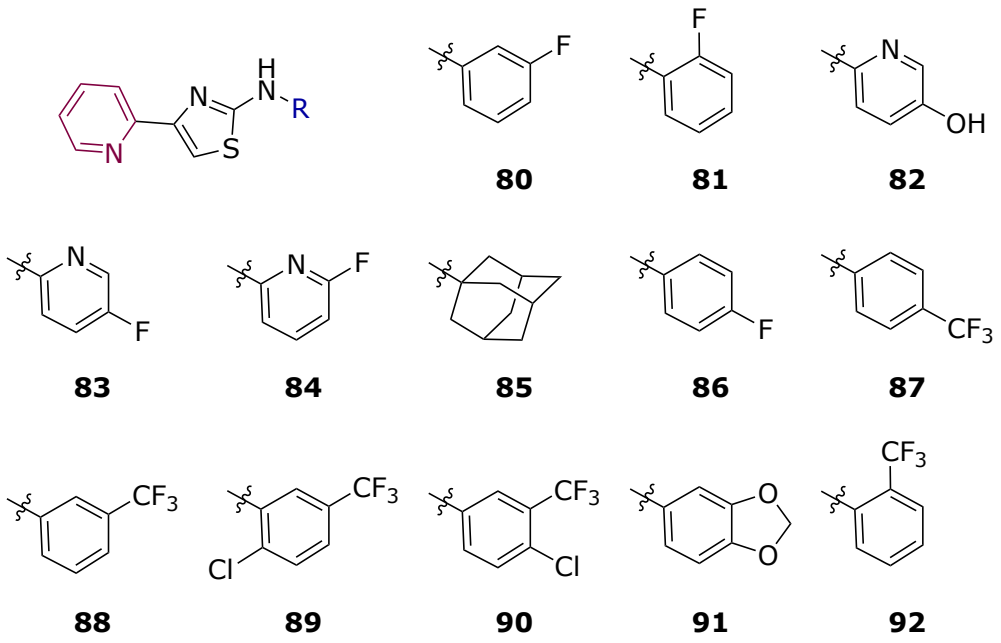

Figure 2.5 – C-2 phenyl and pyridinyl analogues made by high school students in 2022 and 2023.

In 2023, an ambitious goal of 12 target compounds (**80 – 85, 92**) included multiple variations on the C-2 ring (**Figure 2.5**). As the desired thioureas were either unavailable commercially or prohibitively expensive, six thioureas were produced on a ~5 g scale by the Breaking Good team (**93 – 98**, **Figure 2.6**).

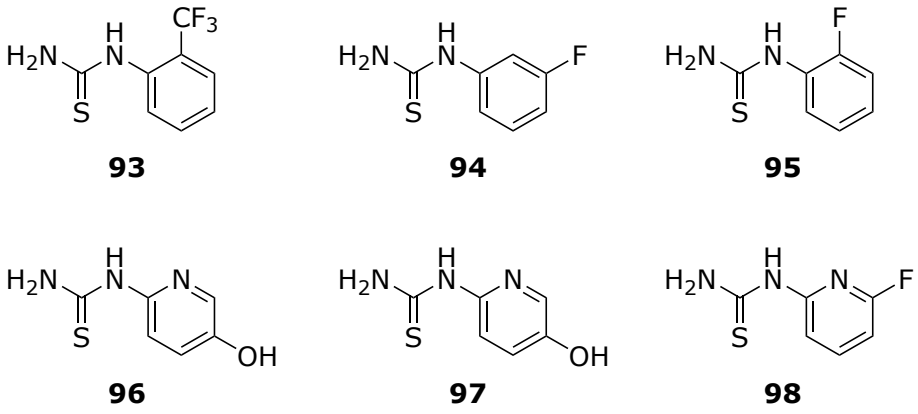

Figure 2.6 – Thioureas **93 – 98** synthesised by the researcher for use in high school workshops in 2023.

Using commercially available bromoketones, the 2023 workshop also targeted compounds with variations on both sides (**99 – 103, Figure 2.7**). Although logistical considerations meant that only a handful of these compounds could be made in one workshop, this demonstrated how a diverse array of molecules can be produced from just a handful of different starting

materials. Ultimately, the necessity of a pyridyl ring on the C-2 side meant that this approach was not continued in the following year, as the necessary bromoketones were not commercially available.

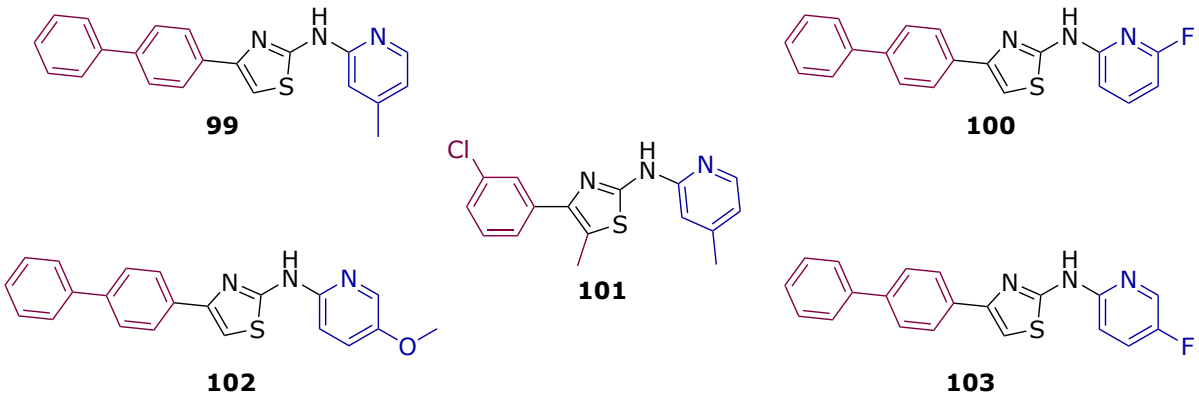

Figure 2.7 – 2-AT analogues with variations at both C-2 and C-4 positions, made by high school students in 2023.

All but one of the 2023 targets were made successfully by students, the exception being the adamantyl derivative **98** made with the commercial adamantyl-thiourea. No precipitate was formed upon addition of HCl, and while LCMS analysis of student filtrates did have a peak that corresponded to the expected mass, no material could be isolated by extraction. When the same reaction was attempted by experienced researchers on the Breaking Good team, similarly disappointing results were initially observed, but with increased reaction times, sufficient product for biological testing purposes was eventually obtained.

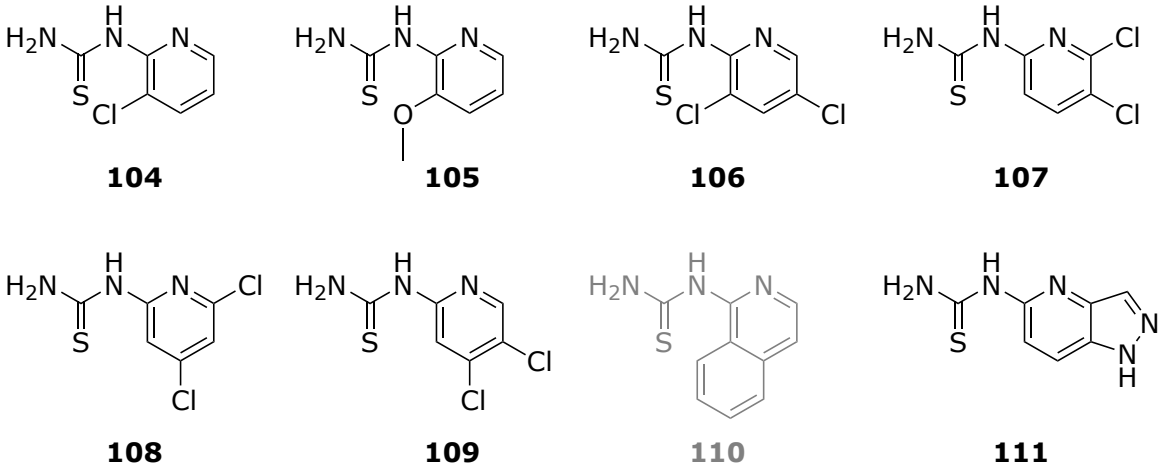

Figure 2.8 – Thioureas **104 – 111** synthesised by the researcher for use in high school workshops in 2024.

By 2024, preliminary biological data showed that compounds with chlorine-substituted pyridine rings at the C-2 position had the most promising activity (see **Chapter 3**, **Table 3.2**). Again, the desired thioureas were not readily available and were therefore synthesised at scale by the Breaking Good team (**105** – **111**, **Figure 2.8**), with the goal of producing four di-chloro-substituted compounds (**114 – 117**), as well as two compounds with C-2 fused ring structures, **118** and **119**, complementary to those being investigated in the Advanced Chemistry program the same year (**Figure 2.9**).

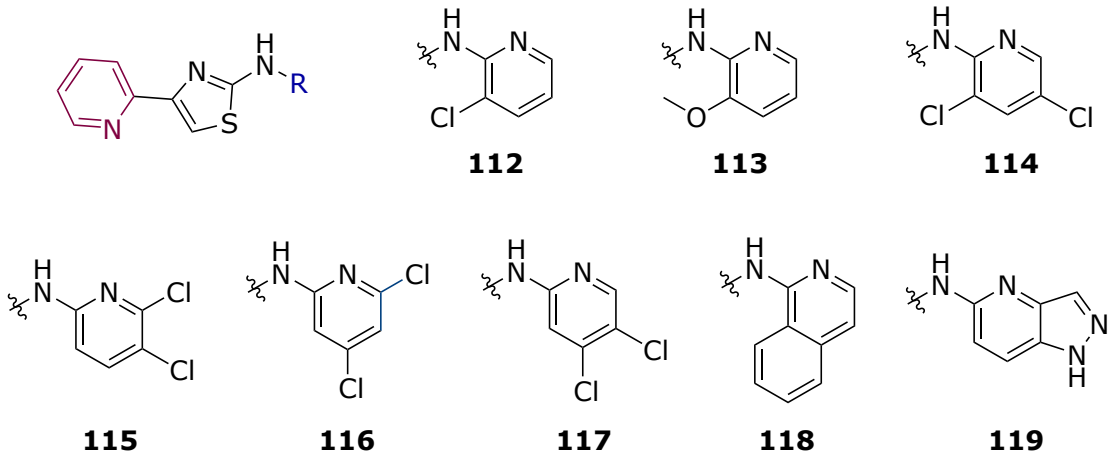

Figure 2.9 – C-2 pyridinyl analogues made by high school students in 2024.

However, during preparation of the intermediates, the quinoline thiourea **110** could not be cleanly hydrolysed from its benzoyl thiourea precursor, and the target **118** thus was not included in the final workshop. The remaining seven analogues were generated successfully with largely excellent purity from precipitation alone, with only **119** presenting a challenge to purify due to its low solubility in most standard solvents.

2.3 Reflections on Breaking Good

From the perspective of the Breaking Good team, both programs were well-received by students and educators alike.[239] The project continues to run in the undergraduate laboratory, and the high school workshops are in the process of being developed into a more sustainable long-term project.

The strength of both programs arguably lies in their adaptation to the different educational settings, with each being tailored to meet the students at their own level of understanding while

also fulfilling the needs of the broader curriculum. Of course, there are differences in output and reach, with the Advanced Chemistry lab program enabling a more comprehensive and personal experience, while the high school workshop reaches a much greater number of students (**Figure 2.10**), reflecting the different roles of the two programs in the greater educational context.

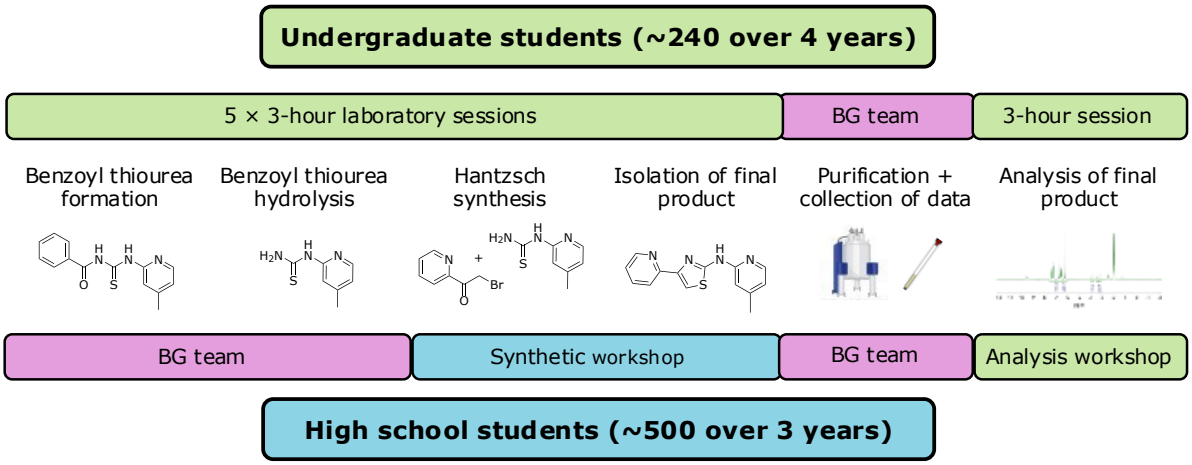

Figure 2.10 – Timeline of the two different iterations of Breaking Good comparing work completed by undergraduates (green), high school students (blue) and Breaking Good (BG) team (pink).

The undergraduate program requires less preparation by the Breaking Good team, as students prepare the thioureas themselves and other logistical factors are handled by the university teaching and technical staff. However, it is only available to students who have already decided to study chemistry at a tertiary level, making it less accessible and reducing the impact it might have on students' career decisions.

By comparison, the high school workshops demand a substantial investment of researcher time to produce the necessary precursors and arrange supervision, access to labs and scheduling for participating schools. This makes them perhaps less accessible from a researcher's point of view, as more effort is required to bring a project into the classroom. Both, though, are valuable examples of how even research areas that have been traditionally considered unapproachable can be made accessible through careful planning and consultation.

2.2.3 Beyond Breaking Good

The merit of the MycetOS/BG collaboration as an OSDD initiative is evident in its adoption beyond the University of Sydney. After the introduction of the 2-AT synthesis to undergraduate labs in 2022, the synthetic processes and details of the program were shared publicly via GitHub, which hosts the MycetOS online community. By 2023, the project had been adapted for third-year undergraduates at the University of York, and separately for chemistry students at the University College London (UCL). **Figure 2.11** summarises how Breaking Good has spurred a network of collaboration that includes partner organisations performing experiments, sharing results and protocols and guiding future research directions.

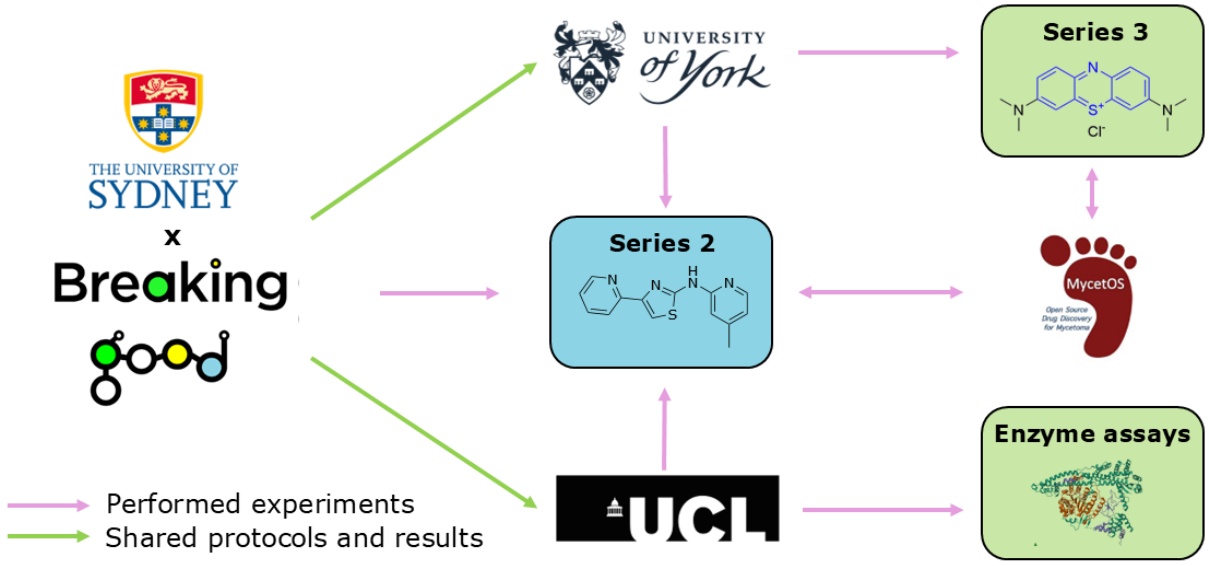

Figure 2.11 – OSDD connections stemming from Breaking Good project.

Both programs differ slightly from Breaking Good, and allow students more freedom in choosing their targets and synthetic methods. The two universities have contributed dozens of 2-AT analogues to the MycetOS project, with those most relevant to SAR shown in **Figure 2.12**. Beyond this, both have embarked on further citizen science endeavours related to the MycetOS project. At UCL, students have begun investigating potential mechanisms of action of these compounds through enzyme assays and molecular modelling. The University of York, on the other hand, has become the main contributor of phenothiazine analogues for MycetOS Series 3, generating these molecules through a similar scheme.

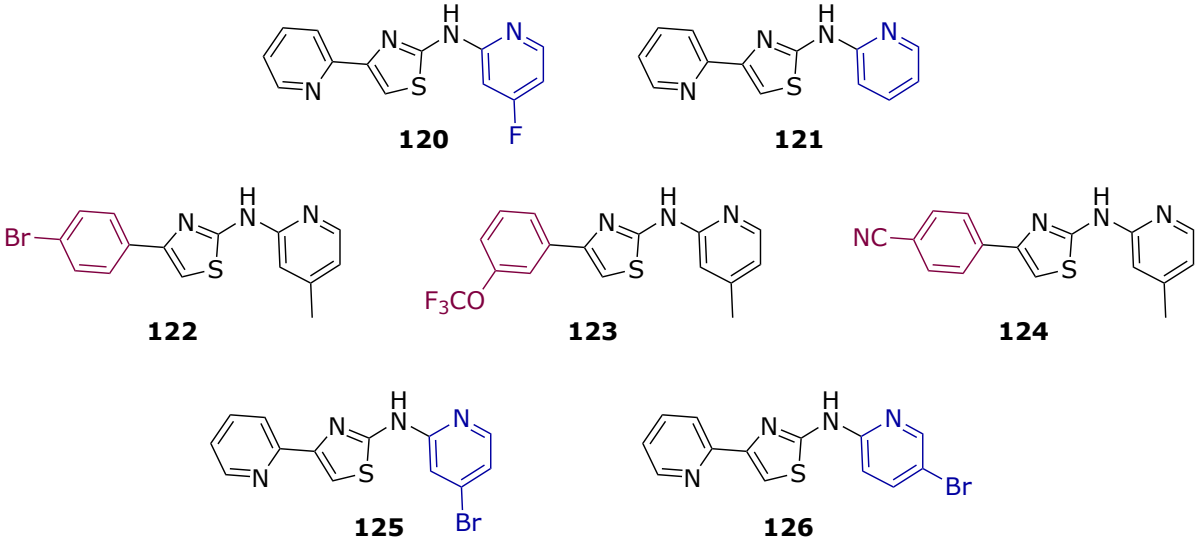

Figure 2.12 – 2-AT analogues contributed to the MycetOS project by UCL (**120 – 124**) and the University of York (**125** and **126**).

Of course, these exciting developments in the citizen science sphere should primarily be attributed to the academic and teaching staff who developed and implemented them. Still, it seems reasonable to assume that Breaking Good was both inspiration and example for these ventures. In turn, the MycetOS community, fostered by open science ideals, provided space for the Breaking Good program to evolve. This interwoven ecosystem of education, research and collaboration thus forms a perfect case study of how OSDD practices led to innovative cross-disciplinary research and education practices.

2.2.4 Impact on citizen science

The Breaking Good project can also be assessed through the lens of citizen science. A good citizen science project results in meaningful contributions to scientific knowledge, and enhanced engagement with the field among participants.[92,232] Both iterations of Breaking Good produced a series of 2-AT analogues that provided valuable information on the SAR of the series and furthered understanding of how these compounds can exert an antifungal effect. Preliminary analysis of both initiatives suggests that students did have improved understanding or interest in topics related to the project, whether this was about drug discovery in particular or the area of synthetic chemistry more generally.[239,240] Therefore, the Breaking Good project succeeded in creating citizen science projects in drug discovery – and in doing so has made

good on its promise to "*empower members of the public to be active researchers in projects that will improve human health*."[241]

While generating a library of related compounds for SAR studies is not a novel concept – engaging school students and undergraduates to synthesise these compounds is the innovation at the centre of this work. A handful of other universities have incorporated drug discovery projects into their practical classes, but there is no precedent in the literature for similar schemes with high school students. Indeed, there is only a scattering of citizen science projects involving synthetic chemistry whatsoever, at any level of education.[242]

The vast majority of compounds investigated in this early-stage drug discovery project were made by citizen scientists. This is a clear step forward for citizen science, and the Breaking Good team is hopeful that this work will illustrate the benefits and possibilities of incorporating citizen science approaches into synthetic chemistry, for both researchers with no experience of participatory science and citizen science practitioners without experience of organic chemistry.

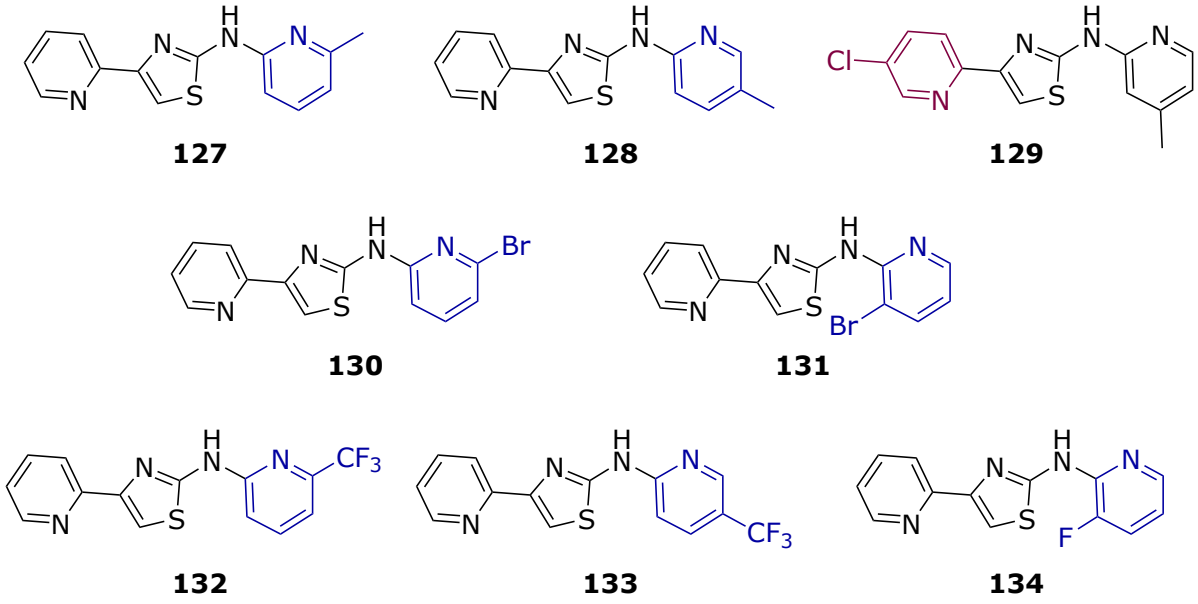

Figure 2.13 – 2-AT analogues **127** – **134** synthesised by the researcher outside of the Breaking Good workshops.

It should be noted that not all compounds discussed in the following analysis of biological activity were generated by students. Occasionally, a desired compound could not be prepared by students, due to concerns with either the safety or the cost of the necessary starting materials. However, this issue was easily circumvented by having these compounds (**127 – 134**) synthesised at a smaller scale by the researcher (**Figure 2.13**). In future workshops, this

synthesis could even be performed by teachers or demonstrators, offering them a chance to practice the skills they would be overseeing and contribute to the project in a more tangible way.

Instead of perceiving this as a barrier to developing citizen science projects in chemistry, it should instead be seen as evidence of their flexibility. Even in fields that have heartily embraced citizen science, like ecology or astronomy, not every project will be suitable for every participant – there is, thus far, no citizen science project encouraging non-experts to milk venomous snakes or fly to Mars. Organic chemistry is no different. Some projects will already be well-suited to crowdsourced approaches, and others may require more adaptation and behind-the-scenes support – but can still be incredibly beneficial to both scientific knowledge and the greater community.

3 Activity of 2-aminothiazole analogues against eumycetoma

The MycetOS working group follows a standard biological screening workflow for testing compounds (**Figure 3.1**). Following a protocol developed by A. Prof. Wendy van de Sande, compounds are first tested *in vitro* at high concentration (100 and 25 µM) against an *M. mycetomatis* type strain, with MIC and IC_{50} values determined for analogues that inhibit >80% of fungal growth. Where possible, MIC_{50} values, which estimate the effectiveness of a drug against the whole species rather than a specific strain, are calculated as well. Selection of compounds to take forward for *in vivo* testing varies slightly depending on the number of hits, but typically only compounds with $IC_{50} \leq 2$ µM are chosen. These are screened in healthy larvae for toxicity, and then in larvae infected with *M. mycetomatis* to determine *in vivo* efficacy.

In 2025, the volume of compounds with activity at 25 µM led to a slight change in protocol, with compounds also being screened at 2 µM before proceeding to IC_{50} determination.

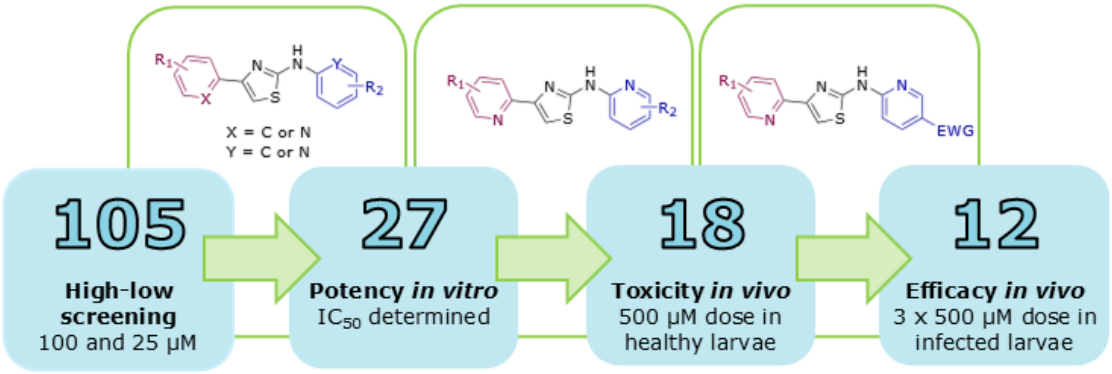

Figure 3.1 – Workflow for screening compounds against *M. mycetomatis* with number of compounds screened at each point (cumulative numbers to date).

A total of 105 compounds have been sourced and screened against *M. mycetomatis* during the investigation of Series 2. From these, 18 were found to be highly potent with $IC_{50} < 2$ µM, and 12 were tested against the *in vivo* model of eumycetoma.

3.1 *In vitro* screening

Since 2004, a colorimetric *in vitro* assay based on the tetrazolium viability dye XTT (2,3-bis-(2-methoxy-4-nitro-5-sulfophenyl)-2H-tetrazolium-5-carboxanilide) has been used to determine fungal susceptibility for *M. mycetomatis*, with recent variations using an alternative tetrazolium dye MTS (3-(4,5-di methyl thiazol-2-yl)-2,5-diphenyltetrazolium bromide).[122,243,244] Both are well-established methods of assessing cell viability as metabolic activity results in the reduction of the dye, turning it from a colourless tetrazolium dye into a bright yellow formazan product (**Scheme 3.1**). Production of the yellow formazan can be measured spectrophotometrically at 490 nm and used as a proxy for cellular growth.[245]

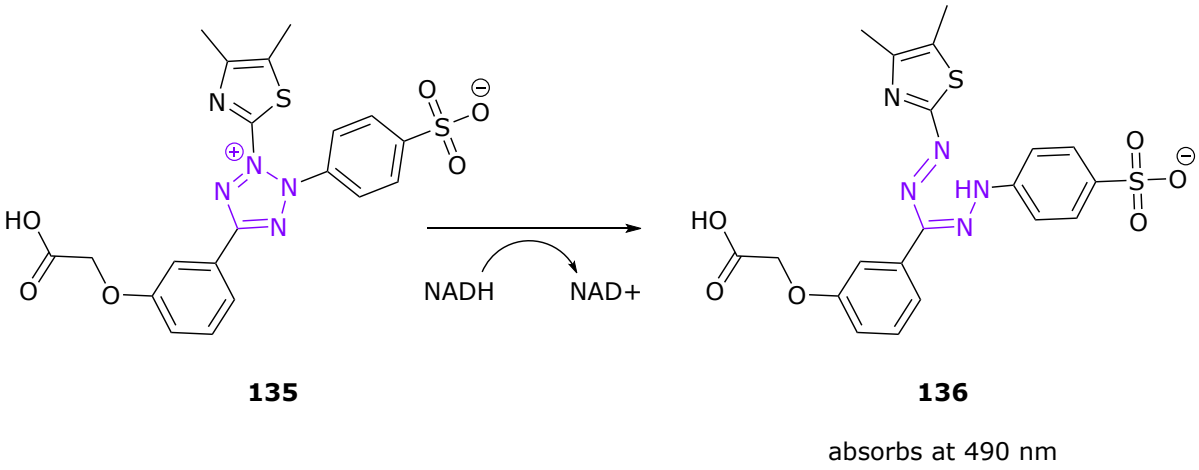

135 **136**

absorbs at 490 nm

Scheme 3.1 – Reduction of colourless tetrazolium dye MTS (**135**) to the yellow formazan product **136** with tetrazolium/formazan motif shown in purple.

Occasionally, *in vitro* testing may be performed using resazurin, a dark blue phenoxazine viability dye that is reduced to bright pink, highly fluorescent resorufin in the presence of NADH or NADPH.[246] While resazurin assays typically have excellent correlation with results from formazan-based assays, and resazurin is generally more affordable than MTS or XTT, the light brown colour of the *M. mycetomatis* fungus can complicate spectrophotometric readings with this dye.[247]

Optical density is typically used to assess the concentration of microorganisms in media, with a measure of CFU/mL referring to colony-forming units (i.e. cells capable of multiplying). CLSI guidelines for antibiotic susceptibility testing of filamentous fungi attempt to standardise results by using a pre-defined dilution of 0.4 – 5.0 × 10^4 CFU/mL. In contrast, the European

Committee on Antimicrobial Susceptibility Testing (EUCAST) endorses a narrower range of $2.0 – 5.0 \times 10^4$ CFU/mL and recommends using a haemocytometer to count cells.[248]

Madurella species are hyphomyetes, a type of conidial mould, within the fungal phylum Ascomyota.[249,250] Under normal conditions, the colony-forming unit of hyphomyetes would be the conidia, a type of spore (**Figure 3.2**).[249,250] However, *M. mycetomatis* only rarely produces conidia when grown *in vitro*,[249,251,252] meaning that an alternative CFU is required.

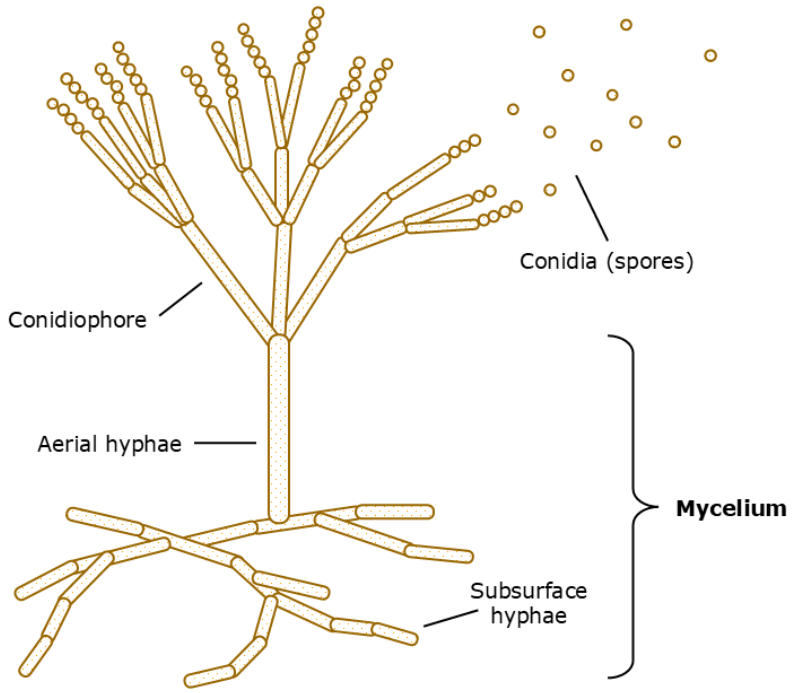

Figure 3.2 – Generalised structure of an ascomycetous fungus. Adapted from Behera *et al.*, 2019 with permission.[253]

The primary mass of any fungus is the mycelium, a network of fine filaments called hyphae which extract nutrients from the environment to sustain fungal growth. When mechanical force is applied to hyphae, they break into tiny pieces known as hyphal fragments, which can develop into a type of CFU called arthrospores.[254,255] These arthrospores are used as the standard CFU when studying *M. mycetomatis,* with dilutions typically measured by turbidimetric analysis using a spectrophotometer to determine the optical density of a given suspension.

3.1.1 Testing against *M. mycetomatis*

M. mycetomatis isolate MM55 was grown on Sabouraud agar for 2–3 weeks before mycelia were harvested and suspended in RPMI 1640 media supplemented with L-glutamine (0.3 g/L) and morpholinepropanesulfonic acid (20 mM) as buffer. The mycelia were broken up *via* sonication and the suspension was incubated for a further 7 days at 37 ºC to allow the growth of hyphal fragments. After incubation, excess media was removed and the fragments were resuspended in fresh RPMI media before sonicating. The final suspension was then prepared by adjusting with fresh RPMI until the final suspension measured 68 – 72 % transmission at 660 nm, which corresponds roughly to the range 0.4 – 5.0 × 10^4 CFU / mL (**Figure 3.3**).

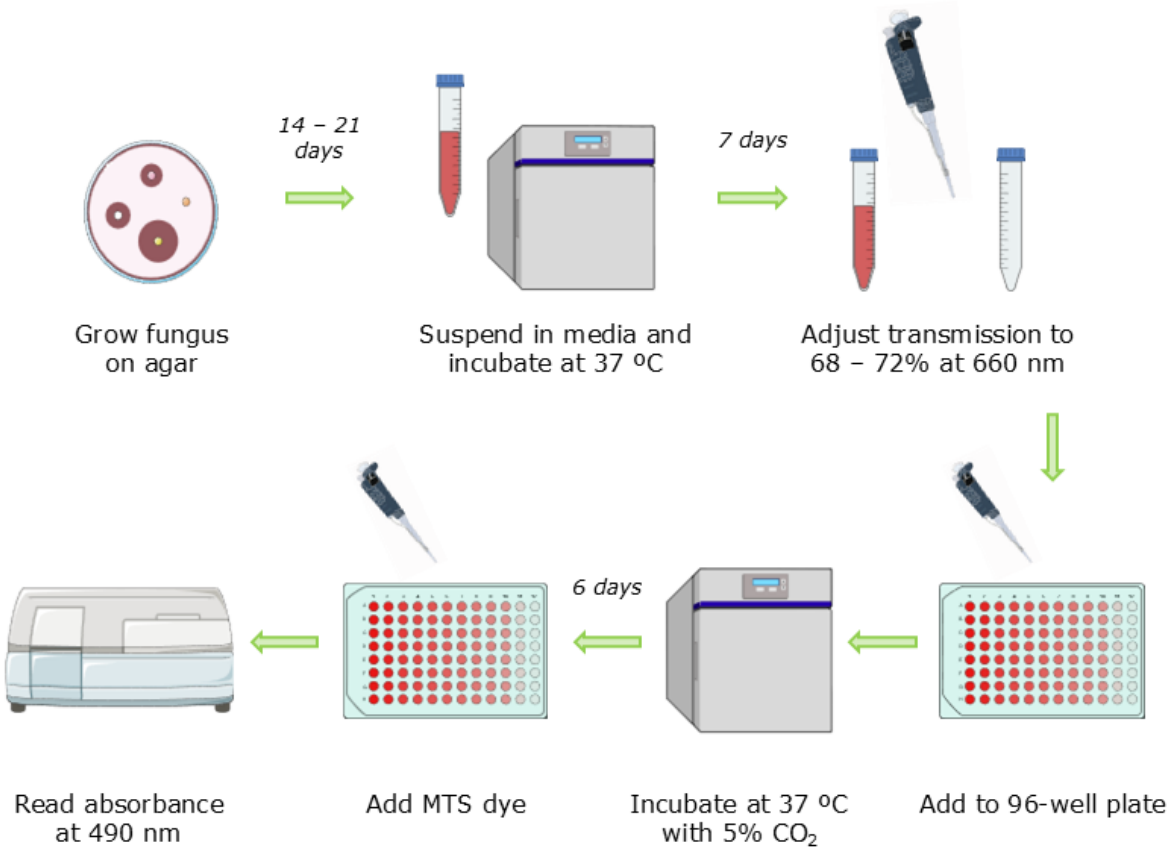

Figure 3.3 – Workflow for *in vitro* testing using MTS dye in a 96-well plate.

The suspension was added to a 96-well plate that already contained the necessary dilutions of compounds being tested. On every plate, a positive growth control of DMSO and a negative control of itraconazole were included in triplicate.

The plate was incubated at for six days (37 ºC, 5% CO_2), then MTS was added to each well and the plate was centrifuged to ensure complete mixing. From each well, approximately 100

uL of solution was transferred to a flat-bottomed 96-well plate, so that fungal growth on the bottom of the original well would not interfere with spectrophotometric readings. The plate was analysed at 490 nm using a BioTek Epoch 2 microplate spectrophotometer and fungal growth was calculated as a percentage according to the formula:

$$100 \times \frac{x_{490} - NC_{490}}{PC_{490} - NC_{490}}$$

Where x = absorbance, NC = averaged absorbance of negative control, PC = averaged absorbance of positive control.

While inhibition for microbes is usually defined as 99.9% reduction in activity,[248] the brown colour of the *M. mycetomatis* mycelium – whether dead or alive – overlaps with the absorbance of the formazan product, making it unclear whether readings are due to inactive fungal remnants or formazan dye. Therefore, fungal inhibition is defined in this work as < 20% growth as measured by the MTS dye.

3.1.2 Activity against *M. mycetomatis*

The first series of analogues to be tested were those with substituted phenyl rings at the C-4 position (**Table 3.1**), made by the 2021 SSP class and various cohorts at UCL and the University of York. Unfortunately, none of these compounds showed activity, even at the highest concentration tested (100 μM). Similarly, any change in the position of the *N* atom within the ring at the C-4 position resulted in complete loss of potency.

Table 3.1 – Substitutions made to C-4 phenyl ring (compound code given). None were able to inhibit fungal growth at 100 μM. Testing performed by Dr Jingyi Ma of the van de Sande lab.

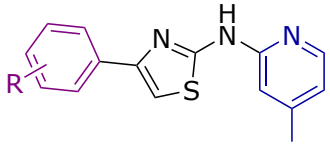

Position	Me	OMe	F	Cl	Br	OCF_3	NO_2	Ph	CN
Ortho	53a	53d	53b	53c	-	-	53e	-	-
Meta	52a	52d	52b	52c	-	123	52e	-	-
Para	51a	51d	51b	51c	122	-	51e	99	124

The next series of compounds to be tested were those made by undergraduate and high school students in 2022 through Breaking Good, incorporating variations on the C-2 ring that included both substituted phenyl and pyridyl rings (**Figure 3.4**). Comparison of matched pairs such as the fluoro analogues **96** and **86** and methyl analogues **11** and **60** suggested that the pyridyl ring was equally necessary on this side of the molecule, and this finding was factored into target choice for the 2023 and 2024 programs.

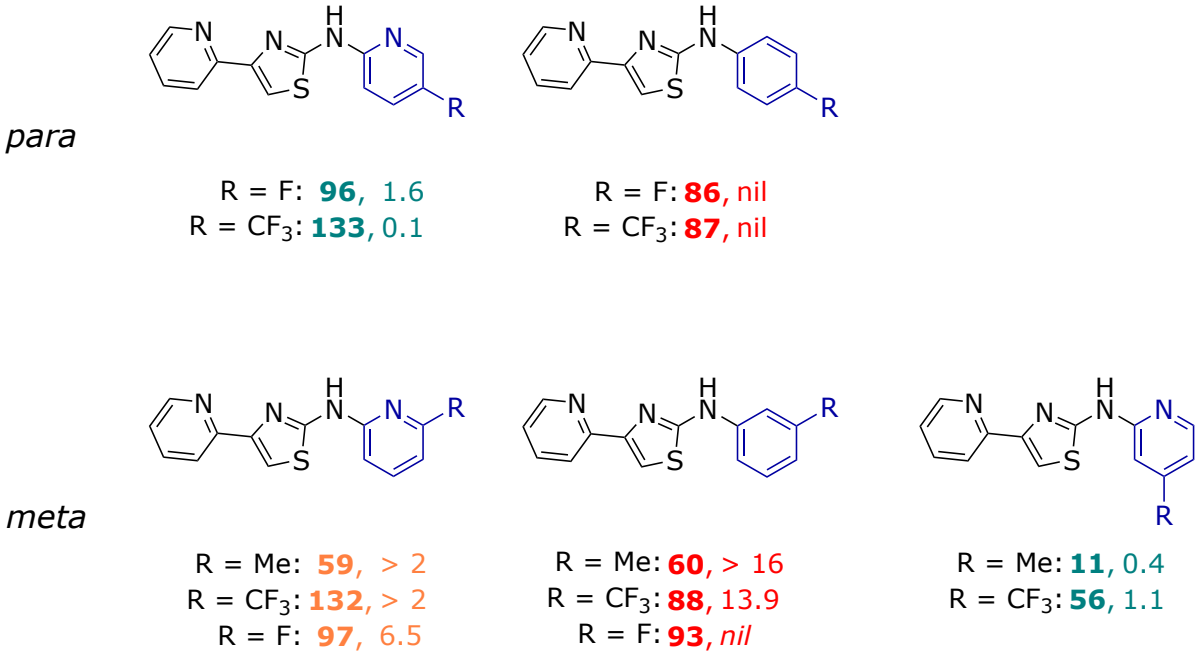

Figure 3.4 – IC_{50} (μM) of selected C-2 phenyl and pyridinyl analogues against *M. mycetomatis*.

By 2023, it had been established that both pyridyl rings were necessary for activity and attention turned to investigating substitution on those rings. On the C-2 pyridyl ring, various electron-withdrawing and donating groups were trialled (**Table 3.2**), with a handful of dichloro-substituted compounds (**114 – 117)** included after the mono-chloro analogues **54**, **57** and **58** were found to have promising activity (**Figure 3.5**).

Table 3.2 – IC_{50} (μM) of C-2 substituted pyridinyl analogues against *M. mycetomatis*. Most potent compound among analogues with the same functional group indicated in blue.

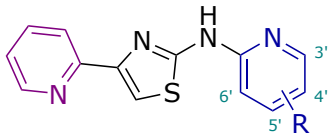

Position	3′	4′	5′	6′
Me	> 2.0	5.4	0.4	-
OMe	4.3	2.2	1.6	3.0
Cl	0.6	0.3	0.6	3.0
F	6.5	1.6	n.a.	1.8
Br	> 2.0	0.4	1.4	1.4
CF_3	> 2.0	0.1	1.1	-
Phenyl	-	0.2	-	-

A handful of these analogues were marginally more potent than the original hit compound **11**, namely those with bromine, chlorine or trifluoromethyl at the 4′ position (**126**, **57** and **133** respectively). In all cases, electronegative substituents showed highest potency at this 4′ position, while the two electron-donating groups, methyl and methoxy, were most potent in the 5′ position (**11** and **55**).

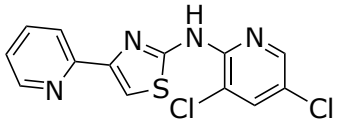

114, 0.6

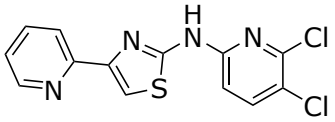

115, nil

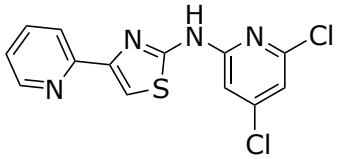

116, 9.7

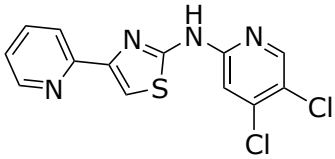

117, nil

Figure 3.5 – IC_{50} (μM) of di-chloro substituted analogues against *M. mycetomatis*.

Disappointingly, very few analogues with pyridine rings substituted at the C-4 position were synthesised, due to challenges sourcing either the methyl ketones or the more desirable bromoketones. Those that were successfully synthesised are shown in **Figure 3.6,** but it is

difficult to draw conclusions from such a small sample, with only **61e** showing activity comparable to the lead compound.

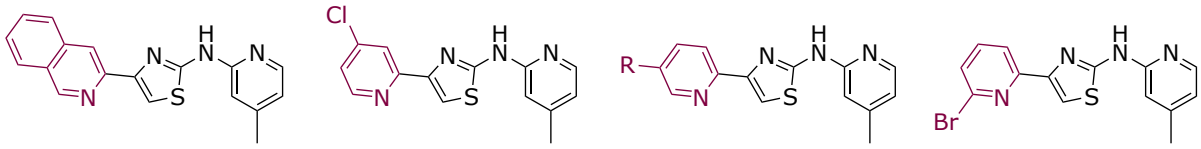

61d, *nil* | **61c**, 5.7 | R = Cl: **129**, > 2; R = Br: **61b**, *nil*; R = Ph: **61e**, **1.6** | **61a**, *nil*

Figure 3.6 – IC_{50} (μM) of C-4 substituted pyridinyl analogues against *M. mycetomatis*.

Finally, the series of cyclic isosteres showed unremarkable activity overall (**Table 3.3**), with some variations having no activity at all at the concentrations tested, and none having IC_{50} values below the 2 μM cutoff point. In some cases, such as **119**, **75** and **85** this could be due to poor solubility, which is an established issue for compounds with these motifs.

Table 3.3 – IC_{50} (μM) of cyclic isosteres at the C-2 position.

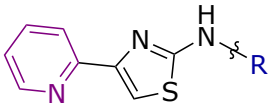

Code	R	IC_{50}	Code	R	IC_{50}
85	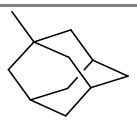	11.5	**74**	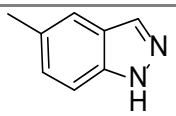	> 25
91	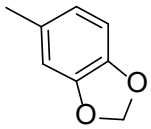	> 25	**78**	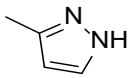	Nil
119	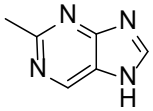	Nil	**77**	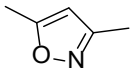	> 25
75	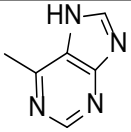	> 2	**76**	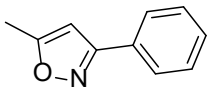	> 2

3.1.3 Species-wide activity

Antimicrobial drugs are often discussed in terms of MIC and IC_{50}, which are both values determined against a single strain of the microbe of interest, usually one that is well-known to the research community. Different strains may be used to assess potency against drug-resistant organisms, or to investigate how known mutations in particular strains might affect drug activity.[256] In contrast, the MIC_{50} measures the activity of a drug against the entire bacterial population within a species, with all the genetic variation that entails.[257]

Table 3.4 – Different measures of potency and their definitions.

Abbreviation	Term	Meaning
MIC	Minimum inhibitory concentration	Lowest concentration required to completely inhibit microbial growth of a given strain.
IC_{50}	Inhibitory concentration "50%"	Concentration required to inhibit 50% of microbial growth of a given strain.
MIC_{50}	Minimum inhibitory concentration "50%"	Lowest concentration required to completely inhibit microbial growth in at least 50% of strains tested.

These three measures of potency are summarised in **Table 3.4**. In comparison to IC_{50} and MIC, MIC_{50} values can be seen as a population-level measure of efficacy and may provide valuable insight into whether a given drug will be effective against strains with acquired or innate drug resistance.

The MIC_{50} is determined by calculating the MIC of a given compound against dozens of isolates of the same species, with the MIC_{50} being the lowest concentration that can inhibit 50% or more of the isolates. Similarly, the MIC_{90} is the concentration that inhibits 90% or more isolates.[258] Individual MIC values for separate isolates are often amalgamated from results from various laboratories.[259]

In the case of eumycetoma, the dearth of research generally has led to MIC_{50} being determined on a smaller scale, with only nine different strains being tested (**Appendix B**). These strains are selected to maximise diversity, including isolates from diverse geographical areas and with different genetic backgrounds.[260]

Table 3.5 – Promising compounds with IC_{50} and MIC_{50} against *M. mycetomatis* shown in µM.

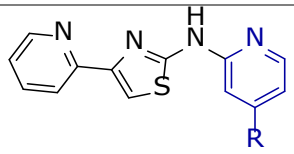

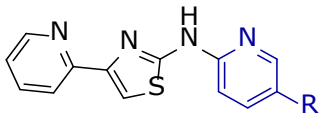

Cmpd	R group	IC_{50}	MIC_{50}	Cmpd	R group	IC_{50}	MIC_{50}
11	Me	0.7	0.25[59]	**128**	Me	5.4	8.0
55	OMe	1.6	2.0	**82**	OMe	2.2	4.0
54	Cl	0.6	2.0	**57**	Cl	0.3	1.0
125	Br	1.4	4.0	**126**	Br	0.4	1.0
56	CF_3	1.1	1.0	**83**	F	1.6	2.0

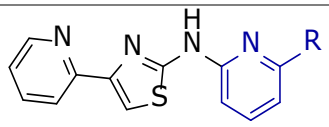

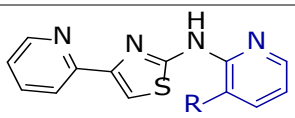

Cmpd	R group	IC_{50}	MIC_{50}	Cmpd	R group	IC_{50}	MIC_{50}
59	OMe	4.3	8.0	**113**	OMe	3.0	4.0
58	Cl	0.6	8.0	**112**	Cl	3.0	4.0
84	F	6.5	16.0	**121**	H	2.7	8.0

MIC_{50} values were determined following the identical protocol described above with *M. mycetomatis* isolates MM14, S01, I1, I3, Parijs1, Peru72012, AL1 and CBS247.48. Values were obtained for 2-AT analogues with IC_{50} values lower than 10 µM, in line with the progression of these compounds into *in vivo* testing, and are shown in **Table 3.5**.

Generally, the IC_{50} calculated against the *mm55* strain fell within a single dilution step of the MIC_{50}, and compounds with the highest activity against a single strain returned MIC_{50} values of 2.0 µM or lower (**11, 54, 57, 126**). The chloro analogue **58** is an exception to this rule, with a reported IC_{50} of 0.6 µM but surprisingly high MIC_{50} of 8.0 µM. Overall, the good agreement between potency against different isolates is an indication that these molecules would be broadly effective against diverse strains of *M. mycetomatis*.[258]

3.1.4 Establishing a pharmacophore

The SAR studies conducted indicate several key requirements for the 2-AT pharmacophore (**Figure 3.7**). Replacement of the pyridine ring at either the C-2 or C-4 position effectively suppresses activity, with the 2-pyridinyl ring being the only isomer tolerated at the C-4 position. There is some evidence that the C-2 aryl ring tolerates greater variety, as analogues **85** and **76**, which contain an adamantane group and 3-phenylisoxazole motif respectively, showed reasonable activity at < 25 μM concentrations.

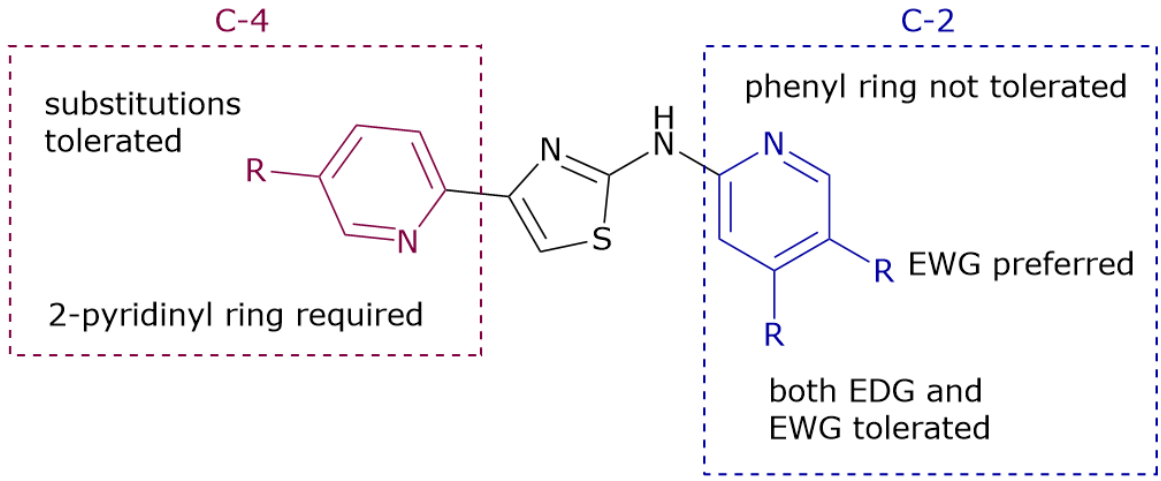

Figure 3.7 – The pharmacophore currently established for *in vitro* activity of 2-ATs against *M. mycetomatis*.

Although substitution on the C-4 ring was trialled, the limited results show no clear trend. Conversely, there is an apparent preference for electron-withdrawing substitutions in the 4′ position on the C-2 ring, while electron-donating groups show greater potency in the 5′ position. However, the differences in potency between different substituents and orientations are generally small.

3.2 Screening in the larval model

The wax moth larvae model used to screen compounds for *in vivo* activity was first developed for eumycetoma in 2015 and has been validated for *M. mycetomatis* and *Falciformispora senegalensis*, two of the most common fungal species responsible for eumycetoma.[261,262] *G. mellonella* larvae are often used as hosts for studying fungal infections as they strike a balance between the benefits and challenges of traditional animal models. The larvae have an immune

system similar enough to that of humans to enable assessment of interactions between drug candidates and the immune response, and can be grown at a temperature of 37°C, mimicking the environment in the human body. In contrast to most mammalian models, they are easy and cost-effective to raise and care for, present fewer ethical complications, and their simple anatomy makes drug delivery and histological studies straightforward.[134]

In the context of eumycetoma drug discovery, the larval model is especially useful as it allows for the development of fungal grains and so evaluation of drug efficacy in this context. It is believed that the inconsistencies observed between *in vitro* potencies and clinical efficacy is at least partially due to formation of these protective fungal grains, which protect the fungus within from fungicidal agents.[131] The drivers and mechanism of grain formation are currently under investigation, but thought to occur through a complex interaction involving both the pathogenic organism and the host immune system. This process, outlined in **Figure 3.8**, ultimately results in the fungus being encapsulated in a layer of near-impenetrable cement-like material.[110]

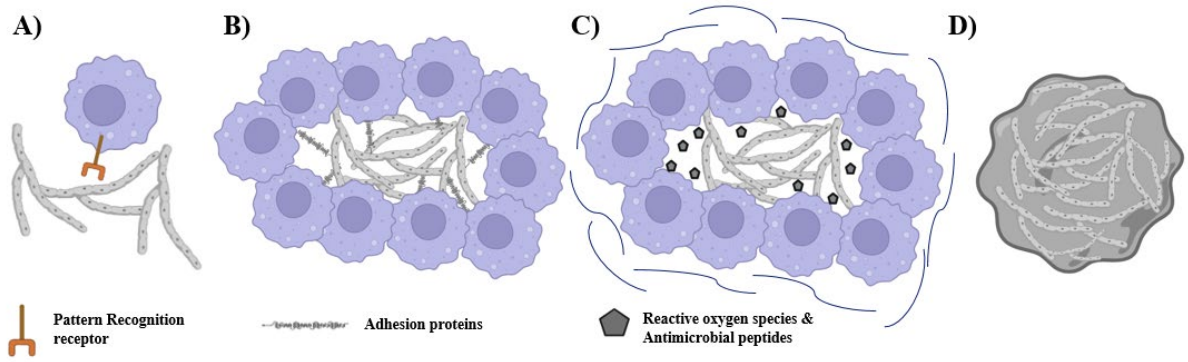

Figure 3.8 – Grain formation over time. A) Fungal hyphae are recognized by Pattern Recognition Receptors as pathogens. B) Immune cells (lilac) aggregate around the hyphae and host cell cross-links and binds to fungal cells. C) Reactive oxygen species are produced by granulated cells. The fungus produces melanin and trehalose and forms a capsule. D). The fungus fully breaks down the host cells and creates cement-like material. Figure and caption adapted from unpublished results of Dounia El-Yachioui with permission.

Researchers have speculated that antifungal compounds with excellent *in vitro* activity are simply unable to reach and interact with the fungus once grains have formed, making the larvae assay an indispensable step in the drug screening process.[261] Although mouse models of eumycetoma do exist, the cost and labour associated with these models makes them unfeasible

for the high volume of testing required in early-stage screening.[263] The *G. mellonella* model is therefore used as a means of identifying the most promising compounds for further study.

3.2.1 Toxicity in *G. mellonella*

Compounds with promising activity (IC_{50} < 2 μM) were first screened in healthy larvae to assess toxicity. A single 20 μL dose (500 μM) of the compound was injected into the bottom left pro-leg of 15 healthy larvae, and their survival was monitored for ten days. Toxicity was defined as a significant decrease in survival compared to a control group treated with a 20 μL dose of the PBS vehicle, using a Log-rank test with a cut-off of p = 0.05.

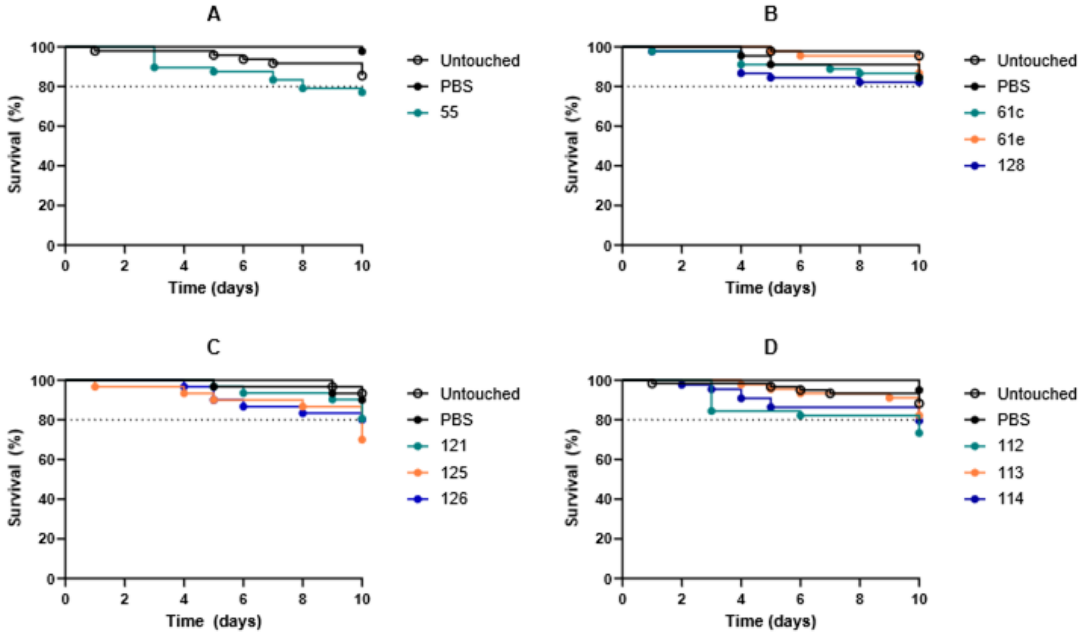

Figure 3.8 – Kaplan-Meier survival plots for ten 2-AT analogues tested in healthy *G. mellonella* larvae, with p-values relative to healthy larvae treated with PBS alone. Panel A: **55**, 0.0028. Panel B: **61c**, 0.9532; **61e**, 0.7183; **128**, 0.7084. Panel C: **121**, 0.3175; **125**, 0.0579; **126**, 0.2630. Panel D: **112**, 0.0013; **113**, 0.0298; **114**, 0.0118.

Three replicates were performed, with a replicate deemed void if more than 20% of the control group died during the observation period. A representative sample of the data is shown through Kaplan-Meier survival plots in **Figure 3.8**.

Eighteen Series 2 compounds were screened for toxicity, with the majority showing excellent tolerability. Even among those that showed some statistical deviation from the PBS control (**55, 112 – 114**) this difference was only observed on the tenth day of observation. While three of

the four compounds exhibiting mild toxicity were dichloro-substituted analogues, singly chloro-substituted analogues **54** and **57** showed no issue, and the sample set of compounds is too small to consider this a meaningful trend.

3.2.2 Efficacy against *M. mycetomatis*

Efficacy testing was performed by treating larvae infected with *M. mycetomatis* with three doses of the compound of interest across 72 hours. *M. mycetomatis* isolate MM55 was grown on Sabouraud agar for three weeks, then mycelia were harvested and suspended in RPMI 1640 media supplemented with chloramphenicol (100 mg/L) and L-glutamine (0.3 g/L) and buffered with MOPS (20 mM). The suspension was sonicated before being incubated at 37 ºC for two weeks with daily agitation. After incubation, the suspension was filtered *in vacuo* to obtain the mycelia as a dry solid, which was suspended in PBS and sonicated.

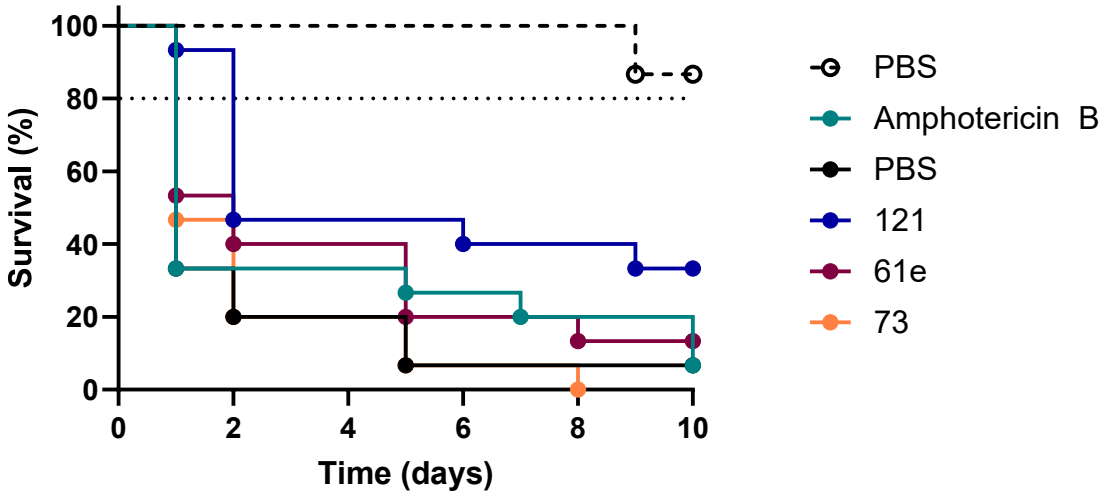

Figure 3.9 – Kaplan-Meier survival plots for 2-AT analogues tested in *G. mellonella* larvae. Solid line indicates infected larvae, dashed line indicates healthy larvae. P-values given relative to infected larvae treated with PBS alone (solid black line), where applicable. **PBS** (black); **Amphotericin B** (teal), 0.5032; **121** (dark blue), 0.0042; **61e** (crimson), 0.2645; **73** (orange), >0.9999. Screening performed by Dounia el-Yachioui.

The suspension was concentrated using centrifugation and adjusted to a concentration of 100 mg/mL with PBS. Healthy *G. mellonella* larvae were injected with a single 40 µL dose of the resulting inoculum, while a control group was injected with an equal volume of PBS vehicle. The larvae were subsequently treated with three 20 µL doses of either the unknown antifungal

agent (500 μM), amphotericin B (25 μg/mL) or PBS buffer delivered 4, 28 and 52 hours after infection.

Survival was monitored for ten days, with infection occurring on day zero. A compound was deemed to be effective if a significant increase in survival compared to the infected controls was detected, using a Log-rank test with a cut-off of $p = 0.05$. Three replicates were performed, with a replicate deemed void if more than 20% of the control group died during the observation period. A representative sample of the data is shown through Kaplan-Meier survival plots in **Figure 3.9**.

A total of 12 Series 2 analogues were tested *in vivo*, but complications with larvae survival meant that efficacy could only be assessed for nine compounds, results for which are given in **Table 3.6**. Apart from the lead compound, only the unsubstituted analogue **121** significantly improves larvae survival. This result was particularly interesting as this derivative has notably lower *in vitro* potency than most of the others tested, with an IC_{50} of 2.7 μM, and typically would not have passed into *in vivo* screening.

Table 3.6 – Raw and corrected survival data, as percentage and area under curve (AUC), of larvae infected with *M. mycetomatis* and treated with Series 2 compounds in 2025. P-values determined by the Log-Rank test, with significant values ($p < 0.05$) indicated by *. All values calculated ten days after infection.

Code	IC_{50} (μM)	Survival (%)	Survival, corrected (%)	AUC	Change in AUC	P-value
11	0.4[59]	28.6	18.6	-	-	0.0012*
56	1.1	2.22	-7.78	286.7	25	0.9383
54	0.6	10	0	304.2	42.5	0.2648
57	0.6	11.11	1.11	326.7	65	0.2814
61c	5.7	3.33	3.33	186.67	-3.32	0.3665
113	3.0	0	0	193.34	3.35	0.3244
121	2.7	33.33	26.67	500.01	273.33	0.0042*
61e	1.6	13.33	6.67	333.33	106.65	0.2645
73	0.2	0	- 6.67	226.68	0	> 0.99

Unfortunately, only limited conclusions can be drawn about the relative *in vivo* activity of this series when so few analogues have demonstrated significant efficacy. Although 2-ATs have

been investigated as potential treatments for several conditions, the mechanism of action is unknown in all cases, and SAR findings are limited. Against both tuberculosis and leishmaniasis, the C-4 pyridine is essential,[47,264] as seen in the current work, while in studies against prion disease, a pyridine ring is required at the C-2 position but not C-4.[265] Additionally, considerable variation in pharmacokinetic profiles has been reported, with analogues prepared for leishmaniasis having insufficient microsomal stability to be effective drug candidates, while those investigated for prion diseases have continued into orally-administered animal studies.[47,265] The thiazole moiety is susceptible to oxidisation at the sulfur, making related analogues like 2-aminooxazoles potentially more attractive targets.[266] Future SAR analysis should therefore incorporate consideration of metabolic stability and toxicity, as well as fungicidal efficacy.

3.2.3 Comparison to other antifungal agents

As with established antifungals, *in vitro* potency does not appear to be strongly correlated to *in vivo* efficacy for the 2-AT series. The control treatment used in larvae experiments, amphotericin B (**137**), has a reported MIC_{50} of 0.5 μM, yet is significantly more effective at increasing larvae survival than olorofim (**138**) and azole-based drugs, which have MIC_{50} values below 0.06 μM (**Figure 3.10**).[122]

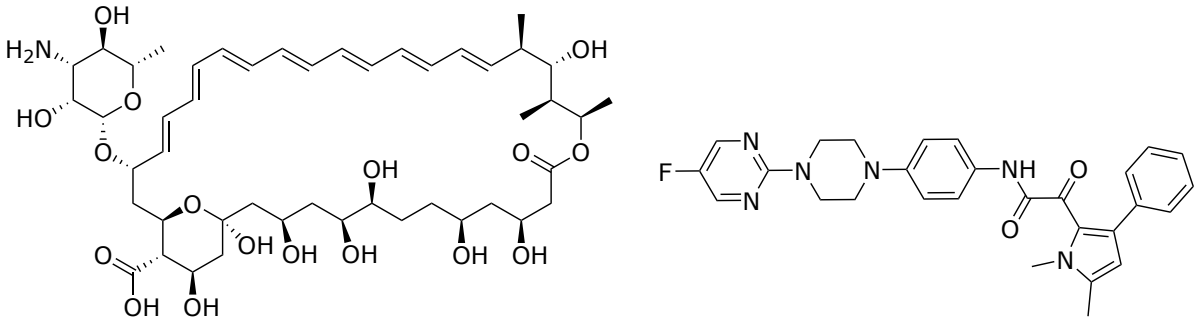

137 **138**

0.5 μM 0.016 μM

Figure 3.10 – Structures of antifungal compounds amphotericin B (**137**) and olorofim (**138**) with reported MIC_{50} against *M. mycetomatis*.

Although azoles and terbinafine are favoured over amphotericin B in the clinic, this is due to the risk of nephrotoxicity associated with amphotericin B therapy.[125,267] Olorofim has not yet been fully approved as a new therapeutic agent, so its clinical efficacy remains unknown.[127]

Broadly, the low efficacy of the compounds discussed above is attributed to the protective effect of the fungal grains in the animal model, with components of the grain like melanin, 1,3-D-glucan, and extracellular DNA thought to bind fungicidal compounds before they can exert their effect. This is supported by the finding that the MICs measured for itraconazole and ketoconazole increase when *M. mycetomatis*-derived melanin is added during *in vitro* studies.[122]

It is possible that amphotericin B can penetrate the fungal grain more effectively due to its highly lipophilic character. In their current state, the 2-AT series are significantly less lipophilic, with calculated logD values mostly between 2 and 4. Extending the molecule at either the C-4 or C-2 ring by incorporating new aromatic rings or fused ring structures is a simple means of increasing overall hydrophobicity, and in this work two of the more potent analogues synthesised are those with an additional phenyl ring on either side of the molecule: **61c** and **73**.

3.3 Understanding the mechanism of action

While SAR studies can on their own enable optimisation of the potency and pharmacokinetic profile of a drug, determining the mechanism of action of a therapeutic provides a more direct route to understanding how structural alterations might impact a compound's efficacy.[268] Unfortunately, there is no clear-cut single approach to determining mechanism of action, although a range of methods can be used.

Methods based on understanding the disease typically involve identifying proteins and pathways that might be relevant to antimicrobial activity. For instance, proteins inhibited by known fungicidal agents are plausible targets for a new antifungal, and more likely to have pre-existing models or assays that can be used to test novel compounds. This avenue can be especially useful if the goal is to develop a treatment for disease strains that are resistant to current drugs.

Alternatively, investigation can be centred on the compounds themselves. Structural similarity to established drugs might hint at a shared mechanism, while previously reported activity or interactions can reveal hitherto unconsidered biological pathways. This approach is complemented by ongoing SAR studies, as structural motifs from the literature can be incorporated and the resulting activity used to refine hypotheses.

3.3.1 Ergosterol biosynthesis

The three classes of antifungal with reported clinical efficacy against eumycetoma all target the cell wall building block ergosterol and its biosynthesis, as outlined in **Figure 3.11**.[117] Terbinafine prevents formation of the squalene epoxide intermediate, azoles inhibit the CYP51 enzyme 14-α-sterol demethylase, and amphotericin B binds ergosterol itself, thus impeding cell wall synthesis.[117] Given the emerging resistance to itraconazole and other azole-based drugs,[123] discovering antifungals that work *via* alternative pathways is of critical importance.[123]

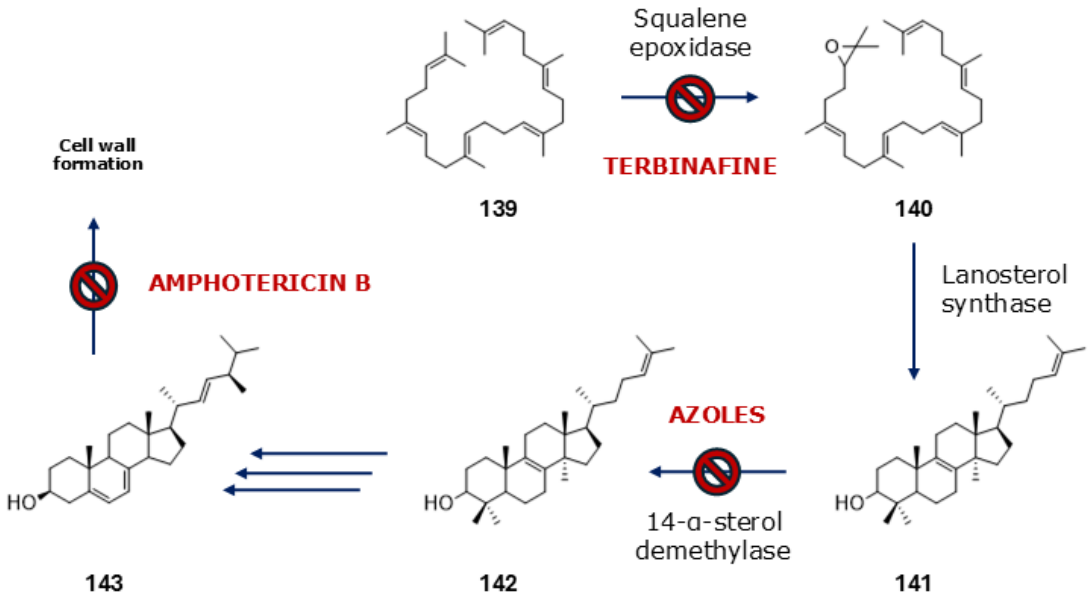

Figure 3.11 – Ergosterol biosynthetic pathway with targets of known antifungals shown. Terbinafine prevents the conversion of squalene (**139**) into squalene epoxide (**140**), azoles prevent conversion of lanosterol (**141**) into 4,4-dimethylcholesta-8,14,24,trienol (**142**), and amphotericin B interferes with the incorporation of ergosterol (**143**) into the fungal cell wall.

Several techniques could be employed to investigate whether 2-ATs act on this pathway, and in particular on CYP51, including molecular modelling, gene knockout experiments, and synergistic studies.

In theory, two drugs which act on the same target will have an unchanged or reduced efficacy when used in combination, while a combination of two drugs with different targets should have unchanged or *increased* efficacy.[269] However, these effects are less clear when drugs act on different targets in the same pathway, as with the ergosterol biosynthesis targeted by terbinafine, azoles, and amphotericin B. For instance, co-administration of amphotericin B and an azole is known to have an antagonistic effect in various fungi, including *M.*

mycetomatis.[122,269] Conversely, terbinafine-azole synergy has been reported in tests with multiple fungi,[269] but using this combination was found to have no significant effect on potency against *M. mycetomatis*.[122] Although co-administration studies cannot definitively rule out certain pathways, they are nonetheless worth pursuing, as discovering a combination therapy with enhanced antifungal activity may still translate into improved clinical outcomes.

Multiple homology models of the *M. mycetomatis* CYP51 enzyme involved in this pathway have already been developed and could be used in docking studies with potent 2-AT analogues to determine whether there are likely to be favourable binding interactions between the two.[123,270,271] While computational approaches do not always reflect *in vivo* activity, modelling can be a useful way to screen compounds of interest with relative speed and low cost. This is particularly relevant in the context of neglected tropical diseases, where funding is often scarce. Computational models could also be extended to other targets beyond the CYP51 enzyme. For instance, recent work by the van de Sande and Fahal groups identified several proteins related to iron transport that are upregulated during infection.[131] These findings could be cross-referenced with machine learning techniques to predict possible binding targets within the known fungal proteome.[272,273]

The creation of gene knockout models for *M. mycetomatis* would likely accelerate drug discovery processes by allowing rapid assessment of the relevance of a given protein to a drug candidate's fungicidal activity.[274,275] Unfortunately, no such models have yet been developed for any proteins in *M. mycetomatis* or *F. senegalensis*, though a CYP51 knockout model is under investigation by others in the MycetOS consortium.

3.3.2 Efflux pump inhibition

Pieroni and colleagues recently proposed that 2-ATs could be used as an adjunct therapy for TB treatment, suggesting that 2-ATs can reduce turnover of antibiotic agents within the cell by inhibiting efflux proteins.[276,277] Phenothiazines such as thioridazine and chlorpromazine (**144**) are already known to function as EPIs which act on type II NADH:quinone oxidoreductase (NDH-2) enzymes and thus reduce ATP levels within the cell. Phenothiazines and 2-ATs share some structural characteristics, with both compound classes having relatively flat, polycyclic structures with a sulfur atom in the central ring. While the 2-ATs investigated in this work consist of three disparate aromatic rings, the lead compound of the series investigated as anti-

tubercular agents (UPAR-174, **145**) boasts a tricyclic fused ring structure that is more obviously comparable to the phenothiazine core (**Figure 3.12**).[277] Fused rings have not been tested against eumycetoma, but have been explored in SAR studies for other conditions.[265]

Pieroni's group suggests that these shared structural elements may facilitate binding of these compounds to NDH-2 to exert an anti-tubercular effect, citing as evidence the fact that bicyclic 2-AT analogues like **11** have reduced activity compared to tricyclic compounds such as **145**.[277] This theory is corroborated by the observation that 2-AT analogues inhibit ethidium bromide efflux, a common proxy for efflux of antibacterial agents.[195,277] Phenothiazines are also under investigation as anti-eumycetoma agents, with their mechanism of action as yet unknown.[278]

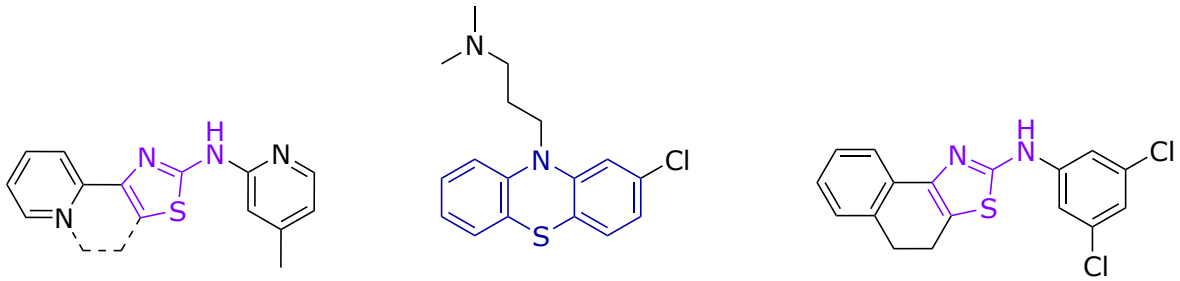

11 **144** **145**

Figure 3.12 – Structures of Series 2 lead **11**, chlorpromazine (**144**) and anti-tubercular EPI lead UPAR-174 (**145**).

Performing ethidium bromide assays with Series 2 analogues would help determine whether these compounds do indeed affect the rate of antibiotic efflux in *M. mycetomatis* and thus provide further insight into their likely mechanism of action. Screening compounds with the same fused-ring motif seen in **145** against eumycetoma might also indicate whether the structural similarity to phenothiazines is as important as has been hypothesised by Pieroni *et al.*. This would be complemented by subjecting MycetOS Series 3 phenothiazines to the same ethidium bromide assays to examine how their activity compares to the 2-ATs.

3.3.3 Calcium channel modulation

One of the only known mechanisms of action of the *N*-aryl-4-aryl-2-aminothiazoles studied here is the modulation of calcium-activated potassium channels (K_{Ca}), observed in neuronal cell assays.[147] Lead compound **11** and several derivatives have previously been reported as inhibitors of these K_{Ca} channels with nanomolar potency. These channel are expressed

primarily in neuronal cells, and their opening is triggered by raised intracellular calcium levels and mediated by the binding of Ca^{2+} to calmodulin proteins.[147]

If the antifungal effect of 2-ATs is related to this pathway, other inhibitors of the same proteins should also inhibit fungal growth. Several large molecule inhibitors with excellent potency have been identified, including the naturally occurring peptide scyllatoxin and smaller cyclic octapeptide apamin.[279,280] Only a handful of small molecule inhibitors are known, many of which are cyclic polyamines derived from dequalinium (**146**, **Figure 3.13**).

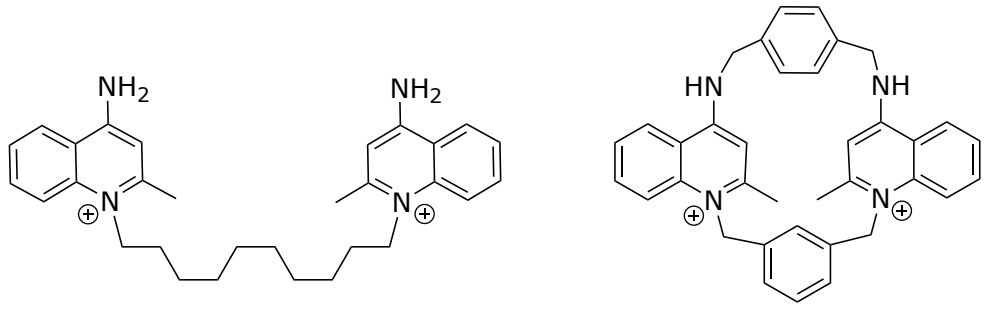

146 1.0 μM

147 3.0 nM

Figure 3.13 – Cyclic polyamine $K_{Ca}2.3$ channel inhibitors dequalinium (**146**) and **147** with IC_{50} against *M. mycetomatis*.

Other compounds that act upon this pathway include pyrazolo[1,5-*a*]pyrimidine **148** (IC_{50} = 350 nM) and 2-aminobenzimidazole derivative NS8593 **149** (IC_{50} ~500 nM, **Figure 3.14**. Although the similarity between NS8593 and MycetOS Series 5 compounds is intriguing, it was decided that the more potent **148** would be synthesised and screened against *M. mycetomatis*.

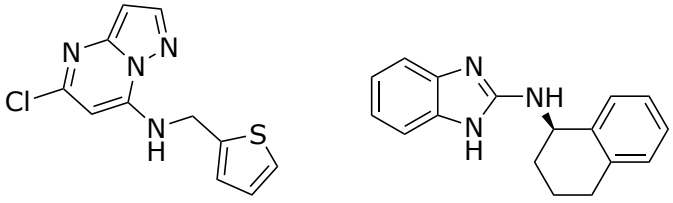

148 350 nM

149 ~ 500 nM

Figure 3.14 – Small molecule $K_{Ca}2.3$ channel inhibitors **148** and **149** (NS8593) with IC_{50} values.

Following an established procedure,[279] commercially available starting materials 5,7-dichloropyrazolo[1,5-*a*]pyrimidine **150** and 2-aminomethylthiophene **151** were heated at

reflux in acetonitrile overnight. The mixture was adjusted to pH ~12 with sodium carbonate solution (saturated), then extracted with petroleum benzine to obtain the crude product as a reddish-brown solid. This material was purified using HPLC, then triturated with cold methanol to give **148** as a red solid in moderate yield (49%) and excellent purity.

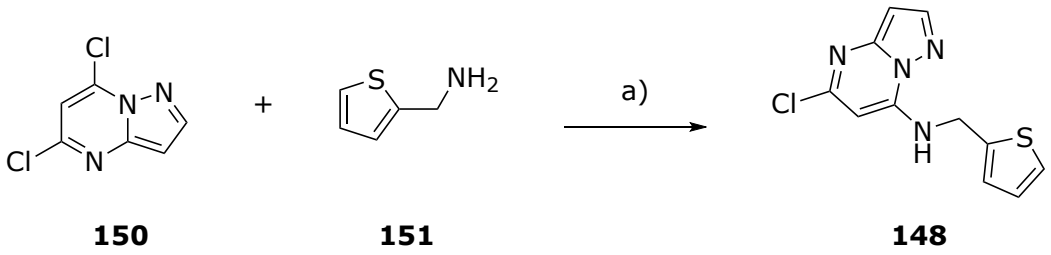

150 **151** **148**

Scheme 3.2 – Synthesis of known K_{Ca} inhibitor **148** from commercially available starting materials **150** and **151**. a) MeCN, 80°C, 18 h, 49%.

The calcium channel inhibitor **148** did not inhibit *M. mycetomatis* growth at 100 μM concentration, though some reduction in growth was observed at all concentrations tested (down to 2 μM). However, there is a 100-fold difference in the reported potency of the two compounds **148** and **149** for K_{Ca} inhibition, so the antifungal effects of **148** would be expected to be considerably lower than those of the 2-AT lead. Screening of other known inhibitors which have more comparable potency at the K_{Ca} channels to Series 2 lead **11** would give a better indication of whether these channels are indeed involved in the inhibition of eumycetoma fungi.

Ultimately, while continued SAR studies may be able to complement other modes of investigation, uncovering the mechanism by which the 2-ATs inhibit *M. mycetomatis* growth is of primary importance. Various plausible mechanisms and assays have been proposed, but have not thus far been examined in detail.

4 Aminothiazoles as antibacterial agents

The 2-aminothiazoles (2-ATs) synthesised in collaboration with Breaking Good as potential treatments for eumycetoma have very similar structures to compounds previously reported to have activity against *Mycobacterium tuberculosis* (*Mtb*) and various gram-positive bacteria.[146,281,282] *Mtb* belongs to the bacterial phylum Actinomycetota, which also includes the five bacteria predominantly responsible for actinomycetoma (**Figure 4.1**).[283–285] It has thus been hypothesised that compounds which inhibit *Mtb* may also show activity against the causative agents of actinomycetoma.

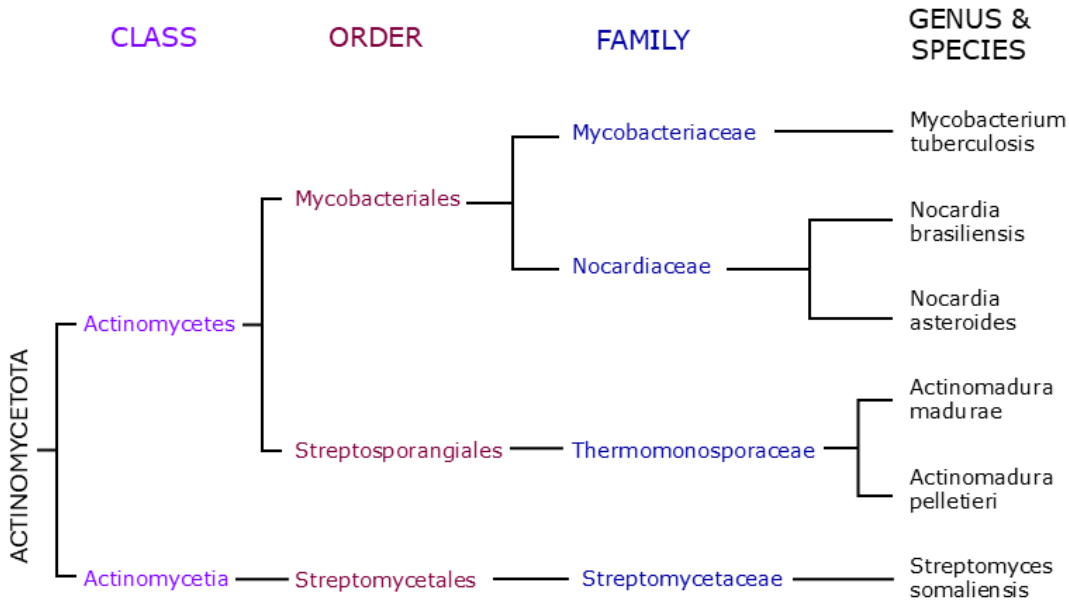

Figure 4.1 – Simplified bacterial taxonomy with the phylum Actinomycetota, showing phylogenetic relationships between actinomycetoma causative agents and *Mtb*.

Thus, a portion of the library of 2-AT analogues produced earlier was screened against *Mtb*, as well as three common actinomycetoma causative agents, *A. madurae*, *N. brasiliensis* and *S. somaliensis*. Globally, *Nocardia* spp. are responsible for the highest number of cases of actinomycetoma, with *N. brasiliensis* dominating in the Americas and *N. asteroides* in south east Asia.[112] *S. somaliensis* causes the most cases in west Asia, while *A. madurae* and *A. pelletieri* are the most reported causative agents in north and west Africa respectively (**Figure 4.2**).[105] While *Streptomyces* spp. are in the class of Actinomycetia, *Actinomadura* spp. diverge at the order level, and *Nocardia* spp. have the closest relationship to *Mtb*, with both being part of the Mycobacteriales order (**Figure 4.1**).

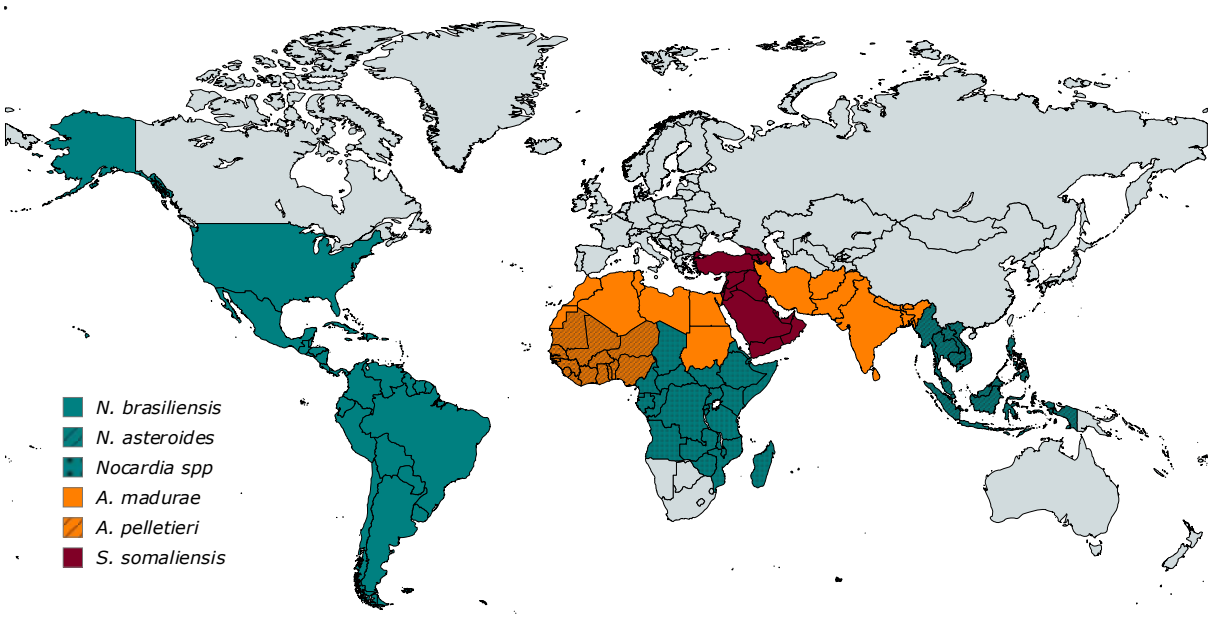

Figure 4.2 – Most common actinomycetoma causative agents in geographical areas around the world, using statistics reported by Emery and Denning, 2020.[105] Made with mapchart.net.

Screening compound libraries against actinomycetoma causative agents currently relies on time-consuming visual analysis of bacterial growth. Therefore, a straightforward, robust colorimetric assay was developed to enable more rapid identification of compounds that display promising antibacterial activity.

4.1 Activity against *Mtb* and actinomycetoma causative agents

The activity of antimicrobials often works on the bacterial cell wall, which means that many drugs are only effective against one of the two main categories of bacteria: either against gram-positive or gram-negative strains. Traditionally, bacteria are classified as gram-positive if they possess a thick (20 – 80 nm) peptidoglycan cell wall that retains the crystal violet dye used in the staining process, making the cell appear blue or purple (**Figure 4.3**).[286] In contrast, gram-negative bacteria have an outer membrane and within that a much thinner (2 – 3 nm) layer of peptidoglycan which doesn't retain the dye as effectively so stains less strongly.

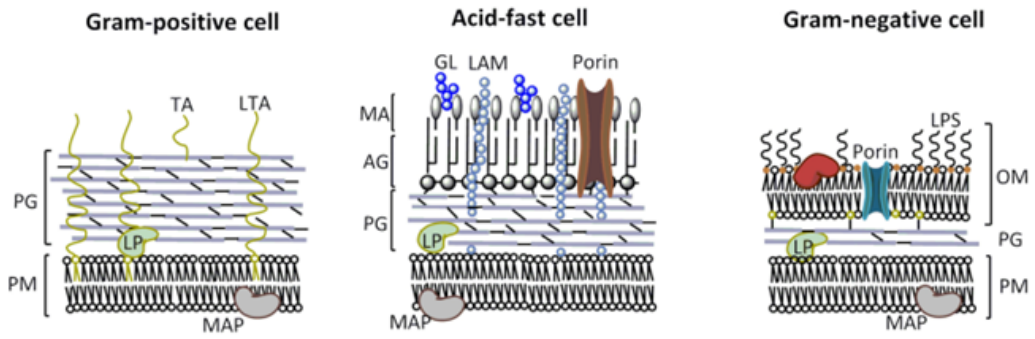

Figure 4.3 – Differences in the cell envelope architecture of gram-positive, acid-fast, and Gram-negative bacteria. AG = arabinogalactan; GL = glycolipid; LAM = lipoarabinomannan; LP = lipoprotein; LPS = lipopolysaccharide; LTA = lipoteichoic acid; MA = mycolic acid; MAP = membrane-associated protein; OM = outer membrane; PG = peptidoglycan; PM = plasma membrane; TA = teichoic acid. Figure and caption reproduced with permission from Maitra *et al.*, 2019.[287]

All five of the predominant actinomycetoma causative agents are gram-positive, meaning that antibacterial agents with activity against one species have a good chance of activity against the other four. However, the Mycobacteria family are an exception to this classification system, as their cell wall structure has characteristics of both categories.[288] Often described as 'acid-fast', the *Mtb* cell wall features a thick peptidoglycan layer in conjunction with a waxy outer membrane made up of the carbohydrate arabinogalactan, functionalised with mycolic acid.[287] This unusual composition results in a significantly different response to antimicrobials, making it more difficult to predict whether compounds with activity against other bacteria will also inhibit *Mtb*.[287,288] While many antibacterial agents cannot penetrate the waxy outer layer of *Mycobacteria*, drugs such as isoniazid, ethionamide and pretomanid achieve excellent selectivity by targeting mycolic acid biosynthesis.[173]

4.1.1 Screening against Mtb

A select number of MycetOS compounds with C-2 variations were tested against *Mtb* H37Rv in a resazurin-based fluorescence assay that is described in detail in Chapter 5. Unfortunately, the slow-growing nature of *Mtb* and associated biological hazards precluded larger-scale screening.

All six of the compounds screened were found to have excellent anti-tubercular activity with IC_{50} values below 1 μM (**Figure 4.4**). The compound with the lowest IC_{90}, **83**, was also one of

just two derivatives that inhibited the growth of all three bacterial species at the lowest concentration tested, the other being the lead compound **11** (activity against actinomycetoma-causative agents is discussed further in **Section 4.1.3** below).

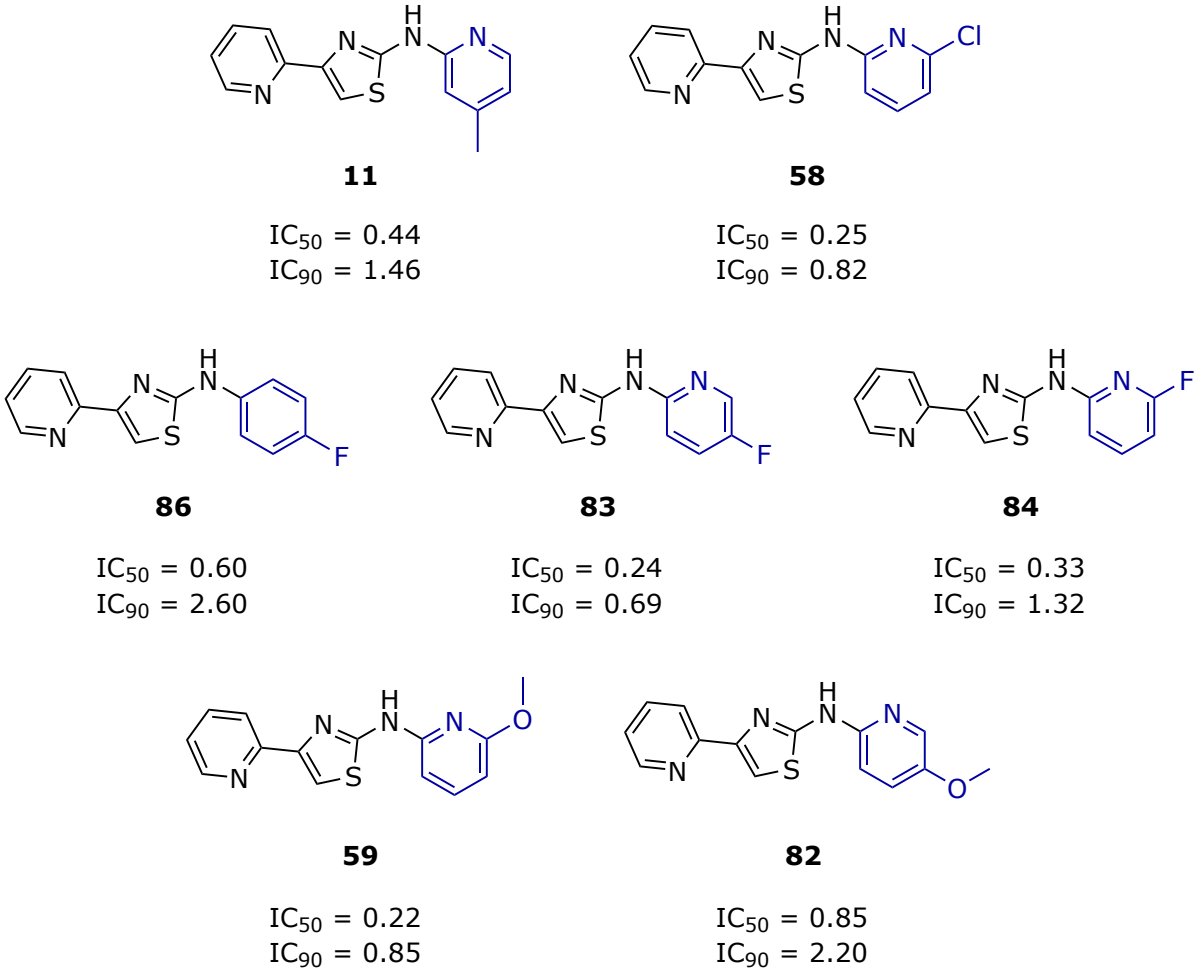

Figure 4.4 – Activity (μM) of 2-AT analogues **11**, **58**, **59**, **82, 83**, **84** and **86** against *Mtb* H37Rv. Testing performed by Dr Diana Quan.

A narrow range of activity was observed for all six compounds, with all IC_{90} values in the range between just 0.69 and 2.20 μM. Nonetheless, these results suggest that 2-AT analogues may have broad application as antimicrobials with activity against multiple strains of pathogenic bacteria.

4.1.2 Potential mechanisms of action against *Mtb*

Most of the 2-AT derivatives detailed in the literature with significant structural similarity to the Breaking Good library are under investigation for anti-tubercular activity. Many of these

analogues feature various substitutions on the C-2 and C-4 phenyl rings, with a handful of derivatives boasting pyridyl rings at either position.[144]

Makam and Kannan reported a series of structurally similar pyridinyl analogues that explore the relationship between lipophilicity and activity (**Figure 4.5**).[289] They found that a 4-fluorophenyl group at the C-2 position and a 4-pyridinyl group at the C-4 position enhanced activity, and that compounds with log *P* values between 4.25 – 6.5 performed best, with an MIC of 6.25 μM.[289] Surprisingly, analogues made with 2-pyridyl groups at the C-2 position had poor activity (IC_{50} > 100 μM),[289] at odds with the finding in this work that all the most active compounds tested featured an unsubstituted 2-pyridinyl in the corresponding position.

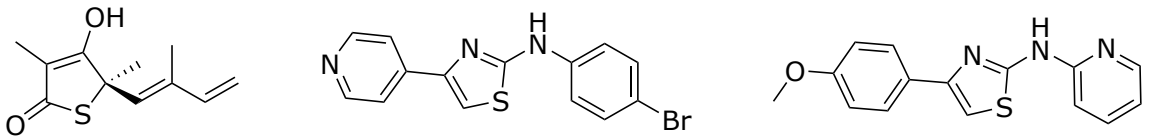

152 **153** **154**

Figure 4.5 – Chemical structures of thiolactomycin **152**, 2-AT **153** which is highly potent against *Mtb*, and 2-pyridinyl analogue **154** which has poor activity.

The 2-AT compound class has some structural similarity to existing antibiotic thiolactomycin (**152**), which is thought to inhibit the KasA protein of *Mtb* and so disrupt mycolic acid biosynthesis.[290] *In silico* docking studies found positive interactions between this protein and the most potent antitubercular 2-AT compounds, including **153**, prompting the authors to propose KasA inhibition as a potential mechanism of action for these 2-AT analogues. However, only the 4-pyridine ring at the C-4 position is described as a specific requirement for inhibition on the basis of this work, with little discussion of how other structural changes might affect protein binding.[289]

Performing similar studies with the promising 2-AT derivatives discovered in this work would allow further exploration of this theory, as the significantly more potent Breaking Good 2-ATs would be expected to have improved binding interactions with the KasA protein, if this is indeed their biomolecular target. Initial confirmation from *in silico* studies could later be followed up by testing within a knock-out model in which KasA protein expression is suppressed, or synergistic studies with known inhibitors.

Alternatively, these compounds may inhibit NDH-2 as proposed by Pieroni and colleagues and discussed in Chapter 3.[195,277] Performing ethidium bromide assays on the 2-ATs synthesised in

this work would therefore be a simple and efficient step towards confirming their mechanism of action. In all cases, understanding the mechanism of action against *Mtb* would provide important insight into how useful these compounds might be as antibacterials against actinomycetoma causative agents.

4.1.3 Screening against actinomycetoma causative agents

Screening of the 2-AT library was performed following a similar workflow to the one used for screening them as anti-eumycetoma agents, following EUCAST guidelines for MIC determination by visual inspection. In short, amikacin hydrate or experimentally produced 2-AT compounds were dissolved in Mueller-Hinton broth (100 µL) and a bacterial suspension adjusted to a McFarland standard of 0.5 (100 µL) was added. A positive growth control consisting of only the bacterial suspension and a negative control consisting of only the Mueller-Hinton broth were included. The plates were sealed and incubated at 37°C ± 2°C for 3 days (*N. brasiliensis* and *S. aureus*) or 7 days (*A. madurae* and *S. somaliensis*). MIC was determined by visual assessment of colony formation.

Initially, 60 compounds were tested against *N. brasiliensis* and *A. madurae* at concentrations of 100 and 25 µM, with 20 identified as complete inhibitors of growth at 25 µM. The 60 original compounds, along with 12 more 2-AT derivatives, were then screened against *S. somaliensis* at a single concentration of 2 µM. The full results of the screening, including nil results, can be found in **Appendix C**.

Of the 72 compounds screened, 32 showed promising activity against one or more bacterial strains, with eight compounds completely inhibiting growth of all three bacteria at the lowest concentrations tested (Panel B, **Figure 4.6**). Twelve compounds inhibited growth of both *A. madurae* and *N. brasiliensis* at 25 µM but failed to inhibit growth of *S. somaliensis* at the lower concentration of 2 µM (Panel A, **Figure 4.6**). A further twelve compounds, including six contributed by our collaborators at the University College London (**136 – 141**), inhibited growth of *S. somaliensis* at 2 µM. Four of these were not tested against the other two bacterial strains while the remaining eight showed some signs of bacterial growth in both *A. madurae* and *N. brasiliensis* at 25 µM (Panel C, **Figure 4.6**).

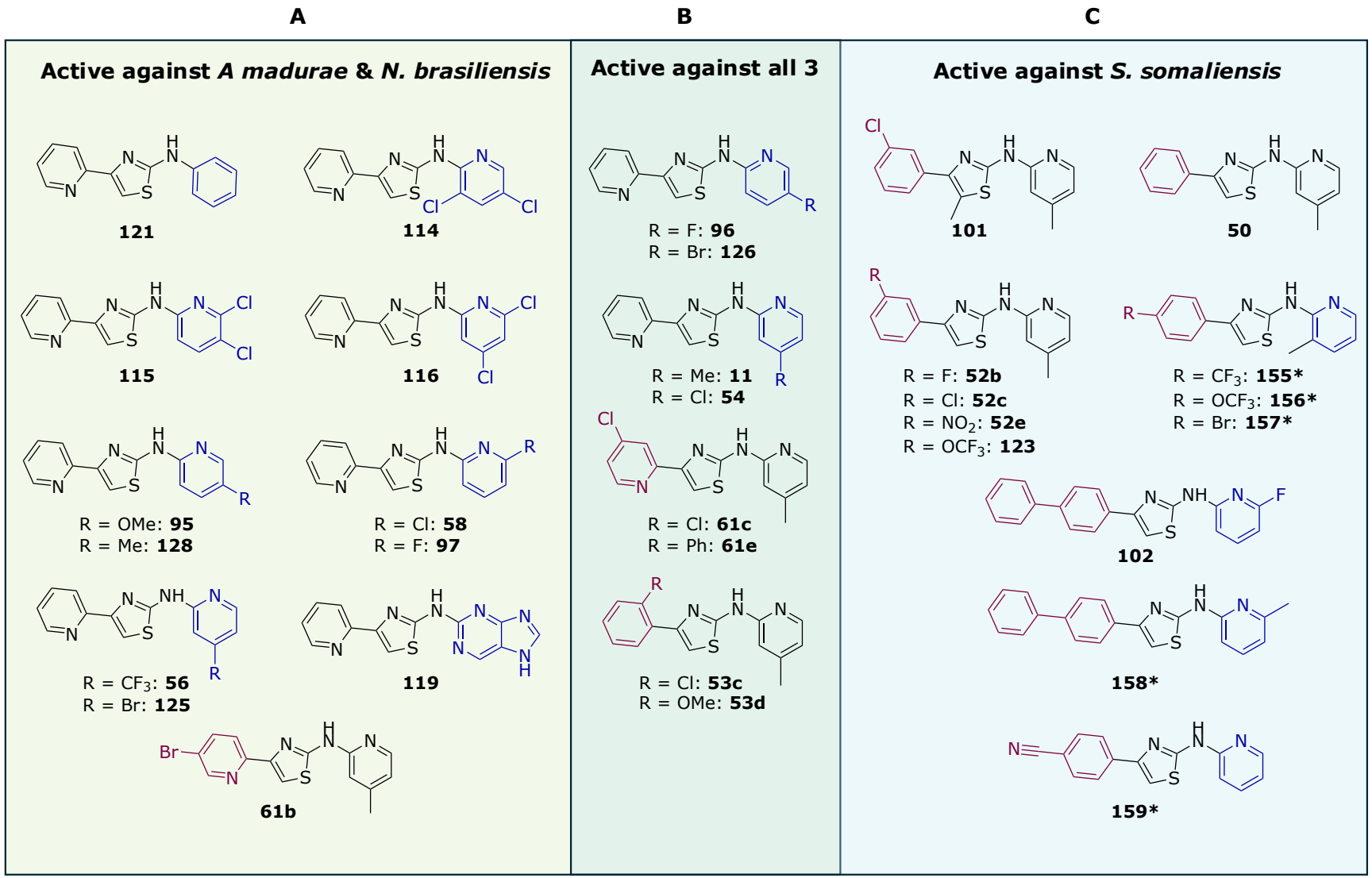

Figure 4.6 – Compounds capable of inhibiting growth of *A. madurae*, *N. brasiliensis* and *S. somaliensis* at lowest tested concentration.

The results obtained from this work are preliminary, and as yet no clear SAR trends are evident in their relative activity against any of the three bacterial strains. The 2-AT core is already a well-known motif in antimicrobial compounds (**Figure 4.7**), forming part of the structure of broad-spectrum cephalosporin antibiotics[143] like cefotiam (**160**) as well as that of monobactams such as azneotram (**161**), which are only effective against gram-negative bacteria. In these contexts, the 2-AT moiety is believed to improve oral absorption and improve affinity for the penicillin-binding proteins targeted by both classes of drug.[143] Interestingly, the C-2 amine is particularly important, with hydroxyl and *N*-methyl substitutions both resulting in reduced antimicrobial activity.[291]

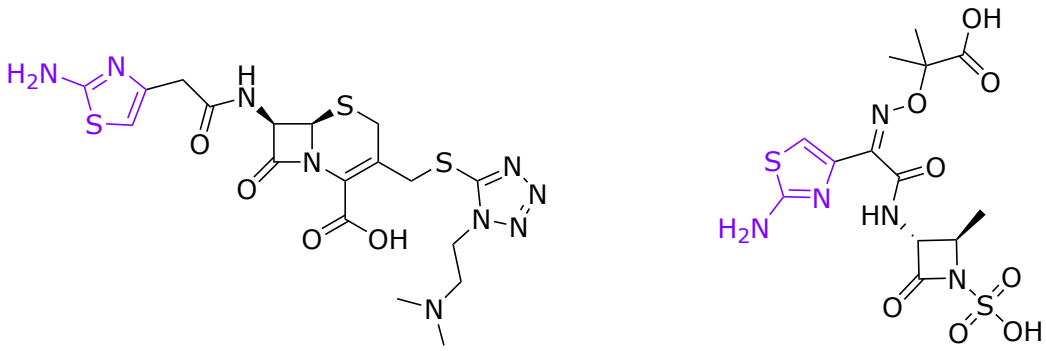

160

cefotiam

161

azneotram

Figure 4.7 – Second-generation cephalosporin antibiotic cefotiam (**160**) and monobactam antibiotic azneotram (**161**) with 2-AT moiety highlighted in purple.

Although many compounds with 2-AT motifs are reported to have promising antibacterial effects, only a few studies have focused on compounds with bis-aryl structures similar to those described in this work. However, a recent study by Chen *et al.* describes the antimicrobial activity of 2-AT analogues[282] very similar to those produced through the Breaking Good project. Initially screened as potentiators of the known antibiotic polymyxin E for gram-negative bacterium *A. baumannii*, promising results prompted an in-depth SAR analysis with the resulting library screened against drug-resistant strains of *S. aureus*, *Bacillus subtilis* and *Enterococcus faecalis*.

The compounds that Chen tested performed well against all four bacterial strains, with four derivatives **162** and **164 – 166** found to have MICs between 1 and 2 μg/mL against each of the gram-positive strains (**Figure 4.8**). The addition of a hydrazone linker between the thiazole and C-4 aryl ring improved activity further, with analogue **163** returning an MIC of 1 μg/mL against

all three strains, and showing comparable activity to the highly potent antimicrobial agent vancomycin in subsequent screening against a further 16 strains of gram-positive MDR bacterial strains.[282]

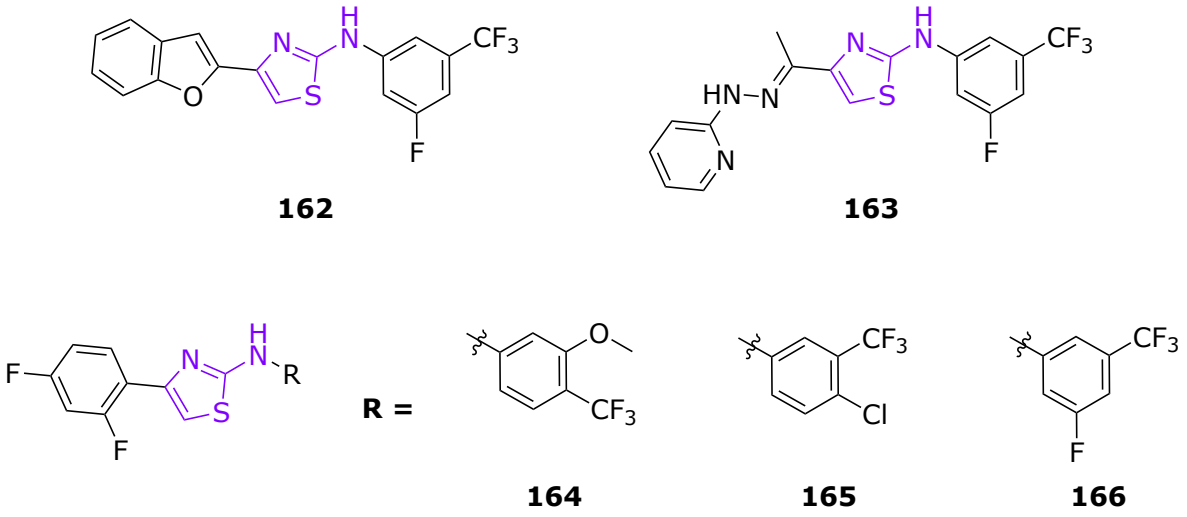

Figure 4.8 – 2-AT analogues **162** – **166** shown to have potent activity against *S. aureus* (MICs = 1 – 4 μg/mL, *B. subtilis* (MICs = 1 – 2 μg/mL) and *E. faecalis* (MICs = 1 – 2 μg/mL).[282]

TEM analysis of the action of **163** on *A. baumannii* suggested that the compound damages the protective outer membrane of the bacteria, especially when administered alongside polymyxin E. However, this mechanism of action does not translate to the gram-positive actinobacteria, which lack this outer membrane and instead rely on the thicker layer of peptidoglycan in their cell wall to defend against external influences.

The mechanism of action of 2-AT derivatives against gram-positive bacteria remains unclear and will likely require considerable further investigation to fully elucidate. A more precise determination of potency against the actinomycetoma causative organisms would provide further evidence of their potential. However, to maximise the limited resources available, testing should prioritise compounds with the most promising range of activity against all three bacteria, *A. madurae*, *N. brasiliensis* and *S. somaliensis*.

Ideally, the eight compounds found to inhibit *S. somaliensis* at 2 μM (**Figure 4.6**) should be screened against *A. madurae* and *N. brasiliensis* at 2 μM, alongside the remaining 2-AT analogues that were not tested against any of these bacteria. MIC and IC_{50} values could then be determined for the subset of compounds which inhibit all three bacteria at 2 μM, which is likely to significantly reduce the volume of testing required.

4.2 Development of a colorimetric assay for MIC determination

Potency screening can be a comparatively lengthy process, especially when relying on human interpretation of bacterial growth. Access to rapid, reliable assays can accelerate drug discovery efforts, and enable more frequent drug susceptibility testing (DST) in the clinic to prevent mistreatment of resistant bacterial strains.[292] The high toxicity and relatively long dosing period of the Welsh regimen (the combination therapy of trimethoprim, sulfamethoxazole, and amikacin sulfate), along with reduced access to the necessary therapeutics for patients in low socioeconomic areas, all increase the likelihood of drug resistance.[158,170,293,294] However, DST is not routinely performed prior to treatment,[113] in part due to a lack of readily available assays.

The gold standard for DST is determination of MIC, usually via liquid broth microdilution or using commercial antibiotic gradient strips. MICs are assessed using a pure culture of the bacteria of interest at a standard concentration, and official clinical breakpoints are calculated by amalgamating data from numerous laboratories.[256] The breakpoint is the concentration at which a strain is deemed to be resistant, while strains with a reported MIC below the breakpoint are defined as susceptible to the antibiotic being tested. Breakpoint values are routinely reviewed by the CLSI and EUCAST when developing testing standards, and are used by clinicians to guide treatment.[256]

MIC determination for DST purposes can also inform further research, from the identification of drug resistance mechanisms to the screening of potential new antibiotics. Broth microdilution methods are more suited to the latter scenario, as antibiotic gradient strips are only available for approved drugs.[295] However, in the protocol outlined by the CLSI, MIC is determined qualitatively by visual inspection of bacterial growth, which is time-consuming and can give subjective results.[296,297] Fluorescent or colorimetric assays provide quantitative data, allowing more detailed analysis of the effects of a given compound.[297,298]

While quantitative assays are more desirable for drug screening, no such methods have been standardized or reviewed for most common causative agents of actinomycetoma. One previous study on the use of resazurin assays for testing antibiotic resistance in *A. madurae* found good agreement between the MICs determined from visual analysis of colour change, absorbance at 600 nm, and MIC values reported by the CLSI guidelines.[113] However, the study focussed on resistance to known antibiotics rather than screening for new drugs, and involved only one of

the causative organisms. Extending this work to other common causative species and refining the parameters of the assay are therefore logical next steps towards developing new drugs to treat actinomycetoma.

4.2.1 Resazurin-based cell viability assay

Many different dyes can be used to quantitatively measure cell growth. Resazurin (**167**), also known as Alamar Blue, is a non-toxic, bright blue dye that changes to fluorescent pink resorufin (**168**) upon reduction. As cellular metabolism produces NADH and other reducing agents, reduction of the blue dye and subsequent increase in the fluorescent pink colour can be used as a proxy for cell viability (**Scheme 4.1**).[246]

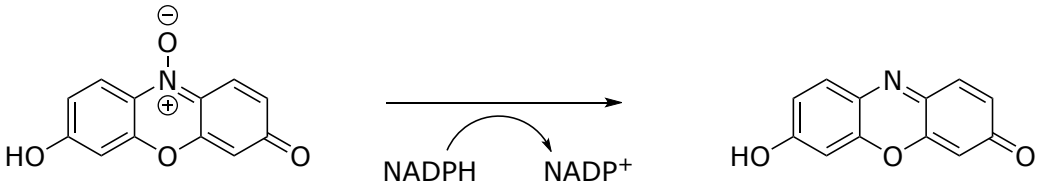

167

resazurin
absorbs at 600 - 620 nm

168

resorufin
absorbs at 570 - 580 nm

Scheme 4.1 – Reduction of resazurin **167** to resorufin **168**.

Resazurin-based assays can be read visually which enables rapid analysis,[297] with blue indicating disruption of cell viability and pink reflecting cellular activity. Alternatively, fluorescence emission between 580 and 620 nm or absorbance at wavelengths corresponding to the blue (600 – 620 nm) or pink (570 – 580 nm) colours can be measured spectrophotometrically.[113,299] Variations in the wavelength measured, volume of inoculum, and concentration of resazurin dye can affect the reliability and ease of reading of results.

Accordingly, this work aimed to develop a straightforward and robust method for determining the potency of drug candidates against the primary causative agents of actinomycetoma. Due to the considerable overlap between eumycetoma and actinomycetoma testing facilities, the established protocol for screening eumycetoma causative agents using resazurin dye was used as a model when developing the method explored here. The assay was trialled against three species of bacteria, *N. brasiliensis*, *A. madurae* and *S. somaliensis*, chosen as a representative

sample of the most frequently reported actinomycetoma pathogens across a wide geographical distribution, with *S. aureus* included as a reference species.

Following the method used previously,[113] amikacin hydrate was dissolved in Mueller-Hinton broth at twice the desired final concentration and added to a round-bottomed 96-well plate. An equal volume of bacterial suspension was added to each well, bringing the total volume in each well to 100, 150 or 200 µL, with positive and negative controls included. Each well was prepared in duplicate, and a set volume of resazurin dye (0.15 g/mL, 5 – 40 µL) was added to one replicate. The plates were sealed and incubated at 37°C ± 2°C for 3 days (*N. brasiliensis* and *S. aureus*) or 7 days (*A. madurae* and *S. somaliensis*), and MIC was determined by all three methods on the same day.

For the replicates without resazurin (dye-free), MIC was determined by visual inspection of each well. For replicates containing the dye, the colorimetric MIC was reported as the lowest concentration of drug that remained blue. Spectrophotometric readings were performed by transferring 100 µL of supernatant to a flat-bottom 96-well plate and measuring absorbance at 580, 600 and 620 nm using a microplate reader.

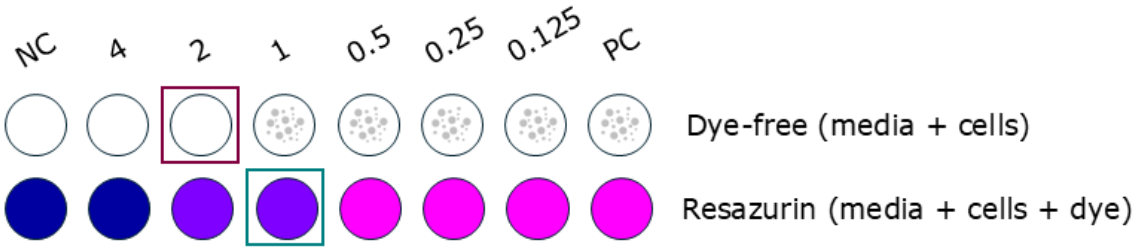

Figure 4.9 – Representation of resazurin assay set up with dilutions from 4 to 0.125 µg/mL, with MIC determined by visual inspection indicated by red box and colorimetric MIC indicated by green box. Dye-free: MIC = 2 µg/mL, Resazurin: MIC = 1 µg/mL. (NC = media only, no cells; PC = cells and media, no drug.)

When comparing results of the resazurin assay, variables were assessed on the level of agreement with the visually inspected replicates, and 'agreement' defined as an MIC within one dilution step of that observed in the dye-free replicate. For example, the two MICs shown in **Figure 4.9** are considered to be in agreement for the purposes of this evaluation.

4.2.2 Optimisation of the resazurin assay

Resazurin viability assays offer significant flexibility as activity can be assessed by measuring fluorescence or absorbance of the pink resorufin product, or absorbance of the blue resazurin itself. Measuring the production of the pink resorufin, which absorbs at 580 nm, approximates cellular activity directly, while the amount of unchanged blue resazurin is a proxy for inhibition. Typically, inhibition and activity are considered inverse to each other, meaning that either measure can be converted to the opposite with simple mathematical manipulation. In this work, results are given as bacterial activity, calculated from absorbance at 580 nm with the following equation:

$$\frac{x_{580} - NC_{580}}{PC_{580} - NC_{580}} \times 100$$

Where x = absorbance of the sample being assessed, NC = averaged absorbance of negative growth control, PC = averaged absorbance of positive control.

When absorbance was measured at 600 or 620 nm, growth was calculated using the inverse equation:

$$\frac{NC_{620} - x_{620}}{NC_{620} - PC_{620}} \times 100$$

Where x = absorbance of the sample being assessed, NC = averaged absorbance of negative growth control, PC = averaged absorbance of positive control.

Usually, MIC is defined as the lowest concentration at which 99.9% inhibition is observed. However, it was recognised in the current study that using a 90% cutoff greatly improved agreement between the spectrophotometric and qualitative analyses. This difference was attributed to the effect of averaging the controls across each plate, which gives a more reliable measure overall.

A series of assays were carried out using resazurin (40 µL) and bacterial inoculum (100 µL) to determine whether there was any difference in accuracy and reproducibility between MICs calculated at the different wavelengths.

Table 4.1 – Results collected for *N. brasiliensis* using three different methods, with overall agreement to visually inspected dye-free replicate reported as a percentage. MICs not in agreement with dye-free replicate indicated by italics.

Method of MIC determination	1	2	3	4	Reproducibility %
Visual inspection (dye-free replicate)	0.5	1.0	1.0	0.5	-
Colorimetric	1.0	1.0	0.5	0.25	100
Spectrophotometric (620 nm)	0.50	0.5	0.5	1.0	100
Spectrophotometric (600 nm)	> 1.0	> 1.0	0.5	1.0	100
Spectrophotometric (580 nm)	0.50	> 1.0	*unclear*	*unclear*	50

The MIC determined by visual inspection for the strain of *N. brasiliensis* varied between 0.50 and 1 μg/mL (**Table 4.1**), in reasonable agreement with the MIC value (0.25 μg/mL) previously established in the group and those reported in the literature (0.25 – 4.0 μg/mL for various strains).[300,301] Pleasingly, 100% agreement with the dye-free MIC was found for both the visual colorimetric method (row 2, **Table 4.1**) and absorbance at 620 nm (row 3). Measuring absorbance at the lower wavelengths, the results were less clear, with the results collected at 580 nm being too difficult to discern a distinct value in some cases, as changes in absorbance did not follow a clear trend. For two replicates, absorbance at 600 nm for the highest concentrations of 1.0 μg/mL showed minimal growth (~ 11%), but were still classified as 'no inhibition' according to the 90% growth inhibition cutoff described earlier. This demonstrates how minor adjustments to the definition of inhibition can affect agreement, and thus reproducibility.

Table 4.2 – Results collected for *A. madurae* with overall agreement reported as a percentage. MICs not in agreement with dye-free replicate indicated by italics.

Method of MIC determination	1	2	3	4	Reproducibility %
Visual inspection (dye-free replicate)	0.008	0.0016	≤ 0.004	≤ 0.004	-
Colorimetric	≤ 0.004	≤ 0.004	≤ 0.004	≤ 0.004	75
Spectrophotometric (620 nm)	*0.016*	0.008	0.008	≤ 0.004	100
Spectrophotometric (600 nm)	*unclear*	0.008	0.008	≤ 0.004	75
Spectrophotometric (580 nm)	≤ 0.004	*unclear*	≤ 0.004	*unclear*	50

Previous results obtained for the *A. madurae* strain used in these experiments did not test concentrations below 0.25 μg/mL, even though amikacin has a much lower MIC against *A. madurae* (0.03 to 2.0 μg/mL).[302] Interpretation of results was complicated by the finding that inhibition was often observed in the lowest concentration tested (0.004 μg/mL), regardless of how activity was measured. In these cases, the true MIC could be even lower again, and could also vary with the method of measurement. However, the range of MICs obtained by visual inspection suggest that the MIC lies between 0.004 and 0.016 μg/mL, and the results have therefore been analysed on the assumption that MICs of 0.004 are correct.

For *A. madurae*, 100% agreement was observed between the dye-free MICs and those determined spectrophotometrically at 620 nm (row 3, **Table 4.2**), while agreement with the colorimetric MICs and absorbance at 600 nm was slightly lower at 75% (rows 2 and 4). As with *N. brasiliensis*, readings at 580 nm could be difficult to determine clearly, though were otherwise in good agreement.

Overall, measurements at 620 nm proved most reliable and this measurement was therefore used in further analysis of other parameters such as resazurin quantity. The literature suggests that the optimal wavelength to use with this dye depends on the assay duration and initial resazurin concentration, with excess residual resazurin a particular concern for fluorometric analysis. Although fluorometric analysis offers higher sensitivity and real-time monitoring, colorimetric analysis is less dependent on equipment parameters and better suited to longer

assays.[303] Using a ratiometric measurement, where activity is calculated from the change in absorbance ratios between the two wavelengths corresponding to resazurin and resorufin, can further improve reproducibility. However, results calculated using different wavelength pairs cannot be compared directly, which may complicate data aggregation.[303]

The effects of changes to the volumes of bacterial inoculum and resazurin dye were assessed by post-hoc analysis of the results obtained during method development. As the volume of inoculum had been iteratively adjusted, the quantity of resazurin present was assessed as a percentage of the total volume in each well. A replicate was described as having *excellent* agreement if the MICs from both colorimetric inspection and spectrophotometric analysis at 620 nm agreed with the visually inspected dye-free replicate, or *good* agreement if only one of those MICs agreed with the dye-free replicate. Otherwise, the agreement was classified as *poor*.

Very similar results were obtained for both bacterial strains, with very low (< 28.4 mM) resazurin concentrations showing no agreement, while *excellent* agreement was observed in at least 50% of replicates using > 126 mM resazurin (**Figure 4.10**). With *A. madurae*, only *good* or *excellent* agreement was observed when using resazurin concentrations of 70.3 – 99.5 mM, and the same trend was seen for *N. brasiliensis* at > 99.5 mM.

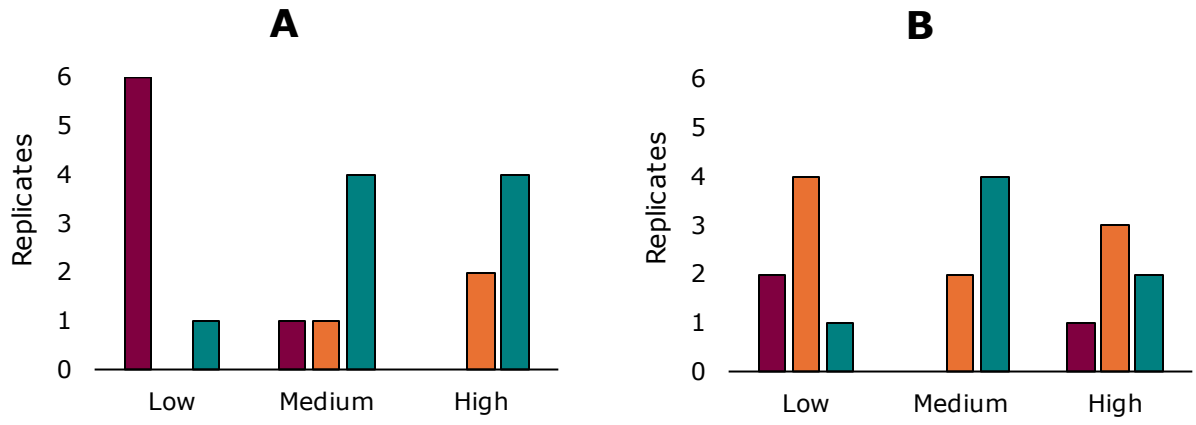

Figure 4.10 – Effect of varying concentrations of resazurin on overall agreement between spectrophotometric analysis at 620 nm and visual inspection. Red = poor, Orange = good, Green = excellent; Low = 14.6 – 54.3 mM, Medium = 70.3 – 99.5 mM, High = 126 – 171 mM. Panel A: Results obtained for *N. brasiliensis*. Panel B: Results obtained for *A. madurae*.

Higher percentages of resazurin were broadly associated with better agreement for both strains of bacteria, although the confounding effect of differing total well volume was not investigated.

While much lower concentrations (0.05 – 0.3 mM) have been reported as optimal in the literature,[303–305] these studies typically measure fluorescence rather than absorbance, meaning that residual resazurin may pose more of a concern. There is also significant variation in optimal concentrations reported for different organisms and applications.[303–305] In this study, there was no indication of toxicity from high resazurin concentrations, and higher concentrations produced a deeper colour that aided in colorimetric analysis.

Resazurin is valued specifically for its flexibility and ease of use, as it yields robust results from many permutations of parameters including the wavelength of measurement, dye concentration, and assay volume. However, reproducibility of experiments relies in no small part on clearly defined protocols, as data collected using slightly different parameters may not be comparable. It is therefore essential to keep variables consistent once an appropriate protocol has been developed, especially when testing options are limited by financial necessity, as is often the case when working with neglected tropical diseases.

This work describes a robust and reproducible protocol suitable for determining the potency of lead compounds against two causative species of actinomycetoma, *A. madurae* and *N. brasiliensis*, that can be used to rapidly and quantitatively assess novel drug candidates such as the 2-ATs studied in this work. In future studies, this method will be extended to other species of interest, including *S. somaliensis*, *N. asteroides* and *A. pelletieri*, with the goal of establishing a single screening protocol appropriate for all the main causative organisms of actinomycetoma.

5 Open Source Tuberculosis

The overarching goal of this work was to further investigate how changes to both the polyamine scaffold and the hydrophobic pendant groups of the cyclam and open cyclam compounds affect activity. Two bulky groups, adamantane and ferrocene, were proposed as potential new pendant groups, and three of the previously investigated linear polyamines were selected as model scaffolds. The most potent open cyclam so far (**36**) is based on the dipropylene triamine skeleton **169**, while the diaminohexane and diaminooctane analogues **170** and **171** were chosen as they are synthetically more accessible while also showing promising activity (**Figure 5.1**).[213] The new pendant groups were also trialled with the original cyclam scaffold **36**, to test the synthetic approach and provide further points of comparison.

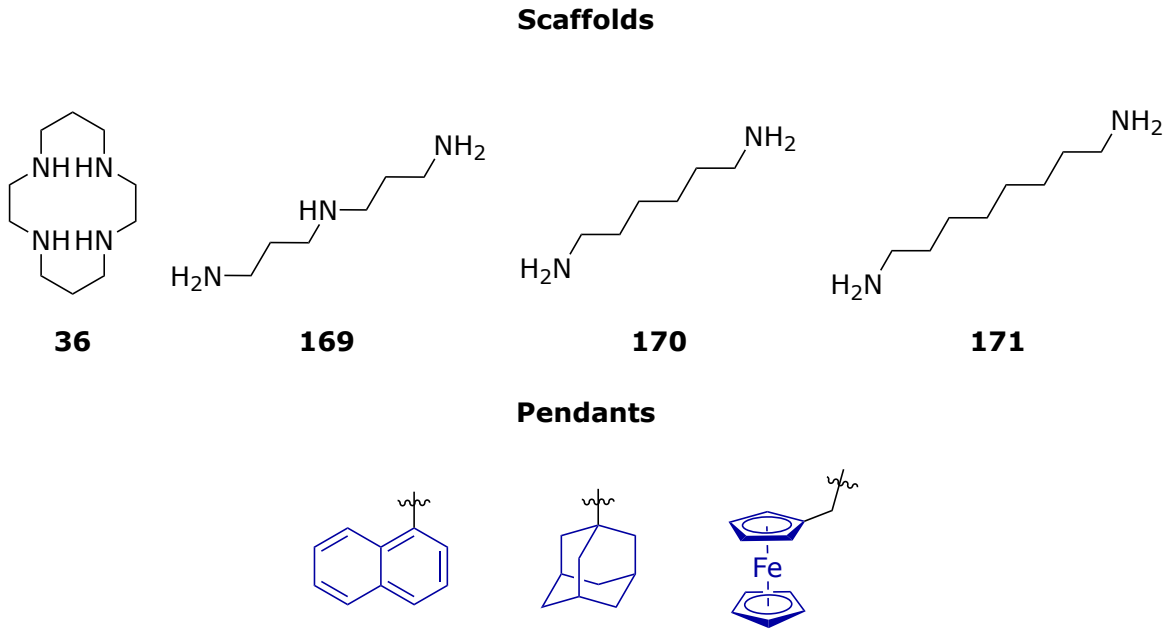

Figure 5.1 – Proposed scaffolds (**36** and **169 – 171)** and pendant groups.

Ferrocene (Fc) and adamantane (Ad) were chosen specifically for their novelty as isosteres for the simpler naphthyl group. Both are bulky, hydrophobic groups, and have found increasing interest among medicinal chemists for their unique structures and properties.[306] As of 2025, eight drugs containing an adamantyl motif have received clinical approval as treatments for ailments as diverse as neurodegenerative diseases, acne, antivirals and type 2 diabetes (**Figure 5.2**).[307] Adamantane has been described as "the lipophilic bullet" as its exceptionally high hydrophobicity substituent constant means that appending just one of these groups can dramatically change the physicochemical properties of a drug.[306] This is exemplified in the

antiviral drug azidothymidine, for which addition of an adamantyl ester in the prodrug **176** significantly increases uptake of the drug across the blood-brain barrier. Enzymatic metabolism then cleaves the adamantyl moiety, revealing the bioactive drug azidothymidine.[307]

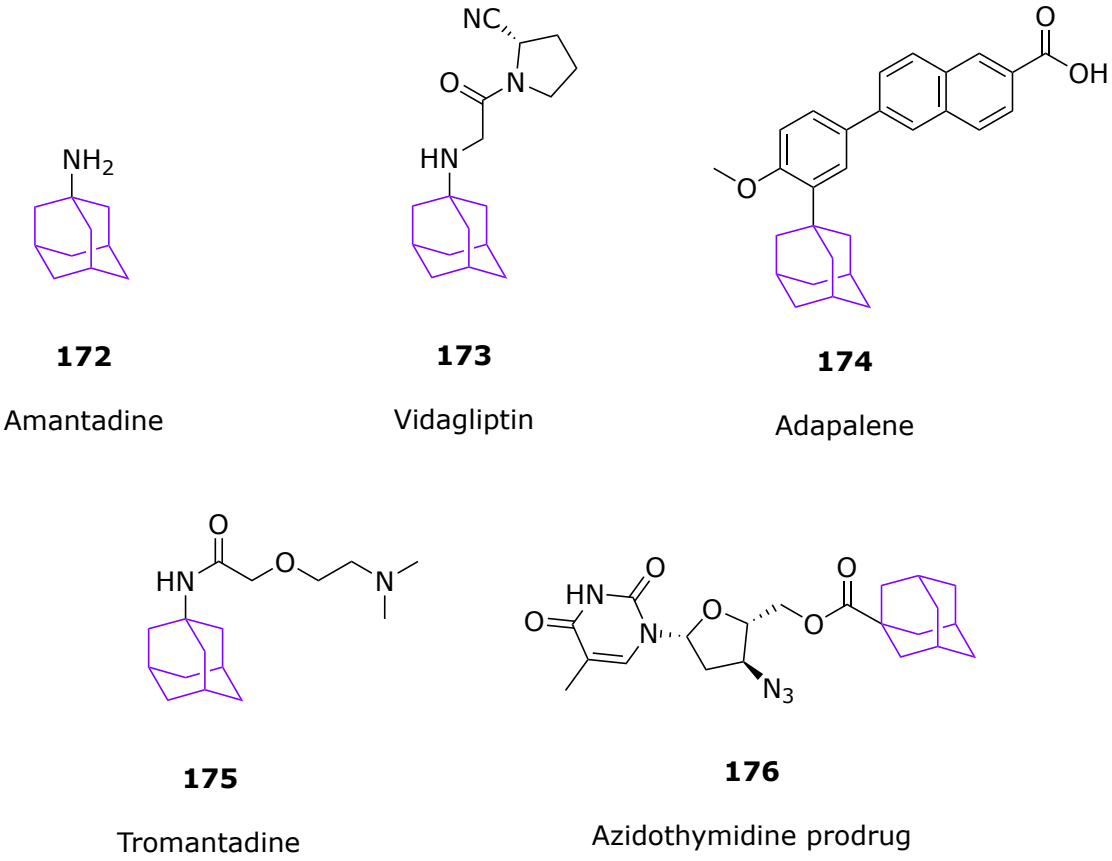

172 Amantadine

173 Vidagliptin

174 Adapalene

175 Tromantadine

176 Azidothymidine prodrug

Figure 5.2 – Clinically approved drugs amantadine **172** (antiviral, Parkinson's disease treatment), vidagliptin **173** (type 2 diabetes), tromantadine **174** (antiviral), adapalene **175** (acne vulgaris), and azidothymidine prodrug **176** (antiviral).

Apart from its hydrophobicity, adamantane is valued as a three-dimensional analogue of the phenyl ring, as it mimics the shape and size of a phenyl ring with rotational freedom. While the absence of aromaticity prevents π-π stacking interactions, its 3D shape and sp^3 hybridisation enable the careful positioning of desired functional groups in three dimensions to probe or enhance binding to a receptor. These properties make it an extremely useful moiety for both investigation and optimisation of potent compounds.[307]

In comparison, ferrocene is an organometallic sandwich complex consisting of two cyclopentadiene rings held together by Fe(II). Ferrocene has a number of applications in both physical and organic chemistry, due to its excellent stability in air and water and reversible oxidation to Fc^+.[308,309] Many drug candidates that incorporate ferrocene are in various stages of

development, with ferroquine and ferrocifen (**177** and **178**, **Figure 5.3**) being the most well-known examples.[308,310]

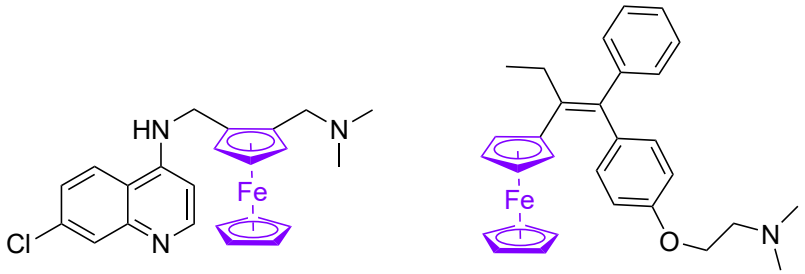

177

Ferroquine

178

Ferrocifen

Figure 5.3 – Clinically approved drugs ferroquine (**177**) and ferrocifen (**178**) with ferrocene shown in purple.

The antimalarial ferroquine is a derivative of the chloroquinine compounds already used against the disease, with ferrocene enabling a secondary mode of action by generating harmful hydroxy radicals inside infected cells. The lipophilicity of ferrocene also improves penetration across membranes and accumulation within the target area compared to the chloroquinine parent, thus improving activity.[311]

Tamoxifen (TAM) is an anti-cancer prodrug, with its metabolic product hydroxytamoxifen able to bind estrogen receptors (ERs) in ER+ breast cancer cells and block DNA transcription. Ferrocifen is a ferrocenyl analogue of TAM, and both the drug itself and its metabolic product can bind the same ER+ cells, as well as binding cells that don't express these receptors. The underlying mechanism is not fully understood, but is believed to involve a stable quinone methide intermediate formed by the oxidised ferrocifen metabolite.[311]

Ferrocene is now an increasingly common choice of bioisostere in drug optimisation, offering potential redox mechanisms alongside increased lipophilicity and three-dimensional space-filling (**Figure 5.4**). Much like adamantane, the cyclopentadiene rings also provide ample opportunity for careful functionalisation to enhance protein binding.[311]

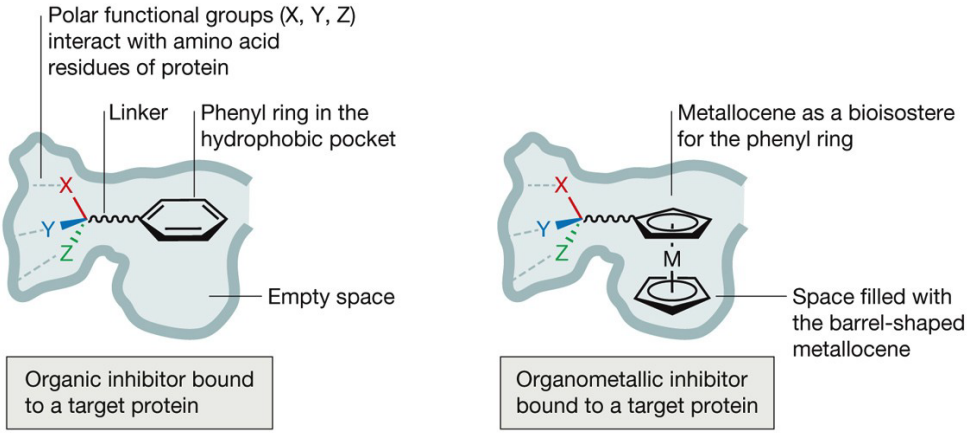

Figure 5.4 – Application of ferrocene as a bioisostere. Reproduced with permission from Patra and Gasser, 2007.[311]

As all the pendant groups previously investigated in the Open Source TB project to date have been aromatic and planar, incorporating three-dimensionally interesting moieties like adamantane and ferrocene offers a chance to explore how changing molecular topology of these drug candidates – and moving them out of the dreaded 'flat land' of traditional drug discovery – might improve activity. If results are promising, decorating the moieties with out-of-plane substituents could further enhance our understanding of the binding mode and target of this compound class.

5.1 Testing new functional groups on the cyclam core

A straight-forward and reliable synthetic route for bis-functionalised cyclam compounds has previously been developed in the group. This approach employs a Cu(I)-catalysed azido-alkyne click coupling reaction (CuAAC) to attach the desired pendant group, using an azido handle on the pendant group and a protected, bis-propargylated cyclam core (**180**).

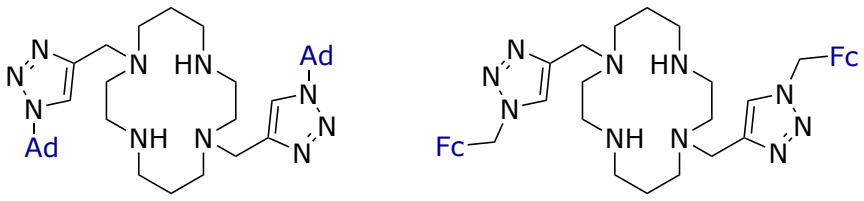

179 **180**

Figure 5.5 – Cyclam target compounds **179** with adamantane pendants and **180** with ferrocene pendants.

Given its demonstrated success, it was decided to use the same method to append the new hydrophobic pendants and make target compounds **179** and **180** (**Figure 5.5**). While 1-azidoadamantane is commercially available, the azidomethylferrocene coupling partner was to be synthesised, along with bis-propargyl cyclam via the well-established protocol.

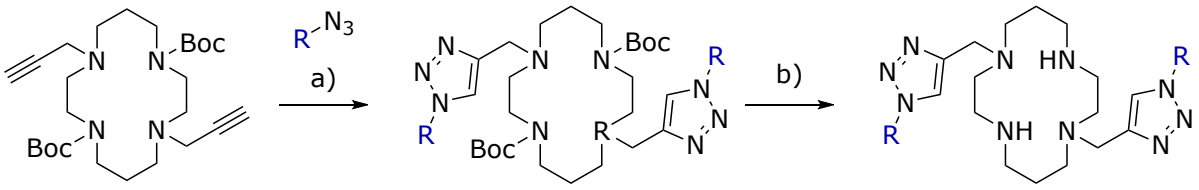

181 **182** R = Ad, **183** R = CH_2Fc **179** R = Ad, **180** R = CH_2Fc

Scheme 5.1 – Generalised route to 1,8-difunctionalised cyclam compounds **179** and **180** *via* the CuAAC reaction. a) $CuSO_4 \cdot 5H_2O$, sodium ascorbate, THF:H_2O. b) HCl in dioxane (4 M), 1,4-dioxane, then Ambersep® 900 hydroxide resin in methanol.

5.1.1 Synthesis of azidomethylferrocene

The azide-decorated ferrocene was not readily available and was therefore prepared synthetically. Concerns about direct reaction on the cyclopentadiene ring prompted the decision to include a methylene group between the ferrocene and azide, so synthesis began with esterification of the commercially available ferrocenecarboxylic acid **184** (anticipating reduction of the resulting ester to ferrocenylmethanol, which could then be transformed directly into the desired azide using diphenylphosphoryl azide (DPPA)).[312] As a first attempt, ferrocenecarboxylic acid **184** was heated at reflux in methanol with acetyl chloride for three hours (**Scheme 5.2**), but this method resulted in a disappointingly low yield of the desired methyl ester **185** (53%).

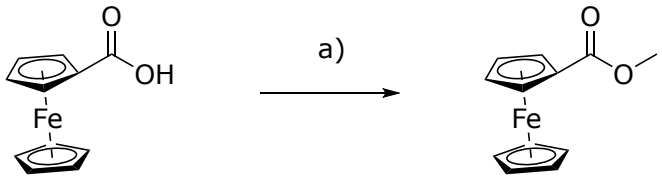

184 **185**

Scheme 5.2 – Methyl esterification of ferrocenecarboxylic acid **184**. a) Acetyl chloride, MeOH, 0°C, 2 h, 53%.

Therefore, an alternative method using 1,8-diazabicyclo(5.4.0)undec-7-ene (DBU) and dimethyl carbonate was trialled. Dimethyl carbonate and DBU (**186**) offer an environmentally friendly alternative to traditional methylating agents, though are not yet used widely. A proposed mechanism (**Scheme 5.3**) involves the DBU driving the base-catalysed acyl bond cleavage ($B_{AC}2$) of dimethyl carbonate to form a carbamate intermediate **187** with methanol as a byproduct. Intermediate **187** is then susceptible to attack from the aryl carboxylate **188** *via* a base-catalysed alkoxy bond cleavage ($B_{AL}2$) mechanism, forming the desired methyl ester. Shieh and colleagues have reported the application of these conditions with various benzylic carboxylic acids, which can be considered analogous to the aromatic cyclopentadiene ring of ferrocenecarboxylic acid.[313]

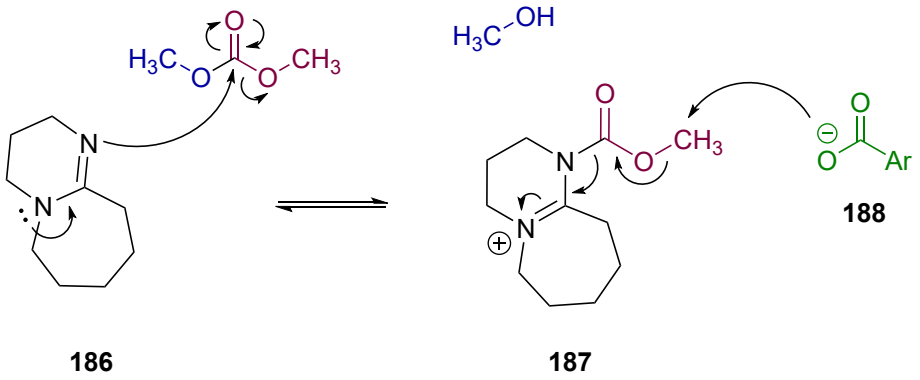

Scheme 5.3 – Mechanism of DBU-catalysed methyl esterification proposed by Shieh and colleagues.[313]

Ferrocenecarboxylic acid **184** and DBU were heated at reflux in dimethyl carbonate overnight. Following workup in which the organic extracts were washed with hydrochloric acid (1 M) and sodium bicarbonate solution, a good quantity of the ferrocenemethyl ester **185** was isolated in good yield (70%) as a dark orange solid that could be used without further purification (**Scheme 5.4**).

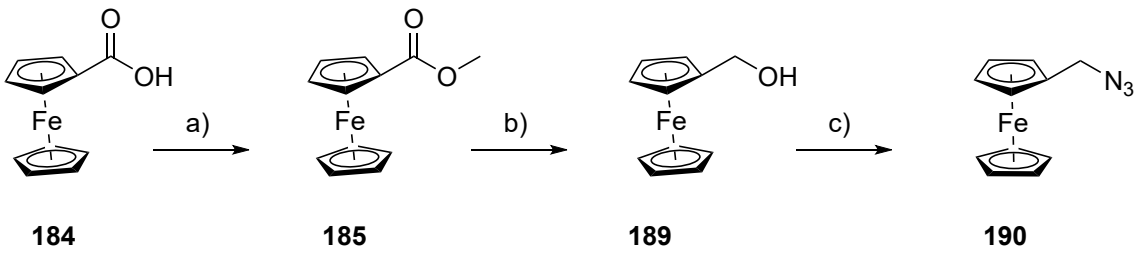

Scheme 5.4 – Synthesis of azidomethylferrocene **190** from ferrocenecarboxylic acid **184**. a) DBU, dimethyl carbonate, 90°C, 18 h, 70%. b) $LiAlH_4$, THF, rt, 3 h, quant. c) DPPA, DBU, NaN_3, THF, 66°C, 30 h, 64%.

Conversion to ferrocenylmethanol **189** was achieved using lithium aluminium hydride as a solution in THF, which was added dropwise to a solution of ferrocene methyl ester in the same solvent. After quenching with ethyl acetate, the formation of an emulsion made it difficult to separate the organic layers and led to an initially low yield. Addition of a saturated Rochelle salt solution improved separation considerably, as the Rochelle salt acts as a high-affinity ligand that can complex the aluminium byproducts in solution. With this improved separation, ferrocenylmethanol **189** was obtained in quantitative yield (**Scheme 5.4**).

The final step was conversion of the alcohol handle into the desired azide, achieved using DPPA. Typically, this conversion is facilitated by either DBU or the Mitsunobu reagent combination of triphenylphosphine and DIAD.[314,315] The DBU method was selected over the latter conditions, which require removal of the triphenylphosphine oxide byproduct. Prior investigation in the group using DPPA and DBU as azidating agents has found that the speed of this reaction can be hampered by the slow rate of nucleophilic attack by the azide anion, and reaction rates can be increased by the addition of sodium azide. Thus alcohol **189** was heated at reflux with DPPA and DBU in DMF for three hours before adding sodium azide and continuing to heat overnight. Extraction with toluene afforded the crude product, which was purified using flash column chromatography to give **190** in moderate yield (64%) as a dark red solid (**Scheme 5.4**).

5.1.2 Synthesis of bis-propargyl cyclam

The protected bis-propargyl cyclam partner had already been synthesised in prior investigations, and the reactions were simply scaled up to provide sufficient material for experimentation. Cyclam reacts with formaldehyde to selectively form 1,4- and 8,11-bridges, and the accumulation of positive charge in the subsequent propargylation step prevents overalkylation. Commercially available cyclam was therefore stirred with formaldehyde in water at 0°C for one hour and bridged cyclam **191** was obtained as a white powder by vacuum filtration. Alkylation was achieved using propargyl bromide to give the desired product **192** as a salt in excellent yields (**Scheme 5.5**).

Removal of the cyclam bridges was combined with protection of the newly freed amines, which could otherwise interfere with the CuAAC reaction by chelating the Cu(I) catalyst. *Tert*-butoxycarbonyl (Boc) is a commonly used protecting group, with straight-forward introduction

and removal, and has been favoured by the Rutledge group as it can be introduced at this point in the sequence via a one-pot procedure.

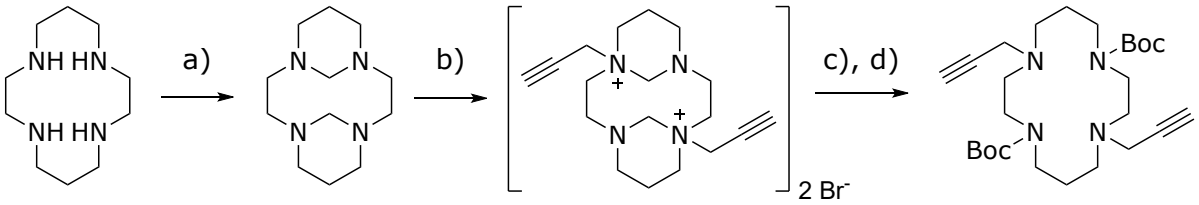

Scheme 5.5 – Synthesis of Boc-protected *bis*-propargyl cyclam **181**. a) Formaldehyde, H_2O, rt, 1 h, 78%. b) Propargyl bromide, MeCN, rt, 17 h, 98%. c) Aqueous NaOH (2.5 M), MeOH, rt, 2 h, then d) Boc_2O, MeOH, rt, 48 h, 54% over two steps.

Treatment of **192** with aqueous NaOH solution hydrolyses the alkyl bridges, before the addition of Boc anhydride sees formation of the Boc-protected, bis-propargyl cyclam **181**. In previous applications of this one-pot process, it was found that excess hydroxide can reduce yields by reacting directly with Boc anhydride to produce *tert*-butanol. Therefore, the pH of the reaction mixture was adjusted to ~11 prior to addition of the Boc anhydride and **181** was obtained in reasonable yield over the two steps and high purity (**Scheme 5.5**).

5.1.3 Click-coupling and deprotection

The term 'click chemistry' was first used in 1991 by Prof Barry Sharpless to describe reactions in which different molecular building blocks could be rapidly, easily connected, like a seatbelt clicking into place.[316] The exemplar click reaction has been the copper(I)-catalysed alkyne-azide cycloaddition, discovered independently by both Sharpless and Prof Morten Meldal (a metal-catalysed variant of the already well known cycloaddition pioneered by Rolf Huisgen).[316–318] This work was significant enough to earn them the Nobel Prize in Chemistry in 2022, along with Prof Carolyn Bertozzi, a pioneer of bio-orthogonal reactions and the application of variant AAC reactions *in vivo*.[319]

Using the CuAAC reaction to join chemical building blocks can dramatically improve the synthetic accessibility of a desired compound by enabling the two halves of the molecule to be synthesised separately and then united, thereby reducing the need for circular processes of protection and deprotection.[320] The reaction relies on Cu(I), usually in the form of either CuI or $CuSO_4$ in conjunction with a reducing agent.[321] The mechanism has been described at length

elsewhere, but in brief involves two copper(I) ions reacting with the alkyne partner to form a Cu(I)-acetylide complex that simultaneously activates the azide functionality on the other reaction partner and is prone to attack by the same group.[322] Ultimately, rearrangement of the ring formed by this attack results in a 1,2,3-triazole that links the two component pieces together.[320]

Thus, bis-propargyl cyclam **181** and 1-azidoadamantane **193** were combined with $CuSO_4$ and sodium ascorbate and stirred at room temperature until TLC analysis indicated complete consumption of the alkyne. After workup, the crude product was purified by flash column chromatography to give **182** as a crystalline golden solid. This was dissolved in dioxane and treated with HCl at 0°C to remove the Boc protecting groups, affording the desired compound **179**·2HCl (**Scheme 5.6**).

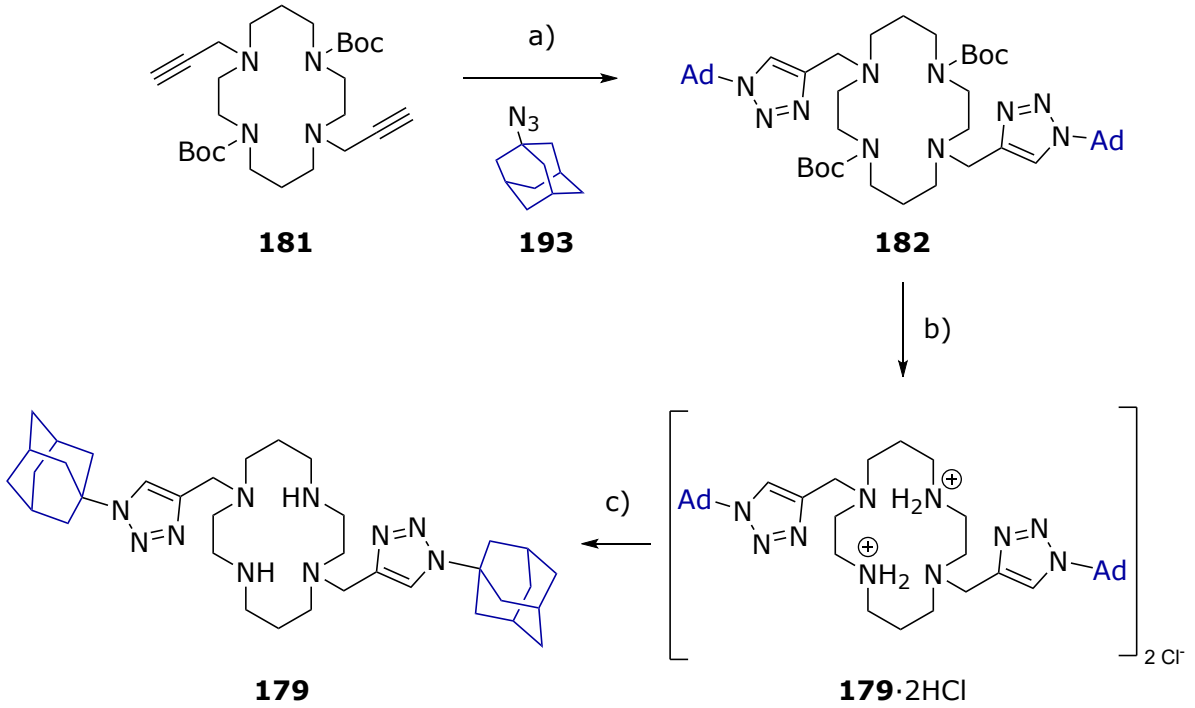

Scheme 5.6 – Synthesis of **179** from cyclam **181** via Boc-protected intermediate **182**. a) $CuSO_4 \cdot 5H_2O$, sodium ascorbate, THF:H_2O, 48 h, 72%. b) HCl in dioxane (4 M), 1,4-dioxane, rt, 1 hr, quant. c) Ambersep® 900 hydroxide resin in methanol, quant.

The corresponding methylferrocenyl derivative was synthesised in much the same way, with the initial click-coupled product **182** obtained as a dark green foam after purification by flash column chromatography (**Scheme 5.7**). Deprotection with HCl furnished **180**·2HCl as a bright yellow solid (**Scheme 5.7**).

While the click-coupling and deprotection steps themselves were routine, and proceeded with good to excellent yields, the subsequent purification proved less straight-forward. Using HCl to remove the Boc groups results in formation of the HCl salt, which can be difficult to characterise by NMR as the charged amines cause broadening of cyclam-derived peaks.

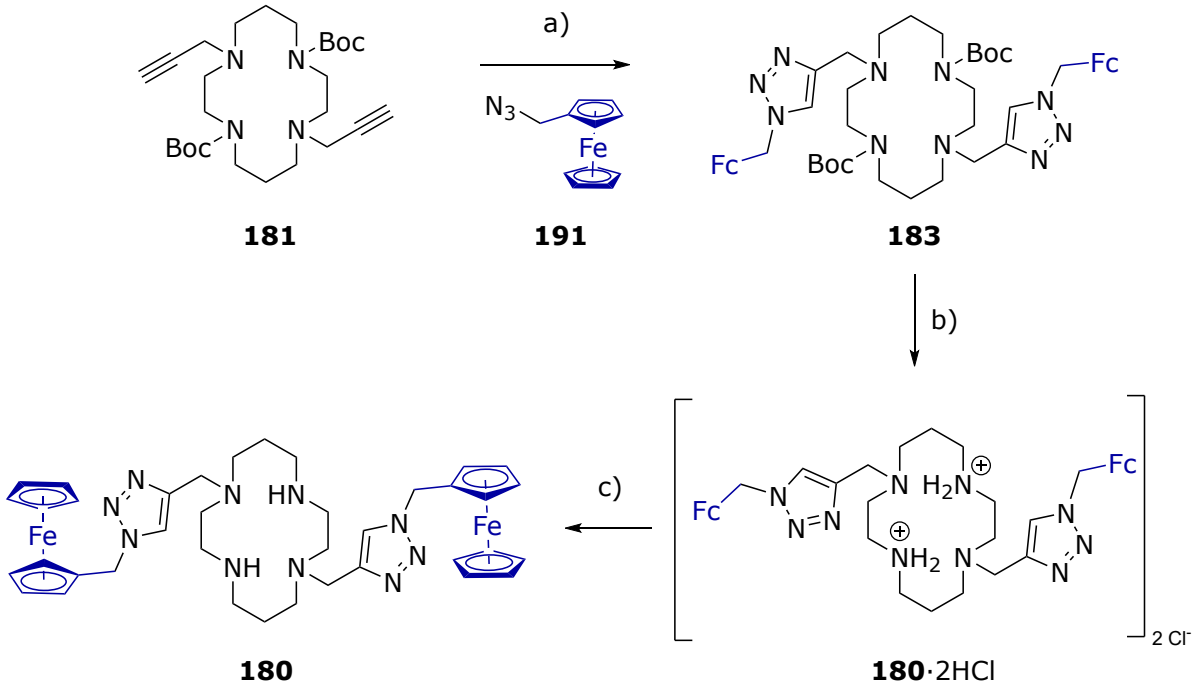

Scheme 5.7 – Synthesis of **180** from cyclam **181** via Boc-protected intermediate **183**. a) $CuSO_4 \cdot 5H_2O$, sodium ascorbate, THF:H_2O, 22 h, 91%. b) HCl in dioxane (4 M), 1,4-dioxane, rt, 1 hr, quant. c) Ambersep® 900 hydroxide resin in methanol, quant.

Functionalised cyclam compounds can be challenging to analyse by NMR in any case, with the limited rotational freedom of the macrocycle often leading to peak broadening and signal overlap.[323] Therefore, a small amount of each compound was converted to the corresponding free base using Ambersep® 900 hydroxide resin, which sequesters chloride ions and neutralises the protonated amines. So, **179**·2HCl was dissolved in methanol and passed through a column containing the resin to obtain the free base as a crystalline brown foam. The same procedure was performed in batch on **180**·2HCl using resin beads pre-swelled in methanol, after which removal of solvent gave the free base as a dark green solid.

In parallel, the remaining portions of both compounds were purified by reversed-phase HPLC to give **179**·2HCl as a fine white powder, and **180**·2HCl as a light green powder. In both cases, conversion to the free base was quantitative, while yields were reduced considerably during the HPLC purification process.

5.2 Open cyclam and new functional groups

Once target compounds **179** and **180** had been synthesised, focus shifted to the corresponding 'open cyclam' analogues. While **41**, the most potent compound made so far, features the propylene triamine core, the triply-substituted diaminohexane analogue **194** (**Figure 5.5**) also showed promising activity, with an MIC_{50} of 12.5 µM, and is synthetically simpler to access.

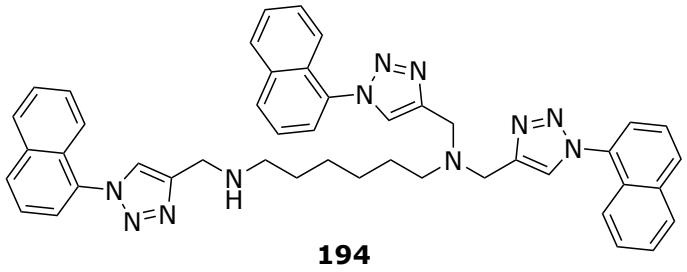

194

12.5 µM

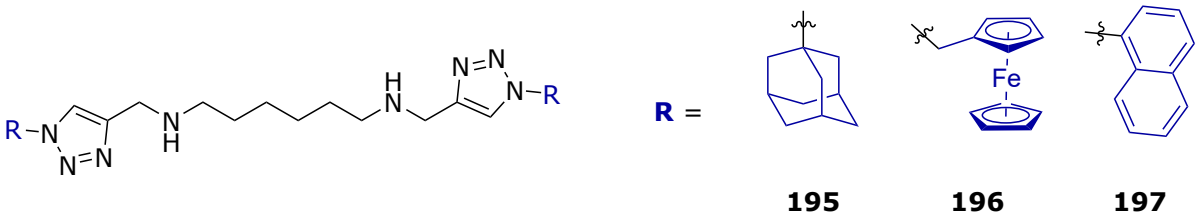

195 **196** **197**

Figure 5.6 – Previously synthesised compound **194** with *minimum* IC_{50} against *Mtb* H37Rv and target compounds featuring the diaminohexane scaffold conjugated with triazolyl-linked adamantane (**195**), ferrocene (**196**) and naphthalene (**197**).

The plan was to apply the same synthetic route used with cyclam to this new core structure, with **170** undergoing Boc protection and propargylation before being clicked with an azide-functionalised pendant group to afford adamantyl- (**195**), ferrocenyl- (**196**) and naphthyl- (**197**) appended 'open cyclam' analogues.

5.2.1 Bis-propargyl amine synthesis

Alkylation of an amine is generally made complicated primarily by the potential for over-alkylation,[324,325] and the Rutledge group has previously reported the *bis*-allylation of diamine **170** using allyl bromide in conjunction with Boc protecting groups, analogous to the method used to prepare the cyclam intermediate **180**.[326] Conversion to a carbamate considerably decreases the nucleophilicity of the nitrogen, as its lone pair participates in resonance with the

carbonyl group.[327] This necessitates the use of strong base to fully deprotonate, thus effectively preventing overalkylation.[328]

Replacing the alkylating agent with the propargyl analogue therefore seemed an obvious means of obtaining desired compound **199**. Boc protection of **170** was achieved facilely by the dropwise addition of Boc anhydride to a solution of **170** in chloroform. The crude product was obtained after overnight reaction and purified using column chromatography to give **198** as a crystalline white powder in good yields (71%, **Scheme 5.8**).

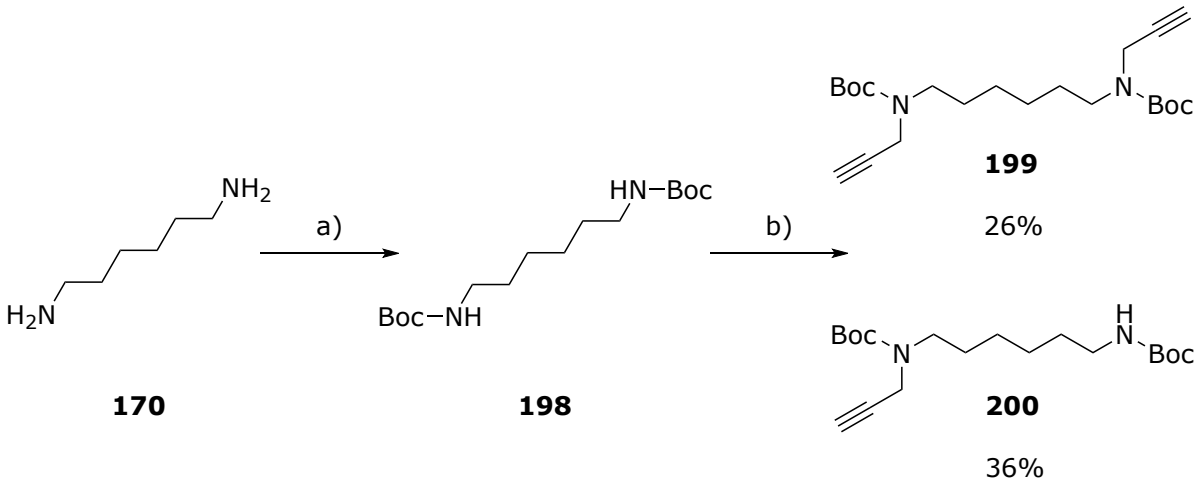

Scheme 5.8 – Boc-protection and bis-propargylation of **170** under optimised conditions, yielding a mixture of the *bis*- and *mono*-alkylated products **199** and **200**. a) Boc anhydride, chloroform, rt, 25 h, 71%. b) Propargyl bromide, sodium hydride, rt, 24 h.

However, propargylation proved more difficult than foreseen. Initially, under similar conditions to those used for allylation, the Boc-protected amine **198**, sodium hydride and propargyl bromide were combined in DMF under anhydrous conditions and stirred at room temperature for 24 hours. TLC analysis indicated consumption of starting material and the formation of two new species, one of which was assumed to be the desired product **199** (**Scheme 5.8**). Upon workup, however only the *mono*-alkylated amine **200** was recovered. Reasoning that the reaction had simply not gone to completion, the *mono*-alkylated product **200** was treated with the same conditions, and after three days of stirring, a new species was observed with a mass corresponding to that of the desired product. After a lengthy purification process, the *bis*-propargylated product **199** was recovered in poor yield as a pale golden oil.

Various modifications to the method were trialled but delivered little improvement, with long reaction times and purification processes compounding the difficulties. As solvent dryness was crucial to preventing deactivation of the hydride base, the less hygroscopic THF was used in

combination with DMF, with a 1:1 ratio of the two solvents resulting in a slightly improved yield of the *bis* product compared to DMF alone. Increasing the ratio of THF, however, resulted in lower yields than before (**Table 5.1**).

Table 5.1 – Results of propargylation reaction under six different conditions. Amounts given as molar percentage calculated from isolated products relative to starting material, unless otherwise stated.

Attempt	Solvent	Time (d)	200 (*mono*)	199 (*bis*)
1	DMF	1	38	Nil
2	DMF	3	Nil*	10
3	DMF:THF 1:1	1	36	26
4	DMF:THF 1:5	5	32	15
5	DMF + crown ether	2	30**	26**
6	DMF	4	32	15

**Mono*-alkylated product of prior reaction used as starting material.
**Amounts calculated from NMR analysis of crude reaction mixture.

A more comprehensive screen of aprotic solvents was then conducted, using LCMS to monitor formation of the desired product after 24 hours of reaction (**Table 5.2**). Acetonitrile was found to deliver the highest conversion to the *bis* product (34%), while DMF boasted the highest total conversion from the starting material (92%). However, a larger scale reaction with acetonitrile was not attempted.

Table 5.2 – Results of solvent screen for the propargylation of **198**. Amounts are molar percentage present after 24 hour reaction time, relative to starting material, calculated from area under curve using LCMS analysis.

Solvent	% of 198 (starting material)	% of 200 (*mono*)	% of 199 (*bis*)	Conversion (%)
DMF	8	72	20	92
THF	39	52	9	61
Acetonitrile	25	41	34	75

The basicity of sodium hydride can be increased by inclusion of 15-crown-5 ether, which complexes the sodium counterion to improve ion pair solvation and accelerate nucleophilic attack.[329] Including a crown ether in the reaction mixture did slightly improve yields of the desired *bis*-propargyl amine, but conversion remained stubbornly low, with significant quantities of both the starting material **198** and *mono* product **200** also obtained (**Table 5.1**, Attempt 5).

Eventually, sufficient material was isolated to carry through to the next steps, and the reaction was not investigated further. The results obtained suggest that the issue is not *N*-alkylation itself but rather forcing a reaction at both ends of the diamine. As a relatively long, flexible molecule, the *mono*-alkylated amine can coil back on itself (**Figure 5.7**), potentially enabling hydrogen bonding between the remaining N–H and the alkylated carbamate that slows or blocks deprotonation at the unreacted end. Alternatively, the deprotonated carbamate may co-ordinate a sodium ion, forming a stable ion pair and causing reaction to stall after the initial alkylation.

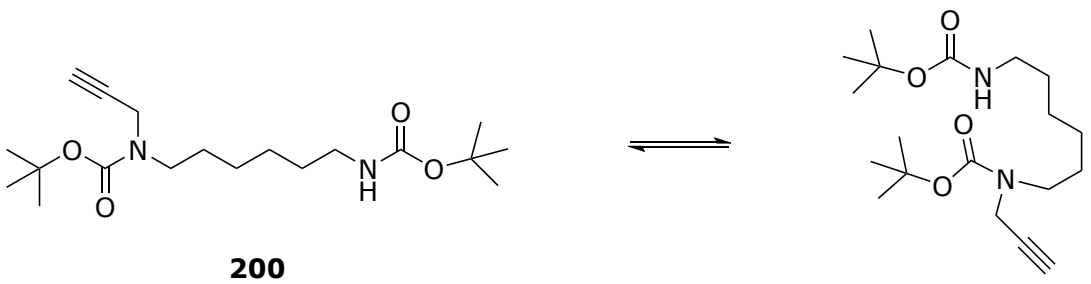

200

Figure 5.7 – Conformational flexibility of **200**.

This second hypothesis is supported by the finding that addition of a crown ether, to preferentially co-ordinate the sodium ion, improved overall conversion rates.

Increasing reaction temperature and using alternative bases, such as alkyl lithium reagents, could probe whether the sluggishness of the second reaction is indeed caused by issues with deprotonation, and our understanding of this reaction would be further enhanced by computational modelling.

5.2.2 Click-coupling and deprotection

Once sufficient quantity of the bis-alkyne **199** had been synthesised, the click-coupling and subsequent deprotection of the triazole-linked compounds was relatively straight-forward, following similar procedures as described for the corresponding cyclam compounds. Methylferrocene azide **190** was click-coupled with **199** under the same conditions used with the cyclam analogues, and **201** was obtained as a red solid in moderate yield after purification *via* automated column chromatography (**Scheme 5.9**). Following the same general procedure, **199** and **193** were reacted to give **202** (**Scheme 5.9**). Initially, purification was attempted using the same solvent system used successfully for **201**, a 0 – 5% gradient of methanol in dichloromethane. Surprisingly, this resulted in the product eluting in the solvent front, and a

gradient of 20 – 100% ethyl acetate in hexane was used instead. This proved more fruitful, and a reasonable quantity of **202** was recovered cleanly as a crystalline white powder.

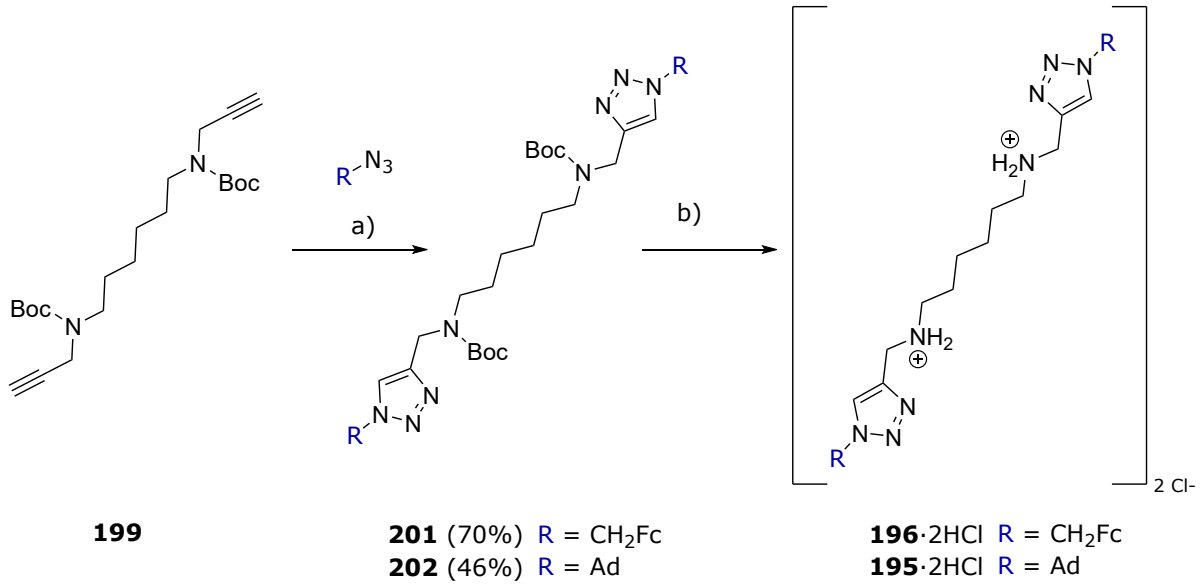

199

201 (70%) R = CH_2Fc
202 (46%) R = Ad

196·2HCl R = CH_2Fc
195·2HCl R = Ad

Scheme 5.9 – Click-coupling of **199** with **193** or **190**, and deprotection of the subsequent products to yield **195·2HCl** and **196·2HCl**. a) $CuSO_4 \cdot 5H_2O$, sodium ascorbate, THF:H_2O, rt, 1 – 3 d. b) HCl in dioxane (4 M), 1,4-dioxane, rt, 1 h, quant.

Deprotection of the click-coupled compounds proceeded smoothly, and a portion of each deprotected compound was again converted to the free base using Ambersep® resin beads. HPLC purification gave the final adamantyl compound **195**·2HCl as a fine white powder, but the ferrocenyl compound **196**·2HCl was not successfully isolated in sufficient purity for biological testing. In both cases, the singly-deprotected amine was also formed and proved difficult to separate from the final product. Nonetheless, isolation of **195**·2HCl demonstrates that the desired product can eventually be obtained through optimisation of the chromatographic conditions.

5.3 *N*-Alkylation method

After the difficulties experienced obtaining *bis*-propargylated intermediate **199**, an alternative reaction sequence to enable variation of the key *N*-alkylation step was envisaged. While direct alkylation using an alkyl halide is arguably the simplest approach, the propensity for over-alkylation has led to a multitude of other routes being devised.[324,330,331] Reductive amination is one alternative, and involves condensation of the amine with a ketone or aldehyde and

reduction of the resulting imine, which is useful for preventing formation of quaternary amines.[332]

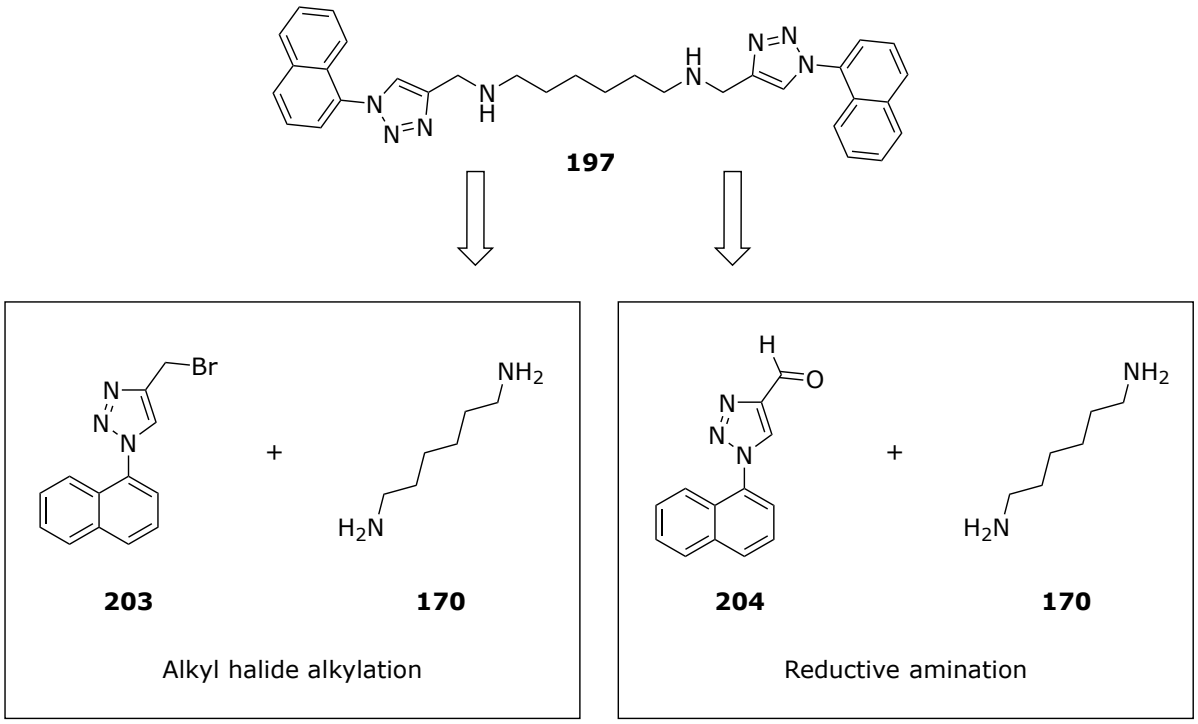

Scheme 5.10 – *N*-alkylation routes using alkyl halides or reductive amination.

A previous study applied this reductive amination approach to eight linear amine scaffolds (**169 – 170, 205 – 209, Figure 5.8**), employing a naphthyl pendant group decorated with a carbonyl handle (**Scheme 5.10**).[213]

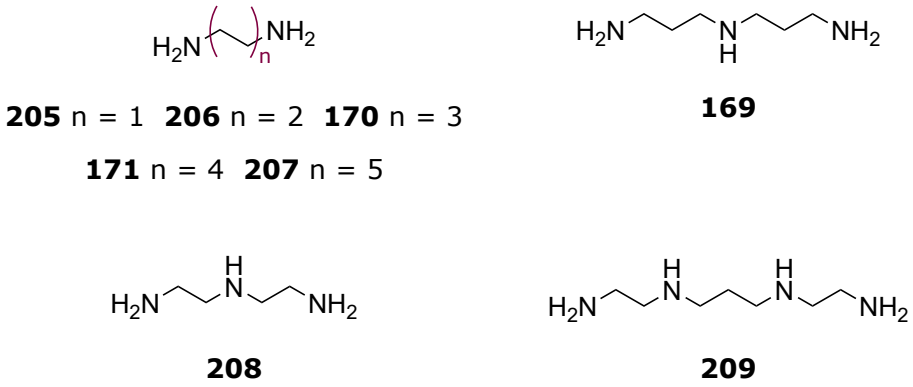

Figure 5.8 – Linear amine scaffolds used in previous studies on open cyclam.

However, reductive amination can also lead to reaction at secondary amines,[333] and in some cases one or both amines were doubly alkylated under these conditions (**Table 5.3**).[213]

Table 5.3 – Open cyclam analogues previously synthesised *via* reductive amination route.

Amines	Carbons	Scaffold	Number of naphthalene-triazole pendants		
			2	**3**	**4**
	2	**205**	**210**	-	-
	4	**206**	**42**	**211**	-
	6	**169**	-	**194**	-
	8	**170**	-	-	**212**
2	10	**207**	**213**	-	-
	4	**208**	**214**	-	
3	6	**169**	-	**41**	-
4	7	**209**	**215**	-	-

Of the five linear diamines trialled by Batten, only three were successfully *bis* functionalised, as only the *tris* and *tetra*-alkylated products **194** and **212** were isolated from reaction of diaminohexane **170** and diaminooctane **171** respectively. Both the *bis* and *tris*-alkylated products (**42** and **211**) were isolated from reaction of the diaminopropane **206**. The 1,4,8,11-tetraazaundecane (**209**), which has a structure most similar to cyclam, was also successfully *bis* functionalised (**215**).

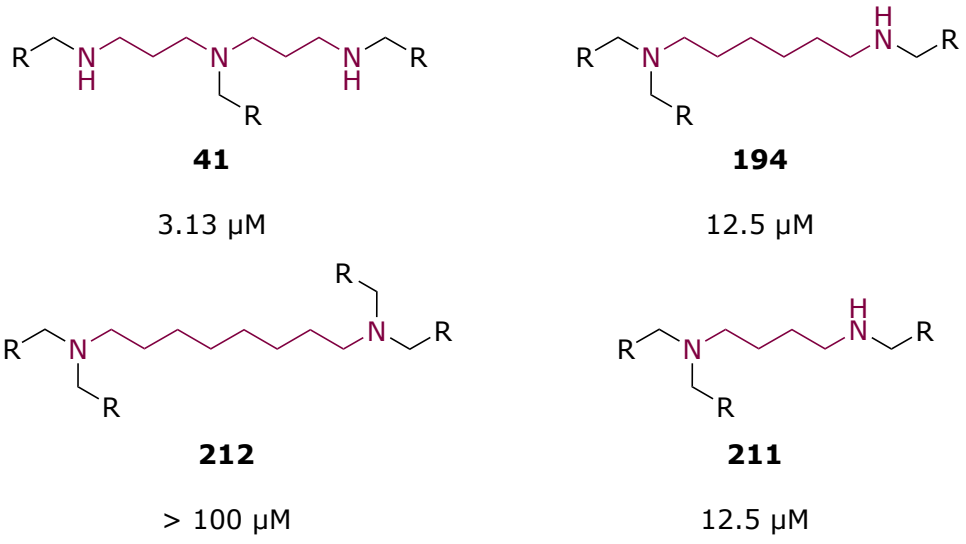

Figure 5.9 – *Tris* and *tetra* products isolated from reductive amination of linear amine substrates (R = triazolo-naphthalene).

Interestingly, the two triamines, which each incorporate two terminal primary amines and a central secondary amine, had different outcomes. The diethylenetriamine **208** yielded the

desired *bis* product **214** while only the *tris* product **41**, with a naphthyl group appended to each amine, was obtained from the dipropylene triamine **169**.

Considering the mixed results obtained *via* the reductive amination route in earlier studies, *N*-alkylation using an alkyl halide was favoured for this work. In theory, direct *N*-alkylation of the unprotected amines can be controlled with strict stoichiometric ratios and low temperatures, while avoiding protecting groups would allow products to be obtained in a single step. This route was therefore selected for initial attempts, with the decision also influenced by the knowledge that two of the unintended multi-alkylated products of reductive amination, **41** and **194**, were among the most potent compounds (**Figure 5.9**). Prior experience also indicated that two linear amines with different degrees of alkylation could be separated, albeit with difficulty, meaning that *tris*- or *tetra*-functionalised side products could potentially be isolated and tested alongside the target compounds.

5.3.1 Pendant synthesis

Following the methods previously described in the group, 1-naphthylamine **216** was combined with sodium azide and sodium nitrite to give the crude azide product **217** as a dark red liquid (**Scheme 5.11**). After purification *via* automated column chromatography, 1-azidonaphthalene **217** was obtained as a viscous golden oil. The azide was then click-coupled with propargyl alcohol under corresponding conditions to the CuAAC reactions described in **Section 5.1.3**.

Low yields and reaction times in excess of 24 hours when using Cu(II) were attributed to the poor solubility of **217** in the THF/water solvent system (**Scheme 5.11a**). This prompted an exchange of reagents, as copper sulfate pentahydrate is insoluble in most organic solvents,[334] whereas copper iodide is somewhat soluble in acetonitrile, as well as being a direct source of the Cu(I) required to catalyse the reaction. The addition of *N*,*N*-diisopropylethylamine (DIPEA) helps to stabilise the active copper species, and has been shown to improve yields,[321,335] while reducing agent sodium ascorbate was retained to prevent *in situ* oxidation of the copper. These conditions greatly improved the yield of **218**, though reaction times remained long.

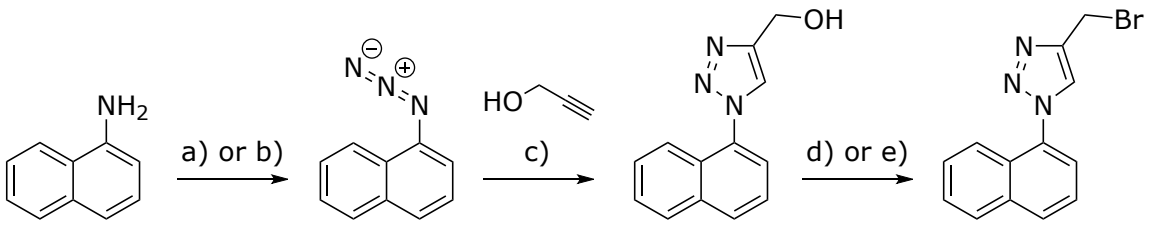

216 **217** **218** **203**

Scheme 5.11 – Synthesis of **218** from 1-aminonapthalene. a) $CuSO_4 \cdot 5H_2O$, sodium ascorbate, THF/H_2O, 50°C, 38 h, 67%. b) CuI, sodium ascorbate, DIPEA, acetonitrile, 50°C, 38 h, 94%. c) $NaNO_2$, NaN_3, HCl (3.4 M), 1 h, 0°C, 73%. d) CBr_4, triphenylphosphine, DCM, rt, 44 h, 75%. e) PBr_3, DCM, rt, 90 min, 62%.

There are many ways to approach bromination of the alcohol handle.[336] The Appel reaction uses carbon tetrabromide as the source of bromine, with the reaction enthalpically driven by the formation of the P=O double bond.[337] A small scale test reaction of **218** under standard conditions showed promising results with good crude yields despite a longer than expected reaction time. However, yields dropped significantly upon scale-up (**Scheme 5.11d**). Some modifications to the conditions were attempted but disappointing results prompted a search for an alternative brominating agent.

Phosphorus tribromide is one of the most common reagents used to brominate alcohols, and has been shown to work on a large range of substrates with excellent yields.[338] Each of the three bromine atoms can react with the alcohol through a simple S_N2 mechanism, and reaction is generally swift and selective.[338]

After stirring **218** and phosphorus tribromide in DCM for 90 minutes, TLC analysis indicated complete consumption of the alcohol and aqueous workup with sodium bicarbonate solution gave the desired alkyl bromide **203** (**Scheme 5.11e**). Generally, the brown solid thus obtained was used without further isolation, though purification with automated column chromatography yielded the pure product as a crystalline golden solid. While yields remained lower than hoped for, this method was preferred over the Appel reaction for its rapidity, reliability and ease of isolation.

5.3.2 Alkylation of unprotected amine

According to standard procedure, the unprotected amine **170** was dissolved in DMF with potassium carbonate and cooled to 0°C, before two equivalents of **203** dissolved in DMF were

added dropwise over 1 hour (**Scheme 5.12**). The reaction was halted after two further hours, when TLC analysis indicated consumption of starting material, and a sticky ochre precipitate was removed from the mixture by filtration. The remaining solvent was removed overnight under a stream of nitrogen, leaving a pale crystalline solid. TLC analysis showed three separate species with R_F values of 0.25, 0.39 and 0.50, which were confirmed by LRMS to be the *bis*, *tris* and *tetra*-alkylated products.

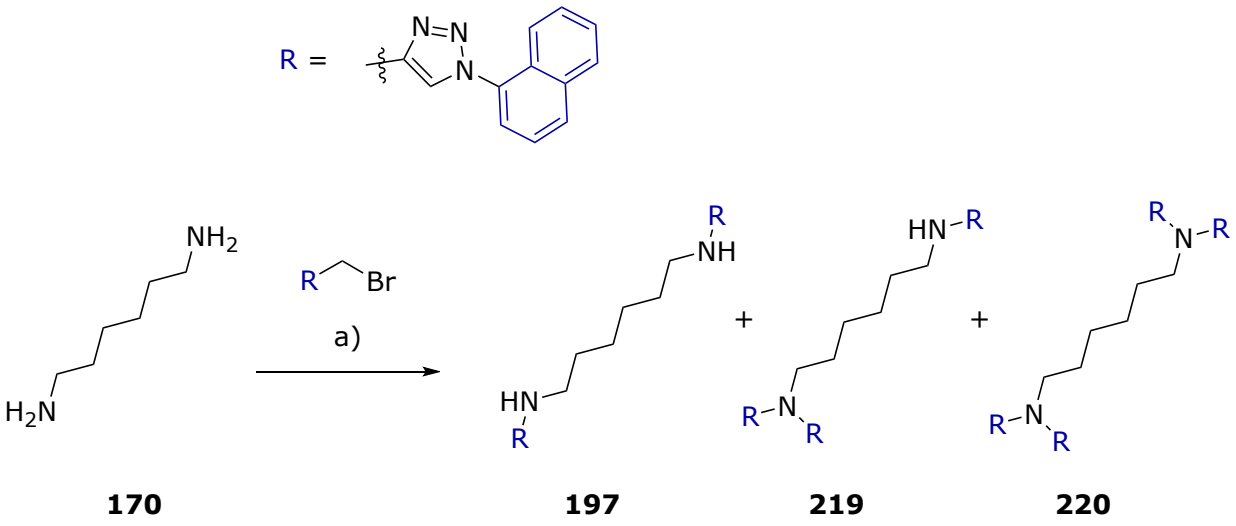

Scheme 5.12 – Synthesis of **198** from **203** and amine **170**. a) Potassium carbonate, DMF, 0°C, 3 h.

Automated column chromatography using a gradient of chloroform and methanol treated with ammonium hydroxide afforded some purification, with a mixture of *bis* and *tris* products (**197** and **219**) being separated from a mixture of *tris* and *tetra* products (**219** and **220**). Surprisingly, the *tetra* product **220** co-eluted with both the *tris* and *bis* products **197** and **219** despite the apparently significant difference in hydrophobicity, and only a small percentage of these latter products could be isolated without contamination from **220**.

This approach could be refined by adjusting the reaction conditions, using a more dilute solution and slower addition of the alkylating agent to prevent overalkylation, as residual amine starting material **170** is likely easier to remove through acid-base manipulations than the *tetra* product **220**. Adjusting the base and solvent could also improve selectivity, however investigation of an alternative reaction path using a protected amine was favoured over optimisation of this route.

5.3.3 Protected *N*-alkylation

The most common strategies for *N*-protection involve converting the amine to a carbamate, amide or sulfonamide, with the latter resulting in a more acidic N-H bond due to increased resonance stabilisation of the conjugate base, enabled by electron delocalisation into the pi system.[339,340] While this acidic N-H proton can be favourable for an *N*-alkylation step, removal of sulfonamides like the frequently employed tosyl group requires harshly acidic or reductive conditions that may not be compatible with the final product.[339] Fukuyama and colleagues therefore developed an alternative sulfonyl reagent, nosyl (Ns), in which an electron-deficient *ortho* or *meta*-nitrobenzene replaces the toluene of tosyl. The nosyl protecting group can be cleaved under much milder conditions, typically achieved *via* nucleophilic aromatic substitution.

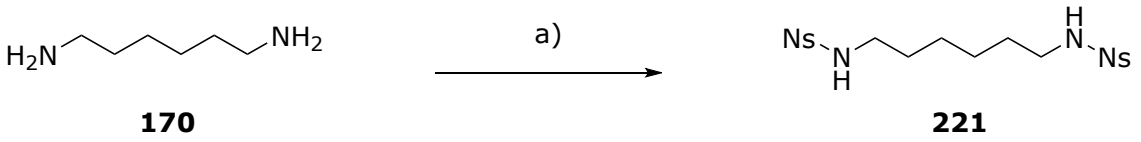

170 **221**

Scheme 5.13 – Nosylation of amine **170**. a) 2-Nitrobenzenesulfonyl chloride, triethylamine, DCM, rt, 22 h, 64%.

Nosylation of **170** was carried out according to well-defined procedures.[333,341,342] Amine **170** was dissolved in DCM with triethylamine, and 2-nitrobenzenesulfonyl chloride was added portion wise (**Scheme 5.13**). The mixture was allowed to stir at room temperature until starting material was no longer observed and a large quantity of pale-yellow precipitate had formed. Excess triethylamine was quenched with ammonium chloride solution, and the mixture was extracted with chloroform. After brine washing, a significant quantity of white precipitate was observed in the organic extracts and filtered out prior to evaporation of the solvent. Subsequent ^{1}H NMR analysis revealed that the white precipitate and the dark green residue obtained after evaporation were the same nosylated amine product. Both crude products were dried under vacuum to remove trace solvents and used without further purification.

The *N*-alkylation step was attempted with the nosyl-protected amine **221** as substrate and DMF as solvent, following Fukuyama's method (**Scheme 5.14**). Initially, a large proportion of the *mono*-alkylated product **223** was obtained, with no evidence of the *bis* product **222** forming at all. It was thought that this may have been due to competing hydrolysis of the alkylating reagent **203** under the reaction conditions, with reaction appearing to stall at the partly alkylated **223**

product. Conducting the reaction in anhydrous DMF yielded more promising results, with LRMS analysis showing evidence of the *bis* product **222** despite incomplete reaction of the starting material. Purification once again proved challenging, and only very small amounts (3 mg, 1%) of the desired **222** could be cleanly isolated by automated column chromatography, and the majority remaining in a mixture of the starting material **221** and the two alkylated products **222** and **223**.

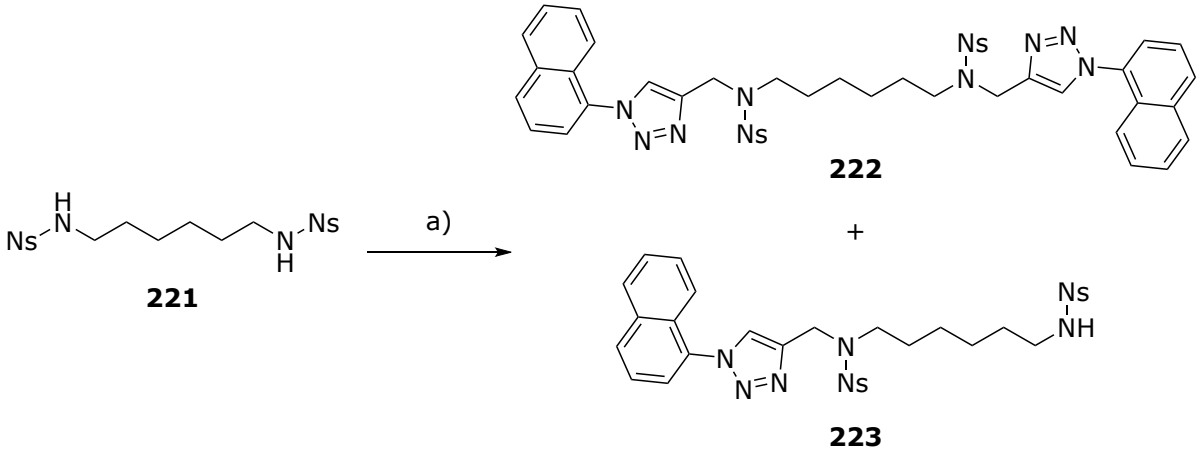

Scheme 5.14 – *N*-Alkylation of **221** to give desired product **222** and unwanted side product **223**. a) **203**, potassium carbonate, DMF, rt, 5 d.

Nonetheless, this modest result spurred further investigation of the reaction conditions, towards the goal of pushing this reaction to completion. Many different combinations of base and solvent have been reported in the literature, usually being described for a highly specific substrate. Aprotic polar solvents like DMF, THF and acetonitrile are broadly preferred for S_N2 reactions, as their lack of interaction with the nucleophile increases its reactivity.[343] Potassium carbonate is widely used as the base, likely due to reasons of cost and accessibility, though stronger bases including hydroxides and hydrides are also frequently utilised.[331,344,345] With this in mind, a different solvent and two bases were screened (**Table 5.4**). Caesium carbonate has been reported to improve both yields and reaction times through the so-called 'caesium effect', whereby the caesium ion slightly stabilises the nucleophile formed *in situ*.[346] The other base tested was sodium hydride, which is well-established as an effective base in *N*-alkylation reactions.[347] The attempted alkylations were run for a 2 day reaction time in each case.

Table 5.4 – Results of solvent and base screen for *N*-alkylation of nosyl-protected amine **221**. Amounts given as molar percentage calculated from NMR analysis.

Attempt	Base	Solvent	% of 223 (*mono*)	% of 222 (*bis*)
1	K_2CO_3	DMF	80	None observed
2	K_2CO_3	DMF	N/A*	< 5**
3	NaH	DMF	~ 16	~ 10
4	Cs_2CO_3	DMF	< 5**	None observed
5	Cs_2CO_3	THF	< 5**	None observed
6	NaH	THF	None observed	None observed

*_Mono_-alkylated product of prior reaction used as starting material.

**Exact quantity could not be determined by NMR.

Formation of **222** and **223** was monitored using LRMS, with NMR analysis performed only if the products were observed as their molecular ions. Formation of the *bis* product **222** was observed only in the sodium hydride/ DMF reaction, with approximately 25% conversion to the alkylated products overall, although poor separation made it difficult to determine exact ratios. A very small amount of the *mono* product **223** was generated in both caesium carbonate reactions, while the sodium hydride/ THF combination showed no reaction at all.

From this limited assessment, the original conditions of potassium carbonate in DMF appear to be the most effective. Other means to improve yields and reaction rates could also be trialled, including microwave reaction or the addition of potassium iodide to amplify the reactivity of **203**. Additional bases and solvents could be explored too, with caesium hydroxide having been particularly cited as an effective base for *N*-alkylation of linear amines.[345]

However, there is little evidence for a specific combination of base, solvent or other variable efficiently controlling the alkylation of multiple nitrogen atoms within a linear polyamine as is required here. Indeed, there is comparatively little precedent in the literature for *bis*-functionalising a polyamine, and in fact more discussion of how to produce unsymmetrically functionalised amines.[310,333,348–351] For instance, Salvatore and colleagues describe a method to prevent secondary alkylation at one nitrogen of a polyamine without even mentioning the possibility of obtaining the symmetric *bis*-functionalised product,[352] while the nosyl protecting group is typically vaunted for enabling protection of just one nitrogen in an amine substrate.[333]

In any case, with the nosyl-protected diaminohexane on hand, the Fukuyama amine synthesis presented an obvious alternative route despite concerns about *bis*-functionalisation. As with

other alkylation methods, the Fukuyama synthesis, which involves a Mitsunobu reaction performed on the nosyl-protected amine, is generally reported for the synthesis of asymmetric amines.[310,353] Still, the high yields and comparatively simple protocol made this an attractive option.

5.4 The Fukuyama method

Discovered in the 1950s, the Mitsunobu reaction refers to the substitution of an alcohol with a nucleophile, facilitated by a dialkyl diazocarboxylate and trialkyl- or triaryl phosphine, with diisopropyl azodicarboxylate (DIAD) and triphenylphosphine being amongst the best-known reagents.[354,355] Mitsunobu conditions are often employed with carboxylic acid nucleophiles to form esters, but can accommodate a diverse range of nucleophiles or 'pronucleophiles', including imides, thiols and sulfonamides.[354]

The reaction relies on the transformation of the alcohol into an alkoxyphosphonium ion, making the carbon adjacent to the alcohol highly susceptible to nucleophilic attack (**Scheme 5.15**). This process begins with the addition of triphenylphosphine (**224**) to one of the nitrogens within the azodicarboxylate **225**, resulting in the resonance-stabilised intermediate **226**. This anion can deprotonate the nucleophile of interest (**222**), while the alcohol **218** attacks the positively charged phosphorus. Proton transfer results in the desired alkoxyphosphium ion **228**, and attack on this by the activated nucleophile **229** produces the final substituted product **223** and triphenylphosphine oxide (**231**) byproduct, with the enthalpic sink of the P=O bond formation helping to drive the reaction forward.

Nosylation is noted as an effective means of activating an amine prior to Mitsunobu alkylation, [314,353–355] with the two-step process of nosylation followed by a Mitsunobu coupling often referred to as the Fukuyama amine synthesis.[310]

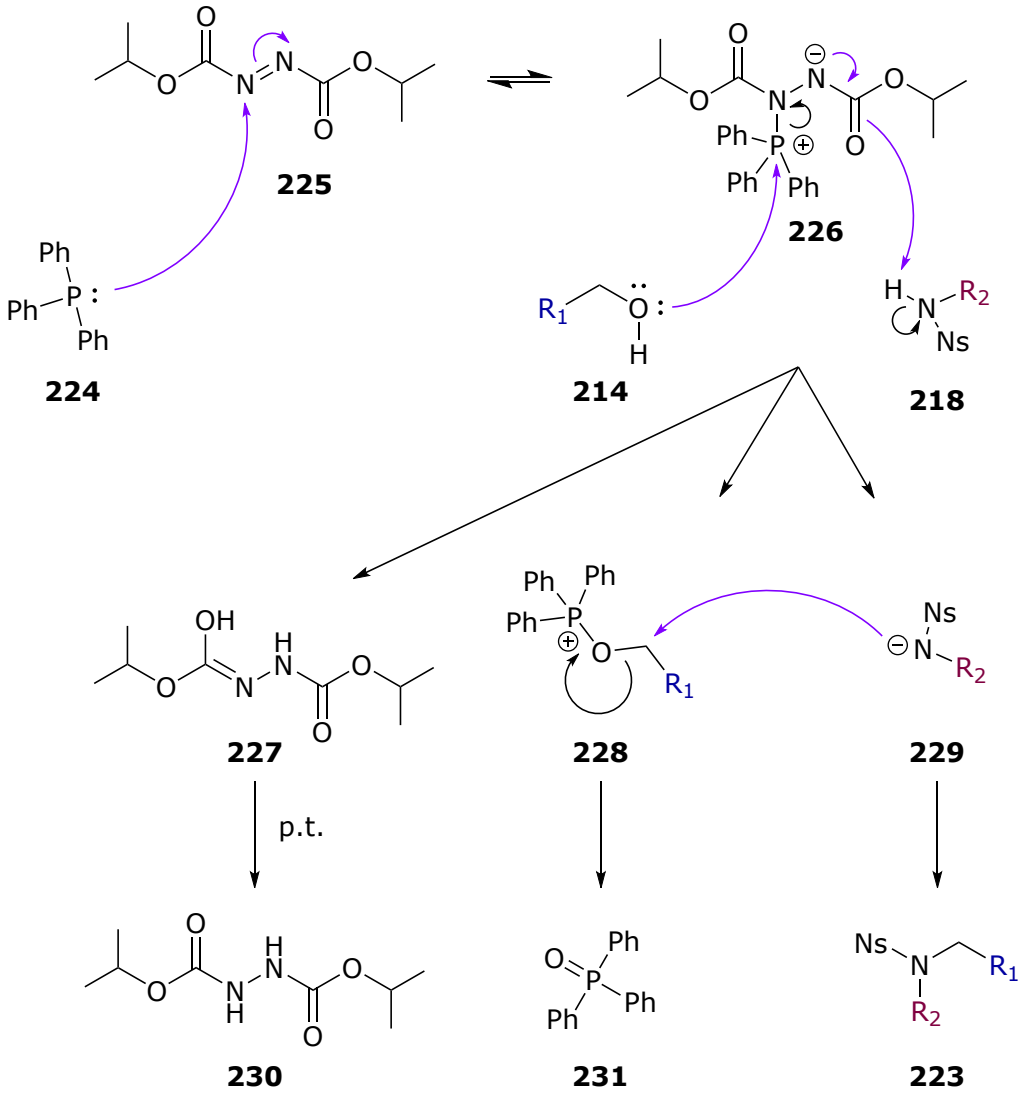

Scheme 5.15 – Mechanism of the Mitsunobu reaction (generalised). For the current study, R_1 = triazolylnaphthyl and $R_2 = (CH_2)_6NHNs$.

5.4.1 Mitsunobu alkylation

Diaminohexane **170** was the first substrate tested with Mitsunobu conditions, as the nosyl-protected derivative was already on hand, and the necessary alcohol **218** had been prepared as a precursor to the brominated pendant used previously. Thus sulfonamide **221** and alcohol **218** were reacted with triphenylphosphine and DIAD at room temperature for 24 hours (**Scheme 5.16**). As large amounts of starting material still remained, the mixture was heated to 60°C for a further 24 hours. Removal of solvent and trituration with cold ether gave the crude product **222**, with both DIAD and its hydrazine product still evident by ^{1}H NMR analysis. A small

quantity of the mono-substituted product **223** was also observed. Most of the residual DIAD was removed by dissolving the sample in DCM and passing the solution through a silica plug, while further purification by automated column chromatography yielded the pure *bis* product **222** as a golden foam.

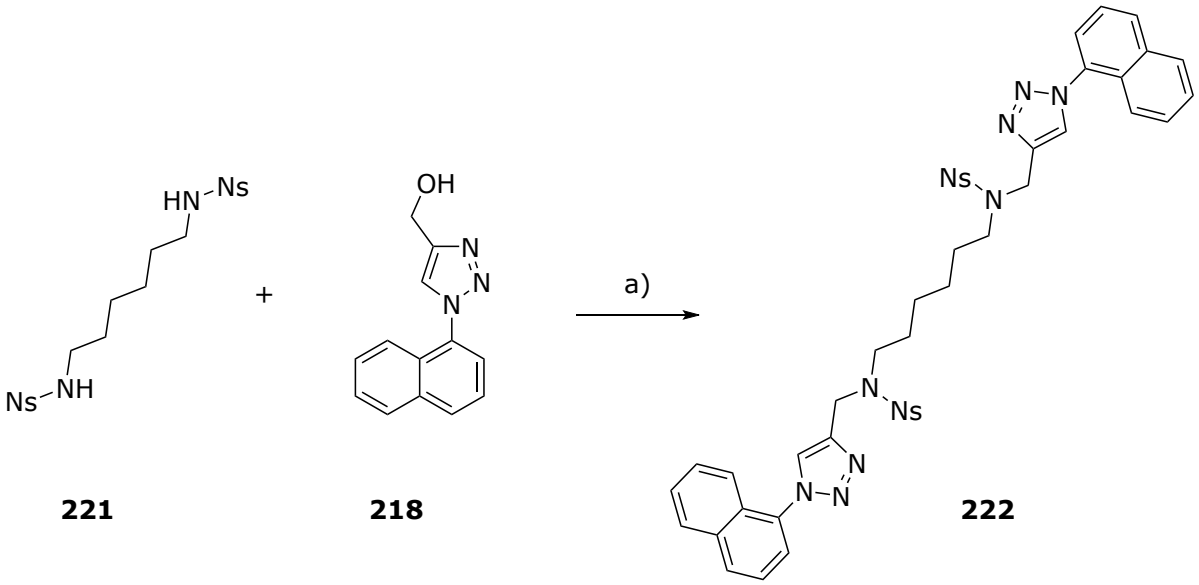

221 **218** **222**

Scheme 5.16 – Mitsunobu reaction of **221** to give **222**. a) Triphenylphosphine, DIAD, THF/toluene, 60°C, 2 d, 37%.

Following the success of this first reaction, the same method was applied to the diaminooctane **180** and dipropylene triamine **169** substrates (**Scheme 5.17**). Diamine **180** was treated with nosyl chloride and triethylamine under the same conditions used previously, and the reaction was complete after just 30 minutes. The *bis*-nosylated product **232** was obtained in excellent purity after aqueous workup alone.

By contrast, reaction of the triamine **169** was sluggish, requiring five days of stirring at 60°C for complete reaction. Analysis by TLC and LRMS during this time indicated the formation of two other species that were not isolated but showed molecular weights corresponding to the *mono* and *bis* nosylated intermediates. Given that the first two nosylation reactions occurred on a similar timeframe to the 'double' reaction of the diaminohexane and diaminooctane substrates, the extended reaction time is presumably due to the central, secondary amine reacting more slowly than the primary amines at each end of the chain. Once the reaction was complete, the black, viscous reaction mixture was washed with water and brine, and removal of solvent then yielded the pure *tris*-nosylated product **233** as a silver-brown foam.

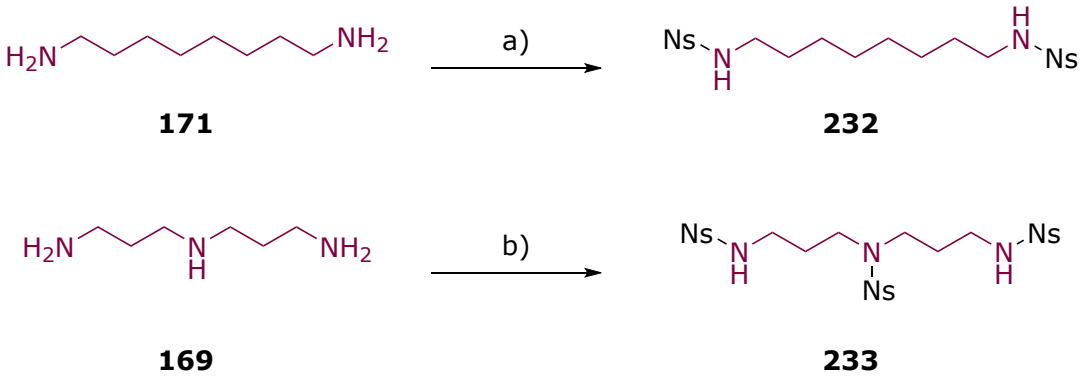

Scheme 5.17 – Nosylation of amines **171** and **169** to give **232** and **233**. a) Nosyl chloride, triethylamine, chloroform, rt, 30 min, 88%. b) 2-Nitrobenzenesulfonyl chloride, triethylamine, dichloromethane, 50°C, 6 d, 88%.

The two nosylated amines **232** and **233** were subjected to the same Mitsunobu conditions that had already been successful (**Scheme 5.18**). As before, diamine **232** was slow to react at both ends, with the singly functionalised product observed as the dominant species on TLC and LRMS after one day of stirring at 60°C. After reacting for a further 24 hours, the *bis* product **234** was clearly evident and the reaction was quenched, even while some of the *mono* product remained. While the triphenylphosphine oxide was easily removed by trituration with ether, separation of the DIAD hydrazine and the two functionalised products proved more challenging. The desired product **234** was eventually obtained in poor yields after multiple rounds of column chromatography, albeit sufficient for subsequent steps (and noting that improved purification would likely increase this yield significantly).

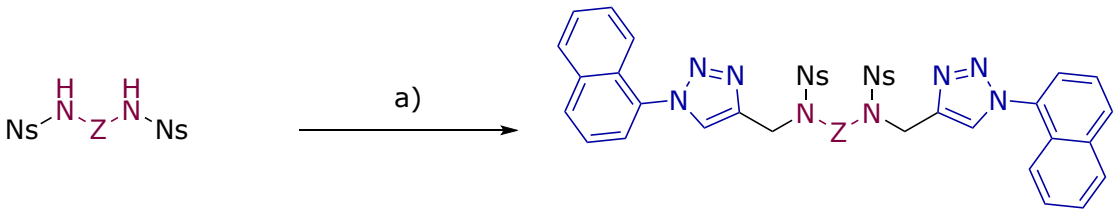

232 Z = $(CH_2)_8$
233 Z = $(CH_2)_3N(CH_2)_3$

234 *(30%)* Z = $(CH_2)_8$
235 *(75%)* Z = $(CH_2)_3N(CH_2)_3$

Scheme 5.18 – Reaction of amines **232** and **233** to give products **234** and **235**. a) Triphenylphosphine, DIAD, THF, rt, 2 d.

The alkylation of triamine **233** progressed similarly, with rapid conversion to a *mono* product and much slower reaction a second time. However, after two days, the reaction appeared complete, and purification was therefore more straightforward. A mixture of the desired *bis* product **235** and DIAD hydrazine was isolated using automated column chromatography with

methanol in DCM, and a second purification step using a gradient of acetone in DCM afforded the pure product **235** in reasonable yield (**Scheme 5.18**).

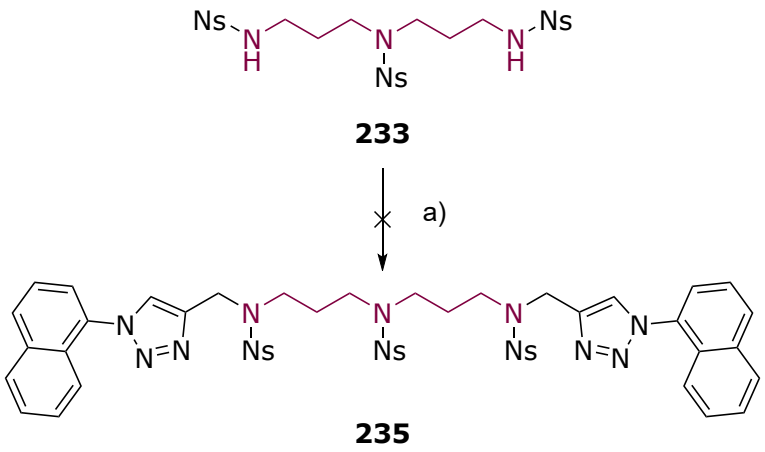

Scheme 5.19 – Attempted alternative Mitsunobu reaction to form **235**. a) Triphenylphosphine, DCAD, THF/toluene, rt, 2 d.

Purification of the products of these Mitsunobu reactions proved complicated, as it generally resulted in three unwanted byproducts: triphenylphosphine oxide **224**, DIAD hydrazine **230**, and the *mono* functionalised sulfonamide. In particular, the structural similarities of the hydrazine and functionalised amines made it difficult to isolate the desired products. An alternative diazocarboxylate reagent, di-*p*-chlorobenzyl azodicarboxylate (DCAD), has been used to circumvent this issue, as the aromatic hydrazine byproduct can be more easily separated by precipitation with DCM.[356] Additionally, DCAD is commercially available as a temperature-stable solid, in comparison to the commonly used liquid reagents DIAD and DEAD.[354]

Trisulfonamide **235** was selected as a test substrate and treated with DCAD under the same conditions used previously (**Scheme 5.19**). However, after two days of reaction, TLC analysis indicated that both starting material and the *mono*-alkylated product were still present alongside the desired product. The incomplete reaction was halted, and isolation of the *bis*-alkylated product was not attempted due to difficulties anticipated in separating the structurally similar products. Given the already sluggish pace of reaction, DIAD was deemed the more appropriate reagent despite the more complicated workup it necessitated.

5.4.2 Deprotection

Removal of the nosyl protecting group is generally straightforward, but requires the use of strong-smelling, toxic thiols, with 2-mercaptoethanol (**236**) and thiophenol (**237**) being well-known reagents (**Figure 5.10**). The nosyl ring undergoes nucleophilic substitution by the thiol, proceeding via a Meisenheimer complex, so stabilisation of the thiolate is desirable. Matoba and colleagues have described the use of various odorless thiols for nosyl group cleavage, finding that *p*-mercaptobenzoic acid and *o*-mercaptobenzoic acid (**238**), also known as thiosalicylic acid, were the two most effective deprotection agents.[357] While these reagents require slightly longer reaction and higher temperatures than the toxic thiols typically used due to the reduction in nucleophilicity caused by the inductive and steric effects of the carboxylic acid group, both thiols boasted high yields on all substrates tested.

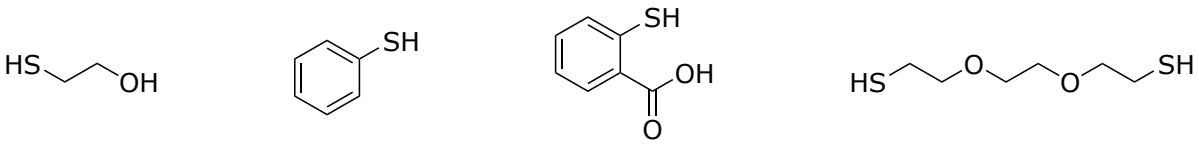

236 **237** **238** **239**

Figure 5.10 – Thiols used for deprotection of nosyl groups: 2-mercaptoethanol (**236**), thiophenol (**237**), thiosalicylic acid (**238**) and (2,2 -(ethylenedioxy)diethanethiol (**239**).

Of these two thiols, thiosalicyclic acid is more affordable and was therefore selected for the deprotection of diaminooctane derivative **234**. Unfortunately, after 24 hours of stirring at 60°C, yields were disappointing, with approximately half of the material being completely deprotected and the remainder only singly deprotected (**Scheme 5.20**). This may have been due to prior dimerization of the thiosalicylic acid, which produces the unreactive 2,2'-dithiosalicylic acid. Although the reagent can be purified by recrystallisation, it was decided that a more nucleophilic thiol would be trialled instead, and deprotection of diaminohexane analogue **197** was attempted with (2,2 -(ethylenedioxy)diethanethiol (**239**) (**Scheme 5.20**). In solid-phase peptide synthesis, this symmetric dithiol has been found to be as effective at nosyl deprotection as the considerably less pleasant 2-mercaptoethanol and thiophenol reagents.[358] However, after three days of stirring at 80°C, this reaction had not gone to completion, with starting material fully consumed but some proportion of the amine remaining singly protected. Despite this frustrating outcome, the deprotected amine **197** was obtained as a brown solid in

sufficient quantity for characterisation and testing, and was isolated in pure form as its TFA salt, a fine white powder, after HPLC purification.

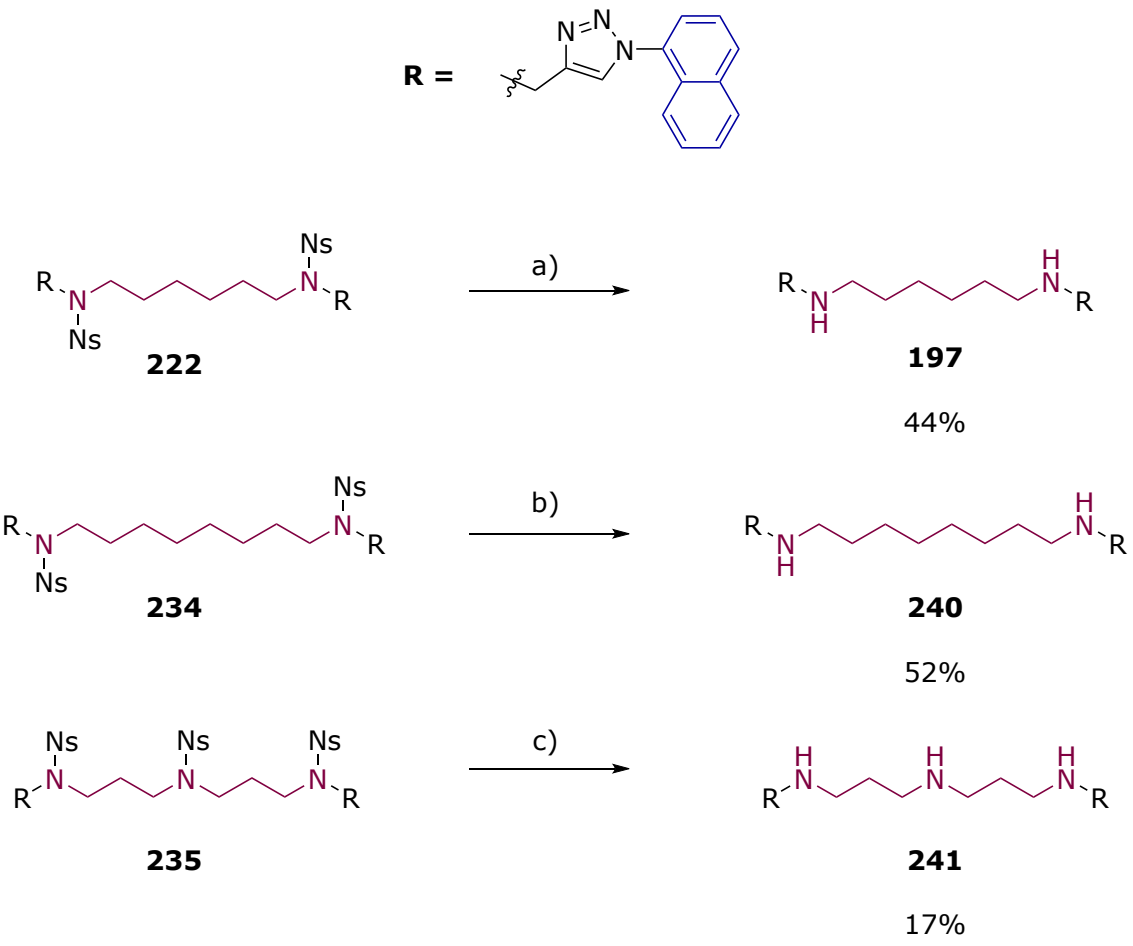

Scheme 5.20 – Deprotection of amines **222, 234** and **235**. a) Potassium carbonate, (2,2 -(ethylenedioxy)diethanethiol, DMF, 80°C, 3 d. b) Potassium carbonate, thiosalicylic acid, DMF, 60°C, 24 h. c) Potassium carbonate, thiophenol, DMF, 80°C, 18 h.

Given the indifferent results achieved with these safer reagents, the final deprotection of triamine derivative **235** was trialled with each of three different thiols: 2-mercaptoethanol, thiophenol, and the (2,2-(ethylenedioxy)diethanethiol used above. Surprisingly, all three produced mixtures of the singly and doubly deprotected amine that were difficult to separate. Eventually, however, treatment with thiophenol yielded the highest proportion of the fully-deprotected product, with reaction time notably shorter than that observed when using the diethanethiol (**Scheme 5.20**). The final product **241** was isolated using HPLC chromatography, with the TFA salt being obtained as a fine white powder.

5.5 Biological activity

Cell viability assays are the most common means of testing novel anti-tubercular agents. Prof Jamie Triccas and Dr Gayathri Nagalingam of the Centenary Institute and Charles Perkins Centre have developed a modified resazurin-based assay for the H37Rv cell line, a virulent strain of drug-susceptible TB widely used as a reference.[359] Antibacterial testing of the compounds described in this chapter was performed by Dr Maxwell Stevens of the Centenary Institute using this protocol. In this method, *Mtb* cells are incubated with the compound under investigation for 7 days, and fluorescence is read at 590 nm after excitation at 544 nm.

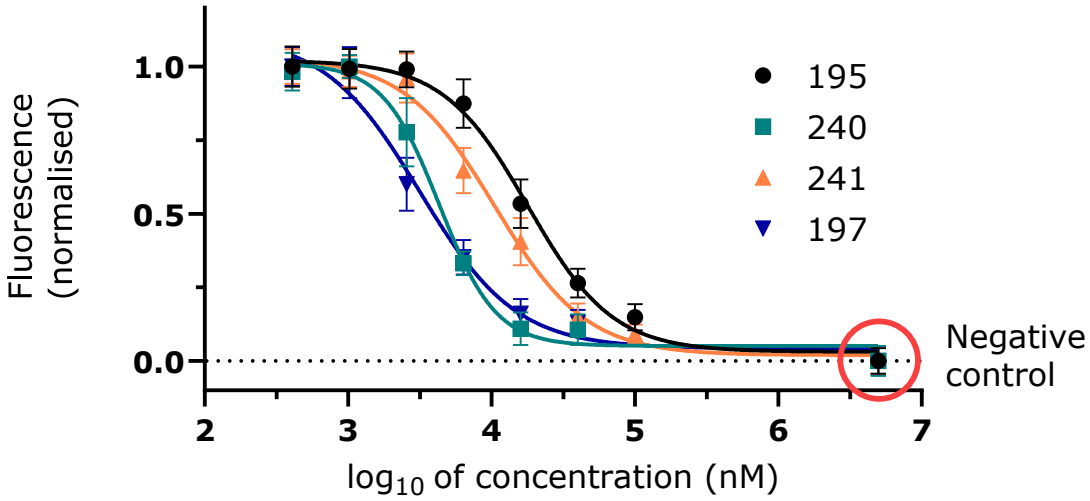

Figure 5.11 – Results for open cyclam compounds **195** (black), **197** (blue), **240** (green) and **241** (orange) tested at 3-fold dilutions from 250 to 0.114 µM. Error bars show 95% confidence interval.

Four of the six final compounds are themselves fluorescent at this wavelength, and results were therefore normalised against the media-only negative control (**Figure 5.11**). The remaining two compounds, **179** and **180**, were normalised internally (**Figure 5.12**). GraphPad Prism was used to fit sigmoidal curves using four-parameter logistic regression and IC_{50} values were calculated.[360,361]

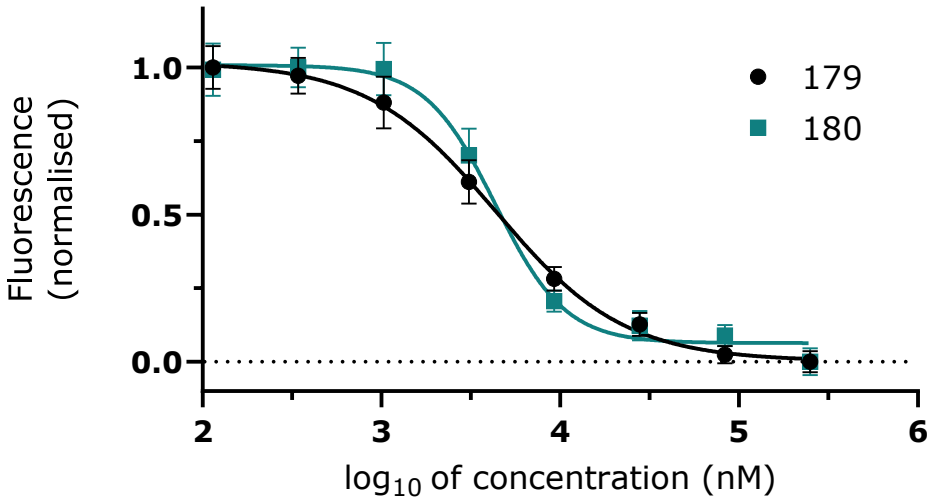

Figure 5.12 – Results for cyclam compounds **179** (black) and **180** (green), tested at 2.5-fold dilutions from 250 to 0.410 µM. Error bars show 95% confidence interval.

In previous assays and reports from the group, activity has been reported as 'MIC_{50} values'.[210,211] While this is the same term used for species-wide MIC_{50} values described in Chapter 3 and discussed further there, in the TB context, this term is used to refer to the lowest tested dose that reliably produced 50% or greater inhibition in a single strain. For clarity, this alternative meaning is referred to as a *minimum IC_{50}* in this work. The *minimum IC_{50}* values have been reported alongside the calculated IC_{50} values for greater ease of comparison (**Table 5.5**).

Table 5.5 – IC_{50} (µM) with 95% confidence interval and *minimum IC_{50}* (µM) of cyclam and open cyclam compounds against *Mtb*.

Compound	IC_{50}	95% CI	*Minimum IC_{50}*
179	4.37	3.49 – 5.49	9.26
180	4.33	3.62 – 5.27	9.26
195	18.0	14.4 – 22.7	40.0
197	3.16	1.92 – 4.39	6.40
240	4.33	3.60 – 5.19	6.40
241	10.6	8.32 – 13.4	40.0

The two cyclam-based compounds showed comparable activity to naphthyl analogues made previously (reported *minimum IC_{50}* = 6.25 µM),[211] with IC_{50} values of 4.37 µM and 4.33 µM reported for the adamantane and ferrocene derivatives **179** and **180** respectively (**Table 5.5**).

However, this didn't hold true for the diaminohexane scaffold, with the adamantane-coupled amine **195** being considerably less potent at 18.0 μM than the naphthyl analogue **197**, which had an IC_{50} of 3.16 μM.

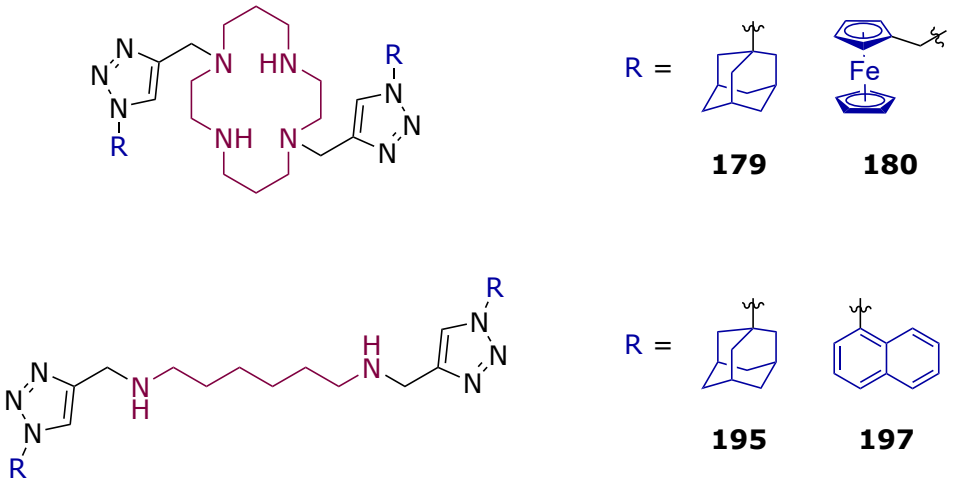

Figure 5.13 – Final compounds based on the cyclam (**179**, **180**) and diaminohexane (**195**, **197**) scaffolds.

Comparison to the open cyclam molecules previously synthesised is further complicated by the number of variables explored. Within the diamine cores, it appears that optimal chain length is between five and eight carbons, with potency dropping off significantly for the diaminobutane and diaminodecane analogues **210** and **213** (previously reported *minimum* IC_{50} = 25.0 and 12.5 μM respectively, **Table 5.6**).[213] Similarly, addition of a third pendant group causes a decrease in potency, as seen with **211** and **194**, both with *minimum* IC_{50} of 12.5 μM.[213] However, in the case of the dipropylene triamine, the opposite result is observed, with triply-substituted **41** (*minimum* IC_{50} = 0.78 μM, **Table 5.6**)[213] far exceeding the potency of the doubly-substituted **241** (IC_{50} = 10.6 μM).

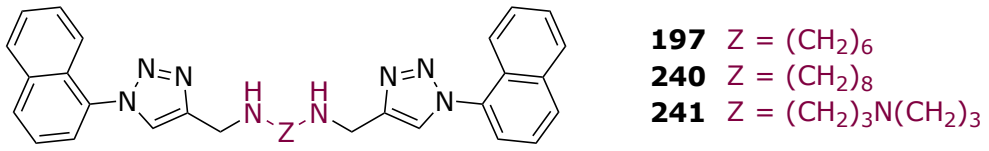

Figure 5.14 – Bis-naphthyl substituted final compounds **197**, **240** and **241**.

Overall, few conclusions can be drawn from the relatively small sample size of analogues explored, and further investigations are required to corroborate and fully elucidate the observations made here. Synthesising more triply-alkylated partners to complement the

doubly-alkylated amines already tested would probe whether these initial findings represent general trends, and should be exploited in future work. The doubly-substituted triamines **214** and **241** have an exposed secondary amine, making them less lipophilic than diamine partners, while **41** is also more hydrophobic overall than **241** by virtue of the additional naphthyl group present. These differences in lipophilicity may impact drug activity by altering compounds' pharmacodynamic profile.

Table 5.6 – Activity (*minimum* IC_{50} in μM) of all open cyclam analogues. Compounds made prior to this work were tested at a 2-fold dilution from 100 to 0.78 μM.[213] Compounds made in this work are shown in blue and tested at a 3-fold dilution from 250 to 0.114 μM.

Amines	Carbons	Chain length	Naphthalene-triazole pendants		
			2	**3**	**4**
2	2	**4**	**210** 25.0		
	4	**6**	**42** 3.13	**211** 12.5	
	6	**8**	**197** 6.40	**194** 12.5	
	8	**10**	**240** 6.40		**212** > 100
	10	**12**	**213** 12.5		
3	4	**7**	**214** 12.5		
	6	**9**	**241** 16.0	**41** 0.78	
4	7	**11**	**215** 6.25		

Interestingly, the eponymous 'open cyclam' compound **215**, the scaffold of which is closest to the macrocycle in chain length, shows very similar potency to its closest cyclam analogue **242** (**Figure 5.15**). Nonetheless, the simpler diamine compounds of a similar total chain length were slightly more active, and without closer comparison it is difficult to assess the effect of the number of amines. Synthesising and testing other variations of substituted tetramines may offer some insight into the relationship between number of amines and potency.

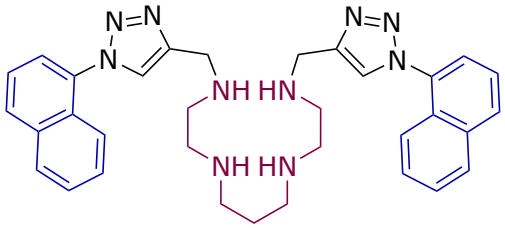

215

6.25 μM

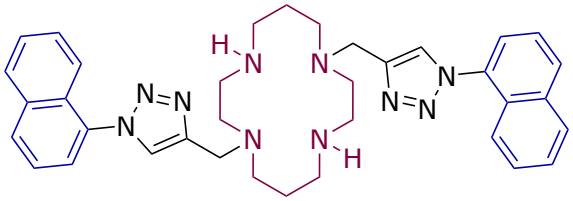

242

3.13 μM

Figure 5.15 – Structures of linear polyamine **215** and previous hit compound **242**, with *minimum* IC_{50} against *Mtb* H37Rv.[211,213]

Although prior studies have found that cyclam analogues with two pendants are more active than those with just one, it would be useful to confirm whether the same holds true for open cyclam derivatives, considering the differences in SAR already observed between the linear amines and their cyclic progenitors. Given that the *mono*-substituted compounds were commonly isolated as side products of the synthetic routes used here, it would require little extra work to isolate and test these *mono* compounds. Unsymmetrically functionalised polyamines with similar structures have been shown to possess various therapeutic effects, while *bis*-functionalised analogues have not been studied as extensively.[310,351,362] Comparing the activity of both *mono* and *bis*-alkylated polyamines with already established polyamine drug candidates could lead to a better understanding of how these open cyclam molecules exert their anti-tubercular effects.

5.6 Mechanisms of action of other polyamine therapeutics

In the field of TB research, these open cyclam polyamines bear most resemblance to the adamantane-conjugated drug candidate SQ109 (**28**), currently in phase 2 clinical trials. However, polyamine drug scaffolds have been investigated for other therapeutic applications, including as anticancer agents and as antibiotics targeting other bacteria.[351,362] Exploration has often started with one or more of the naturally occurring compounds putrescine **239**, spermidine **243**, and spermine **241** (**Figure 5.16**), with previous studies on open cyclam being no exception.

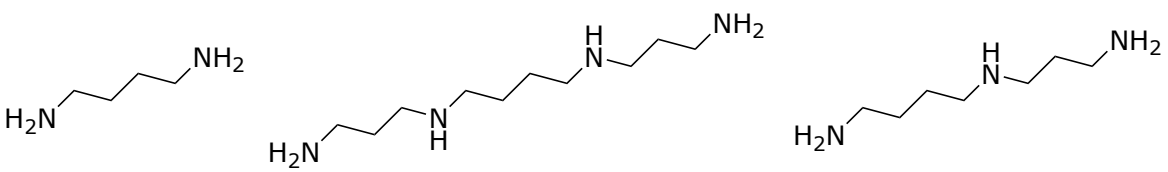

206 **209** **243**

Putrescine Spermine Spermidine

Figure 5.16 – Naturally occurring linear polyamines putrescine (**239**), spermidine (**243**) and spermine (**241**).

These linear polyamines are ubiquitous in living organisms and involved in various cellular processes required for cell homeostasis.[362] In some cases, therapeutic effect may be derived by hijacking or inhibiting the biosynthesis or transport pathways of these naturally occurring linear amines.[362] Alternatively, interactions between the positively charged protonated polyamines and negatively charged macromolecules like DNA, RNA and some proteins may be more relevant, particularly for anticancer agents.[310,351,362]

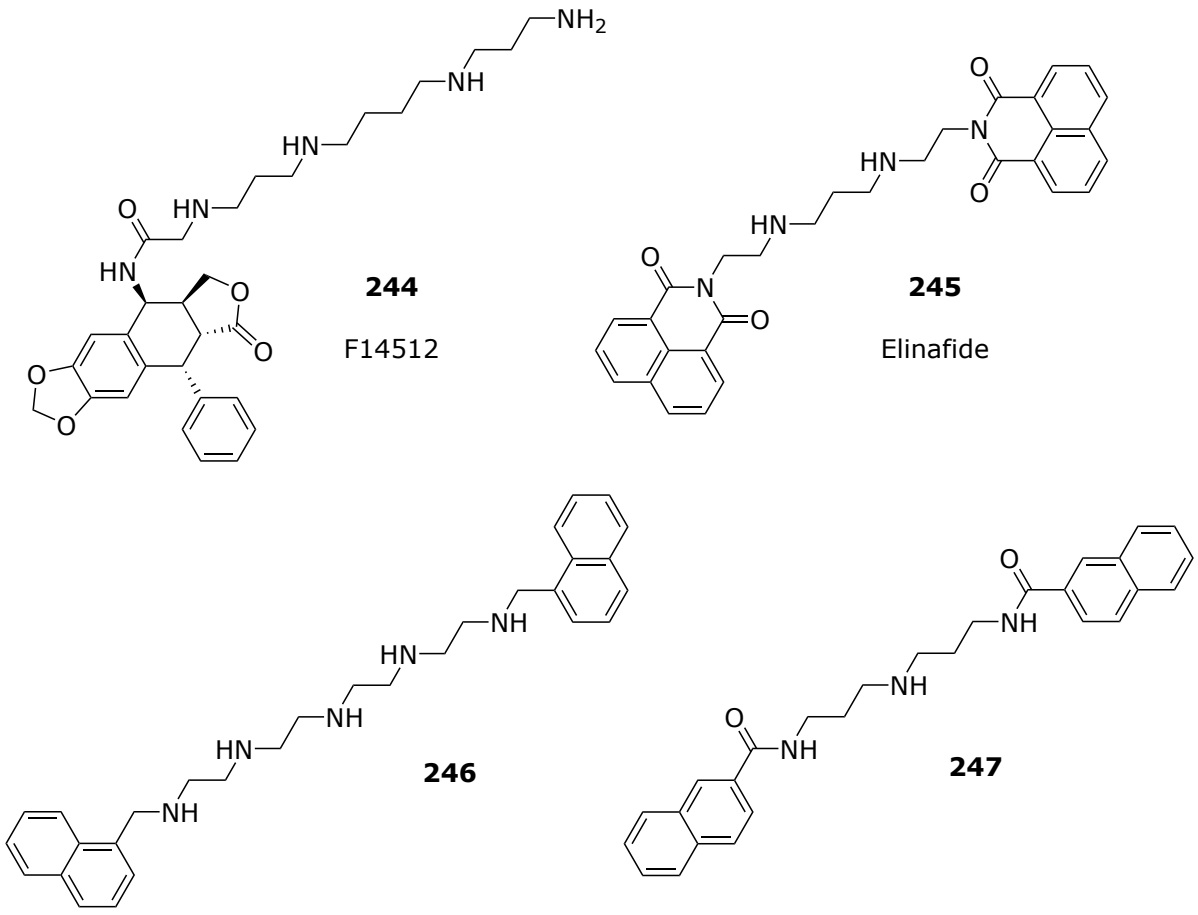

244 F14512

245 Elinafide

246 **247**

Figure 5.17 – Structures of functionalised linear polyamines **244** – **247** under investigation as anticancer agents.

Anticancer drug candidate F14512 (**244**) is a mono-functionalised tetramine that exerts its effect through increased senescence and apoptosis of cancer cells, both effects known to arise from DNA damage (**Figure 5.17**).[350] Similarly, the *bis*-naphthalimide-conjugated polyamine elinafide (**245**) and related compounds **246** and **247** are thought to suppress tumour growth and metastasis through DNA intercalation enabled by the naphthalimide pendant, as well as interactions with cell proliferation proteins.[363] Symmetric polyamines with naphthalene pendants, very similar in structure to the open cyclams investigated in the current study, have also shown anticancer activity, though research remains preliminary.[364,365]

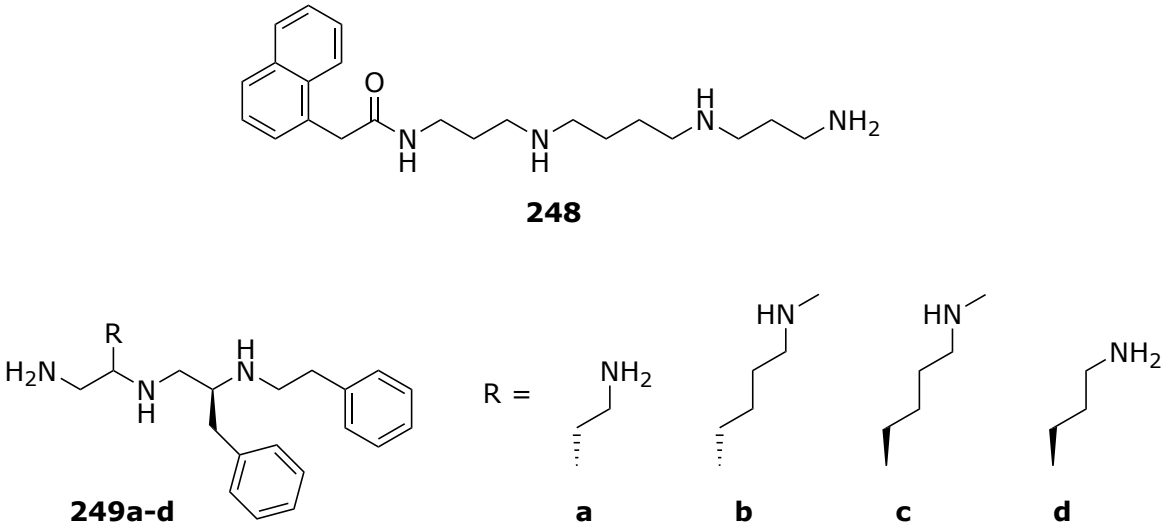

Figure 5.18 – Structures of functionalised linear polyamines **248** and **249a-d** investigated as potential antimicrobial agents.

In antibiotic drug discovery, polyamines have shown activity against both Gram-positive bacteria like *Staphyloccus aureus* and Gram-negative bacteria including *Pseudomonas aeruginosa* and *Escherichia coli*, but their mechanism of action is not well-understood.[351,362] Some polyamines appear to increase the antimicrobial activity of established antibiotics; for example, naphthylacetylspermine **248** improves the activity of erythromycin and novobiocin against *E. coli*, with the authors of the study proposing that the positively charged polyamines may alter membrane integrity by displacing other divalent cations from the membrane (**Figure 5.18**).[351] Various permutations of benzyl-conjugated polyamines **249a-d** have also been found to potentiate the bactericidal effect of chloramphenicol and tetracycline against *P. aeruginosa*, *S. aureus* and *A. baumannii*.[366] In this case, non-specific depolarisation of membrane potential

was not observed and their adjuvant effect has been attributed to direct inhibition of efflux pumps, with ethidium bromide assays supporting this hypothesis.[366]

Elucidating a mechanism for the antitubercular action of the open cyclam series and parent cyclam analogues will require new avenues of investigation beyond SAR studies. For instance, cell localisation assays would narrow down possible modes of action by indicating where these compounds accumulate,[367,368] and synergistic studies might reveal the biological pathways are involved.[369] Another powerful, though time consuming and expensive, approach to target identification is to induce resistance, and then execute genomic or proteomic sequencing.[370,371] Treating the organism with sub-lethal doses enables bacteria to develop resistance mechanisms specific to the drug being used, and identifying the mutations responsible for resistance can indicate the protein(s) or pathway(s) on which the drug acts.[274] Ultimately, continued exploration of this series will require a multidisciplinary approach that combines further SAR analysis with a strong focus on target identification through biological assays.

6 Conclusions and future work

6.1 Breaking Good and MycetOS

In this work, a synthetic chemistry citizen science project was developed and implemented successfully at both the undergraduate and secondary school level to produce novel compounds for a drug discovery program. Through the Breaking Good program, students synthesised dozens of 2-AT analogues to be tested for activity against *M. mycetomatis*, while additional compounds were synthesised in the research laboratory or sourced from international collaborators as part of the MycetOS open source drug discovery consortium. Evaluating the educational and social impact of this program falls outside the scope of this study (and is being investigated by others in the group), but initial analysis has shown positive outcomes for the students and teachers involved. Having already evolved significantly from its inception in 2016, Breaking Good has significant potential to develop further in several different directions. These include: shifting towards a new series of targets for the treatment of mycetoma or another disease; continuing to work with educators to develop robust workshops with greater alignment to curriculum; or trialling workshops that focus on another aspect of drug discovery such as biological testing.

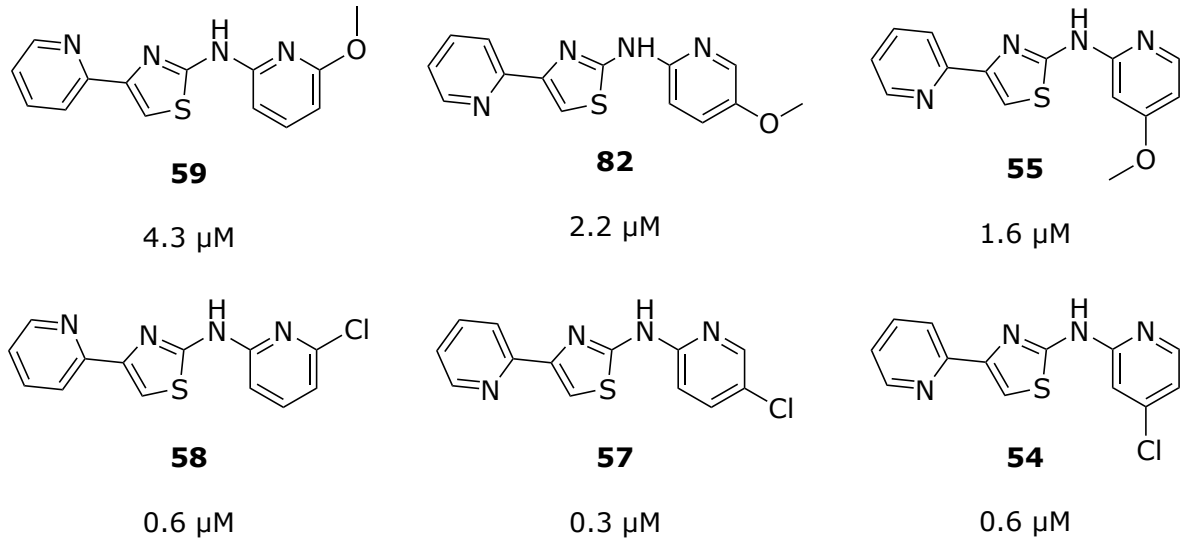

Figure 6.1 – Representative sample of 2-AT compounds with IC_{50} against *M. mycetomatis*.

The 2-AT analogues were subjected to *in vitro* testing, including determination of MIC_{50} and standard evaluation of potency for SAR analysis. Investigation of the C-2 and C-4 aryl rings

revealed that the 2-pyridyl moiety is crucial for activity at both positions. A small number of substituents on this ring were trialled, with chloride and phenyl substituents showing moderate and promising activity respectively. At the C-2 position, a broad range of substitutions on the 2-pyridine ring showed a slight preference for electron-donating groups in the 5′ position or electron-withdrawing groups in the 4′ position, but observed differences in activity were small (**Figure 6.1**).

Eighteen of the most promising compounds were assessed for toxicity in the *G. mellonella* larval model, with the majority well tolerated at a concentration of 20 µM. Efficacy assays were completed for nine of these compounds, revealing that lead compound **11** and the unsubstituted **121** were the only analogues that improved larval survival relative to a PBS control.

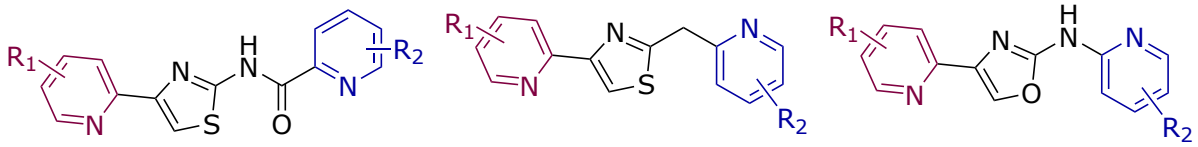

Figure 6.2 – Potential future targets for MycetOS Series 2.

Future SAR studies would most usefully focus on an increased range of synthetic variation, such as swapping the amine linker for an amide or methylene group, or altering the thiazole ring to an oxazole (**Figure 6.2**). The analogues synthesised so far also offer ample opportunity to extend the most active molecules *via* coupling reactions, such as Buchwald-Hartwig amination or Suzuki couplings combining halide-decorated analogues with appropriate amine or boronic acid/ boronate partners.

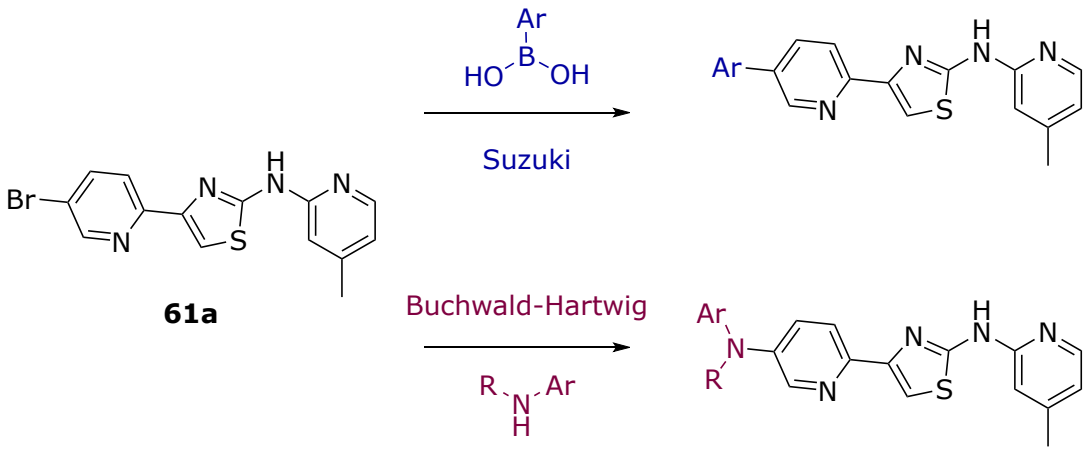

Scheme 6.1 – Examples of potential coupling reactions with brominated analogue **61a**.

Ultimately, a deeper understanding of the activity of 2-aminothiazoles against *M. mycetomatis* will require further biological evaluation to elucidate the mechanism(s) of action. Synergistic studies, molecular modelling and gene knockout experiments would offer insight into the effect of 2-ATs on identified proteins of interest, including those involved in the ergosterol biosynthesis pathway targeted by azole-based antifungals.[122,269,270,274] Ethidium bromide assays, commonly used to study efflux pump activity, may clarify whether the 2-ATs impact the transport of antimicrobial compounds out of the cell, while thallium flux studies could reveal any effect on calcium-activated potassium channels.[147,276] In combination, these studies would furnish a comprehensive overview of 2-aminothiazoles' potential mechanisms of action.

6.2 Activity of 2-aminothiazoles as antibacterials

A significant portion of the library of 2-ATs developed for the treatment of eumycetoma was also cross-screened *in vitro* against three causative organisms of actinomycetoma, *A. madurae*, *N. brasiliensis* and *S. somaliensis*, and a small subset was additionally screened against *Mtb*. All seven compounds screened against *Mtb* showed excellent potency, consistent with broader findings in the literature, but the small sample size precluded any significant SAR analysis. Activity against the Gram-positive bacteria was more varied, with eight of the 72 analogues showing inhibition of all three bacterial species at the lowest concentration tested. Ideally, the complete library would be tested against all three species at concentrations of 100, 25 and 2 μM, to enable more accurate analysis of SAR trends. Biological assays akin to those suggested earlier (**Section 6.1**) to evaluate mechanism of action in fungi should also illuminate the mode of action of these compounds as antibacterial agents, with ethidium bromide assays and molecular modelling being most crucial.

A resazurin-based assay was also developed to improve the quality and efficiency of antibacterial testing for mycetoma. The protocol allows rapid visual analysis by colour as well as providing quantitative spectrophotometric data that can be used to more precisely quantify potency. This assay was trialled with *A. madurae* and *N. brasiliensis* strains. It could now be broadened to include other relevant bacterial species or used to determine the specific activity of the most promising 2-AT compounds described above. Optimising the protocol with a greater number of strains and different antibiotics would also improve the robustness and overall usefulness of this assay.

6.3 Polyamines for tuberculosis

This work aimed to synthesise a series of polyamine analogues (built on cyclam and 'open cyclam' amine cores) to explore the effects of the polyamine backbone and pendant groups on anti-tubercular activity. The cyclam-based targets **179** and **180** were successfully synthesised and tested against *Mtb* in a resazurin-based fluorescence assay, and shown to have antimycobacterial activity comparable to previously described analogues with naphthyl and naphthalimide pendants, returning IC_{50} values of 4.37 and 4.33 µM respectively. The synthetic procedure used to prepare the cyclam compounds was modified slightly to produce the open cyclam analogues **195** and **196**, although only **195** was obtained in sufficient yield and purity for biological testing, and it proved to have disappointing activity with an IC_{50} of just 18.0 µM (**Figure 6.3**).

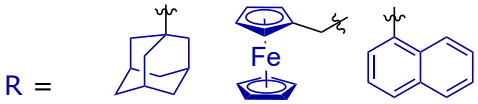

Cyclam	**179**	**180**	**242**
Minimum IC_{50}:	9.26	9.26	6.25
Actual IC_{50}:	4.37	4.33	-
Diaminohexane	**195**	**196**	**197**
Minimum IC_{50}:	40.0	-	6.40
Actual IC_{50}:	18.0	-	3.16

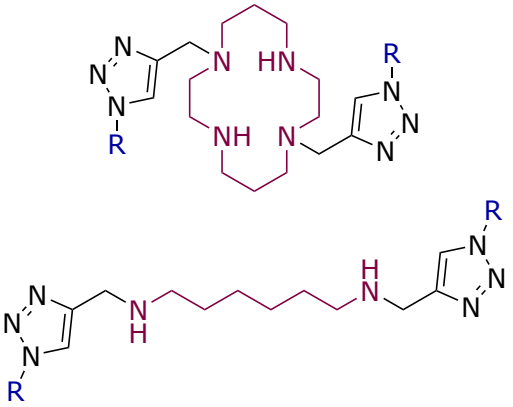

Figure 6.3 – Activity (µM) of cyclam and diaminohexane analogues against *Mtb* H37Rv.

Alternative routes to the naphthyl-decorated open cyclam targets were investigated, with alkylation of unprotected and protected linear amines both yielding unsatisfactory results. The desired compounds were ultimately synthesised using nosyl groups to simultaneously activate and protect the terminal amines from overalkylation in a Mitsunobu reaction, with the protecting groups then readily cleaved by addition of a thiol. This route worked reliably with the three different substrates tested, and the relatively low yields obtained could likely be improved by optimisation of the purification process at each step.

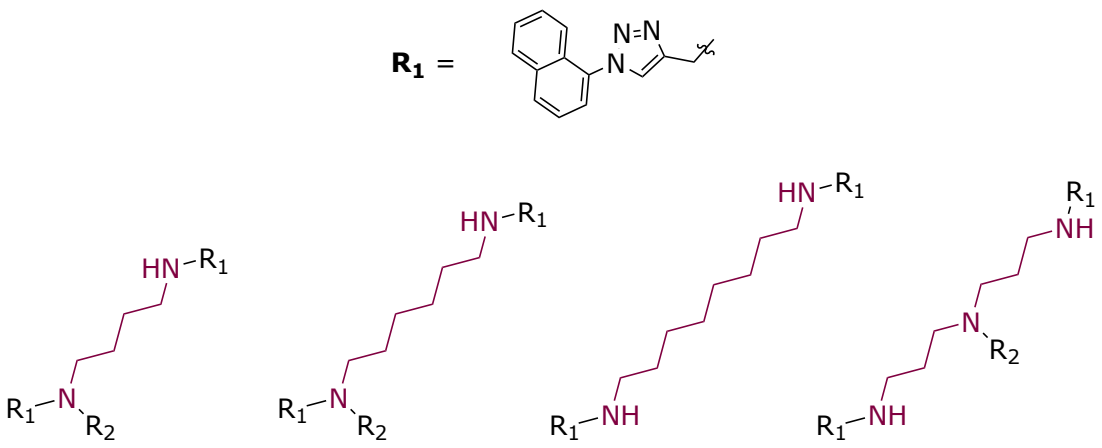

R_2 = H:	**42**, 3.13	**197**, 6.4	**240**, 6.4	**241**, 16
R_2 = R_1:	**211**, 12.5	**194**, 12.5	-	**41**, 3.13

Figure 6.4 – Activity (*minimum* IC_{50} in μM) of selected open cyclam analogues against *Mtb* H37Rv.

The slow reaction times observed for the key alkylation step could also be exploited to enable access to the *mono*- and *tris*-alkylated analogues, thus offering additional opportunity for comparison across the different open cyclams. Currently, chain length is the most well-studied factor, with diamines **42** (C_4 chain between *N*s), **197** (C_6 chain) and **240** (C_8 chain) being the most potent doubly alkylated compounds, while activity is diminished for the *bis*-alkylated diaminoethane and diaminodecane analogues. Interestingly, although addition of a third pendant group reduces potency in the diamines (compare, for example, **211** and **194**, to **42** and **197** respectively in **Figure 6.4**), the triply-alkylated dipropylene triamine **41** remains one of the most potent compounds tested to date, while the corresponding *bis*-alkylated analogue **241** showed only modest activity. Future studies should thus prioritise synthesis of the *tris*-alkylated analogues of the diaminooctane and diethylene triamine derivatives to further investigate these trends. Overall, there is considerable scope to synthesise additional analogues to further develop this preliminary SAR analysis, alongside the suite of biological experiments focused on target identification discussed in greater detail in the final section of Chapter 5.

7 Experimental

7.1 General materials and instrumentation - Chemistry

Anhydrous solvents were dried over 3 Å or 4 Å molecular sieves. Commercially available reagents and solvents were purchased from Sigma-Aldrich, Merck, Alfa Aesar, Ajax Finechem, Combi-Blocks, Ambeed or Arctom and used without purification unless otherwise specified. Automated flash column chromatography was performed on a Biotage Isolera One using refillable cartridges obtained from either Biotage or Velocity Scientific Solutions packed with silica gel 60 (0.040–0.063 nm) obtained from ChemSupply. TLC was performed on Merck silica gel 60 F254 pre-coated aluminium plates (0.2 mm) and visualised with UV (254 and 365 nm) or staining with potassium permanganate, ninhydrin or vanillin solutions.

Melting points were recorded on an Optimelt 100 automated melting point apparatus and are uncorrected. Infrared spectra were recorded on a Bruker ALPHA FT-IR spectrophotometer (ZnSe or diamond ATR) using OPUS software. Low resolution mass spectrometry was recorded on a Bruker Amazon SL mass spectrometer using electrospray ionisation (ESI) or atmospheric-pressure chemical ionization (APCI). LRMS measurements are reported with observed mass-to-charge ratios and their assignment. High resolution mass spectrometry was performed on a Bruker 7 T Fourier-transform ion cyclotron resonance using ESI or APCI. Analytical HPLC was used to determine the purity of the compounds tested for biological activity and only compounds with > 95% purity were screened.

Nuclear magnetic resonance (NMR) spectroscopy on small molecules was carried out on a Bruker AVANCE 300, Bruker AVANCE III 400 or Bruker NEO 500 instrument. Spectra obtained were processed using MestReNova. Deuterated solvents were obtained from either Cambridge Isotope Laboratories, Novachem or Sigma-Aldrich. Spectra were referenced to either TMS or residual solvent peaks.

7.2 General materials and instrumentation - Biology

Fungal strains (MM55, MM14, S01, I1, I3, Parijs1, Peru72012, AL1, CBS247.48) were obtained from the library maintained by the van de Sande group at Erasmus Medical Center (Rotterdam, the Netherlands), and include samples isolated from patients at the Mycetoma

Research Center in Sudan, Hospital General de Mexico Dr Eduardo Liceaga in Mexico, and Westerdijk Fungal Biodiversity Institute in the Netherlands. Morphology and sequencing of the ITS regions was used to identify the isolates to the species level. Fungi were cultured on Saboraud agar (Difco Laboratories, Becton Dickinson).

Sonication was performed at 10 μM using a Soniprep 160 (Beun de Ronde, the Netherlands). RPMI 1640 media was supplemented with *L*-glutamine (0.3 g/L; Gibco, ThermoFisher, Bleiswijk, the Netherlands) in MOPS buffer (3-(*N*-morpholino)propanesulfonic acid, 20 mM; Sigma-Aldrich, Zwijndrecht, the Netherlands). Fungal suspensions grown for *in vivo* testing were additionally supplemented with chloramphenicol (100 mg/L; Oxoid, Basingstroke, United Kingdom), with mycelia separated by vacuum filtration (Nalgene, Abcoude, the Netherlands). Mycelia suspensions were otherwise separated by centrifugation (Rotana 460R, Hettich Zentrifuger, Germany) and transmission was measured at 660 nm (Novaspec II; Pharmacia Biotech, Uppsala, Sweden).

G. mellonella larvae were selected based on size and activity, with the average volume of each larva being 0.5 mL. Initial or single injections were administered to the bottom left pro-leg using an insulin 29G U-100 needle (BD diagnostics, Sparsk, USA) with any repeated injections being administered a different pro-leg, starting with the bottom right.

Experimentally produced 2-aminothiazole compounds were dissolved in sterile DMSO (10 mM; Merck, Darmstadt, Germany) and diluted with PBS (pH 7.4) as required. Amphotericin B Fungizone, Bristol Myers Squibb, Utrecht, The Netherlands), itraconazole (Janssen Pharmaceutica, Beerse, Belgium), resazurin (Sigma-Aldrich, R7017) and amikacin hydrate (Sigma-Aldrich, A3650) were purchased as solids and dissolved in sterile distilled water to the appropriate concentrations. MTS (Promega Benelux BV, G3581) was purchased as a ready-to-use reagent.

Bacterial strains (*Actinomadura madurae* DSM43067T, *Nocardia brasiliensis* DSM43758T and *Streptomyces somaliensis* DSM40738T) were purchased from the German Collection of Microorganisms and Cell Cultures GmbH (DSMZ). Staphylococcus aureus ATCC 29213 was included as a quality control. All strains were molecularly identified to the species level by 16S rRNA sequencing. Bacteria were cultured on blood agar (tryptic soy agar with 5% sheep blood; Difco Laboratories, Becton Dickinson) and suspensions were prepared according to CLSI

guidelines in Mueller-Hinton II broth (Sigma-Aldrich, Zwijndrecht, the Netherlands), adjusted to a McFarland standard of 0.5 (equivalent to 1.5 × 108 CFU/mL).

Fungal and bacterial suspensions were grown in round-bottomed 96-well plates (Corning® Costar 3799; Fisher Scientific, Breda, the Netherlands) and transferred to flat-bottomed 96-well plates for reading (Corning® Costar 3439454; Fisher Scientific, Breda, the Netherlands). Absorbance was read at various wavelengths using an Epoch 2 plate reader (BioTek, United States).

7.3 General chemical procedures

General Synthetic Procedure A: Preparation of thiourea intermediates from amines.

Benzoyl chloride (1.3 mL, 11 mmol, 1.1 equiv.) was added to a solution of potassium thiocyanate (1.17 g, 12 mmol, 1.2 equiv.) in acetone (50 mL), heated to reflux and stirred for 15–30 minutes. The aniline or aminopyridine (10 mmol, 1.0 equiv.) was added and the reaction mixture was heated and stirred at reflux for 1–2 hours until the aniline starting material was no longer evident on TLC. The mixture was poured onto ice water, and the resulting precipitate was collected by filtration and washed with water and isopropanol. The crude benzoyl thiourea intermediate was then added to NaOH (2.5 M aq., 10 mL) and heated to 80°C for 15–30 minutes, until completely dissolved. After cooling, the mixture was poured onto ice water and adjusted to pH 7 using HCl (1.0 M aq.) and sodium carbonate solution (sat. aq.). The precipitate was collected by vacuum filtration and washed with water. The thiourea compounds were generally obtained in excellent yield (65–90% over two steps) and were used without further purification. When made by undergraduate students, the thiourea compounds were identified by TLC analysis only and not further characterised.

General Synthetic Procedure B: NBS bromination of ketones.

N-Bromosuccinimide (2.15 g, 12 mmol, 1.2 equiv.) and (*p*-toluenesulfonic acid (2.6 g, 15 mmol, 1.5 equiv.) were added to a solution of the ketone (10 mmol, 1.0 equiv.) in acetonitrile (300 mL). The reaction was stirred at 85°C for 24 hours or until TLC analysis indicated consumption of the ketone starting material. The acetonitrile was removed by rotary evaporation and the crude material was redissolved in dichloromethane (200 mL), and washed

with water (150 mL) and brine (150 mL). The organic layer was then dried over magnesium sulfate, filtered, and the filtrate concentrated under reduced pressure to yield the desired bromoacetophenone (35–95%). The bromoacetophenone intermediates were used without further purification.

General Synthetic Procedure C: Hantzsch synthesis of 2-aminothiazoles.

The thiourea (10 mmol, 1.0 equiv.) was combined with the bromoacetophenone (10 mmol, 1.0 equiv.) in ethanol (50 mL) and heated and stirred at reflux for 1–3 hours or until TLC analysis indicated completion. The mixture was then cooled to room temperature, poured over ice water and adjusted to pH 8 with sodium carbonate solution (sat. aq.). The resulting precipitate was collected by vacuum filtration and washed with water and hexanes. Many of the products were obtained in excellent purity (> 95% by HPLC) and good yield (60–95%). Otherwise, analogues were purified using flash column chromatography (90:9:1 CH_2Cl_2:MeOH:10% $NH_4OH_{(aq)}$ on silica gel).

General Synthetic Procedure D: Copper(I)-catalysed azide-alkyne cycloaddition.

For a 0.1–4.0 mmol scale

Procedure adapted from Spain et al.[211] Alkyne (1.0 equiv.), azide (2.2 equiv.), sodium ascorbate (0.5 equiv.) and $CuSO_4 \cdot 5H_2O$ (0.2 equiv.) were dissolved in THF:water (1:1, 5–10 mL) and the mixture was stirred at room temperature under a nitrogen gas atmosphere for 18–48 hours until TLC analysis indicated consumption of alkyne starting material. The mixture was concentrated under reduced pressure, diluted with ammonium chloride solution (sat. aq., 15 mL) and extracted with dichloromethane (3 × 20 mL). The combined organic layers were dried over magnesium sulfate, filtered, and the filtrate concentrated under reduced pressure to yield the crude product.

General Synthetic Procedure E: HCl-mediated Boc deprotection.

For a 0.1–4.0 mmol scale

Procedure adapted from Spain *et al.*[211] The Boc-protected compound was dissolved in 1,4-dioxane (3 mL) and water (1 mL) and cooled to 0°C. HCl solution (4.0 M in dioxane, 1.00 mL, 4.00 mmol) was added and the reaction was warmed to room temperature and stirred for 1 hour, when TLC analysis indicated complete conversion. The mixture was concentrated under reduced pressure to give the crude product as the HCl salt.

7.4 Compounds described in chapters 2 and 3

Yields are not provided for compounds made by students, as samples were often amalgamated prior to purification and characterisation.

*Indicates compound made by undergraduate students.

**Indicates compound made by high school students.

7.4.1 Intermediates

2-Bromo-6-(bromoacetyl)pyridine (62a)

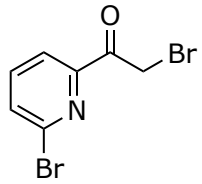

Prepared according to **General Synthetic Procedure B** from 1-(6-bromopyridin-2-yl)ethan-1-one (2.01 g, 10.0 mmol) and obtained as a dark brown solid (2.75 g, 95%). **LRMS** (APCI+) *m/z* 278.98, 279.95, 281.93 $[M+H]^+$. **HRMS** (APCI+) *m/z* calcd for $C_7H_5Br_2NO$, 277.88107, found 277.88103 (Error = 0.14 ppm). **^{1}H NMR** (300 MHz, Chloroform-*d*) δ 8.01 – 7.95 (m, 1H), 7.74 – 7.59 (m, 2H), 4.75 (d, *J* = 0.9 Hz, 2H). **^{13}C NMR** (75 MHz, Chloroform-*d*) δ 191.07, 152.01, 141.50, 139.47, 132.63, 121.59, 32.16. **FTIR** (ATR) ν_{max}/cm^{-1}: 3081, 3006, 2946, 1715, 1554, 1426, 1397, 1385, 1307, 1196, 1155, 1127, 998, 985, 814, 794, 663, 624.

5-Bromo-2-(bromoacetyl)pyridine (62b)

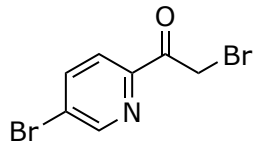

Prepared according to **General Synthetic Procedure B** from 1-(5-bromopyridin-2-yl)ethan-1-one (1.02 g, 5.09 mmol) and obtained as a dark brown solid (1.53 g, 94%). **LRMS** (APCI+) *m/z* 277.98, 279.96, 281.95 $[M+H]^+$. **HRMS** (APCI+) *m/z* calcd for $C_7H_5Br_2NO$, 277.88107, found 277.88101 (error = 0.22). **^{1}H NMR** (300 MHz, Chloroform-*d*) δ 8.71 (dq, *J* = 3.2, 1.2 Hz, 1H), 8.06 – 7.97 (m, 1H), 8.03 – 7.84 (m, 1H), 7.48 (d, *J* = 1.1 Hz, 1H), 4.75 (d, *J* = 1.1 Hz, 2H). The spectroscopic data were in agreement with the literature.[372]

4-Chloro-2-(bromoacetyl)pyridine (62c)

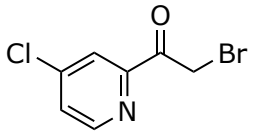

Prepared according to **General Synthetic Procedure B** from 1-(4-chloropyridin-2-yl)ethan-1-one (2.06 g, 13.2 mmol) and obtained as a dark brown solid (2.37 g, 77%). **LRMS** (APCI+) *m/z* 233.99, 236.01 $[M+H]^+$. **HRMS** (APCI+) *m/z* calcd for $C_7H_5BrClNO$, 233.93158, found 233.93153 (error = 0.21). **^{1}H NMR** (300 MHz, Chloroform-*d*) δ 8.54 (d, *J* = 5.2 Hz, 1H), 8.03 (d, *J* = 2.0 Hz, 1H), 7.52 – 7.46 (m, 1H), 4.76 (d, *J* = 0.9 Hz, 2H). The spectroscopic data were in agreement with the literature.[373]

2-Acetyl-5-phenylpyridine (63d)

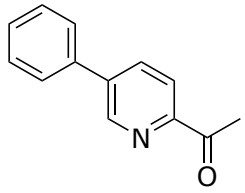

Prepared according to a procedure by Huo *et al.*[221] Phenylboronic acid (778 mg, 6.38 mmol, 1.2 equiv.), 2-acetyl-5-bromopyridine (1.060 g, 5.29 mmol, 1.0 equiv.), potassium carbonate (1.4619 g, 10.58 mmol, 2.0 equiv.) and $Pd(PPh_3)_4$ (31.8 mg, 0.028 mmol, cat.) were combined

in an oxygen-free environment and dissolved in toluene (25 mL) and water (5 mL). The resulting mixture was stirred at 105°C for 22 hours until TLC analysis indicated completion. The mixture was then diluted with additional water (40 mL) and extracted with ethyl acetate (3 × 60 mL), and the combined organic extracts were washed with brine and dried over magnesium sulfate. Concentrating the extracts under reduced pressure gave the crude product as a lumpy orange-white solid, which was dissolved in petroleum benzine and filtered through a silica plug to give the final product in quantitative yield. **LRMS** (ESI+) *m/z* 219.97 $[M+Na]^+$. **^{1}H NMR** (300 MHz, Chloroform-*d*) δ 8.93 – 8.86 (m, 1H), 8.11 (d, J = 8.1 Hz, 1H), 8.04 – 7.95 (m, 1H), 7.62 (dd, J = 7.9, 1.7 Hz, 2H), 7.56 – 7.38 (m, 3H), 2.75 (d, J = 1.0 Hz, 3H). **FTIR** (ATR) ν_{max}/cm^{-1}: 3068, 3001, 2961, 1688, 1582, 1369, 1276, 1232, 1025, 958, 855, 768, 743, 691, 592, 543. The spectroscopic data were in agreement with the literature.[221]

2-(Bromoacetyl)-5-phenylpyridine (62d)

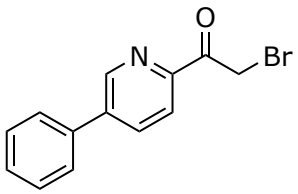

Prepared according to **General Synthetic Procedure B** from **63d** (2.78 g, 14.1 mmol) and obtained as a dark brown solid (3.02 g, 77%). **LRMS** (APCI+) *m/z* 276.06, 277.88 $[M+H]^+$. **FTIR** (ATR) ν_{max}/cm^{-1}: 3081, 3006, 2946, 1714, 1553, 1426, 1397, 1386, 1307, 1196, 1155, 1128, 1075, 998, 985, 794, 722, 663, 624. Used without further purification.

Methyl quinoline-2-carboxylate (66)

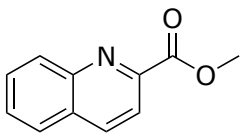

Prepared according to a procedure from Abramova *et al.*[223] Quinoline-2-carboxylic acid (22 mg, 3.01 mmol) was dissolved in methanol (5 mL) and sulfuric acid (98%, 0.15 mL) was added. The mixture was stirred at 65°C for 22 hours then neutralised with sodium bicarbonate solution (sat. aq., 15 mL), upon which a white precipitate formed. The mixture was extracted with

chloroform (4 × 5 mL) and the combined organic extracts were dried over magnesium sulfate, filtered, and the filtrate concentrated under reduced pressure to yield the crude product as a brittle beige solid. This was triturated with chloroform to give the final product as a white crystalline solid (462 mg, 82%). **LRMS** (ESI+) *m/z* 188.16 $[M+H]^+$, 210.12 $[M+Na]^+$. **^{1}H NMR** (300 MHz, Chloroform-*d*) δ 8.29 (dd, J = 8.5, 1.9 Hz, 2H), 8.18 (d, J = 8.5 Hz, 1H), 7.86 (dd, J = 8.2, 1.5 Hz, 1H), 7.77 (ddd, J = 8.4, 6.8, 1.5 Hz, 1H), 7.63 (ddd, J = 8.1, 6.9, 1.2 Hz, 1H), 4.07 (s, 3H). **FTIR** (ATR) ν_{max}/cm^{-1}: 3066, 3001, 2951, 2853, 1709, 1448, 1316, 1195, 1140, 1105, 972, 850, 771, 625, 592, 475. The spectroscopic data were in agreement with the literature.[223,374]

Ethyl 3-oxo-3-(quinolin-2-yl)propanoate (67)

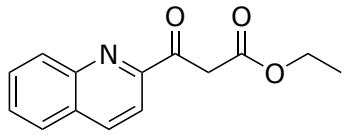

Prepared according to a procedure by Chan and Ciufolini.[222] Potassium *tert*-butoxide (1.097 g, 9.78 mmol, 1.2 equiv.) was added to a solution of **66** (1.5143 g, 8.09 mmol, 1.0 equiv.) in ethyl acetate (30 mL) and the reaction mixture was stirred for 1 hour at room temperature. Once TLC analysis indicated both absence of starting material and formation of a less polar product, the mixture was neutralised with water (100 mL) and extracted with ethyl acetate (3 × 100 mL). The combined organic extracts were washed with brine, dried over magnesium sulfate and concentrated under reduced pressure to yield a crude product with a mass of 1.7 g. This was purified by automated column chromatography (ethyl acetate in hexanes) to give the final product as an off-white solid (898.9 mg, 46%). **LRMS** (ESI+) *m/z* 244.14 $[M+H]^+$, 266.12 $[M+Na]^+$, 509.05 $[2M+Na]^+$. **^{1}H NMR** (300 MHz, Chloroform-*d*) δ 8.30 – 8.16 (m, 2H), 8.10 (d, *J* = 8.5 Hz, 1H), 7.78 (dd, *J* = 8.2, 1.5 Hz, 1H), 7.70 (ddd, *J* = 8.5, 6.9, 1.5 Hz, 1H), 7.55 (ddd, *J* = 8.1, 6.9, 1.2 Hz, 1H), 4.49 (q, *J* = 7.1 Hz, 2H), 1.42 (t, *J* = 7.1 Hz, 3H). **FTIR** (ATR) ν_{max}/cm^{-1}: 2980, 2938, 1736, 1701, 1367, 1320, 1264, 1241, 1195, 1148, 1115, 1034, 840, 753, 732. The spectroscopic data were in agreement with the literature.[222]

2-Acetyl-quinoline (63e)

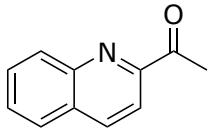

Prepared according to a procedure by Chan and Ciufolini.[222] **67** (149 mg, 0.61 mmol) was dissolved in 1,4-dioxane (3 mL). HCl (1.0 M aq., 2.5 mL, 2.5 mmol) was added. The reaction mixture was stirred at 100°C for 18 hours until TLC analysis indicated consumption of starting material, then the volatiles were removed by rotary evaporation and the crude material was redissolved in water. This solution was extracted with ethyl acetate (3 × 10 mL), washed with sodium bicarbonate solution (sat. aq., 20 mL), then dried over magnesium sulfate, filtered, and the filtrate concentrated under reduced pressure to yield a dark brown solid (79.6 mg, 76%), which was used without further purification. **LRMS** (ESI+) *m/z* 172.15 $[M+H]^+$, 194.13 $[M+Na]^+$. **^{1}H NMR** (300 MHz, Chloroform-*d*) δ 8.21 (dd, J = 14.3, 8.5 Hz, 2H), 8.11 (d, J = 8.5 Hz, 1H), 7.85 (dd, J = 8.1, 1.5 Hz, 1H), 7.77 (ddd, J = 8.5, 6.9, 1.5 Hz, 1H), 7.63 (ddd, J = 8.1, 6.8, 1.2 Hz, 1H), 2.86 (s, 3H). **FTIR** (ATR) ν_{max}/cm^{-1}: 3367, 3058, 3003, 1688, 1540, 1456, 1354,1276, 1234, 1208, 1122, 940, 879, 836, 790, 767, 692, 657, 614, 575, 482. The spectroscopic data were in agreement with the literature.[223,375]

3-(Bromoacetyl)isoquinoline (62e)

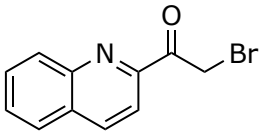

Prepared according to **General Synthetic Procedure B** from **63e** (811 mg, 4.74 mmol) and obtained as a brown gum (418 mg, 35%). **LRMS** (APCI+) *m/z* 250.06, 252.08 $[M+H]^+$. **HRMS** (APCI+) *m/z* calcd for $C_{11}H_8BrNO$, 249.98620, found 249.98620 (Error = 0.00 ppm). **^{1}H NMR** (300 MHz, Chloroform-*d*) δ 8.34 – 8.08 (m, 3H), 7.94 – 7.74 (m, 2H), 7.66 (ddd, *J* = 9.6, 8.2, 6.9 Hz, 1H), 5.07 (d, *J* = 1.1 Hz, 2H). The spectroscopic data were in agreement with the literature.[376]

5-Chloro-2-(bromoacetyl)pyridine (129b)

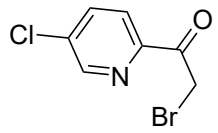

LRMS (APCI+) *m/z* 233.99, 235.99 $[M+H]^+$. **HRMS** (APCI+) *m/z* calcd for $C_7H_6BrClNO$, 233.93158, found 233.93160 (error = 0.1 ppm). **^{1}H NMR** (300 MHz, Chloroform-*d*) δ 8.64 (t, *J* = 2.4 Hz, 1H), 8.10 (dd, *J* = 24.2, 8.4 Hz, 1H), 7.87 (ddd, *J* = 11.2, 8.4, 2.4 Hz, 1H), 4.80 (s, 2H). The spectroscopic data were in agreement with the literature.[376]

7.4.2 Thiourea intermediates

All following compounds made according to **General Synthetic Procedure B** unless otherwise indicated.

1-(4-Fluorophenyl)thiourea (93)

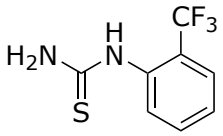

LRMS (ESI-) *m/z* 219.02 $[M-H]^-$.**^{1}H NMR** (500 MHz, DMSO-d_6) δ 9.25 (s, 1H), 7.72 (dd, J = 8.0, 1.5 Hz, 1H), 7.68 (td, J = 7.7, 1.5 Hz, 1H), 7.57 (d, J = 8.0 Hz, 1H), 7.50 – 7.45 (m, 1H). **^{13}C NMR** (126 **MHz, DMSO-d_6)** δ 183.57, 137.41, 133.16, 132.36, 127.47, 127.28, 126.49 (q), 125.91 (q), 125.11, 122.93, 120.76. **^{19}FNMR** (471 **MHz, DMSO-d_6)** δ -59.56. *White Beige powder (527 mg, 94% over two steps).* Spectroscopic data were in agreement with the literature.[377]

1-(3-Fluorophenyl)thiourea (94)

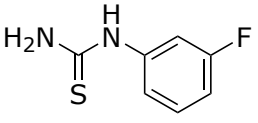

LRMS (ESI+) *m/z* 193.07 $[M+Na]^+$. **^{1}H NMR** (500 MHz, DMSO-d_6) δ 9.86 (s, 1H), 7.56 (dt, J = 11.5, 2.3 Hz, 1H), 7.35 (td, J = 8.2, 6.8 Hz, 1H), 7.18 (ddd, J = 8.1, 2.0, 0.9 Hz, 1H), 6.93 (tdd, J = 8.5, 2.6, 0.9 Hz, 1H). **^{13}C NMR** (126 MHz, DMSO-d_6) δ 181.12, 162.84, 160.91,

141.12 (d), 130.14 (d), 118.17 (d), 110.53 (d), 109.21 (d). **^{19}F NMR** (471 MHz, DMSO-d_6) δ -112.31. *White powder (4.89 g, 63% over two steps).* Spectroscopic data were in agreement with the literature.[378]

1-(2-fluorophenyl)thiourea (95)

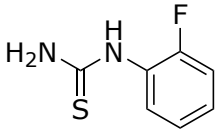

LRMS (ESI+) *m/z* 193.09 [M+Na]$^+$. **^{1}H NMR** (500 MHz, DMSO-d6) δ 9.38 (s, 1H), 7.72 – 7.65 (m, 1H), 7.28 – 7.19 (m, 2H), 7.19 – 7.13 (m, 1H). **^{13}C NMR** (126 MHz, DMSO-d_6) δ 182.12, 156.85, 154.90, 127.92, 126.97 (d), 126.70 (d), 124.15 (d) 115.77 (d). **^{19}F NMR** (471 MHz, DMSO) δ -123.27. *White precipitate (1.20 g, 84% over two steps).*

1-(5-Methoxypyridin-2-yl)-thiourea (96)

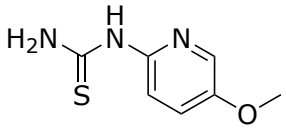

LRMS (ESI+) *m/z* 206.11 [M+Na]$^+$,184.13 [M+H]$^+$. **^{1}H NMR** (500 MHz, DMSO-d_6) δ 10.41 (s, 1H), 10.33 – 10.29 (m, 1H), 8.68 (s, 1H), 7.95 (d, J = 3.0 Hz, 1H), 7.46 (dd, J = 9.1, 3.1 Hz, 1H), 7.16 (d, J = 9.1 Hz, 1H), 3.79 (s, 3H). **^{13}C NMR** (126 **MHz, DMSO-d_6)** δ 180.33, 151.62, 148.11, 131.61, 126.35, 114.07, 56.35. *White powder (5.28 g, 83% over two steps).* Spectroscopic data were in agreement with the literature.[265] [265]

1-(5-Fluoropyridin-2-yl)-thiourea (97)

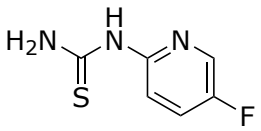

LRMS (ESI-) *m/z* 170.05 [M-H]$^-$. **^{1}H NMR** (500 MHz, DMSO-d_6) δ 10.62 (s, 1H), 10.19 (s, 1H), 8.86 (s, 1H), 8.24 (d, J = 2.9 Hz, 1H), 7.77 (tq, J = 9.0, 3.3, 2.6 Hz, 1H), 7.25 (dd, J = 9.2, 3.9 Hz, 1H). **^{13}C NMR** (126 **MHz, DMSO-d_6)** δ 180.69, 156.33, 154.37, 150.64 (d), 133.46 (d), 127.40 (d), 114.68 (d). **^{19}F NMR** (471 **MHz, DMSO-d_6)** δ -135.09. **FTIR** (ATR) ν_{max}/cm^{-1}: 3197, 3107, 3032, 1595, 1536, 1491, 1442, 1396, 1337, 1317, 1280, 1223, 1121, 1062, 1014, 822, 727, 650, 640, 620. *White powder (378 mg, 75% over two steps).*

1-(6-Fluoropyridin-2-yl)-thiourea (98)

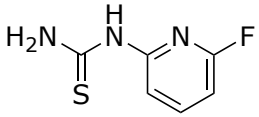

LRMS (ESI-) *m/z* 170.03 [M-H]$^-$. **^{1}H NMR** (300 MHz, DMSO-d_6) δ 10.77 (s, 1H), 9.55 (s, 1H), 8.99 (s, 1H), 7.95 (q, J = 8.2 Hz, 1H), 7.14 (dd, J = 8.1, 1.9 Hz, 1H), 6.81 (dd, J = 8.0, 2.0 Hz, 1H). **^{13}C NMR** (126 MHz, DMSO-d_6) δ 180.86, 161.84, 159.94, 151.95 (d), 144.39 (t), 109.96 (d), 102.16 (d). *Beige powder (6.13 g, 80% over two steps).* Spectroscopic data were in agreement with the literature.[379]

1-(3-Chloropyridin-2-yl)-thiourea (104)

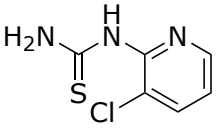

^{1}H NMR (400 MHz, DMSO-d_6) δ 10.15 (s, 1H), 9.28 (s, 1H), 8.64 (s, 1H), 8.27 (dd, *J* = 4.9, 1.6 Hz, 1H), 8.03 (dd, *J* = 8.0, 1.6 Hz, 1H), 7.18 (dd, *J* = 7.9, 4.9 Hz, 1H). **^{13}C NMR** (101 MHz, DMSO-d_6) δ 180.61, 148.55, 145.69, 139.47, 120.29, 117.48. **FTIR** (ATR) ν_{max}/cm^{-1}: 3070, 2834, 2666, 2604, 2554, 1678, 1600, 1582, 1452, 1420, 1323, 1289, 1178, 1126, 1071, 1026, 932, 704, 683, 665, 544.

1-(3-Methoxypyridin-2-yl)-thiourea (105)

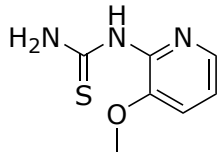

FTIR (ATR) ν_{max}/cm^{-1}: 3322, 3251, 3098, 2460, 2397, 2347, 2301, 1604, 1584, 1568, 1495, 1437, 1361, 1314, 1272, 1212, 1133, 1074, 1055, 1040, 775, 722, 652, 606.

1-(3,5-Dichloropyridin-2-yl)thiourea (106)

^{1}H NMR (500 MHz, DMSO-d_6) δ 9.65 (s, 1H), 9.25 (s, 1H), 8.81 (s, 1H), 7.95 (d, J = 7.6 Hz, 1H), 7.51 (t, J = 7.6 Hz, 1H). **^{13}C NMR** (101 MHz, DMSO-d_6) δ 180.50, 147.32, 144.15, 138.81, 125.47, 119.03.

1-(5,6-Dichloropyridin-2-yl)thiourea (107)

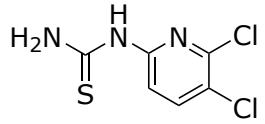

^{1}H NMR (300 MHz, DMSO-d_6) δ 10.88 (s, 1H), 9.44 (s, 1H), 9.11 (s, 1H), 8.06 (d, J = 8.7 Hz, 1H), 7.27 (d, J = 8.7 Hz, 1H). **^{13}C NMR** (126 MHz, DMSO-d_6) δ 180.76, 151.56, 144.10, 142.01, 121.94, 113.77.

1-(4,6-Dichloropyridin-2-yl)thiourea (108)

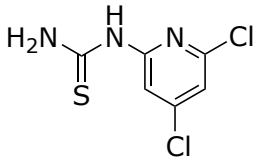

^{1}H NMR (500 MHz, DMSO-d_6) δ 10.84 (s, 1H), 9.53 (s, 1H), 9.16 (s, 1H), 7.41 (d, J = 1.5 Hz, 1H), 7.34 (d, J = 1.6 Hz, 1H). **^{13}C NMR** (126 MHz, DMSO-d_6) δ 180.95, 153.78, 148.20, 146.45, 117.76, 111.41.

1-(4,5-Dichloropyridin-2-yl)thiourea (109)

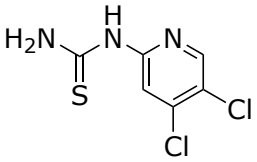

LRMS (ESI-) *m/z* 219.91, 221.96 223.89 [M-H]$^-$. **^{1}H NMR** (500 MHz, DMSO-d_6) δ 10.72 (d, J = 4.9 Hz, 1H), 10.00 (s, 1H), 9.08 (s, 1H), 8.48 – 8.43 (m, 1H), 7.47 (t, J = 3.0 Hz, 1H). **^{13}C NMR** (101 MHz, DMSO-d_6) δ 180.94, 152.97, 146.92, 142.69, 122.80, 114.06.

1-(6-Methylpyridin-2-yl)-thiourea (127b)

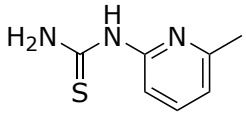

LRMS (ESI+) *m/z* 190.10 [M+Na]$^+$, (ESI-) *m/z* 166.02 [M-H]$^-$. **^{1}H NMR** (500 MHz, DMSO-d_6) δ 10.66 (s, 1H), 10.44 (s, 1H), 8.83 (s, 1H), 7.67 – 7.61 (m, 1H), 6.97 (d, J = 8.2 Hz, 1H), 6.89 (d, J = 7.4 Hz, 1H), 2.39 (s, 3H). **^{13}C NMR** (126 MHz, DMSO-d_6) δ 181.10, 155.36, 153.62, 139.55, 117.54, 110.03, 40.50, 40.34, 40.17, 40.00, 39.84, 39.67, 39.50, 24.15. *White precipitate (576 mg, 59% over two steps).* Spectroscopic data were in agreement with the literature.[265]

1-(6-Bromopyridin-2-yl)-thiourea (130b)

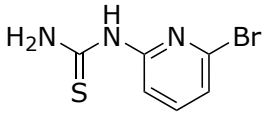

LRMS (ESI-) *m/z* 229.86, 231.86 $[M-H]^-$, 267.84 $[M+Cl]^-$. **HRMS** (ESI-) *m/z* calcd for $C_6H_5BrN_3S$, 229.93930, found 229.93930 (error < 0.1 ppm). **^{1}H NMR** (500 MHz, DMSO-d_6) δ 10.75 (s, 1H), 9.70 (s, 1H), 9.04 (s, 1H), 7.72 (t, *J* = 7.9 Hz, 1H), 7.29 (d, *J* = 7.6 Hz, 1H), 7.23 (d, *J* = 8.2 Hz, 1H). **^{13}C NMR** (126 MHz, DMSO-d_6) δ 180.93, 153.67, 142.06, 137.35, 121.89, 112.09. **FTIR** (ATR) ν_{max}/cm^{-1}: 3294, 3214, 3149, 3068, 3025, 1581, 1528, 1428, 1312, 1242, 1158, 1128, 1081, 1057, 987, 902, 829, 777, 678, 568, 481. *Beige powder (375 mg, 59% over two steps).*

1-(3-bromopyridin-2-yl)thiourea (131b)

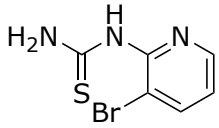

LRMS (ESI+) *m/z* 255.94 $[M+Na]^+$, 486.78 $[2M+Na]^+$. **HRMS** (ESI-) *m/z* calcd for $C_6H_5BrN_3S$, 229.93930, found 229.93934 (error = 0.2 ppm). **^{1}H NMR** (500 MHz, DMSO-d_6) δ 10.17 (s, 1H), 9.30 (s, 1H), 8.53 (s, 1H), 8.30 (dd, *J* = 4.9, 1.5 Hz, 1H), 8.18 (dd, *J* = 7.9, 1.6 Hz, 1H), 7.10 (dd, *J* = 7.9, 4.9 Hz, 1H). **^{13}C NMR** (126 MHz, DMSO) δ 180.53, 149.34, 146.31, 142.84, 120.67, 107.47. **FTIR** (ATR) ν_{max}/cm^{-1}: 3388, 3306, 3215, 3151, 3066, 1582, 1511, 1408, 1309, 1126, 1065, 1018, 833, 795, 723, 622, 581, 475, 408. *Pale brown powder (388 mg, 68% over two steps).*

1-(6-(Trifluoromethyl)pyridin-2-yl)thiourea (132b)

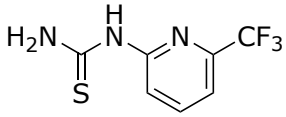

LRMS (ESI-) *m/z* 219.97 $[M-H]^-$. **HRMS** (ESI-) *m/z* calcd for $C_7H_5F_3N_3S$, 220.01618, found 220.1619 (error < 0.1 ppm). **^{1}H NMR** (500 MHz, DMSO-d_6) δ 10.92 (s, 1H), 9.92 (s, 1H), 9.14 (s, 1H), 8.04 (t, *J* = 8.0 Hz, 1H), 7.54 (d, *J* = 7.5 Hz, 1H), 7.50 (d, *J* = 8.5 Hz, 1H). **^{13}C NMR** (126 MHz, DMSO-d_6) δ 181.35, 153.76, 143.21 (q, *J* = 34.2 Hz), 141.24, 121.66 (q, *J* = 273.7 Hz), 117.24, 115.15 (d, *J* = 2.9 Hz). **^{19}F NMR** (471 MHz, DMSO-d_6) δ -67.24. **FTIR** (ATR) ν_{max}/cm^{-1}: 3290, 3225, 3162, 3112, 3053, 1603, 1545, 1454, 1420, 1354, 1257, 1123, 1083, 1061, 994, 934, 832, 804, 703, 664, 602, 483, 429. *Pale powder (372 mg, 61% over two steps).* The spectroscopic data were in agreement with the literature.[380]

1-(5-(Trifluoromethyl)pyridin-2-yl)thiourea (133b)

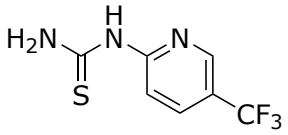

LRMS (ESI-) *m/z* 220.00 $[M-H]^-$, 255.90 $[M+Cl]^-$. **HRMS** (ESI-) *m/z* calcd for $C_7H_5F_3N_3S$, 220.01618, found 220.01626 (error = 0.4 ppm). **^{1}H NMR** (500 MHz, DMSO-d_6) δ 10.90 (s, 1H), 10.40 – 10.36 (m, 1H), 9.15 (d, *J* = 3.8 Hz, 1H), 8.62 (dt, *J* = 2.2, 1.0 Hz, 1H), 8.13 (dd, *J* = 8.8, 2.6 Hz, 1H), 7.33 (d, *J* = 8.8 Hz, 1H). **^{13}C NMR** (126 MHz, DMSO-d_6) δ 181.29, 156.30, 144.46 (d, *J* = 4.5 Hz), 136.43 (d, *J* = 3.2 Hz), 124.30 (q, *J* = 271.3 Hz), 119.33 (q, *J* = 32.8 Hz), 113.27. **^{19}F NMR** (471 MHz, DMSO-d_6) δ -60.36. *Beige powder (192 mg, 38% over two steps).* The spectroscopic data were in agreement with the literature.[265]

1-(3-Fluoropyridin-2-yl)-thiourea (134b)

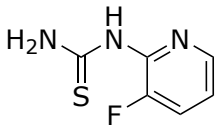

LRMS (ESI+) *m/z* 194.01 $[M+H]^+$, 364.93 $[2M+Na]^+$. **HRMS** (ESI-) *m/z* calcd for $C_6H_5FN_3S$, 170.01937, found 170.01953 (error < 0.1 ppm). **^{1}H NMR** (500 MHz, DMSO-d_6) δ 10.06 (s, 1H), 9.66 (s, 1H), 8.99 (s, 1H), 8.12 (dd, *J* = 5.0, 1.4 Hz, 1H), 7.77 (ddd, *J* = 10.8, 8.1, 1.4 Hz, 1H), 7.18 (ddd, *J* = 8.3, 4.9, 3.6 Hz, 1H). **^{13}C NMR** (126 MHz, DMSO-d_6) δ 181.01, 148.03,

145.97, 142.42, 124.82, 119.99. **^{19}F NMR** (471 MHz, DMSO-d_6) δ -131.49. **FTIR** (ATR) ν_{max}/cm^{-1}: 2242, 2120, 1607, 1522, 1446, 1333, 1262, 1232, 1171, 1100, 1053, 1023, 997, 850, 826, 798, 738, 614, 540, 515. *Beige powder (529 mg, 74% over two steps).*

7.4.3 Final compounds

All following compounds made according to **General Synthetic Procedure C** unless otherwise indicated.

***N*-(4-Methylpyridin-2-yl)-4-(pyridin-2-yl)thiazol-2-amine (11)**

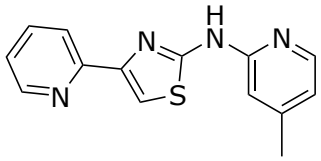

LRMS (ESI+) *m/z* 269.08 $[M+H]^+$, 291.06 $[M+Na]^+$, 559.11 $[2M+Na]^+$. **HRMS** (ESI+) *m/z* calcd for $C_{14}H_{13}N_4S$, 269.08554, found 269.08558 (error = 0.1 ppm). **^{1}H NMR** (500 MHz, DMSO-d_6) δ 11.36 (s, 1H), 8.59 (ddd, *J* = 4.8, 1.8, 0.9 Hz, 1H), 8.18 (d, *J* = 5.2 Hz, 1H), 7.97 (dt, *J* = 7.8, 1.1 Hz, 1H), 7.87 (td, *J* = 7.7, 1.8 Hz, 1H), 7.64 (s, 1H), 7.30 (ddd, *J* = 7.4, 4.7, 1.2 Hz, 1H), 6.91 (q, *J* = 1.1 Hz, 1H), 6.79 (dd, *J* = 5.2, 1.4 Hz, 1H), 2.29 (s, 3H). **^{13}C NMR** (126 MHz, DMSO-d_6) δ 159.96, 152.49, 151.95, 149.41, 148.86, 148.54, 146.10, 137.11, 122.47, 119.83, 117.52, 110.61, 109.50, 20.71.

***N*-(4-Methylpyridin-2-yl)-4-(pyridin-4-yl)thiazol-2-amine (48) ***

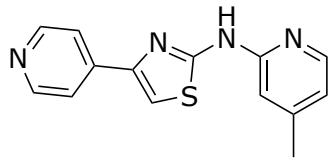

HPLC purity: 100%. **LRMS** (ESI+) *m/z* 269.06 $[M+H]^+$, 559.07 $[2M+Na]^+$. **HRMS** (ESI+) *m/z* calcd for $C_{14}H_{13}N_4S$, 269.08554, found 269.08558 (error = 0.1 ppm)**. ^{1}H NMR** (400 MHz, DMSO-d_6) δ 11.31 (s, 1H), 8.57 (d, *J* = 5.0 Hz, 2H), 8.15 (d, *J* = 5.1 Hz, 1H), 7.83 (d, *J* = 5.0 Hz, 2H), 7.71 (s, 1H), 6.88 (s, 1H), 6.80 (d, *J* = 5.2 Hz, 1H), 2.27 (s, 3H). **^{13}C NMR** (101 MHz, DMSO-d_6) δ 160.70, 152.16, 150.41, 149.41, 146.54, 146.47, 142.02, 120.47, 118.31, 111.14,

110.77, 21.10. **FTIR** (ATR) ν_{max}/cm^{-1}: 3147, 2914, 1600, 1544, 1440, 1386, 1300, 750, 445. *Beige powder*.

N*-(4-Methylpyridin-2-yl)-4-(pyridin-3-yl)thiazol-2-amine (49)

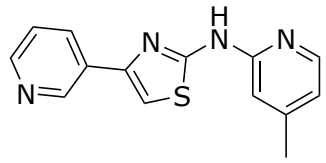

HPLC purity: 100%. **LRMS** (ESI+) *m/z* 269.17 $[M+H]^+$, 291.07 $[M+Na]^+$. **HRMS** (ESI+) *m/z* calcd for $C_{14}H_{12}N_4NaS$, 291.06749, found 291.06741 (error = 0.26 ppm). **^{1}H NMR** (400 MHz, DMSO-d_6) δ 11.28 (s, 1H), 9.08 (dd, *J* = 2.3, 0.9 Hz, 1H), 8.47 (dd, *J* = 4.8, 1.6 Hz, 1H), 8.22 (dt, *J* = 8.0, 1.9 Hz, 1H), 8.15 (d, *J* = 5.2 Hz, 1H), 7.53 (s, 1H), 7.45 (ddd, *J* = 8.0, 4.8, 0.9 Hz, 1H), 6.88 (q, *J* = 1.1 Hz, 1H), 6.79 (dd, *J* = 5.4, 1.5 Hz, 1H), 2.27 (s, 3H). **^{13}C NMR** (101 MHz, DMSO-d_6) δ 160.76, 152.20, 149.34, 148.62, 147.08, 146.56, 146.00, 133.44, 130.87, 124.42, 118.23, 111.12, 107.97, 21.10. **FTIR** (ATR) ν_{max}/cm^{-1}: 3102, 3050, 2950, 2893, 2824, 2773, 1616, 1545, 1486, 1335, 1310, 1164, 1025, 905, 848, 801, 724, 715, 695, 690, 658.

N*-(4-Methylpyridin-2-yl)-4-phenylthiazol-2-amine (50)

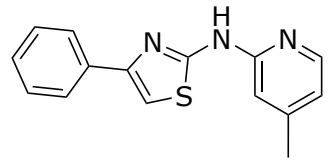

LRMS (ESI+) *m/z* 268.17 $[M+H]^+$, 290.16 $[M+Na]^+$. **HRMS** (ESI+) *m/z* calcd for $C_{15}H_{13}N_3NaS$, 290.07224, found 290.07216 (error = 0.26 ppm). **^{1}H NMR** (400 MHz, DMSO-d_6) δ 11.18 (s, 1H), 8.14 (d, *J* = 5.2 Hz, 1H), 7.91 – 7.84 (m, 2H), 7.40 (dd, *J* = 8.4, 7.0 Hz, 2H), 7.34 (s, 1H), 7.33 – 7.24 (m, 1H), 6.88 (q, *J* = 1.0 Hz, 1H), 6.78 (dd, *J* = 5.4, 1.5 Hz, 1H), 2.27 (s, 3H). **^{13}C NMR** (101 MHz, DMSO-d_6) δ 160.24, 152.35, 149.22, 149.01, 146.59, 135.10, 129.14, 127.99, 126.02, 118.09, 111.07, 106.26, 21.10. **FTIR** (ATR) ν_{max}/cm^{-1}: 3233, 3155, 3051, 3026, 2956, 2918, 1616, 1442, 1382, 1323, 1299, 1267, 1239, 1168, 1117, 1073, 1066, 1061, 992, 912, 907, 861, 854, 842, 819, 806, 798, 770, 709, 685, 671.

4-(4-Fluorophenyl)-*N*-(4-methylpyridin-2-yl)thiazol-2-amine (51b)*

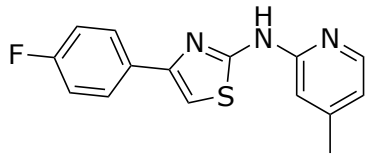

LRMS (ESI+) *m/z* 286.05 $[M+H]^+$, 308.3 $[M+Na]^+$, 593.05 $[2M+Na]^+$. **HRMS** (ESI+) *m/z* calcd for $C_{15}H_{13}FN_3S$, 286.08087, found 286.08087**.** **^{1}H NMR** (400 MHz, DMSO-d_6) δ 8.16 (d, *J* = 5.4 Hz, 1H), 7.96 – 7.87 (m, 2H), 7.34 (s, 1H), 7.26 – 7.15 (m, 2H), 6.91 (s, 1H), 6.86 – 6.80 (m, 1H), 2.28 (s, 3H). **^{13}C NMR** (101 MHz, DMSO-d_6) δ 163.34, 160.91, 160.49, 151.51, 150.78, 148.15, 144.93, 131.39 (d, *J* = 3.0 Hz), 128.14 (d, *J* = 8.1 Hz), 118.33, 115.90 (d, *J* = 21.4 Hz).111.59, 106.33, 40.16, 39.95, 39.74, 39.54, 39.33, 39.12, 38.91, 21.24. **^{19}F NMR** (376 MHz, DMSO-d_6) δ -114.42. **FTIR** (ATR) ν_{max}/cm^{-1}: 3391, 3103, 3050, 2925, 2360, 1610, 1540, 1484, 1366, 1315, 1266, 1213, 1168, 1155, 1117, 1096, 1074, 1059, 1012, 903, 875, 865, 844, 812, 803, 782, 745, 737, 710, 666. *Off-white powder.*

4-(4-Chlorophenyl)-*N*-(4-methylpyridin-2-yl)thiazol-2-amine (51c)*

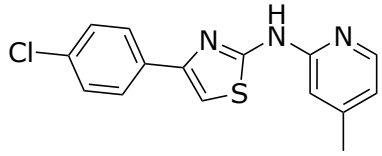

HPLC purity: 100%. **LRMS** (ESI+) *m/z* 302.05 $[M+H]^+$, 324.04 $[M+Na]^+$, 625.03 $[2M+Na]^+$. **HRMS** (ESI+) *m/z* calcd for $C_{15}H_{13}ClN_3S$, 302.05132, found 302.05134 (error < 0.1 ppm). **^{1}H NMR** (400 MHz, DMSO-d_6) δ 8.13 (d, *J* = 5.2 Hz, 1H), 7.92 – 7.84 (m, 2H), 7.47 – 7.39 (m, 2H), 7.36 (s, 1H), 6.87 (s, 1H), 6.76 (d, *J* = 5.1 Hz, 1H), 2.25 (s, 3H). **^{13}C NMR** (101 MHz, DMSO-d_6) δ 160.44, 152.29, 149.24, 147.77, 146.54, 133.99, 132.36, 129.08, 127.73, 118.12, 111.11, 106.97, 21.08. **FTIR** (ATR) ν_{max}/cm^{-1}: 3393, 3100, 2917, 1607, 1537, 1299, 1165, 1104, 1088, 1058, 1011, 964, 900, 864, 847, 828, 811, 736, 700, 666, 583, 445. *Off-white powder.*

4-(4-Methoxyphenyl)-*N*-(pyridin-2-yl)thiazol-2-amine (51d)*

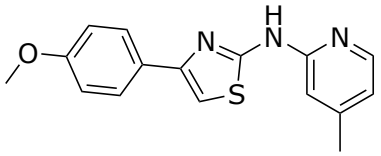

HPLC purity: 100%. **LRMS** (ESI+) *m/z* 298.07 $[M+H]^+$, 320.05 $[M+Na]^+$, 617.10 $[2M+Na]^+$. **HRMS** (ESI+) *m/z* calcd for $C_{16}H_{16}N_3OS$, 298.10086, found 298.10090 (error = 0.1 ppm). **^{1}H NMR** (400 MHz, DMSO-d_6) δ 8.22 (d, *J* = 5.7 Hz, 1H), 7.84 (d, *J* = 8.6 Hz, 2H), 7.30 (s, 1H), 7.02 – 6.91 (m, 4H), 3.76 (s, 3H), 2.33 (s, 3H). **^{13}C NMR** (101 MHz, DMSO-d_6) δ 160.54, 159.49, 150.53, 149.04, 142.88, 127.71, 127.05, 118.66, 114.51, 112.27, 105.04, 55.61, 21.49. **FTIR** (ATR) ν_{max}/cm^{-1}: 3108, 3054, 3029, 2954, 2912, 2833, 2754, 2362, 1610, 1543, 1482, 1382, 1323, 1302, 1245, 1198, 1168, 1112, 1065, 1025, 989, 844, 809, 710. *Pale yellow powder.*

N*-(4-Methylpyridin-2-yl)-4-(4-nitrophenyl)thiazol-2-amine (51e)

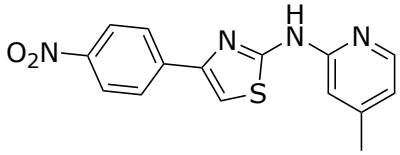

LRMS (ESI+) *m/z* 313.11 $[M+H]^+$. **HRMS** (ESI+) *m/z* calcd for $C_{15}H_{13}N_4O_2S$, 313.07537, found 313.07537 (error = 0.01 ppm). **^{1}H NMR** (500 MHz, DMSO-d_6) δ 11.47 (s, 1H), 8.30 (d, J = 8.5 Hz, 2H), 8.18 (dd, J = 10.9, 7.0 Hz, 3H), 7.79 (s, 1H), 6.91 (s, 1H), 6.80 (s, 1H), 3.35 (s, 1H), 2.31 (s, 3H). **^{13}C NMR** (101 MHz, DMSO-d_6) δ 160.68, 152.26, 149.20, 146.93, 146.66, 146.57, 141.30, 126.83, 124.60, 118.20, 111.17, 111.08, 21.18. **FTIR** (ATR) ν_{max}/cm^{-1}: 3384, 3105, 1613, 1593, 1500, 1329. *Bright yellow-orange powder.*

4-(3-Fluorophenyl)-*N*-(4-methylpyridin-2-yl)thiazol-2-amine (52b)*

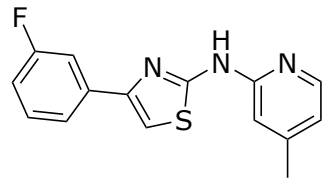

HPLC purity: 100%. **LRMS** (ESI+) *m/z* 286.05 $[M+H]^+$, 593.05 $[2M+Na]^+$. **HRMS** (ESI+) *m/z* calcd for $C_{15}H_{13}FN_3S$, 286.08087, found 286.08089 (error < 0.1 ppm). **^{1}H NMR** (400 MHz, DMSO-d_6) δ 11.21 (s, 1H), 8.12 (d, *J* = 5.2 Hz, 1H), 7.71 (dt, *J* = 7.8, 1.2 Hz, 1H), 7.64 (ddd, *J* = 10.7, 2.7, 1.5 Hz, 1H), 7.48 – 7.38 (m, 2H), 7.13 – 7.03 (m, 1H), 6.89 – 6.84 (m, 1H), 6.76 (dd, *J* = 5.2, 1.4 Hz, 1H), 2.25 (s, 3H). **^{13}C NMR** (101 MHz, DMSO-d_6) δ 164.21, 161.80, 160.36, 152.25, 149.26, 147.66 (d, *J* = 2.7 Hz), 146.50, 137.54 (d, *J* = 8.1 Hz), 131.11 (d, *J* = 8.5 Hz), 122.01 (d, *J* = 2.5 Hz), 118.14, 114.52 (d, *J* = 21.1 Hz), 112.48 (d, *J* = 22.8 Hz), 111.09, 107.66, 21.06. **^{19}F NMR** (376 MHz, DMSO-d_6) δ -113.04. **FTIR** (ATR) ν_{max}/cm^{-1}: 3244, 3107, 3056, 3023, 2919, 1613, 1376, 1151, 804, 443. *Crystalline yellow solid.*

4-(3-Chlorophenyl)-*N*-(4-methylpyridin-2-yl)thiazol-2-amine (52c)*

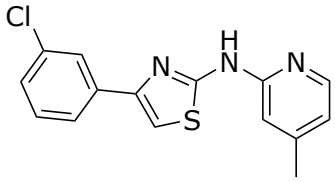

HPLC purity: 99.6%. **LRMS** (ESI+) *m/z* 302.04 $[M+H]^+$, 625.00 $[2M+Na]^+$. **HRMS** (ESI+) *m/z* calcd for $C_{15}H_{13}ClN_3S$, 302.05132, found 302.05135 (error = 0.1 ppm). **^{1}H NMR** (400 MHz, DMSO-d_6) δ 8.18 (d, *J* = 5.5 Hz, 1H), 7.94 (d, *J* = 2.0 Hz, 1H), 7.85 (d, *J* = 7.9 Hz, 1H), 7.54 (s, 1H), 7.42 (t, *J* = 7.9 Hz, 1H), 7.33 (dd, *J* = 7.9, 2.0 Hz, 1H), 6.95 (s, 1H), 6.88 (d, *J* = 5.5 Hz, 1H), 2.30 (s, 3H). **^{13}C NMR** (101 MHz, DMSO-d_6) δ 160.59, 151.88, 150.90, 147.70, 143.90, 136.56, 134.00, 131.04, 127.89, 125.84, 124.71, 118.55, 111.94, 108.35, 21.37. **FTIR** (ATR) ν_{max}/cm^{-1}: 3039, 2735, 1651, 1587, 1517, 1201, 1078, 866, 779, 729. *Off-white powder.*

4-(3-Methoxyphenyl)-*N*-(pyridin-2-yl)thiazol-2-amine (52d)*

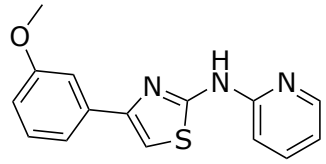

HPLC purity: 100%. **LRMS** (ESI+) *m/z* 298.17 $[M+H]^+$. **HRMS** (ESI+) *m/z* calcd for $C_{32}H_{30}N_6NaO_2S_2$, 617.17639, found 617.17598 (error = 0.65 ppm). **^{1}H NMR** (400 MHz, DMSO-d_6) δ 11.17 (s, 1H), 8.14 (d, J = 5.2 Hz, 1H), 7.49 – 7.41 (m, 2H), 7.37 (s, 1H), 7.31 (t, J = 7.9 Hz, 1H), 6.90 – 6.82 (m, 2H), 6.78 (dd, J = 5.3, 1.4 Hz, 1H), 3.76 (s, 3H), 2.26 (s, 3H). **^{13}C NMR** (101 MHz, DMSO-d_6) δ 160.15, 159.98, 152.34, 149.23, 148.80, 146.57, 136.54, 130.25, 118.49, 118.10, 113.79, 111.22, 111.08, 106.70, 55.54, 21.10. **FTIR** (ATR) ν_{max}/cm^{-1}: 3391, 3241, 3096, 3054, 2955, 2920, 2833, 2360, 1611, 1581, 1543, 1482, 1382, 1317, 1281, 1163, 1066, 1046, 930, 842, 809, 795, 775, 727. *Pale beige powder*.

N*-(4-Methylpyridin-2-yl)-4-(3-nitrophenyl)thiazol-2-amine (52e)

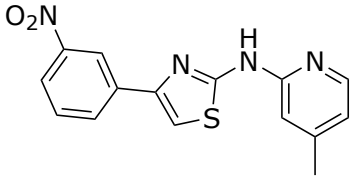

HPLC purity: 96.78%. **LRMS** (ESI+) *m/z* 313.12 $[M+H]^+$, 335.00 $[M+Na]^+$. **HRMS** (ESI+) *m/z* calcd for $C_{15}H_{13}N_4O_2S$, 313.07537, found 313.07538 (error = 0.02 ppm). **^{1}H NMR** (300 MHz, Chloroform-*d*) δ 9.20 (s, 1H), 8.72 (t, J = 2.0 Hz, 1H), 8.27 – 8.05 (m, 3H), 7.53 (t, J = 8.0 Hz, 1H), 7.18 (s, 1H), 6.77 – 6.66 (m, 1H), 6.48 (s, 1H), 2.21 (s, 3H). **^{13}C NMR** (101 MHz, Chloroform-*d*) δ 161.54, 151.29, 149.04, 148.70, 146.99, 146.41, 136.58, 131.84, 129.62, 122.12, 120.99, 118.19, 110.70, 108.01, 20.97.). **FTIR** (ATR) ν_{max}/cm^{-1}: 3246, 3053, 1671, 1613, 1536, 1348. *Bright yellow-orange powder.*

4-(2-Fluorophenyl)-*N*-(4-methylpyridin-2-yl)thiazol-2-amine (53b)*

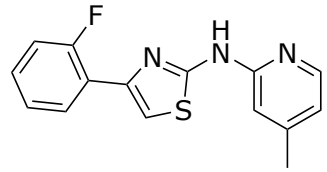

LRMS (ESI+) *m/z* 286.06 $[M+H]^+$, 308.03 $[M+Na]^+$, 593.03 $[2M+Na]^+$. **HRMS** (ESI+) *m/z* calcd for $C_{15}H_{13}FN_3S$, 286.08087, found 286.08082 (error = 0.2 ppm). **^{1}H NMR** (400 MHz, DMSO-d_6) δ 8.18 (d, *J* = 5.5 Hz, 1H), 8.08 (td, *J* = 8.1, 2.0 Hz, 1H), 7.41 – 7.32 (m, 2H), 7.32 – 7.22 (m, 2H), 6.95 (s, 1H), 6.87 (d, *J* = 5.5 Hz, 1H), 2.30 (s, 3H). **^{13}C NMR** (101 MHz, DMSO-d_6) δ 161.20, 159.81, 158.73, 151.29, 144.54, 142.92, 129.87, 129.78, 125.20, 122.22, 118.48, 116.59, 111.75, 111.10, 21.31. **^{19}FNMR** (376 MHz, DMSO-d_6) δ -114.41. **FTIR** (ATR) ν_{max}/cm^{-1}: 3083, 2745, 1613, 1563, 1545, 1439, 1382, 1315, 1218, 1067, 749. *Off-white powder.*

4-(2-Chlorophenyl)-*N*-(4-methylpyridin-2-yl)thiazol-2-amine (53c)*

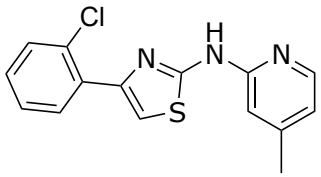

HPLC purity: 100%. **LRMS** (ESI+) *m/z* 302.04 $[M+H]^+$, 624.97 $[2M+Na]^+$. **HRMS** (ESI+) *m/z* calcd for $C_{15}H_{13}ClN_3S$, 302.05132, found 302.05134 (error < 0.1 ppm). **^{1}H NMR** (400 MHz, DMSO-d_6) δ 11.19 (s, 1H), 8.14 (d, *J* = 5.2 Hz, 1H), 7.87 (dd, *J* = 7.7, 1.8 Hz, 1H), 7.50 (dd, *J* = 7.9, 1.4 Hz, 1H), 7.44 – 7.28 (m, 3H), 6.87 (d, *J* = 1.4 Hz, 1H), 6.77 (dd, *J* = 5.2, 1.4 Hz, 1H), 2.25 (s, 3H). **^{13}C NMR** (101 MHz, DMSO-d_6) δ 159.34, 152.29, 149.25, 146.57, 145.69, 133.82, 131.54, 131.27, 130.78, 129.44, 127.68, 118.09, 111.06, 111.04, 21.08. **FTIR** (ATR) ν_{max}/cm^{-1}: 2916, 1616, 1542, 1382, 1167, 1044. *Off-white powder.*

4-(2-Methoxyphenyl)-*N*-(pyridin-2-yl)thiazol-2-amine (53d)*

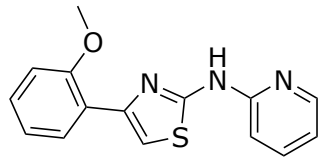

HPLC purity: 100%. **LRMS** (ESI+) *m/z* 298.08 $[M+H]^+$, 320.06 $[M+Na]^+$, 617.08 $[2M+Na]^+$. **HRMS** (ESI+) *m/z* calcd for $C_{16}H_{16}N_3OS$, 298.10086, found 298.10089 (error = 0.1 ppm). **^{1}H NMR** (400 MHz, DMSO-d_6) δ 11.23 (s, 1H), 8.20 – 8.10 (m, 2H), 7.48 (s, 1H), 7.29 (ddd, *J* = 8.3, 7.3, 1.8 Hz, 1H), 7.11 (dd, *J* = 8.4, 1.1 Hz, 1H), 7.03 (td, *J* = 7.5, 1.1 Hz, 1H), 6.90 (dt, *J* = 1.7, 0.9 Hz, 1H), 6.77 (dd, *J* = 5.3, 1.4 Hz, 1H), 3.92 (s, 3H), 2.29 (s, 3H). **^{13}C NMR** (101 MHz, DMSO-d_6) δ 158.48, 157.11, 152.60, 148.91, 146.63, 144.91, 129.36, 128.82, 123.53, 120.84, 117.82, 112.06, 111.04, 110.24, 55.88, 21.20. **FTIR** (ATR) ν_{max}/cm^{-1}: 2917, 2835, 1613, 1541, 1250, 751, 442. *Pale grey powder.*

N*-(4-Methylpyridin-2-yl)-4-(2-nitrophenyl)thiazol-2-amine (53e)

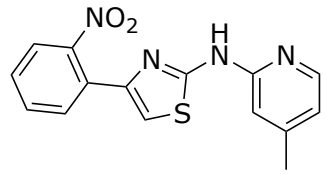

HPLC purity: 99.79%. **LRMS** (ESI+) *m/z* 313.11 $[M+H]^+$, 335.07 $[M+Na]^+$. **HRMS** (ESI+) *m/z* calcd for $C_{15}H_{13}N_4O_2S$, 313.07537, found 313.07537 (error = 0.02 ppm). **^{1}H NMR** (400 MHz, Chloroform-*d*) δ 9.25 (s, 1H), 8.17 (d, *J* = 4.6 Hz, 1H), 7.74 (d, *J* = 9.0 Hz, 1H), 7.69 (d, *J* = 8.0 Hz, 1H), 7.55 (t, *J* = 8.2 Hz, 1H), 7.42 (t, *J* = 7.7 Hz, 1H), 6.95 (s, 1H), 6.69 (d, *J* = 5.2 Hz, 1H), 6.53 (s, 1H), 2.24 (s, 3H). **^{13}C NMR** (101 MHz, DMSO-d_6) δ 160.35, 151.90, 149.99, 149.11, 145.72, 145.20, 132.80, 131.09, 129.44, 128.98, 124.29, 118.29, 111.46, 110.34, 21.28. **FTIR** (ATR) ν_{max}/cm^{-1}: 3241, 3133, 3045, 2944, 1607, 1525, 1477, 1366, 1158, 857, 809, 776, 758, 735, 693, 584, 520, 441. *Yellow brown solid.*

N*-(4-Chloropyridin-2-yl)-4-(pyridin-2-yl)thiazol-2-amine (54)

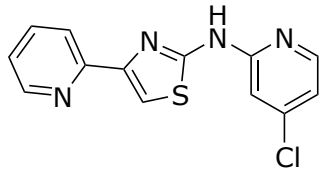

HPLC purity: 96.13%. **LRMS** (ESI+) *m/z* 289.08, 291.07 $[M+H]^+$, 311.03, 313.02 $[M+Na]^+$. **HRMS** (ESI+) *m/z* calcd for $C_{13}H_9ClN_4NaS$, 311.01287, found 311.01288 (error < 0.1 ppm). **^{1}H NMR** (500 MHz, DMSO-d_6) δ 11.63 (s, 1H), 8.61 (d, J = 5.5 Hz, 1H), 8.31 (d, J = 5.5 Hz, 1H), 7.97 (d, J = 7.9 Hz, 1H), 7.92 – 7.86 (m, 1H), 7.71 (s, 1H), 7.36 – 7.30 (m, 1H), 7.19 (d, J = 1.6 Hz, 1H), 7.05 (s, 1H).**^{13}C NMR** (126 MHz, DMSO-d_6) δ 159.95, 153.39, 152.76, 149.91, 149.48, 148.69, 144.00, 137.68, 123.09, 120.35, 116.64, 110.66, 110.46. **FTIR** (ATR) νmax/cm^{-1}: 2959, 1590, 1531, 1418, 1342. *Sandy beige powder.*

N*-(4-Methoxypyridin-2-yl)-4-(pyridin-2-yl)thiazol-2-amine (55)

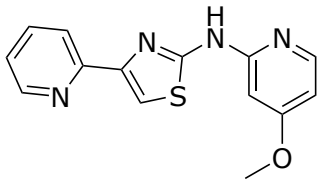

LRMS (ESI+) *m/z* 285.13 $[M+H]^+$, 307.11 $[M+Na]^+$. **HRMS** (ESI+) *m/z* calcd for $C_{14}H_{13}N_4OS$, 285.08046, found 285.08052 (error = 0.2 ppm). **^{1}H NMR** (500 MHz, DMSO-d_6) δ 11.28 (s, 1H), 8.58 (ddd, J = 4.7, 1.8, 0.9 Hz, 1H), 8.13 (d, J = 5.8 Hz, 1H), 7.95 (dt, J = 7.9, 1.2 Hz, 1H), 7.86 (td, J = 7.7, 1.8 Hz, 1H), 7.62 (s, 1H), 7.29 (ddd, J = 7.5, 4.7, 1.2 Hz, 1H), 6.64 (d, J = 2.3 Hz, 1H), 6.58 (dd, J = 5.9, 2.3 Hz, 1H), 3.81 (s, 3H). **^{13}C NMR** (126 MHz, DMSO-d_6) δ 166.95, 160.59, 154.05, 152.94, 149.90, 149.29, 148.21, 137.63, 122.97, 120.32, 110.11, 105.27, 94.79, 55.67. **FTIR** (ATR) ν_{max}/cm^{-1}: 3238, 3116, 3054, 3009, 2969, 2944, 1603, 1542, 1479.

4-(Pyridin-2-yl)-*N*-(4-(trifluoromethyl)pyridin-2-yl)thiazol-2-amine (56)*

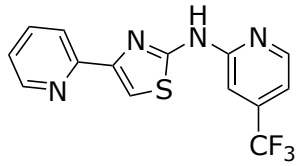

HPLC purity: 95.95%. **LRMS** (ESI+) *m/z* 323.05 $[M+H]^+$, 345.01 $[M+Na]^+$. **HRMS** (ESI+) *m/z* calcd for $C_{14}H_{10}F_3N_4S$, 323.05728, found 323.05734 (error = 0.2 ppm). **^{1}H NMR** (500 MHz, DMSO-d_6) δ 11.86 (s, 1H), 8.60 (dd, J = 14.9, 4.7 Hz, 2H), 8.00 (d, J = 7.8 Hz, 1H), 7.91 (t, J = 7.6 Hz, 1H), 7.43 (s, 1H), 7.38 – 7.32 (m, 1H), 7.26 (d, J = 5.1 Hz, 1H). **^{13}C NMR** (126 MHz, DMSO-d_6) δ 159.76, 152.94, 152.60, 149.82, 149.43, 149.17, 137.85, 123.18, 120.45, 111.34, 110.91, 107.00. **FTIR** (ATR) ν_{max}/cm^{-1}: 3252, 3128, 3045, 1618, 1588, 1548, 1522, 1471, 1432. *Pale yellow powder*.

N*-(5-Chloropyridin-2-yl)-4-(pyridin-2-yl)thiazol-2-amine (57)

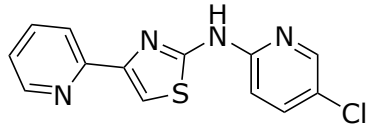

HPLC purity: 99.62%. **LRMS** (ESI+) *m/z* 289.07 $[M+H]^+$, 311.02 $[M+Na]^+$. **HRMS** (ESI+) *m/z* calcd for $C_{13}H_{10}ClN_4S$, 289.03092, found 289.03095 (error = 0.1 ppm). **^{1}H NMR** (300 MHz, Chloroform-*d*) δ 9.28 (s, 1H), 8.62 (d, *J* = 5.5 Hz, 1H), 8.31 (d, *J* = 2.2 Hz, 1H), 7.94 (d, *J* = 7.9 Hz, 1H), 7.71 (t, *J* = 8.6 Hz, 1H), 7.60 (s, 1H), 7.48 (dd, *J* = 8.8, 2.5 Hz, 1H), 7.24 – 7.15 (m, 1H), 6.72 (d, *J* = 8.8 Hz, 1H). **^{13}C NMR** (126 MHz, DMSO-d_6) δ 160.07, 152.81, 150.99, 149.92, 149.54, 145.09, 138.37, 137.65, 123.07, 122.61, 120.37, 112.75, 110.27. **FTIR** (ATR) ν_{max}/cm^{-1}: 2748, 1593, 1536, 1473, 1442, 1372, 1219, 1108, 1067, 1001, 887, 817, 731, 699, 665, 621, 508, 416. *Sandy beige powder.* Spectroscopic data were in agreement with literature.[47]

N*-(6-Chloropyridin-2-yl)-4-(pyridin-2-yl)thiazol-2-amine (58)

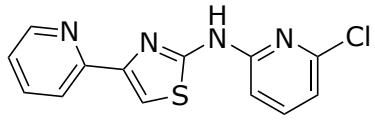

LRMS (ESI+) *m/z* 289.07 $[M+H]^+$, 311.05 $[M+Na]^+$. **HRMS** (ESI+) *m/z* calcd for $C_{13}H_9ClN_4NaS$, 311.01287, found 311.01288 (error = 0.5 ppm). **^{1}H NMR** (500 MHz, DMSO-d_6) δ 11.75 (s, 1H), 8.61 (s, 1H), 7.98 (d, J = 7.8 Hz, 1H), 7.89 (t, J = 7.6 Hz, 1H), 7.80 – 7.73 (m, 2H), 7.36 – 7.29 (m, 1H), 7.12 (d, J = 8.2 Hz, 1H), 7.04 (d, J = 7.6 Hz, 1H). **^{13}C NMR** (126 MHz, DMSO-d_6) δ 159.84, 152.75, 152.37, 149.92, 149.54, 147.57, 141.38, 137.67, 123.10, 120.37, 115.70, 110.73, 109.83. **FTIR** (ATR) νmax/cm^{-1}: 2952, 1595, 1534, 1444, 1390. *Beige powder.*

N*-(6-Methoxypyridin-2-yl)-4-(pyridin-2-yl)thiazol-2-amine (59)

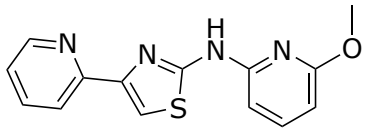

LRMS (ESI+) *m/z* 285.13 $[M+H]^+$, 307.10 $[M+Na]^+$. **HRMS** (ESI+) *m/z* calcd for $C_{14}H_{13}N_4OS$, 285.08046, found 285.08049 (error = 0.1 ppm). **^{1}H NMR** (500 MHz, DMSO-d_6) δ 11.42 (s, 1H), 8.61 (d, J = 4.4 Hz, 1H), 7.98 (d, J = 7.9 Hz, 1H), 7.89 (t, J = 7.8 Hz, 1H), 7.63 (t, J = 7.9 Hz, 1H), 7.35 – 7.29 (m, 1H), 6.67 (d, J = 7.7 Hz, mnj,./:n,1H), 6.34 (d, J = 7.9 Hz, 1H), 4.14 (s, 1H), 4.05 (s, 3H). **^{13}C NMR** (126 MHz, DMSO-d_6) δ 163.18, 160.26, 152.86, 151.12, 149.88, 149.59, 141.14, 137.63, 123.03, 120.39, 109.95, 101.15, 56.12, 55.08. **FTIR** (ATR) νmax/cm^{-1}: 3275, 3052, 3012, 2872, 1677, 1618, 1401, 1343. *Fawn-coloured powder.*

4-(Pyridin-2-yl)-*N*-(*m*-tolyl)thiazol-2-amine (60)*

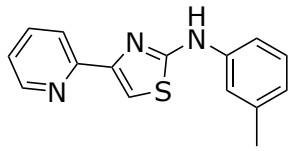

LRMS (ESI+) *m/z* 268.12 $[M+H]^+$, 290.10 $[M+Na]^+$. **HRMS** (ESI+) *m/z* calcd for $C_{15}H_{14}N_3S$, 268.09030, found 268.09038 (error = 0.31 ppm). **^{1}H NMR** (500 MHz, DMSO-d_6) δ 10.23 (s, 1H), 8.59 (ddd, *J* = 4.7, 1.8, 0.9 Hz, 1H), 7.99 (dt, *J* = 7.8, 1.1 Hz, 1H), 7.91 (td, *J* = 7.7, 1.8 Hz, 1H), 7.59 (dd, *J* = 8.0, 2.2 Hz, 1H), 7.54 (s, 1H), 7.48 (t, *J* = 2.0 Hz, 1H), 7.32 (ddd, *J* = 7.5, 4.7, 1.2 Hz, 1H), 7.24 (t, *J* = 7.8 Hz, 1H), 6.81 (ddt, *J* = 7.4, 1.6, 0.9 Hz, 1H), 2.33 (s, 3H).**^{13}C NMR** (101 MHz, DMSO-d_6) δ 163.95, 152.64, 150.81, 149.88, 141.57, 138.64, 137.76, 129.39, 123.09, 122.61, 120.77, 117.97, 114.61, 107.12, 21.85. **FTIR** (ATR) νmax/cm^{-1}: 2918, 1593, 1528, 1421. *Fawn-coloured powder.* Spectroscopic data were in agreement with literature.[378]

4-(6-Bromopyridin-2-yl)-*N*-(4-methylpyridin-2-yl)thiazol-2-amine (61a)*

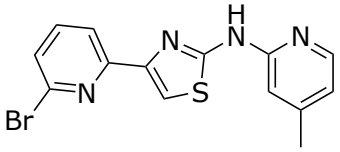

HPLC purity: 99.91%. **LRMS** (ESI+) *m/z* 346.96, 348.98 $[M+H]^+$, 368.95, 370.95 $[M+Na]^+$. **HRMS** (ESI+) *m/z* calcd for $C_{14}H_{12}BrN_4S$, 346.99606, found 346.99614 (error = 0.3 ppm). **^{1}H NMR** (500 MHz, DMSO-d_6) δ 11.79 (s, 1H), 8.25 (d, *J* = 5.5 Hz, 1H), 8.06 (d, *J* = 7.8 Hz, 1H), 7.85 (t, *J* = 7.8 Hz, 1H), 7.73 (s, 1H), 7.56 (d, *J* = 7.9 Hz, 1H), 7.01 (s, 1H), 6.92 (d, *J* = 5.5 Hz, 1H), 2.35 (s, 3H). **^{13}C NMR** (101 MHz, DMSO-d_6) δ 160.75, 153.93, 150.04, 147.67, 145.74, 141.63, 141.03, 138.56, 127.02, 119.72, 118.30, 111.92, 111.43, 21.29. **FTIR** (ATR) ν_{max}/cm^{-1}: 3017, 2801, 2642, 1649, 1611, 1540, 1208, 1158, 1110, 994, 930, 853, 834, 796, 746, 723, 581, 430. *Beige poder.*

4-(5-Bromopyridin-2-yl)-*N*-(4-methylpyridin-2-yl)thiazol-2-amine (61b)*

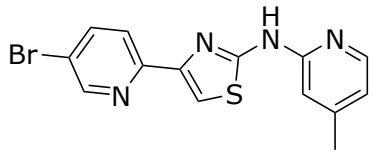

HPLC purity: 99.67%. **LRMS** (ESI+) *m/z* 346.99, 348.98 $[M+H]^+$, 368.94, 370.97 $[M+Na]^+$. **HRMS** (ESI+) *m/z* calcd for $C_{14}H_{12}BrN_4S$, 346.99606, found 346.99611 (error = 0.2 ppm). **^{1}H NMR** (500 MHz, DMSO-d_6) δ 11.39 (s, 1H), 8.71 (d, J = 2.3 Hz, 1H), 8.19 (d, J = 5.2 Hz, 1H), 8.13 (dt, J = 8.6, 1.9 Hz, 1H), 7.92 (d, J = 8.5 Hz, 1H), 7.67 (s, 1H), 6.91 (s, 1H), 6.80 (d, J = 5.2 Hz, 1H), 2.31 (s, 3H). **^{13}C NMR** (126 MHz, DMSO-d_6) δ 160.62, 152.32, 151.71, 150.53, 149.11, 148.20, 146.57, 140.24, 122.04, 118.89, 118.10, 111.12, 110.85, 21.19. **FTIR** (ATR) ν_{max}/cm^{-1}: 3421, 3119, 3032, 2804, 2712, 1646, 1594, 1528, 1452, 1363, 1264, 1243, 1191, 1089, 1052, 1004, 857, 791, 724, 631, 481. *Yellow powder.*

4-(4-Chloropyridin-2-yl)-*N*-(4-methylpyridin-2-yl)thiazol-2-amine (61c)*

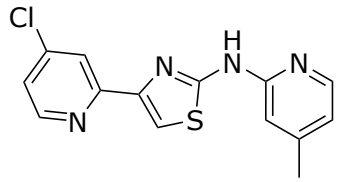

LRMS (ESI+) *m/z* 303.15, 305.14 $[M+H]^+$, 325.05 $[M+Na]^+$. **HRMS** (ESI+) *m/z* calcd for $C_{14}H_{11}ClN_4NaS$, 325.02852, found 325.02860 (error = 0.2 ppm). **^{1}H NMR** (500 MHz, DMSO-d_6) δ 11.38 (s, 1H), 8.57 (d, J = 5.2 Hz, 1H), 8.18 (d, J = 5.2 Hz, 1H), 7.98 (d, J = 2.0 Hz, 1H), 7.72 (s, 1H), 7.46 (dd, J = 5.3, 2.1 Hz, 1H), 6.90 (s, 1H), 6.81 (dd, J = 5.3, 1.3 Hz, 1H), 2.30 (s, 3H). **^{13}C NMR** (126 MHz, DMSO-d_6) δ 160.63, 154.52, 152.27, 151.49, 149.17, 147.83, 146.56, 144.14, 122.78, 120.20, 118.15, 111.55, 111.12, 21.19. **FTIR** (ATR) ν_{max}/cm^{-1}: 3081, 2917, 1646, 1594, 1528, 1452, 1363, 1264, 1243, 1191, 1089, 1052, 1004, 857, 791, 724, 631, 481. *Brown-orange solid.*

4-(Isoquinolin-3-yl)-*N*-(4-methylpyridin-2-yl)thiazol-2-amine (61d)*

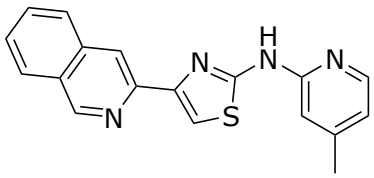

LRMS (ESI+) *m/z* 319.14 $[M+H]^+$, 341.10 $[M+Na]^+$. **HRMS** (ESI+) *m/z* calcd for $C_{18}H_{14}N_4NaS$, 341.08314, found 341.08322 (error = 0.2 ppm). **^{1}H NMR** (400 MHz, DMSO-d_6) δ 11.48 (s, 1H), 8.46 (d, *J* = 8.6 Hz, 1H), 8.24 – 8.17 (m, 2H), 8.07 – 7.96 (m, 2H), 7.88 (s, 1H), 7.79 (ddd, *J* = 8.5, 6.8, 1.5 Hz, 1H), 7.60 (ddd, *J* = 8.0, 6.8, 1.2 Hz, 1H), 6.93 (s, 1H), 6.86 – 6.79 (m, 1H), 2.33 (s, 3H). **^{13}C NMR** (101 MHz, DMSO-d_6) δ 160.46, 152.43, 149.47, 149.11, 148.04, 146.61, 137.45, 130.36, 129.22, 128.36, 127.57, 126.65, 119.43, 118.06, 111.52, 111.12, 21.21. **FTIR** (ATR) ν_{max}/cm^{-1}: 3397, 2910, 1609, 1532, 1483, 1363, 1300, 1160, 846, 809, 773, 760, 578, 521, 478, 461. *Brown-orange solid.*

N*-(4-Methylpyridin-2-yl)-4-(5-phenylpyridin-2-yl)thiazol-2-amine (61e)

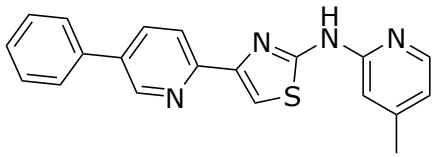

LRMS (ESI+) *m/z* 345.16 $[M+H]^+$, 367.09 $[M+Na]^+$. **HRMS** (ESI+) *m/z* calcd for $C_{20}H_{16}N_4NaS$, 367.09879, found 367.09917 (error = 1 ppm). **^{1}H NMR** (500 MHz, DMSO-*d6*) δ 11.39 (s, 1H), 8.93 (d, J = 2.4 Hz, 1H), 8.22 – 8.15 (m, 2H), 8.06 (d, J = 8.2 Hz, 1H), 7.78 (d, J = 7.4 Hz, 2H), 7.69 (s, 1H), 7.53 (t, J = 7.6 Hz, 2H), 7.47 – 7.40 (m, 1H), 6.94 (s, 1H), 6.80 (d, J = 5.2 Hz, 1H), 2.31 (s, 3H). **^{13}C NMR** (126 MHz, DMSO-d_6) δ 160.52, 152.41, 151.93, 149.08, 149.06, 147.94, 146.59, 137.36, 135.45, 134.42, 129.63, 128.53, 127.08, 120.37, 118.05, 111.12, 110.15, 21.19. **FTIR** (ATR) ν_{max}/cm^{-1}: 3398, 3310, 3138, 3013, 2835, 1609, 1533, 1483, 1365, 1160, 846, 806, 747, 693, 579, 464, 443. *Dark yellow solid.*

N*-(5-Phenylpyridin-2-yl)-4-(pyridin-2-yl)thiazol-2-amine (73)

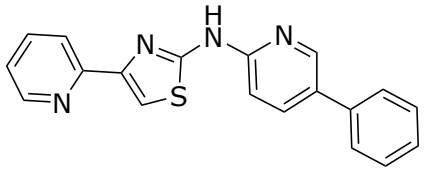

LRMS (ESI+) *m/z* 331.14 $[M+H]^+$. **HRMS** (ESI+) *m/z* calcd for 331.10119, found 331.10083 (error = 1.1 ppm). **^{1}H NMR** (300 MHz, DMSO-d_6) δ 11.75 (s, 1H), 8.80 (d, *J* = 5.7 Hz, 1H), 8.68 (d, *J* = 2.3 Hz, 1H), 8.64 – 8.49 (m, 1H), 8.45 (d, *J* = 8.1 Hz, 1H), 8.29 (s, 1H), 8.13 (dd, *J* = 8.6, 2.5 Hz, 1H), 7.87 (t, *J* = 6.6 Hz, 1H), 7.77 – 7.68 (m, 2H), 7.49 (t, *J* = 7.5 Hz, 2H), 7.36 (dd, *J* = 20.1, 8.0 Hz, 2H). **^{13}C NMR** (101 MHz, DMSO-d_6) δ 161.08, 159.12, 150.85, 150.43, 144.28, 144.13, 143.22, 137.23, 129.53, 129.28, 127.93, 126.64, 125.26, 124.41, 123.79, 116.78, 111.80. **FTIR** (ATR) ν_{max}/cm^{-1}: 3339, 3081, 3057, 3035, 3014, 2997, 2809, 2654, 1590, 1536, 1416, 1294, 1190, 1096, 842, 754, 682, 479. *Lumpy yellow powder.*

N*-(1*H*-Indazol-5-yl)-4-(pyridin-2-yl)thiazol-2-amine (74)

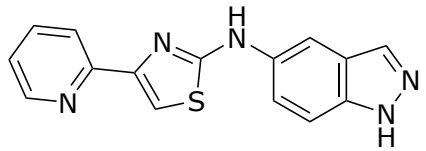

LRMS (ESI-) *m/z* 292.02 $[M-H]^-$. **HRMS** (ESI-) *m/z* calcd for $C_{15}H_{12}N_5S$, 294.08079, found 294.08070 (error = 0.3 ppm). **^{1}H NMR** (500 MHz, Methanol-d_4) δ 8.72 (dd, *J* = 6.2, 1.5 Hz, 1H), 8.57 (td, *J* = 7.8, 7.3, 1.5 Hz, 1H), 8.56 – 8.50 (m, 1H), 8.41 (d, *J* = 2.0 Hz, 1H), 8.12 (s, 1H), 8.08 (s, 1H), 7.92 (ddd, *J* = 7.4, 5.9, 1.4 Hz, 1H), 7.58 (d, *J* = 8.9 Hz, 1H), 7.50 (dd, *J* = 8.9, 2.1 Hz, 1H). **^{13}C NMR** (126 MHz, Methanol-d_4) δ 166.77, 146.08, 145.52, 141.41, 140.40, 137.38, 134.04, 133.27, 124.67, 123.56, 123.14, 120.83, 114.55, 110.68, 109.09. **FTIR** (ATR) ν_{max}/cm^{-1}: 3373, 3211, 3043, 1596, 1549, 1506, 1448, 1294, 1223, 1068, 946, 805, 741, 646, 525. *Dark brown solid.*

N*-(7*H*-Purin-6-yl)-4-(pyridin-2-yl)thiazol-2-amine (75)

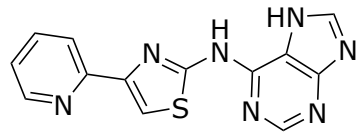

LRMS (ESI+) *m/z* 296.13 $[M+H]^+$. **HRMS** (ESI+) *m/z* calcd for $C_{13}H_9N_7S$, 296.07129, found 296.02514 (error = 156 ppm). **^{1}H NMR** (400 MHz, Methanol-d_4) δ 8.59 – 8.53 (m, 1H), 8.27 (d, *J* = 8.2 Hz, 1H), 8.19 (t, *J* = 7.9 Hz, 1H), 7.88 (s, 1H), 7.83 – 7.74 (m, 2H), 7.57 (t, *J* = 6.5 Hz, 1H), 7.41 (dd, *J* = 5.1, 2.0 Hz, 3H), 6.78 (s, 1H). **^{13}C NMR** (101 MHz, Methanol-d_4) δ 163.78, 160.99, 149.75, 146.05, 140.72, 129.94, 129.18, 128.64, 126.43, 123.67, 122.22, 111.70, 83.21. **FTIR** (ATR) ν_{max}/cm^{-1}: 3204, 3136, 3078, 1673, 1612, 1541, 1409, 1196, 1121, 948, 798, 751. *Pale yellow powder.*

3-Phenyl-*N*-(4-(pyridin-2-yl)thiazol-2-yl)isoxazol-5-amine (76)*

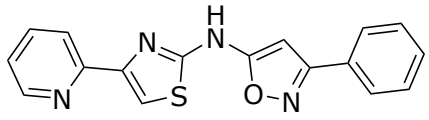

LRMS (ESI-) *m/z* 319.05 $[M-H]^-$. **HRMS** (ESI+) *m/z* calcd for 663.13559 $[2M+Na]^+$, found 663.13416 (error = 2.2 ppm). **^{1}H NMR** (300 MHz, DMSO-d_6) δ 12.12 (s, 1H), 8.62 (ddd, *J* = 4.8, 1.8, 0.9 Hz, 1H), 8.13 (d, *J* = 7.9 Hz, 1H), 8.00 – 7.88 (m, 3H), 7.76 (s, 1H), 7.54 (dd, *J* = 5.1, 1.9 Hz, 3H), 7.36 (ddd, *J* = 7.6, 4.8, 1.2 Hz, 1H), 6.76 (s, 1H). **^{13}C NMR** (101 MHz, DMSO-d_6) δ 163.82, 163.29, 160.44, 151.99, 149.86, 138.01, 130.64, 129.49, 127.07, 123.46, 121.17, 109.98, 83.37. **FTIR** (ATR) ν_{max}/cm^{-1}: 3120, 3057, 3010, 2896, 2791, 1644, 1587, 1481, 1445, 1344, 1293, 1065, 993, 950, 921, 816, 759, 744, 719, 690. *Brown powder.*

3-Methyl-*N*-(4-(pyridin-2-yl)thiazol-2-yl)isoxazol-5-amine (77)*

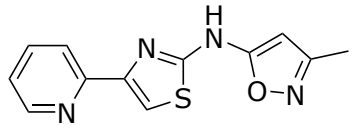

LRMS (ESI+) *m/z* 281.09 $[M+Na]^+$. **HRMS** (ESI+) *m/z* calcd for 281.04675, found 281.04690 (error = 0.5 ppm). **^{1}H NMR** (400 MHz, Methanol-d_4) δ 8.58 – 8.52 (m, 1H), 8.10 (d, J = 7.8 Hz, 1H), 7.91 (td, J = 7.8, 1.8 Hz, 1H), 7.62 (s, 1H), 7.35 (ddd, J = 7.6, 4.9, 1.2 Hz, 1H), 6.25 (s, 1H), 4.59 (s, 1H), 2.29 (s, 3H). **^{13}C NMR** (126 MHz, Methanol-d_4) δ 163.13, 161.63, 161.58, 160.28, 152.09, 148.71, 137.56, 122.79, 121.29, 108.58, 85.50, 10.32. **FTIR** (ATR) ν_{max}/cm^{-1}: 3382, 3196, 3152, 3128, 3078, 2998, 2929, 2788, 2656, 1588, 1415, 1065, 826, 752, 716. *Beige powder.*

N*-(1*H*-Pyrazol-3-yl)-4-(pyridin-2-yl)thiazol-2-amine (78)

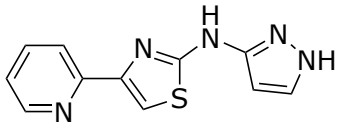

LRMS (ESI-) *m/z* 242.00 $[M-H]^-$. **HRMS** (ESI-) *m/z* calcd for $C_{11}H_{10}N_5S$, 244.06514, found 244.06458 (error = 2.7 ppm). **^{1}H NMR** (400 MHz, DMSO-d_6) δ 11.80 (s, 1H), 9.00 (s, 1H), 8.64 (d, J = 5.0 Hz, 1H), 8.46 (s, 1H), 8.12 (d, J = 7.8 Hz, 1H), 8.05 (q, J = 8.0, 7.6 Hz, 2H), 7.87 (s, 1H), 7.45 (t, J = 6.3 Hz, 1H), 7.25 (s, 1H), 7.12 (s, 1H), 6.99 (s, 1H). ^{13}C NMR (101 MHz, DMSO-d_6) δ 153.66, 148.46, 147.02, 145.18, 139.38, 133.58, 130.15, 123.55, 121.29, 111.91. **FTIR** (ATR) ν_{max}/cm^{-1}: 3360, 3243, 3082, 2926, 1621, 1568, 1411, 1351, 1283, 1197, 946, 791, 740, 719, 613, 579, 456. *Fine beige powder.*

N*-(3-Fluorophenyl)-4-(pyridin-2-yl)thiazol-2-amine (80)*

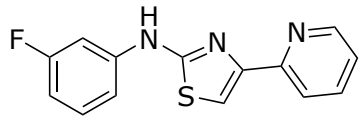

LRMS (ESI+) *m/z* 272.05 $[M+H]^+$, 294.02 $[M+Na]^+$. **HRMS** (ESI+) *m/z* calcd for $C_{14}H_{10}FN_3S$, [M+Na], 294.04717, found 294.04709 (error = 0.3 ppm). **^{1}H NMR** (400 MHz, DMSO-d_6) δ 10.56 (s, 1H), 8.60 (ddd, *J* = 4.8, 1.8, 0.9 Hz, 1H), 7.99 (dt, *J* = 7.8, 1.2 Hz, 1H), 7.93 (td, *J* = 7.6, 1.8 Hz, 1H), 7.81 (dt, *J* = 12.3, 1.9 Hz, 1H), 7.61 (s, 1H), 7.44 – 7.30 (m, 3H), 6.85 – 6.74 (m, 1H). **^{13}C NMR** (101 MHz, DMSO-d_6) δ 164.26, 163.43, 161.87, 152.47, 150.84, 149.93, 143.22 (d), 137.83, 131.04 (d), 123.20, 120.75, 113.26 (d), 107.93, 104.01 (d). **^{19}F NMR** (471 MHz, DMSO-d_6) δ -111.57. **FTIR** (ATR) ν_{max}/cm^{-1}: 3255, 3203, 3126, 3067, 3022, 1619, 1594, 1481, 1447, 1424, 1336, 1279, 1260, 1250, 1197, 1129, 1093, 1065, 997, 963, 922, 856, 810, 792, 769, 753, 743, 706, 679. *Beige powder.* Spectroscopic data were in agreement with literature.[378,381]

N*-(5-Methoxypyridin-2-yl)-4-(pyridin-2-yl)thiazol-2-amine (82)*

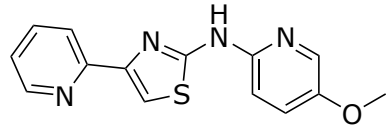

m.p. = 204–212°C. **LRMS** (ESI+) *m/z* 285.14 $[M+H]^+$, 307.12 $[M+Na]^+$. **HRMS** (ESI+) *m/z* calcd for $C_{28}H_{24}N_8NaO_2S_2$, 591.13559, found 591.13533 (error = 0.4 ppm). **^{1}H NMR** (400 MHz, DMSO-d_6) δ 11.24 (s, 1H), 8.59 (d, *J* = 4.7 Hz, 1H), 8.05 (d, *J* = 2.6 Hz, 1H), 7.96 (d, *J* = 7.9 Hz, 1H), 7.87 (td, *J* = 7.7, 1.8 Hz, 1H), 7.58 (s, 1H), 7.45 (dd, *J* = 9.0, 3.0 Hz, 1H), 7.34 – 7.28 (m, 1H), 7.11 (d, *J* = 9.4 Hz, 1H), 3.81 (s, 3H). **^{13}C NMR** (101 MHz, DMSO-d_6) δ 160.29, 152.50, 150.25, 149.37, 148.89, 146.09, 137.08, 131.24, 125.85, 122.43, 119.83, 111.45, 108.41, 55.96. **FTIR** (ATR) ν_{max}/cm^{-1}: 3128, 3003, 2943, 2909, 2839, 2764, 1619, 1593, 1545, 1516, 1492, 1422, 1343, 1323, 1293, 1275, 1178, 1066, 1033, 1002, 898, 814, 724, 706, 667. *Light brown powder.* Spectroscopic data were in agreement with literature.[47]

N*-(5-Fluoropyridin-2-yl)-4-(pyridin-2-yl)thiazol-2-amine (83)*

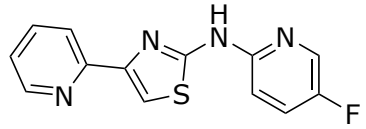

m.p. = 198–207°C. **LRMS** (ESI+) *m/z* (ESI-) *m/z* 271.03 $[M-H]^-$. **HRMS** (ESI-) *m/z* calcd for $C_{13}H_8FN_4S$, 271.04592, found 271.04604 (error = 0.4 ppm). **^{1}H NMR** (400 MHz, DMSO-d_6) δ 11.51 (s, 1H), 8.61 (d, *J* = 3.9 Hz, 1H), 8.33 (d, *J* = 3.0 Hz, 1H), 7.98 (d, *J* = 7.9 Hz, 1H), 7.89 (td, *J* = 7.7, 1.8 Hz, 1H), 7.78 – 7.71 (m, 1H), 7.65 (s, 1H), 7.35 – 7.30 (m, 1H), 7.20 (dd, *J* = 9.2, 3.5 Hz, 1H). **^{13}C NMR** (101 MHz, DMSO-d_6) δ 159.99, 155.55, 153.12, 152.37, 149.40, 148.99, 148.63, 137.12, 133.04 (d), 126.28 (d), 122.52, 119.86, 111.96, 108.98. **^{19}F NMR** (376 MHz, DMSO-d_6) δ -138.48. **FTIR** (ATR) ν_{max}/cm^{-1}: 3120, 3022, 2915, 1594, 1494, 1477, 1449, 1424, 1379, 1289, 1226, 1068, 1002, 820, 808, 741, 725, 705, 667. *Crystalline brown solid.*

N*-(6-Fluoropyridin-2-yl)-4-(pyridin-2-yl)thiazol-2-amine (84)*

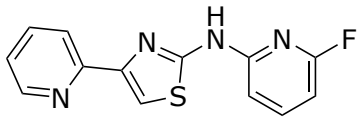

m.p. = 202–220°C. **LRMS** (ESI-) *m/z* 271.00 $[M-H]^-$. **HRMS** (ESI-) *m/z* calcd for $C_{13}H_8FN_4S$, 271.04592, found 271.04574 (error = 0.7 ppm).**^{1}H NMR** (400 MHz, DMSO-d_6) δ 11.71 (s, 1H), 8.62 (d, *J* = 6.5 Hz, 1H), 7.98 (d, *J* = 7.9 Hz, 1H), 7.90 (d, *J* = 24.5 Hz, 2H), 7.74 (s, 1H), 7.38 – 7.30 (m, 1H), 7.08 (d, *J* = 9.9 Hz, 1H), 6.67 (d, *J* = 9.8 Hz, 1H). **^{13}C NMR** (101 MHz, DMSO-d_6) δ 162.61, 160.25, 159.57, 152.21, 151.04 (d), 149.44, 149.13, 142.99 (d), 137.17, 122.63, 119.90, 110.06, 107.52 (d), 99.18. **^{19}F NMR** (376 MHz, DMSO-d_6) δ -70.72. **FTIR** (ATR) ν_{max}/cm^{-1}: 3051, 2922, 2854, 2796, 1657, 11624, 1594, 1572, 1518, 1472, 1417, 1343, 1278, 1208, 1160, 1092, 1069, 1030, 1000, 916, 890, 781, 741, 722, 709. *Light brown powder.*

***N*-(1-adamantyl)-4-(pyridin-2-yl)thiazol-2-amine (85)**

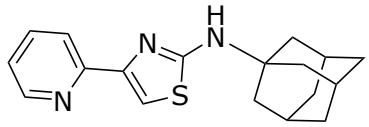

LRMS (ESI+) *m/z* 312.21 $[M+H]^+$, 334.14 $[M+Na]^+$. **^{1}H NMR**: (300 MHz, Chloroform-*d* δ 8.53 (dt, *J* = 1.40, 4.91, 1H), 8.17-8.06 (m, 1H), 7.78-7.76 (m, 2H), 7.19-7.10 (m, 1H), 5.90 (s, 1H), 2.04 (d, *J* = 6.35, 4H), 1.94 (t, *J* = 3.16, 6H), 1.64 (t, *J* = 3.37, 6H).

N*-(4-Fluorophenyl)-4-(pyridin-2-yl)thiazol-2-amine (86)*

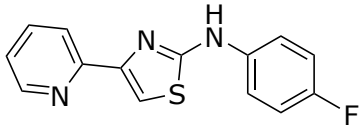

LRMS (ESI+) *m/z* 272.12 $[M+H]^+$, 294.08 $[M+Na]^+$. **HRMS** (ESI+) *m/z* calcd for $C_{14}H_{11}FN_3S$, 272.06522, found 272.06489 (error = 1.2 ppm). **^{1}H NMR** (500 MHz, DMSO-d_6) δ 10.34 (s, 1H), 8.59 (ddd, *J* = 4.8, 1.8, 0.9 Hz, 1H), 8.01 (dt, *J* = 7.9, 1.1 Hz, 1H), 7.90 (td, *J* = 7.7, 1.8 Hz, 1H), 7.82 – 7.73 (m, 2H), 7.56 (s, 1H), 7.32 (ddd, *J* = 7.5, 4.7, 1.2 Hz, 1H), 7.25 – 7.16 (m, 2H). **^{13}C NMR** (126 MHz, DMSO-d_6) δ 163.96, 158.33, 156.44, 152.51, 150.69, 149.80, 138.13 (d, *J* = 2.2 Hz), 137.79, 123.13, 120.87, 118.91 (d, *J* = 7.7 Hz),116.09, 115.91, 107.31. **FTIR** (ATR) ν_{max}/cm^{-1}: 3251, 3207, 3121, 3034, 2996, 2936, 2857, 2811, 1620, 1541, 1538, 1204, 1065, 827, 744. *Dark brown powder.* The spectroscopic data were in agreement with the literature.[381]

4-(Pyridin-2-yl)-*N*-(4-(trifluoromethyl)phenyl)thiazol-2-amine (87)**

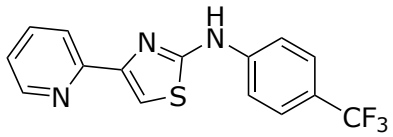

LRMS (ESI+) *m/z* 322.08 $[M+H]^+$, 344.09 $[M+Na]^+$. **HRMS** (ESI+) *m/z* calcd for $C_{15}H_{10}F_3N_3NaS$, 344.04397, found 344.04385 (error = 0.35 ppm). **^{1}H NMR** (500 MHz, DMSO-d_6) δ 10.68 (s, 1H), 8.54 (dt, *J* = 4.7, 1.3 Hz, 1H), 8.00 (dt, *J* = 8.0, 1.2 Hz, 1H), 7.89 (d, *J* = 8.5 Hz, 2H), 7.88 – 7.81 (m, 1H), 7.64 (d, *J* = 8.5 Hz, 2H), 7.60 (s, 1H), 7.27 (ddd, *J* = 7.5, 4.7,

1.2 Hz, 1H). **^{13}C NMR** (126 MHz, DMSO-d_6) δ 163.14, 152.40, 150.87, 149.89, 144.80, 137.80, 126.83 (q, J = 3.8 Hz), 126.21, 124.06, 123.26, 122.01 – 121.04 (m), 120.97, 117.07, 108.50. **FTIR** (ATR) ν_{max}/cm^{-1}: 3237, 3187, 3121, 3035, 2938, 2859, 2809, 1615, 1524, 1416, 1321, 1258, 1152, 1108, 1062, 1003, 835, 792, 751, 713, 593. *Beige powder.* The spectroscopic data were in agreement with the literature.[381]

4-(Pyridin-2-yl)-*N*-(3-(trifluoromethyl)phenyl)thiazol-2-amine (88)**

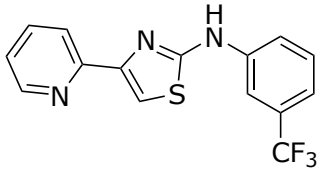

LRMS (ESI+) *m/z* 322.09 $[M+H]^+$, 344.08 $[M+Na]^+$. **HRMS** (ESI+) *m/z* calcd for $C_{15}H_{11}F_3N_3S$, 322.06203, found 322.06151 (error = 1.6 ppm). **^{1}H NMR** (500 MHz, DMSO-d_6) δ 10.70 (s, 1H), 8.61 (dt, J = 4.6, 1.4 Hz, 1H), 8.33 (t, J = 2.0 Hz, 1H), 8.00 – 7.89 (m, 3H), 7.64 (s, 1H), 7.59 (t, J = 8.0 Hz, 1H), 7.37 – 7.28 (m, 2H). **^{13}C NMR** (126 MHz, DMSO-d_6) δ 163.38, 152.44, 150.74, 149.97, 142.15, 137.80, 130.66, 130.22 (q, J = 31.4 Hz), 124.75 (d, J = 272.3 Hz), 123.24, 120.80, 120.53, 117.82 (q, J = 3.8 Hz), 113.24 (q, J = 4.2 Hz),108.21. **FTIR** (ATR) ν_{max}/cm^{-1}: 3301, 3120, 3097, 3061, 3019, 1613, 1548, 1452, 1338, 1158, 1117, 747, 700. *Light brown powder.* The spectroscopic data were in agreement with the literature.[381]

***N*-(2-chloro-5-(trifluoromethyl)phenyl)-4-(pyridin-2-yl)thiazol-2-amine (89)**

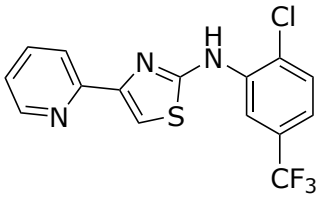

HRMS (ESI+) *m/z* calcd for $C_{15}H_{10}ClF_3N_3S$, 356.02306, found 356.02243 (error = 1.8 ppm). **^{1}H NMR** (300 MHz, Chloroform-*d*) δ 8.97 (d, J = 2.1 Hz, 1H), 8.62 (ddd, J = 4.8, 1.9, 0.9 Hz, 1H), 8.03 (dt, J = 7.9, 1.0 Hz, 1H), 7.80 (td, J = 7.7, 1.8 Hz, 1H), 7.61 (s, 2H), 7.52 (d, J = 8.3 Hz, 1H), 7.28 – 7.18 (m, 2H). **^{13}C NMR** (126 MHz, Chloroform-*d*) δ 162.9, 151.9, 149.5, 138.1, 137.3, 130.6, 128.7 – 127.9 (q, J = 32.8 MHz), 125.0, 124.7, 122.9, 122.7, 119.6, 118.8

– 118.7 (q, J = 3.8 MHz), 116.0 – 115.9 (q, J = 5.0 MHz), 109.5. **FTIR** (ATR) ν_{max}/cm^{-1}: 3398, 3283, 3146, 1592, 1555, 1548, 1531, 1432, 1307, 1301, 1281, 1272, 1161, 1138, 1149, 1118, 1108, 1092, 1085, 1068, 1045.

***N*-(4-Chloro-3-(trifluoromethyl)phenyl)-4-(pyridin-2-yl)thiazol-2-amine (90)**

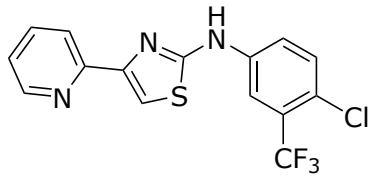

HRMS (ESI+) *m/z* calcd for $C_{13}H_6F_4N_5OS$, 356.02237, found 356.02259 (error = 0.6 ppm). **^{1}H NMR** (300 MHz, Chloroform-*d*) δ 8.61 (ddd, J = 4.8, 1.9, 1.0 Hz, 1H), 8.09 (d, J = 2.8 Hz, 1H), 8.01 (dt, J = 7.9, 1.1 Hz, 1H), 7.78 (td, J = 7.7, 1.8 Hz, 1H), 7.62 (dd, J = 8.8, 2.8 Hz, 1H), 7.50 (s, 1H), 7.55 – 7.42 (m, 2H), 7.23 (ddd, J = 7.5, 4.8, 1.2 Hz, 1H). **^{13}C NMR** (126 MHz, Chloroform-*d*) δ 162.6, 151.6, 150.2, 149.5, 140.3, 137.3, 132.2, 127.2 – 126.5 (q, J = 30.2 Hz), 126.1, 124.0, 122.8, 121.8, 121.4, 121.3, 120.0, 115.4 – 115.2 (q, J = 5.0 MHz), 108.0. **FTIR** (ATR) ν_{max}/cm^{-1}: 3233, 3120, 3063, 2969, 2744, 1605, 1545, 1481, 1454, 1422, 1355, 1285, 1262, 1244, 1208, 1171, 1112, 1065, 1051, 1029, 1002.

N*-(Benzo[d][1,3]dioxol-5-yl)-4-(pyridin-2-yl)thiazol-2-amine (91)*

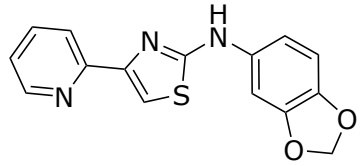

LRMS (ESI+) *m/z* 298.11 $[M+H]^+$. **HRMS** (ESI+) *m/z* calcd for $C_{15}H_{12}N_3O_2S$, 298.06447, found 298.06396 (error = 1.7 ppm). **^{1}H NMR** (300 MHz, Chloroform-*d*) δ 8.64 – 8.55 (m, 1H), 8.01 – 7.92 (m, 1H), 7.74 (td, J = 7.8, 1.8 Hz, 1H), 7.37 (s, 1H), 7.20 (ddd, J = 7.6, 4.8, 1.2 Hz, 1H), 7.06 (dd, J = 1.7, 0.9 Hz, 1H), 6.81 (d, J = 1.7 Hz, 2H), 5.99 (s, 2H). **^{13}C NMR** (126 MHz, Chloroform-*d*) δ 163.73, 152.11, 150.25, 149.37, 147.37, 141.67, 137.23, 135.92, 122.56,

120.22, 109.63, 108.33, 106.31, 100.84, 99.54. **FTIR** (ATR) ν_{max}/cm^{-1}: 3233, 3120, 2970, 2886, 2774, 1533, 1500, 1421, 1205, 1034, 928, 802, 790.

4-(Pyridin-2-yl)-*N*-(2-(trifluoromethyl)phenyl)thiazol-2-amine (92)**

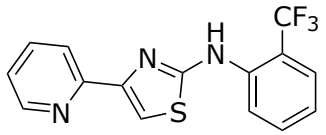

LRMS (ESI+) *m/z* 322.06 $[M+H]^+$. **HRMS** (ESI+) *m/z* calcd for $C_{15}H_{10}F_3N_3S$, $[M+Na]^+$, 344.04397, found 344.04413 (error = 0.5 ppm). **^{1}H NMR** (400 MHz, DMSO-d_6) δ 9.56 (s, 1H), 8.60 – 8.54 (m, 1H), 8.14 (d, *J* = 8.2 Hz, 1H), 7.89 – 7.79 (m, 2H), 7.78 – 7.67 (m, 2H), 7.55 (s, 1H), 7.42 – 7.24 (m, 2H). **^{13}C NMR** (101 MHz, DMSO-d_6) δ 166.03, 152.54, 150.47, 149.83, 139.06, 137.64, 133.92, 127.05, 126.99, 126.14, 124.88, 123.08, 121.73, 120.77, 108.62. **^{19}F NMR** (376 MHz, DMSO-d_6) δ -59.21. **FTIR** (ATR) ν_{max}/cm^{-1}: 3194, 3123, 3061, 3009, 2930, 2852, 1586, 1471, 1454, 1424, 1320, 1281, 1198, 1169, 1104, 1056, 1035, 886, 843, 794, 768, 742, 710, 682. *Brown powder.* Spectroscopic data were in agreement with literature.[378]

4-([1,1'-Biphenyl]-4-yl)-*N*-(4-methylpyridin-2-yl)thiazol-2-amine (99)**

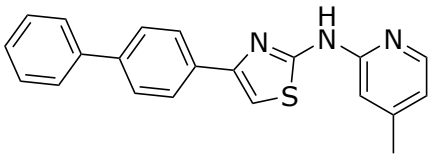

LRMS (ESI-) *m/z* 342.10 $[M-H]^-$. **HRMS** (ESI-) *m/z* calcd for $C_{21}H_{16}N_3S$, 342.10704, found 342.10700 (error = 0.1 ppm). **^{1}H NMR** (400 MHz, DMSO-d_6) δ 11.36 (s, 1H), 8.20 (d, *J* = 5.2 Hz, 1H), 8.02 (d, *J* = 8.5 Hz, 2H), 7.75 (dd, *J* = 7.7, 5.6 Hz, 4H), 7.54 – 7.46 (m, 3H), 7.39 (t, *J* = 7.3 Hz, 1H), 6.93 (s, 1H), 6.81 (d, *J* = 6.0 Hz, 1H), 2.32 (s, 3H). **^{13}C NMR** (101 MHz, DMSO-d_6) δ 159.73, 151.97, 148.47, 148.14, 146.11, 139.66, 138.91, 133.92, 128.92, 127.39, 126.81, 126.41, 126.11, 117.44, 110.58, 106.08, 20.69. **FTIR** (ATR) ν_{max}/cm^{-1}: 3118, 3055, 2926, 2848, 2775, 1655, 1616, 1520, 1478, 1406, 1378, 1348, 1294, 1264, 1243, 1202, 1073, 1040, 1005, 993, 916, 878, 837, 792, 738, 692, 668. *Yellow solid.*

4-([1,1'-biphenyl]-4-yl)-*N*-(6-fluoropyridin-2-yl)thiazol-2-amine (100)

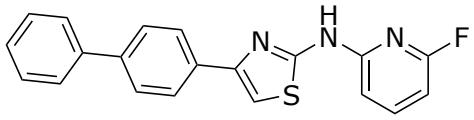

LRMS (ESI+) *m/z* 348.09 $[M+H]^+$, 370.07 $[M+Na]^+$. **HRMS** (ESI+) *m/z* calcd for $C_{20}H_{15}FN_3S$, 348.09652, found 348.09667 (error = 0.4 ppm). **^{1}H NMR** (300 MHz, DMSO-d6) δ 11.71 (s, 1H), 8.02 (d, J = 8.4 Hz, 2H), 7.89 (q, J = 8.1 Hz, 1H), 7.80 – 7.69 (m, 4H), 7.58 (s, 1H), 7.49 (dd, J = 8.2, 6.8 Hz, 2H), 7.44 – 7.33 (m, 1H), 7.07 (dd, J = 8.1, 2.1 Hz, 1H), 6.65 (dd, J = 7.8, 2.1 Hz, 1H). **^{13}C NMR** (75 MHz, DMSO) δ 163.78, 159.83, 151.63, 148.99, 143.56, 140.11, 139.61, 134.12, 129.46, 127.97, 127.39, 126.96, 126.67, 108.06, 107.15, 99.68. *Yellow powder.*

4-(3-chlorophenyl)-5-methyl-N-(4-methylpyridin-2-yl)thiazol-2-amine (101)

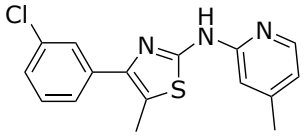

HPLC purity: 99.4%. **LRMS** (ESI+) *m/z* 316.07 $[M+H]^+$, 652.89 $[2M+Na]^+$. **^{1}H NMR** (500 MHz, DMSO-d6) δ 11.14 (s, 1H), 8.13 (d, J = 5.3 Hz, 1H), 7.71 (t, J = 1.9 Hz, 1H), 7.63 (dt, J = 7.8, 1.3 Hz, 1H), 7.47 (t, J = 7.9 Hz, 1H), 7.38 (ddd, J = 8.0, 2.2, 1.0 Hz, 1H), 6.83 (d, J = 1.4 Hz, 1H), 6.76 (dd, J = 5.3, 1.5 Hz, 1H), 2.47 (s, 3H), 2.27 (s, 3H). **^{13}C NMR** (126 MHz, DMSO) δ 156.35, 152.34, 148.99, 146.57, 142.38, 137.95, 133.56, 130.68, 127.93, 127.14, 126.68, 120.51, 117.83, 110.87, 21.17, 12.22. *Off white powder.*

4-([1,1'-biphenyl]-4-yl)-*N*-(5-methoxypyridin-2-yl)thiazol-2-amine (102)

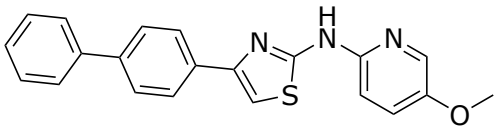

LRMS (ESI+) *m/z* 360.16 $[M+H]^+$, 382.08 $[M+Na]^+$, 741.99 $[2M+Na]^+$. **HRMS** (ESI+) *m/z* calcd for $C_{21}H_{18}N_3OS$, 360.11651, found 360.11611 (error = 1.1 ppm). **^{1}H NMR** (400 MHz, DMSO-d6) δ 11.28 (s, 1H), 8.09 (dd, J = 3.0, 0.6 Hz, 1H), 8.08 – 8.01 (m, 2H), 7.82 – 7.73 (m, 4H), 7.57 – 7.43 (m, 4H), 7.46 – 7.37 (m, 1H), 7.17 (d, J = 9.0 Hz, 1H), 3.86 (s, 3H). **^{13}C NMR** (101 MHz, DMSO-d6) δ 160.60, 150.72, 148.71, 146.65, 140.18, 139.40, 134.46, 131.77, 129.43, 127.90, 127.30, 126.92, 126.62, 126.33, 111.95, 105.54, 56.45. *Crystalline yellow-green solid.*

4-([1,1'-biphenyl]-4-yl)-*N*-(5-fluoropyridin-2-yl)thiazol-2-amine (103)

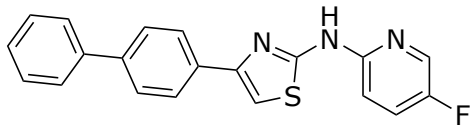

LRMS (ESI+) *m/z* 346.09 $[M-H]^-$. **HRMS** (ESI+) *m/z* calcd for $C_{20}H_{14}FN_3NaS$, 370.07847, found 370.07806 (error = 8.6 ppm). **^{1}H NMR** (400 MHz, DMSO-d6) δ 11.49 (s, 1H), 8.32 (d, J = 3.0 Hz, 1H), 8.05 – 7.97 (m, 2H), 7.78 – 7.68 (m, 5H), 7.53 – 7.44 (m, 3H), 7.42 – 7.33 (m, 1H), 7.19 (dd, J = 9.1, 3.7 Hz, 1H). **^{13}C NMR** (101 MHz, DMSO-d6) δ 160.28, 149.17, 148.83, 140.15, 139.52, 134.30, 133.68, 133.43, 129.44, 127.93, 127.35, 126.94, 126.65, 112.46, 112.41, 106.10. **^{19}F NMR** (471 MHz, DMSO) δ -138.53. *Yellow-green powder.*

N*-(3-Chloropyridin-2-yl)-4-(pyridin-2-yl)thiazol-2-amine (112)*

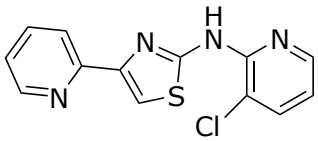

HPLC purity: 99.85%. **LRMS** (ESI-) *m/z* 286.99, 288.92 $[M-H]^-$. **HRMS (ESI-)** *m/z* calcd for $C_{13}H_8ClN_4S$, 287.01637, found 287.01641 (error = 0.1 ppm). **^{1}H NMR** (500 MHz, DMSO-d_6) δ 10.69 (s, 1H), 8.61 (d, J = 4.5 Hz, 1H), 8.34 (d, J = 4.8 Hz, 1H), 8.07 (d, J = 8.0 Hz, 1H), 7.96 – 7.86 (m, 2H), 7.76 (s, 1H), 7.33 (t, J = 6.3 Hz, 1H), 7.05 (t, J = 6.6 Hz, 1H). **^{13}C NMR** (126 MHz, DMSO-d_6) δ 159.84, 152.71, 149.89, 149.28, 148.29, 145.14, 138.64, 137.66, 123.15, 120.63, 117.85, 116.44, 111.10. **FTIR** (ATR) νmax/cm^{-1}: 3420, 3120, 3050, 1589, 1528, 1374, 1296, 1035. *White powder.* Spectroscopic data were in agreement with literature.[382]

N*-(3-Methoxypyridin-2-yl)-4-(pyridin-2-yl)thiazol-2-amine (113)*

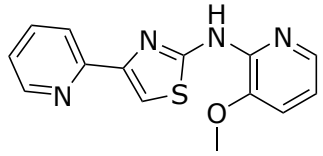

HPLC purity: 99.25%. **LRMS** (ESI-) *m/z* 283.27 $[M-H]^-$. **HRMS (ESI-)** *m/z* calcd for $C_{14}H_{11}N_4OS$, 283.06591, found 283.06593 (error < 0.1 ppm). **^{1}H NMR** (500 MHz, DMSO-d_6) δ 10.19 (d, J = 7.3 Hz, 1H), 8.63 – 8.57 (m, 1H), 8.03 (t, J = 7.5 Hz, 1H), 7.97 (s, 2H), 7.89 (dq, J = 14.4, 6.9, 6.3 Hz, 2H), 7.74 – 7.66 (m, 1H), 7.37 (t, J = 7.1 Hz, 1H), 7.31 (q, J = 6.4 Hz, 1H), 6.98 (td, J = 7.6, 4.9 Hz, 1H), 3.91 (dd, J = 6.1, 2.0 Hz, 3H). **^{13}C NMR** (126 MHz, DMSO-d_6) δ 159.81, 152.91, 149.86, 149.36, 143.08, 142.76, 137.59, 137.30, 123.03, 120.55, 117.44, 116.96, 110.32, 56.30. **FTIR** (ATR) νmax/cm^{-1}: 3427, 3406, 3374, 3250,3129, 3078, 1607, 1590, 1571, 1530, 1463, 1390, 1280, 1230, 1112, 1013, 778, 744, 712, 586, 573, 503. *Brown powder.* Spectroscopic data were in agreement with literature.[382]

N*-(3,5-Dichloropyridin-2-yl)-4-(pyridin-2-yl)thiazol-2-amine (114)*

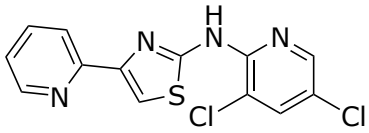

HPLC purity: 99.77%. **LRMS** (ESI+) *m/z* 322.98, 325.06 $[M+H]^+$, 344.98, 346.98 $[M+Na]^+$. **HRMS** (ESI+) *m/z* calcd for $C_{13}H_7Cl_2N_4S$, 320.97740, found 320.97757 (error = 0.5 ppm). **^{1}H NMR** (500 MHz, DMSO-d_6) δ 10.73 (s, 1H), 8.74 (dt, J = 5.6, 1.3 Hz, 1H), 8.44 – 8.34 (m, 3H), 8.28 – 8.18 (m, 2H), 7.76 (ddd, J = 7.1, 5.3, 1.8 Hz, 1H). **^{13}C NMR** (126 MHz, DMSO-d_6) δ 160.44, 147.62, 146.78, 146.75, 144.88, 144.01, 143.38, 138.26, 125.04, 123.28, 123.19, 117.36, 116.37. **FTIR** (ATR) ν_{max}/cm^{-1}: 1589, 1523, 1409, 1375, 1345, 1271, 1240, 1056, 787, 767, 731, 708, 657, 630, 576, 484, 453, 424.

N*-(5,6-Dichloropyridin-2-yl)-4-(pyridin-2-yl)thiazol-2-amine (115)*

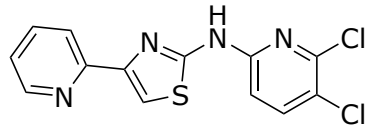

HPLC purity: 97.63%. **LRMS** (ESI+) *m/z* 323.02, 325.01 $[M+H]^+$, 344.96, 346.93 $[M+Na]^+$. **HRMS** (ESI+) *m/z* calcd for $C_{13}H_7Cl_2N_4S$, 320.97740, found 320.97801 (error = 1.9 ppm). **^{1}H NMR** (500 MHz, DMSO-d_6) δ 11.91 (s, 1H), 8.64 (d, J = 4.9 Hz, 1H), 8.07 – 7.97 (m, 3H), 7.87 (s, 1H), 7.45 – 7.39 (m, 1H), 7.17 (d, J = 8.6 Hz, 1H). **^{13}C NMR** (126 MHz, DMSO-d_6) δ 159.91, 151.40, 150.48, 148.64, 148.11, 144.49, 141.27, 139.34, 123.63, 121.11, 119.61, 112.19, 111.84. **FTIR** (ATR) ν_{max}/cm^{-1}: 3310, 3232, 3009, 2791, 1602, 1525, 1448, 1139, 847, 818, 787, 738, 715, 697, 657, 636, 440. *Beige powder.*

N*-(4,6-Dichloropyridin-2-yl)-4-(pyridin-2-yl)thiazol-2-amine (116)*

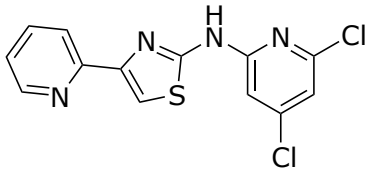

LRMS (ESI+) *m/z* 344.94, 346.94 $[M+Na]^+$. **HRMS** (ESI+) *m/z* calcd for $C_{13}H_7Cl_2N_4S$, 320.97740, found 320.97754 (error = 0.4 ppm). **^{1}H NMR** (500 MHz, DMSO-d_6) δ 11.97 (s, 1H), 8.73 (d, J = 5.5 Hz, 1H), 8.33 (s, 1H), 8.27 (d, J = 8.3 Hz, 1H), 7.70 (s, 1H), 7.30 (t, J = 1.8 Hz, 1H), 7.23 (s, 1H). **^{13}C NMR** (126 MHz, DMSO-d_6) δ 160.29, 152.42, 148.63, 146.95, 145.83, 145.12, 144.06, 142.67, 125.23, 123.54, 117.08, 116.01, 109.60. **FTIR** (ATR) ν_{max}/cm^{-1}: 3335, 1578, 1525, 1439, 1367, 1152, 1093, 844, 817, 786, 747, 689, 654, 618, 485, 437. *Pale yellow powder.*

N*-(4,5-Dichloropyridin-2-yl)-4-(pyridin-2-yl)thiazol-2-amine (117)*

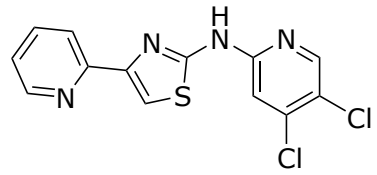

HPLC purity: 99.99%. **LRMS** (ESI+) *m/z* 323.04, 324.92 $[M+H]^+$, 344.94, 346.92 $[M+Na]^+$. **HRMS** (ESI+) *m/z* calcd for $C_{13}H_7Cl_2N_4S$, 320.97740, found 320.97757 (error = 0.5 ppm). **^{1}H NMR** (500 MHz, DMSO-d_6) δ 11.75 (s, 1H), 8.62 (d, J = 4.7 Hz, 1H), 8.54 (s, 1H), 8.03 – 7.92 (m, 2H), 7.79 (s, 1H), 7.38 (d, J = 5.2 Hz, 2H). **^{13}C NMR** (126 MHz, DMSO-d_6) δ 160.02, 151.70, 151.18, 148.38, 147.77, 147.20, 141.98, 139.67, 123.71, 121.23, 120.96, 112.38, 112.14. **FTIR** (ATR) νmax/cm^{-1}: 3405, 3223, 3010, 2798, 1580, 1525, 1447, 1425, 1212, 906, 848, 787, 748, 740, 716, 697, 660, 440. *Beige powder.*

N*-(7*H*-Purin-2-yl)-4-(pyridin-2-yl)thiazol-2-amine (119)*

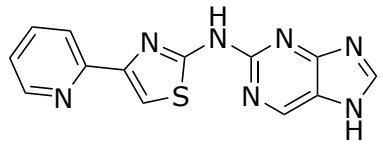

LRMS (ESI-) *m/z* 294.05 $[M-H]^-$. **HRMS** (ESI-) *m/z* calcd for $C_{13}H_8N_7S$, 294.05674, found 294.05680 (error = 0.2 ppm). **^{1}H NMR** (400 MHz, DMSO-d_6) δ 11.74 (s, 1H), 8.99 (s, 1H), 8.64 – 8.58 (m, 1H), 8.42 (s, 1H), 8.10 – 8.00 (m, 1H), 7.98 – 7.89 (m, 1H), 7.77 (s, 1H), 7.66 (d, *J* = 8.3 Hz, 1H), 7.36 (dd, *J* = 7.4, 4.9 Hz, 1H), 7.22 (s, 1H), 7.09 (s, 1H), 6.96 (s, 1H). **FTIR** (ATR) ν_{max}/cm^{-1}: 3404, 3050, 2922, 1618, 1591, 1563, 1391, 1348, 1243, 791, 741, 713, 616, 578, 454.

***N*-(6-Methylpyridin-2-yl)-4-(pyridin-2-yl)thiazol-2-amine (127)**

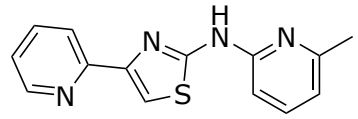

HPLC purity: 98.63%. **LRMS** (ESI-) *m/z* 267.01 $[M-H]^-$. **HRMS** (ESI-) *m/z* calcd for $C_{14}H_{11}N_4S$, 267.07099, found 267.07098 (error = 0.1 ppm). **^{1}H NMR** (500 MHz, DMSO-d_6) δ 11.37 (s, 1H), 8.62 – 8.57 (m, 1H), 8.00 – 7.94 (m, 1H), 7.87 (td, *J* = 7.6, 1.8 Hz, 1H), 7.66 (s, 1H), 7.60 (t, *J* = 7.7 Hz, 1H), 7.30 (ddd, *J* = 7.5, 4.7, 1.2 Hz, 1H), 6.91 (d, *J* = 8.2 Hz, 1H), 6.79 (d, *J* = 7.3 Hz, 1H), 2.48 (s, 3H).**^{13}C NMR** (126 MHz, DMSO-d_6) δ 160.35, 155.62, 153.02, 151.55, 149.86, 149.27, 138.65, 137.61, 122.94, 120.30, 115.46, 110.13, 107.99, 23.86. **FTIR** (ATR) ν_{max}/cm^{-1}: 3233, 3176, 3113, 3060, 2981, 2915, 2857, 2820, 2755, 1612, 1549, 1454, 1421, 1340, 1274, 1212, 1166, 1072, 1000, 912, 784, 723, 657. *Grey powder (250 mg, 66%).* Spectroscopic data were in agreement with literature.[47,381]

***N*-(5-Methylpyridin-2-yl)-4-(pyridin-2-yl)thiazol-2-amine (128)**

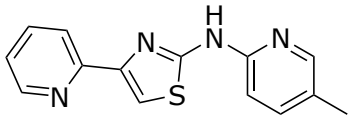

HPLC purity: 95.41%. **LRMS** (ESI+) *m/z* 269.15 $[M+H]^+$, 291.15 $[M+Na]^+$. **HRMS** (ESI+) *m/z* calcd for $C_{14}H_{12}N_4NaS$, 291.06749, found 291.06739 (error = 0.3 ppm). **^{1}H NMR** (400 MHz, DMSO-d_6) δ 11.32 (s, 1H), 8.60 (ddd, *J* = 4.8, 1.9, 1.0 Hz, 1H), 8.17 (d, *J* = 2.3 Hz, 1H), 7.97 (dt, *J* = 7.9, 1.2 Hz, 1H), 7.89 (td, *J* = 7.7, 1.8 Hz, 1H), 7.63 (s, 1H), 7.58 (dd, *J* = 8.3, 2.4 Hz, 1H), 7.32 (ddd, *J* = 7.5, 4.7, 1.3 Hz, 1H), 7.05 (d, *J* = 8.4 Hz, 1H), 2.25 (s, 3H).**^{13}C NMR** (101 MHz, DMSO-d_6) δ 160.50, 153.00, 150.34, 149.88, 149.37, 146.27, 139.29, 137.60, 125.26, 122.95, 120.33, 110.87, 109.64, 17.65. **FTIR** (ATR) ν_{max}/cm^{-1}: 3220, 3153, 3010, 2954, 2921, 2854, 1674, 1598, 1536, 1493, 1371, 1316, 1224, 1152, 1024, 818, 736, 707, 627, 512. *Brown powder.* Spectroscopic data were in agreement with literature.[47]

4-(5-Chloropyridin-2-yl)-*N*-(4-methylpyridin-2-yl)thiazol-2-amine (129)

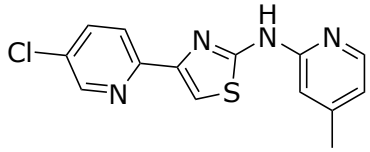

HPLC purity: 99.65%. **LRMS** (ESI+) *m/z* 303.09 $[M+H]^+$, 325.01 $[M+Na]^+$. **HRMS** (ESI+) *m/z* calcd for $C_{14}H_{12}ClN_4S$, 303.04657, found 303.04662 (error = 0.2 ppm). **^{1}H NMR** (400 MHz, Methanol-d_4) δ 8.61 (d, *J* = 2.5 Hz, 1H), 8.28 (d, *J* = 6.0 Hz, 1H), 8.16 (d, *J* = 8.6 Hz, 1H), 7.97 (dd, *J* = 8.6, 2.5 Hz, 1H), 7.84 (s, 1H), 7.14 – 7.06 (m, 2H), 2.51 (s, 3H). **^{13}C NMR** (101 MHz, Methanol-d_4) δ 161.23, 150.15, 149.89, 147.50, 137.14, 130.84, 121.97, 118.41, 112.04, 111.22, 66.73, 20.27. **FTIR** (ATR) ν_{max}/cm^{-1}: 3409, 3234, 3053, 2921, 1618, 1544, 1488, 1455, 1386, 1238, 1167, 1108, 1010, 847, 804, 756. *Pale brown powder (1.8 mg, 0.4%).*

***N*-(6-Bromopyridin-2-yl)-4-(pyridin-2-yl)thiazol-2-amine (130)**

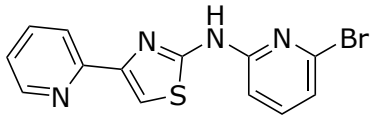

HPLC purity: 99.88%. **LRMS** (ESI+) *m/z* 332.99, 334.99 $[M+H]^+$, 354.92, 356.93 $[M+Na]^+$. **HRMS** (ESI+) *m/z* calcd for $C_{13}H_9BrN_4NaS$, 354.96235, found 354.96238 (error = 0.1 ppm). **^{1}H NMR** (500 MHz, DMSO-d_6) δ 11.72 (s, 1H), 8.60 (ddd, *J* = 4.7, 1.8, 0.9 Hz, 1H), 7.97 (dt, *J* = 7.9, 1.2 Hz, 1H), 7.88 (td, *J* = 7.7, 1.8 Hz, 1H), 7.74 (s, 1H), 7.69 – 7.62 (m, 1H), 7.32 (ddd, *J* = 7.5, 4.8, 1.3 Hz, 1H), 7.17 – 7.10 (m, 2H). **^{13}C NMR** (126 MHz, DMSO-d_6) δ 159.96, 152.80, 152.57, 149.91, 149.51, 141.10, 138.09, 137.67, 123.08, 120.38, 119.35, 110.60, 110.21. **FTIR** (ATR) ν_{max}/cm^{-1}: 3424, 3206, 3124, 3010, 2897, 2811, 1591, 1523, 1445, 1396, 1329, 1271, 1168, 1132, 106, 1001, 984, 943, 781, 725, 646. *Beige powder (232 mg, 64%).*

***N*-(3-Bromopyridin-2-yl)-4-(pyridin-2-yl)thiazol-2-amine (131)**

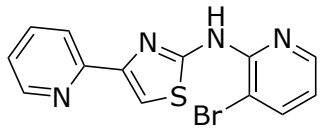

HPLC purity: 95.26%. **LRMS** (ESI+) *m/z* 334.97 $[M+H]^+$, 354.94, 356.94 $[M+Na]^+$. **HRMS** (ESI-) *m/z* calcd for $C_{13}H_8BrN_4S$, 330.96585, found 330.96586 (error < 0.1 ppm). **^{1}H NMR** (400 MHz, DMSO-d_6) δ 8.72 (d, *J* = 5.6 Hz, 1H), 8.46 – 8.35 (m, 3H), 8.25 (s, 1H), 8.15 (d, *J* = 7.8 Hz, 1H), 7.76 (t, *J* = 6.4 Hz, 1H), 7.09 – 7.00 (m, 1H). **^{13}C NMR** (101 MHz, DMSO-d_6) δ 160.72, 148.29, 147.42, 145.79, 144.67, 143.92, 142.79, 142.43, 125.10, 123.14, 119.16, 116.47, 106.31. **FTIR** (ATR) ν_{max}/cm^{-1}: 3386, 3219, 3093, 3050, 1590, 1530, 1443, 1384, 1285, 1226, 1014, 736, 593. *Yellow powder.* Spectroscopic data were in agreement with the literature.[382]

4-(Pyridin-2-yl)-*N*-(6-(trifluoromethyl)pyridin-2-yl)thiazol-2-amine (132)

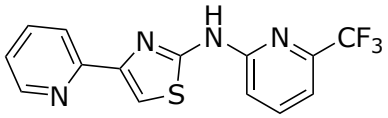

HPLC purity: 97.56%. **LRMS** (ESI-) *m/z* 320.99 $[M-H]^-$. **HRMS** (ESI-) *m/z* calcd for $C_{14}H_8F_3N_4S$, 321.04273, found 321.04269 (error = 0.1 ppm). **^{1}H NMR** (500 MHz, DMSO-d_6) δ 8.60 (ddd, *J* = 4.9, 1.8, 0.9 Hz, 1H), 8.01 – 7.93 (m, 2H), 7.88 (td, *J* = 7.7, 1.8 Hz, 1H), 7.77 (s, 0H), 7.38 (dd, *J* = 9.2, 7.8 Hz, 2H), 7.32 (ddd, *J* = 7.5, 4.7, 1.2 Hz, 1H). **^{13}C NMR** (126 MHz, DMSO-d_6) δ 160.07, 152.78 (d, *J* = 8.6 Hz), 149.90, 149.55, 143.98 (q, *J* = 34.1 Hz), 139.91, 137.66, 123.19, 123.08, 121.01, 120.40, 115.39, 112.74 (d, *J* = 3.3 Hz), 110.84. **^{19}F NMR** (471 MHz, DMSO-d_6) δ -67.00. **FTIR** (ATR) ν_{max}/cm^{-1}: 3171, 3114, 3056, 2999, 2958, 1613, 1515, 1462, 1427, 1372, 1313, 1278, 1179, 1158, 1133, 1072, 991, 965, 803, 738, 718, 645. *Ivory powder (273 mg, 78%).*

4-(Pyridin-2-yl)-*N*-(5-(trifluoromethyl)pyridin-2-yl)thiazol-2-amine (133)

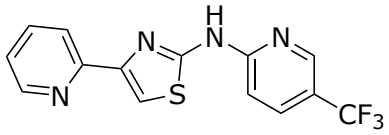

HPLC purity: 97.27%. **LRMS** (ESI+) *m/z* 323.08 $[M+H]^+$. **HRMS** (ESI+) *m/z* calcd for $C_{14}H_9F_3N_4NaS$, 345.03922, found 345.03984 (error = 1.8 ppm). **^{1}H NMR** (500 MHz, DMSO-d_6) δ 8.67 (d, *J* = 2.4 Hz, 1H), 8.62 – 8.57 (m, 1H), 8.03 (dd, *J* = 8.9, 2.5 Hz, 1H), 7.98 (d, *J* = 7.8 Hz, 1H), 7.92 – 7.85 (m, 1H), 7.74 (s, 1H), 7.32 (dd, *J* = 7.5, 4.8 Hz, 1H), 7.24 (d, *J* = 8.8 Hz, 1H). **^{13}C NMR** (126 MHz, DMSO-d_6) δ 160.01, 155.16, 152.77, 149.92, 149.55, 144.85 (d, *J* = 4.6 Hz), 137.71, 135.27 (d, *J* = 3.2 Hz), 125.93 (t, *J* = 270.9 Hz), 123.13, 120.44, 117.25 (q, *J* = 32.3 Hz), 111.65, 110.98. **^{19}F NMR** (471 MHz, DMSO-d_6) δ -59.78. **FTIR** (ATR) ν_{max}/cm^{-1}: 3014, 1617, 1542, 1457, 1391, 1324, 1160, 1132, 1102, 1078, 934, 831, 739, 675, 627. *Ivory powder.*

***N*-(3-Fluoropyridin-2-yl)-4-(pyridin-2-yl)thiazol-2-amine (134)**

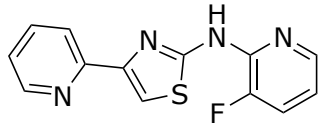

HPLC purity: 97.36%. **LRMS** (ESI+) *m/z* 273.08 $[M+H]^+$, 295.07 $[M+Na]^+$, 566.99 $[2M+Na]^+$. **HRMS** (ESI+) *m/z* calcd for $C_{13}H_9FN_4NaS$, 295.04242, found 295.04242 (error < 0.1 ppm). **^{1}H NMR** (500 MHz, DMSO-d_6) δ 11.45 (s, 1H), 8.62 – 8.57 (m, 1H), 8.17 (dd, *J* = 4.9, 1.4 Hz, 1H), 8.03 (d, *J* = 7.9 Hz, 1H), 7.89 (td, *J* = 7.7, 1.8 Hz, 1H), 7.74 – 7.64 (m, 2H), 7.35 – 7.29 (m, 1H), 7.03 (ddd, *J* = 8.1, 4.9, 3.3 Hz, 1H). **^{13}C NMR** (126 MHz, DMSO-d_6) δ 159.72, 152.73, 149.86, 149.32, 147.73, 145.68, 142.14, 141.83, 137.73, 123.20, 120.62, 117.15, 110.64. **^{19}F NMR** (471 MHz, DMSO-d_6) δ -134.37. **FTIR** (ATR) ν_{max}/cm^{-1}: 3414, 1620, 1590, 1537, 1456, 1411, 1335, 1298, 1262, 1230, 1095, 778, 738, 706, 536, 448. *Beige powder (537 mg, 72%)*. Spectroscopic data were in agreement with literature.[382]

5-Chloro-N-(thiophen-2-ylmethyl)pyrazolo[1,5-a]pyrimidin-7-amine (148)

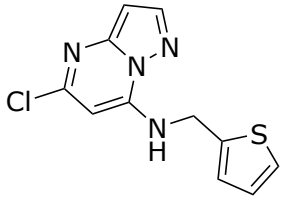

Prepared according a procedure by Gentles *et al.*[279] A solution of 5,7-dichloropyrazolo[1,5-*a*]pyrimidine (404 mg, 2.15 mmol) and thiophen-2-ylmethanamine (240 µL, 2.33 mmol) in acetonitrile (10 mL) was heated to 80°C for 24 hours. The reaction mixture was then cooled to room temperature and diluted with sodium carbonate solution (sat. aq., 10 mL) and extracted with ethyl acetate (2 × 25 mL). The combined organic layers were dried over magnesium sulfate and concentrated under reduced pressure, then purified by automated flash column chromatography (0–40%, EtOAc/hexanes with 0.1% NEt_3) (ethyl acetate in hexane with 0.1% triethylamine). The fractions containing the product were concentrated and triturated with cold methanol to yield the product as a red solid (279 mg, 49%). **LRMS** (ESI+) *m/z* 265.06, 267.09 $[M+H]^+$. **HRMS** (ESI+) *m/z* calcd for $C_{11}H_{10}ClN_4S$, 265.03092, found 265.03090 (error < 0.1 ppm). **^{1}H NMR** (400 MHz, Chloroform-*d*) δ 7.89 (d, *J* = 2.2 Hz, 1H), 7.23 (dd, *J* = 5.1, 1.2 Hz, 1H), 7.01 (dd, *J* = 3.5, 1.2 Hz, 1H), 6.93 (dd, *J* = 5.1, 3.5 Hz, 1H), 6.80 (d, *J* = 5.9 Hz, 1H), 6.37 (d, *J* = 2.2 Hz, 1H), 5.96 (s, 1H), 4.68 (dd, *J* = 5.8, 0.9 Hz, 2H). **^{13}C NMR** (101 MHz, Chloroform-*d*) δ 150.52, 146.59, 145.63, 143.32, 137.08, 126.28, 125.68, 125.05, 95.14, 84.11, 40.28. **FTIR** (ATR) ν_{max}/cm^{-1}: 3344, 3086, 2924, 2851, 1581, 1434, 1365, 1331, 1252, 1230, 1173, 1111, 894, 849, 797, 763, 706, 629, 564, 465.

7.5 Compounds described in chapter 5

7.5.1 Intermediates

1,4,8,11-Tetraazatricyclo[9.3.1.14,8]hexadecane (191)

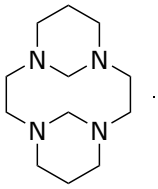

Prepared according to a previously described method.[383] Cyclam (1.05 g, 5.2 mmol, 1.0 equiv.) was dissolved in water (80 mL), and then formaldehyde (37% aq., 0.8 mL, 10.6 mmol, 2.0 equiv.) was added. The mixture was stirred at 0°C for one hour before being filtered under reduced pressure and washed with ice cold water (3 × 20 mL) to yield the bridged cyclam as a white powder (0.877 g, 78%). **m.p.** 104–107°C (lit. 106–108°C).[384] **LRMS** (ESI+) *m/z* 225.2 $[M+H]^+$. **^{1}H NMR** (300 MHz, Chloroform-*d*) δ 5.43 (dt, *J* = 10.9, 2.3 Hz, 2H), 3.22 – 3.08 (m, 4H), 2.89 (d, *J* = 10.9 Hz, 2H), 2.87 – 2.79 (m, 3H), 2.68 – 2.55 (m, 4H), 2.41 – 2.34 (m, 6H), 1.18 (dtt, *J* = 13.5, 3.6, 1.6 Hz, 2H). Spectroscopic values were in agreement with those reported in the literature.[384]

1,8-Di-prop-2-ynyl-1,4,8,11-tetraaza-tricyclo[9.3.1.14,8]hexadecane bromide salt (192)

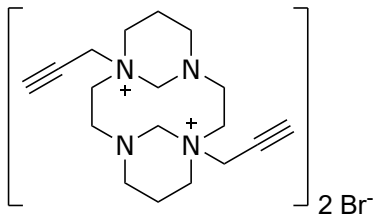

Prepared according to a previously described method.[383] **191** (1.00 g, 4.46 mmol) was dissolved in acetonitrile (64 mL), and then propargyl bromide (3.4 mL, 22.9 mmol) was added. The mixture was stirred for 17 hours at room temperature. The white precipitate formed was collected by filtration under reduced pressure and washed with ice-cold acetonitrile (2 × 50 mL) to yield an off-white powder (1.89 g, 98%). **LRMS** (ESI-) *m/z* 301.2 $[M-H]^-$. **^{1}H NMR** (300 MHz, Deuterium Oxide) δ 3.50 (s, 4H), 3.40 – 3.27 (m, 7H), 2.88 (dq, *J* = 18.3, 7.2, 6.3

Hz, 9H), 2.03 – 1.89 (m, 4H). Spectroscopic values were in agreement with those reported in the literature.

1,8-Di-(Boc)-4,11-di(propargyl)cyclam (181)

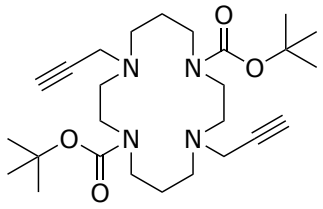

Prepared according to a literature procedure.[384] **192-2** (1.89 g, 4.34 mmol) was suspended in methanol (30 mL) and then NaOH (2.5 M aq., 30 mL) was added. The mixture was stirred for 2 hours at room temperature before di-*tert*-butyl dicarbonate (2 mL, 8.71 mmol) was added. The mixture was stirred at room temperature for 24 hours before additional di-*tert*-butyl dicarbonate (1 mL, 4.35 mmol) was added. After an additional 24 hours of stirring at room temperature, the mixture was filtered under reduced pressure, washed with water (3 × 20 mL) and dried under reduced pressure to yield a white powder (1.12 g, 54%).

LRMS (ESI+) *m/z* 477.33 $[M+H]^+$, 499.3 $[M+Na]^+$. **^{1}H NMR** (300 MHz, Chloroform-*d*) δ 3.36 (d, *J* = 17.5 Hz, 12H), 2.65 (t, *J* = 5.7 Hz, 4H), 2.52 (t, *J* = 6.5 Hz, 4H), 2.16 (s, 2H), 1.70 (q, *J* = 6.8 Hz, 4H), 1.46 (s, 18H). Spectroscopic values were in agreement with those reported in the literature.[384]

Ferrocenyl methyl ester (185)

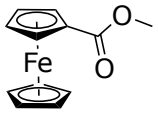

Ferrocenecarboxylic acid (208 mg, 0.904 mmol, 1.0 equiv.) was dissolved in dimethyl carbonate (4 mL) and then DBU (0.210 mL, 1.39 mmol, 1.6 equiv.) was added before the mixture was heated and stirred at reflux for 18 hours. The solution was then cooled to room temperature, diluted with water (50 mL) and brine (30 mL), and extracted with ethyl acetate (3 × 40 mL). The combined organic extracts were washed with HCl solution (1.0 M aq.,

2 × 100 mL) and sodium bicarbonate solution (sat. aq., 2 × 100 mL), then dried over magnesium sulfate and concentrated under reduced pressure to yield the product as a red-orange solid (155 mg, 70%). The material was used without further purification.

LRMS (ESI+) *m/z* 244.03 $[M+H]^+$, 267.03 $[M+Na]^+$. **^{1}H NMR** (300 MHz, Chloroform-*d*) δ 4.80 (t, *J* = 2.0 Hz, 2H), 4.39 (t, *J* = 2.0 Hz, 2H), 4.21 (s, 5H), 3.81 (s, 3H). **FTIR** (ATR) ν_{max}/cm^{-1}: 3088, 2997, 2953, 2923, 2853, 1696, 1462, 1277, 1136, 1104, 960, 819, 771, 503, 482, 460. Spectroscopic data were in agreement with the literature.[385]

Ferrocenylmethanol (189)

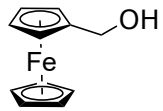

Ferrocenyl methyl ester **185** (396 mg, 1.62 mmol, 1.0 equiv.) was dissolved in anhydrous THF (10 mL) under nitrogen and then $LiAlH_4$ (2.0 mL, 1.0 M in THF, 2.0 mmol, 1.23 equiv.) was added dropwise. The reaction mixture was stirred for 3 hours before being quenched with ethyl acetate (15 mL) and poured over Rochelle's salts (sat., aq., 40 mL). The mixture was extracted with ethyl acetate (4 × 40 mL) and washed with brine (100 mL). The combined organic layers were dried over magnesium sulfate and concentrated under reduced pressure to yield a red-orange solid (332 mg, 95%).

LRMS (APCI+) *m/z* 199.84 $[M-OH]^+$. **HRMS** (APCI+) *m/z* calcd for $C_{11}H_{11}Fe$, 199.0204, found 199.02040 (error = 0.3 ppm). **^{1}H NMR** (500 MHz, Chloroform-*d*) δ 4.35 – 4.30 (m, 2H), 4.25 (d, *J* = 15.8 Hz, 2H), 4.17 (s, 5H), 4.12 (d, *J* = 11.7 Hz, 2H). **^{13}C NMR** (126 MHz, Chloroform-*d*) δ 88.47, 83.76, 69.36, 68.45, 68.29, 67.88, 60.78. **FTIR** (ATR) ν_{max}/cm^{-1}: 3087, 2953, 1696, 1462, 1048. Spectroscopic data were in agreement with the literature.[386,387]

Azidomethylferrocene (190)

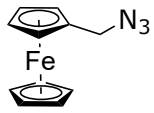

Following a method by Liubimtsev *et al.*,[388] **189** (332 mg, 1.54 mmol, 1.0 equiv.) was dissolved in anhydrous THF (10 mL), and then DPPA (0.4 mL, 1.85 mmol, 1.2 equiv.) and DBU (0.28 mL, 1.85 mmol, 1.2 equiv.) were added. The reaction mixture was stirred for one hour, then heated and stirred at reflux for two hours, before sodium azide (117 mg, 1.69 mmol, 1.1 equiv.) was added. The mixture was heated and stirred at reflux for a further 21 hours, and further DPPA (0.26 mL, 1.23 mmol, 0.8 equiv.) and DBU (0.18 mL, 1.23, 0.8 equiv.) was added. After six hours of further heating stirring at reflux, the reaction mixture was quenched with water (40 mL) and extracted with toluene (3 × 60 mL), before being washed with brine (150 mL), dried over magnesium sulfate and concentrated under reduced pressure. The crude product was purified by flash column chromatography (ethyl acetate in hexanes, 0–10%) to yield a dark red solid (236 mg, 64%).

LRMS (ESI+) *m/z* 241.08 $[M+H]^+$. **HRMS** (ESI+) *m/z* calcd for $C_{11}H_{11}FeN_3$, 241.02969, found 241.02966 (error = 0.10 ppm). **^{1}H NMR** (300 MHz, Chloroform-*d*) δ 4.24 (s, 2H), 4.20 (s, 2H), 4.17 (s, 5H), 4.12 (s, 2H). **FTIR** (ATR) ν_{max}/cm^{-1}: 3092, 2962, 2925, 2869, 2089, 1258, 1105, 1000, 801, 480. Spectroscopic data were in agreement with the literature.[388,389]

1,8-Di-(Boc)-4,11-bis((1-(1-adamantyl)-1*H*-1,2,3-triazol-4-yl)methyl)cyclam (182)

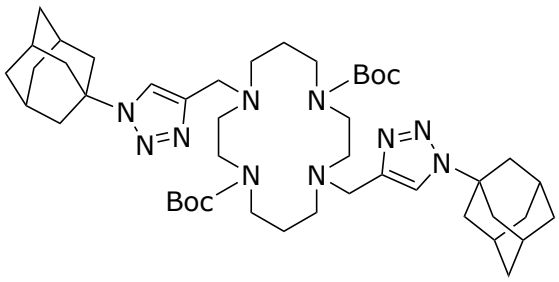

181 (768 mg, 1.61 mmol, 1.0 equiv.) and **1911** (565 mg, 3.19 mmol, 2.0 equiv.) were combined according to **General Synthetic Procedure D** and the crude product was purified by flash column chromatography (5:95, MeOH:CH_2Cl_2,) to yield a golden crystalline solid (970 mg, 72%).

LRMS (ESI+) *m/z* 831.74 $[M+H]^+$. **HRMS** (ESI+) *m/z* calcd for $C_{46}H_{75}N_{10}O_4$, 831.59673, found 831.59658 (error = 0.2 ppm). **^{1}H NMR** (400 MHz, Chloroform-*d*) δ 7.45 (s, 2H), 3.76 (s, 4H), 3.33 (d, *J* = 19.3 Hz, 8H), 2.57 (t, *J* = 5.9 Hz, 4H), 2.46 (t, *J* = 6.4 Hz, 4H), 2.22 (d, *J* = 7.6 Hz, 24H), 2.15 (s, 6H), 1.85 – 1.69 (m, 4H), 1.40 (s, 18H). **^{13}C NMR** (101 MHz, Chloroform-*d*) δ 185.47, 155.77, 118.42, 79.25, 59.32, 53.02, 51.60, 46.45, 42.99, 41.53, 35.94, 30.87, 29.81, 29.46, 28.48, 26.95. **FTIR** (ATR) ν_{max}/cm^{-1}: 2908, 2852, 2085, 1684.

1,8-Di-(Boc)-4,11-bis((1-(methylferrocenyl)-1*H*-1,2,3-triazol-4-yl)methyl)-1,4,8,11-tetraazacyclotetradecane (183)

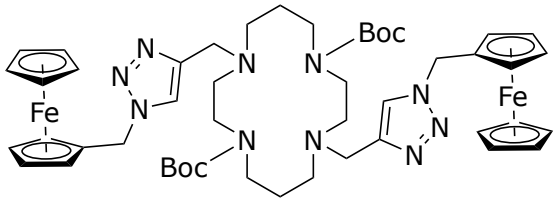

183 was synthesised from **181** (132 mg, 0.276 mmol, 1.0 equiv.) and **190** (112 mg, 0.466 mmol, 1.7 equiv.) according to **General Synthetic Procedure D**, and purified *via* automated column chromatography to yield the product as a green foam (182 mg, 81%).

LRMS (ESI+) *m/z* 959.44 $[M+H]^+$, 981.42 $[M+Na]^+$. **HRMS** (ESI+) *m/z* calcd for $C_{48}H_{67}Fe_2N_{10}O_4$, 959.40400, found 959.40404 (error < 0.1 ppm). **^{1}H NMR** (300 MHz, Chloroform-*d*) δ 7.30 (s, 2H), 5.24 (s, 4H), 4.27 (s, 4H), 4.19 (t, *J* = 1.9 Hz, 4H), 4.17 (s, 10H), 3.69 (s, 4H), 3.28 (s, 8H), 2.55 (s, 4H), 2.47 – 2.37 (m, 4H), 1.69 (s, 4H), 1.40 (s, 18H). **^{13}C NMR** (126 MHz, Chloroform-*d*) δ 155.86, 122.07, 121.64, 81.24, 79.40, 69.18, 69.06, 53.84, 53.59, 52.20, 50.61, 50.11, 47.11, 46.66, 30.49, 28.63. **FTIR** (ATR) ν_{max}/cm^{-1}: 3089, 2971, 2930, 2811, 1683, 1456, 1365, 1156, 1106, 1045, 483.

***N*,*N*'-Di-(Boc)-1,6-diaminohexane (198)**

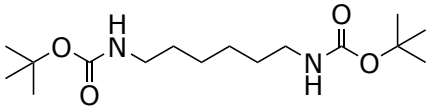

Prepared according to a previously described method.[326] Di-*tert*-butyl dicarbonate (9 mL, 39.2 mmol) in chloroform (20 mL) was added dropwise to a solution of 1,6-diaminohexane (2.18 g, 18.8 mmol) in chloroform (10 mL). The mixture was stirred for 18 hours at room

temperature before being concentrated at reduced pressure. The residue was diluted with water (50 mL) and extracted with chloroform (3 × 25 mL). The combined organic extracts were washed with sodium bicarbonate solution (sat. aq., 75 mL) and brine (85 mL), dried over magnesium sulfate and then filtered. The filtrate was concentrated under reduced pressure to yield the product as a white powder (5.93 g, 99%).

m.p. *102–105*°C (lit. 101–103°C).[390]). **LRMS** (ESI+) *m/z* 339.2 $[M+Na]^+$, 655.4 $[2M+Na]^+$. **^{1}H NMR** (300 MHz, Chloroform-*d*) δ 4.54 (s, 2H), 3.12 (q, *J* = 6.7 Hz, 4H), 1.46 (s, 20H), 1.35 (q, *J* = 4.2, 3.8 Hz, 4HSpectroscopic values were in agreement with those reported in the literature.[391]

_N_,_N_'-Di-(Boc)-_N_,_N_'-dipropargyl-1,6-diaminohexane (199)

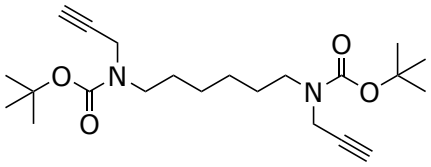

Sodium hydride (60% in mineral oil dispersion, 449 mg, 11.2 mmol, 8.7 equiv.) and **198** (407 mg, 1.29 mmol, 1.0 equiv.) were combined in an oxygen-free environment and dissolved in anhydrous solvent (DMF:THF, 1:5, 18 mL). After 5 minutes of stirring at room temperature, propargyl bromide (80% in toluene, 0.5 mL, 4.67 mmol, 3.6 equiv.) was added and the mixture was stirred at room temperature for 24 hours until it turned black. Despite incomplete consumption of starting material indicated by TLC, the mixture was diluted with ammonium chloride solution (sat. aq., 25 mL) and water (55 mL) and extracted with toluene (4 × 50 mL). The combined organic extracts were washed with water (3 × 125 mL) and brine (150 mL) and dried over magnesium sulfate before being concentrated under reduced pressure to yield the crude product as a light brown gum. This material was purified by manual column chromatography (ethyl acetate in hexanes, 5–30%) to obtain the desired product as a thick yellow oil (129 mg, 26%).

LRMS (ESI+) *m/z* 415.25 $[M+Na]^+$. **HRMS** (ESI+) *m/z* calcd for $C_{22}H_{36}N_2NaO_4$, 415.25673, found 415.25638 (error = 0.8 ppm). **^{1}H NMR** (300 MHz, Chloroform-*d*) δ 4.01 (s, 4H), 3.29 (t, *J* = 7.4 Hz, 4H), 2.17 (t, *J* = 2.4 Hz, 2H), 1.63 – 1.50 (m, 4H), 1.46 (s, 18H), 1.36 – 1.26 (m,

4H). **FTIR** (ATR) ν_{max}/cm^{-1}: 3245, 2916, 2848, 1687, 1468, 1411, 1366, 1246, 1159, 773, 718. Spectroscopic data were in agreement with the literature.[392]

N,*N*'-Di(Boc)-*N*-propargyl-1,6-diaminohexane (200)

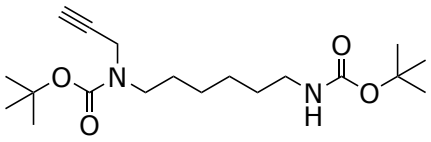

The mono-propargylated side product ***200*** was also isolated from the above procedure as a yellow oil (164 mg, 36%).

LRMS (ESI+) *m/z* 377.24 $[M+Na]^+$. **HRMS** (ESI+) *m/z* calcd for $C_{19}H_{34}N_2NaO_4$, 377.24108, found 377.24095 (error = 0.3 ppm). **^{1}H NMR** (500 MHz, Chloroform-*d*) δ 8.99 (d, *J* = 5.5 Hz, 1H), 4.83 – 4.78 (m, 1H), 3.87 – 3.82 (m, 2H), 3.13 (q, *J* = 6.2, 5.2 Hz, 2H), 2.93 (t, *J* = 7.0 Hz, 2H), 1.39 (dh, *J* = 11.0, 6.7 Hz, 4H), 1.33 – 1.25 (m, 18H), 1.22 – 1.09 (m, 4H). **^{13}C NMR** (126 MHz, Chloroform-*d*) δ 162.83, 155.95, 79.80, 79.79, 79.70, 78.58, 71.28, 53.37, 46.23, 40.27, 29.87, 28.30, 28.23, 27.88, 26.30. **FTIR** (ATR) ν_{max}/cm^{-1}: 3311, 2976, 2932, 2861, 1685, 1365, 1245, 1163, 774.

N,*N*'-Di-(Boc)-*N*,*N*'-bis(1-(1-adamantyl)-1*H*-1,2,3-triazol-4-yl)methyl-1,6-diaminohexane (202)

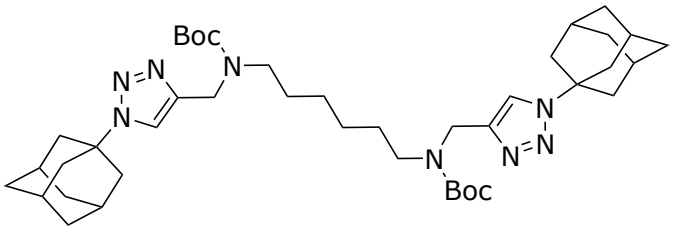

202 was prepared from **199** (123 mg, 0.313 mmol, 1.0 equiv.) and 1-azidoadamantane (128 mg, 0.720 mmol, 2.3 equiv.) according to **General Synthetic Procedure D**. The crude material was purified *via* automated column chromatography to give **202** as a white crystalline solid (107 mg, 46%).

LRMS (ESI+) *m/z* 747.56 ($[M+H]^+$), 769.53 $[M+Na]^+$. **HRMS** (ESI+) *m/z* calcd for $C_{42}H_{66}N_8NaO_4$, 769.50992, found 769.50901 (error = 1.19 ppm). **^{1}H NMR** (300 MHz,

Chloroform-*d*) δ 7.51 (d, *J* = 40.5 Hz, 2H), 4.45 (s, 4H), 3.22 (t, *J* = 7.3 Hz, 4H), 2.25 (s, 6H), 2.21 (d, *J* = 2.7 Hz, 12H), 1.86 – 1.71 (m, 12H), 1.52 (d, *J* = 12.2 Hz, 4H), 1.45 (s, 18H), 1.25 (td, *J* = 9.5, 4.2 Hz, 4H). **^{13}C NMR** (126 MHz, Chloroform-*d*) δ 155.80, 144.40, 119.00, 79.59, 59.43, 47.00, 43.00, 41.94, 35.93, 29.46, 28.53, 28.30, 28.04, 26.59. **FTIR** (ATR) ν_{max}/cm^{-1}: 2910, 2854, 1688, 1411, 1364, 1245, 1166, 1013, 878, 777.

_N_,_N_'-Di-(Boc)-_N_,_N_'-bis(1-(methylferrocenyl)-1_H_-1,2,3-triazol-4-yl)methyl-1,6-diaminohexane (201)

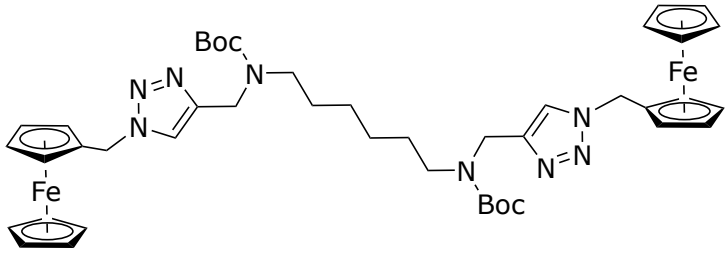

201 was prepared from **199** (42 mg, 0.107 mmol, 1.0 equiv.) and **190** (58.2 mg, 0.241 mmol, 2.3 equiv.) according to **General Synthetic Procedure D**. The crude material was purified *via* automated column chromatography to give **201** as a red solid (62 mg, 70%).

LRMS (ESI+) *m/z* 897.34 ([M+H]$^+$). **HRMS** (ESI+) *m/z* calcd for $C_{44}H_{58}Fe_2N_8NaO_4$, 897.31720, found 897.31736 (error = 0.2 ppm). **^{1}H NMR** (400 MHz, Chloroform-*d*) δ 7.46 (dt, *J* = 24.2, 13.5 Hz, H), 5.26 (d, *J* = 7.2 Hz, 4H), 4.40 (s, 4H), 4.24 (s, 4H), 4.20 (d, *J* = 3.8 Hz, 4H), 4.16 (d, *J* = 8.8 Hz, 10H), 3.19 (t, *J* = 7.4 Hz, 4H), 1.41 (s, 18H), 1.28 – 1.10 (m, 4H). **^{13}C NMR** (101 MHz, Chloroform-*d*) δ 163.00, 156.00, 145.28, 81.27, 80.84, 79.63, 68.87, 64.38, 49.96, 40.49, 30.00, 28.46, 28.06, 26.53, 26.34. **FTIR (ATR)** ν_{max}/cm^{-1}: 3350, 3096, 2930, 2857, 1680, 1541, 1340, 1160, 1042, 774, 731, 584, 482.

1-Azidonaphthalene (217)

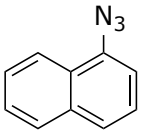

Prepared according to a procedure by Spain *et al.*[211] 1-Napthylamine (1.00 g, 6.98 mmol, 1.0 equiv.) was dissolved in hydrochloric acid (3.4 M, 7 mL), and then sodium nitrite (629 mg,

9.12 mmol, 1.3 equiv.) dissolved in water (2 mL) was added. The mixture was stirred at 0°C for 15 minutes before sodium azide (628 mg, 9.66 mmol, 1.4 equiv.) dissolved in water (2 mL) was added. The reaction was stirred at 0°C for 1 hour, then diluted with water (5 mL) and extracted with diethyl ether (4 × 30 mL). The resulting dark red solution was washed with sodium bicarbonate (2 × 50 mL) and brine (2 × 50 mL), dried over magnesium sulfate and concentrated under reduced pressure to yield a dark red liquid, which was purified *via* automated column chromatography to yield **217** as a thick golden oil (897 mg, 73%).

^{1}H NMR (300 MHz, Chloroform-*d*) δ 8.19 – 8.10 (m, 1H), 7.92 – 7.80 (m, 1H), 7.67 (d, *J* = 8.2 Hz, 1H), 7.62 – 7.44 (m, 3H), 7.29 (dd, *J* = 7.4, 1.1 Hz, 1H). **^{13}C NMR** (126 MHz, Chloroform-*d*) δ 136.53, 134.36, 127.72, 126.88, 126.43, 126.13, 125.66, 124.70, 122.54, 113.91. **FTIR** (ATR) ν_{max}/cm^{-1}: 3049, 2103, 1574, 1389, 1283, 962, 790, 765, 655, 531, 481. Spectroscopic data were in agreement with the literature.[211]

4-Hydroxymethyl-1-(1-naphthyl)-(1,2,3-triazole) (218)

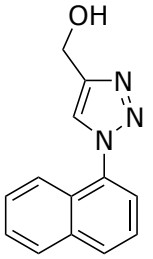

Prepared according to a procedure by Batten.[213] Copper iodide (314.6 mg, 0.2 equiv.) and sodium ascorbate (813.6 mg, 0.5 equiv.) were combined and the flask was backfilled with nitrogen. **217** (1.3727 g, 8.12 mmol, 1.0 equiv.) dissolved in acetonitrile (15 mL) was added, followed by propargyl alcohol (0.56 mL, 9.69 mmol, 1.2 equiv.), and DIPEA (2.8 mL, 16.1 mmol, 2.0 equiv.). The resulting mixture was stirred for 22 hours at room temperature, then heated to 50°C for 16 hours. Despite the presence of starting material by TLC, the incomplete reaction was diluted with EDTA solution (50 mM aq., 50 mL), extracted with dichloromethane (3 × 50 mL), and washed with water (2 × 100 mL) and brine to give a dark red solid (1.725 g, 94%).

LRMS (ESI+) *m/z* 226.15 9 $[M+H]^+$, 248.14 $[M+Na]^+$. **HRMS** (ESI+) *m/z* calcd for $C_{13}H_{11}N_3NaO$, 248.07943, found 248.07920 (error = 0.93 ppm). **^{1}H NMR** (300 MHz,

Chloroform-*d*) δ 8.05 – 7.89 (m, 3H), 7.63 – 7.42 (m, 5H), 4.98 (s, 2H). Spectroscopic data were in agreement with the literature.[213,393]

4-Bromomethyl-1-(1-naphthyl)-(1,2,3-triazole) (203)

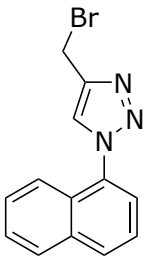

Adapted from a procedure by Shi.[393] **218** (43 mg, 1.08 mmol, 1.0 equiv.) was dissolved in dichloromethane (2 mL) and carbon tetrabromide (427 mg, 1.30 mmol, 1.2 equiv.) and triphenylphosphine (338 mg, 1.30 mmol, 1.2 equiv.) were added. The reaction mixture was stirred under nitrogen at room temperature for 24 hours, then additional tetrabromoethane (214 mg, 0.653 mmol, 0.6 equiv.) and triphenylphosphine (166 mg, 0.633 mmol, 0.6 equiv.) were added. The reaction was stirred for a further 20 hours at room temperature, then was concentrated under reduced pressure to yield the crude product as a brown gum. This was purified *via* automated column chromatography to obtain **203** as a dark brown solid (235 mg, 75%).

LRMS (APCI+) *m/z* 279.20 $[M+H]^+$. **HRMS** (APCI+) *m/z* calcd for $C_{13}H_{11}BrN_3$ 288.01309, found 288.01300, 290.01096. **^{1}H NMR** (300 MHz, Chloroform-*d*) δ 8.04 (p, *J* = 3.6 Hz, 1H), 8.00 – 7.94 (m, 2H), 7.67 – 7.51 (m, 5H), 4.74 (s, 2H). **FTIR** (ATR) ν_{max}/cm^{-1}: 3139, 3056, 1596, 1512, 1218, 1043, 800, 766. Spectroscopic data were in agreement with the literature.[394]

Alternative method for 4-Bromomethyl-1-(1-naphthyl)-(1,2,3-triazole) (203)

Following a procedure adapted from Simmons *et al*,[395] **218** (202 mg, 0.897 mmol, 1.0 equiv.) was dissolved in dichloromethane (5 mL) and phosphorus tribromide (101 μL, 88 mg, 1.076 mmol, 1.2 equiv.) was added. The reaction mixture was stirred at room temperature for 90 minutes, turning from clear straw yellow to a pale cloudy yellow. Upon completion, the mixture was quenched with sodium bicarbonate solution (sat. aq., 10 mL), then was extracted with dichloromethane (3 × 10 mL) and washed with sodium bicarbonate solution (sat. aq., 10 mL).

The combined organic layers were dried over magnesium sulfate and concentrated under reduced pressure to give the product as a light brown solid (159.6 mg, 62%). It was generally used without purification but could be further purified by column chromatography to give a golden crystalline solid (35% yield).

***N*,*N*'-(octane-1,8-diyl)bis(2-nitrobenzenesulfonamide) (232)**

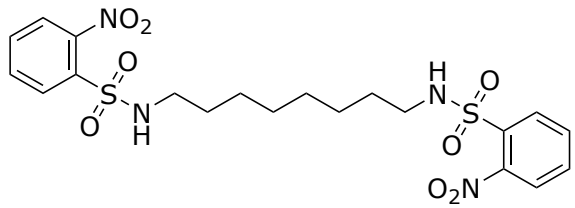

Adapted from a method by Deane *et al.*[342] 2-Nitrobenzenesulfonyl chloride (960.6 mg, 4.34 mmol, 2.4 equiv.) and 1,8-diaminooctane (260.4 mg, 1.81 mmol, 1.0 equiv.) were dissolved in chloroform (6 mL). Triethylamine (0.8 mL, 5.42 mmol, 3.0 equiv.) was added and the mixture was stirred at room temperature for 30 minutes until a white precipitate formed and reaction completion was indicated by TLC (90:9:1 CH_2Cl_2:MeOH:$NH_4OH_{(aq)}$). The mixture was then quenched with ammonium chloride solution (sat. aq., 10 mL) and extracted with chloroform (3 × 25 mL). The combined organic layers were washed with water (50 mL) and brine (50 mL), dried over magnesium sulfate and concentrated under reduced pressure to yield **232** as a white powder (818 mg, 88%).

LRMS (ESI+) *m/z* 537.08 $[M+Na]^+$. **HRMS** (ESI+) *m/z* calcd for $C_{20}H_{26}N_4NaO_8S_2$, 537.10843, found 537.10828 (error = 0.3 ppm). **^{1}H NMR** (500 MHz, DMSO-d_6) δ 8.06 – 7.97 (m, 4H), 8.00 – 7.91 (m, 2H), 7.90 – 7.81 (m, 4H), 2.88 (q, J = 6.6 Hz), 1.37 (p, J = 7.2 Hz, 4H), 1.19 – 1.13 (m, 4H), 1.15 – 1.07 (m, 4H). **^{13}C NMR** (126 MHz, DMSO-d_6) δ 148.22, 134.39, 133.35, 133.01, 129.89, 124.75, 43.10, 29.46, 28.77, 26.24. **FTIR** (ATR) ν_{max}/cm^{-1}: 3288, 2947, 2889, 2846, 1537, 1413, 1362, 1328, 1161, 1128, 1064, 855, 780, 729, 657, 596, 565, 511.

***N*,*N*'-(hexane-1,6-diyl)bis(2-nitrobenzenesulfonamide) (221)**

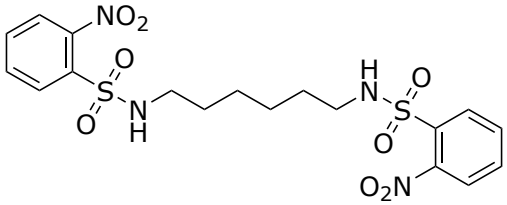

Adapted from a method by Deane *et al.*[342] 1,6-Diaminohexane (1.985 g, 17.1 mmol, 1.0 equiv.) was dissolved in dichloromethane (150 mL) and then triethylamine (7.2 mL, 51.3 mmol, 3.0 equiv.) was added. The mixture was cooled to 0°C and 2-nitrobenzenesulfonyl chloride (9.029 g, 40.9 mmol, 2.4 equiv.) was added portionwise. The reaction was stirred at room temperature for 22 hours until TLC indicated consumption of starting material and a large quantity of white precipitate had formed, upon which the mixture was quenched with ammonium chloride solution (sat., aq., 80 mL) and extracted with chloroform (3 × 80 mL). The combined organic extracts were washed with brine and dried over magnesium sulfate, and a white precipitate was separated from the yellow reaction mixture *via* vacuum filtration. This white precipitate was washed with water and dried *via* vacuum filtration to give the desired product as a white powder (5.313 g, 64%). It was sufficiently pure to use in the next step.

LRMS (ESI-) *m/z* 485.11 $[M-H]^-$. **HRMS** (ESI-) *m/z* calcd for $C_{18}H_{21}N_4O_8S_2$, 485.08063, found 485.08072 (error = 0.2 ppm). **^{1}H NMR** (500 MHz, DMSO-d_6) δ 8.05 – 7.97 (m, 4H), 7.99 – 7.91 (m, 2H), 7.90 – 7.81 (m, 4H), 2.86 (t, J = 7.1 Hz, 4H), 1.34 (t, J = 6.9 Hz, 4H), 1.19 – 1.11 (m, 4H). **^{13}C NMR** (126 MHz, DMSO-d_6) δ 148.22, 134.39, 133.33, 133.02, 129.87, 124.76, 43.03, 29.43, 25.88. **FTIR** (ATR) ν_{max}/cm^{-1}: 3286, 2950, 2892, 2864, 1537, 1414, 1363, 1338, 1321, 1161, 1128, 1063, 855, 779, 729, 657, 592, 562, 523.

2-Nitro-*N*,*N*-bis(3-((2-nitrophenyl)sulfonamido)propyl)benzenesulfonamide (233)

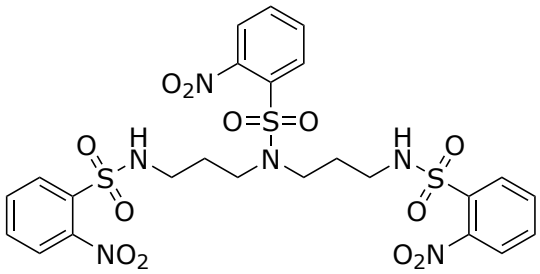

Adapted from a method by Deane *et al.*[342] Bis(3-aminopropyl)amine (577.8 g, 4.40 mmol, 1.0 equiv.) was dissolved in dichloromethane (10 mL) and triethylamine (3.0 mL, 21.78 mmol, 5.0 equiv.) was added. The mixture was cooled to 0°C before the addition of 2-nitrobenzenesulfonyl chloride (3.2284 g, 14.6 mmol, 3.3 equiv.), after which the mixture was stirred for 22 hours at room temperature and a further 5 hours at 30 C. Additional triethylamine (1.5 mL, 10.9 mmol, 2.5 equiv.) was added and the mixture was stirred at 60°C for 5 days until starting material was consumed. The viscous, black mixture was diluted with dichloromethane (150 mL) and washed with water (4 × 80 mL) and brine (80 mL), then concentrated under reduced pressure to yield the product as a silvery brown foam (2.6531 g, 88%). It was sufficiently pure to use in the next step.

LRMS (ESI-) *m/z* 685.10 ([M-H]$^-$). **HRMS** (ESI-) *m/z* calcd for $C_{24}H_{25}N_6O_{12}S_3$, 685.06981, found 685.07029 (error = 0.7 ppm). **FTIR (ATR) ν_{max}/cm^{-1}:** 3328, 3098, 2944, 1534, 1336, 1160, 1123, 852, 779, 731, 653, 577. **^{1}H NMR** (500 MHz, DMSO-d_6) δ 8.17 – 8.09 (m, 2H), 8.01 (tdd, J = 5.8, 3.6, 1.9 Hz, 4H), 8.01 – 7.95 (m, 2H), 7.95 – 7.89 (m, 4H), 7.92 – 7.82 (m, 2H), 3.26 (dd, J = 8.6, 6.5 Hz, 4H), 2.90 (t, J = 7.0 Hz, 4H), 1.68 (p, J = 7.2 Hz, 4H). **^{13}C NMR** (101 MHz, Chloroform-*d*) δ 147.90, 133.93, 133.70, 133.25, 132.77, 132.33, 132.09, 130.72, 130.53, 125.15, 124.25, 76.79, 48.97, 40.55, 28.69.

***N*-((1-(1-Naphthyl)-1*H*-1,2,3-triazol-4-yl)methyl)-*N*-(6-((*N*-((1-(1-naphthyl)-1*H*-1,2,3-triazol-4-yl)methyl)-2-nitrophenyl)sulfonamido)hexyl)-2-nitrobenzenesulfonamide (222)**

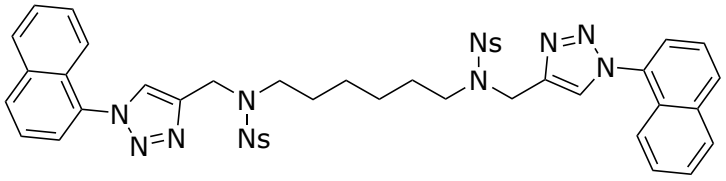

Following a procedure adapted from Ghotekar *et al,*[396] **221** (204.7 mg, 0.421 mmol, 1.0 equiv.), and **218** (228.9 mg, 1.02 mmol, 2.4 equiv.) were combined with triphenylphosphine (243 mg, 0.926 mmol, 2.2 equiv.). The flask was evacuated and backfilled with nitrogen before the addition of anhydrous THF (3 mL) and anhydrous toluene (3 mL). The resulting solution was cooled to 0°C and DIAD (0.18 mL, 0.917 mmol, 2.2 equiv.) was added. The reaction was stirred at room temperature for 24 hours, then at 60°C for 24 hours, until TLC analysis indicated consumption of starting material. The mixture was concentrated under reduced pressure and the solid obtained was triturated with cold diethyl ether (5 × 3 mL) then purified *via* automated column chromatography to yield **222** as a golden foam (139 mg, 37%).

LRMS (ESI-) *m/z* 935.25 $[M+Cl]^-$. **HRMS** (ESI+) *m/z* calcd for $C_{44}H_{40}N_{10}NaO_8S_2$, 923.23642, found 923.23575 (error = 0.7 ppm). **^{1}H NMR** (500 MHz, Chloroform-*d*) δ 8.11 – 8.03 (m, 2H), 8.01 (dd, *J* = 8.1, 1.1 Hz, 2H), 7.99 – 7.92 (m, 4H), 7.74 – 7.68 (m, 2H), 7.71 – 7.66 (m, 2H), 7.68 – 7.61 (m, 2H), 7.63 – 7.48 (m, 10H), 4.76 (s, 4H), 3.43 – 3.36 (m, 4H), 1.60 (d, *J* = 10.1 Hz, 4H), 1.30 – 1.17 (m, 4H). **^{13}C NMR** (126 MHz, Chloroform-*d*) δ 148.02, 143.52, 134.15, 133.71, 133.50, 131.92, 130.83, 130.52, 128.37, 128.32, 128.00, 127.13, 126.05, 124.98, 124.31, 123.57, 122.15, 47.77, 42.21, 27.48, 25.81. **FTIR** (ATR) ν_{max}/cm^{-1}: 3140, 3092, 2999, 2928, 2859, 1707,1542, 1437, 1346, 1221, 1160, 1039, 851, 772, 651, 582.

***N*-((1-(1-Naphthyl)-1*H*-1,2,3-triazol-4-yl)methyl)-*N*-(8-((*N*-((1-(1-naphthyl)-1*H*-1,2,3-triazol-4-yl)methyl)-2-nitrophenyl)sulfonamido)octyl)-2-nitrobenzenesulfonamide (234)**

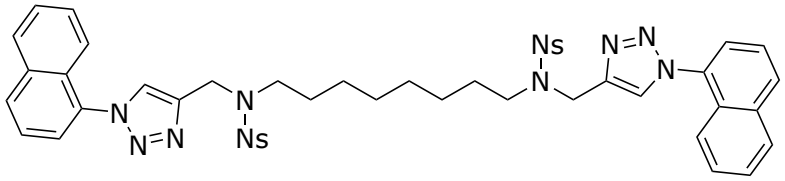

Following a procedure adapted from Ghotekar *et al*,[396] **232** (202 mg, 0.393 mmol, 1.0 equiv.), **218** (228.8 mg, 1.016 mmol, 2.6 equiv.) and PPh3 (364.3 mg, 1.389 mmol, 3.5 equiv.) were combined and the flask was evacuated and backfilled with nitrogen. Anhydrous THF (4 mL) and anhydrous toluene (4 mL) were added, and the solution was cooled to 0°C before the addition of DIAD (0.27 mL, 1.362 mmol, 3.5 equiv.). The mixture was stirred at room temperature for 48 hours, before being concentrated under reduced pressure and triturated with cold diethyl ether (5 × 3 mL). The resulting red-brown solid was purified *via* automated column chromatography to yield the desired product **234** as a red solid (108 mg, 30%).

LRMS (ESI-) *m/z* 963.25 $[M+Cl]^-$. **HRMS** (ESI+) *m/z* calcd for $C_{46}H_{44}N_{10}NaO_8S_2$, 951.26772, found 951.26784. **^{1}H NMR** (500 MHz, Chloroform-*d*) δ 8.09 – 8.04 (m, 2H), 8.02 (dd, *J* = 8.0, 1.4 Hz, 2H), 7.98 (s, 2H), 7.96 (d, *J* = 8.2 Hz, 2H), 7.73 – 7.67 (m, 4H), 7.66 (s, 2H), 7.61 – 7.50 (m, 10H), 4.77 (s, 4H), 3.47 – 3.33 (m, 4H), 1.61 (t, *J* = 7.7 Hz, 4H), 1.18 (s, 8H). **^{13}C NMR** (126 MHz, Chloroform-*d*) δ 148.05, 143.66, 134.17, 133.68, 133.59, 133.53, 131.84, 130.82, 130.54, 128.39, 128.34, 127.98, 127.14, 126.04, 124.97, 124.31, 123.55, 122.16, 48.00, 42.29, 28.84, 27.67, 26.24. **FTIR** (ATR) ν_{max}/cm^{-1}: 3351, 3097, 2930, 2856, 1539, 1338, 1160, 1124, 1040, 909, 772, 729, 652, 582.

***N*-((1-(1-Naphthyl)-1*H*-1,2,3-triazol-4-yl)methyl)-*N*-(3-((*N*-(3-((*N*-((1-(1-naphthyl)-1*H*-1,2,3-triazol-4-yl)methyl)-2-nitrophenyl)sulfonamido)propyl)-2-nitrophenyl)sulfonamido)propyl)-2-nitrobenzenesulfonamide (235)**

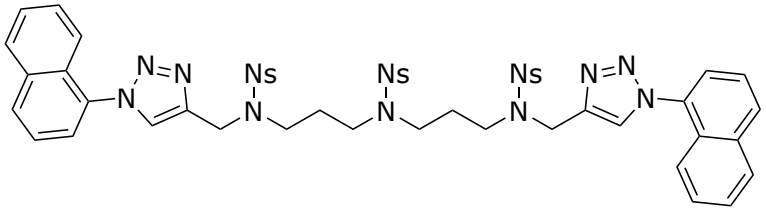

Following a procedure adapted from Ghotekar *et al*,[396] **233** (269.9 mg, 0.393 mmol, 1.0 equiv.) and **218** (211.4 mg, 0.939 mmol, 2.4 equiv.) were combined and triphenylphosphine (310.4 mg, 1.18 mmol, 3.0 equiv.) was added. The flask was evacuated and backfilled with nitrogen before the addition of anhydrous THF (5 mL). The resulting solution was cooled to 0°C and DIAD (0.23 mL, 1.17 mmol, 3.0 equiv.) was added. The reaction was stirred at room temperature for 48 hours until TLC analysis indicated consumption of starting material, then was concentrated under reduced pressure. The gummy solid obtained was triturated with cold diethyl ether (5 × 3 mL) then purified *via* automated column chromatography to yield **235** as a brown solid (323 mg, 75%).

LRMS (ESI-) *m/z* 1135.27([M+Cl]$^-$). **HRMS** (ESI+) *m/z* calcd for $C_{50}H_{44}N_{12}O_{12}S_3$, [M+Na], 1123.22560, found 1123.22407 (error = 1.4 ppm). **^{1}H NMR** (300 MHz, Chloroform-*d*) δ 8.15 – 8.02 (m, 2H), 7.99 (s, 4H), 8.07 – 7.89 (m, 4H), 7.76 – 7.60 (m, 6H), 7.66 – 7.52 (m, 4H), 7.58 – 7.44 (m, 8H), 4.77 (s, 4H), 3.42 (t, *J* = 7.4 Hz, 4H), 3.31 (t, *J* = 7.4 Hz, 4H), 2.02 (d, *J* = 15.8 Hz, 4H). **^{13}C NMR** (126 MHz, Chloroform-*d*) δ 148.14, 143.09, 134.24, 133.97, 133.78, 133.57, 133.03, 132.27, 131.20, 130.62, 128.41, 128.16, 127.24, 126.34, 125.12, 124.45, 123.76, 122.31, 45.59, 45.38, 42.52, 26.85. **FTIR** (ATR) ν_{max}/cm^{-1}: 3007, 1707, 1533, 1334, 1222, 1154, 991, 850, 744, 651, 549.

7.5.2 Final compounds

1,8-Bis((1-(1-adamantyl)-1*H*-1,2,3-triazol-4-yl)methyl)-1,4,8,11-tetraazacyclotetradecane (179)

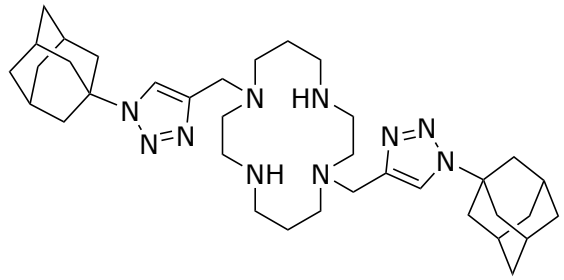

182 (203 mg, 0.244 mmol) was deprotected according to **General Synthetic Procedure E** and obtained in quantitative yield as a golden foam. One portion (105 mg, 0.149 mmol) of the crude product was dissolved in methanol and passed through a column containing Ambersep® 900 hydroxide form resin, then concentrated under reduced pressure to give the product as a free base, a crystalline brown foam (91 mg, 0.144 mmol, 97% from crude material).

LRMS (ESI+) *m/z* 631.49 $[M+H]^+$. **HRMS** (ESI+) *m/z* calcd for $C_{36}H_{59}N_{10}$, 631.49187, found 631.49332 (error = 2.3 ppm). **^{1}H NMR** (400 MHz, Methanol-d_4) δ 7.77 (s, 2H), 3.66 (s, 4H), 3.10 (s, 4H), 2.96 – 2.86 (m, 4H), 2.79 (s, 4H), 2.55 (t, J = 5.4 Hz, 4H), 2.18 – 2.07 (m, 18H), 1.86 (s, 4H), 1.72 (q, J = 12.4 Hz, 12H). **^{13}C NMR** (101 MHz, Methanol-d_4) δ 173.23, 143.35, 119.43, 81.59, 59.68, 55.31, 51.01, 45.34, 42.69, 35.52, 29.57, 27.45, 27.08, 27.00, 23.63. **FTIR** (ATR) ν_{max}/cm^{-1}: 3099, 2911, 2852, 2706, 1556, 1451, 1429, 1142, 1133, 1091, 1051, 1009, 828, 742, 699.

1,8-Bis((1-(1-adamantyl)-1*H*-1,2,3-triazol-4-yl)methyl)-1,4,8,11-tetraazacyclotetradecane · 2 HCl (179·2HCl salt)

A 50 mg (0.071 mmol) portion of the crude product obtained after deprotection was purified *via* HPLC to give the HCl salt as a fine white powder (9.9 mg, 0.012 mmol, 16%). **^{1}H NMR** (300 MHz, Deuterium Oxide) δ 7.93 (s, 2H), 3.73 (s, 4H), 3.39 (s, 4H), 3.24 (s, 4H), 2.96 (s, 4H), 2.77 (t, J = 5.5 Hz, 4H), 2.22 (s, 6H), 2.14 (d, J = 2.9 Hz, 12H), 2.01 (d, J = 7.2 Hz, 4H), 1.77 (q, J = 13.0 Hz, 12H).

1,8-Bis((1-(methylferrocenyl)-1*H*-1,2,3-triazol-4-yl)methyl)-1,4,8,11-tetraazacyclotetradecane (180)

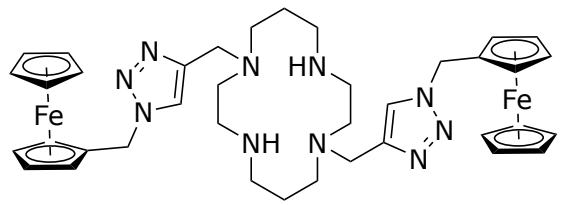

183 (188 mg, 0.196 mmol) was deprotected according to **General Synthetic Procedure E** to give a bright mustard yellow precipitate. One portion (63 mg, 0.076 mmol) of the crude product) was converted to the free base using Ambersep® 900 hydroxide form resin beads, pre-swelled with methanol (57 mg, 0.75 mmol, 99% from crude).

LRMS (ESI+) *m/z* 759.30 $[M+H]^+$. **HRMS** (ESI+) *m/z* calcd for $C_{38}H_{51}Fe_2N_{10}$, 759.29914, found 759.29846 (error = 0.9 ppm). **^{1}H NMR** (300 MHz, Chloroform-*d*) δ 7.31 (d, *J* = 4.6 Hz, 2H), 5.13 (d, *J* = 4.6 Hz, 4H), 4.31 – 4.24 (m, 4H), 4.13 (dd, *J* = 3.4, 1.2 Hz, 14H), 4.10 – 4.06 (m, 4H), 3.31 – 2.75 (m, 12H), 2.57 (t, *J* = 5.2 Hz, 4H), 1.92 (d, *J* = 35.3 Hz, 4H). **^{13}C NMR** (126 MHz, Chloroform-*d*) δ 143.63, 134.30, 122.15, 81.35, 69.36, 69.12, 69.09, 69.01, 68.97, 50.20, 49.04, 48.46, 29.81, 23.38. **FTIR** (ATR) ν_{max}/cm^{-1}: 3419, 3089, 2968, 2905, 2847, 1673, 1647, 1195, 1117, 1042, 1000, 774, 697.

1,8-Bis((1-(methylferrocenyl)-1*H*-1,2,3-triazol-4-yl)methyl)-1,4,8,11-tetraazacyclotetradecane · 2 TFA (180·2TFA)

An 80 mg (0.096 mmol) portion of the crude product obtained after deprotection was purified *via* HPLC to give the HCl salt as a light green powder (19.8 mg, 0.020 mmol, 21%).

***N*^{1},*N*^{6}-Bis((1-(1-adamantyl)-1*H*-1,2,3-triazol-4-yl)methyl)hexane-1,6-diamine (195)**

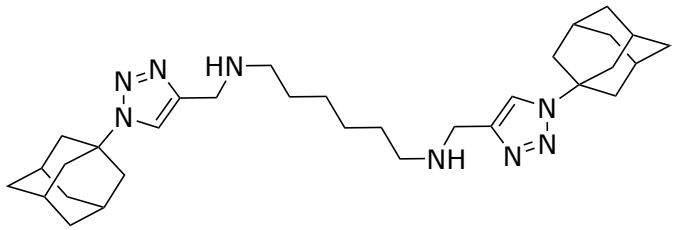

202 (86.1 mg, 0.115 mmol) was deprotected according to **General Synthetic Procedure E**. A portion of the crude product (35 mg, 0.056 mmol) was converted to the free base using Ambersep® 900 hydroxide form resin beads pre-swelled with methanol (29 mg, 0.053 mmol, 94%). *Obtained as an off-white solid*. **LRMS** (ESI+) *m/z* 547.40 $[M+H]^+$. **HRMS** (ESI-) *m/z* calcd for $C_{32}H_{50}ClN_8$, 581.38524, found 581.38617 (error = 1.6 ppm). **^{1}H NMR** (400 MHz, Methanol-d_4) δ 8.17 (d, *J* = 7.3 Hz, 2H), 4.20 (s, 4H), 2.98 (q, *J* = 10.3, 7.7 Hz, 4H), 2.31 (s, 18H), 1.89 (s, 12H), 1.72 (s, 4H), 1.52 – 1.41 (m, 4H). **^{13}C NMR** (101 MHz, Methanol-d_4) δ 140.05, 120.80, 60.00, 42.55, 42.24, 35.52, 35.47, 29.59, 26.60, 25.94. **FTIR** (ATR) ν_{max}/cm^{-1}: 2910, 2853, 1646, 1453, 1142, 1103, 1056, 1017.

***N*^{1},*N*^{6}-Bis((1-(adamantan-1-yl)-1*H*-1,2,3-triazol-4-yl)methyl)hexane-1,6-diamine · 2 HCl (195·2HCl)**

A second portion (18 mg, 0.029 mmol) of the crude product obtained after deprotection was purified *via* HPLC to give the HCl salt as a white powder (3.4 mg, 4.0 µmol, 15%).

***N*^{1},*N*^{6}-Bis((1-(methylferrocenyl)-1*H*-1,2,3-triazol-4-yl)methyl)hexane-1,6-diamine (196)**

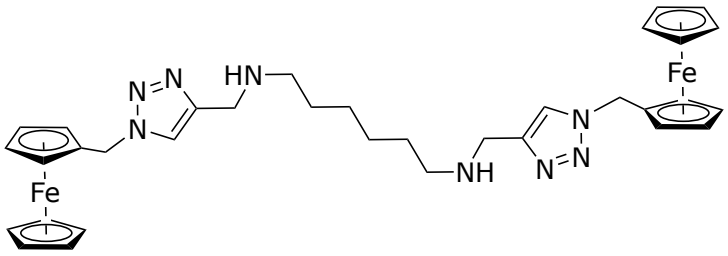

201 (75.8 mg, 0.0867 mmol) was deprotected according to **General Synthetic Procedure E** and obtained as a dark brown solid in quantitative yield (65 mg, 0.087 mmol, 100%). **LRMS** (ESI+) *m/z* 675.23 $[M+H]^+$. **HRMS** (ESI+) *m/z* calcd for $C_{34}H_{43}Fe_2N_8$, 675.23039, found

675.23002 (error = 0.6 ppm). **^{1}H NMR** (500 MHz, Methanol-d_4) δ 8.02 (s, 2H), 5.42 (s, 4H), 4.37 (s, 4H), 4.31 (s, 4H), 4.24 (s, 10H), 3.37 (s, 4H), 1.71 (s, 4H), 1.43 (s, 4H). **^{13}C NMR** (101 MHz, Methanol-d_4) δ 42.60, 35.49, 29.60, 27.33. **FTIR** (ATR) ν_{max}/cm^{-1}: 3388, 3082, 2927, 2855, 2776, 1655, 1604, 1459, 1253, 1105, 1051, 1001, 814, 484.

N^1,*N*^{8}-Bis((1-(1-naphthyl)-1*H*-1,2,3-triazol-4-yl)methyl)octane-1,8-diamine (240)

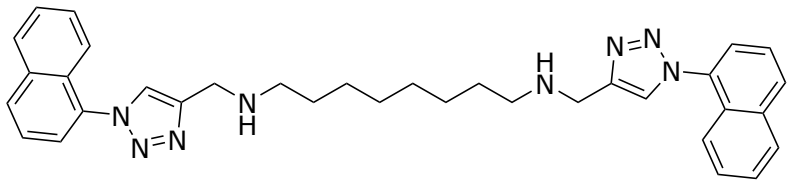

Adapted from a procedure by Matoba *et al.*[357] Thiosalicyclic acid (69.2 mg, 0.449 mmol, 4.1 equiv.) was added to a solution of **234** (101.2 mg, 0.109 mmol, 1.0 equiv.) in anhydrous DMF (3 mL) and the mixture was stirred at 60°C for 24 hours. Once TLC analysis confirmed the consumption of starting material, the mixture was diluted with diethyl ether (25 mL), washed with lithium chloride solution (5% w/v, aq., 3 × 20 mL), sodium carbonate solution (sat. aq., 2 × 20 mL) and brine (25 mL) before being dried over magnesium sulfate and concentrated under reduced pressure to give the crude product as a red-orange solid.

LRMS (ESI+) *m/z* 559.32 [M+H]$^+$, 571.31 [M+Na]$^+$. **HRMS** (ESI+) *m/z* calcd for $C_{34}H_{39}N_8$, 559.32922, found 559.32920 (error < 0.1 ppm). **^{1}H NMR** (400 MHz, Methanol-d_4) δ 8.53 (s, 2H), 8.20 (dd, *J* = 6.6, 2.9 Hz, 2H), 8.14 – 8.07 (m, 2H), 7.75 – 7.64 (m, 6H), 7.62 (ddd, *J* = 8.1, 6.7, 1.4 Hz, 2H), 7.61 – 7.53 (m, 2H), 4.56 (s, 4H), 3.29 – 3.21 (m, 4H), 1.84 (p, *J* = 7.9, 7.2 Hz, 4H), 1.52 (d, *J* = 13.7 Hz, 8H). **^{13}C NMR** (101 MHz, Methanol-d_4) δ 161.19, 138.52, 134.31, 133.12, 130.65, 128.34, 128.19, 127.75, 127.65, 126.95, 124.85, 123.57, 121.44, 41.43, 28.49, 26.03, 25.69. **FTIR** (ATR) ν_{max}/cm^{-1}: 3055, 2925, 2852, 1674, 1469, 1433, 1219, 1127, 1103, 1038, 1018, 799, 770, 733, 701.

N^1,*N*^{8}-Bis((1-(1-naphthyl)-1*H*-1,2,3-triazol-4-yl)methyl)octane-1,8-diamine · 2 TFA (**240**·2TFA salt)

The crude product **240** was purified *via* automated column chromatography and HPLC to yield **240·2TFA** as a white powder (1.03 mg, 1.0 μmol, 2%).

***N*^{1},*N*^{6}-Bis((1-(1-naphthyl)-1*H*-1,2,3-triazol-4-yl)methyl)hexane-1,6-diamine (197)**

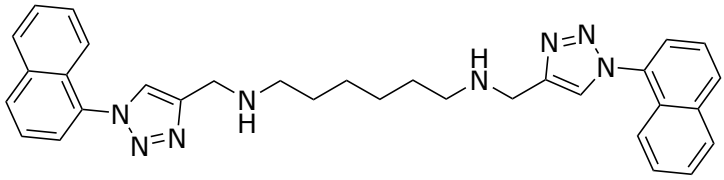

Adapted from a procedure by Matoba *et al.*[357] 2,2-(Ethylenedioxy)diethanethiol (67 µL, 0.411 mmol, 4.0 equiv.) was added to a solution of anhydrous potassium carbonate (117.5 mg, 0.821 mmol, 8.0 equiv.) and **222** (92.4 mg, 0.103 mmol, 1.0 equiv.). The solution was stirred at 80°C for 3 days until TLC analysis indicated consumption of **222**. The mixture was then diluted with ethyl acetate (20 mL), washed with lithium chloride solution (5% w/v, aq., 3 × 20 mL), sodium carbonate solution (sat. aq., 20 mL) and brine (25 mL) before being dried over magnesium sulfate, filtered, and the filtrate concentrated under reduced pressure. The crude product **197** was obtained as a red-brown solid after partial purification *via* automated column chromatography.

LRMS (ESI+) *m/z* 531.32 $[M+H]^+$. **HRMS** (ESI+) *m/z* calcd for $C_{32}H_{35}N_8$, 531.29792, found 531.29747 (error = 0.9 ppm). **^{1}H NMR** (400 MHz, Methanol-d_4) δ 8.53 (s, 2H), 8.20 (dd, *J* = 6.9, 2.6 Hz, 2H), 8.11 (d, *J* = 8.1 Hz, 2H), 7.76 – 7.68 (m, 4H), 7.71 – 7.59 (m, 4H), 7.57 (d, *J* = 8.4 Hz, 2H), 4.57 (s, 4H), 3.32 – 3.24 (m, 4H), 1.88 (d, *J* = 8.0 Hz, 4H), 1.64 – 1.56 (m, 4H). **^{13}C NMR** (101 MHz, Methanol-d_4) δ 161.23, 138.47, 134.32, 133.11, 130.67, 128.33, 128.20, 127.75, 127.63, 126.96, 124.84, 123.56, 121.42, 41.42, 25.68, 25.52. **FTIR** (ATR) ν_{max}/cm^{-1}: 3138, 3056, 2925, 2853, 1669, 1470, 1434, 1221, 1169, 1123, 1039, 1018, 800, 771, 731, 698.

***N*^{1},*N*^{6}-Bis((1-(1-naphthyl)-1*H*-1,2,3-triazol-4-yl)methyl)hexane-1,6-diamine · 2 TFA (197·2TFA salt)**

The crude product **197** was purified by HPLC to yield **197** as the TFA salt (7.2 mg, 9.5 µmol, 21%.

N^1-((1-(1-Naphthyl)-1*H*-1,2,3-triazol-4-yl)methyl)-N^3-(3-(((1-(1-naphthyl)-1*H*-1,2,3-triazol-4-yl)methyl)amino)propyl)propane-1,3-diamine (241)

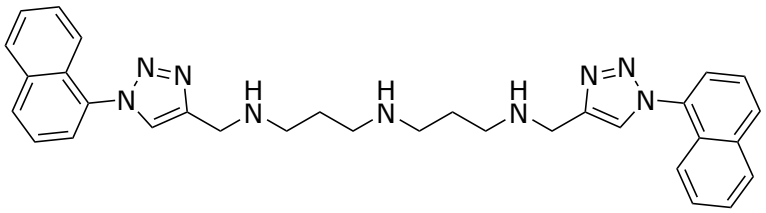

Adapted from a procedure by Matoba *et al.*[357] Anhydrous potassium carbonate (318 mg, 2.30 mmol, 18 equiv.) was combined with **235** (140 mg, 0.127 mmol, 1.0 equiv.) and dissolved in anhydrous DMF (5 mL). Thiophenol (0.11 mL, 1.08 mmol, 8.5 equiv.) was added and the mixture was stirred at 80°C for 18 hours until TLC analysis indicated consumption of **235**. The mixture was diluted with ethyl acetate (40 mL), washed with lithium chloride solution (5%, 3 × 20 mL), sodium carbonate solution (sat. aq., 2 × 20 mL) and dried over magnesium sulfate before concentrating under reduced pressure. The resulting material was redissolved in water and adjusted to pH 8 before being extracted with dichloromethane (2 × 50 mL). This solution was extracted with hydrochloric acid (0.1 M aq., pH 1, 3 × 60 mL) and the combined aqueous extracts were basified to pH 14 using NaOH solution (2.5 M aq.) resulting in white precipitate. This aqueous solution was extracted once again with dichloromethane (3 × 60 mL) and washed with brine before being dried over magnesium sulfate and concentrated under reduced pressure. The crude product **241** was obtained as a brown solid after partial purification *via* automated column chromatography (14.3 mg, 0.026 mmol, 17%).

LRMS (ESI+) *m/z* 546.30 $[M+H]^+$. **HRMS** (ESI+) *m/z* calcd for $C_{32}H_{35}N_9$, $[M+H]^+$, 546.30882, found 546.30984 (error = 1.87 ppm). **^{1}H NMR** (500 MHz, Methanol-d_4) δ 8.52 (s, 2H), 8.20 (dd, J = 7.5, 2.1 Hz, 2H), 8.11 (d, J = 8.1 Hz, 2H), 7.74 – 7.65 (m, 6H), 7.62 (ddd, J = 8.2, 6.7, 1.3 Hz, 2H), 7.59 – 7.55 (m, 2H), 4.58 (s, 4H), 3.43 – 3.37 (m, 4H), 3.34 – 3.25 (m, 4H), 2.34 – 2.25 (m, 4H). **^{13}C NMR** (126 MHz, Methanol-d_4) δ 139.93, 135.71, 134.49, 132.08, 129.70, 129.61, 129.16, 129.03, 128.37, 126.24, 124.96, 122.84, 46.24, 45.58, 42.94, 24.20. **FTIR (ATR)** ν_{max}/cm^{-1}: 3057, 2978, 2924, 2850, 1514, 1475, 1438, 1334, 1302, 1104, 1056, 1041, 733, 688.

***N*^{1}-((1-(1-Naphthyl)-1*H*-1,2,3-triazol-4-yl)methyl)-*N*^{3}-(3-(((1-(1-naphthyl)-1*H*-1,2,3-triazol-4-yl)methyl)amino)propyl)propane-1,3-diamine · 2 TFA** (240·2TFA salt)

The crude product **241** was purified by HPLC to yield **241** as the TFA salt (3.1 mg, 3.5 μmol, 15%).

8 References

(1) Korbmacher, M.; Azevedo, F.; Pennington, C. R.; Hartmann, H.; Pownall, M.; Schmidt, K.; Elsherif, M.; Breznau, N.; Robertson, O.; Kalandadze, T.; Yu, S.; Baker, B. J.; O'Mahony, A.; Olsnes, J. Ø.-S.; Shaw, J. J.; Gjoneska, B.; Yamada, Y.; Röer, J. P.; Murphy, J.; Alzahawi, S.; Grinschgl, S.; Oliveira, C. M.; Wingen, T.; Yeung, S. K.; Liu, M.; König, L. M.; Albayrak-Aydemir, N.; Lecuona, O.; Micheli, L.; Evans, T. The Replication Crisis Has Led to Positive Structural, Procedural, and Community Changes. *Commun Psychol* **2023**, *1* (1), 1–13. https://doi.org/10.1038/s44271-023-00003-2.

(2) Baker, M. 1,500 Scientists Lift the Lid on Reproducibility. *Nature* **2016**, *533* (7604), 452–454. https://doi.org/10.1038/533452a.

(3) Herb, U. Sociological Implications of Scientific Publishing: Open Access, Science, Society, Democracy and the Digital Divide. *First Monday* **2010**. https://doi.org/10.5210/fm.v15i2.2599.

(4) Laine, H. Afraid of Scooping – Case Study on Researcher Strategies against Fear of Scooping in the Context of Open Science. *Data Science Journal* **2017**, *16* (0). https://doi.org/10.5334/dsj-2017-029.

(5) Jablonka, K. M.; Patiny, L.; Smit, B. Making the Collective Knowledge of Chemistry Open and Machine Actionable. *Nat. Chem.* **2022**, *14* (4), 365–376. https://doi.org/10.1038/s41557-022-00910-7.

(6) Palomo, M. New Insight into the Origins of the Calculus War. *Annals of Science* **2021**, *78* (1), 22–40. https://doi.org/10.1080/00033790.2020.1794038.

(7) Maedche, A.; Elshan, E.; Höhle, H.; Lehrer, C.; Recker, J.; Sunyaev, A.; Sturm, B.; Werth, O. Open Science. *Bus Inf Syst Eng* **2024**, *66* (4), 517–532. https://doi.org/10.1007/s12599-024-00858-7.

(8) UNESCO Recommendation on Open Science - UNESCO Digital Library, 2022. https://unesdoc.unesco.org/ark:/48223/pf0000379949 (accessed 2025-04-29).

(9) Méndez, E. Open Science por defecto. La nueva normalidad para la investigación. *Arbor* **2021**, *197* (799), a587–a587. https://doi.org/10.3989/arbor.2021.799002.

(10) So, D.; Joly, Y.; Knoppers, B. M. Clinical Trial Transparency and Orphan Drug Development: Recent Trends in Data Sharing by the Pharmaceutical Industry. *Public Health Genomics* **2014**, *16* (6), 322–335. https://doi.org/10.1159/000355941.

(11) Federer, L. M.; Lu, Y.-L.; Joubert, D. J.; Welsh, J.; Brandys, B. Biomedical Data Sharing and Reuse: Attitudes and Practices of Clinical and Scientific Research Staff. *PLOS ONE* **2015**, *10* (6), e0129506. https://doi.org/10.1371/journal.pone.0129506.

(12) Beck, M. W.; O'Hara, C.; Lowndes, J. S. S.; Mazor, R. D.; Theroux, S.; Gillett, D. J.; Lane, B.; Gearheart, G. The Importance of Open Science for Biological Assessment of Aquatic Environments. *PeerJ* **2020**, *8*, e9539. https://doi.org/10.7717/peerj.9539.

(13) Forscher, P. S.; Wagenmakers, E.-J.; Coles, N. A.; Silan, M. A.; Dutra, N.; Basnight-Brown, D.; IJzerman, H. The Benefits, Barriers, and Risks of Big-Team Science. *Perspect Psychol Sci* **2023**, *18* (3), 607–623. https://doi.org/10.1177/17456916221082970.

(14) Colavizza, G.; Cadwallader, L.; LaFlamme, M.; Dozot, G.; Lecorney, S.; Rappo, D.; Hrynaszkiewicz, I. An Analysis of the Effects of Sharing Research Data, Code, and Preprints on Citations. *PLOS ONE* **2024**, *19* (10), e0311493. https://doi.org/10.1371/journal.pone.0311493.

(15) Fell, M. J. The Economic Impacts of Open Science: A Rapid Evidence Assessment. *Publications* **2019**, *7* (3), 46. https://doi.org/10.3390/publications7030046.

(16) COVID Moonshot: Open Science Discovery of SARS-CoV-2 Main Protease Inhibitors by Combining Crowdsourcing, High-Throughput Experiments, Computational Simulations, and Machine Learning.

(17) Klebel, T.; Traag, V.; Grypari, I.; Stoy, L.; Ross-Hellauer, T. The Academic Impact of Open Science: A Scoping Review. *Royal Society Open Science* **2025**, *12* (3), 241248. https://doi.org/10.1098/rsos.241248.

(18) Manco, A. Open Science Policies as Regarded by the Communities of Researchers from the Basic Sciences in the Scientific Periphery. *Online Information Review* **2023**, *48* (6), 1065–1087. https://doi.org/10.1108/OIR-03-2023-0135.

(19) Vicente-Saez, R.; Martinez-Fuentes, C. Open Science Now: A Systematic Literature Review for an Integrated Definition. *Journal of Business Research* **2018**, *88*, 428–436. https://doi.org/10.1016/j.jbusres.2017.12.043.

(20) Smart, P.; Holmes, S.; Lettice, F.; Pitts, F. H.; Zwiegelaar, J. B.; Schwartz, G.; Evans, S. Open Science and Open Innovation in a Socio-Political Context: Knowledge Production for Societal Impact in an Age of Post-Truth Populism. *R&D Management* **2019**, *49* (3), 279–297. https://doi.org/10.1111/radm.12377.

(21) Wilkinson, M. D.; Dumontier, M.; Aalbersberg, Ij. J.; Appleton, G.; Axton, M.; Baak, A.; Blomberg, N.; Boiten, J.-W.; da Silva Santos, L. B.; Bourne, P. E.; Bouwman, J.; Brookes, A. J.; Clark, T.; Crosas, M.; Dillo, I.; Dumon, O.; Edmunds, S.; Evelo, C. T.; Finkers, R.; Gonzalez-Beltran, A.; Gray, A. J. G.; Groth, P.; Goble, C.; Grethe, J. S.; Heringa, J.; 't Hoen, P. A. C.; Hooft, R.; Kuhn, T.; Kok, R.; Kok, J.; Lusher, S. J.; Martone, M. E.; Mons, A.; Packer, A. L.; Persson, B.; Rocca-Serra, P.; Roos, M.; van Schaik, R.; Sansone, S.-A.; Schultes, E.; Sengstag, T.; Slater, T.; Strawn, G.; Swertz, M. A.; Thompson, M.; van der Lei, J.; van Mulligen, E.; Velterop, J.; Waagmeester, A.; Wittenburg, P.; Wolstencroft, K.; Zhao, J.; Mons, B. The FAIR Guiding Principles for Scientific Data Management and Stewardship. *Sci Data* **2016**, *3* (1), 160018. https://doi.org/10.1038/sdata.2016.18.

(22) Bouter, L. Why Research Integrity Matters and How It Can Be Improved. *Accountability in Research* **2024**, *31* (8), 1277–1286. https://doi.org/10.1080/08989621.2023.2189010.

(23) Sheikh, A.; Richardson, J. Open Access Movement in the Scholarly World: Pathways for Libraries in Developing Countries. *Journal of Information Science* **2023**, 01655515231202758. https://doi.org/10.1177/01655515231202758.

(24) Arthur, P. L.; Hearn, L.; Ryan, J. C.; Menon, N.; Khumalo, L. Making Open Scholarship More Equitable and Inclusive. *Publications* **2023**, *11* (3), 41. https://doi.org/10.3390/publications11030041.

(25) Bohannon, J. Who's Downloading Pirated Papers? Everyone. *Science* **2016**, *352* (6285), 508–512. https://doi.org/10.1126/science.352.6285.508.

(26) Jeschke, J. M.; Börner, K.; Stodden, V.; Tockner, K. Open Access Journals Need to Become First Choice, in Invasion Ecology and Beyond. *NeoBiota* **2019**, *52*, 1–8. https://doi.org/10.3897/neobiota.52.39542.

(27) Wang, Z.; Chen, Y.; Yang, C. The Role of Preprints in Open Science: Accelerating Knowledge Transfer from Science to Technology. *Journal of Informetrics* **2025**, *19* (2), 101663. https://doi.org/10.1016/j.joi.2025.101663.

(28) Pagliaro, M. Did You Ask for Citations? An Insight into Preprint Citations En Route to Open Science. *Publications* **2021**, *9* (3), 26. https://doi.org/10.3390/publications9030026.

(29) Heiser, R. E. The Emergence of the Open Research University Through International Research Collaboration. *The International Review of Research in Open and Distributed Learning* **2023**, *24* (3), 99–124. https://doi.org/10.19173/irrodl.v24i3.7328.

(30) Forte, A.; Lampe, C. Defining, Understanding, and Supporting Open Collaboration: Lessons From the Literature. *American Behavioral Scientist* **2013**, *57* (5), 535–547. https://doi.org/10.1177/0002764212469362.

(31) Kumari, P.; Gakhar, H.; Sinhababu, D. A.; Sharma, D. J.; Chakravarty, P. R. Libre Open Access in Science Journals: An Analytical Study of DOAJ. *Library Philosophy and Practice (e-journal)* **2021**.

(32) Directorate-General for Research and Innovation (European Commission). *Turning FAIR into Reality: Final Report and Action Plan from the European Commission Expert Group on FAIR Data*; Publications Office of the European Union, 2018.

(33) *Data Management | Data Sharing*. https://sharing.nih.gov/data-management-and-sharing-policy/data-management#fair-principles (accessed 2025-04-29).

(34) *Australian FAIR Access Working Group*. https://www.fair-access.net.au/fair-statement (accessed 2025-04-29).

(35) Pagliaro, M. Open Access Publishing in Chemistry: A Practical Perspective Informing New Education. *Insights* **2021**, *34* (1). https://doi.org/10.1629/uksg.540.

(36) Wang, X.; Cui, Y.; Xu, S.; Hu, Z. The State and Evolution of Gold Open Access: A Country and Discipline Level Analysis. *Aslib Journal of Information Management* **2018**, *70* (5), 573–584. https://doi.org/10.1108/AJIM-02-2018-0023.

(37) Looking Back and Moving Forward in Medicinal Chemistry. *Nat Commun* **2023**, *14* (1), 4299. https://doi.org/10.1038/s41467-023-39949-6.

(38) Drewry, D. H.; Wells, C. I.; Zuercher, W. J.; Willson, T. M. A Perspective on Extreme Open Science: Companies Sharing Compounds without Restriction. *SLAS Discovery* **2019**, *24* (5), 505–514. https://doi.org/10.1177/2472555219838210.

(39) Hendrickx, K.; Dooms, M. Orphan Drugs, Compounded Medication and Pharmaceutical Commons. *Front. Pharmacol.* **2021**, *12*. https://doi.org/10.3389/fphar.2021.738458.

(40) Martinez-Sevillano, M.; Falaguera, M. J.; Mestres, J. CIPSI: An Open Chemical Intellectual Property Service for Medicinal Chemists. *Molecular Informatics* **2024**, *43* (1), e202300221. https://doi.org/10.1002/minf.202300221.

(41) Miljković, F.; Bajorath, J. Kinase Drug Discovery: Impact of Open Science and Artificial Intelligence. *Mol. Pharmaceutics* **2024**, *21* (10), 4849–4859. https://doi.org/10.1021/acs.molpharmaceut.4c00659.

(42) Todd, M. H. Open Access and Open Source in Chemistry. *Chemistry Central Journal* **2007**, *1* (1), 1–4. https://doi.org/10.1186/1752-153X-1-3.

(43) Årdal, C.; Røttingen, J.-A. Open Source Drug Discovery in Practice: A Case Study. *PLoS Negl Trop Dis* **2012**, *6* (9), e1827. https://doi.org/10.1371/journal.pntd.0001827.

(44) Weng, H.-B.; Chen, H.-X.; Wang, M.-W. Innovation in Neglected Tropical Disease Drug Discovery and Development. *Infect Dis Poverty* **2018**, *7*, 67. https://doi.org/10.1186/s40249-018-0444-1.

(45) *Ending the neglect to attain the Sustainable Development Goals: A road map for neglected tropical diseases 2021–2030*. https://www.who.int/publications/i/item/9789240010352 (accessed 2025-05-06).

(46) Lim, W.; Verbon, A.; van de Sande, W. Identifying Novel Drugs with New Modes of Action for Neglected Tropical Fungal Skin Diseases (Fungal skinNTDs) Using an Open Source Drug Discovery Approach. *Expert Opinion on Drug Discovery* **2022**, *17* (6), 641–659. https://doi.org/10.1080/17460441.2022.2080195.

(47) Bhuniya, D.; Mukkavilli, R.; Shivahare, R.; Launay, D.; Dere, R. T.; Deshpande, A.; Verma, A.; Vishwakarma, P.; Moger, M.; Pradhan, A.; Pati, H.; Gopinath, V. S.; Gupta, S.; Puri, S. K.; Martin, D. Aminothiazoles: Hit to Lead Development to Identify Antileishmanial Agents. *European Journal of Medicinal Chemistry* **2015**, *102*, 582–593. https://doi.org/10.1016/j.ejmech.2015.08.013.

(48) Bhardwaj, A.; Scaria, V.; Raghava, G. P. S.; Lynn, A. M.; Chandra, N.; Banerjee, S.; Raghunandanan, M. V.; Pandey, V.; Taneja, B.; Yadav, J.; Dash, D.; Bhattacharya, J.; Misra, A.; Kumar, A.; Ramachandran, S.; Thomas, Z.; Open Source Drug Discovery Consortium; Brahmachari, S. K. Open Source Drug Discovery– A New Paradigm of Collaborative Research in Tuberculosis Drug Development. *Tuberculosis* **2011**, *91* (5), 479–486. https://doi.org/10.1016/j.tube.2011.06.004.

(49) *State of inequality: HIV, tuberculosis and malaria*. https://www.who.int/publications/i/item/9789240039445 (accessed 2025-05-06).

(50) Harding, R. J. Open Notebook Science Can Maximize Impact for Rare Disease Projects. *PLOS Biology* **2019**, *17* (1), e3000120. https://doi.org/10.1371/journal.pbio.3000120.

(51) Wells, T. N. C.; Willis, P.; Burrows, J. N.; van Huijsduijnen, R. H. Open Data in Drug Discovery and Development: Lessons from Malaria. *Nat Rev Drug Discov* **2016**, *15* (10), 661–662. https://doi.org/10.1038/nrd.2016.154.

(52) *Traditional medicine has a long history of contributing to conventional medicine and continues to hold promise*. https://www.who.int/news-room/feature-stories/detail/traditional-medicine-has-a-long-history-of-contributing-to-conventional-medicine-and-continues-to-hold-promise (accessed 2025-05-01).

(53) Tulchinsky, T. H. John Snow, Cholera, the Broad Street Pump; Waterborne Diseases Then and Now. *Case Studies in Public Health* **2018**, 77–99. https://doi.org/10.1016/B978-0-12-804571-8.00017-2.

(54) Duffy Sandra; Sykes Melissa L.; Jones Amy J.; Shelper Todd B.; Simpson Moana; Lang Rebecca; Poulsen Sally-Ann; Sleebs Brad E.; Avery Vicky M. Screening the Medicines for Malaria Venture Pathogen Box across Multiple Pathogens Reclassifies Starting Points for Open-Source Drug Discovery. *Antimicrobial Agents and Chemotherapy* **2017**, *61* (9), e00379-17. https://doi.org/10.1128/AAC.00379-17.

(55) Woelfle, M.; Seerden, J.-P.; de Gooijer, J.; Pouwer, K.; Olliaro, P.; Todd, M. H. Resolution of Praziquantel. *PLoS Negl Trop Dis* **2011**, *5* (9), e1260. https://doi.org/10.1371/journal.pntd.0001260.

(56) Williamson, A. E.; Ylioja, P. M.; Robertson, M. N.; Antonova-Koch, Y.; Avery, V.; Baell, J. B.; Batchu, H.; Batra, S.; Burrows, J. N.; Bhattacharyya, S.; Calderon, F.; Charman, S. A.; Clark, J.; Crespo, B.; Dean, M.; Debbert, S. L.; Delves, M.; Dennis, A. S. M.; Deroose, F.; Duffy, S.; Fletcher, S.; Giaever, G.; Hallyburton, I.; Gamo, F.-J.; Gebbia, M.; Guy, R. K.; Hungerford, Z.; Kirk, K.; Lafuente-Monasterio, M. J.; Lee, A.; Meister, S.; Nislow, C.; Overington, J. P.; Papadatos, G.; Patiny, L.; Pham, J.; Ralph, S. A.; Ruecker, A.; Ryan, E.; Southan, C.; Srivastava, K.; Swain, C.; Tarnowski, M. J.; Thomson, P.; Turner, P.; Wallace, I. M.; Wells, T. N. C.; White, K.; White, L.; Willis, P.; Winzeler, E. A.; Wittlin, S.; Todd, M. H. Open Source Drug Discovery: Highly Potent Antimalarial Compounds Derived from the Tres Cantos Arylpyrroles. *ACS Cent. Sci.* **2016**, *2* (10), 687–701. https://doi.org/10.1021/acscentsci.6b00086.

(57) Guardia, A.; Baiget, J.; Cacho, M.; Pérez, A.; Ortega-Guerra, M.; Nxumalo, W.; Khanye, S. D.; Rullas, J.; Ortega, F.; Jiménez, E.; Pérez-Herrán, E.; Fraile-Gabaldón, M. T.; Esquivias, J.; Fernández, R.; Porras-De Francisco, E.; Encinas, L.; Alonso, M.; Giordano, I.; Rivero, C.; Miguel-Siles, J.; Osende, J. G.; Badiola, K. A.; Rutledge, P. J.; Todd, M. H.; Remuiñán, M.; Alemparte, C. Easy-To-Synthesize Spirocyclic Compounds Possess Remarkable in Vivo Activity against Mycobacterium Tuberculosis. *J. Med. Chem.* **2018**, *61* (24), 11327–11340. https://doi.org/10.1021/acs.jmedchem.8b01533.

(58) Klug, D. M.; Tse, E. G.; Silva, D. G.; Cao, Y.; Charman, S. A.; Chauhan, J.; Crighton, E.; Dichiara, M.; Drake, C.; Drewry, D.; da Silva Emery, F.; Ferrins, L.; Graves, L.; Hopkins, E.; Kresina, T. A. C.; Lorente-Macías, Á.; Perry, B.; Phipps, R.; Quiroga, B.; Quotadamo, A.; Sabatino, G. N.; Sama, A.; Schätzlein, A.; Simpson, Q. J.; Steele, J.; Shanu-Wilson, J.; Sjö, P.; Stapleton, P.; Swain, C. J.; Vaideanu, A.; Xie, H.; Zuercher, W.; Todd, M. H. Open Source Antibiotics: Simple Diarylimidazoles Are Potent against Methicillin-Resistant Staphylococcus Aureus. *ACS Infect Dis* **2023**, *9* (12), 2423–2435. https://doi.org/10.1021/acsinfecdis.3c00286.

(59) Lim, W.; Melse, Y.; Konings, M.; Duong, H. P.; Eadie, K.; Laleu, B.; Perry, B.; Todd, M. H.; Ioset, J.-R.; Sande, W. W. J. van de. Addressing the Most Neglected Diseases through an Open Research Model: The Discovery of Fenarimols as Novel Drug Candidates for

Eumycetoma. *PLOS Neglected Tropical Diseases* **2018**, *12* (4), e0006437. https://doi.org/10.1371/journal.pntd.0006437.

(60) Scott, W. L.; O'Donnell, M. J. *Distributed Drug Discovery, Part 1: Linking Academia and Combinatorial Chemistry to Find Drug Leads for Developing World Diseases*. ACS Publications. https://doi.org/10.1021/cc800183m.

(61) Desselle, M. R.; Neale ,Ruth; Hansford ,Karl A; Zuegg ,Johannes; Elliott ,Alysha G; Cooper ,Matthew A; and Blaskovich, M. A. Institutional Profile: Community for Open Antimicrobial Drug Discovery – Crowdsourcing New Antibiotics and Antifungals. *Future Science OA* **2017**, *3* (2), FSO171. https://doi.org/10.4155/fsoa-2016-0093.

(62) Samby, K.; Willis, P. A.; Burrows, J. N.; Laleu, B.; Webborn, P. J. H. Actives from MMV Open Access Boxes? A Suggested Way Forward. *PLOS Pathogens* **2021**, *17* (4), e1009384. https://doi.org/10.1371/journal.ppat.1009384.

(63) *Strategy | DNDi*. https://dndi.org/about/strategy/ (accessed 2025-05-06).

(64) Harky, A.; Mishra, V.; Ansari, D. M.; Melamed, N. Are Open-Source Approaches the Most Efficient Way Forward for COVID-19 Drug Discovery? *Expert Opinion on Drug Discovery* **2020**.

(65) Boby, M. L.; Fearon, D.; Ferla, M.; Filep, M.; Koekemoer, L.; Robinson, M. C.; The COVID Moonshot Consortium; Chodera, J. D.; Lee, A. A.; London, N.; von Delft, A.; von Delft, F. Open Science Discovery of Potent Noncovalent SARS-CoV-2 Main Protease Inhibitors. *Science* **2023**, *382* (6671), eabo7201. https://doi.org/10.1126/science.abo7201.

(66) Team, D. D. W. *The COVID-19 antiviral race: we're all in this together*. Drug Discovery World (DDW). https://www.ddw-online.com/the-covid-19-antiviral-race-were-all-in-this-together-1243-202008/ (accessed 2025-05-15).

(67) An Introduction to the UNESCO Recommendation on Open Science, 2022. https://doi.org/10.54677/XOIR1696 (accessed 2025-08-01).

(68) *10 Principles of Citizen Science – Australian Citizen Science Association*. https://citizenscience.org.au/10-principles-of-citizen-science/ (accessed 2025-05-06).

(69) O'Reilly, W.; Starrs, D. Science Citizen: Shifting to a "Science-First" Approach and Recognising the Trade-Offs between Objectives in a Long-Term Citizen Science Program. *Front. Environ. Sci.* **2023**, *11*. https://doi.org/10.3389/fenvs.2023.1270247.

(70) Njue, N.; Stenfert Kroese, J.; Gräf, J.; Jacobs, S. R.; Weeser, B.; Breuer, L.; Rufino, M. C. Citizen Science in Hydrological Monitoring and Ecosystem Services Management: State of the Art and Future Prospects. *Science of The Total Environment* **2019**, *693*, 133531. https://doi.org/10.1016/j.scitotenv.2019.07.337.

(71) Mesaglio, T.; Callaghan, C. T. An Overview of the History, Current Contributions and Future Outlook of iNaturalist in Australia. *Wildl. Res.* **2021**, *48* (4), 289–303. https://doi.org/10.1071/WR20154.

(72) Hota, A.; Konar, C.; Stalin, C. S.; Vaddi, S.; Mohanty, P. K.; Dabhade, P.; Dharmik Bhoga, S. A.; Rajoria, M.; Sethi, S. Tracking Galaxy Evolution Through Low-Frequency Radio Continuum Observations Using SKA and Citizen-Science Research Using Multi-Wavelength Data. *J Astrophys Astron* **2016**, *37* (4), 41. https://doi.org/10.1007/s12036-016-9415-8.

(73) Roche, J.; Bell, L.; Galvão, C.; Golumbic, Y. N.; Kloetzer, L.; Knoben, N.; Laakso, M.; Lorke, J.; Mannion, G.; Massetti, L.; Mauchline, A.; Pata, K.; Ruck, A.; Taraba, P.; Winter, S. Citizen Science, Education, and Learning: Challenges and Opportunities. *Front. Sociol.* **2020**, *5*. https://doi.org/10.3389/fsoc.2020.613814.

(74) Wehn, U.; Gharesifard, M.; Ceccaroni, L.; Joyce, H.; Ajates, R.; Woods, S.; Bilbao, A.; Parkinson, S.; Gold, M.; Wheatland, J. Impact Assessment of Citizen Science: State of the Art and Guiding Principles for a Consolidated Approach. *Sustain Sci* **2021**, *16* (5), 1683–1699. https://doi.org/10.1007/s11625-021-00959-2.

(75) Strasser, B. J.; Tancoigne, E.; Baudry, J.; Piguet, S.; Spiers, H.; Marquez, J. L.-F.; Kasparian, J.; Grey, F.; Anderson, D.; Lintott, C. Quantifying Online Citizen Science: Dynamics and Demographics of Public Participation in Science. *PLOS ONE* **2023**, *18* (11), e0293289. https://doi.org/10.1371/journal.pone.0293289.

(76) Hindle, M. Vital Matters: Mary Shelley's Frankenstein and Romantic Science. *Critical Survey* **1990**, *2* (1), 29–35.

(77) Tauber, A. I. On Ways of Knowing. In *The Triumph of Uncertainty*; Science and Self in the Postmodern Age; Central European University Press, 2022; pp 33–54. https://doi.org/10.7829/j.ctv2cw0s3h.7.

(78) Serjeant, S.; Pearson, J.; Dickinson, H.; Jarvis, J. Citizen Science in European Research Infrastructures. *Eur. Phys. J. Plus* **2024**, *139* (5), 418. https://doi.org/10.1140/epjp/s13360-024-05223-x.

(79) de Sherbinin, A.; Bowser, A.; Chuang, T.-R.; Cooper, C.; Danielsen, F.; Edmunds, R.; Elias, P.; Faustman, E.; Hultquist, C.; Mondardini, R.; Popescu, I.; Shonowo, A.; Sivakumar, K. The Critical Importance of Citizen Science Data. *Front. Clim.* **2021**, *3*. https://doi.org/10.3389/fclim.2021.650760.

(80) Riley, J.; Mason-Wilkes, W. Dark Citizen Science. *Public Underst Sci* **2024**, *33* (2), 142–157. https://doi.org/10.1177/09636625231203470.

(81) Harwell, T. A.; Low ,Russanne; Mattheis ,Allison; Riedinger ,Kelly; and Fischer, H. Is Citizen Science Queering Science? An Exploration of the Personal Dimensions of Engaging LGBTQ+ Citizen Science Volunteers. *International Journal of Science Education, Part B* **2023**, *13* (2), 116–130. https://doi.org/10.1080/21548455.2022.2137706.

(82) Cole, N. L.; Kormann, E.; Klebel, T.; Apartis, S.; Ross-Hellauer, T. The Societal Impact of Open Science: A Scoping Review. *Royal Society Open Science* **2024**, *11* (6), 240286. https://doi.org/10.1098/rsos.240286.

(83) Waugh, J. K.; Lindsey, J. K.; Stewart, M. Z.; Winter, J. C.; Parrish, J. K. Demographics of Public Participation in Science: A Meta-Analytic Approach. *Citizen Science: Theory and Practice* **2023**, *8* (1). https://doi.org/10.5334/cstp.610.

(84) Koepnick, B.; Flatten, J.; Husain, T.; Ford, A.; Silva, D.-A.; Bick, M. J.; Bauer, A.; Liu, G.; Ishida, Y.; Boykov, A.; Estep, R. D.; Kleinfelter, S.; Nørgård-Solano, T.; Wei, L.; Players, F.; Montelione, G. T.; DiMaio, F.; Popović, Z.; Khatib, F.; Cooper, S.; Baker, D. De Novo Protein Design by Citizen Scientists. *Nature* **2019**, *570* (7761), 390–394. https://doi.org/10.1038/s41586-019-1274-4.

(85) *Press release: The Nobel Prize in Chemistry 2024*. NobelPrize.org. https://www.nobelprize.org/prizes/chemistry/2024/press-release/ (accessed 2025-05-06).

(86) *HHMI's David Baker Wins 2024 Nobel in Chemistry | HHMI*. https://www.hhmi.org/hhmi-david-baker-wins-2024-nobel-chemistry (accessed 2025-04-25).

(87) Xue, K. *Citizen science draws amateurs into scientific research | Harvard Magazine*. https://www.harvardmagazine.com/2013/12/popular-science (accessed 2025-04-25).

(88) Haklay, M.; Fraisl, D.; Greshake Tzovaras, B.; Hecker, S.; Gold, M.; Hager, G.; Ceccaroni, L.; Kieslinger, B.; Wehn, U.; Woods, S.; Nold, C.; Balázs, B.; Mazzonetto, M.; Ruefenacht, S.; Shanley, L. A.; Wagenknecht, K.; Motion, A.; Sforzi, A.; Riemenschneider, D.; Dorler, D.; Heigl, F.; Schaefer, T.; Lindner, A.; Weißpflug, M.; Mačiulienė, M.; Vohland, K. Contours of Citizen Science: A Vignette Study. *Royal Society Open Science* **2021**, *8* (8), 202108. https://doi.org/10.1098/rsos.202108.

(89) *Zooniverse*. https://www.zooniverse.org/ (accessed 2025-11-28).

(90) Solé, C.; Couso, D.; Hernández, M. I. Citizen Science in Schools: A Systematic Literature Review. *International Journal of Science Education, Part B* **2023**, *0* (0), 1–17. https://doi.org/10.1080/21548455.2023.2280009.

(91) Stuckey, M.; Hofstein ,Avi; Mamlok-Naaman ,Rachel; and Eilks, I. The Meaning of 'Relevance' in Science Education and Its Implications for the Science Curriculum. *Studies in Science Education* **2013**, *49* (1), 1–34. https://doi.org/10.1080/03057267.2013.802463.

(92) Lüsse, M.; Brockhage, F.; Beeken, M.; Pietzner, V. Citizen Science and Its Potential for Science Education. *International Journal of Science Education* **2022**, *44* (7), 1120–1142. https://doi.org/10.1080/09500693.2022.2067365.

(93) West, J. D.; Bergstrom, C. T. Misinformation in and about Science. *Proceedings of the National Academy of Sciences* **2021**, *118* (15), e1912444117. https://doi.org/10.1073/pnas.1912444117.

(94) *Why We Must Rebuild Trust in Science*. https://pew.org/2MoiYlW (accessed 2025-08-01).

(95) *Widespread distrust in science: Is the way we communicate to blame?*. AAMC. https://www.aamc.org/news/widespread-distrust-science-way-we-communicate-blame (accessed 2025-08-01).

(96) Kozlov, M.; Ryan, C. How Trump 2.0 Is Slashing NIH-Backed Research — in Charts. *Nature* **2025**, *640* (8060), 863–865. https://doi.org/10.1038/d41586-025-01099-8.

(97) Hwang, I.; Huang, J.; Anthes, E.; Migliozzi, B.; Mueller, B. The Gutting of America's Medical Research: Here Is Every Canceled or Delayed N.I.H. Grant. *The New York Times*. June 4, 2025. https://www.nytimes.com/interactive/2025/06/04/health/trump-cuts-nih-grants-research.html (accessed 2025-08-01).

(98) Pizzolato, L. A. V.; Tsuji, L. J. S. Citizen Science in K–12 School-Based Learning Settings. *School Science and Mathematics* **2022**, *122* (4), 222–231. https://doi.org/10.1111/ssm.12528.

(99) Vitone, T.; Stofer, K.; Steininger, M. S.; Hulcr, J.; Dunn, R.; Lucky, A. School of Ants Goes to College: Integrating Citizen Science into the General Education Classroom Increases Engagement with Science. *JCOM* **2016**, *15* (1), A03. https://doi.org/10.22323/2.15010203.

(100) Burrell-Sander, K.; Firmer, G.; Marfavi, A.; Rutledge, P.; Motion, A.; Scroggie, K. Breaking Good: A Citizen Science Approach to Developing New Treatments for Mycetoma. *unpublished*.

(101) *Pioneering education and research program leads to international conference at IUPUI*. news. https://medicine.iu.edu/news/2013/07/distributed-drug (accessed 2025-05-05).

(102) User, P. *Bush medicine project*. https://federation.edu.au/institutes-and-schools/iiss/research/bush-medicine-project (accessed 2025-05-15).

(103) Tse, E. G.-O. Open Source Malaria: Potent Triazolopyrazine-Based Antiplasmodium Agents That Probe an Important Mechanism of Action. PhD, University of Sydney, Sydney, NSW, 2020.

(104) *Mycetoma*. https://www.who.int/news-room/fact-sheets/detail/mycetoma (accessed 2025-05-19).

(105) Emery, D.; Denning, D. W. The Global Distribution of Actinomycetoma and Eumycetoma. *PLOS Neglected Tropical Diseases* **2020**, *14* (9), e0008397. https://doi.org/10.1371/journal.pntd.0008397.

(106) Nenoff, P.; van de Sande, W. w. j.; Fahal, A. h.; Reinel, D.; Schöfer, H. Eumycetoma and Actinomycetoma – an Update on Causative Agents, Epidemiology, Pathogenesis,

Diagnostics and Therapy. *Journal of the European Academy of Dermatology and Venereology* **2015**, *29* (10), 1873–1883. https://doi.org/10.1111/jdv.13008.

(107) Abushouk, A.; Nasr, A.; Masuadi, E.; Allam, G.; Siddig, E. E.; Fahal, A. H. The Role of Interleukin-1 Cytokine Family (IL-1β, IL-37) and Interleukin-12 Cytokine Family (IL-12, IL-35) in Eumycetoma Infection Pathogenesis. *PLOS Neglected Tropical Diseases* **2019**, *13* (4), e0007098. https://doi.org/10.1371/journal.pntd.0007098.

(108) Musa, E. A.; Abdoon, I. H.; Bakhiet, S. M.; Osman, B.; Abdalla, S. A.; Fahal, A. H. Mycetoma Management and Clinical Outcomes: The Mycetoma Research Center Experience. *Transactions of The Royal Society of Tropical Medicine and Hygiene* **2023**, *117* (1), 12–21. https://doi.org/10.1093/trstmh/trac069.

(109) van de Sande, W. W. J. Global Burden of Human Mycetoma: A Systematic Review and Meta-Analysis. *PLoS Negl Trop Dis* **2013**, *7* (11), e2550. https://doi.org/10.1371/journal.pntd.0002550.

(110) van de Sande, W. W. J.; Fahal, A. H. An Updated List of Eumycetoma Causative Agents and Their Differences in Grain Formation and Treatment Response. *Clinical Microbiology Reviews* **2024**, *37* (2), e00034-23. https://doi.org/10.1128/cmr.00034-23.

(111) Hao, X.; Cognetti, M.; Burch-Smith, R.; Mejia, E. O.; Mirkin, G. Mycetoma: Development of Diagnosis and Treatment. *Journal of Fungi* **2022**, *8* (7), 743. https://doi.org/10.3390/jof8070743.

(112) Welsh, O.; Salinas-Carmona, M. C.; la Garza, J. A. C.-D.; Rodriguez-Escamilla, I. M.; Sanchez-Meza, E. Current Treatment of Mycetoma. *Curr Treat Options Infect Dis* **2018**, *10* (3), 389–396. https://doi.org/10.1007/s40506-018-0171-y.

(113) Abd Algaffar, S. O.; Verbon, A.; Khalid, S. A.; van de Sande, W. W. J. Development and Validation of a Resazurin Assay for in Vitro Susceptibility Testing of Actinomadura Madurae: A Common Causative Agent of Actinomycetoma. *Journal of Antimicrobial Chemotherapy* **2023**, *78* (1), 155–160. https://doi.org/10.1093/jac/dkac367.

(114) *M24 | Susceptibility Testing of Mycobacteria, Nocardia spp., and Other Aerobic Actinomycetes*. https://clsi.org/shop/standards/m24/ (accessed 2025-06-24).

(115) Chandler, D. J.; Bonifaz, A.; van de Sande, W. W. J. An Update on the Development of Novel Antifungal Agents for Eumycetoma. *Front. Pharmacol.* **2023**, *14*. https://doi.org/10.3389/fphar.2023.1165273.

(116) Fahal, A. H.; Ahmed, E. S.; Bakhiet, S. M.; Bakhiet, O. E.; Fahal, L. A.; Mohamed, A. A.; Mohamedelamin, E. S. W.; Bahar, M. E. N.; Attalla, H. Y.; Siddig, E. E.; Mhmoud, N. A.; Musa, A. M.; van de Sande, W. W. J.; Scherrer, B.; Oyieko, P.; Egondi, T. W.; Onyango, K. O.; Hata, K.; Chu, W.-Y.; Dorlo, T. P. C.; Brüggemann, R. J.; Nyaoke, B. A.; Strub-Wourgaft, N.; Zijlstra, E. E. Two Dose Levels of Once-Weekly Fosravuconazole versus Daily Itraconazole in Combination with Surgery in Patients with Eumycetoma in Sudan: A Randomised, Double-Blind, Phase 2, Proof-of-Concept Superiority Trial. *The Lancet Infectious Diseases* **2024**, *24* (11), 1254–1265. https://doi.org/10.1016/S1473-3099(24)00404-3.

(117) Vanreppelen, G.; Wuyts, J.; Van Dijck, P.; Vandecruys, P. Sources of Antifungal Drugs. *Journal of Fungi* **2023**, *9* (2), 171. https://doi.org/10.3390/jof9020171.

(118) Hammoudi Halat, D.; Younes, S.; Mourad, N.; Rahal, M. Allylamines, Benzylamines, and Fungal Cell Permeability: A Review of Mechanistic Effects and Usefulness against Fungal Pathogens. *Membranes (Basel)* **2022**, *12* (12), 1171. https://doi.org/10.3390/membranes12121171.

(119) Shafiei, M.; Peyton, L.; Hashemzadeh, M.; Foroumadi, A. History of the Development of Antifungal Azoles: A Review on Structures, SAR, and Mechanism of Action. *Bioorganic Chemistry* **2020**, *104*, 104240. https://doi.org/10.1016/j.bioorg.2020.104240.

(120) Akinosoglou, K.; Papageorgiou ,Despoina; Gogos ,Charalambos; and Dimopoulos, G. An Update on Newer Antifungals. *Expert Review of Anti-infective Therapy* **2025**, *23* (2–4), 149–158. https://doi.org/10.1080/14787210.2025.2461566.

(121) Estrada, R.; Chávez-López, G.; Estrada-Chávez, G.; López-Martínez, R.; Welsh, O. Eumycetoma. *Clinics in Dermatology* **2012**, *30* (4), 389–396. https://doi.org/10.1016/j.clindermatol.2011.09.009.

(122) van de Sande, W. W. J. In Vitro Susceptibility Testing for Black Grain Eumycetoma Causative Agents. *Transactions of The Royal Society of Tropical Medicine and Hygiene* **2021**, *115* (4), 343–354. https://doi.org/10.1093/trstmh/traa184.

(123) Yoshioka, I.; Fahal, A. H.; Kaneko, S.; Cao, W.; Yaguchi, T. Itraconazole Resistance in Madurella Fahalii Linked to a Distinct Homolog of the Gene Encoding Cytochrome P450 14-α Sterol Demethylase (CYP51). *PLOS Neglected Tropical Diseases* **2025**, *19* (3), e0012623. https://doi.org/10.1371/journal.pntd.0012623.

(124) Sow, D.; Ndiaye, M.; Sarr, L.; Kanté, M. D.; Ly, F.; Dioussé, P.; Faye, B. T.; Gaye, A. M.; Sokhna, C.; Ranque, S.; Faye, B. Mycetoma Epidemiology, Diagnosis Management, and Outcome in Three Hospital Centres in Senegal from 2008 to 2018. *PLOS ONE* **2020**, *15* (4), e0231871. https://doi.org/10.1371/journal.pone.0231871.

(125) Siddig, E. E.; Ahmed, A.; Ali, Y.; Bakhiet, S. M.; Mohamed, N. S.; Ahmed, E. S.; Fahal, A. H. Eumycetoma Medical Treatment: Past, Current Practice, Latest Advances and Perspectives. *Microbiology Research* **2021**, *12* (4), 899–906. https://doi.org/10.3390/microbiolres12040066.

(126) Oliver, J. D.; Sibley, G. E. M.; Beckmann, N.; Dobb, K. S.; Slater, M. J.; McEntee, L.; du Pré, S.; Livermore, J.; Bromley, M. J.; Wiederhold, N. P.; Hope, W. W.; Kennedy, A. J.; Law, D.; Birch, M. F901318 Represents a Novel Class of Antifungal Drug That Inhibits Dihydroorotate Dehydrogenase. *Proceedings of the National Academy of Sciences* **2016**, *113* (45), 12809–12814. https://doi.org/10.1073/pnas.1608304113.

(127) Vanbiervliet, Y.; Van Nieuwenhuyse, T.; Aerts, R.; Lagrou, K.; Spriet, I.; Maertens, J. Review of the Novel Antifungal Drug Olorofim (F901318). *BMC Infectious Diseases* **2024**, *24* (1), 1256. https://doi.org/10.1186/s12879-024-10143-3.

(128) Lim, W.; Eadie, K.; Konings, M.; Rijnders, B.; Fahal, A. H.; Oliver, J. D.; Birch, M.; Verbon, A.; van de Sande, W. Madurella Mycetomatis, the Main Causative Agent of Eumycetoma, Is Highly Susceptible to Olorofim. *Journal of Antimicrobial Chemotherapy* **2020**, *75* (4), 936–941. https://doi.org/10.1093/jac/dkz529.

(129) van de Sande, W. W. J.; Luijendijk, A.; Ahmed, A. O. A.; Bakker-Woudenberg, I. A. J. M.; van Belkum, A. Testing of the In Vitro Susceptibilities of Madurella Mycetomatis to Six Antifungal Agents by Using the Sensititre System in Comparison with a Viability-Based 2,3-Bis(2-Methoxy-4-Nitro-5-Sulfophenyl)-5- [(Phenylamino)Carbonyl]-2H-Tetrazolium Hydroxide (XTT) Assay and a Modified NCCLS Method. *Antimicrobial Agents and Chemotherapy* **2005**, *49* (4), 1364–1368. https://doi.org/10.1128/aac.49.4.1364-1368.2005.

(130) Kloezen, W.; Parel, F.; Brüggemann, R.; Asouit, K.; Helvert-van Poppel, M.; Fahal, A.; Mouton, J.; van de Sande, W. Amphotericin B and Terbinafine but Not the Azoles Prolong Survival in Galleria Mellonella Larvae Infected with Madurella Mycetomatis. *Medical Mycology* **2018**, *56* (4), 469–478. https://doi.org/10.1093/mmy/myx064.

(131) Abugessaisa, I.; Konings, M.; Manabe, R.-I.; Murphy, C. M.; Kawashima, T.; Hasegawa, A.; Takahashi, C.; Tagami, M.; Okazaki, Y.; Eadie, K.; Lim, W.; Doyle, S.; Verbon, A.; Fahal, A. H.; Kasukawa, T.; van de Sande, W. W. J. Iron Regulatory Pathways Differentially Expressed during Madurella Mycetomatis Grain Development in Galleria Mellonella. *Nat Commun* **2025**, *16* (1), 5324. https://doi.org/10.1038/s41467-025-60875-2.

(132) Sheehan, G.; Konings, M.; Lim, W.; Fahal, A.; Kavanagh, K.; Sande, W. W. J. van de. Proteomic Analysis of the Processes Leading to Madurella Mycetomatis Grain Formation in Galleria Mellonella Larvae. *PLOS Neglected Tropical Diseases* **2020**, *14* (4), e0008190. https://doi.org/10.1371/journal.pntd.0008190.

(133) Lim, W.; Nyuykonge, B.; Eadie, K.; Konings, M.; Smeets, J.; Fahal, A.; Bonifaz, A.; Todd, M.; Perry, B.; Samby, K.; Burrows, J.; Verbon, A.; Sande, W. van de. Screening the Pandemic Response Box Identified Benzimidazole Carbamates, Olorofim and Ravuconazole as Promising Drug Candidates for the Treatment of Eumycetoma. *PLOS Neglected Tropical Diseases* **2022**, *16* (2), e0010159. https://doi.org/10.1371/journal.pntd.0010159.

(134) Marena, G. D.; Thomaz, L.; Nosanchuk, J. D.; Taborda, C. P. Galleria Mellonella as an Invertebrate Model for Studying Fungal Infections. *Journal of Fungi* **2025**, *11* (2), 157. https://doi.org/10.3390/jof11020157.

(135) *Sudan war destroys world's only research centre on skin disease mycetoma: director*. France 24. https://www.france24.com/en/live-news/20250424-sudan-war-destroys-world-s-only-research-centre-on-skin-disease-mycetoma-director (accessed 2025-06-02).

(136) Abd Algaffar, S. O.; Satyal, P.; Ashmawy, N. S.; Verbon, A.; van de Sande, W. W. J.; Khalid, S. A. In Vitro and In Vivo Wide-Spectrum Dual Antimycetomal Activity of Eight Essential Oils Coupled with Chemical Composition and Metabolomic Profiling. *Microbiology Research* **2024**, *15* (3), 1280–1297. https://doi.org/10.3390/microbiolres15030086.

(137) Esteves, L. *MycetOS | DNDi*. https://dndi.org/research-development/portfolio/mycetos/ (accessed 2025-06-02).

(138) Ma, J.; van Doodewaerd, B. R.; Biersack, B.; Verbon, A.; Geurink, P. P.; van de Sande, W. W. J. A Drug-Repurposing Screen of FDA- and EMA-Approved Drugs Identifies Two NF-κB Inhibitors Active against Eumycetoma. *J Antimicrob Chemother* **2025**, dkaf369. https://doi.org/10.1093/jac/dkaf369.

(139) Duong, H. P.; Melechov, D.; Lim, W.; Ma, J.; Scroggie, K. R.; Rajendra, L.; Perry, B.; Cruz, L. R.; Saleem, R. S. Z.; Rutledge, P. J.; Motion, A.; Sande, W. W. J. van de; Todd, M. H. Structure–Activity Relationships of Fenarimol Analogues with Potent in Vitro and in Vivo Activity against Madurella Mycetomatis, the Main Causative Agent of Mycetoma. *RSC Med. Chem.* **2025**. https://doi.org/10.1039/D5MD00427F.

(140) Silva, V. K. A.; May, R. C.; Rodrigues, M. L. Pyrifenox, an Ergosterol Inhibitor, Differentially Affects Cryptococcus Neoformans and Cryptococcus Gattii. *Medical Mycology* **2020**, *58* (7), 928–937. https://doi.org/10.1093/mmy/myz132.

(141) Xu, Y.; Sheng, C.; Wang, W.; Che, X.; Cao, Y.; Dong, G.; Wang, S.; Ji, H.; Miao, Z.; Yao, J.; Zhang, W. Structure-Based Rational Design, Synthesis and Antifungal Activity of Oxime-Containing Azole Derivatives. *Bioorganic & Medicinal Chemistry Letters* **2010**, *20* (9), 2942–2945. https://doi.org/10.1016/j.bmcl.2010.03.014.

(142) Kosmalski, T.; Kupczyk, D.; Baumgart, S.; Paprocka, R.; Studzińska, R. A Review of Biologically Active Oxime Ethers. *Molecules* **2023**, *28* (13), 5041. https://doi.org/10.3390/molecules28135041.

(143) Jakopin, Ž. 2-Aminothiazoles in Drug Discovery: Privileged Structures or Toxicophores? *Chemico-Biological Interactions* **2020**, *330*, 109244. https://doi.org/10.1016/j.cbi.2020.109244.

(144) Das, D.; Sikdar, P.; Bairagi, M. Recent Developments of 2-Aminothiazoles in Medicinal Chemistry. *European Journal of Medicinal Chemistry* **2016**, *109*, 89–98. https://doi.org/10.1016/j.ejmech.2015.12.022.

(145) Girardini, M.; Ferlenghi, F.; Annunziato, G.; Degiacomi, G.; Papotti, B.; Marchi, C.; Sammartino, J. C.; Rasheed, S. S.; Contini, A.; Pasca, M. R.; Vacondio, F.; Evans, J. C.; Dick, T.; Müller, R.; Costantino, G.; Pieroni, M. Expanding the Knowledge around Antitubercular 5-(2-Aminothiazol-4-Yl)Isoxazole-3-Carboxamides: Hit–to–Lead Optimization and Release of

a Novel Antitubercular Chemotype via Scaffold Derivatization. *European Journal of Medicinal Chemistry* **2023**, *245*, 114916. https://doi.org/10.1016/j.ejmech.2022.114916.

(146) Mjambili, F.; Njoroge, M.; Naran, K.; De Kock, C.; Smith, P. J.; Mizrahi, V.; Warner, D.; Chibale, K. Synthesis and Biological Evaluation of 2-Aminothiazole Derivatives as Antimycobacterial and Antiplasmodial Agents. *Bioorganic & Medicinal Chemistry Letters* **2014**, *24* (2), 560–564. https://doi.org/10.1016/j.bmcl.2013.12.022.

(147) Gentles, R. G.; Grant-Young, K.; Hu, S.; Huang, Y.; Poss, M. A.; Andres, C.; Fiedler, T.; Knox, R.; Lodge, N.; Weaver, C. D.; Harden, D. G. Initial SAR Studies on Apamin-Displacing 2-Aminothiazole Blockers of Calcium-Activated Small Conductance Potassium Channels. *Bioorganic & Medicinal Chemistry Letters* **2008**, *18* (19), 5316–5319. https://doi.org/10.1016/j.bmcl.2008.08.023.

(148) Ferrins, L.; Buskes, M. J.; Kapteyn, M. M.; Engels, H. N.; Enos, S. E.; Lu, C.; Klug, D. M.; Singh, B.; Quotadamo, A.; Bachovchin, K.; Tear, W. F.; Spaulding, A. E.; Forbes, K. C.; Bag, S.; Rivers, M.; LeBlanc, C.; Burchfield, E.; Armand, J. R.; Diaz-Gonzalez, R.; Ceballos-Perez, G.; García-Hernández, R.; Pérez-Moreno, G.; Bosch-Navarrete, C.; Gómez-Liñán, C.; Ruiz-Pérez, L. M.; Gamarro, F.; González-Pacanowska, D.; Navarro, M.; Mensa-Wilmot, K.; Pollastri, M. P.; Kyle, D. E.; Rice, C. A. Identification of Novel Anti-Amoebic Pharmacophores from Kinase Inhibitor Chemotypes. *Front. Microbiol.* **2023**, *14*. https://doi.org/10.3389/fmicb.2023.1149145.

(149) Dreikorn, B. A.; Owen, W. J. Fungicides, Agricultural. In *Kirk-Othmer Encyclopedia of Chemical Technology*; John Wiley & Sons, Ltd, 2000. https://doi.org/10.1002/0471238961.0621140704180509.a01.

(150) Starkey, L. A.; Blagburn, B. L. 13 - Antiparasitic Drugs. In *Greene's Infectious Diseases of the Dog and Cat (Fifth Edition)*; Sykes, J. E., Ed.; W.B. Saunders: Philadelphia, 2021; pp 149–160. https://doi.org/10.1016/B978-0-323-50934-3.00013-6.

(151) Elkheir, L. Y. M.; Delaye, P.-O.; Penichon, M.; Eadie, K.; Mohamed, M. A.; Besson, P.; Chesnay, A.; Desoubeaux, G.; Roger, S.; van de Sande, W. W. J.; Fahal, A. H.; Enguehard-Gueiffier, C. Emerging Therapeutics: The Imidazo[1,2-*b*]Pyridazine Scaffold as a Novel Drug Candidate for Eumycetoma, a Neglected Tropical Disease. *European Journal of Medicinal Chemistry* **2024**, *277*, 116720. https://doi.org/10.1016/j.ejmech.2024.116720.

(152) Malik, M. S.; Alshareef, H. F.; Alfaidi, K. A.; Ather, H.; Abduljaleel, Z.; Hussein, E. M.; Moussa, Z.; Ahmed, S. A. Exploring the Untapped Pharmacological Potential of Imidazopyridazines. *RSC Adv 14* (6), 3972–3984. https://doi.org/10.1039/d3ra07280k.

(153) Law, C. S. W.; Yeong, K. Y. Benzimidazoles in Drug Discovery: A Patent Review. *ChemMedChem* **2021**, *16* (12), 1861–1877. https://doi.org/10.1002/cmdc.202100004.

(154) Faville, S. C.; Harris-Hamdscomb, K.; Harker, O.; Mattison, S.; Tamorite, H.; Bristowe, J.; Daly, D.; Ege, R.; He, H.; Jones, J.; McCorkindale, A.; Mei, K.; Monson, A.; Moree, L.; Perkovic, F.; Rickerby, G.; Robinson, J.; Rudkin, F.; Whibley, L.; Worthington, R.; Ennis, C.; de la Harpe, S.; Brind, T.; Hopkins, A.; Winefield, K.; Hendrickx, S.; Caljon, G.; Perry, B.; Vernall, A. J. Open Synthesis Network Research in an Undergraduate Laboratory: Development of Benzoxazole Amide Derivatives against Leishmania Parasite. *J. Chem. Educ.* **2022**, *99* (4), 1682–1690. https://doi.org/10.1021/acs.jchemed.1c01213.

(155) Daniel, T. M. The History of Tuberculosis. *Respiratory Medicine* **2006**, *100* (11), 1862–1870. https://doi.org/10.1016/j.rmed.2006.08.006.

(156) *Global Tuberculosis Report 2024*. https://www.who.int/teams/global-programme-on-tuberculosis-and-lung-health/tb-reports/global-tuberculosis-report-2024 (accessed 2025-06-16).

(157) Sharma, A.; De Rosa, M.; Singla, N.; Singh, G.; Barnwal, R. P.; Pandey, A. Tuberculosis: An Overview of the Immunogenic Response, Disease Progression, and Medicinal Chemistry Efforts in the Last Decade toward the Development of Potential Drugs for Extensively Drug-Resistant Tuberculosis Strains. *J. Med. Chem.* **2021**, *64* (8), 4359–4395. https://doi.org/10.1021/acs.jmedchem.0c01833.

(158) Alsayed, S. S. R.; Gunosewoyo, H. Tuberculosis: Pathogenesis, Current Treatment Regimens and New Drug Targets. *Int J Mol Sci* **2023**, *24* (6), 5202. https://doi.org/10.3390/ijms24065202.

(159) Sharma, S. K.; Mohan ,Alladi; and Kohli, M. Extrapulmonary Tuberculosis. *Expert Review of Respiratory Medicine* **2021**, *15* (7), 931–948. https://doi.org/10.1080/17476348.2021.1927718.

(160) Houben, R. M. G. J.; Dodd, P. J. The Global Burden of Latent Tuberculosis Infection: A Re-Estimation Using Mathematical Modelling. *PLOS Medicine* **2016**, *13* (10), e1002152. https://doi.org/10.1371/journal.pmed.1002152.

(161) Singh, S.; Zahiruddin, Q. S.; Lakhanpal, S.; Ballal, S.; Kumar, S.; Bhat, M.; Sharma, S.; Kumar, M. R.; Dhandh, Y. K.; Rustagi, S.; Alissa, M.; Halwani, M. A.; Garout, M.; Alrasheed, H. A.; Al-Subaie, M. F.; Al Kaabi, N. A.; Rabaan, A. A.; Sah, S.; Shabil, M.; Khatib, M. N.; Satapathy, P. Wealth-Based Inequalities in Tuberculosis Prevalence among Households Having Children and Young Adults in India: Insights from Indian Demographic and Health Surveys (2015–2021). *BMC Infectious Diseases* **2025**, *25* (1), 21. https://doi.org/10.1186/s12879-024-10301-7.

(162) *Global Health Sector Strategies*. https://www.who.int/teams/global-hiv-hepatitis-and-stis-programmes/strategies/global-health-sector-strategies (accessed 2025-06-16).

(163) Pareek, M.; Greenaway, C.; Noori, T.; Munoz, J.; Zenner, D. The Impact of Migration on Tuberculosis Epidemiology and Control in High-Income Countries: A Review. *BMC Medicine* **2016**, *14* (1), 48. https://doi.org/10.1186/s12916-016-0595-5.

(164) Żukowska, L.; Zygała-Pytlos, D.; Struś, K.; Zabost, A.; Kozińska, M.; Augustynowicz-Kopeć, E.; Dziadek, J.; Minias, A. An Overview of Tuberculosis Outbreaks Reported in the Years 2011–2020. *BMC Infectious Diseases* **2023**, *23* (1), 253. https://doi.org/10.1186/s12879-023-08197-w.

(165) Furlow, B. Historic TB Outbreak a Wake-up Call for US Policy Makers. *The Lancet Respiratory Medicine* **2025**, *13* (4), e23. https://doi.org/10.1016/S2213-2600(25)00050-5.

(166) Smith, I. Mycobacterium Tuberculosis Pathogenesis and Molecular Determinants of Virulence. *Clin Microbiol Rev* **2003**, *16* (3), 463–496. https://doi.org/10.1128/CMR.16.3.463-496.2003.

(167) Shin, H.-J.; Kwon, Y.-S. Treatment of Drug Susceptible Pulmonary Tuberculosis. *Tuberc Respir Dis (Seoul)* **2015**, *78* (3), 161–167. https://doi.org/10.4046/trd.2015.78.3.161.

(168) Lambert, M.-L.; Hasker, E.; Deun, A. V.; Roberfroid, D.; Boelaert, M.; Van der Stuyft, P. Recurrence in Tuberculosis: Relapse or Reinfection? *The Lancet Infectious Diseases* **2003**, *3* (5), 282–287. https://doi.org/10.1016/S1473-3099(03)00607-8.

(169) Sotgiu, G.; Centis, R.; D'ambrosio, L.; Migliori, G. B. Tuberculosis Treatment and Drug Regimens. *Cold Spring Harb Perspect Med* **2015**, *5* (5), a017822. https://doi.org/10.1101/cshperspect.a017822.

(170) Patel, M. N.; Patel, A. J.; Nandpal, M. N.; Raval, M. A.; Patel, R. J.; Patel, A. A.; Paudel, K. R.; Hansbro, P. M.; Singh, S. K.; Gupta, G.; Dua, K.; Patel, S. G. Advancing against Drug-Resistant Tuberculosis: An Extensive Review, Novel Strategies and Patent Landscape. *Naunyn-Schmiedeberg's Arch Pharmacol* **2025**, *398* (3), 2127–2150. https://doi.org/10.1007/s00210-024-03466-0.

(171) Conradie, F.; Diacon, A. H.; Ngubane, N.; Howell, P.; Everitt, D.; Crook, A. M.; Mendel, C. M.; Egizi, E.; Moreira, J.; Timm, J.; McHugh, T. D.; Wills, G. H.; Bateson, A.; Hunt, R.; Van Niekerk, C.; Li, M.; Olugbosi, M.; Spigelman, M. Treatment of Highly Drug-Resistant Pulmonary Tuberculosis. *New England Journal of Medicine* **2020**, *382* (10), 893–902. https://doi.org/10.1056/NEJMoa1901814.

(172) Varshney, K.; Anaele, B.; Molaei, M.; Frasso, R.; Maio, V. <p>Risk Factors for Poor Outcomes Among Patients with Extensively Drug-Resistant Tuberculosis (XDR-TB): A Scoping Review</P>. *IDR* **2021**, *14*, 5429–5448. https://doi.org/10.2147/IDR.S339972.

(173) Dookie, N.; Rambaran, S.; Padayatchi, N.; Mahomed, S.; Naidoo, K. Evolution of Drug Resistance in Mycobacterium Tuberculosis: A Review on the Molecular Determinants of Resistance and Implications for Personalized Care. *J Antimicrob Chemother* **2018**, *73* (5), 1138–1151. https://doi.org/10.1093/jac/dkx506.

(174) Lange, C.; Abubakar, I.; Alffenaar, J.-W. C.; Bothamley, G.; Caminero, J. A.; Carvalho, A. C. C.; Chang, K.-C.; Codecasa, L.; Correia, A.; Crudu, V.; Davies, P.; Dedicoat, M.; Drobniewski, F.; Duarte, R.; Ehlers, C.; Erkens, C.; Goletti, D.; Günther, G.; Ibraim, E.; Kampmann, B.; Kuksa, L.; Lange, W. de; Leth, F. van; Lunzen, J. van; Matteelli, A.; Menzies, D.; Monedero, I.; Richter, E.; Rüsch-Gerdes, S.; Sandgren, A.; Scardigli, A.; Skrahina, A.; Tortoli, E.; Volchenkov, G.; Wagner, D.; Werf, M. J. van der; Williams, B.; Yew, W.-W.; Zellweger, J.-P.; Cirillo, D. M. Management of Patients with Multidrug-Resistant/Extensively Drug-Resistant Tuberculosis in Europe: A TBNET Consensus Statement. *European Respiratory Journal* **2014**, *44* (1), 23–63. https://doi.org/10.1183/09031936.00188313.

(175) Rana, H. K.; Singh, A. K.; Kumar, R.; Pandey, A. K. Antitubercular Drugs: Possible Role of Natural Products Acting as Antituberculosis Medication in Overcoming Drug Resistance and Drug-Induced Hepatotoxicity. *Naunyn-Schmiedeberg's Arch Pharmacol* **2024**, *397* (3), 1251–1273. https://doi.org/10.1007/s00210-023-02679-z.

(176) Wang, F.; Langley, R.; Gulten, G.; Dover, L. G.; Besra, G. S.; Jacobs, W. R.; Sacchettini, J. C. Mechanism of Thioamide Drug Action against Tuberculosis and Leprosy. *J Exp Med* **2007**, *204* (1), 73–78. https://doi.org/10.1084/jem.20062100.

(177) Alfarisi, O.; Alghamdi ,Wael A.; Al-Shaer ,Mohammad H.; Dooley ,Kelly E.; and Peloquin, C. A. Rifampin vs. Rifapentine: What Is the Preferred Rifamycin for Tuberculosis? *Expert Review of Clinical Pharmacology* **2017**, *10* (10), 1027–1036. https://doi.org/10.1080/17512433.2017.1366311.

(178) Zifodya, J. S.; Kreniske, J. S.; Schiller, I.; Kohli, M.; Dendukuri, N.; Schumacher, S. G.; Ochodo, E. A.; Haraka, F.; Zwerling, A. A.; Pai, M.; Steingart, K. R.; Horne, D. J. Xpert Ultra versus Xpert MTB/RIF for Pulmonary Tuberculosis and Rifampicin Resistance in Adults with Presumptive Pulmonary Tuberculosis. *Cochrane Database Syst Rev* **2021**, *2021* (2), CD009593. https://doi.org/10.1002/14651858.CD009593.pub5.

(179) Farhat, M.; Cox, H.; Ghanem, M.; Denkinger, C. M.; Rodrigues, C.; Abd El Aziz, M. S.; Enkh-Amgalan, H.; Vambe, D.; Ugarte-Gil, C.; Furin, J.; Pai, M. Drug-Resistant Tuberculosis: A Persistent Global Health Concern. *Nat Rev Microbiol* **2024**, *22* (10), 617–635. https://doi.org/10.1038/s41579-024-01025-1.

(180) Nguyen, T. V. A.; Anthony, R. M.; Bañuls, A.-L.; Nguyen, T. V. A.; Vu, D. H.; Alffenaar, J.-W. C. Bedaquiline Resistance: Its Emergence, Mechanism, and Prevention. *Clin Infect Dis* **2018**, *66* (10), 1625–1630. https://doi.org/10.1093/cid/cix992.

(181) Mudde, S. E.; Upton, A. M.; Lenaerts, A.; Bax, H. I.; De Steenwinkel, J. E. M. Delamanid or Pretomanid? A Solomonic Judgement! *J Antimicrob Chemother* **2022**, *77* (4), 880–902. https://doi.org/10.1093/jac/dkab505.

(182) Hoelscher, M.; Barros-Aguirre, D.; Dara, M.; Heinrich, N.; Sun, E.; Lange, C.; Tiberi, S.; Wells, C. Candidate Anti-Tuberculosis Medicines and Regimens under Clinical Evaluation. *Clinical Microbiology and Infection* **2024**, *30* (9), 1131–1138. https://doi.org/10.1016/j.cmi.2024.06.016.

(183) Majalekar, P. P.; Shirote, P. J. Fluoroquinolones: Blessings Or Curses. *Current Drug Targets 21* (13), 1354–1370. https://doi.org/10.2174/1389450121666200621193355.

(184) Poulikakos, P.; Falagas, M. E. Aminoglycoside Therapy in Infectious Diseases. *Expert Opinion on Pharmacotherapy* **2013**, *14* (12), 1585–1597. https://doi.org/10.1517/14656566.2013.806486.

(185) *The selection and use of essential medicines, 2025: WHO Model List of Essential Medicines, 24th list*. https://www.who.int/publications/i/item/B09474 (accessed 2025-11-28).

(186) Brown, K. L.; Wilburn, K. M.; Montague, C. R.; Grigg, J. C.; Sanz, O.; Pérez-Herrán, E.; Barros, D.; Ballell, L.; VanderVen, B. C.; Eltis, L. D. Cyclic AMP-Mediated Inhibition of Cholesterol Catabolism in Mycobacterium Tuberculosis by the Novel Drug Candidate GSK2556286. *Antimicrobial Agents and Chemotherapy* **2023**, *67* (1), e01294-22. https://doi.org/10.1128/aac.01294-22.

(187) Benedetta, S.; Vallini ,Francesco; Guida ,Michela; Tammaro ,Chiara; Biava ,Mariangela; and Poce, G. Mycobacterium Tuberculosis Inhibitors: An Updated Patent Review (2021–Present). *Expert Opinion on Therapeutic Patents* **2024**, *34* (12), 1215–1230. https://doi.org/10.1080/13543776.2024.2419826.

(188) *Safety, Tolerability, Pharmacokinetics, and Metabolism of Telacebec (Q203) for the Treatment of Tuberculosis: a Randomized, Placebo-Controlled, Multiple Ascending Dose Phase 1B Trial | Antimicrobial Agents and Chemotherapy*. https://journals.asm.org/doi/10.1128/aac.01123-22 (accessed 2025-06-18).

(189) Janssen, S.; Upton, C.; Jager, V. R. de; Niekerk, C. van; Dawson, R.; Hutchings, J.; Kim, J.; Choi, J.; Nam, K.; Sun, E.; Diacon, A. H. Telacebec, A Potent Agent in the Fight Against Tuberculosis: Findings from A Randomized, Phase 2 Clinical Trial and Beyond. *American Journal of Respiratory and Critical Care Medicine* **2025**. https://doi.org/10.1164/rccm.202408-1632OC.

(190) dos Reis, D. B.; Linhares, E. P. M.; dos Santos e Silva, G.; do Carmo Ferreira, F. H.; Costa, L. A. S.; Ávila, E. P.; de Almeida, M. V.; de Souza, M. V. N.; da Silva Lourenço, M. C.; Saraiva, M. F. Synthesis, Antituberculosis Evaluation and Structure–Activity Relationships of New SQ109 Analogs. *Archiv der Pharmazie* **2025**, *358* (4), e3130. https://doi.org/10.1002/ardp.202400665.

(191) Heinrich, N.; Jager, V. de; Dreisbach, J.; Gross-Demel, P.; Schultz, S.; Gerbach, S.; Kloss, F.; Dawson, R.; Narunsky, K.; Matt, L.; Wildner, L.; McHugh, T. D.; Fuhr, U.; Aldana, B. H.; Mouhdad, C.; Brake, L. te; Boeree, M. J.; Aarnoutse, R. E.; Svensson, E. M.; Gong, X.; Phillips, P. P. J.; Diacon, A. H.; Hoelscher, M.; Dreisbach, J.; Demel, P. G.-; Wagnerberger, L.; Heinrich, N.; Razid, A.; Lutchmun, W.; Noreña, I.; Diaz, L. P.; Sloan, D.; Sabiiti, W.; Gillespie, S.; Brake, L. te; Svensson, E.; Mouhdad, C.; Aarnoutse, R.; Boeree, M.; Stemkens, R.; Koele, S.; Bateson, A.; Hunt, R.; McHugh, T. D.; Wildner, L. M.; Solanki, P.; Phillips, P.; Gong, X.; Aldana, B.; Crook, A.; Dawson, R.; Narunsky, K.; Arnolds, S.; Diacon, A.; Jager, V. de; Friedrich, S.; Sanne, I.; Rassool, M.; Churchyard, G.; Sebe, M.; Makkan, H.; Mokaba, L.; Madikizela, N.; Mdluli, J.; Sithole, J.; Wallis, R.; Beattie, T.; Ntinginya, N. E.; Mangu, C.; Manyama, C.; Sabi, I.; Mtafya, B.; Minja, L. T.; Mhimbira, F.; Mbeya, B.; Zumba, T.; Chibunu, N.; Sasamalo, M.; Reither, K.; Jugheli, L.; Sam, N.; Kibiki, G.; Semvua, H.; Mpagama, S.; Liyoyo, A.; Adegbite, B. R.; Adegnika, A. A.; Grobusch, M. P.; Kirenga, B.; Khosa, C.; Timana, I.; Nliwasa, M.; Mukoka, M. Safety, Bactericidal Activity, and Pharmacokinetics of the Antituberculosis Drug Candidate BTZ-043 in South Africa (PanACEA-BTZ-043–02): An Open-Label, Dose-Expansion, Randomised, Controlled, Phase 1b/2a Trial. *The Lancet Microbe* **2025**, *6* (2). https://doi.org/10.1016/j.lanmic.2024.07.015.

(192) Nearmedic Plus LLC. *Multicenter, Open, Randomized Study With Active Control to Evaluate the Early Bactericidal Activity, Safety and Pharmacokinetics of the Drug PBTZ169 When Used in Patients With First-Diagnosed Tuberculosis of the Respiratory System With Bacterial Excretion and Saved Bacterial Susceptibility to Isoniazid and Rifampicin*; Clinical trial registration NCT03334734; clinicaltrials.gov, 2020. https://clinicaltrials.gov/study/NCT03334734 (accessed 2025-06-18).

(193) Diacon, A. H.; Barry, C. E.; Carlton, A.; Chen, R. Y.; Davies, M.; de Jager, V.; Fletcher, K.; Koh, G. C. K. W.; Kontsevaya, I.; Heyckendorf, J.; Lange, C.; Reimann, M.; Penman, S. L.; Scott, R.; Maher-Edwards, G.; Tiberi, S.; Vlasakakis, G.; Upton, C. M.; Aguirre, D. B. A First-in-Class Leucyl-tRNA Synthetase Inhibitor, Ganfeborole, for Rifampicin-Susceptible Tuberculosis: A Phase 2a Open-Label, Randomized Trial. *Nat Med* **2024**, *30* (3), 896–904. https://doi.org/10.1038/s41591-024-02829-7.

(194) Worthington, R. J.; Melander, C. Combination Approaches to Combat Multidrug-Resistant Bacteria. *Trends in Biotechnology* **2013**, *31* (3), 177–184. https://doi.org/10.1016/j.tibtech.2012.12.006.

(195) Laws, M.; Jin, P.; Rahman, K. M. Efflux Pumps in Mycobacterium Tuberculosis and Their Inhibition to Tackle Antimicrobial Resistance. *Trends in Microbiology* **2022**, *30* (1), 57–68. https://doi.org/10.1016/j.tim.2021.05.001.

(196) Krishnamurthy, N.; Grimshaw, A. A.; Axson, S. A.; Choe, S. H.; Miller, J. E. Drug Repurposing: A Systematic Review on Root Causes, Barriers and Facilitators. *BMC Health Services Research* **2022**, *22* (1), 970. https://doi.org/10.1186/s12913-022-08272-z.

(197) Adeniji, A. A.; Knoll, K. E.; Loots, D. T. Potential Anti-TB Investigational Compounds and Drugs with Repurposing Potential in TB Therapy: A Conspectus. *Appl Microbiol Biotechnol* **2020**, *104* (13), 5633–5662. https://doi.org/10.1007/s00253-020-10606-y.

(198) Chen, C.; Gardete, S.; Jansen, R. S.; Shetty, A.; Dick, T.; Rhee, K. Y.; Dartois, V. Verapamil Targets Membrane Energetics in Mycobacterium Tuberculosis. *Antimicrobial Agents and Chemotherapy* **2018**, *62* (5), 10.1128/aac.02107-17. https://doi.org/10.1128/aac.02107-17.

(199) Machado, D.; Pires, D.; Perdigão, J.; Couto, I.; Portugal, I.; Martins, M.; Amaral, L.; Anes, E.; Viveiros, M. Ion Channel Blockers as Antimicrobial Agents, Efflux Inhibitors, and Enhancers of Macrophage Killing Activity against Drug Resistant Mycobacterium Tuberculosis. *PLOS ONE* **2016**, *11* (2), e0149326. https://doi.org/10.1371/journal.pone.0149326.

(200) Rodrigues, L.; Parish, T.; Balganesh, M.; Ainsa, J. A. Antituberculosis Drugs: Reducing Efflux = Increasing Activity. *Drug Discovery Today* **2017**, *22* (3), 592–599. https://doi.org/10.1016/j.drudis.2017.01.002.

(201) Badiola, K. A.; Quan, D. H.; Triccas, J. A.; Todd, M. H. Efficient Synthesis and Anti-Tubercular Activity of a Series of Spirocycles: An Exercise in Open Science. *PLOS ONE* **2014**, *9* (12), e111782. https://doi.org/10.1371/journal.pone.0111782.

(202) Ballell, L.; Bates, R. H.; Young, R. J.; Alvarez-Gomez, D.; Alvarez-Ruiz, E.; Barroso, V.; Blanco, D.; Crespo, B.; Escribano, J.; González, R.; Lozano, S.; Huss, S.; Santos-Villarejo, A.; Martín-Plaza, J. J.; Mendoza, A.; Rebollo-Lopez, M. J.; Remuiñan-Blanco, M.; Lavandera, J. L.; Pérez-Herran, E.; Gamo-Benito, F. J.; García-Bustos, J. F.; Barros, D.; Castro, J. P.; Cammack, N. Fueling Open-Source Drug Discovery: 177 Small-Molecule Leads against Tuberculosis. *ChemMedChem* **2013**, *8* (2), 313–321. https://doi.org/10.1002/cmdc.201200428.

(203) Warrier, T.; Martinez-Hoyos, M.; Marin-Amieva, M.; Colmenarejo, G.; Porras-De Francisco, E.; Alvarez-Pedraglio, A. I.; Fraile-Gabaldon, M. T.; Torres-Gomez, P. A.; Lopez-Quezada, L.; Gold, B.; Roberts, J.; Ling, Y.; Somersan-Karakaya, S.; Little, D.; Cammack, N.; Nathan, C.; Mendoza-Losana, A. Identification of Novel Anti-Mycobacterial Compounds by Screening a Pharmaceutical Small-Molecule Library against Nonreplicating Mycobacterium Tuberculosis. *ACS Infect Dis* **2015**, *1* (12), 580–585. https://doi.org/10.1021/acsinfecdis.5b00025.

(204) Tawil, S.; Seelajaroen, H.; Petsom, A.; Sariciftci, N. S.; Thamyongkit, P. Clam-Shaped Cyclam-Functionalized Porphyrin for Electrochemical Reduction of Carbon Dioxide. *Journal of Porphyrins and Phthalocyanines* **2019**. https://doi.org/10.1142/S1088424619500548.

(205) Wong, J. K.-H.; Todd, M. H.; Rutledge, P. J. Recent Advances in Macrocyclic Fluorescent Probes for Ion Sensing. *Molecules* **2017**, *22* (2), 200. https://doi.org/10.3390/molecules22020200.

(206) Chang, H.; Qiao, R.; Li, C. Recent Advances in Functionalized Macrocyclic Polyamines for Medicine Applications. *Chinese Chemical Letters* **2025**, *36* (7), 110675. https://doi.org/10.1016/j.cclet.2024.110675.

(207) Schols, D.; Esté, J. A.; Henson, G.; De Clercq, E. Bicyclams, a Class of Potent Anti-HIV Agents, Are Targeted at the HIV Coreceptor Fusin/CXCR-4. *Antiviral Res* **1997**, *35* (3), 147–156. https://doi.org/10.1016/s0166-3542(97)00025-9.

(208) Sakyiamah, M. M.; Kobayakawa, T.; Fujino, M.; Konno, M.; Narumi, T.; Tanaka, T.; Nomura, W.; Yamamoto, N.; Murakami, T.; Tamamura, H. Design, Synthesis and Biological Evaluation of Low Molecular Weight CXCR4 Ligands. *Bioorganic & Medicinal Chemistry* **2019**, *27* (6), 1130–1138. https://doi.org/10.1016/j.bmc.2019.02.013.

(209) Pilon, A.; Lorenzo, J.; Rodriguez-Calado, S.; Adão, P.; Martins, A. M.; Valente, A.; Alves, L. G. New Cyclams and Their Copper(II) and Iron(III) Complexes: Synthesis and Potential Application as Anticancer Agents. *ChemMedChem* **2019**, *14* (7), 770–778. https://doi.org/10.1002/cmdc.201800702.

(210) Yu, M.; Nagalingam, G.; Ellis, S.; Martinez, E.; Sintchenko, V.; Spain, M.; Rutledge, P. J.; Todd, M. H.; Triccas, J. A. Nontoxic Metal–Cyclam Complexes, a New Class of Compounds

with Potency against Drug-Resistant Mycobacterium Tuberculosis. *J. Med. Chem.* **2016**, *59* (12), 5917–5921. https://doi.org/10.1021/acs.jmedchem.6b00432.

(211) Spain, M.; Wong, J. K.-H.; Nagalingam, G.; Batten, J. M.; Hortle, E.; Oehlers, S. H.; Jiang, X. F.; Murage, H. E.; Orford, J. T.; Crisologo, P.; Triccas, J. A.; Rutledge, P. J.; Todd, M. H. Antitubercular Bis-Substituted Cyclam Derivatives: Structure–Activity Relationships and in Vivo Studies. *J. Med. Chem.* **2018**, *61* (8), 3595–3608. https://doi.org/10.1021/acs.jmedchem.7b01569.

(212) Smith, N.; Quan, D.; Nagalingam, G.; Triccas, J. A.; Rendina, L. M.; Rutledge, P. J. Carborane Clusters Increase the Potency of Bis-Substituted Cyclam Derivatives against Mycobacterium Tuberculosis. *RSC Med. Chem.* **2022**, *13* (10), 1234–1238. https://doi.org/10.1039/D2MD00150K.

(213) Batten, J. On the Antibiotic Potential of Azamacrocycles. Doctoral thesis, The University of Sydney, 2022.

(214) Tallapragada, N. P. Off-Patent Drugs at Brand-Name Prices: A Puzzle for Policymakers. *Journal of Law and the Biosciences* **2016**, *3* (1), 238–247. https://doi.org/10.1093/jlb/lsw008.

(215) Strom, M. *Sydney schoolboys take down Martin Shkreli, the "most hated man in the world."* The Sydney Morning Herald. https://www.smh.com.au/technology/sydney-schoolboys-take-down-martin-shkreli-the-most-hated-man-in-the-world-20161125-gsxcu5.html (accessed 2025-05-15).

(216) Walker, D. W.; Smigaj, M.; Tani, M. The Benefits and Negative Impacts of Citizen Science Applications to Water as Experienced by Participants and Communities. *WIREs Water* **2021**, *8* (1), e1488. https://doi.org/10.1002/wat2.1488.

(217) Rasmussen, C. R.; Jr, F. J. V.; Weaner, L. E.; Reynolds, B. E.; Hood, A. R.; Hecker, L. R.; Nortey, S. O.; Hanslin, A.; Costanzo, M. J.; Powell, E. T.; Molinari, A. J. Improved Procedures for the Preparation of Cycloalkyl-, Arylalkyl-, and Arylthioureas. *Synthesis* **1988**, *1988* (06), 456–459. https://doi.org/10.1055/s-1988-27605.

(218) Linton, B. R.; Carr, A. J.; Orner, B. P.; Hamilton, A. D. A Versatile One-Pot Synthesis of 1,3-Substituted Guanidines from Carbamoyl Isothiocyanates. *J. Org. Chem.* **2000**, *65* (5), 1566–1568. https://doi.org/10.1021/jo991458q.

(219) Wang, Y.; Sun, J.; Qiao, J.; Ouyang, J.; Na, N. A "Soft" and "Hard" Ionization Method for Comprehensive Studies of Molecules. *Anal. Chem.* **2018**, *90* (24), 14095–14099. https://doi.org/10.1021/acs.analchem.8b04437.

(220) Thomas, A.; Gasch, B.; Olivieri, E.; Quintard, A. Trichloroacetic Acid Fueled Practical Amine Purifications. *Beilstein J Org Chem* **2022**, *18*, 225–231. https://doi.org/10.3762/bjoc.18.26.

(221) Huo, J.; Arulsamy, N.; Hoberg, J. O. Facile Synthesis and Platinum Complexes of 4′,5,5′′-Trisubstituted-2,2′:6′,2′′-Terpyridines. *Dalton Trans.* **2011**, *40* (29), 7534–7540. https://doi.org/10.1039/C1DT10465A.

(222) Chan, B. K.; Ciufolini, M. A. Total Synthesis of Streptonigrone. *J. Org. Chem.* **2007**, *72* (22), 8489–8495. https://doi.org/10.1021/jo701435p.

(223) Abramova, E. O.; Paderina, A. V.; Slavova, S. O.; Kostenko, E. A.; Eliseenkov, E. V.; Petrovskii, S. K.; Gitlina, A. Yu.; Boyarskiy, V. P.; Grachova, E. V. Just Add the Gold: Aggregation-Induced-Emission Properties of Alkynylphosphinegold(I) Complexes Functionalized with Phenylene–Terpyridine Subunits. *Inorg. Chem.* **2021**, *60* (24), 18715–18725. https://doi.org/10.1021/acs.inorgchem.1c02125.

(224) Bellale, E.; Naik, M.; VB, V.; Ambady, A.; Narayan, A.; Ravishankar, S.; Ramachandran, V.; Kaur, P.; McLaughlin, R.; Whiteaker, J.; Morayya, S.; Guptha, S.; Sharma, S.; Raichurkar, A.; Awasthy, D.; Achar, V.; Vachaspati, P.; Bandodkar, B.; Panda, M.; Chatterji, M. Diarylthiazole: An Antimycobacterial Scaffold Potentially Targeting PrrB-PrrA Two-Component System. *J. Med. Chem.* **2014**, *57* (15), 6572–6582. https://doi.org/10.1021/jm500833f.

(225) Xing, Y.; Zhang, M.; Ciccarelli, S.; Lee, J.; Catano, B. AuIII-Catalyzed Formation of α-Halomethyl Ketones from Terminal Alkynes. *European Journal of Organic Chemistry* **2017**, *2017* (4), 781–785. https://doi.org/10.1002/ejoc.201601416.

(226) Vražič, D.; Jereb, M.; Laali, K. K.; Stavber, S. Brønsted Acidic Ionic Liquid Accelerated Halogenation of Organic Compounds with N-Halosuccinimides (NXS). *Molecules* **2013**, *18* (1), 74–96. https://doi.org/10.3390/molecules18010074.

(227) Mohan, R. B.; Reddy, N. C. G. Regioselective α-Bromination of Aralkyl Ketones Using N-Bromosuccinimide in the Presence of Montmorillonite K-10 Clay: A Simple and Efficient

Method. *Synthetic Communications* **2013**, *43* (19), 2603–2614. https://doi.org/10.1080/00397911.2012.725264.

(228) Mohan Reddy, B.; Venkata Ramana Kumar, V.; Chinna Gangi Reddy, N.; Mahender Rao, S. Silica Gel Catalyzed *α*-Bromination of Ketones Using *N*-Bromosuccinimide: An Easy and Rapid Method. *Chinese Chemical Letters* **2014**, *25* (1), 179–182. https://doi.org/10.1016/j.cclet.2013.09.014.

(229) Rodríguez, J. C.; Maldonado, R. A.; Ramírez-García, G.; Díaz Cervantes, E.; de la Cruz, F. N. Microwave-Assisted Synthesis and Luminescent Activity of Imidazo[1,2-a]Pyridine Derivatives. *Journal of Heterocyclic Chemistry* **2020**, *57* (5), 2279–2287. https://doi.org/10.1002/jhet.3950.

(230) Tan, H.; Laishram, R. D.; Zhang, X.; Shi, G.; Li, K.; Chen, J. Rhodium-Catalyzed Spiro Indenyl Benzoxazine Synthesis via C-H Activation/Annulation of 3-Aryl-2H-Benzo[b][1,4]Oxazines and Alkynes. *European Journal of Organic Chemistry* **2020**, *2020* (29), 4542–4546. https://doi.org/10.1002/ejoc.202000668.

(231) Angeles-Dunham, V. V.; Nickerson, D. M.; Ray, D. M.; Mattson, A. E. Nitrimines as Reagents for Metal-Free Formal C(Sp2)–C(Sp2) Cross-Coupling Reactions. *Angewandte Chemie International Edition* **2014**, *53* (52), 14538–14541. https://doi.org/10.1002/anie.201408613.

(232) Koomen, M. H.; Rodriguez, E.; Hoffman, A.; Petersen, C.; Oberhauser, K. Authentic Science with Citizen Science and Student-Driven Science Fair Projects. *Science Education* **2018**, *102* (3), 593–644. https://doi.org/10.1002/sce.21335.

(233) Braz Sousa, L.; Zhang, W.; Ho, T.; Preston, C.; Golumbic, Y.; Rutledge, P.; Motion, A. School-Based Citizen Science: History and Future Outlook.

(234) Zoellick, B.; Nelson, S. J.; Schauffler, M. Participatory Science and Education: Bringing Both Views into Focus. *Frontiers in Ecology and the Environment* **2012**, *10* (6), 310–313. https://doi.org/10.1890/110277.

(235) *Project Finder | Australian Citizen Science Projects*. https://biocollect.ala.org.au/acsa/#isCitizenScience%3Dtrue%26projectId%3Df3fd3e83-ff39-4cbe-b8f7-3ddbc89546a9%26max%3D30%26sort%3DdateCreatedSort%26fq%3DscienceType%253A

Chemical%2520sciences%26queryList%3DscienceType%253AChemical%2520sciences (accessed 2025-11-25).

(236) Sousa, L. B.; Kenneally, C.; Golumbic, Y.; Martin, J. M.; Preston, C.; Rutledge, P.; Motion, A. Teacher Experiences and Understanding of Citizen Science in Australian Classrooms. *PLOS ONE* **2024**, *19* (11), e0312680. https://doi.org/10.1371/journal.pone.0312680.

(237) *Chemistry Stage 6 Syllabus (2017) | NSW Education Standards*. https://educationstandards.nsw.edu.au/wps/portal/nesa/11-12/stage-6-learning-areas/stage-6-science/chemistry-2017 (accessed 2025-07-08).

(238) de Ridder, D. Inquiry-Based Learning in Years 11 and 12 Secondary Science. *Teaching Science: The Journal of the Australian Science Teachers Association* **2021**, *67* (2), 11–21.

(239) Braz Sousa, L. Breaking Good in Schools: Integrating Citizen Science Medicinal Chemistry into Secondary Education. *unpublished*.

(240) Golumbic, Y. N.; Motion, A. Expanding the Scope of Citizen Science: Learning and Engagement of Undergraduate Students in a Citizen Science Chemistry Lab. *Citizen Science: Theory and Practice* **2021**, *6* (1). https://doi.org/10.5334/cstp.431.

(241) *Breaking Good*. Breaking Good. https://www.breakinggoodproject.com (accessed 2025-08-19).

(242) Urválková, E. S.; Janoušková, S. Citizen Science – Bridging the Gap between Scientists and Amateurs. *Chemistry Teacher International* **2019**, *1* (2). https://doi.org/10.1515/cti-2018-0032.

(243) Ahmed, A. O. A.; van de Sande, W. W. J.; van Vianen, W.; van Belkum, A.; Fahal, A. H.; Verbrugh, H. A.; Bakker-Woudenberg, I. A. J. M. In Vitro Susceptibilities of Madurella Mycetomatis to Itraconazole and Amphotericin B Assessed by a Modified NCCLS Method and a Viability-Based 2,3-Bis(2-Methoxy-4-Nitro-5- Sulfophenyl)-5-[(Phenylamino)Carbonyl]-2H- Tetrazolium Hydroxide (XTT) Assay. *Antimicrobial Agents and Chemotherapy* **2004**, *48* (7), 2742–2746. https://doi.org/10.1128/aac.48.7.2742-2746.2004.

(244) Ahmed, S. A.; de Hoog, G. S.; Stevens, D. A.; Fahal, A. H.; van de Sande, W. W. J. In Vitro Antifungal Susceptibility of Coelomycete Agents of Black Grain Eumycetoma to Eight Antifungals. *Medical Mycology* **2015**, *53* (3), 295–301. https://doi.org/10.1093/mmy/myu098.

(245) Riss, T. L.; Moravec, R. A.; Niles, A. L.; Duellman, S.; Benink, H. A.; Worzella, T. J.; Minor, L. Cell Viability Assays. In *Assay Guidance Manual*; Markossian, S., Grossman, A., Baskir, H., Arkin, M., Auld, D., Austin, C., Baell, J., Brimacombe, K., Chung, T. D. Y., Coussens, N. P., Dahlin, J. L., Devanarayan, V., Foley, T. L., Glicksman, M., Gorshkov, K., Grotegut, S., Hall, M. D., Hoare, S., Inglese, J., Iversen, P. W., Lal-Nag, M., Li, Z., Manro, J. R., McGee, J., Norvil, A., Pearson, M., Riss, T., Saradjian, P., Sittampalam, G. S., Tarselli, M. A., Trask, O. J., Weidner, J. R., Wildey, M. J., Wilson, K., Xia, M., Xu, X., Eds.; Eli Lilly & Company and the National Center for Advancing Translational Sciences: Bethesda (MD), 2004.

(246) O'Brien, J.; Wilson, I.; Orton, T.; Pognan, F. Investigation of the Alamar Blue (Resazurin) Fluorescent Dye for the Assessment of Mammalian Cell Cytotoxicity. *European Journal of Biochemistry* **2000**, *267* (17), 5421–5426. https://doi.org/10.1046/j.1432-1327.2000.01606.x.

(247) Abd Algaffar, S. O.; Verbon, A.; van de Sande, W. W. J.; Khalid, S. A. Development and Validation of an In Vitro Resazurin-Based Susceptibility Assay against Madurella Mycetomatis. *Antimicrobial Agents and Chemotherapy* **2021**, *65* (3), 10.1128/aac.01338-20. https://doi.org/10.1128/aac.01338-20.

(248) Balouiri, M.; Sadiki, M.; Ibnsouda, S. K. Methods for in Vitro Evaluating Antimicrobial Activity: A Review. *J Pharm Anal* **2016**, *6* (2), 71–79. https://doi.org/10.1016/j.jpha.2015.11.005.

(249) *Madurella mycetomatis*. Mycology | University of Adelaide. https://www.adelaide.edu.au/mycology/fungal-descriptions-and-antifungal-susceptibility/hyphomycetes-conidial-moulds/madurella (accessed 2025-07-10).

(250) de Hoog, G. S.; Adelmann, D.; Ahmed, A. O. A.; van Belkum, A. Phylogeny and Typification of Madurella Mycetomatis, with a Comparison of Other Agents of Eumycetoma. *Mycoses* **2004**, *47* (3–4), 121–130. https://doi.org/10.1111/j.1439-0507.2004.00964.x.

(251) Desnos-Ollivier, M.; Bretagne, S.; Dromer, F.; Lortholary, O.; Dannaoui, E. Molecular Identification of Black-Grain Mycetoma Agents. *Journal of Clinical Microbiology* **2006**, *44* (10), 3517–3523. https://doi.org/10.1128/jcm.00862-06.

(252) Borman, A. M.; Desnos-Ollivier, M.; Campbell, C. K.; Bridge, P. D.; Dannaoui, E.; Johnson, E. M. Novel Taxa Associated with Human Fungal Black-Grain Mycetomas: Emarellia Grisea Gen. Nov., Sp. Nov., and Emarellia Paragrisea Sp. Nov. *Journal of Clinical Microbiology* **2016**, *54* (7), 1738–1745. https://doi.org/10.1128/jcm.00477-16.

(253) Behera, S. S.; Ray, R. C.; Das, U.; Panda, S. K.; Saranraj, P. Microorganisms in Fermentation. In *Essentials in Fermentation Technology*; Berenjian, A., Ed.; Springer International Publishing: Cham, 2019; pp 1–39. https://doi.org/10.1007/978-3-030-16230-6_1.

(254) Sammon, N. B.; Harrower, K. M.; Fabbro, L. D.; Reed, R. H. Three Potential Sources of Microfungi in a Treated Municipal Water Supply System in Sub-Tropical Australia. *Int J Environ Res Public Health* **2011**, *8* (3), 713–732. https://doi.org/10.3390/ijerph8030713.

(255) Shakil A Saghir, M. S.; Jeremiah Bancroft, I. H.; Rais Ansari, P. D. Molds and Mycotoxins Indoors II: Toxicological Perspective. *Arch Clin Toxicol* **2025**, *Volume 7* (Issue 1), 8–40. https://doi.org/10.46439/toxicology.7.033.

(256) Kadeřábková, N.; Mahmood, A. J. S.; Mavridou, D. A. I. Antibiotic Susceptibility Testing Using Minimum Inhibitory Concentration (MIC) Assays. *npj Antimicrob Resist* **2024**, *2* (1), 37. https://doi.org/10.1038/s44259-024-00051-6.

(257) Schwarz, S.; Silley, P.; Simjee, S.; Woodford, N.; van Duijkeren, E.; Johnson, A. P.; Gaastra, W. Editorial: Assessing the Antimicrobial Susceptibility of Bacteria Obtained from Animals†. *Journal of Antimicrobial Chemotherapy* **2010**, *65* (4), 601–604. https://doi.org/10.1093/jac/dkq037.

(258) Khanafer, N.; Daneman, N.; Greene, T.; Simor, A.; Vanhems, P.; Samore, M.; Brown, K. A. Susceptibilities of Clinical *Clostridium Difficile* Isolates to Antimicrobials: A Systematic Review and Meta-Analysis of Studies since 1970. *Clinical Microbiology and Infection* **2018**, *24* (2), 110–117. https://doi.org/10.1016/j.cmi.2017.07.012.

(259) EUCAST. *MIC distributions and the setting of epidemiological cut- off (ECOFF) values.*
https://www.eucast.org/fileadmin/src/media/PDFs/EUCAST_files/EUCAST_SOPs/2025/EU

CAST_SOP_10.2_MIC_distributions_and_epidemiological_cut-off_value__ECOFF__setting_20250512.pdf (accessed 2025-07-15).

(260) Duong, H. P.; Melechov, D.; Lim, W.; Ma, J.; Scroggie, K.; Rajendra, L.; Perry, B.; Cruz, L.; Rutledge, P.; Motion, A.; Sande, W. van de; Todd, M. Structure–Activity Relationships of Fenarimol Analogues with Potent in Vitro and in Vivo Activity against Madurella Mycetomatis, the Main Causative Agent of Eumycetoma. ChemRxiv May 5, 2025. https://doi.org/10.26434/chemrxiv-2025-kj5x1.

(261) Kloezen, W.; Poppel, M. van H.; Fahal, A. H.; Sande, W. W. J. van de. A Madurella Mycetomatis Grain Model in Galleria Mellonella Larvae. *PLOS Neglected Tropical Diseases* **2015**, *9* (7), e0003926. https://doi.org/10.1371/journal.pntd.0003926.

(262) Ma, J.; Konings, M.; Verbon, A.; van de Sande, W. W. J. A Falciformispora Senegalensis Grain Model in Galleria Mellonella Larvae. *Medical Mycology* **2023**, *61* (8), myad070. https://doi.org/10.1093/mmy/myad070.

(263) Ahmed, A. O.; van Vianen, W.; ten Kate, M. T.; van de Sande, W. W. J.; van Belkum, A.; Fahal, A. H.; Verbrugh, H. A.; Bakker-Woudenberg, I. A. J. M. A Murine Model of Madurella Mycetomatis Eumycetoma. *FEMS Immunology & Medical Microbiology* **2003**, *37* (1), 29–36. https://doi.org/10.1016/S0928-8244(03)00096-8.

(264) Kesicki, E. A.; Bailey, M. A.; Ovechkina, Y.; Early, J. V.; Alling, T.; Bowman, J.; Zuniga, E. S.; Dalai, S.; Kumar, N.; Masquelin, T.; Hipskind, P. A.; Odingo, J. O.; Parish, T. Synthesis and Evaluation of the 2-Aminothiazoles as Anti-Tubercular Agents. *PLOS ONE* **2016**, *11* (5), e0155209. https://doi.org/10.1371/journal.pone.0155209.

(265) Gallardo-Godoy, A.; Gever, J.; Fife, K. L.; Silber, B. M.; Prusiner, S. B.; Renslo, A. R. 2-Aminothiazoles as Therapeutic Leads for Prion Diseases. *J. Med. Chem.* **2011**, *54* (4), 1010–1021. https://doi.org/10.1021/jm101250y.

(266) Azzali, E.; Girardini, M.; Annunziato, G.; Pavone, M.; Vacondio, F.; Mori, G.; Pasca, M. R.; Costantino, G.; Pieroni, M. 2-Aminooxazole as a Novel Privileged Scaffold in Antitubercular Medicinal Chemistry. *ACS Med. Chem. Lett.* **2020**, *11* (7), 1435–1441. https://doi.org/10.1021/acsmedchemlett.0c00173.

(267) Laniado-Laborín, R.; Cabrales-Vargas, M. N. Amphotericin B: Side Effects and Toxicity. *Revista Iberoamericana de Micología* **2009**, *26* (4), 223–227. https://doi.org/10.1016/j.riam.2009.06.003.

(268) Strelow, J.; Dewe, W.; Iversen, P. W.; Brooks, H. B.; Radding, J. A.; McGee, J.; Weidner, J. Mechanism of Action Assays for Enzymes. In *Assay Guidance Manual [Internet]*; Eli Lilly & Company and the National Center for Advancing Translational Sciences, 2012.

(269) Campitelli, M.; Zeineddine, N.; Samaha, G.; Maslak, S. Combination Antifungal Therapy: A Review of Current Data. *J Clin Med Res* **2017**, *9* (6), 451–456. https://doi.org/10.14740/jocmr2992w.

(270) Elsaman, T.; Awadalla, M. K. A.; Mohamed, M. S.; Eltayib, E. M.; Mohamed, M. A. Identification of Microbial-Based Natural Products as Potential CYP51 Inhibitors for Eumycetoma Treatment: Insights from Molecular Docking, MM-GBSA Calculations, ADMET Analysis, and Molecular Dynamics Simulations. *Pharmaceuticals* **2025**, *18* (4), 598. https://doi.org/10.3390/ph18040598.

(271) Mohamed, M. A.; Awadalla, M. K. A.; Mohamed, M. S.; Elsaman, T.; Eltayib, E. M. Repurposing FDA-Approved Drugs for Eumycetoma Treatment: Homology Modeling and Computational Screening of CYP51 Inhibitors. *International Journal of Molecular Sciences* **2025**, *26* (1), 315. https://doi.org/10.3390/ijms26010315.

(272) Bonetta, R.; Valentino, G. Machine Learning Techniques for Protein Function Prediction. *Proteins: Structure, Function, and Bioinformatics* **2020**, *88* (3), 397–413. https://doi.org/10.1002/prot.25832.

(273) Guo, Z.; Yamaguchi, R. Machine Learning Methods for Protein-Protein Binding Affinity Prediction in Protein Design. *Front. Bioinform.* **2022**, *2*. https://doi.org/10.3389/fbinf.2022.1065703.

(274) Gonçalves, E.; Segura-Cabrera, A.; Pacini, C.; Picco, G.; Behan, F. M.; Jaaks, P.; Coker, E. A.; Van Der Meer, D.; Barthorpe, A.; Lightfoot, H.; Mironenko, T.; Beck, A.; Richardson, L.; Yang, W.; Lleshi, E.; Hall, J.; Tolley, C.; Hall, C.; Mali, I.; Thomas, F.; Morris, J.; Leach, A. R.; Lynch, J. T.; Sidders, B.; Crafter, C.; Iorio, F.; Fawell, S.; Garnett, M. J. Drug Mechanism-of-action Discovery through the Integration of Pharmacological and CRISPR

Screens. *Molecular Systems Biology* **2020**, *16* (7), e9405. https://doi.org/10.15252/msb.20199405.

(275) McCall, L.-I.; Aroussi, A. E.; Choi, J. Y.; Vieira, D. F.; Muylder, G. D.; Johnston, J. B.; Chen, S.; Kellar, D.; Siqueira-Neto, J. L.; Roush, W. R.; Podust, L. M.; McKerrow, J. H. Targeting Ergosterol Biosynthesis in Leishmania Donovani: Essentiality of Sterol 14alpha-Demethylase. *PLOS Neglected Tropical Diseases* **2015**, *9* (3), e0003588. https://doi.org/10.1371/journal.pntd.0003588.

(276) Machado, D.; Azzali, E.; Couto, I.; Costantino, G.; Pieroni, M.; Viveiros, M. Adjuvant Therapies against Tuberculosis: Discovery of a 2-Aminothiazole Targeting Mycobacterium Tuberculosis Energetics. *Future Microbiology* **2018**, *13* (12), 1383–1402. https://doi.org/10.2217/fmb-2018-0110.

(277) Girardini, M.; Machado, D.; Annunziato, G.; Papotti, B.; Palumbo, M.; Spaggiari, C.; Costantino, G.; Viveiros, M.; Pieroni, M. Preliminary Structure−activity Relationships Analysis on N-(3,5-Dichlorophenyl)-4,5-Dihydronaphtho[1,2-d]Thiazol-2-Amine, a Disruptor of Mycobacterial Energetics. *Med Chem Res* **2024**, *33* (3), 518–531. https://doi.org/10.1007/s00044-024-03198-z.

(278) Duong, H. P. Chemistry with the Community: Fenarimols Open-Source Drug Discovery for Eumycetoma and Evaluation of a High School Chemistry Outreach Program. Doctoral thesis, University of Sydney, Sydney, NSW, 2025.

(279) Gentles, R. G.; Hu, S.; Huang, Y.; Grant-Young, K.; Poss, M. A.; Andres, C.; Fiedler, T.; Knox, R.; Lodge, N.; Weaver, C. D.; Harden, D. G. Preliminary SAR Studies on Non-Apamin-Displacing 4-(Aminomethylaryl)Pyrrazolopyrimidine KCa Channel Blockers. *Bioorganic & Medicinal Chemistry Letters* **2008**, *18* (20), 5694–5697. https://doi.org/10.1016/j.bmcl.2008.08.026.

(280) Auguste, P.; Hugues, M.; Mourre, C.; Moinier, D.; Tartar, A.; Lazdunski, M. Scyllatoxin, a Blocker of Calcium-Activated Potassium Channels: Structure-Function Relationships and Brain Localization of the Binding Sites. *Biochemistry* **1992**, *31* (3), 648–654. https://doi.org/10.1021/bi00118a003.

(281) Pieroni, M.; Wan, B.; Cho, S.; Franzblau, S. G.; Costantino, G. Design, Synthesis and Investigation on the Structure–Activity Relationships of N-Substituted 2-Aminothiazole

Derivatives as Antitubercular Agents. *European Journal of Medicinal Chemistry* **2014**, *72*, 26–34. https://doi.org/10.1016/j.ejmech.2013.11.007.

(282) Chen, Y.; Li, Z.; Lin, T.; Li, Z.; Chen, D.; Xu, X. Novel 2-Aminothiazole Analogues Both as Polymyxin E Synergist and Antimicrobial Agent against Multidrug-Resistant Gram-Positive Bacteria. *European Journal of Medicinal Chemistry* **2024**, *279*, 116879. https://doi.org/10.1016/j.ejmech.2024.116879.

(283) Zhang, Z.; Kudo, T.; Nakajima, Y.; Wang, Y. Clarification of the Relationship between the Members of the Family Thermomonosporaceae on the Basis of 16S rDNA, 16S-23S rRNA Internal Transcribed Spacer and 23S rDNA Sequences and Chemotaxonomic Analyses. *International Journal of Systematic and Evolutionary Microbiology* **2001**, *51* (2), 373–383. https://doi.org/10.1099/00207713-51-2-373.

(284) Goodfellow, M.; Williams, S. T. Ecology of Actinomycetes. *Annu Rev Microbiol* **1983**, *37*, 189–216. https://doi.org/10.1146/annurev.mi.37.100183.001201.

(285) Goodfellow, M.; Alderson, G.; Lacey, J. Numerical Taxonomy of Actinomadura and Related Actinomycetes. *Microbiology* **1979**, *112* (1), 95–111. https://doi.org/10.1099/00221287-112-1-95.

(286) Sizar, O.; Leslie, S. W.; Unakal, C. G. Gram-Positive Bacteria. In *StatPearls*; StatPearls Publishing: Treasure Island (FL), 2025.

(287) Maitra, A.; Munshi, T.; Healy, J.; Martin, L. T.; Vollmer, W.; Keep, N. H.; Bhakta, S. Cell Wall Peptidoglycan in Mycobacterium Tuberculosis: An Achilles' Heel for the TB-Causing Pathogen. *FEMS Microbiol Rev* **2019**, *43* (5), 548–575. https://doi.org/10.1093/femsre/fuz016.

(288) Fu, L. M.; Fu-Liu, C. S. Is *Mycobacterium Tuberculosis* a Closer Relative to Gram-Positive or Gram–Negative Bacterial Pathogens? *Tuberculosis* **2002**, *82* (2), 85–90. https://doi.org/10.1054/tube.2002.0328.

(289) Makam, P.; Kannan, T. 2-Aminothiazole Derivatives as Antimycobacterial Agents: Synthesis, Characterization, in Vitro and in Silico Studies. *European Journal of Medicinal Chemistry* **2014**, *87*, 643–656. https://doi.org/10.1016/j.ejmech.2014.09.086.

(290) Luckner, S. R.; Machutta, C. A.; Tonge, P. J.; Kisker, C. Crystal Structures of Mycobacterium Tuberculosis KasA Show Mode of Action within Cell Wall Biosynthesis and Its Inhibition by Thiolactomycin. *Structure* **2009**, *17* (7), 1004–1013. https://doi.org/10.1016/j.str.2009.04.012.

(291) Neu, H. C. Beta-Lactam Antibiotics: Structural Relationships Affecting in Vitro Activity and Pharmacologic Properties. *Rev Infect Dis* **1986**, *8 Suppl 3*, S237-259. https://doi.org/10.1093/clinids/8.supplement_3.s237.

(292) Carroll, G. F.; Brown, J. M.; Haley, L. D. A Method for Determining In-Vitro Drug Susceptibilities of Some Nocardiae and Actinomadurae Results with 17 Antimicrobial Agents. *American Journal of Clinical Pathology* **1977**, *68* (2), 279–283. https://doi.org/10.1093/ajcp/68.2.279.

(293) Infections, I. of M. (US) F. on E.; Knobler, S. L.; Lemon, S. M.; Najafi, M.; Burroughs, T. Factors Contributing to the Emergence of Resistance. In *The Resistance Phenomenon in Microbes and Infectious Disease Vectors: Implications for Human Health and Strategies for Containment: Workshop Summary*; National Academies Press (US), 2003.

(294) Franklin, B. D.; Abel, G.; Shojania, K. G. Medication Non-Adherence: An Overlooked Target for Quality Improvement Interventions. *BMJ Qual Saf* **2020**, *29* (4), 271–273. https://doi.org/10.1136/bmjqs-2019-009984.

(295) Mayrhofer, S.; Domig, K. J.; Mair, C.; Zitz, U.; Huys, G.; Kneifel, W. Comparison of Broth Microdilution, Etest, and Agar Disk Diffusion Methods for Antimicrobial Susceptibility Testing of Lactobacillus Acidophilus Group Members. *Appl Environ Microbiol* **2008**, *74* (12), 3745–3748. https://doi.org/10.1128/AEM.02849-07.

(296) Zheng, L.; Guo, Y.; Liang, Y.; Wang, L.; Meng, S.; Song, Y.; Tang, Y. TrCL-AGS: A Universal Sequential Triple-Stage Contrastive Learning Framework for Bacterial Detection With Across-Growth-Stage Information. *IEEE Internet of Things Journal* **2025**, *12* (10), 14886–14896. https://doi.org/10.1109/JIOT.2025.3527021.

(297) Raro, O. H. F.; Bouvier, M.; Kerbol, A.; Decousser, J.-W.; Poirel, L.; Nordmann, P. Rapid Detection of Cefiderocol Susceptibility/Resistance in Acinetobacter Baumannii. *Eur J Clin Microbiol Infect Dis* **2023**, *42* (12), 1511–1518. https://doi.org/10.1007/s10096-023-04691-w.

(298) Srikanth, S.; Jayapiriya, U. S.; Dubey, S. K.; Javed, A.; Goel, S. A Lab-on-Chip Platform for Simultaneous Culture and Electrochemical Detection of Bacteria. *iScience* **2022**, *25* (11). https://doi.org/10.1016/j.isci.2022.105388.

(299) Petiti, J.; Revel, L.; Divieto, C. Standard Operating Procedure to Optimize Resazurin-Based Viability Assays. *Biosensors* **2024**, *14* (4), 156. https://doi.org/10.3390/bios14040156.

(300) Toyokawa, M.; Ohana, N.; Ueda, A.; Imai, M.; Tanno, D.; Honda, M.; Takano, Y.; Ohashi, K.; Saito, K.; Shimura, H. Identification and Antimicrobial Susceptibility Profiles of Nocardia Species Clinically Isolated in Japan. *Sci Rep* **2021**, *11* (1), 16742. https://doi.org/10.1038/s41598-021-95870-2.

(301) Gomez-Flores, A.; Welsh, O.; Said-Fernández, S.; Lozano-Garza, G.; Tavarez-Alejandro, R. E.; Vera-Cabrera, L. In Vitro and In Vivo Activities of Antimicrobials against Nocardia Brasiliensis. *Antimicrob Agents Chemother* **2004**, *48* (3), 832–837. https://doi.org/10.1128/AAC.48.3.832-837.2004.

(302) Vera-Cabrera, L.; Ochoa-Felix, E. Y.; Gonzalez, G.; Tijerina, R.; Choi, S. H.; Welsh, O. In Vitro Activities of New Quinolones and Oxazolidinones against Actinomadura Madurae. *Antimicrobial Agents and Chemotherapy* **2004**, *48* (3), 1037–1039. https://doi.org/10.1128/aac.48.3.1037-1039.2004.

(303) Lavogina, D.; Lust, H.; Tahk, M.-J.; Laasfeld, T.; Vellama, H.; Nasirova, N.; Vardja, M.; Eskla, K.-L.; Salumets, A.; Rinken, A.; Jaal, J. Revisiting the Resazurin-Based Sensing of Cellular Viability: Widening the Application Horizon. *Biosensors (Basel)* **2022**, *12* (4), 196. https://doi.org/10.3390/bios12040196.

(304) Balbaied, T.; Moore, E. Resazurin-Based Assay for Quantifying Living Cells during Alkaline Phosphatase (ALP) Release. *Applied Sciences* **2020**, *10* (11), 3840. https://doi.org/10.3390/app10113840.

(305) Escribano, A. I.; Marcel, A. M.; Tugores, Y. M.; Ruiz, J. J. N.; Redó, V. J. A.; García-Trevijano, J. A. E.; Barrio, A. G. Validation of a Modified Fluorimetric Assay for the Screening of Trichomonacidal Drugs. *Mem. Inst. Oswaldo Cruz* **2012**, *107*, 637–643. https://doi.org/10.1590/S0074-02762012000500010.

(306) Wanka, L.; Iqbal, K.; Schreiner, P. R. The Lipophilic Bullet Hits the Targets: Medicinal Chemistry of Adamantane Derivatives. *Chem. Rev.* **2013**, *113* (5), 3516–3604. https://doi.org/10.1021/cr100264t.

(307) Dane, C.; Montgomery, A. P.; Kassiou, M. The Adamantane Scaffold: Beyond a Lipophilic Moiety. *European Journal of Medicinal Chemistry* **2025**, *291*, 117592. https://doi.org/10.1016/j.ejmech.2025.117592.

(308) Sharma, A.; Rana, R.; Kumar, N.; gulati, H. kaur; Jyoti; Khanna, A.; Sharma, S.; Pooja; Singh, J. V.; Bedi, P. M. S. Ferrocene-Based Compounds: Promising Anticancer and Antimalarial Agents in Modern Therapeutics. *Med Chem Res* **2025**, *34* (6), 1177–1199. https://doi.org/10.1007/s00044-025-03408-2.

(309) Astruc, D. Why Is Ferrocene so Exceptional? *European Journal of Inorganic Chemistry* **2017**, *2017* (1), 6–29. https://doi.org/10.1002/ejic.201600983.

(310) Nichugovskiy, A.; Tron, G. C.; Maslov, M. Recent Advances in the Synthesis of Polyamine Derivatives and Their Applications. *Molecules* **2021**, *26* (21), 6579. https://doi.org/10.3390/molecules26216579.

(311) Patra, M.; Gasser, G. The Medicinal Chemistry of Ferrocene and Its Derivatives. *Nat Rev Chem* **2017**, *1* (9), 1–12. https://doi.org/10.1038/s41570-017-0066.

(312) Adamson, J. Cyclam Conjugates for the Modulation of Amyloid-β Aggregation. Honours Thesis, The University of Sydney, Sydney, NSW, 2018.

(313) Shieh, W.-C.; Dell, S.; Repič, O. Nucleophilic Catalysis with 1,8-Diazabicyclo[5.4.0]Undec-7-Ene (DBU) for the Esterification of Carboxylic Acids with Dimethyl Carbonate. *J. Org. Chem.* **2002**, *67* (7), 2188–2191. https://doi.org/10.1021/jo011036s.

(314) Bouzina, A.; Aouf, Z.; Amira, A.; Bouone, Y. O.; Bentoumi, H.; Chemam, Y.; Ibrahim-Ouali, M.; Zerrouki, R.; Aouf, N.-E. Recent Advances in the Mitsunobu and Related Reactions: A Review from 2010 to 2024. *Top Curr Chem (Z)* **2025**, *383* (2), 15. https://doi.org/10.1007/s41061-025-00501-3.

(315) Thompson, A. S.; Humphrey, G. R.; DeMarco, A. M.; Mathre, D. J.; Grabowski, E. J. J. Direct Conversion of Activated Alcohols to Azides Using Diphenyl Phosphorazidate. A

Practical Alternative to Mitsunobu Conditions. *J. Org. Chem.* **1993**, *58* (22), 5886–5888. https://doi.org/10.1021/jo00074a008.

(316) Kolb, H. C.; Finn, M. G.; Sharpless, K. B. Click Chemistry: Diverse Chemical Function from a Few Good Reactions. *Angewandte Chemie International Edition* **2001**, *40* (11), 2004–2021. https://doi.org/10.1002/1521-3773(20010601)40:11%253C2004::AID-ANIE2004%253E3.0.CO;2-5.

(317) Meldal, M.; Tornøe, C. W. Cu-Catalyzed Azide−Alkyne Cycloaddition. *Chem. Rev.* **2008**, *108* (8), 2952–3015. https://doi.org/10.1021/cr0783479.

(318) Tornøe, C. W.; Christensen, C.; Meldal, M. Peptidotriazoles on Solid Phase: [1,2,3]-Triazoles by Regiospecific Copper(I)-Catalyzed 1,3-Dipolar Cycloadditions of Terminal Alkynes to Azides. *J. Org. Chem.* **2002**, *67* (9), 3057–3064. https://doi.org/10.1021/jo011148j.

(319) *Press release: The Nobel Prize in Chemistry 2022*. NobelPrize.org. https://www.nobelprize.org/prizes/chemistry/2022/press-release/ (accessed 2025-09-09).

(320) Kumar, V.; Lal, K.; Naveen; Tittal, R. K. The Fate of Heterogeneous Catalysis & Click Chemistry for 1,2,3-Triazoles: Nobel Prize in Chemistry 2022. *Catalysis Communications* **2023**, *176*, 106629. https://doi.org/10.1016/j.catcom.2023.106629.

(321) Haldón, E.; Nicasio, M. C.; Pérez, P. J. Copper-Catalysed Azide–Alkyne Cycloadditions (CuAAC): An Update. *Org. Biomol. Chem.* **2015**, *13* (37), 9528–9550. https://doi.org/10.1039/C5OB01457C.

(322) Silva, P. J.; Bernardo, C. E. P. Influence of Alkyne and Azide Substituents on the Choice of the Reaction Mechanism of the Cu+-Catalyzed Addition of Azides to Iodoalkynes. *J. Phys. Chem. A* **2018**, *122* (37), 7497–7507. https://doi.org/10.1021/acs.jpca.8b06894.

(323) Wyrwał, J.; Schroeder, G.; Kowalewski, J.; Aski, S. N. The Effect of Pendant-Arm Modification and Ring Size on the Dynamics of Cyclic Polyamines. *Journal of Molecular Structure* **2006**, *792–793*, 274–279. https://doi.org/10.1016/j.molstruc.2005.10.061.

(324) Tripathi, R.; Verma, S.; Pandey, J.; Tiwari, V. Recent Development on Catalytic Reductive Amination and Applications. *COC* **2008**, *12* (13), 1093–1115. https://doi.org/10.2174/138527208785740283.

(325) Neelarapu, R.; Petukhov, P. A. A One-Pot Selective Synthesis of N-Boc Protected Secondary Amines: Tandem Direct Reductive Amination/N-Boc Protection. *Tetrahedron* **2012**, *68* (35), 7056–7062. https://doi.org/10.1016/j.tet.2012.06.055.

(326) McCubbin, L. Diversity Oriented Synthesis as a Tool for the Development of Anti-Tubercular Compounds. Honours Thesis, The University of Sydney, Sydney, NSW, 2019.

(327) Chankeshwara, S. V.; Chakraborti, A. K. Catalyst-Free Chemoselective N-Tert-Butyloxycarbonylation of Amines in Water. *Org. Lett.* **2006**, *8* (15), 3259–3262. https://doi.org/10.1021/ol0611191.

(328) Agami, C.; Couty, F. The Reactivity of the *N*-Boc Protecting Group: An Underrated Feature. *Tetrahedron* **2002**, *58* (14), 2701–2724. https://doi.org/10.1016/S0040-4020(02)00131-X.

(329) Aspinall, H. C.; Greeves, N.; Lee, W.-M.; McIver, E. G.; Smith, P. M. An Improved Williamson Etherification of Hindered Alcohols Promoted by 15-Crown-5 and Sodium Hydride. *Tetrahedron Letters* **1997**, *38* (26), 4679–4682. https://doi.org/10.1016/S0040-4039(97)00965-9.

(330) Yang, B. H.; Buchwald, S. L. Palladium-Catalyzed Amination of Aryl Halides and Sulfonates. *Journal of Organometallic Chemistry* **1999**, *576* (1), 125–146. https://doi.org/10.1016/S0022-328X(98)01054-7.

(331) Ma, X.; Su, C.; Xu, Q. N-Alkylation by Hydrogen Autotransfer Reactions. *Top Curr Chem (Z)* **2016**, *374* (3), 27. https://doi.org/10.1007/s41061-016-0027-1.

(332) Podyacheva, E.; Afanasyev, O. I.; Tsygankov, A. A.; Makarova, M.; Chusov, D. Hitchhiker's Guide to Reductive Amination. *Synthesis* **2019**, *51* (13), 2667–2677. https://doi.org/10.1055/s-0037-1611788.

(333) Kan, T.; Fukuyama, T. Ns Strategies: A Highly Versatile Synthetic Method for Amines. *Chem. Commun.* **2004**, No. 4, 353–359. https://doi.org/10.1039/B311203A.

(334) PubChem. *Hazardous Substances Data Bank (HSDB) : 2968*. https://pubchem.ncbi.nlm.nih.gov/source/hsdb/2968 (accessed 2025-08-20).

(335) Díez-González, S. Well-Defined Copper(i) Complexes for Click Azide–Alkyne Cycloaddition Reactions: One Click Beyond. *Catal. Sci. Technol.* **2011**, *1* (2), 166. https://doi.org/10.1039/c0cy00064g.

(336) Cui, X.-M.; Guan, Y.-H.; Li, N.; Lv, H.; Fu, L.-A.; Guo, K.; Fan, X. A Mild and Efficient Method for Bromination of Alcohols Using α,α-Dibromo-β-Dicarbonyl Compounds as Halogen Sources. *Tetrahedron Letters* **2014**, *55* (1), 90–93. https://doi.org/10.1016/j.tetlet.2013.10.120.

(337) Appel, R. Tertiäres Phosphan/Tetrachlormethan, ein vielseitiges Reagens zur Chlorierung, Dehydratisierung und PN-Verknüpfung. *Angewandte Chemie* **1975**, *87* (24), 863–874. https://doi.org/10.1002/ange.19750872403.

(338) Mundy, B. P.; Stewart, C. A. Phosphorus(III) Bromide. In *Encyclopedia of Reagents for Organic Synthesis*; John Wiley & Sons, Ltd, 2008. https://doi.org/10.1002/047084289X.rp154.pub2.

(339) Spieß, P.; Sirvent, A.; Tiefenbrunner, I.; Sargueil, J.; Fernandes, A. J.; Arroyo-Bondía, A.; Meyrelles, R.; Just, D.; Prado-Roller, A.; Shaaban, S.; Kaiser, D.; Maulide, N. Nms-Amides: An Amine Protecting Group with Unique Stability and Selectivity. *Chemistry – A European Journal* **2023**, *29* (41), e202301312. https://doi.org/10.1002/chem.202301312.

(340) Wilden, J. D. The Sulfonamide Motif as a Synthetic Tool. *Journal of Chemical Research* **2010**, *34* (10), 541–548. https://doi.org/10.3184/030823410X12857514635822.

(341) Fukuyama, T.; Jow, C.-K.; Cheung, M. 2- and 4-Nitrobenzenesulfonamides: Exceptionally Versatile Means for Preparation of Secondary Amines and Protection of Amines. *Tetrahedron Letters* **1995**, *36* (36), 6373–6374. https://doi.org/10.1016/0040-4039(95)01316-A.

(342) Deane, F. M.; Lin, A. J. S.; Hains, P. G.; Pilgrim, S. L.; Robinson, P. J.; McCluskey, A. FD5180, a Novel Protein Kinase Affinity Probe, and the Effect of Bead Loading on Protein Kinase Identification. *ACS Omega* **2017**, *2* (7), 3828–3838. https://doi.org/10.1021/acsomega.7b00020.

(343) Soderberg, T. Organic Chemistry with a Biological Emphasis Volume I. *Chemistry Publications* **2019**.

(344) Salvatore, R. N.; Nagle, A. S.; Jung, K. W. Cesium Effect: High Chemoselectivity in Direct N-Alkylation of Amines. *J. Org. Chem.* **2002**, *67* (3), 674–683. https://doi.org/10.1021/jo010643c.

(345) Salvatore, R. N.; Nagle, A. S.; Schmidt, S. E.; Jung, K. W. Cesium Hydroxide Promoted Chemoselective N-Alkylation for the Generally Efficient Synthesis of Secondary Amines. *Org. Lett.* **1999**, *1* (12), 1893–1896. https://doi.org/10.1021/ol9910417.

(346) Salvatore, R. N.; Chu, F.; Nagle, A. S.; Kapxhiu, E. A.; Cross, R. M.; Jung, K. W. Efficient Cs2CO3-Promoted Solution and Solid Phase Synthesis of Carbonates and Carbamates in the Presence of TBAI. *Tetrahedron* **2002**, *58* (17), 3329–3347. https://doi.org/10.1016/S0040-4020(02)00286-7.

(347) Gawley, R. E.; Hennings, D. D. Sodium Hydride. In *Encyclopedia of Reagents for Organic Synthesis*; John Wiley & Sons, Ltd, 2006. https://doi.org/10.1002/047084289X.rs073.pub2.

(348) Tian, Z.-Y.; Li, J.-H.; Li, Q.; Zang, F.-L.; Zhao, Z.-H.; Wang, C.-J. Study on the Synthesis, Biological Activity and Spectroscopy of Naphthalimide-Diamine Conjugates. *Molecules* **2014**, *19* (6), 7646–7668. https://doi.org/10.3390/molecules19067646.

(349) Li, J.; Tian, R.; Ge, C.; Chen, Y.; liu, X.; Wang, Y.; Yang, Y.; Luo, W.; Dai, F.; Wang, S.; Chen, S.; Xie, S.; Wang, C. Discovery of the Polyamine Conjugate with Benzo[Cd]Indol-2(1H)-One as a Lysosome-Targeted Antimetastatic Agent. *J. Med. Chem.* **2018**, *61* (15), 6814–6829. https://doi.org/10.1021/acs.jmedchem.8b00694.

(350) Kruczynski, A.; Pillon, A.; Créancier, L.; Vandenberghe, I.; Gomes, B.; Brel, V.; Fournier, E.; Annereau, J.-P.; Currie, E.; Guminski, Y.; Bonnet, D.; Bailly, C.; Guilbaud, N. F14512, a Polyamine-Vectorized Anti-Cancer Drug, Currently in Clinical Trials Exhibits a Marked Preclinical Anti-Leukemic Activity. *Leukemia* **2013**, *27* (11), 2139–2148. https://doi.org/10.1038/leu.2013.108.

(351) Blanchet, M.; Borselli, D.; Brunel, J. M. Polyamine Derivatives: A Revival of an Old Neglected Scaffold to Fight Resistant Gram-Negative Bacteria? *Future Medicinal Chemistry* **2016**, *8* (9), 963–973. https://doi.org/10.4155/fmc-2016-0011.

(352) Salvatore, R. N.; Schmidt, S. E.; Shin, S. I.; Nagle, A. S.; Worrell, J. H.; Jung, K. W. CsOH-Promoted Chemoselective Mono-N-Alkylation of Diamines and Polyamines.

Tetrahedron Letters **2000**, *41* (50), 9705–9708. https://doi.org/10.1016/S0040-4039(00)01747-0.

(353) Sikandar, S.; Zahoor, A. F.; Naheed, S.; Parveen, B.; Ali, K. G.; Akhtar, R. Fukuyama Reduction, Fukuyama Coupling and Fukuyama–Mitsunobu Alkylation: Recent Developments and Synthetic Applications. *Mol Divers* **2022**, *26* (1), 589–628. https://doi.org/10.1007/s11030-021-10194-7.

(354) Fletcher, S. The Mitsunobu Reaction in the 21 St Century. *Organic Chemistry Frontiers* **2015**, *2* (6), 739–752. https://doi.org/10.1039/C5QO00016E.

(355) Swamy, K. C. K.; Kumar, N. N. B.; Balaraman, E.; Kumar, K. V. P. P. Mitsunobu and Related Reactions: Advances and Applications. *Chem. Rev.* **2009**, *109* (6), 2551–2651. https://doi.org/10.1021/cr800278z.

(356) Lipshutz, B. H.; Chung, D. W.; Rich, B.; Corral, R. Simplification of the Mitsunobu Reaction. Di- *p* -Chlorobenzyl Azodicarboxylate: A New Azodicarboxylate. *Org. Lett.* **2006**, *8* (22), 5069–5072. https://doi.org/10.1021/ol0618757.

(357) Matoba, M.; Kajimoto, T.; Node, M. Application of Odorless Thiols for the Cleavage of 2- and 4-Nitrobenzenesulfonamides. *Synthetic Communications* **2008**, *38* (8), 1194–1200. https://doi.org/10.1080/00397910701866098.

(358) Fang, W.-J.; Yakovleva, T.; Aldrich, J. V. A Convenient Approach to Synthesizing Peptide C-Terminal N-Alkyl Amides. *Peptide Science* **2011**, *96* (6), 715–722. https://doi.org/10.1002/bip.21600.

(359) Quan, D. H.; Wang, T.; Martinez, E.; Kim, H. Y.; Sintchenko, V.; Britton, W. J.; Triccas, J. A.; Alffenaar, J.-W. Beta-Lactam Combination Treatment Overcomes Rifampicin Resistance in Mycobacterium Tuberculosis. *Eur J Clin Microbiol Infect Dis* **2025**, *44* (5), 1279–1284. https://doi.org/10.1007/s10096-025-05062-3.

(360) Bindslev, N. Hill in Hell. In *Drug-Acceptor Interactions*; CRC Press, 2008.

(361) Cumberland, W. N.; Fong, Y.; Yu, X.; Defawe, O.; Frahm, N.; De Rosa, S. Nonlinear Calibration Model Choice between the Four and Five-Parameter Logistic Models. *Journal of Biopharmaceutical Statistics* **2015**, *25* (5), 972–983. https://doi.org/10.1080/10543406.2014.920345.

(362) Basagni, F.; Marotta, G.; Rosini, M.; Minarini, A. Polyamine–Drug Conjugates: Do They Boost Drug Activity? *Molecules* **2023**, *28* (11), 4518. https://doi.org/10.3390/molecules28114518.

(363) Dai, F.; He, H.; Xu, X.; Chen, S.; Wang, C.; Feng, C.; Tian, Z.; Dong, H.; Xie, S. Synthesis and Biological Evaluation of Naphthalimide-Polyamine Conjugates Modified by Alkylation as Anticancer Agents through P53 Pathway. *Bioorganic Chemistry* **2018**, *77*, 16–24. https://doi.org/10.1016/j.bioorg.2017.12.036.

(364) Szumilak, M.; Galdyszynska, M.; Dominska, K.; Bak-Sypien, I. I.; Merecz-Sadowska, A.; Stanczak, A.; Karwowski, B. T.; Piastowska-Ciesielska, A. W. Synthesis, Biological Activity and Preliminary in Silico ADMET Screening of Polyamine Conjugates with Bicyclic Systems. *Molecules* **2017**, *22* (5), 794. https://doi.org/10.3390/molecules22050794.

(365) Pont, I.; Felipe, R.; Frías, J. C.; Chicote, J. U.; García-España, A.; García-España, E.; Albelda, M. T. An Effective Liposome-Based Nanodelivery System for Naphthalene Derivative Polyamines with Antitumor Activity. *Biomolecules* **2024**, *14* (11), 1347. https://doi.org/10.3390/biom14111347.

(366) Fleeman, R. M.; Debevec, G.; Antonen, K.; Adams, J. L.; Santos, R. G.; Welmaker, G. S.; Houghten, R. A.; Giulianotti, M. A.; Shaw, L. N. Identification of a Novel Polyamine Scaffold With Potent Efflux Pump Inhibition Activity Toward Multi-Drug Resistant Bacterial Pathogens. *Front. Microbiol.* **2018**, *9*. https://doi.org/10.3389/fmicb.2018.01301.

(367) Rutkowska, A.; Thomson, D. W.; Vappiani, J.; Werner, T.; Mueller, K. M.; Dittus, L.; Krause, J.; Muelbaier, M.; Bergamini, G.; Bantscheff, M. A Modular Probe Strategy for Drug Localization, Target Identification and Target Occupancy Measurement on Single Cell Level. *ACS Chem. Biol.* **2016**, *11* (9), 2541–2550. https://doi.org/10.1021/acschembio.6b00346.

(368) Pang, Z.; Cravatt, B. F.; Ye, L. Deciphering Drug Targets and Actions with Single-Cell and Spatial Resolution. *Annual Review of Pharmacology and Toxicology* **2024**, *64* (Volume 64, 2024), 507–526. https://doi.org/10.1146/annurev-pharmtox-033123-123610.

(369) Dou, L.; Zhang, Z.; liu, D.; Qian, Y.; Zhang, Q. BCM-DTI: A Fragment-Oriented Method for Drug–Target Interaction Prediction Using Deep Learning. *Computational Biology and Chemistry* **2023**, *104*, 107844. https://doi.org/10.1016/j.compbiolchem.2023.107844.

(370) Du, P.; Fan, R.; Zhang, N.; Wu, C.; Zhang, Y. Advances in Integrated Multi-Omics Analysis for Drug-Target Identification. *Biomolecules* **2024**, *14* (6), 692. https://doi.org/10.3390/biom14060692.

(371) Tabana, Y.; Babu, D.; Fahlman, R.; Siraki, A. G.; Barakat, K. Target Identification of Small Molecules: An Overview of the Current Applications in Drug Discovery. *BMC Biotechnology* **2023**, *23* (1), 44. https://doi.org/10.1186/s12896-023-00815-4.

(372) Reck, F.; Zhou, F.; Eyermann, C. J.; Kern, G.; Carcanague, D.; Ioannidis, G.; Illingworth, R.; Poon, G.; Gravestock, M. B. Novel Substituted (Pyridin-3-Yl)Phenyloxazolidinones: Antibacterial Agents with Reduced Activity against Monoamine Oxidase A and Increased Solubility. *J. Med. Chem.* **2007**, *50* (20), 4868–4881. https://doi.org/10.1021/jm070428+.

(373) Emde, U.; Buchstaller, H. P.; Klein, M.; Esdar, C.; Bomke, J. Pyridinylimidazolone Derivatives for the Inhibition of Pi3 Kinases. US2012220587A1, August 30, 2012.

(374) Largy, E.; Hamon, F.; Rosu, F.; Gabelica, V.; De Pauw, E.; Guédin, A.; Mergny, J.-L.; Teulade-Fichou, M.-P. Tridentate N-Donor Palladium(II) Complexes as Efficient Coordinating Quadruplex DNA Binders. *Chemistry – A European Journal* **2011**, *17* (47), 13274–13283. https://doi.org/10.1002/chem.201102300.

(375) Müller, S.; Schohe-Loop, R.; Ortega, H.; Süssmeier, F.; Jimenez Nunez, E.; Brumby, T.; Lindner, N.; Gerdes, C.; Pook, E.; Buchmüller, A.; Gaugaz, F.; Lang, D.; Zimmermann, S.; Ehrmann, A.; Gerisch, M.; Lehmann, L.; Timmermann, A.; Schäfer, M.; Schmidt, G.; Schlemmer, K.-H.; Follmann, M.; Kersten, E.; Wang, V.; Gao, X.; Wang, Y. Substituted Dihydropyrazolo Pyrazine Carboxamide Derivatives, November 21, 2019. https://patentscope.wipo.int/search/en/detail.jsf?docId=WO2019219517 (accessed 2025-10-27).

(376) Nakao, K.; Stevens, R. W. Tetrazolylalkyl Indole Compounds as Anti-Inflammatory and Analgesic Agents. EP1065206A1, January 3, 2001.

(377) Bagherzadeh, N.; Sardarian, A. R.; Inaloo, I. D. Green and Efficient Synthesis of Thioureas, Ureas, Primary O-Thiocarbamates, and Carbamates in Deep Eutectic Solvent/Catalyst Systems Using Thiourea and Urea. *New J. Chem.* **2021**, *45* (26), 11852–11858. https://doi.org/10.1039/D1NJ01827B.

(378) Hay, M. P.; Turcotte, S.; Flanagan, J. U.; Bonnet, M.; Chan, D. A.; Sutphin, P. D.; Nguyen, P.; Giaccia, A. J.; Denny, W. A. 4-Pyridylanilinothiazoles That Selectively Target von Hippel−Lindau Deficient Renal Cell Carcinoma Cells by Inducing Autophagic Cell Death. *J. Med. Chem.* **2010**, *53* (2), 787–797. https://doi.org/10.1021/jm901457w.

(379) Wang, J.; Takahashi, K.; Shoup, T. M.; Gong, L.; Li, Y.; El Fakhri, G.; Zhang, Z.; Brownell, A.-L. Organomediated Cleavage of Benzoyl Group Enables an Efficient Synthesis of 1-(6-Nitropyridin-2-Yl)Thiourea and Its Application for Developing 18F-Labeled PET Tracers. *Bioorganic Chemistry* **2022**, *124*, 105804. https://doi.org/10.1016/j.bioorg.2022.105804.

(380) Castro, A. C.; Mcgovern, K. J.; Burke, M. 4-Phenyl-N-(Phenyl)Thiazol-2-Amine Derivatives and Related Compounds as Aryl Hydrocarbon Receptor (Ahr) Agonists for the Treatment of E.g. Angiogenesis Implicated or Inflammatory Disorders, June 24, 2021. https://patentscope.wipo.int/search/en/detail.jsf?docId=WO2021127301 (accessed 2025-10-27).

(381) Meissner, A.; Boshoff, H. I.; Vasan, M.; Duckworth, B. P.; Barry, C. E.; Aldrich, C. C. Structure–Activity Relationships of 2-Aminothiazoles Effective against Mycobacterium Tuberculosis. *Bioorganic & Medicinal Chemistry* **2013**, *21* (21), 6385–6397. https://doi.org/10.1016/j.bmc.2013.08.048.

(382) Mathew, B.; Ruiz, P.; Dutta, S.; Entrekin, J. T.; Zhang, S.; Patel, K. D.; Simmons, M. S.; Augelli-Szafran, C. E.; Cowell, R. M.; Suto, M. J. Structure-Activity Relationship (SAR) Studies of N-(3-Methylpyridin-2-Yl)-4-(Pyridin-2-Yl)Thiazol-2-Amine (SRI-22819) as NF-κB Activators for the Treatment of ALS. *European Journal of Medicinal Chemistry* **2021**, *210*, 112952. https://doi.org/10.1016/j.ejmech.2020.112952.

(383) Smith, N. Carborane-Cyclam Conjugates with Potent Anti-Tubercular Activity. Honours Thesis, The University of Sydney, Sydney, NSW, 2018.

(384) *Antitubercular Bis-Substituted Cyclam Derivatives: Structure–Activity Relationships and in Vivo Studies | Journal of Medicinal Chemistry*. https://pubs.acs.org/doi/10.1021/acs.jmedchem.7b01569 (accessed 2021-04-20).

(385) Barišić, L.; Rapić, V.; Pritzkow, H.; Pavlović, G.; Nemet, I. Ferrocene Compounds: Part XXXIII. Synthesis and Characterization of Amino Acids Containing Skeletal 1,1′-

Ferrocenylene Unit. *Journal of Organometallic Chemistry* **2003**, *682* (1), 131–142. https://doi.org/10.1016/S0022-328X(03)00774-5.

(386) Zimmermann, B. M.; Ngoc, T. T.; Tzaras, D.-I.; Kaicharla, T.; Teichert, J. F. A Bifunctional Copper Catalyst Enables Ester Reduction with H2: Expanding the Reactivity Space of Nucleophilic Copper Hydrides. *J. Am. Chem. Soc.* **2021**, *143* (40), 16865–16873. https://doi.org/10.1021/jacs.1c09626.

(387) Iyer, K. S.; Nelson, C.; Lipshutz, B. H. Facile, Green, and Functional Group-Tolerant Reductions of Carboxylic Acids…in, or with, Water. *Green Chem.* **2023**, *25* (7), 2663–2671. https://doi.org/10.1039/D3GC00517H.

(388) Liubimtsev, N.; Kösterke, T.; Che, Y.; Appelhans, D.; Gaitzsch, J.; Voit, B. Redox-Sensitive Ferrocene Functionalised Double Cross-Linked Supramolecular Hydrogels. *Polymer Chemistry* **2022**, *13* (3), 427–438. https://doi.org/10.1039/D1PY01211H.

(389) Casas-Solvas, J. M.; Vargas-Berenguel, A.; Capitán-Vallvey, L. F.; Santoyo-González, F. Convenient Methods for the Synthesis of Ferrocene−Carbohydrate Conjugates. *Org. Lett.* **2004**, *6* (21), 3687–3690. https://doi.org/10.1021/ol048665j.

(390) Krapcho, A. P.; Kuell, C. S. Mono-Protected Diamines. N-Tert-Butoxycarbonyl-α,ω-Alkanediamines from α,ω-Alkanediamines. *Synthetic Communications* **1990**, *20* (16), 2559–2564. https://doi.org/10.1080/00397919008053205.

(391) Prinsell, M. R.; Everson, D. A.; Weix, D. J. Nickel-Catalyzed, Sodium Iodide-Promoted Reductive Dimerization of Alkyl Halides, Alkyl Pseudohalides, and Allylic Acetates. *Chem. Commun.* **2010**, *46* (31), 5743–5745. https://doi.org/10.1039/C0CC01716G.

(392) Sinha, M. K.; Reany, O.; Yefet, M.; Botoshansky, M.; Keinan, E. Bistable Cucurbituril Rotaxanes Without Stoppers. *Chemistry – A European Journal* **2012**, *18* (18), 5589–5605. https://doi.org/10.1002/chem.201103434.

(393) Shi, M. Functionalised Azamacrocycles for Modulating Amyloid Aggregation. Masters thesis, The University of Sydney, 2020.

(394) Nielsen, B. E.; Stabile, S.; Vitale, C.; Bouzat, C. Design, Synthesis, and Functional Evaluation of a Novel Series of Phosphonate-Functionalized 1,2,3-Triazoles as Positive

Allosteric Modulators of A7 Nicotinic Acetylcholine Receptors. *ACS Chem. Neurosci.* **2020**, *11* (17), 2688–2704. https://doi.org/10.1021/acschemneuro.0c00348.

(395) *Integrated and Passive 1,2,3-Triazolyl Groups in Fluorescent Indicators for Zinc(II) Ions: Thermodynamic and Kinetic Evaluations | Inorganic Chemistry*. https://pubs.acs.org/doi/10.1021/ic302798u (accessed 2025-10-21).

(396) Ghotekar, G. S.; Mujahid, M.; Muthukrishnan, M. Total Synthesis of Marine Natural Products Serinolamide A and Columbamide D. *ACS Omega* **2019**, *4* (1), 1322–1328. https://doi.org/10.1021/acsomega.8b03417.

9 Appendices

These data can all be found on the researcher's publicly accessible electronic lab notebook, hosted on GitHub at the following link:

https://github.com/KlementineJBS/USYD_PhD_ELN/wiki/PhD-Thesis-data

Appendix A: Compounds described in this work

Appendix A.1 – Compounds tested against *M. mycetomatis* as part of the MycetOS consortium.

Thesis	Internal	MYOS	SMILES
9	DM34-1	193	CC1=CC=NC(NC2=NC(C3=CC=CC(OC)=C3)=CS2)=C1
11	KRS_021_002	176	CC1=CC=NC(NC2=NC(C3=CC=CC=N3)=CS2)=C1
12	Methylene blue (chloride)	386	O=C(CC1=CC=CC(Cl)=C1)NC2=NC3=CC(Cl)=CC=C3O2
13	NEU-0006878=AA-001=C	627	CC1=CC=NC(NC2=NC(C3=CC=C(C4=CC=CC=C4)C=N3)=CS2)=C1
14	n.a. (University of York)	752	C12=CN=C(N=C1N=CN2)NC3=NC(C4=CC=CC=N4)=CS3
18	HH01	326	C1(C2=CSC(NC3=CC4=C(OCO4)C=C3)=N2)=CC=CC=N1
48	SSP_2020_8a	179	CC1=CC=NC(NC2=NC(C3=CC=CN=C3)=CS2)=C1
49	SSP_2020_8j	177	CC1=CC=NC(NC2=NC(C3=CC=C(OC)C=C3)=CS2)=C1
50	SSP_2020_Demos	178	FC1=C(C(N2CCNCC2)C3=CN=CC=C3)C=CC(Cl)=C1
51a	KRS_040	309	CC1=CC=NC(NC2=NC(C3=CC=CC(C)=C3)=CS2)=C1
51b	SSP_2020_8g	185	CC1=CC=NC(NC2=NC(C3=CC=CC=C3F)=CS2)=C1
51c	SSP_2020_8d	182	CC1=CC=NC(NC2=NC(C3=CC=CC=C3Cl)=CS2)=C1
51d	SSP_2020_8k	188	CC1=CC=NC(NC2=NC(C3=CC=CC=C3OC)=CS2)=C1
51e	2022_SSP_8I	429	CC1=CC(NC2=NC(C3=CC([N+]([O-])=O)=CC=C3)=CS2)=NC=C1
52a	KRS_039	308	CC1=CC=NC(NC2=NC(C3=CC=CC=C3C)=CS2)=C1
52b	SSP_2020_8f	184	CC1=CC=NC(NC2=NC(C3=CC=C(Cl)C=C3)=CS2)=C1
52c	SSP_2020_8c	181	CC1=CC=NC(NC2=NC(C3=CC=NC=C3)=CS2)=C1
52d	SSP_2020_8i	187	CC1=CC=NC(NC2=NC(C3=CC=C(F)C=C3)=CS2)=C1

52e	2022_SSP_8H	428	CC1=CC(NC2=NC(C3=C(C=CC=C3)[N+]([O-])=O)=CS2)=NC=C1
53a	KRS_038	307	ClC1=CC=C(C(Cl)=C1)C(CC2=CN=CC=C2)=NOC
53b	SSP_2020_8e	183	CC1=CC=NC(NC2=NC(C3=CC=CC(Cl)=C3)=CS2)=C1
53c	SSP_2020_8b	180	CC1=CC=NC(NC2=NC(C3=CC=CC=C3)=CS2)=C1
53d	SSP_2020_8h	186	CC1=CC=NC(NC2=NC(C3=CC=CC(F)=C3)=CS2)=C1
53e	2022_SSP_8G	427	ClC1=CN=C(NC2=NC(C3=CC=CC=N3)=CS2)C=C1
54	2022_SSP_8E	425	ClC1=CC=CC(NC2=NC(C3=CC=CC=N3)=CS2)=N1
55	2022_SSP_8C	423	COC1=CC=CC(NC2=NC(C3=CC=CC=N3)=CS2)=N1
56	2022_SSP_8A	421	CC1=CC(NC2=NC(C3=CC=CC=N3)=CS2)=CC=C1
57	2022_SSP_8F	426	ClC1=CC(NC2=NC(C3=CC=CC=N3)=CS2)=NC=C1
58	2022_SSP_8D	424	COC1=CC(NC2=NC(C3=CC=CC=N3)=CS2)=NC=C1
59	2022_SSP_8B	422	FC(F)(C1=CC(NC2=NC(C3=CC=CC=N3)=CS2)=NC=C1)F
60	2022_SSP_8A	420	CN(C)C1=CC2=[S+]C3=CC(N(C)C)=CC=C3N=C2C=C1.[Cl-]
61a	2023_SSP_8A	615	CC1=CC=CC(NC2=NC(C3=CC=C(OC(F)(F)F)C=C3)=CS2)=N1
61b	2023_SSP_8B	616	CC1=CC=NC(NC2=NC(C3=CC=CC(Br)=N3)=CS2)=C1
61c	2023_SSP_8C	617	CC1=CC=NC(NC2=NC(C3=CC=C(Br)C=N3)=CS2)=C1
61d	2023_SSP_8D	618	CC1=CC=NC(NC2=NC(C3=CC(Cl)=CC=N3)=CS2)=C1
61e	2023_SSP_8E	619	CC1=CC=NC(NC2=NC(C3=CC(C=CC=C4)=C4C=N3)=CS2)=C1
73	2024_SSP_8A	773	BrC1=CN=C(NC2=NC(C3=NC=CC=C3)=CS2)C=C1
74	2024_SSP_8G	779	C1(NC2=NC=CN2)=NC(C3=CC=CC=N3)=CS1
75	2024_SSP_8D	776	C1(C2=CSC(NC3=NNC=C3)=N2)=CC=CC=N1
76	2024_SSP_8E	777	C12=NC=NC(NC3=NC(C4=CC=CC=N4)=CS3)=C1NC=N2
77	2024_SSP_8B	774	C1(NC2=NC(C3=CC=CC=N3)=CS2)=NC=C(C4=CC=CC=C4)C=C1
78	2024_SSP_8C	775	CC1=NOC(NC2=NC(C3=CC=CC=N3)=CS2)=C1
79	2024_SSP_8F	778	C1(C2=CC=CC=C2)=NOC(NC3=NC(C4=CC=CC=N4)=CS3)=C1
80	2023_BG_2C	533	FC1=CC=CC=C1NC2=NC(C3=CC=CC=N3)=CS2
81	2023_BG_1C	532	CC1=CC=C(NC2=NC(C3=CC=CC=N3)=CS2)N=C1
82	2023_BG_8C	536	C1(C2=CSC(NC3(C4)CC5CC4CC(C5)C3)=N2)=CC=CC=N1
83	2023_BG_10C	538	FC1=CC=CC(NC2=NC(C3=CC=CC=N3)=CS2)=N1
84	2023_BG_9C	537	COC1=CC=C(NC2=NC(C3=CC=CC=N3)=CS2)N=C1

85	2022_BG_4C	535	FC(F)(F)C1=CC=CC=C1NC2=NC(C3=CC=CC=N3)=CS2
86	2022_BG_4C	315	CC1=CC=NC(NC2=NC(C3=CC=C(C)C=C3)=CS2)=C1
87	2022_BG_4E	316	FC1=CC=C(C=C1)NC2=NC(C3=CC=CC=N3)=CS2
88	2022_BG_4F	317	FC(C1=CC=C(C=C1)NC2=NC(C3=CC=CC=N3)=CS2)(F)F
89	2022_BG_4H	319	ClC1=C(C(F)(F)F)C=C(C=C1)NC2=NC(C3=CC=CC=N3)=CS2
90	2022_BG_4G	318	FC(C1=CC=CC(NC2=NC(C3=CC=CC=N3)=CS2)=C1)(F)F
91	2022_BG_4I	320	ClC1=CC=C(C(F)(F)F)C=C1NC2=NC(C3=CC=CC=N3)=CS2
92	2023_BG_3C	534	FC1=CC(NC2=NC(C3=CC=CC=N3)=CS2)=CC=C1
99	2023_BG_13C	540	CC1=CC=NC(NC2=NC(C3=CC(Cl)=CC=C3)=C(C)S2)=C1
100	2023_BG_15C	542	COC(C=N1)=CC=C1NC2=NC(C3=CC=C(C4=CC=CC=C4)C=C3)=CS2
101	2023_BG_12C	539	FC1=CN=C(NC2=NC(C3=CC=CC=N3)=CS2)C=C1
102	2023_BG_14C	541	CC1=CC=NC(NC2=NC(C3=CC=C(C4=CC=CC=C4)C=C3)=CS2)=C1
103	2023_BG_16C	543	FC1=NC(NC2=NC(C3=CC=C(C4=CC=CC=C4)C=C3)=CS2)=CC=C1
112	2024_BG_1C	726	CC1=CC=NC(NC2=NC(C3=CC=C(C#N)C=C3)=CS2)=C1
113	2024_BG_2C	727	ClC1=C(NC2=NC(C3=CC=CC=N3)=CS2)N=CC=C1
114	2024_BG_6C	731	ClC1=CC(Cl)=NC(NC2=NC(C3=CC=CC=N3)=CS2)=C1
115	2024_BG_4C	729	ClC1=C(Cl)C=NC(NC2=NC(C3=CC=CC=N3)=CS2)=C1
116	2024_BG_5C	730	ClC1=CC=C(NC2=NC(C3=CC=CC=N3)=CS2)N=C1Cl
117	2024_BG_3C	728	COC1=C(NC2=NC(C3=CC=CC=N3)=CS2)N=CC=C1
118	2024_BG_7C	732	ClC1=CC(Cl)=C(NC2=NC(C3=CC=CC=N3)=CS2)N=C1
119	2024_BG_8C	733	C1(NC2=NC(C3=NC=CC=C3)=CS2)=CC=C(C=CC=C4)C4=N1
120	n.a. (UCL)	815	CC1=CC=CC(NC2=NC(C3=CC=CC=N3)=CS2)=N1
121	n.a. (UCL × Whitgift)	605	C1(C2=CSC(NC3=CC=CC=N3)=N2)=CC=CC=N1
122	A3B8	606	BrC(C=C1)=CC=C1C2=CSC(NC3=NC=CC(C)=C3)=N2
123	A3B2	612	N#CC(C=C1)=CC=C1C2=CSC(NC3=CC=CC=N3)=N2
124	n.a. (University of York)	645	CN(C)CCNCCN1C2=CC=C(OC(F)(F)F)C=C2C2=C1C=CC(OC(F)(F)F)=C2
125	n.a. (University of York)	771	O=S(N1C2=C(C=CC=C2)SC3=CC=CC=C31)(C4=CC=CN=C4)=O
126	n.a. (University of York)	772	BrC1=CC(NC2=NC(C3=NC=CC=C3)=CS2)=NC=C1

127	KBS76	798	BrC1=CC=CC(NC2=NC(C3=CC=CC=N3)=CS2)=N1
128	KBS33	432	CC1=CC(NC2=NC(C3=CC=C(C=C3)[N+]([O-])=O)=CS2)=NC=C1
129	KBS58	792	C1(C=C2)=C(C=NN1)C=C2NC3=NC(C4=NC=CC=C4)=CS3
130	KBS73	797	BrC1=C(NC2=NC(C3=CC=CC=N3)=CS2)N=CC=C1
131	KBS70	796	FC(C1=NC(NC2=NC(C3=CC=CC=N3)=CS2)=CC=C1)(F)F
132	KBS67	795	FC(C1=CC=C(NC2=NC(C3=CC=CC=N3)=CS2)N=C1)(F)F
133	KBS64	794	FC1=C(NC2=NC(C3=CC=CC=N3)=CS2)N=CC=C1
134	KBS61	793	CC1=CC=NC(NC2=NC(C3=CC=C(Cl)C=N3)=CS2)=C1
148	KBS56	799	ClC1=NC2=CC=NN2C(NCC3=CC=CS3)=C1
155	A2B1	597	FC(C=N1)=CC=C1NC2=NC(C3=CC=C(C4=CC=CC=C4)C=C3)=CS2
156	A2B2	598	CC1=CC=CN=C1NC2=NC(C3=CC=C(OC(F)(F)F)C=C3)=CS2
157	A2B8	603	CC1=CC=CN=C1NC2=NC(C3=CC=C(OC(F)(F)F)C=C3)=CS2
158	A5B3	607	CC1=CC=NC(NC2=NC(C3=CC=C(Br)C=C3)=CS2)=C1
159	A3B3	610	CC1=CC(NC2=NC(C3=CC=C(C4=CC=CC=C4)C=C3)=CS2)=NC=C1

Appendix A.2 – Compounds synthesised in this work as part of Open Source TB Series 4.

Thesis	Internal	SMILES
179	KBS13	N1(CC2=CN(C3(C4)CC(C5)CC4CC5C3)N=N2)CCCNCCN(CC6=CN(C7(C8)CC9CC8CC(C9)C7)N=N6)CCCNCC1
180	KBS19	[][Fe][].[][Fe][].N1(CC2=CN(Cc3cccc3)N=N2)CCCNCCN(CC4=CN(Cc5cccc5)N=N4)CCCNCC1.c6cccc6.c7cccc7
181	KBS10	C#CCN1CCCN(C(OC(C)(C)C)=O)CCN(CC#C)CCCN(C(OC(C)(C)C)=O)CC1
182	KBS12	CC(OC(N1CCN(CC2=CN(C3(C4)CC(C5)CC4CC5C3)N=N2)CCCN(C(OC(C)(C)C)=O)CCN(CC6=CN(C7(C8)CC9CC8CC(C9)C7)N=N6)CCC1)=O)(C)C
183	KBS18	[][Fe][].[][Fe][].CC(OC(N1CCCN(CC2=CN(Cc3cccc3)N=N2)CCN(C(OC(C)(C)C)=O)CCCN(CC4=CN(Cc5cccc5)N=N4)CC1)=O)(C)C.c6cccc6.c7cccc7
185	KBS14	[][Fe][].O=C(OC)c1cccc1.c2cccc2
189	KBS15	[][Fe][].OCc1cccc1.c2cccc2
190	KBS16	[][Fe][].[N-]=[N+]=NCc1cccc1.c2cccc2
191	KBS1	N1(CCN(CCC2)CN2CC3)CCCN3C1
192	KBS9	C#CC[N+]1(C2)CCCN2CC[N+]3(CC#C)CCCN(C3)CC1.C#CC[N+]4(C5)CCCN5CC[N+]6(CC#C)CCCN(C6)CC4
195	KBS26	C1(CNCCCCCCNCC2=CN(C3(C4)CC5CC4CC(C5)C3)N=N2)=CN(C67CC8CC(C7)CC(C8)C6)N=N1
196	KBS27	[][Fe][].[][Fe][].C1(CNCCCCCCNCC2=CN(Cc3cccc3)N=N2)=CN(Cc4cccc4)N=N1.c5cccc5.c6cccc6
197	KBS53	C1(N2C=C(CNCCCCCCNCC3=CN(N=N3)C4=C5C=CC=CC5=CC=C4)N=N2)=C6C=CC=CC6=CC=C1
198	KBS3	CC(OC(NCCCCCCNC(OC(C)(C)C)=O)=O)(C)C
199	KBS17	C#CCN(C(OC(C)(C)C)=O)CCCCCCN(CC#C)C(OC(C)(C)C)=O
200	KBS17 *mono*	C#CCN(C(OC(C)(C)C)=O)CCCCCCNC(OC(C)(C)C)=O

201	KBS24	[][Fe][].[][Fe][].CC(OC(N(CC1=CN(Cc2cccc2)N=N1)CCCCCCN(C(OC(C)(C)C)=O)CC3=CN(Cc4cccc4)N=N3)=O)(C)C.c5cccc5.c6cccc6
202	KBS22	CC(OC(N(CC1=CN(C23CC4CC(C3)CC(C4)C2)N=N1)CCCCCCN(C(OC(C)(C)C)=O)CC5=CN(C6(C7)CC8CC7CC(C8)C6)N=N5)=O)(C)C
203	KBS29	BrCC(N=N1)=CN1C2=CC=CC3=CC=CC=C32
217	KBS23	[N-]=[N+]=NC1=CC=CC2=CC=CC=C21
218	KBS28	OCC(N=N1)=CN1C2=CC=CC3=CC=CC=C32
221	KBS43	O=S(NCCCCCCNS(C1=C([N+]([O-])=O)C=CC=C1)(=O)=O)(C2=C([N+]([O-])=O)C=CC=C2)=O
222	KBS48	O=S(N(CC1=CN(N=N1)C2=C3C=CC=CC3=CC=C2)CCCCCCN(S(C4=C([N+]([O-])=O)C=CC=C4)(=O)=O)CC5=CN(N=N5)C6=C7C=CC=CC7=CC=C6)(C8=CC=CC=C8[N+]([O-])=O)=O
232	KBS45	O=S(NCCCCCCCCCNS(C1=C([N+]([O-])=O)C=CC=C1)(=O)=O)(C2=CC=CC=C2[N+]([O-])=O)=O
233	KBS50	O=S(NCCCN(S(C1=CC=CC=C1[N+]([O-])=O)(=O)=O)CCCNS(C2=CC=CC=C2[N+]([O-])=O)(=O)=O)(C3=C([N+]([O-])=O)C=CC=C3)=O
234	KBS49	O=S(N(CC1=CN(N=N1)C2=C3C=CC=CC3=CC=C2)CCCCCCCCN(S(C4=CC=CC=C4[N+]([O-])=O)(=O)=O)CC5=CN(N=N5)C6=C7C=CC=CC7=CC=C6)(C8=CC=CC=C8[N+]([O-])=O)=O
235	KBS51	O=S(N(CC1=CN(N=N1)C2=C3C=CC=CC3=CC=C2)CCCN(S(C4=CC=CC=C4[N+]([O-])=O)(=O)=O)CCCN(CC5=CN(N=N5)C6=C7C=CC=CC7=CC=C6)S(C8=C([N+]([O-])=O)C=CC=C8)(=O)=O)(C9=CC=CC=C9[N+]([O-])=O)=O
240	KBS44	C1(N2C=C(CNCCCCCCCCNCC3=CN(N=N3)C4=C5C=CC=CC5=CC=C4)N=N2)=C6C=CC=CC6=CC=C1
241	KBS52	C1(N2C=C(CNCCCCCCCCNCC3=CN(N=N3)C4=C5C=CC=CC5=CC=C4)N=N2)=C6C=CC=CC6=CC=C1

Appendix B: Activity of 2-aminothiazoles as antifungals

Compounds are denoted by their MycetOS codes, which can be cross-referenced with **Appendix A.1**.

Table B.1 – Raw absorbance at 490 nm for MycetOS compounds **617**, **619**, **420**, **423**, **432_1** and **726** tested by the researcher at concentrations between 16.0 and 0.031 µM.

	617			**619**			**420**			**423**			**432_1**			**726**		
	1	2	3	1	2	3	1	2	3	1	2	3	1	2	3	1	2	3
(µM)																		
NC	0.325	0.092	0.106	0.27	0.091	0.139	0.164	0.078	0.17	0.237	0.063	0.226	0.127	0.08	0.134	0.117	0.109	0.257
16.0	0.257	0.215	0.248	0.217	0.192	0.225	0.64	0.658	0.748	0.179	0.184	0.243	0.251	0.154	0.242	0.235	0.189	0.221
8.00	0.252	0.213	0.222	0.228	0.183	0.212	0.606	0.614	0.725	0.21	0.159	0.23	0.228	0.181	0.933	0.208	0.161	0.212
4.00	0.688	0.177	1.176	0.236	0.2	0.191	0.695	0.666	0.667	0.223	0.154	0.197	0.656	0.229	0.778	0.199	0.176	0.214
2.00	0.64	0.612	0.773	0.354	0.178	0.202	0.712	0.578	0.725	0.214	0.119	0.214	0.768	0.574	0.715	0.839	0.374	0.723
1.00	0.716	0.7	0.704	0.533	0.639	0.881	0.577	0.525	0.684	0.487	0.674	0.958	0.536	0.538	0.63	0.594	0.664	0.704
0.50	0.627	0.717	0.655	0.463	0.512	0.62	0.531	0.551	0.67	0.492	0.542	0.686	0.527	0.592	0.679	0.537	0.569	0.694
0.250	0.602	0.556	0.82	0.568	0.482	0.654	0.632	0.514	0.659	0.51	0.489	0.69	0.606	0.474	0.782	0.555	0.482	0.706
0.125	0.661	0.645	0.713	0.596	0.534	0.645	0.583	0.506	0.699	0.57	0.544	0.699	0.595	0.549	0.73	0.539	0.559	0.727
0.063	0.908	0.508	0.822	0.596	0.599	0.788	0.524	0.588	0.83	0.576	0.519	0.758	0.558	0.47	0.784	0.493	0.594	0.793
0.031	0.654	0.601	0.689	0.808	0.561	0.637	0.503	0.558	0.643	0.515	0.612	0.657	0.561	0.586	0.624	0.548	0.635	0.716
PC	0.767	0.565	0.769	0.923	0.544	0.72	0.639	0.585	0.524	0.761	0.569	0.734	1.012	0.565	0.75	1.031	0.611	0.754

Table B.2 – Raw absorbance at 490 nm for MycetOS compounds **727**, **728**, **730**, **731** and **535** tested by the researcher at concentrations between 16.0 and 0.031 µM.

	727			**728**			**730**			**731**			**535**		
	1	2	3	1	2	3	1	2	3	1	2	3	1	2	3
(µM)															
NC	0.093	0.18	0.148	0.109	0.071	0.195	0.196	0.184	0.296	0.182	0.208	0.213	0.179	0.189	0.231
16.0	0.209	0.17	0.155	0.397	0.423	0.717	0.472	0.409	0.298	0.194	0.171	0.147	0.207	0.211	0.775
8.00	0.227	0.195	0.258	0.427	0.403	0.791	0.646	0.539	0.418	0.239	0.201	0.3	0.591	0.614	0.52
4.00	0.293	0.127	0.201	0.682	0.495	0.643	0.556	0.591	0.477	0.181	0.319	0.239	0.518	0.575	0.532
2.00	0.724	0.272	0.886	0.628	0.58	0.688	0.583	0.699	0.471	0.136	0.136	0.179	0.56	0.585	0.556
1.00	0.601	0.627	0.64	0.639	0.576	0.708	0.619	0.632	0.559	0.215	0.142	0.475	0.566	0.591	0.524
0.50	0.595	0.568	0.693	0.529	0.538	0.707	0.568	0.596	0.747	0.481	0.349	0.499	0.532	0.551	0.513
0.250	0.569	0.515	0.82	0.591	0.461	0.949	0.617	0.65	0.58	0.573	0.584	0.496	0.523	0.572	0.48
0.125	0.563	0.558	0.787	0.615	0.574	0.957	0.561	0.591	0.873	0.552	0.545	0.533	0.505	0.548	0.496
0.063	0.584	0.593	0.749	0.637	0.616	0.961	0.681	0.593	0.566	0.604	0.587	0.514	0.621	0.594	0.514
0.031	0.716	0.626	0.736	0.657	0.7	0.804	0.631	0.582	0.541	0.59	0.606	0.496	0.572	0.58	0.514
PC	0.606	0.691	0.748	0.84	0.709	0.95	0.632	0.586	0.602	0.576	0.592	0.498	0.708	0.579	0.555

Table B.3 – Raw absorbance at 490 nm for MycetOS compounds **752**, **771**, **772**, **432_2**, **605** and **420** tested by the researcher at concentrations between 16.0 and 0.031 µM.

	752			**771**			**772**			**432_2**			**605**			**420 (repeat)**		
	1	2	3	1	2	3	1	2	3	1	2	3	1	2	3	1	2	3
(µM)																		
NC	0.159	0.281	0.164	0.21	0.261	0.132	0.21	0.256	0.167	0.212	0.249	0.122	0.163	0.247	0.226	0.225	0.251	0.11
16.0	0.742	0.22	0.554	0.176	0.232	0.19	0.204	0.247	0.207	0.162	0.219	0.278	0.177	0.248	0.105	0.186	1.036	0.692
8.00	0.798	1.104	0.662	0.173	0.25	0.113	0.235	0.263	0.112	0.191	0.292	0.183	0.182	0.194	0.117	0.209	0.283	0.512
4.00	0.481	1.155	0.538	0.218	0.224	0.131	0.23	0.239	0.154	0.206	1.149	0.686	0.189	0.975	0.131	0.211	0.253	0.198
2.00	0.489	0.898	0.789	0.212	0.96	0.127	0.182	0.245	0.151	0.644	0.775	0.394	0.225	0.805	0.481	0.236	1.026	0.186
1.00	0.46	0.965	1.245	0.33	0.9	0.535	0.284	0.276	0.176	0.553	0.803	0.492	0.512	1.075	0.449	0.67	1.077	1.059
0.50	0.668	0.98	0.775	0.572	0.903	0.582	0.337	0.733	0.299	0.742	1.029	0.596	0.461	0.994	0.52	1.034	1.006	1.028
0.250	0.548	0.984	0.782	0.675	0.915	0.556	0.334	0.958	0.475	0.451	0.86	0.361	0.466	0.99	0.402	0.758	0.919	0.764
0.125	0.34	0.936	0.663	0.446	0.921	0.608	0.482	0.853	0.35	0.407	0.597	0.351	0.368	0.953	0.422	0.501	0.978	0.782
0.063	0.462	0.947	0.586	0.426	1.046	0.421	0.378	1.052	0.361	0.398	0.778	0.532	0.374	1.104	0.457	0.751	1.046	0.72
0.031	0.602	0.963	0.641	0.644	1.043	0.506	0.435	0.941	0.416	0.558	0.848	0.411	0.363	0.938	0.424	0.601	0.977	0.56
PC	0.539	1.055	0.643	0.507	0.981	0.702	0.624	0.877	0.572	0.478	0.872	0.34	0.627	0.981	0.41	0.641	1.02	0.715

Table B.4 – MICs (µM) obtained against nine strains of *M. mycetomatis*. All results shown were confirmed in triplicate.

Strain	mm14	mm55	SO1	I1	I3	P1	Peru	Parijs	CBS247
Compound									
420	0	> 16	0	0	0	< 12	> 16	-	> 16
423	2	2	2	-	2	0.5	2	2	2
432_1	16	8	8	8	8	0.5	8	4	4
432_2	8	8	8	8	8	0.5	16	4	8
605	8	4	8	8	8	2	8	8	8
617	8	8	4	-	4	0.5	4	-	8
619	4	2	4	2	1	1	4	-	4
726	4	4	4	4	4	1	4	-	4
727	4	4	8	16	4	2	4	16	8
731	1	1	1	1	1	0.5	> 16	> 16	> 16
752	8	> 16	16	8	16	8	> 16	> 16	> 16
771	4	2	4	4	4	0.5	4	4	2
772	1	1	1	2	1	0.5	2	4	4

The normalised activity of all compounds at 100 and 25 µM can be found in the masterlist maintained by the MycetOS consortium, which can be accessed at the following link: https://github.com/OpenSourceMycetoma/General-Start-Here/wiki/MycetOS-masterlist

Appendix C: Activity of 2-aminothiazoles against bacteria

Table C.1 – MIC values (μM) obtained for 2-ATs against *A. madurae*, *N. brasiliensis* and *S. somaliensis*. Compounds which were not active against any of the three species at the lowest concentration tested shown separately.

Code	*N. brasiliensis*	*A. madurae*	*S. somaliensis*
Active at lowest concentrations tested			
176	25	25	2
180	25	25	2
186	25	25	2
617	25	25	2
619	25	25	2
772	25	25	2
425	25	25	2
538	25	25	2
Active against Am and Nb at lowest concentrations tested			
424	25	25	> 2
432_01	25	25	> 2
605_01	25	25	> 2
616	25	25	> 2
421	25	25	> 2
536	25	25	> 2
537	25	25	> 2
729	25	25	> 2
730	25	25	> 2
731	25	25	> 2
733	> 100	25	> 2
771	25	25	> 2
Active against Ss at lowest concentration tested			
178	> 100	> 100	2
181	> 100	25	2
184	> 100	> 100	2
428	> 100	> 100	2

539	> 100	> 100	2
542	> 100	> 100	2
597	> 100	> 100	2
598	> 100	> 100	2
603	n.a.	n.a.	2
612	n.a.	n.a.	2
607	n.a.	n.a.	2
610	n.a.	n.a.	2

Table C.2 – MIC values (μM) obtained for 2-ATs against *A. madurae*, *N. brasiliensis* and *S. somaliensis*. Compounds failed to inhibit any of the three species at the lowest concentration tested.

Code	Nb	Am	Ss
177	> 100	> 100	> 2
179	> 100	> 100	> 2
182	> 100	> 100	> 2
185	> 100	> 100	> 2
188	> 100	> 100	> 2
420	100	100	> 2
422	> 100	> 100	> 2
426	> 100	> 100	> 2
427	> 100	> 100	> 2
429	> 100	> 100	> 2
533	100	100	> 2
534	> 100	> 100	> 2
540	> 100	> 100	> 2
541	> 100	> 100	> 2
543	> 100	> 100	> 2
592	> 100	> 100	> 2
593	> 100	> 100	> 2
594	> 100	> 100	> 2
595	> 100	> 100	> 2
596	> 100	> 100	> 2
599	> 100	> 100	> 2
600	> 100	> 100	> 2
601	> 100	> 100	> 2
602	100	100	> 2
606	n.a.	n.a.	> 2
608	n.a.	n.a.	> 2
609	n.a.	n.a.	> 2
613	n.a.	n.a.	> 2
614	n.a.	n.a.	> 2
615	> 100	> 100	> 2
618	> 100	> 100	> 2
726	100	100	> 2
727	> 100	> 100	> 2
728	> 100	> 100	> 2

Appendix D: Resazurin-based assay optimisation

Table D.1 – MIC results collected for *N. brasiliensis* using three different methods, with overall agreement to visually inspected dye-free replicate reported qualitatively.

Resazurin (mM)	Volume inoculum (µL)	Volume resazurin solution (µL)	Visual inspection	Colorimetric	620 nm	Agreement
14.6	200	5	2	unclear	> 4	poor
19.3	150	5	1	unclear	0.125	poor
19.3	150	5	1	unclear	1	poor
28.4	200	10	2	unclear	unclear	poor
37.3	150	10	1	unclear	> 1	poor
37.3	150	10	1	unclear	>4	poor
54.3	200	20	2	2	2	excellent
70.3	150	20	1	unclear	> 1	poor
70.3	150	20	1	1	2	excellent
77.9	200	30	2	2	2	excellent
99.5	150	30	1	1	> 1	excellent
99.5	150	30	1	1	> 4	good
99.5	150	30	1	1	0.5	excellent
126	150	40	1	1	0.5	excellent
138	100	30	0.5	1	0.5	excellent
171	100	40		1	0.5	excellent
171	100	40	1	1	0.5	excellent
171	100	40	1	0.5	0.5	good
171	100	40	0.5	0.25	1	good

Table D.2 – MIC results collected for *A. madurae* using three different methods, with overall agreement to visually inspected dye-free replicate reported qualitatively.

Resazurin (mM)	Volume inoculum (µL)	Volume resazurin solution (µL)	Visual inspection	Colorimetric	620 nm	Agreement
14.6	5	200	0.0156	unclear	0.008	poor
19.3	5	150	≤ 0.03	unclear	≤ 0.03	**good**
19.3	5	150	0.008	unclear	0.008	**good**
28.4	10	200	0.0156	unclear	0.008	**poor**
37.3	10	150	≤ 0.03	unclear	≤ 0.03	**excellent**
37.3	10	150	0.008	unclear	0.008	**good**
54.3	20	200	0.0156	0.008	0.008	**good**
70.3	20	150	≤ 0.03	unclear	≤ 0.03	**excellent**
70.3	20	150	0.008	0.008	0.008	**excellent**
77.9	30	200	0.0156	0.008	0.008	**good**
99.5	30	150	≤ 0.03	unclear	0.5	**good**
99.5	30	150	0.008	0.008	0.008	**excellent**
99.5	30	150	0.008	0.008	≤ 0.004	**excellent**
126	40	150	0.008	≤ 0.004	0.008	**good**
138	30	100	0.008	≤ 0.004	0.06	**poor**
171	40	100	0.008	≤ 0.004	0.0156	**good**
171	40	100	0.0016	≤ 0.004	0.008	**good**
171	40	100	≤ 0.004	≤ 0.004	0.008	**excellent**
171	40	100	≤ 0.004	≤ 0.004	≤ 0.004	**excellent**

Appendix E: Activity of cyclam and open cyclam against *Mtb*

Table E.1 – Raw data from resazurin fluorescence assays on cyclam-based compounds **KBS13 (179)** and **KBS19 (180)**.

Concentration	KBS13 (179)			KBS19 (180)		
(uM)	1	2	3	1	2	3
250	120834	125365	122071	111856	108848	104668
83.3	122269	126023	124746	114991	118481	112872
27.8	128124	132253	132907	121025	119778	113619
9.26	138342	143265	142476	126766	125814	121506
3.09	157502	165094	166529	168591	166785	155400
1.03	174560	182070	186004	189847	191533	178650
0.343	182738	190728	187158	191197	188979	181161
0.114	183253	190534	192291	192556	188144	178846
0	181373	187245	184840	185835	182279	177857

Table E.2 – Raw data from resazurin fluorescence assays on linear amine compounds **KBS26 (195)**, **KBS52 (241)**, **KBS44 (240)** and **KBS53 (197)**.

Concentration	KBS26 (195)			KBS52 (241)			KBS44 (240)			KBS53 (197)		
(μM)	1	2	3	1	2	3	1	2	3	1	2	3
250	*136402**	*139836**	*141435**	*129041**	*132059**	*133922**	*152892**	*150762**	*146231**	*148632**	*147680**	*143482**
100	132357	137526	137106	128567	132548	130947	*138719**	*141001**	*135428**	*140284**	*139678**	*134147**
40.0	139564	143846	145590	130866	135482	136432	133727	133073	127688	134436	133237	129141
16.0	154115	163474	162785	144735	152602	154102	134608	132780	127827	136770	135134	130603
6.40	175815	185803	183321	160220	167669	169280	147433	146880	142773	148565	148710	142105
2.56	184694	190183	192082	179575	187477	189667	179030	176740	165387	167180	163759	155888
1.02	184200	191333	191867	183155	188568	189290	189350	188917	184853	191947	186459	180825
0.410	184631	192321	191901	183811	190924	189309	188366	189436	181998	191299	188744	183180
0	181878	186954	182696	173470	181436	181156	186150	182480	173981	180038	185128	173641
5000	123093	128034	127686	121667	126681	126327	127393	125936	121199	126165	125179	120529

Appendix F: NMR spectra of 2-aminothiazoles

All NMR spectra (including raw data files) for compounds described in Chapter 2 can be found on GitHub at the following link:

https://github.com/KlementineJBS/USYD_PhD_ELN/wiki/Characterisation-data-%E2%80%90-MycetOS

Sample spectra are provided for 2-aminothiazole **109**.

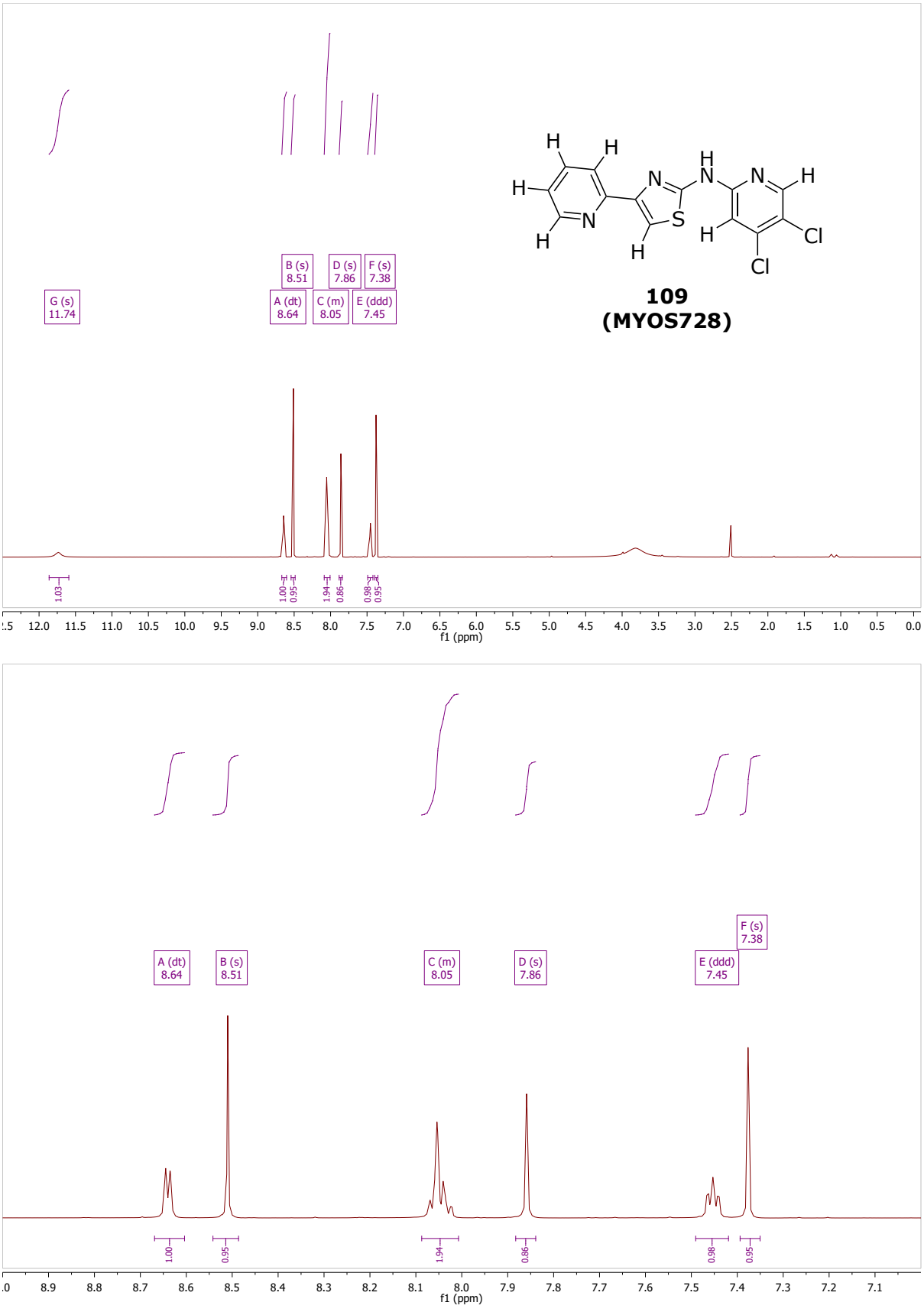

Figure F.1 – ^{1}H NMR (500 MHz) spectrum of **109** (MYOS728) in DMSO.

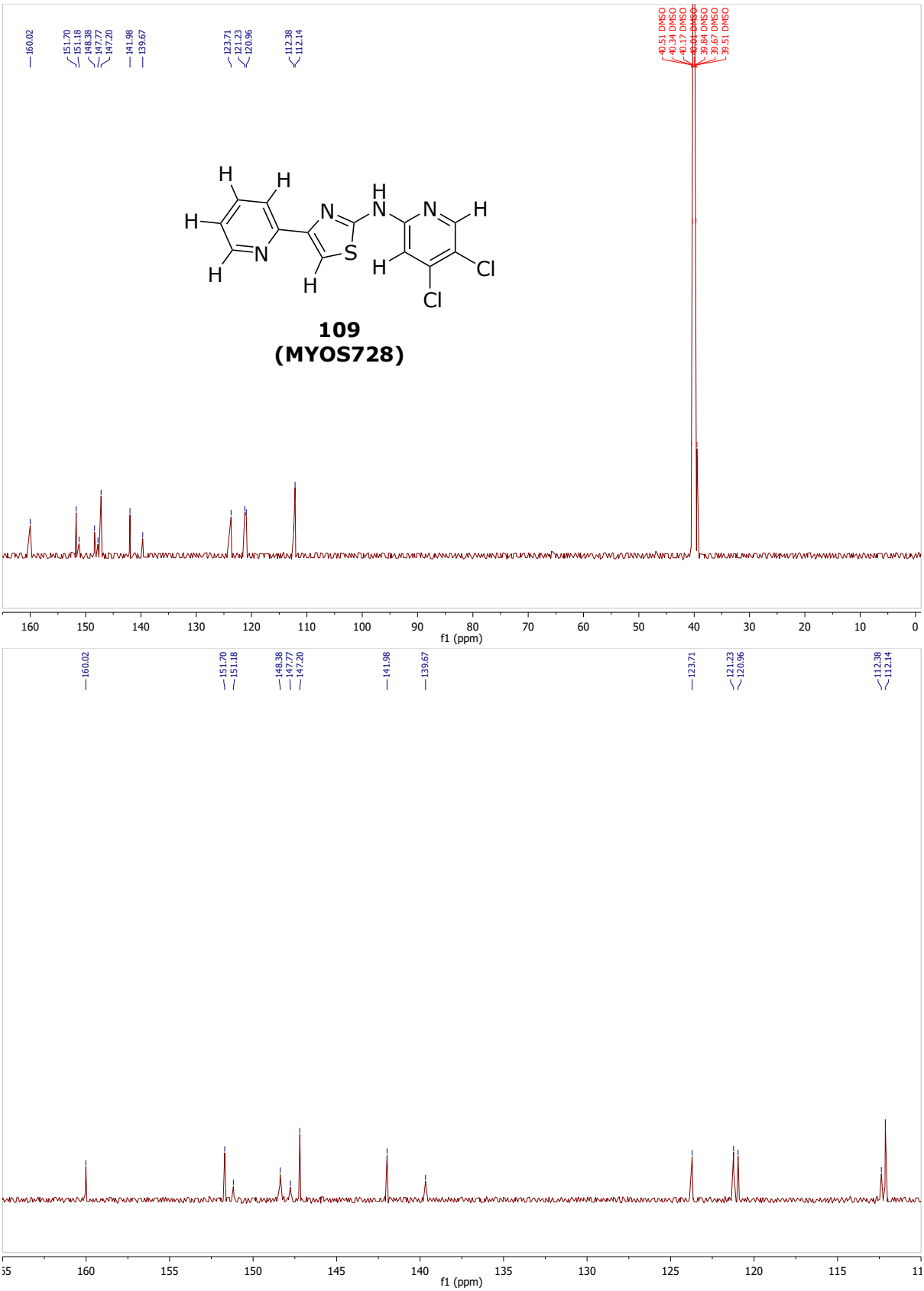

Figure F.2 – ^{13}C NMR (126 MHz) spectrum of **109** (MYOS728) in DMSO.

Appendix G: NMR spectra of OSTB compounds

^{1}H NMR spectra for all final compounds are provided here. Additional NMR spectra (including raw data files) for novel compounds described in Chapter 5 can be found on GitHub at the following link:

https://github.com/KlementineJBS/USYD_PhD_ELN/wiki/Characterisation-data-%E2%80%90-OSTB

The annotated spectra of Boc-protected compound **182** and final compound **179** are shown as an example of cyclam compounds with ferrocene and adamantane pendant groups made using the click-coupling method (**Figures G.1** and **G.2**).

The annotated spectra of nosyl-protected diaminohexane **221**, nosyl-protected compound **222** and final compound **197** are shown as an example of linear polyamines with naphthyl pendant groups made using the Fukuyama amine synthesis method (**Figures G.5** – **G.7**).

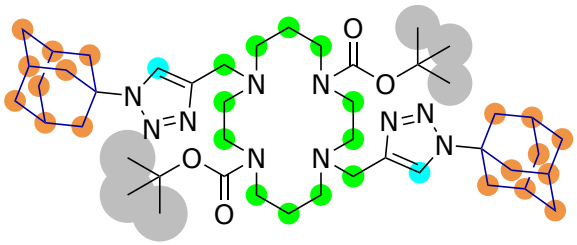

182

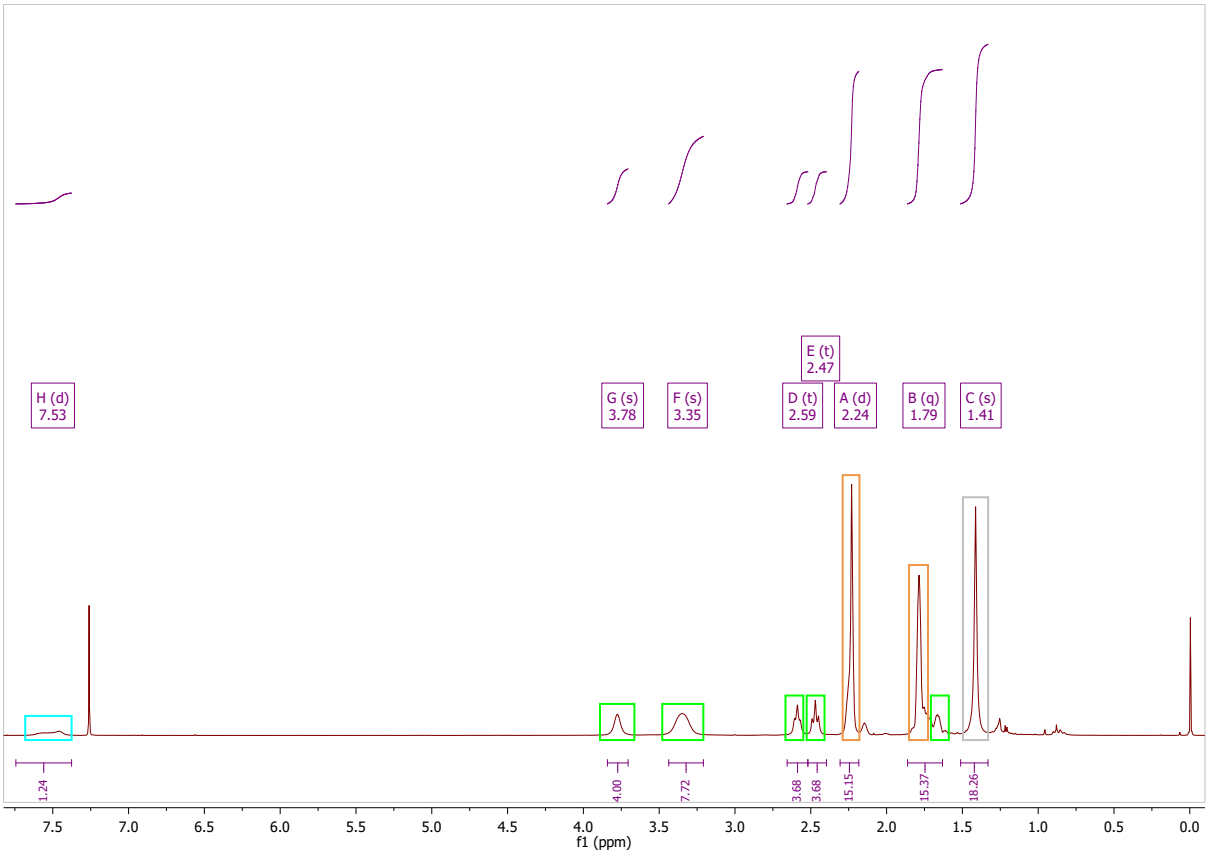

Appendix G.1 – ^{1}H NMR (300 MHz) spectrum of **182** in $CDCl_3$.

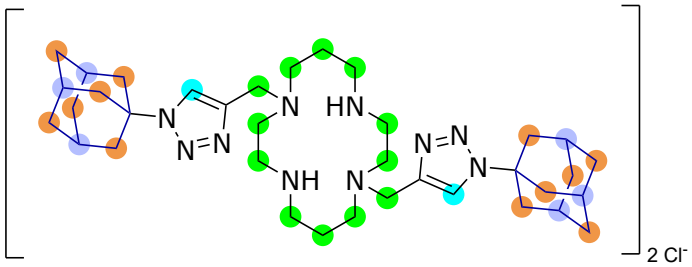

179·2HCl

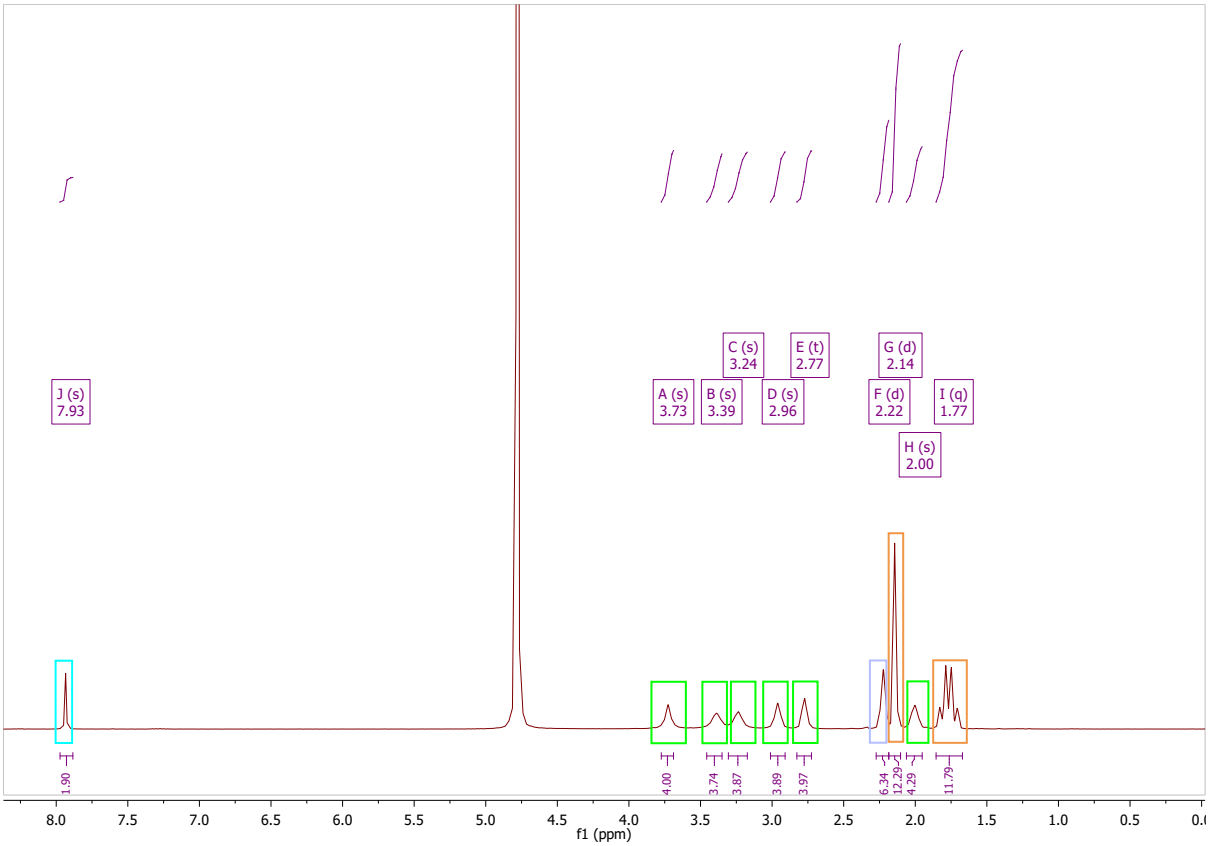

Appendix G.2 – ^{1}H NMR (300 MHz) spectrum of **179·2HCl** in D_2O.

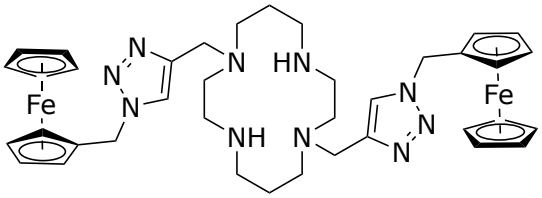

180

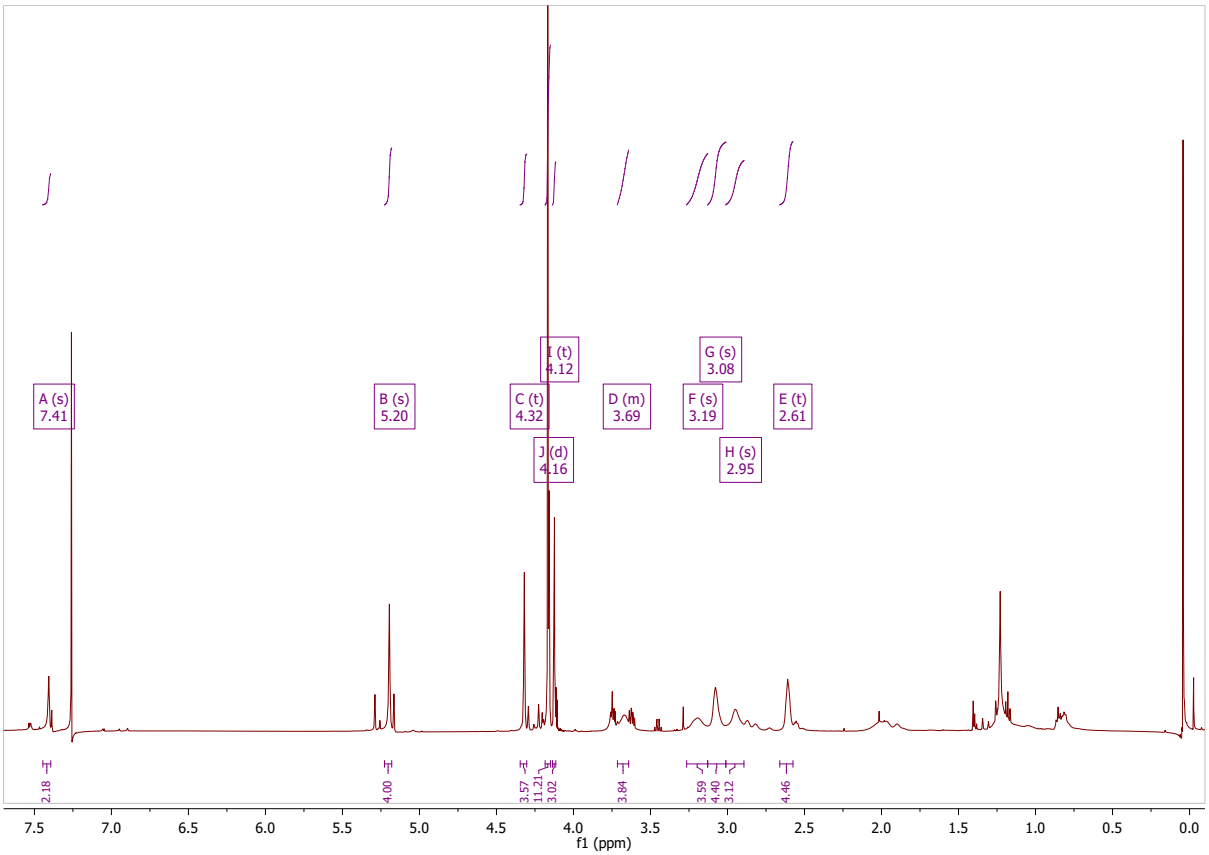

Appendix G.3 – ^{1}H NMR (500 MHz) spectrum of **180** in $CDCl_3$.

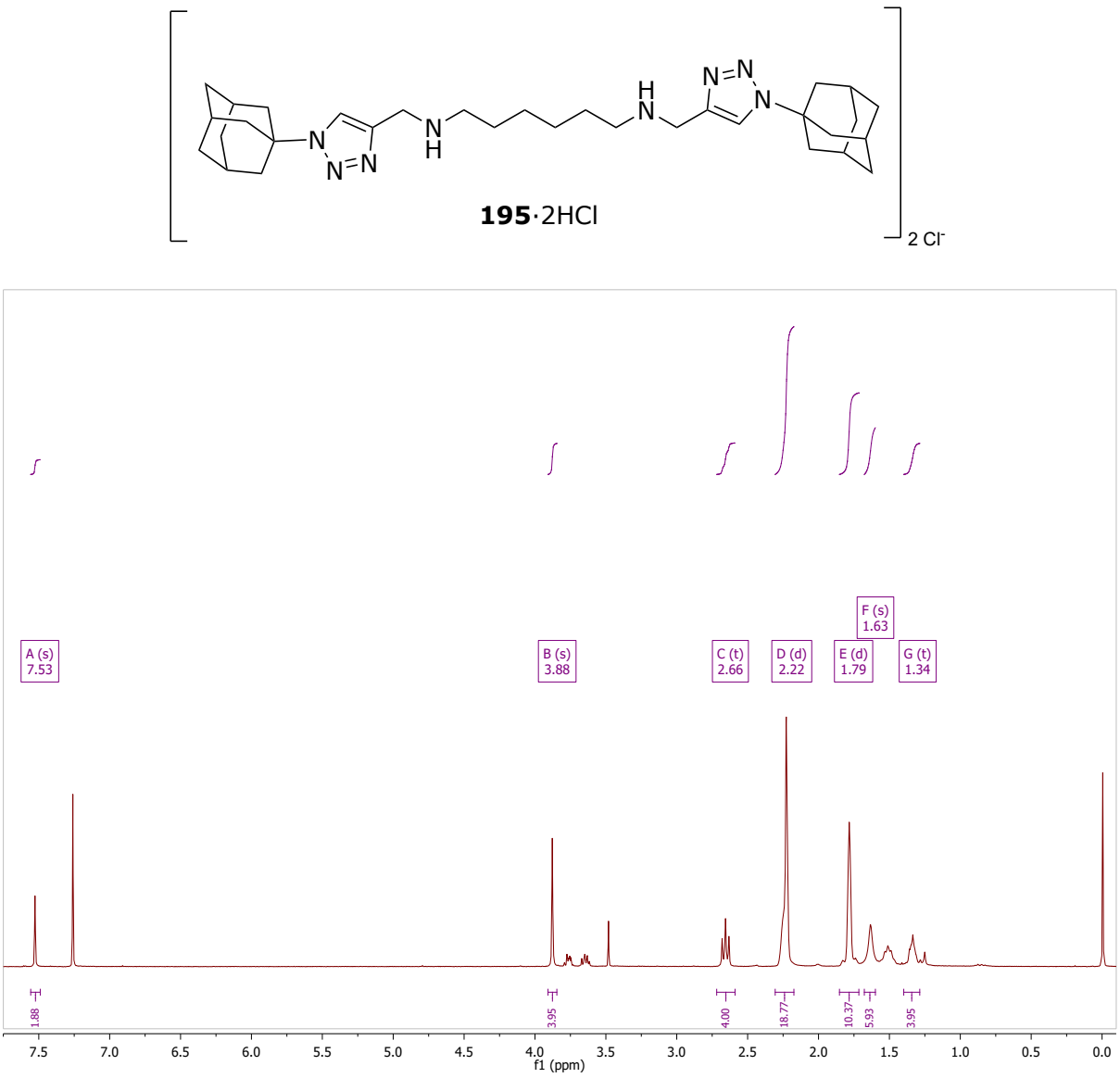

Appendix G.4 – ^{1}H NMR (300 MHz) spectrum of **195·2HCl** in $CDCl_3$.

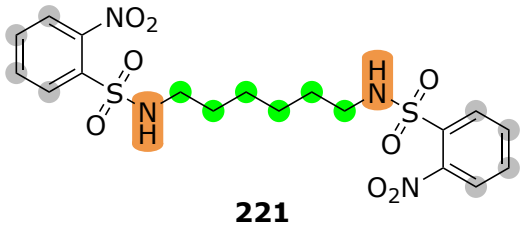

221

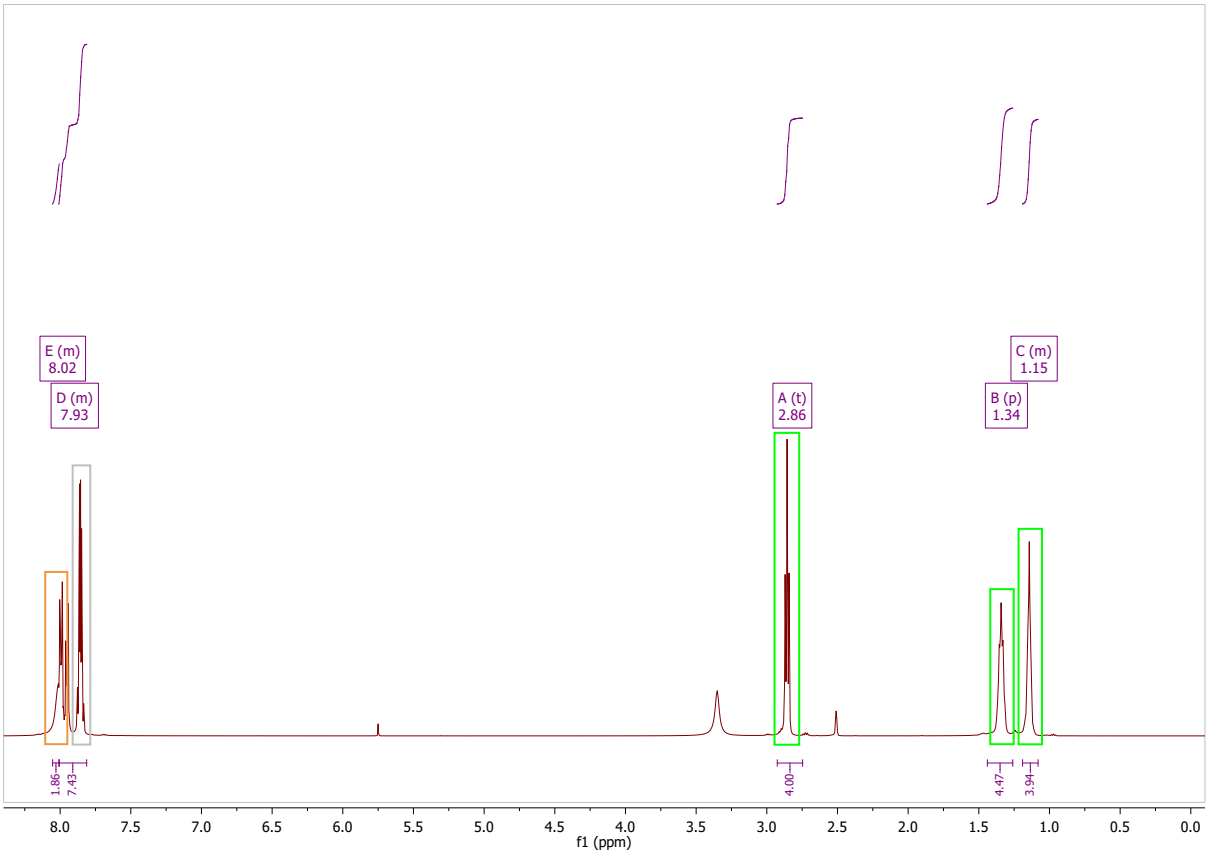

Appendix G.5 – ^{1}H NMR (500 MHz) spectrum of **221** in DMSO.

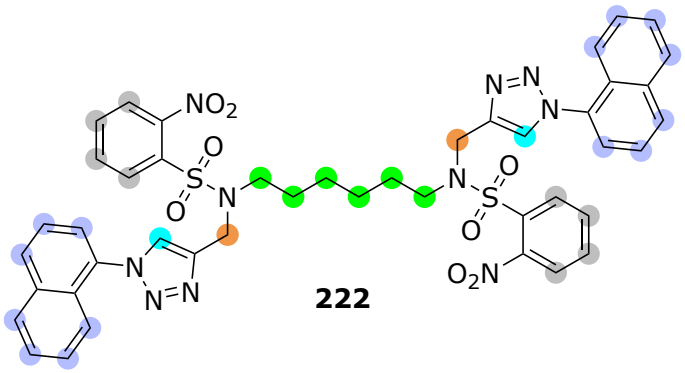

222

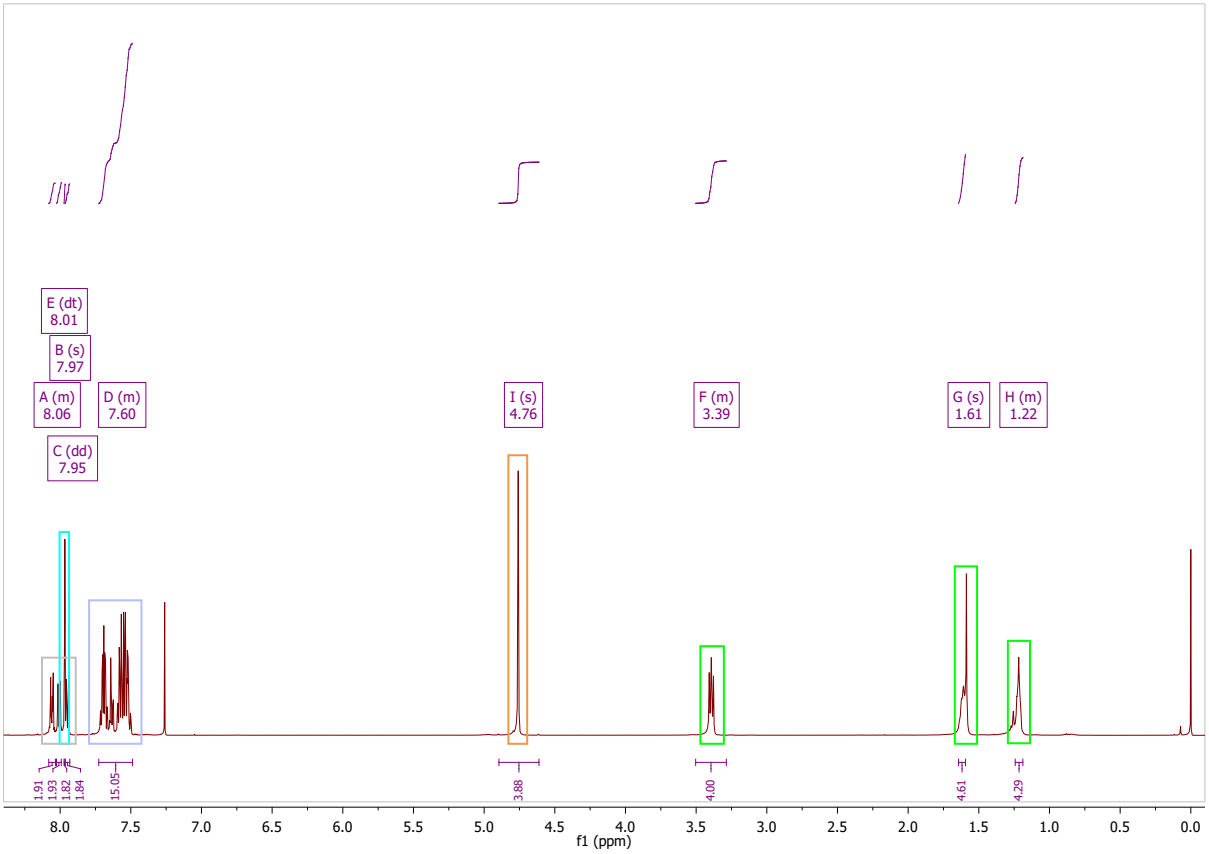

Appendix G.6 – ^{1}H NMR (500 MHz) spectrum of **222** in $CDCl_3$.

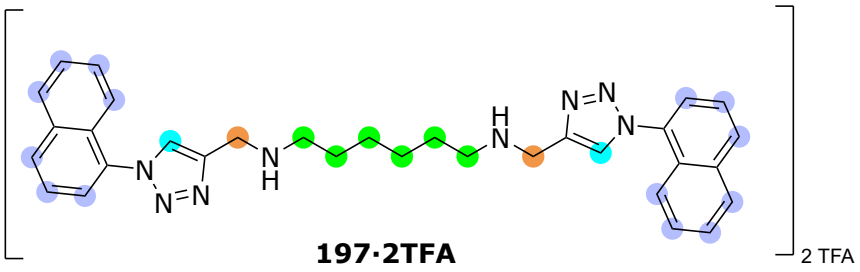

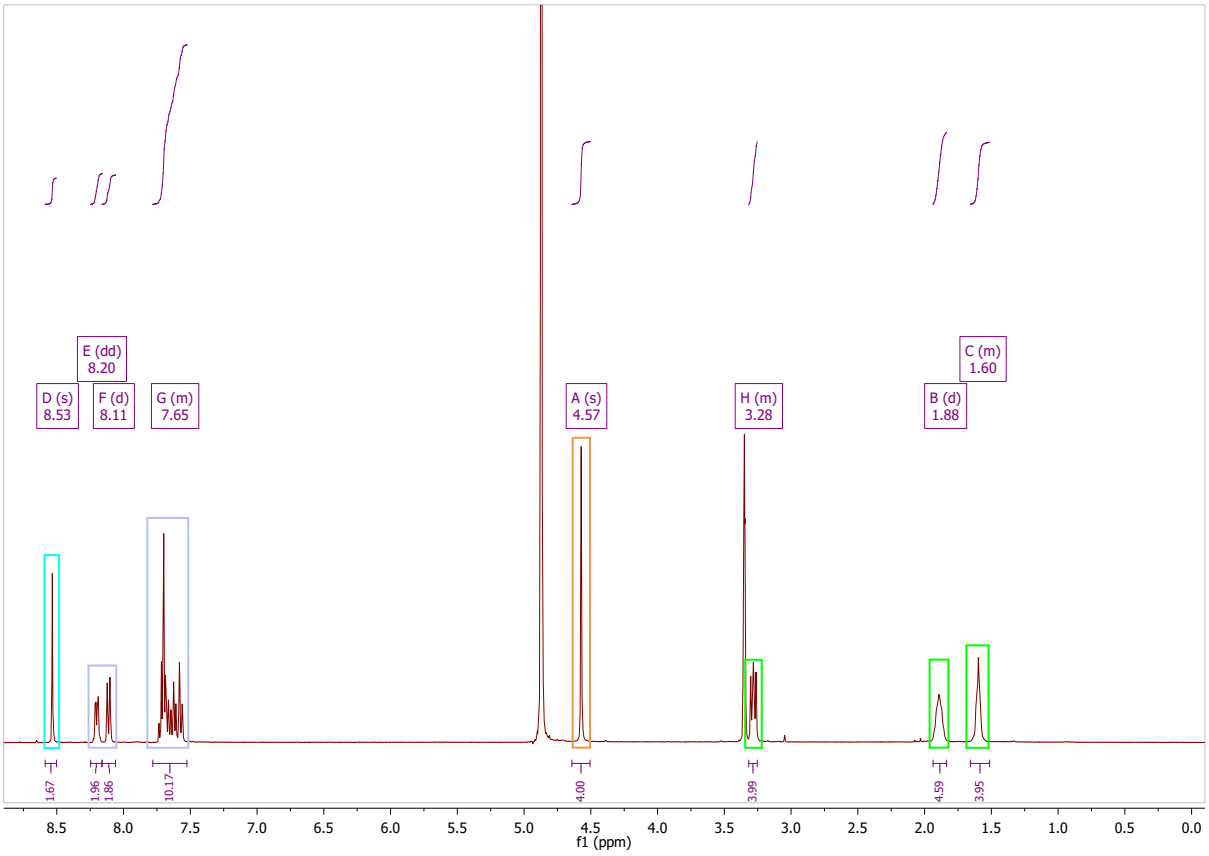

Appendix G.7 – ^{1}H NMR (400 MHz) spectrum of **197·2TFA** in MeOD.

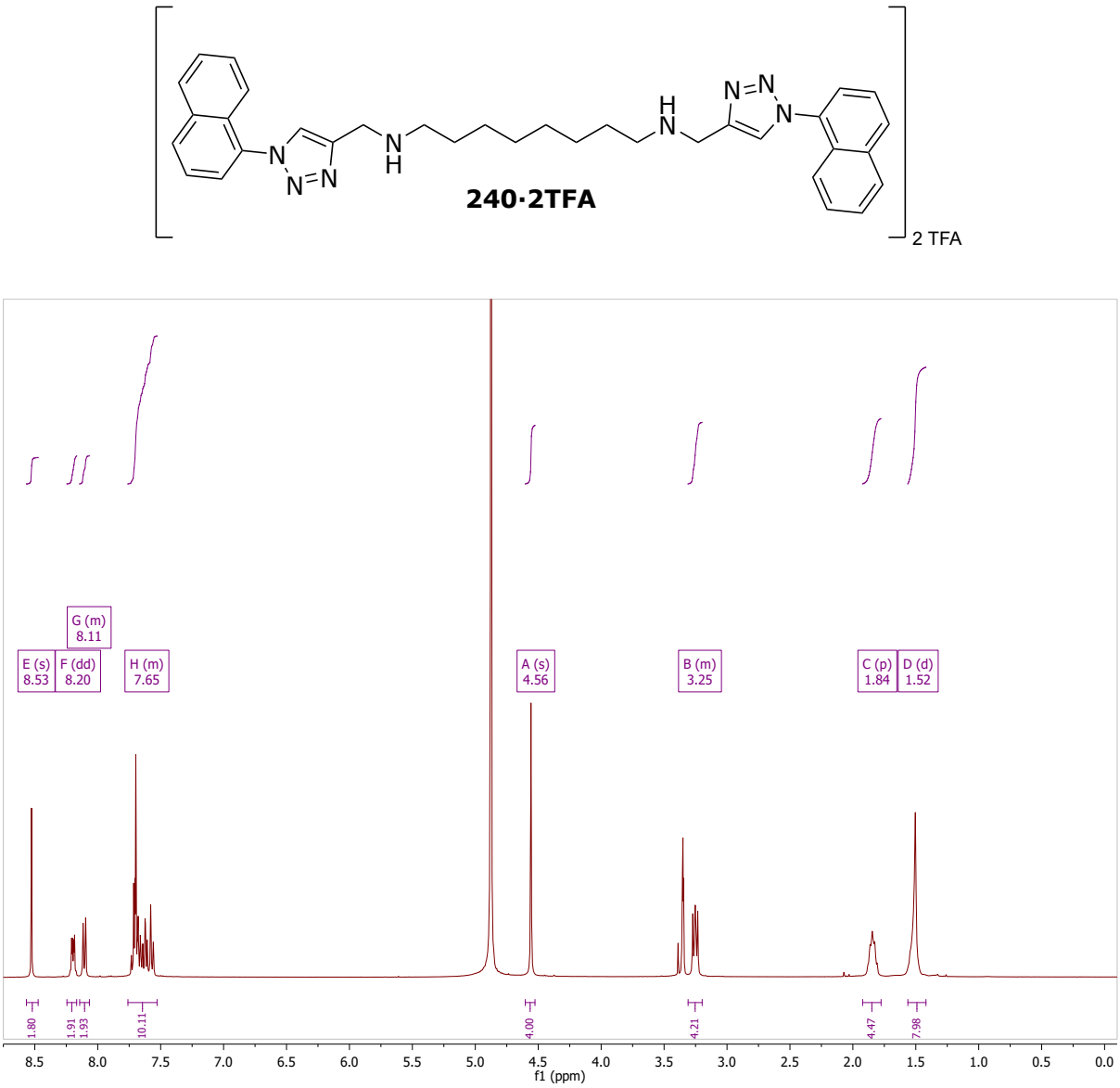

Appendix G.8 – ^{1}H NMR (400 MHz) spectrum of **240·2TFA** in MeOD.

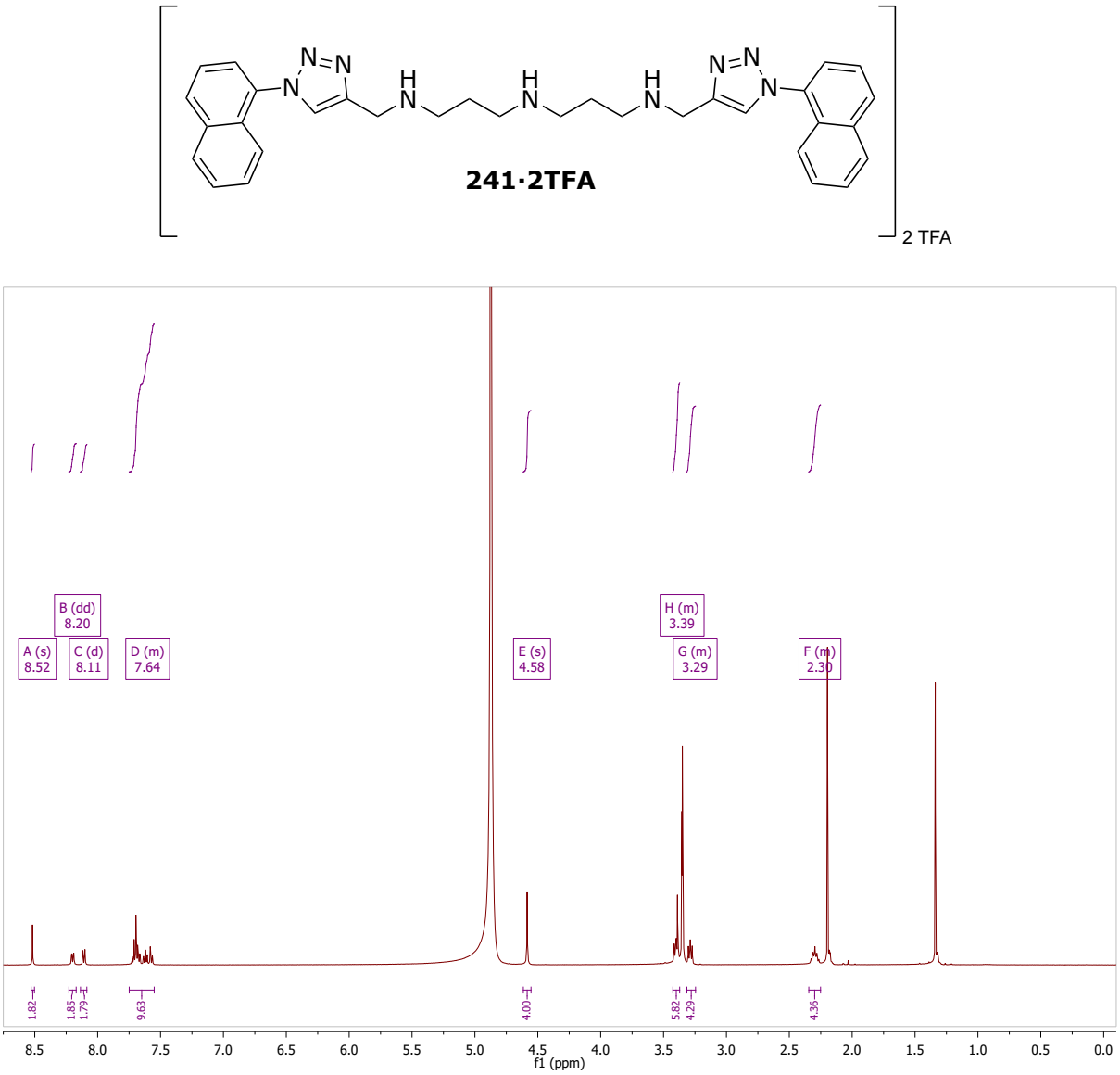

Appendix G.9 – ^{1}H NMR (500 MHz) spectrum of **241·2TFA** in MeOD.